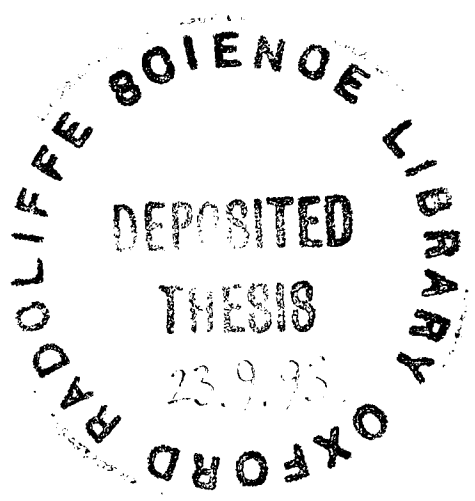
THE VALIDITY OF OPTICAL DATING BASED ON FELDSPAR

Nigel A. Spooner

Linacre College, Oxford

A thesis dissertation submitted for the degree of Doctor of Philosophy.

Hilary Term, 1993



© N. A. Spooner 1993

ABSTRACT

The potential for valid dating using feldspar minerals has recently been increasingly questioned with the recognition of a range of effects capable of giving rise to age shortfalls. The intention here was to investigate the more serious of these, and to simultaneously extend the surprisingly meagre body of knowledge on the luminescence of the feldspar minerals.

A suite of feldspars representative of all major mineral species of the feldspar ternary system was assembled and mineralogically classified by XRD and SEM techniques. Characterization of some luminescence properties relevant to dating (radiation dose-sensitivities, emission spectra, thermal sensitization and bleaching by IR and green light) was conducted to enable comparison of these properties with the anomalous fading behaviour in each feldspar (IRSL and OSL intensities being subsequently measured as a function of storage duration at 10°C and 100°C). Examples of feldspars representative of each major compositional regime of the ternary system were found to fade, and similarly some were stable; no luminescence characteristics or storage duration at these temperatures permitted reliable separation of stable signals. A new method for analysis of localised transition-type anomalous fading was successfully tested on zircon; however the fading mechanism operant in feldspars was found to be tunnelling-type fading. Such fading cannot be circumvented by any feasible laboratory procedure and it was concluded that monitoring of samples for the presence of fading is essential: discovery of fading is a rejection criteria.

The long-term trapping stability of the IRSL source traps was investigated by "conventional" kinetic means, and also by a combined optical and thermal approach in which the bleaching response curves of five selected feldspars were measured along with their low temperature (≈ 100-400 K) response. It was concluded that the IRSL signal originates from one trap type only in all feldspars, which possesses a constant ground state-to-excited state transition energy of 1.44 ± 0.01 eV. However, the excited state-to-conduction band energy varies depending on the major element composition of the feldspar. Lifetimes of microcline TL from glow curve temperatures > 300°C greatly exceed the minimum required for dating and this work and complementary experiments showed no physical basis for the existence of an age limit for coarse grain feldspars, other than dose saturation. Supplementary work supported the existence of an upper age limit of ≈ 100 ka for fine grain materials.

ACKNOWLEDGEMENTS

I thank Prof. M.J. Aitken for his supervision of this project and valuable discussions and advice. Encouragement from Prof. M.S. Tite in the latter stages of this work was also appreciated.

The work presented in this thesis would not have been possible without the expert assistance of M. Franks, D. Seeley, J. Fenton and A. Bowley, and I am pleased to express my great appreciation of their efforts.

Valuable discussions with Dr. G. Hütt, Dr. B.W. Smith, Dr. A.M. Stoneham, Dr. R.H. Templer, Dr. R. Visocekas and Dr. A.G. Wintle are gratefully acknowledged.

The friendship and help with apparatus given by D. Stoneham, M. Winter and Dr. A. Allsop throughout the time of my stay in RLAHA are also gratefully remembered, as are the help of the other staff at RLAHA.

It is also a great pleasure to acknowledge the friendship of Cate McElroy, Xie Jun, Fraser Hunter, Sara Hall, C. McFee, Dr. G.C.W.S. Wheeler and Dr. E.J. Rhodes.

I am indebted to my benevolent landlord Dr. Simon Mercer, and to P. Clark for casting a lifeline in the turmoil.

I am profoundly indebted to D.G. Questiaux-Spooner for much valued discussion and tireless help with data analyses.

Finally I thank the ORS award scheme, and RLAHA for financial assistance throughout the course of this work.

TABLE OF CONTENTS

CHAPTER 1 INTRODUCTION 1

1.1 INTRODUCTION 1

1.2 LUMINESCENCE AND LUMINESCENCE DATING 1

1.3 THE STABILITY OF LUMINESCENCE SIGNALS 2

1.4 AGE SHORTFALLS IN DATING BASED ON FELDSPATHIC MATERIALS 4

1.4.1 FINE-GRAIN MATERIALS 4

1.4.2 COARSE GRAIN FELDSPAR 6

1.5 INTRODUCTION TO THE THESIS 6

1.5.1 A THESIS OVERVIEW 6

CHAPTER 2 THE DEVELOPMENT OF AN OPTICAL DATING SYSTEM BASED ON IR DIODE ARRAYS 9

2.1 INTRODUCTION 9

2.2 THE EARLY DIODE MODULES 11

2.3 INTERCOMPARISON OF HIGH-POWER INFRARED LEDs 15

2.4 THE SHUTTERED DIODE ARRAY "Mk IV" 18

2.5 THE AUTOMATED OPTICAL DATING SYSTEM INTRODUCTION . 22

2.6 A SYSTEM OVERVIEW 23

2.7 DESIGN CONSIDERATIONS 23

2.8 SYSTEM PERIPHERALS 27

CHAPTER 3 FELDSPAR LUMINESCENCE CHARACTERISTICS 29

3.1 INTRODUCTION 29

3.2 THE FELDSPAR SAMPLES 31

3.3 LUMINESCENCE SENSITIVITIES 33

3.3.1 DISCUSSION 34

3.4 IRSL EMISSION SPECTRA 36

3.4.1 INTRODUCTION 36

3.4.2 EXPERIMENTAL 39

3.4.3 RESULTS AND DISCUSSION 40

3.4.4 RELEVANCE TO FADING 41

3.5 BLEACHING OF FELDSPAR LUMINESCENCE 43

3.5.1 INTRODUCTION 43

3.5.2 EXPERIMENTAL 44

3.5.3 RESULTS AND DISCUSSION 45

3.5.3.1 INITIAL DECAY RATES 49
3.5.3.2 ABSENCE OF PEAK-SPECIFIC BLEACHING 50
3.5.3.3 RELEVANCE TO STABILITY 51
3.6 THERMAL ACTIVATION CHARACTERISTIC (TAC) CURVES 52
3.6.1 RESULTS AND DISCUSSION 53
3.7 SUMMARY. 54
CHAPTER 4 ANOMALOUS FADING OF FELDSPAR LUMINESCENCE 55
4.1 INTRODUCTION - AN OVERVIEW AND NOMENCLATURE 55
4.2 ANOMALOUS FADING 61
4.2.1 INTRODUCTION AND PRELIMINARY RESULTS 61
4.2.2 THE FADING SURVEY 63
4.2.2.1 FADING OF IRSL AT 10°C AND 100°C 64
4.2.2.2 FADING OF OSL AT 10°C AND 100°C 65
4.2.2.3 FADING OF IRSL OF LABRADORITE AT 77 K 67
4.2.2.4 DISCUSSION 68
4.2.3 FADING OF TL IN SANIDINE 73
4.2.3.1 INTRODUCTION 73
4.2.3.2 THERMAL ACCELERATION OF FADING IN 12. PATMOS SANIDINE 73
4.2.3.3 DATING OF 12. PATMOS SANIDINE 76
4.2.4 A NEW APPROACH FOR INVESTIGATING LOCALISED TRANSITION FADING - THE METHOD OF VARIATION OF HEATING RATE 78
4.2.4.1 INTRODUCTION 78
4.2.4.2 EXPERIMENTAL 80
4.2.4.3 THE EFFECT OF ALPHA IRRADIATION 83
4.2.4.4 RESULTS AND CONCLUSIONS 87
4.2.5 A SEARCH FOR LOCALISED TRANSITION MEDIATED FADING IN FELDSPAR USING THE METHOD OF VARIATION OF HEATING RATE. 89
4.2.5.1 INTRODUCTION 89
4.2.5.2 EXPERIMENTAL 89
4.2.5.3 RESULTS AND DISCUSSION 90
4.2.6 FADING MONITORING 96
4.2.6.1 INTRODUCTION 96
4.2.6.2 THE FADING MONITORING PROCEDURE 97
4.2.7 SUMMARY 100
CHAPTER 5 THERMAL STABILITY OF LUMINESCENCE FROM SELECTED FELDSPARS 103
5.1 INTRODUCTION 103

5.2 OPTICAL BLEACHING OF THE IRSL SIGNAL BY VARIOUS WAVEBANDS (MONITORED BY 880 ▲ 80 nm STIMULATION) 104
5.2.1 INTRODUCTION 104
5.2.2 EXPERIMENTAL 107
5.2.3 IRSL DECAY CURVES FOR VARIOUS STIMULATION WAVEBANDS 108
5.2.4 BLEACHING RESPONSE OF THE IRSL SIGNAL 110
5.2.5 DISCUSSION 112
5.2.6 OPTICAL BLEACHING OF THE OSL FROM A MICROCLINE (MONITORED BY 514.5 nm STIMULATION) 118
5.2.6.1 INTRODUCTION 118
5.2.6.2 EXPERIMENTAL 119
5.2.6.3 RESULTS 120
5.2.6.4 OPTICAL BLEACHING OF MICROCLINE TL 120
5.2.6.5 DISCUSSION 121
5.2.7 SUMMARY OF THE BLEACHING RESULTS 123
5.3 TEMPERATURE DEPENDENCE OF THE IRSL SIGNAL 125
5.3.1 INTRODUCTION 125
5.3.2 EXPERIMENTAL 126
5.3.3 RESULTS AND DISCUSSION 128
5.3.4 SUMMARY 131
5.4 DEPENDENCE OF THE IRSL ON PHOTON FLUX DENSITY. 132
5.4.1 EXPERIMENTAL 133
5.4.2 DISCUSSION 134
5.5 A KINETIC STUDY OF A MICROCLINE FELDSPAR 135
5.5.1 INTRODUCTION 135
5.5.2 EXPERIMENTAL 139
5.5.3 TL PEAK STRIPPING BY STORAGE AT 220°C AND 260°C: GLOW CURVES AND INITIAL RISE MEASUREMENTS 140
5.5.4 THE 380°C TL PEAK 144
5.5.4.1 INTRODUCTION 144
5.5.4.2 THE 380°C TL PEAK AS AN IRSL SOURCE 144
5.5.4.2.1 EXPERIMENTAL 145
5.5.4.2.2 RESULTS AND DISCUSSION 146
5.5.4.3 THE ISOLATED 380°C TL PEAK: ANALYSIS BY THE METHOD OF HEATING RATE VARIATIONS (HOOGENSTRAATEN'S METHOD) 150
5.5.4.4 ISOTHERMAL DECAY AT 0.01 K/s 154

5.5.4.5 ANALYSIS OF THE 380°C TL PEAK FOLLOWING STORAGE AT 300°C: CHEN'S METHOD AND THE INITIAL RISE METHOD 155
5.5.5 SOME TRAP PARAMETERS OF SCANDINAVIAN FELDSPAR Z10b 158
5.6 DISCUSSION AND SUMMARY 159

CHAPTER 6 SOME INVESTIGATIONS ON LONG-TERM STABILITY 164
6.1 INTRODUCTION 164
6.2 AN ATTEMPT AT LONG RANGE OPTICAL DATING USING POLYMINERAL FINE GRAIN MATERIAL 164
6.3 CIRCUMVENTION OF FADING OF IRSL BY CHOICE OF STIMULATION WAVELENGTH - A DATING TEST OF THE SINGLE-EXCITED STATE HYPOTHESIS. 166
6.3.1 INTRODUCTION 166
6.3.2 IRSL LIGHT SUMS AND TL BLEACHING - EFFECT OF DIFFERENT IR WAVELENGTHS 168
6.3.3 A DATING COMPARISON OF THE IRSL STIMULATED BY DIFFERENT IR WAVEBANDS 172
6.4 AN INVESTIGATION OF A POSSIBLE INTERMEDIARY TRAP ACCESSIBLE BY PHOTOTRANSFER 176
6.4.1 INTRODUCTION 176
6.4.2 EXPERIMENTAL 177
6.4.3 DISCUSSION 178
6.5 BLEACHING BY ENVIRONMENTAL BLACKBODY RADIATION 180
6.5.1 INTRODUCTION 180
6.5.2 THERMAL RADIATION DOSAGE IN ANTIQUITY AND IN LABORATORY PROCEDURES 181
6.6 DISCUSSION AND SUMMARY 184

CHAPTER 7 CONCLUSIONS ON OPTICAL DATING USING FELDSPAR 188

APPENDICES

APPENDIX A A FLUORESCENT MONITOR FOR OSL READERS
APPENDIX B AN INVESTIGATION OF CERAMIC-SUBSTRATE SOURCES FOR BETA IRRADIATIONS
APPENDIX C CIRCUIT DIAGRAM FOR THE MK III LED MODULE
APPENDIX D CIRCUIT DIAGRAMS FOR THE MK IV LED MODULE
APPENDIX E THE ELSEC OPTICAL DATING SYSTEM

APPENDIX E THE ELSEC OPTICAL DATING SYSTEM

APPENDIX F CIRCUIT DIAGRAMS FOR SHUTTER DRIVERS

APPENDIX G FELDSPAR SAMPLE COMPOSITION

APPENDIX H FELDSPAR EMISSION SPECTRA DATA

APPENDIX I "NATURAL" AND REGENERATED FELDSPAR GLOW CURVES

I.1 EXPERIMENTAL

I.2 RESULTS AND DISCUSSION : POTENTIAL FOR RECUPERATION

BIBLIOGRAPHY 195

INCLUDED PUBLICATIONS

ACHENHEIM BEYOND THE EEMIAN USING GREEN AND INFRA-RED STIMULATION

ARCHAEOLOGICAL DATING BY INFRA-RED STIMULATED LUMINESCENCE USING A DIODE ARRAY

SOME CHARACTERISTICS OF INFRA-RED EMITTING DIODES RELEVANT TO LUMINESCENCE DATING

OPTICAL DATING : PRELIMINARY RESULTS ON THE ANOMALOUS FADING OF LUMINESCENCE FROM FELDSPARS

CHAPTER 1 INTRODUCTION

1.1 INTRODUCTION

Progress towards the acceptance of luminescence dating as a valid geochronological tool has been stymied by the successive identifications of age shortfalls from feldspathic materials. It remained unknown whether these shortfalls arose from deficiencies in the dating methodologies so far applied, or in the failure of feldspar luminescence to fulfil the fundamental requirement of a dating method - that of the predictability of the "clock phenomenon". In luminescence dating the "clock" is the accumulation of trapped charge within the crystal lattice and "predictability" includes the successful retention - stability - of the trapped charge.

The intention of this thesis then was to investigate the stabilities of luminescence signals from feldspathic materials in order to determine whether or not fundamental limitations of stability were at work, and if not, to attempt to refine existing dating methodologies so as to permit more accurate dating.

1.2 LUMINESCENCE AND LUMINESCENCE DATING

The luminescence phenomena of concern in this thesis are those resulting from the recombination of an electron and hole, accompanied by the emission of a detectable photon. Creation of the electron-hole pair originally took place in the process of deposition of energy into the crystal lattice by ionizing radiation; following which each charge species diffused in the conduction and valence bands respectively until metastably

trapped at mid-band defect sites. Release from these trapping sites may be activated either by thermal means - phonon absorption - (thermoluminescence (TL)), or by absorption of a suitably energetic photon, giving rise to optically stimulated luminescence (OSL), or infrared stimulated luminescence (IRSL). Acceptably accurate dating application of luminescence requires these trapping sites to retain the electron and hole, prior to this laboratory untrapping event, over at least an order of magnitude of time greater than the timespan to be dated.

Equally strong requirements are that the concentration of this trapped charge grows with dose, and that the environmental radiation field produces ionizing radiation at a constant (or at least determinable) rate over the dating age range. These fundamental criteria underpin luminescence dating, the tenets of which have been amply covered elsewhere (i.e., Aitken 1985) and will not be further reiterated here.

1.3 THE STABILITY OF LUMINESCENCE SIGNALS

While TL dating has the facility of the plateau test, in which the "flatness" of the ratio of natural to additive-dose glow curves reveals the temperature regimes in which the luminescence has sufficient thermal stability for that dating application, optical dating has no such convenient tool (as the influence of interactive kinetics during measurement can cause the ratio of Natural/(Natural+added dose) "shine" curves to deviate from a "plateau", even when only stable signal is present - pers. comm. D.G. Questiaux, Dec. 1988). Alternative means have been proposed for assessing the thermal stability of the signals in optical dating by Huntley *et al* (1985) and Questiaux (pers. comm., 1988). The former suggests use of successively higher temperature preheats of equal duration, whereas the

latter demonstrated a preheat "plateaux" constructed from repeated palaeodose evaluations made following incrementally longer storages at one preheat temperature. Both methods rely on reaching a sufficiently "hard" preheat after which only thermally stable luminescence remains. Although these empirical methods are essential in the practical application of optical dating, they cannot reliably reveal the presence of fading, and hence are of limited use in addressing age shortfalls, beyond determining its presence in known age samples.

Consequently, to quantify the parameters of the traps exploited for optical dating it was necessary to turn to analytical means (kinetic methods). Although the application of kinetic methods is fraught with uncertainty, on account of the analysis methods themselves being derived under a series of approximations (Lewandowski and McKeever, 1991), they remain the only analytical means of measuring trap stability. (The empirical approach of determining lifetimes from the signal levels in "infinitely" old samples (Mejdahl, 1988), is in practice vulnerable to unknown systematic errors such as long-timescale diffusion processes not ordinarily significant over dating age ranges, and also to recently recognised problems such as internal absorption of UV emissions (Wintle and Duller, 1991)).

The lifetime, (for thermal untrapping), of an electron at a trapping site is given by $\tau = S^{-1} * e^{E/kT}$ seconds. The escape frequency factor S and the trap depth E are characteristic of each trap type and may be experimentally determined by a range of analytical techniques. Full descriptions of the kinetic methods applied in this work are given in Chen and Winer (1970), Chen and Kirsh (1981), Fleming (1990), Kirsh (1992), Lewandowski and McKeever (1991) and McKeever (1985).

Unfortunately, the simple picture alluded to above in which straightforward and reliable estimates may be made of trapping stabilities is not universally obeyed. The

phenomenon of anomalous fading was identified through the discovery of drastic age underestimations from feldspathic samples (Wintle, 1973) which also showed loss of luminescence on laboratory timescales from TL glow curve temperatures presumed thermally stable on kinetic grounds. Some mechanisms by which this fading may occur, and of which there is extensive experimental evidence, are quantum mechanical tunnelling (i.e., Delbecq *et al* (1974), Visocekas *et al* (1976) and Visocekas (1979)) and localised transitions (Templer (1986a and 1986b)). Various other mechanisms, such as defect diffusion have been postulated but confirmation of their presence in the minerals commonly used for luminescence dating has not yet been reported.

The existence of these fading mechanisms gives a physical basis for expectation that some, at least, of the reported age shortfalls may not be methodological artifacts. Generally, a brief overview of the described types of age shortfall and some possible causes is given in section 4.1.

1.4 AGE SHORTFALLS IN DATING BASED ON FELDSPATHIC MATERIALS

1.4.1 FINE-GRAIN MATERIALS

Following the work of Debenham (1985) and Wintle (1985), in which an old age limit (the so-called "100 ka" limit) for the dating of fine-grain feldspathic samples was identified, this limit has come to appear to be a fundamental restraint on maximum age obtainable from these materials. The widespread geographical localities from which old age shortfalls have recently been reported (i.e., Europe; Packman and Grün, (1989 and 1992), Spooner and Questiaux, (1989), using optical dating with both green and IR

stimulation; Pakistan; Rendell (1988); China; Lu et al (1988) and Zhou and Wintle, (1989)) strongly suggest that the limitation is fundamental and possibly ubiquitous. Although some claims have been made for dates well in excess of 100 ka, notably those by Zöller and Wagner (1989) and Berger *et al* (1992), in the former case a systematic dating study of those same loess deposits from the Middle Rhine Area, (Frechen, (1992), and Frechen *et al* (1992)) failed to substantiate the claimed ages. The success reported in dating a 800 ka loess deposit from New Zealand by Berger *et al* (1992) must also be questioned, as some of the explanations invoked for this success (such as selection of filters so as to exclude the self-attenuated UV emissions) are invalid (see Wintle *et al* (1993) for a critical discussion of this work). However, the possibility exists that there is a peculiarity of the local geology at the sites sampled by Berger *et al* (1992) which permits such great ages to be attained. Unfortunately, the absence of credible reports of similar ages elsewhere to set against the unanimity of old age dating failures leads to the conclusion that this success, if true, is only significant as a geophysical curiosity.

The lack of success experienced by Spooner and Questiaux, (1989), using an extensive range of temperature and storage-time combinations, coupled with detection of the full spectral range of IRSL and OSL emissions available to a bialkali photomultiplier (PMT), was taken as verification of the above perception regarding the long-term stability of luminescence signals in fine grain loessic material. Consequently further work on this aspect of the stability problem was discontinued by the author.

Regarding younger samples: self-consistent results in accord with geological expectation were found by Questiaux (1991) in a comprehensive optical dating study using both IRSL and OSL from various grain size fractions and emission bands from European loessic material. Similarly, promising results on the thermal stability of IRSL signals were reported by Li (1992) for loess samples from different global regions.

1.4.2 COARSE GRAIN FELDSPAR

Although age shortfalls have been widely described from the use of coarse grain (potassium) feldspars, (i.e., Dijkmans and Wintle (1989), Grün *et al* (1989) and Balescu *et al* (1989)), it appears to be a different phenomenon to that seen in fine grain samples. In these and other reports there is a consistent fractional age underestimate of ≈ 30 %. Balescu and Lamothe (1992) overcame this by use of blue-pass filters which rejected UV emissions, a success attributed by Wintle and Duller (1991) to avoidance of dosimetric problems posed by the internal absorption of UV-wavelength luminescence by the coarse grain K-feldspars.

However, it is also proposed by Mejdahl (1986), (1988) and (1989) that long-term thermal instability is another cause of age shortfalls, setting a definite upper limit on the age range available using coarse grain alkali feldspars. (These findings are taken as support for the hypothesis that grain-size-dependent processes could be responsible for the "100 ka" limit but inconsequential for larger grain sizes).

1.5 INTRODUCTION TO THE THESIS

1.5.1 A THESIS OVERVIEW

From a consideration of the above reports it was apparent that demonstrating the fundamental stability of the luminescence stimulated from feldspathic materials was of primary importance to the successful and confident establishment of feldspathic-based luminescence techniques as mature geochronological tools. Consequently, systematic study of signal stability in the feldspar minerals using known-composition museum specimens

was considered to be the most productive approach.

The initial stage was the characterization of the feldspars from both the mineralogical and luminescence standpoints (see chapter 3).

Highest priority was then given to investigating the "anomalous fading" (first reported by Wintle, (1973)). This was partly because of its potential for manifestation in any feldspathic sample, regardless of age, and partly because it was hoped that the "short-term" fading, i.e., that seen in the laboratory over timescales of days (Wintle, 1973, Visocekas, 1985), and the "long-term" fading giving rise to the 100 ka limit and possibly to age shortfalls in general, were all various manifestations of the same phenomenon. At the outset of this study it was optimistically anticipated from the work of Templer (1986a,b) on zircon that the fading was of a kind in which the trapped electrons could "leak" by sub-conduction band shared excited levels to spatially adjacent hole traps, and thereby be lost by recombination. A feature of the findings of Templer (1986a,b) was that only about a third of the traps possessed this pathway; the remaining two-thirds were energetically disconnected, and so stable; the crucial consequence of this for dating applications was that a suitable laboratory treatment (such as illumination by red light, or storage at $\approx$ 100°C for several days) would activate the "fading" centres to undergo recombination and leave the stable component untouched. The expectation was that if anomalous fading of the OSL and IRSL was detected, it would be of this type and therefore amenable to similarly convenient treatments. This study, originally expected to entail little more than optimising the thermal wash (preheat) procedure required to eliminate the fading component, is described in chapter 4.

A central hypothesis investigated next (see chapter 5) was that feldspathic signals may not possess the stabilities determined for them from earlier kinetic studies (i.e., Strickertsson, 1985) and so display long-term fading simply due to charge loss by

"normal" thermal untrapping at ambient temperatures (Mejdahl, 1988). The approach here was to determine the energy levels of the IRSL source traps in selected feldspar samples by "conventional" kinetic methods, then to compare the findings with those obtained by combined optical and thermal techniques.

Finally, a range of other possible causes of long-term age shortfalls were investigated; among these were bleaching by the IR photons of the environmental thermal radiation field, "leakage" from IRSL source traps via a "ladder" of excited states and the possible role in fading played by the apparent phototransfer IRSL described by Spooner and Questiaux (1989).

Although the thesis is concerned with "optical dating" in general, the emphasis throughout is on IRSL in preference to OSL. This emphasis evolved slowly: the expectation at the commencement of the study was that the IRSL signal would prove to be an unstable, anomalously fading component (generalizing from the findings of (Templer, 1985) who used bleaching by long-wavelength light to remove anomalously fading luminescence from zircon). However, early experiments showed this was not the case (Spooner and Questiaux, (1989) and Spooner *et al*, (1990)), and given the two signals possessed similar stabilities, the IRSL was not only easier to bleach, but also permitted greater detection efficiency due to the greater spectral range (UV and visible) made available by the relative ease of rejection of IR photons: effort was then accordingly directed towards the IRSL signal.

CHAPTER 2 THE DEVELOPMENT OF AN OPTICAL DATING SYSTEM BASED ON IR DIODE ARRAYS

2.1 INTRODUCTION

The dating application of IR for the stimulation of luminescence from K-feldspar was first reported by Hütt *et al* (1988) at the TL and ESR Dating Seminar, Cambridge, July 1987, the apparatus being a xenon lamp and monochromator assembly. In the proceedings of the same conference Godfrey-Smith *et al* (1988) reported the detection of luminescence stimulated from feldspar and quartz by means of a single IR LED. These findings, with hindsight, are implicit in the work of Kronbørg (1983) where significant bleaching (45% loss of TL at the 330°C abscissa) was observed in feldspar TL following exposure to light passed by 700 nm long-pass Kodak Wratten filters.

In September 1988, following commissioning of the Oxford xenon lamp set (see Fig.1, Spooner and Questiaux, 1989), luminescence was observed from a polymineralic 'natural' portion of loess (4-11 μm, from Val Sorda, Italy, of middle palaeolithic age (Accorsi *et al*, 1990) under stimulation by 861.1Δ12.5 nm IR. Luminescence was also detected from a coarse grain sedimentary extract of potassium feldspar (Scandinavia, provided by V. Mejdahl), both from untreated portions and as a dose dependent signal following incremental β dosing. Additional measurements showed that the IRSL could be zeroed by exposure to green light (514.5 nm), so demonstrating its potential as a sediment dating signal.

Further applications of IRSL became apparent after trials on quartz. Quartz was found to emit no detectable luminescence under IR stimulation, or show any depletion of

the OSL light sum detected during green light stimulation following prolonged IR exposure. This stimulation wavelength resolution between quartz and feldspar raised two immediate possibilities additional to the dating prospect, as outlined in Spooner and Questiaux, (1989). Firstly the testing of quartz separates for feldspar contamination - no detected IRSL signal being interpreted as showing the absence of feldspar. Secondly the possibility of using a long IR bleach to remove the feldspathic signal from polymineral fine grain samples and so permit a "quartz only" optical date to be obtained, in addition to which the IRSL, if recorded, could provide a "feldspar only" date.

The xenon lamp set with which this early work was performed was required for other work, so an alternative more convenient source of IR illumination was sought. Laser diodes, as used for example by Mathur et al (1986) for dosimetry, were considered and rejected as being underpowered, expensive and presenting a significant laser eye hazard.

Following the report of Godfrey-Smith *et al* (1988), a simple ring of 12 TEMT 8850 infrared emitting LEDs (880Δ80 nm, 50 mW/SR at 100 mA, in use as illumination for hand picking zircons by image intensifier (Smith, *et al* 1991)) was assembled as a bleaching light source by B.W. Smith. Modifications were then made to enable IRSL emitted from a single sample disc positioned at the focus of the diode beams to be observed by a PMT, the diode array being inserted between the PMT and a standard TL glow oven. Development of an optimized dating tool based on an array of these diodes was then commenced, paralleling similar work underway at Durham University (Poolton and Bailiff, 1989). Other IRSL readers based on diode arrays have subsequently been reported, by Galloway (1991) and Bøtter-Jensen *et al* (1991).

Problems in producing a stable controllable IR beam soon obtruded, and a comparative study of IR LED characteristics had to be undertaken to select a diode type

more suitable for this application. The sections that follow describe this study and the diode modules resulting, and the subsequent incorporation of a diode module as the stimulation source in an automated IRSL reader developed in commercial collaboration with Littlemore Scientific Engineering (Elsec). Finally, the expansion to a comprehensive optical dating system based on the automated reader is described.

2.2 THE EARLY DIODE MODULES

This section describes the design of diode arrays based on the TEMT 8850 devices and refinements developed from experience with them.

Some requirements desirable or necessary to be addressed in the design of luminescence readers for optical dating applications are :

1) Choice of stimulation waveband

2) Illumination characteristics

   (a) adequate intensity

   (b) uniform intensity across the disc

   (c) omnidirectional (to minimize pseudo-recuperation effects (Aitken and Smith, 1988)

3) Illumination control

   (a) constant intensity

   (b) constant wavelength

   (c) rapid, complete and "spike-free" on/off switching (<10 ms)

4) Sample positioning and orientation - reproducible and precise

5) Sample temperature control (IRSL exhibits about 1 %/°C temperature dependence)

6) Sample-detector geometry to maximise luminescence collection efficiency

The choice of stimulation wavelength was limited to those obtainable from the commercially available high powered IR emitting LEDs of either GaAlAs (880 nm) or GaAs (950 nm) type. Fortuitously both wavebands lay on the IR resonance peak of the optical stimulation response spectra published by Hütt *et al* (1988), and as the 880 nm diode output spectrum was a better match to that data it was decided to retain the TEMT 8850 diodes. The arrangement of 12 diodes in a ring was also retained, though with their beam centres redirected to intercept the sample disc in a circle centred on the disc and of approximately 4 mm radius. This defocussing was necessary so as to prevent a central "hot spot" of overlapping beams giving significant centre-edge illumination intensity drop-off. The ring arrangement of diodes appeared satisfactory as regards illumination quality, and a TL glow oven provided a convenient isothermal sample plate for positioning the discs. Diode response time following switch-on/off, though extended slightly by the circuit response, was nevertheless only of the order of microseconds, and free of significant spikes.

However, as shown in Fig. 2.2.1 the intensity of the output beam of the simple 12 diode ring appeared to drop rapidly following switch-on when monitored by an EMI 9635 PMT (with 2 mm thick Schott RG 830 sharp cut and 1.0 neutral density filters) measuring IR scattered from a ground glass disc placed at the array focus. The percentage drop in intensity increased with increasing diode current, (a finding later attributed to increase in LED junction temperature - GE/RCA Optoelectronics Data Book, 1987, and Melles Griot, Optics Guide 4, (1988)). This finding posed difficulties for the use of this diode array for dating as the illumination intensity would depend critically on diode current and pulse

duration and so vary with time during a long exposure. Even more importantly the diode temperature at the commencement of each individual long exposure in a series of dating measurements must be the same to ensure equivalent illumination over a fixed period exposure. This led to the construction of a new diode module ("Mk III") incorporating features intended to negate intensity changes by delivering compensating changes in diode current.

Fig. 2.2.2 shows the diode module, the circuit diagram is given in Appendix C. The principal development from the previous module is the addition of a photofeedback control facility based on a silicon photodiode (initially Radio Spares cat # 303-674, active area 100 mm^2, later replaced by a Siemens BPW-34 silicon photodiode due to weaker temperature dependence). This photodiode was positioned in the module so as to detect scattered IR - the intensity of which was taken as being proportional to the total IR intensity incident on the sample. Illumination control could then be operated in two ways - "light control", in which the current to the LEDs was adjusted so as to maintain a constant photocurrent from the photodiode or "current control" in which the LED current was set constant and the photodiode was a passive monitor of IR beam intensity.

However it was anticipated, and later shown, that differences in reflectivity between discs would manifest as differences in the level of scattered IR detected by the photodiode and so be treated as real variations in beam power, causing erroneous adjustment to diode current. To minimize the scattered IR contribution originating from reflections off the sample disc an annular white diffusion screen (Lee Filter 251, quarter white diffusion) was interposed between the diodes and the sample. The back reflections off this screen thus constituted a sample of the output beam of each individual LED, the sum being the dominant source of scattered IR "seen" by the photodiode and independent

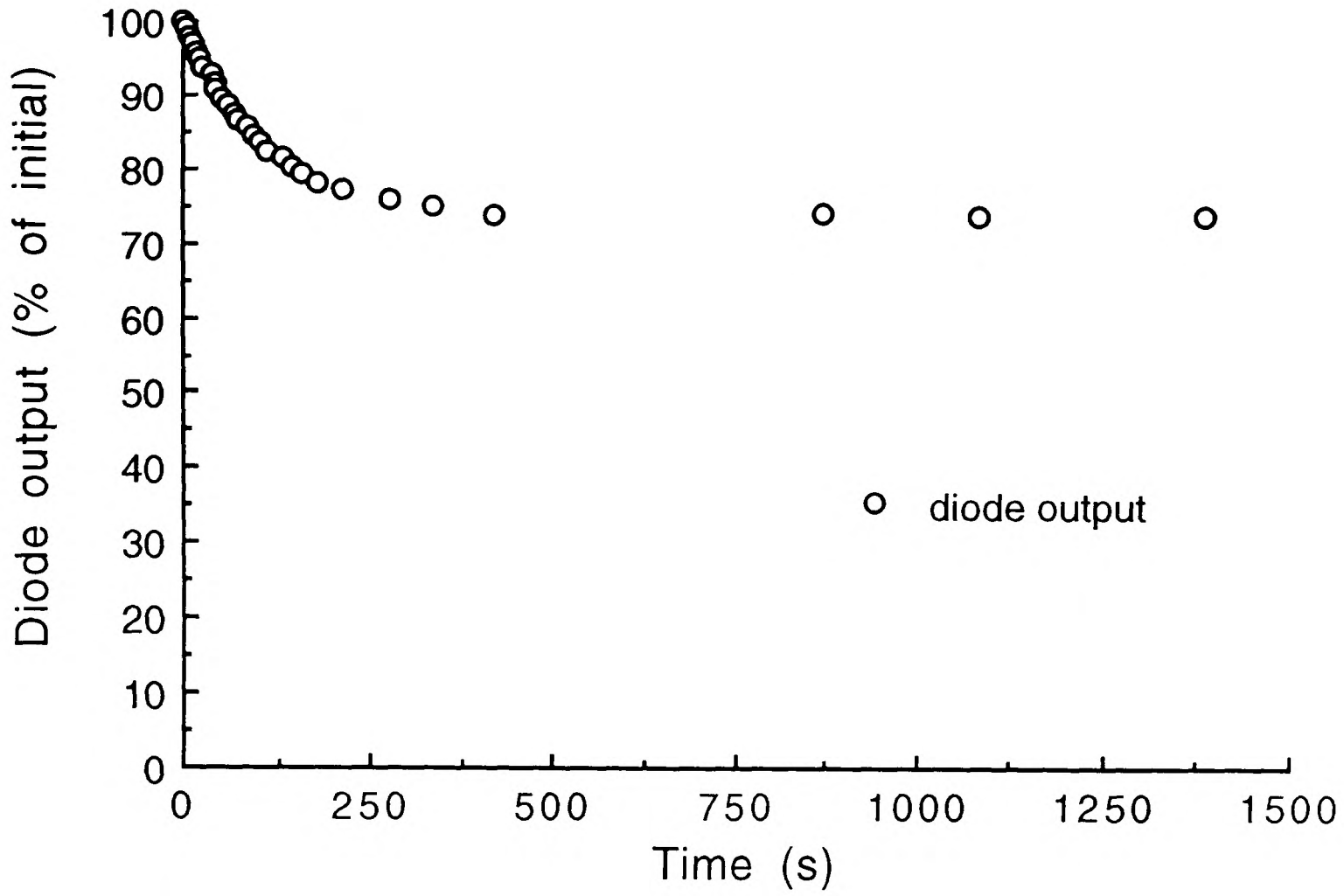


Fig.2.2.1 The variation with time of the output beam from a ring of twelve TEMT 8850 LEDs, at 40 mA. Beam stabilization requires at least 1000 seconds continuous operation.

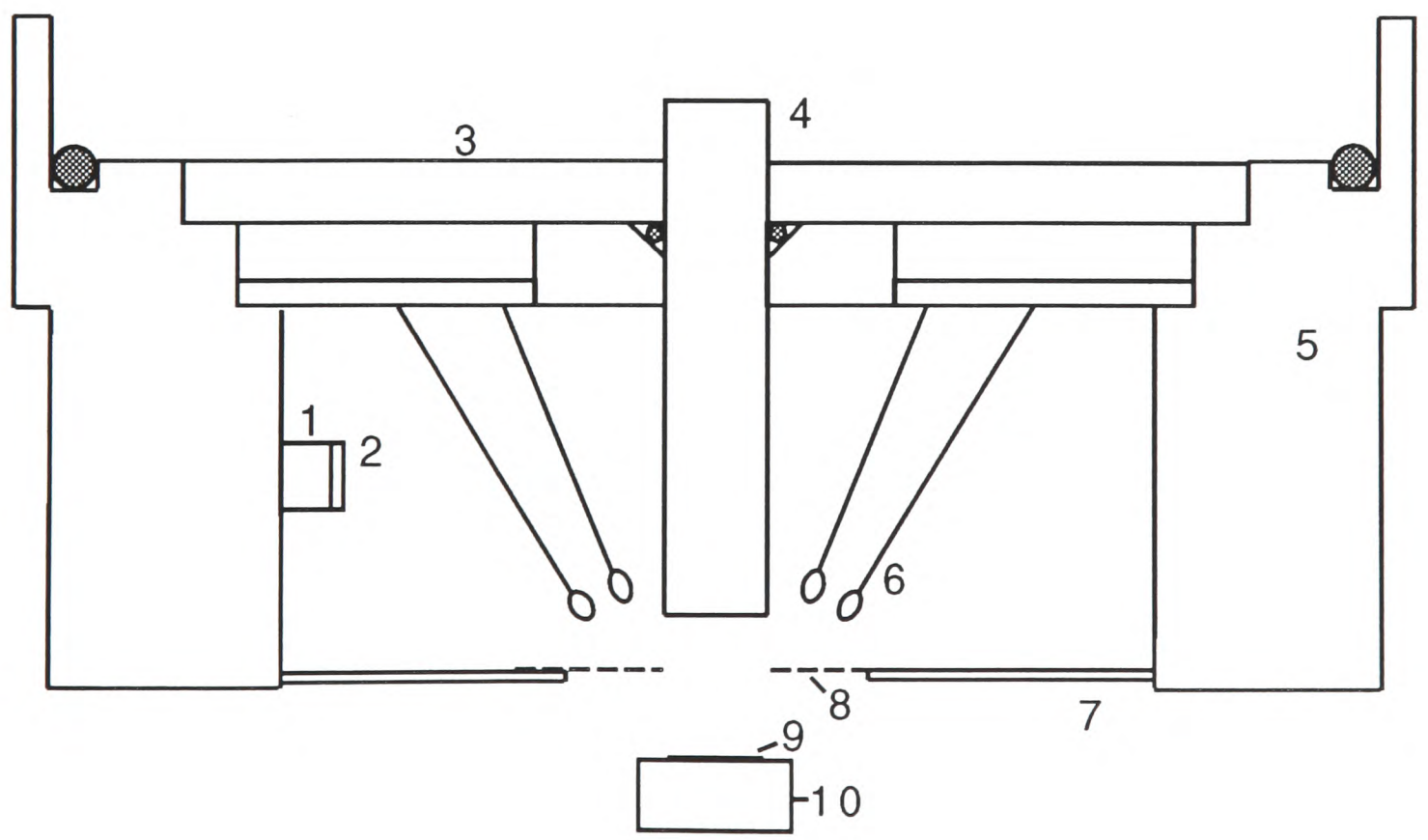


Fig.2.2.2 The MK III diode module, showing (1) photodiode, (2) 2 ND Kodak Wratten filter, (3) light guide mount, (4) 12 mm ϕ spectrasil B light guide, (5) aluminium body, (6) LED array, (7) diffusion screen mount, (8) diffusion screen, (9) sample disc, (10) TL oven plate.

of sample disc reflectivity. Improved uniformity of sample illumination was an additional benefit though at the expense of beam power at the sample. Adequate power was ensured by the addition of a second 12 diodes, giving a total of 24 diodes in two concentric rings of twelve.

Operational procedures were also developed to minimize intensity drift problems. As the percentage intensity drop was proportional to diode current, better IR beam stability was obtained by underrunning the diodes, typically at 30 mA (series connection) rather than the 100 mA maximum rating. Data were recorded using a Silena MCA (model 7922-1024), triggered from the diode array timer. Exposure time units were of 10 msec and exposure durations could be either continuous or pulsed (10 msec minimum period).

However, while the photofeedback control was successful for short exposures (<1s) it proved unable to control the beam for longer exposures (>1s). (It was later shown that the LED output spectrum was temperature dependent (see section 2.3), complicating the use of spectrally sensitive photodiodes; no fast response "blackbody" detectors were available). This problem could be largely circumvented by a measurement regime which used photofeedback control (light control) only for short exposures, relying on the time elapsed between each measurement being sufficient for the diodes to cool to ambient - "cold mode". For long exposures, the photodiode output was used only at the start of a measurement run to set the diode current to a constant level (current control). The diodes then heated towards thermal equilibrium with the relative effects of intensity drifts being removed by the operator maintaining a timed schedule of disc changing with constant time intervals between successive diode usage - "hot mode". Operated in light control mode the Mk III module, though laborious to use, performed well enough to permit dating application (Aitken 1992, Aitken and Xie, 1992), although considerable improvement

would follow from successful photofeedback control. To this end a comprehensive survey of the behaviour of commercially available LEDs was undertaken to find a stable diode or, failing this, a more controllable diode type for dating using the Oxford module design.

2.3 INTERCOMPARISON OF HIGH-POWER INFRARED LEDs

Temperature dependent drifts in the LED output spectrum coupled to the wavelength dependent response of the silicon photodiode prevented long exposure photofeedback control of TEMT 8850-based modules of Mk III design, and instigated an intercomparison of various high power IR emitting LEDs commercially available in the UK (as of 1989). The findings are reported elsewhere ("Some characteristics of infrared emitting diodes relevant to luminescence dating", Spooner, N.A. and Franks, M., Ancient TL, Vol. 8, No. 3, 16-19) and will not be fully recapitulated here. A brief account of aspects of the methodology and supporting experiments follows.

Fig. 2.3.1. shows the change with time of the output intensity of one LED of each type tested, operated at 28.6 mA and measured using an EMI 9635 PMT with 1.0 ND and 2 mm thick RG 830 Schott glass sharp cut filters. The diode beams were aimed directly into the PMT. This initial test demonstrated that all types of diodes tested, with the exception of CQX19, showed monotonic decrease in output with time, attributable to warming towards thermal equilibrium at that operating current (the CQX19 diode was operating at only 10 % of its rated maximum power and emitting just 2 mW/diode, the lack of strong warming effects are therefore not surprising).

It was noted that the magnitude of the observed intensity drops might have been exacerbated by the spectral response of the PMT - reliance on the residual red sensitivity

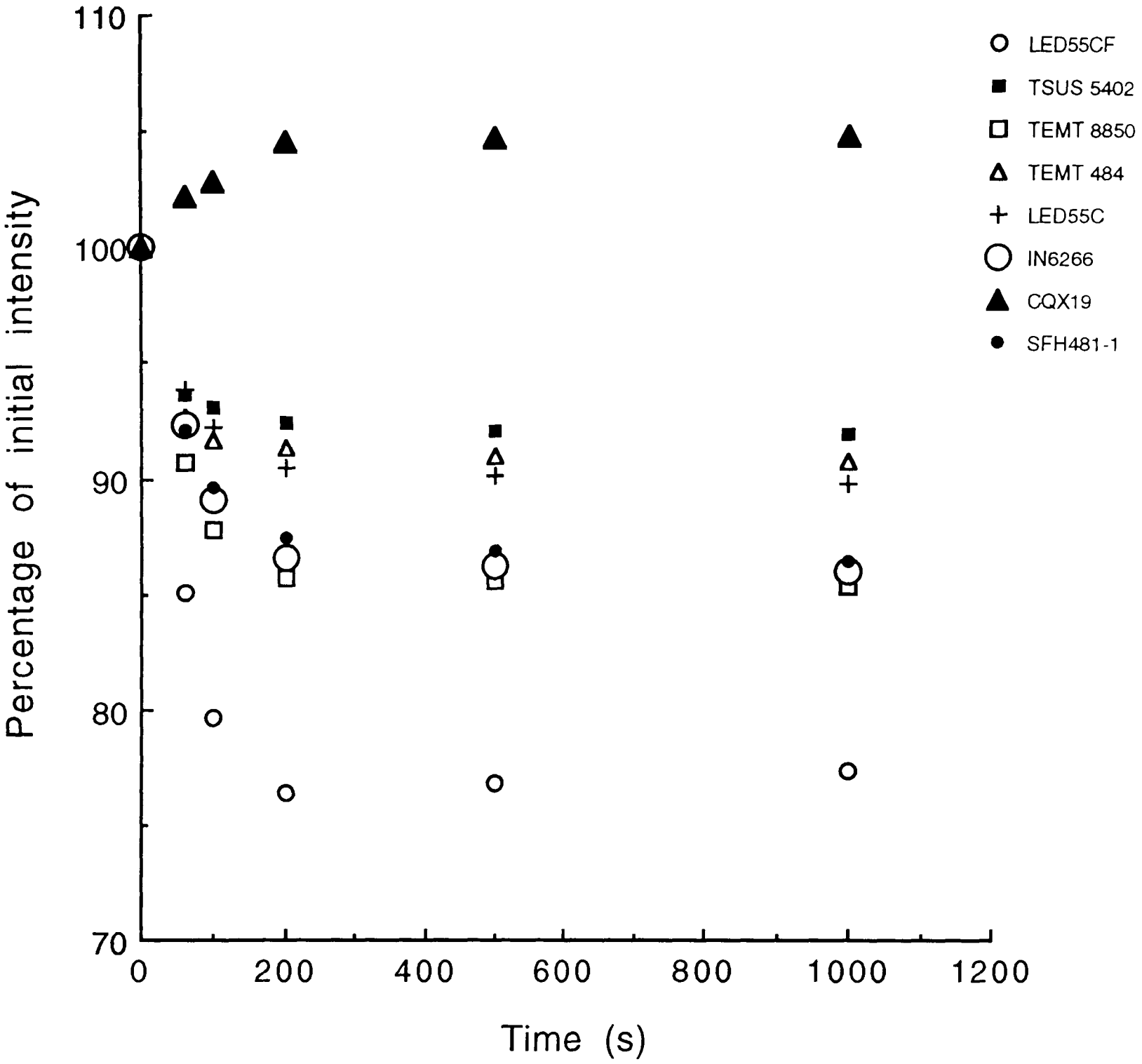


Fig. 2.3.1 The output intensity variation with time for one diode of each type tested. the diodes were operated at 28.6 mA and monitored by filtered PMT. Note the performance of the resin packaged diodes are TEMT 484 and TSUS 5402.

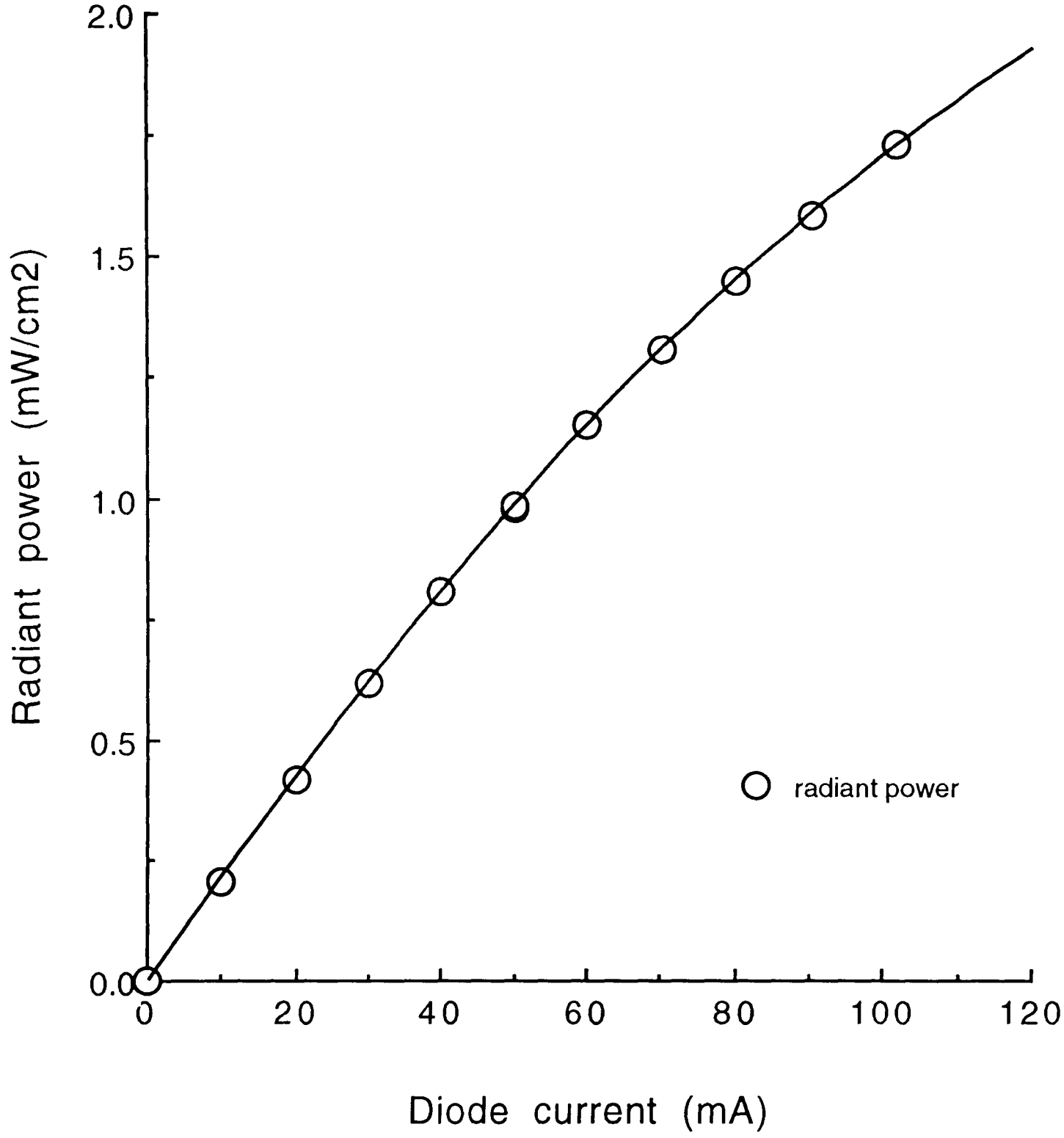
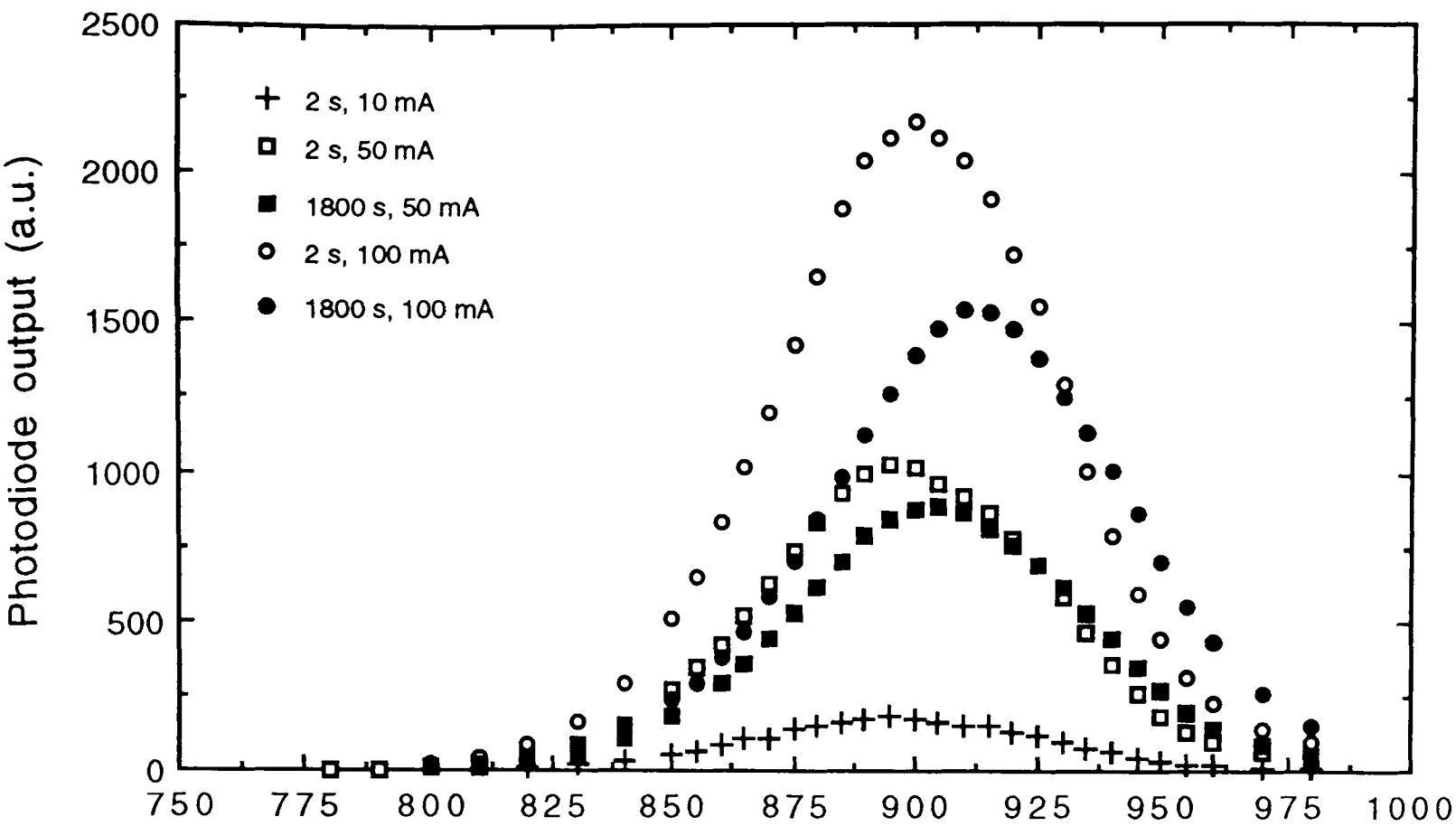


Fig. 2.3.2 The relation of diode current to radiant IR power emitted for a single TSUS 5402 LED. Measurements were made using a Molectron radiometer, following a 600 second warm-up period for stabilization at each current. Note the sublinearity of the response.

of the bialkali photocathode to detect the IR photons passing the filters made the experiment vulnerable to drifts in the diode output spectrum. This possibility was tested by measuring LED radiant power dependence on current using a spectrally insensitive pyroelectric radiometer (Molectron Corporation, model PR-20). Fig. 2.3.2 shows a typical result, from which the conclusion was drawn that the intensity drop was not wholly an artifact of the monitoring procedure and led to the use of a calibrated monochromator (Oriel, model 7240) and photodiode (Radio Spares cat # 303-674, large area silicon photodiode) to produce unambiguous data on the diode output intensity relation to operating current, warm-up time and wavelength.

The monochromator and photodiode assembly was calibrated using 12 discrete wavebands of visible and IR light selected from the output of a filament lamp by narrow band interference filters (400 nm through to 961 nm, FWHM typically 8 nm) and, additionally, a low pressure sodium lamp provided a known spectral line (589 nm). Diode spectral measurements: for each diode type the beam from a single LED was directed into the monochromator and the photodiode at the exit slit detected the transmitted light, photocurrent being manually recorded at 5 nm intervals and corrected using the manufacturer's photodiode spectral response data.

Two routines intended to measure the initial and stabilized spectra were followed, and also to replicate closely hot and cold mode operation. The initial spectra ("cold" mode) routine involved manually setting the monochromator to the wavelength of interest, switching on the LED and recording the photodiode output two seconds after switch-on. LED current was then switched off and the diodes given at least 3 minutes to return to ambient temperature prior to measurement at the next wavelength. Stabilized spectra ("hot" mode) were measured during a scan of the 800 nm to 980 nm waveband following



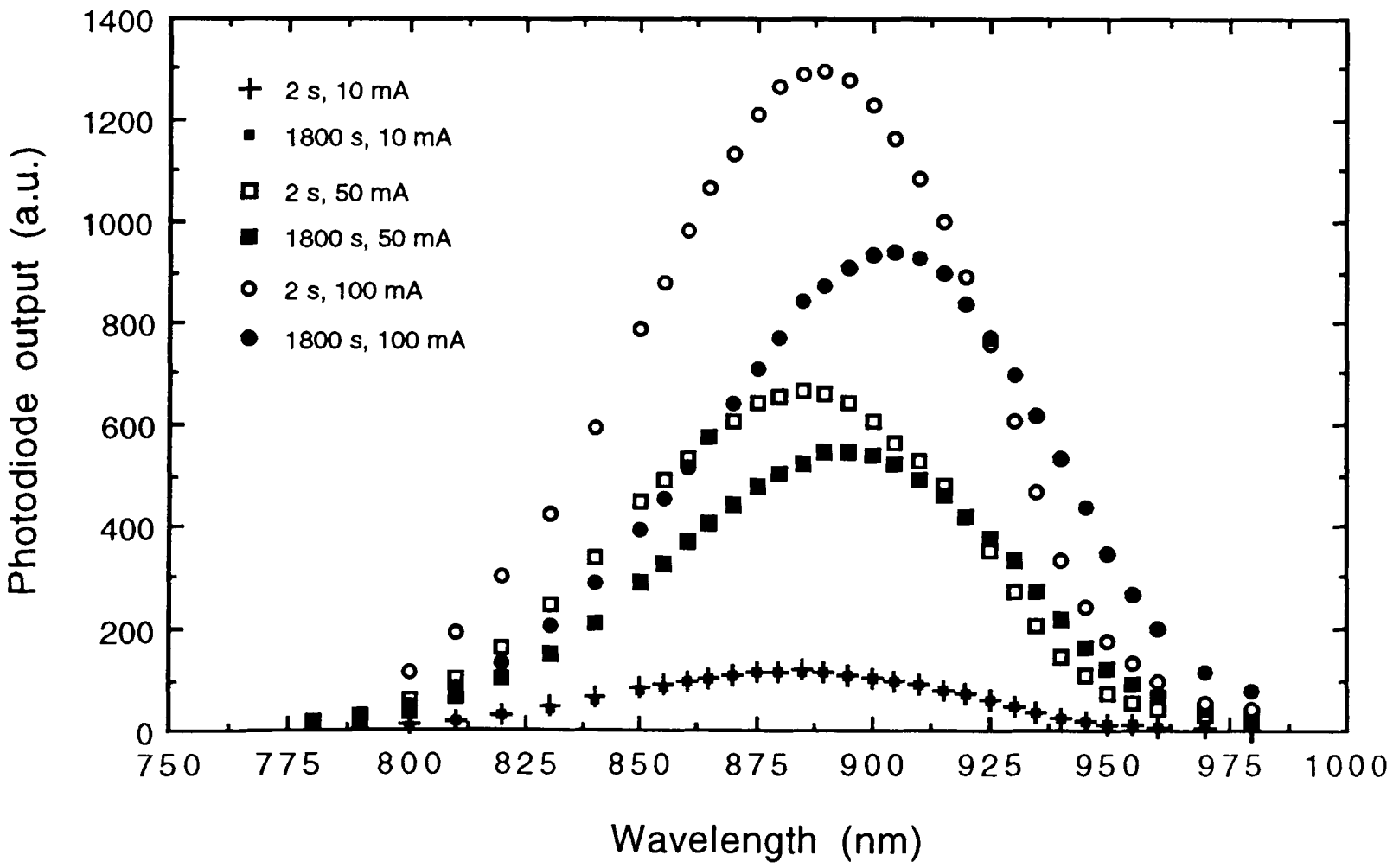
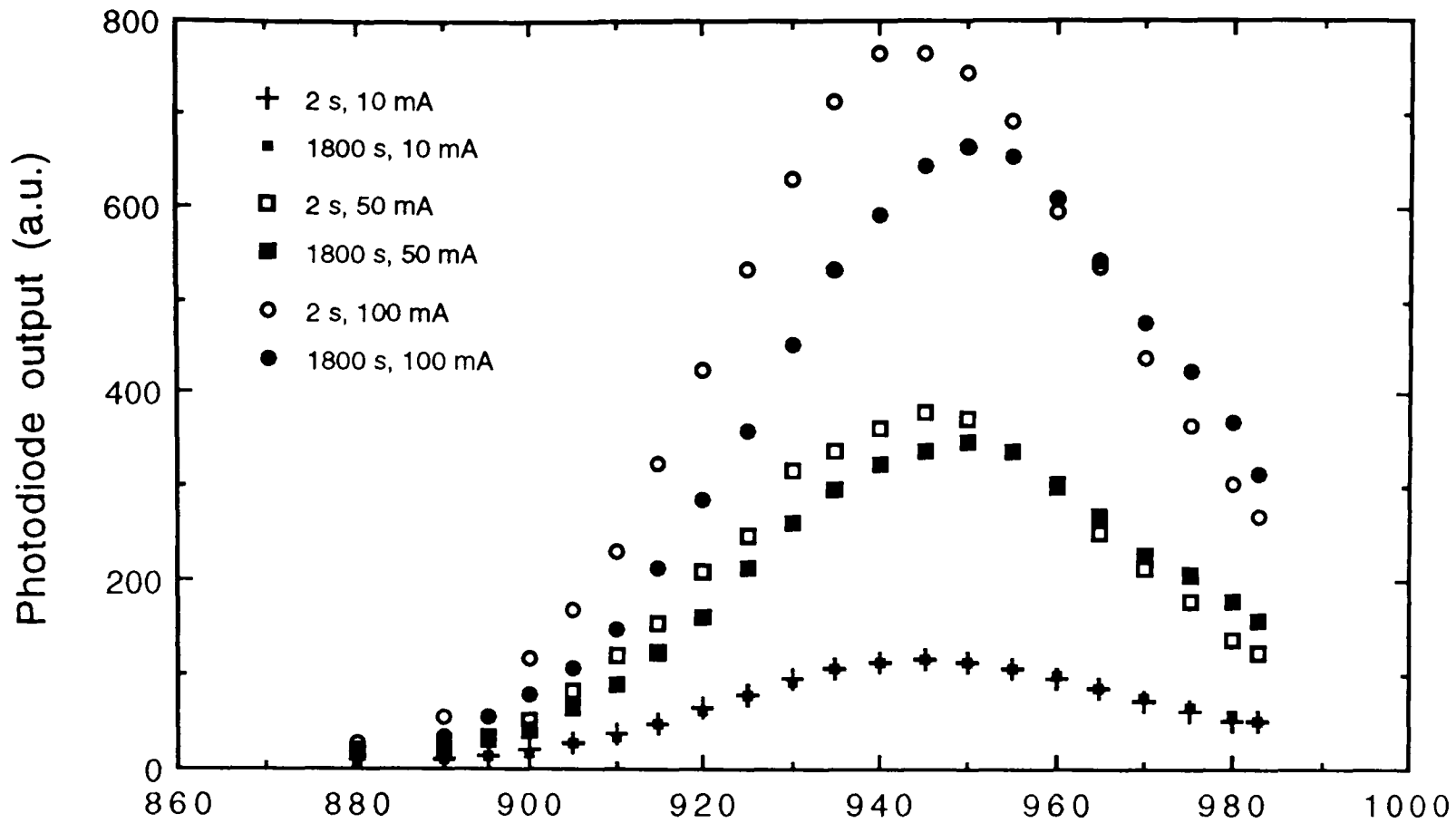
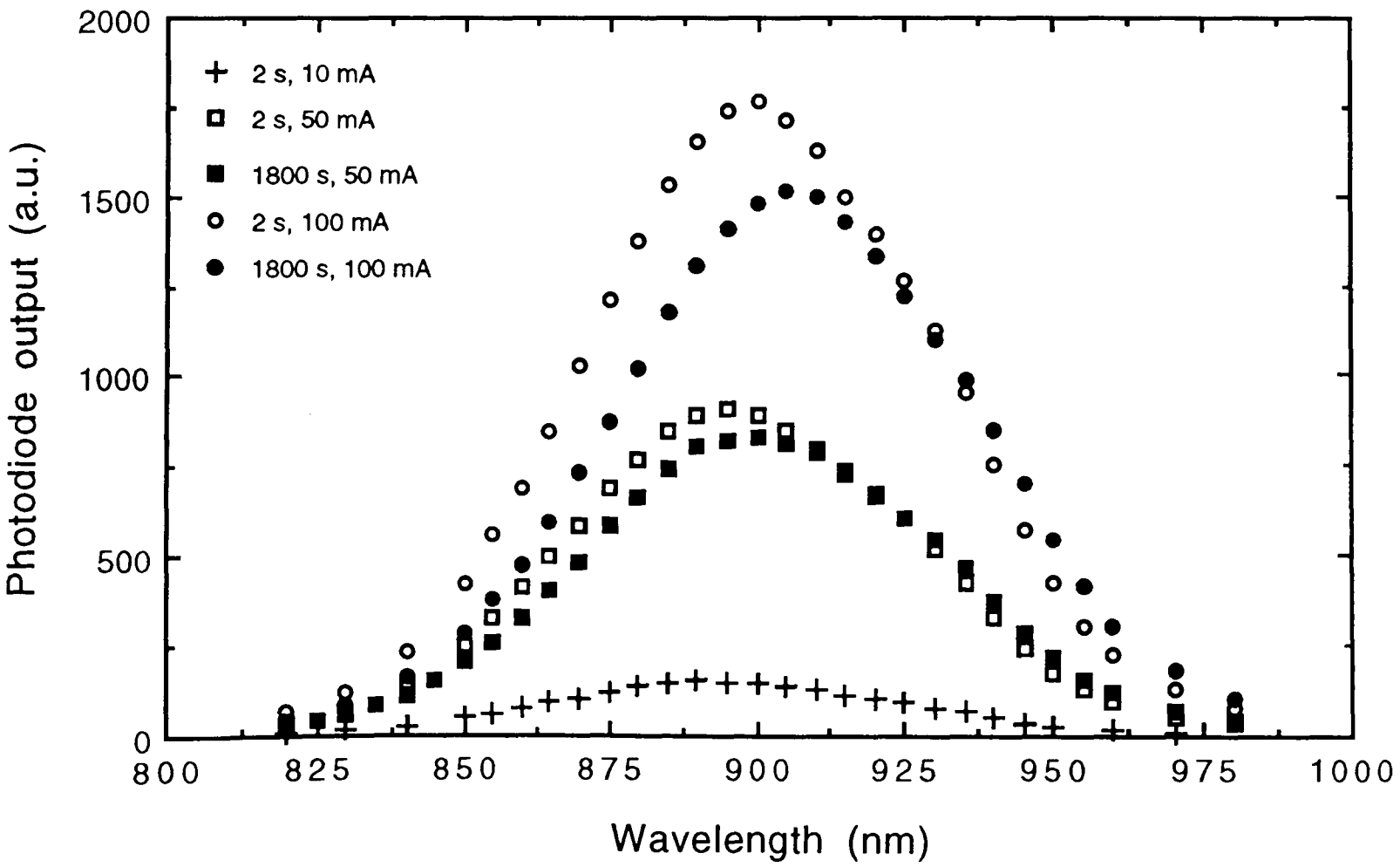


Fig. 2.3.3.(a)-(h) The emission spectra for each diode measured at various currents. Data were recorded either 2 seconds ("initial") or 1800 seconds ("stabilized") after diode actuation and are corrected for photodiode spectral response.

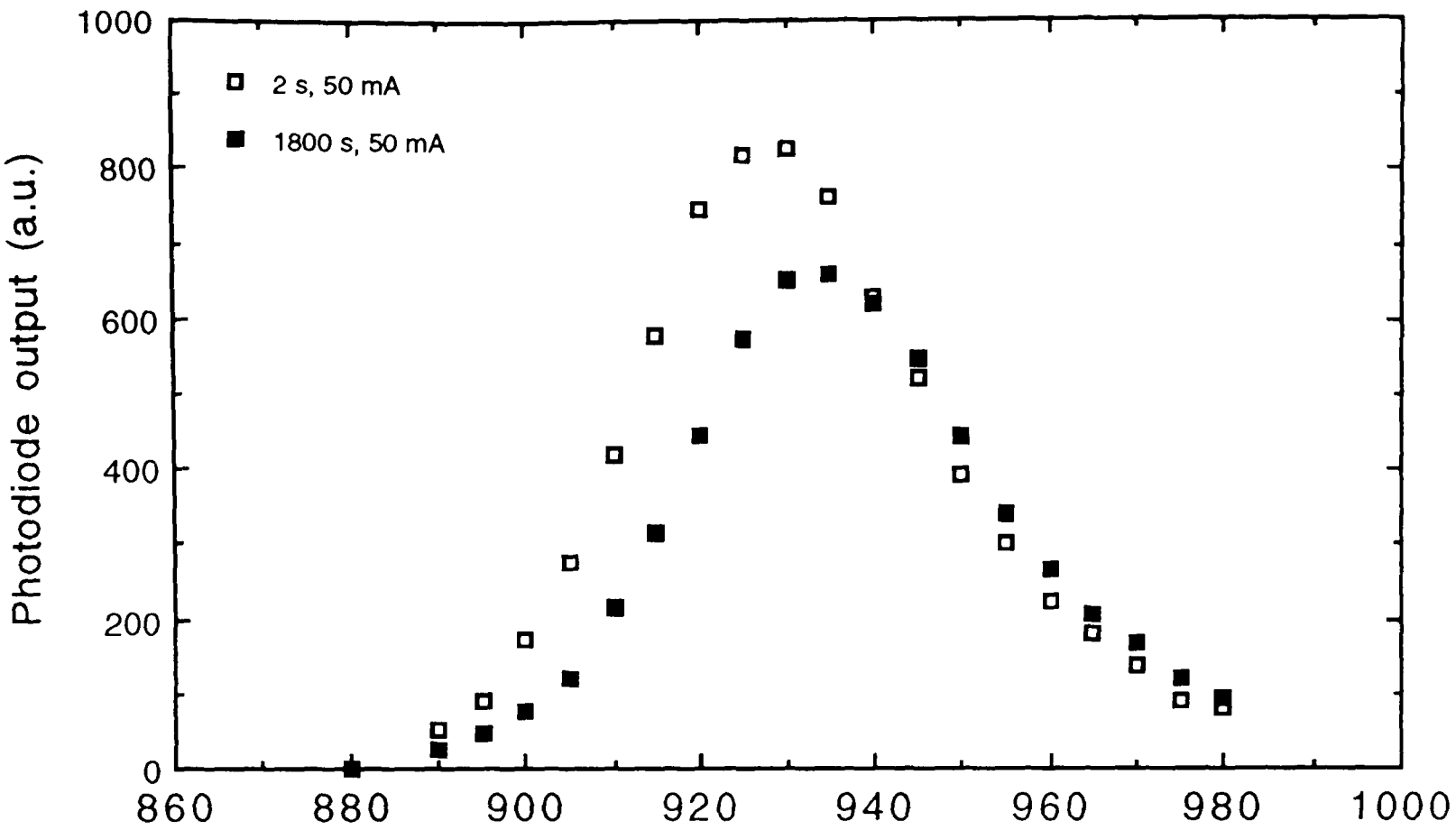
(c) TSUS 5402



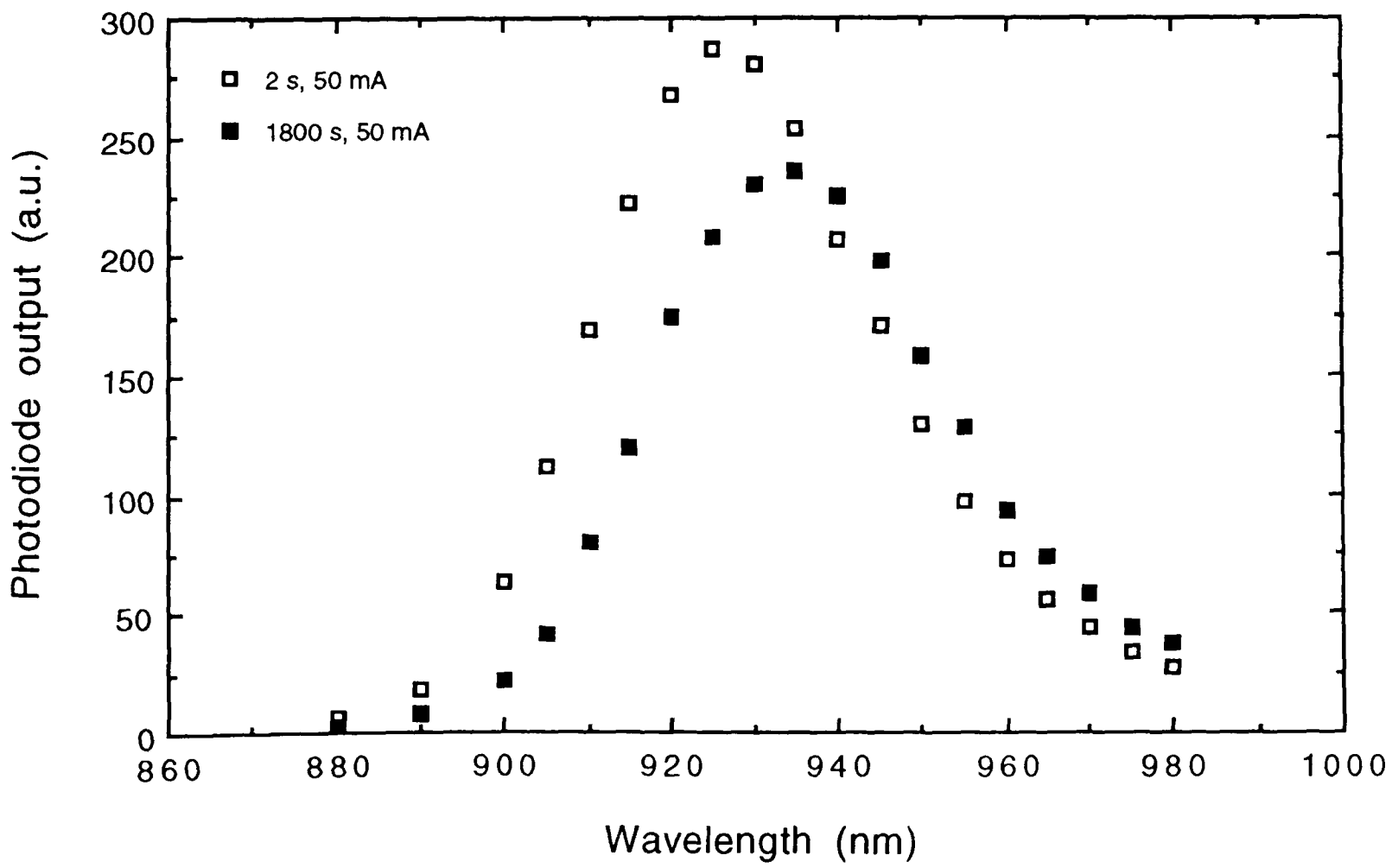
(d) TEMT 484



(e) LED55C



(f) LED55CF



30 minutes operation of the diode. Some results are shown in Fig. 2.3.3 (a)-(h), though only at 50 mA current for the four diode types for which investigation was discontinued.

Radiant power decrease and spectral shifts to longer wavelengths are seen in all cases, the magnitude increasing with diode current. However, though all diodes displayed output variations with current, the resin bodied types were least affected (presumably the shiny metal jackets of the remaining diodes impede radiative heat dissipation).

The significance of these findings for diode choice and IR reader design led to a second confirmatory series of measurements using the same monochromator-photodiode combination. The monochromator was now set to a selected wavelength and the beam intensity recorded as a function of time elapsed following switch-on. Data were taken over periods of typically 1200 seconds, then after a similar period of cooling to ambient the procedure was repeated at a different wavelength. This routine was then further repeated at different currents. Some results are shown in Fig.2.3.4 (a)-(d). Note that even at low current (10 mA) slight spectral changes occur, indicating that the low current "Durham mode" (see Poolton and Bailiff, 1989) does not fully avoid this problem, even at the sacrifice of radiant power.

Intensity increases at the longer wavelengths are seen in all cases along with commensurate intensity decreases at shorter wavelengths, in accord with the earlier findings. Table 2.3.1 summarizes some diode characteristics. A major conclusion was that metallic-jacketed diodes were less suited to the dating application and so were discarded. The choice between the two resin-bodied diodes remaining (TEMT 484 and TSUS 5402) was settled in favour of the type TEMT 484 (880 Δ 80 nm) due its output spectrum match to the data of Hütt *et al* (1988). Fig.1 of Spooner *et al* (1990) shows the stabilized output spectrum of a single such diode overplotted on the similar data of Hütt and Jaek (1989) -

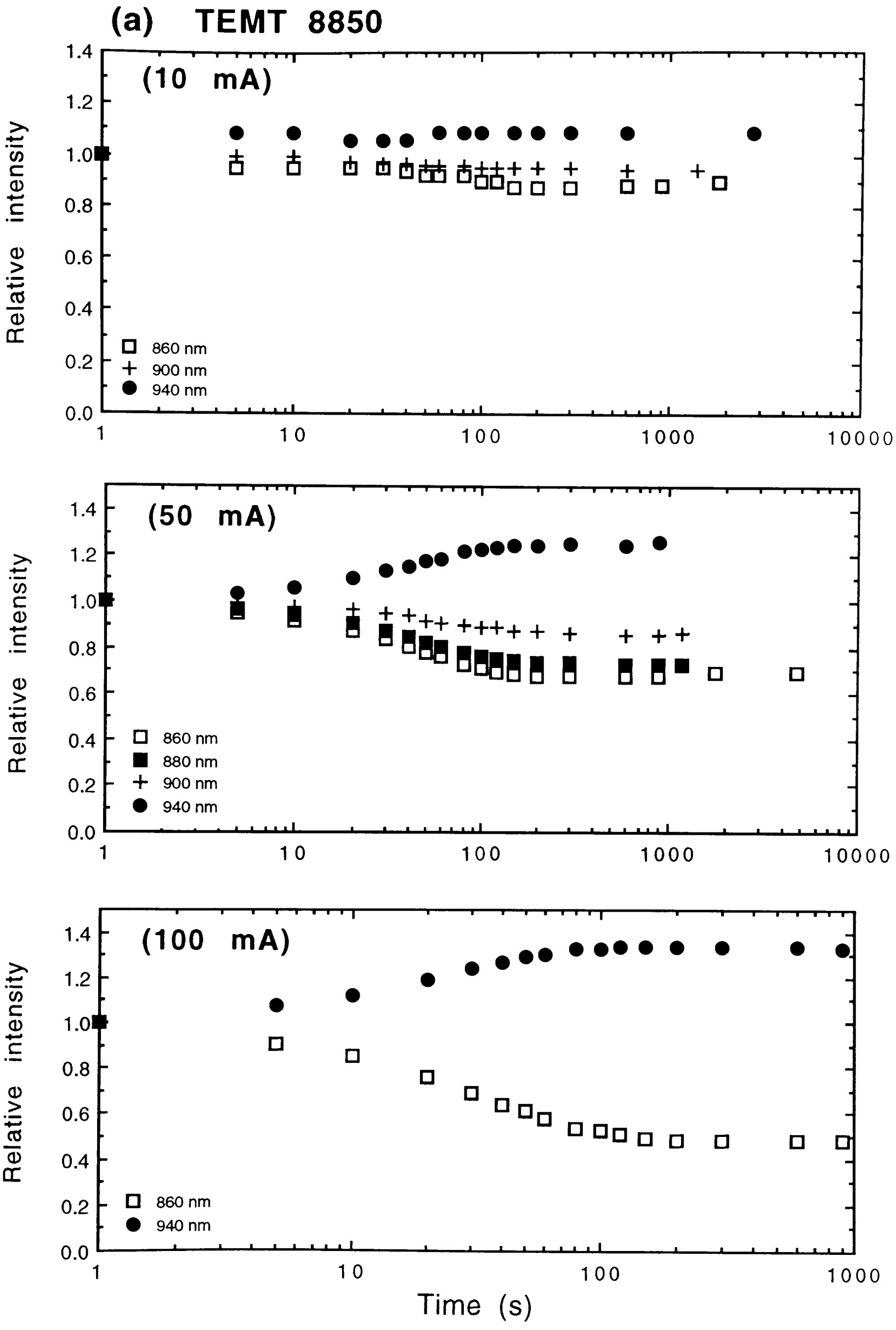
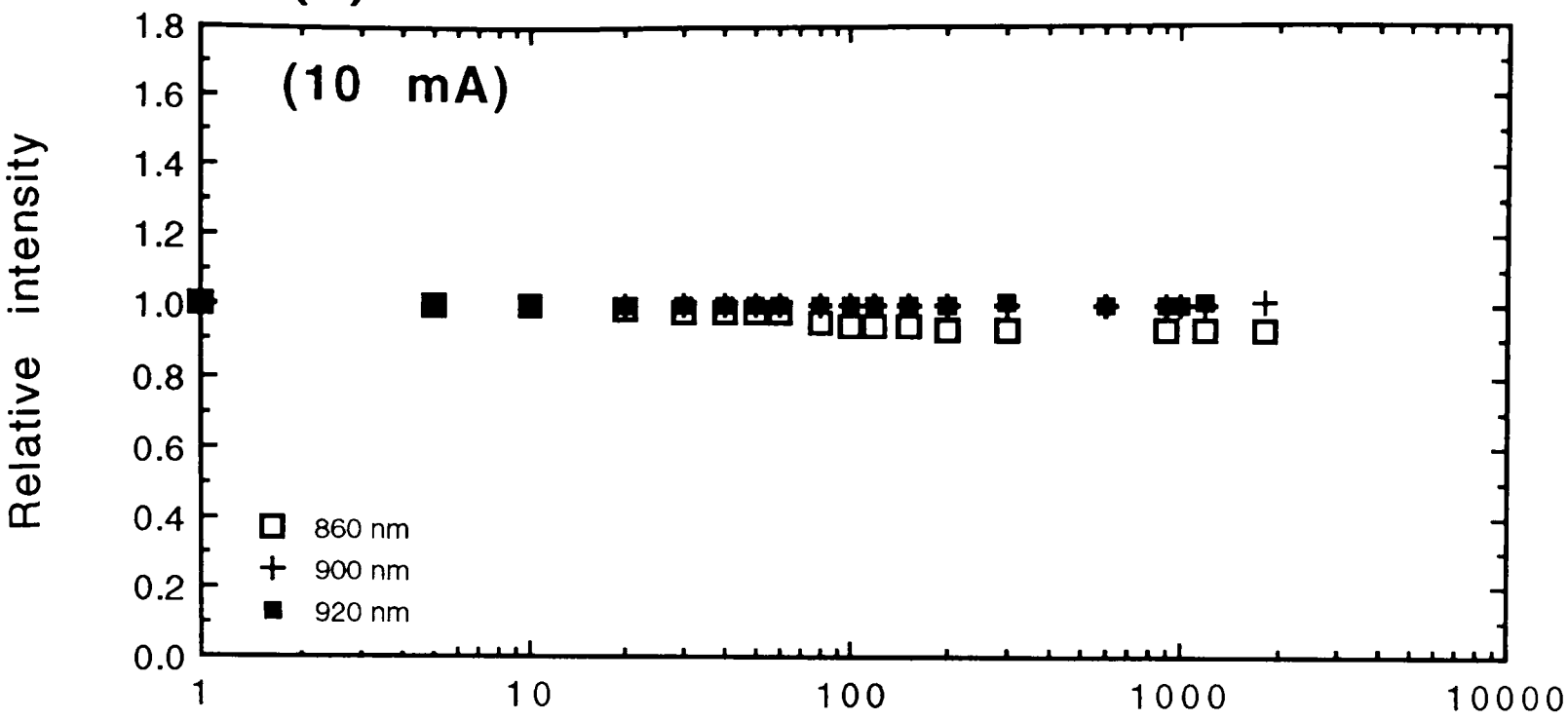
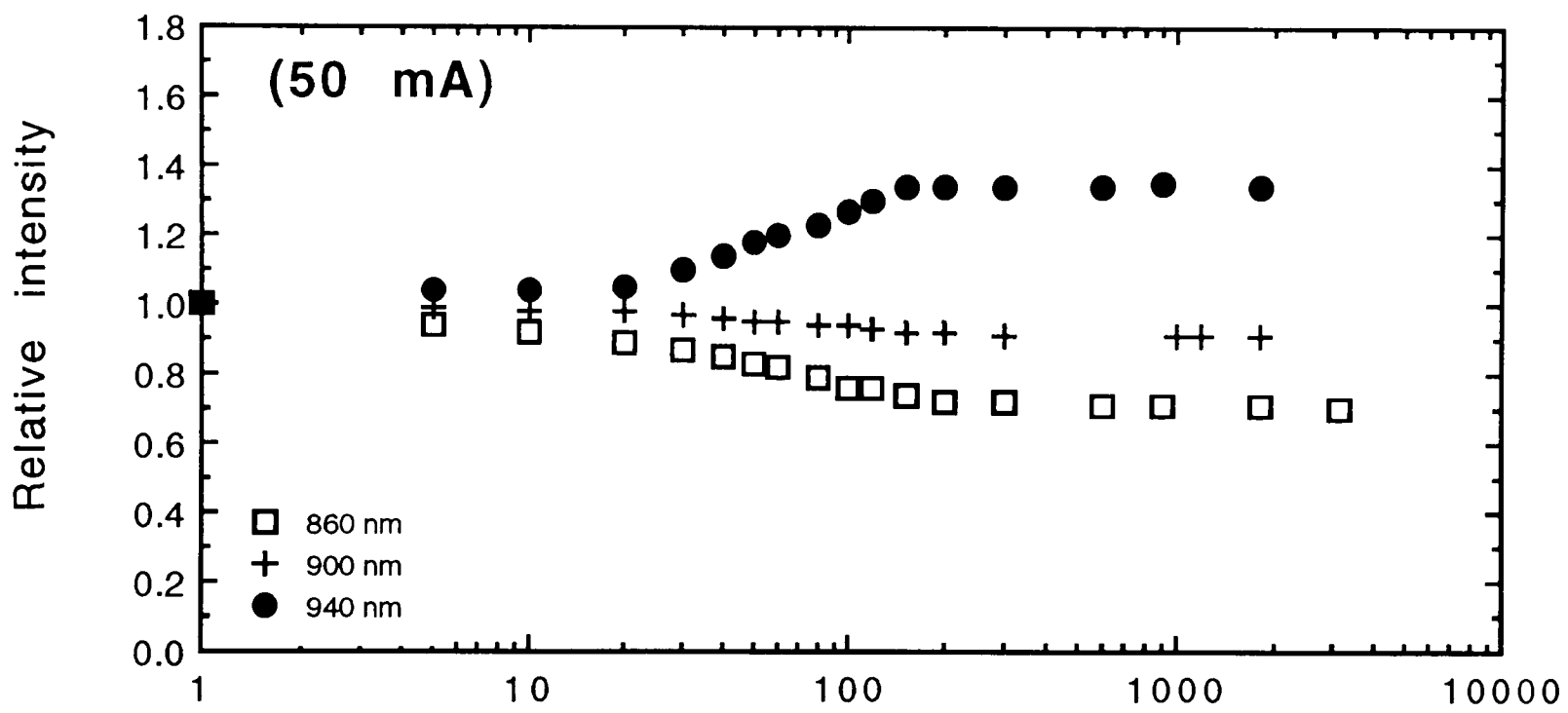
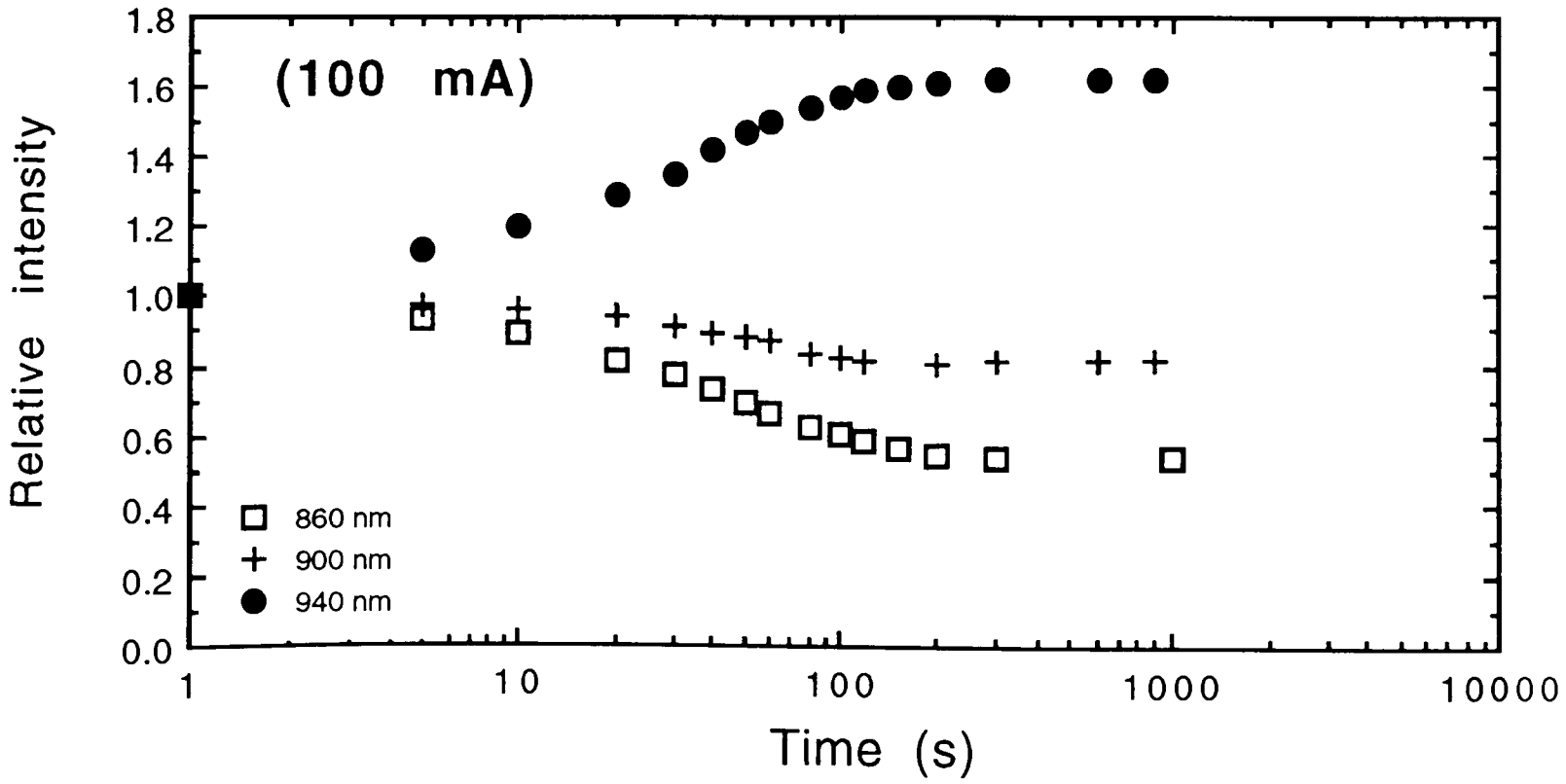


Fig. 2.3.4.(a)-(d) The changes with time of relative beam intensities at selected wavelengths for various LEDs. Data are corrected for photodiode spectral response. Beam stabilization is reached simultaneously across the spectrum, and typically requires at least 300 seconds for these single diodes.

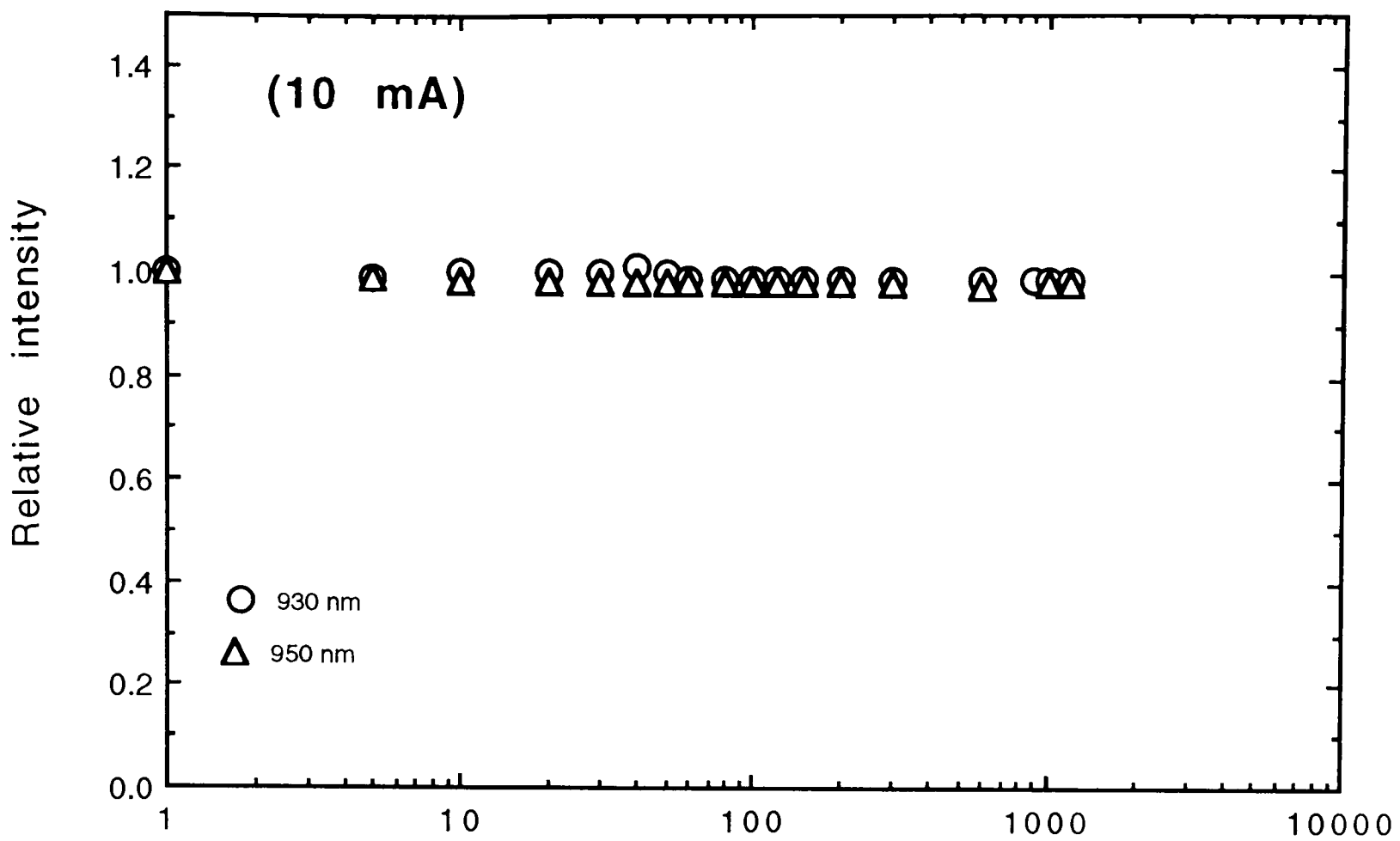
(b) SFH481-1

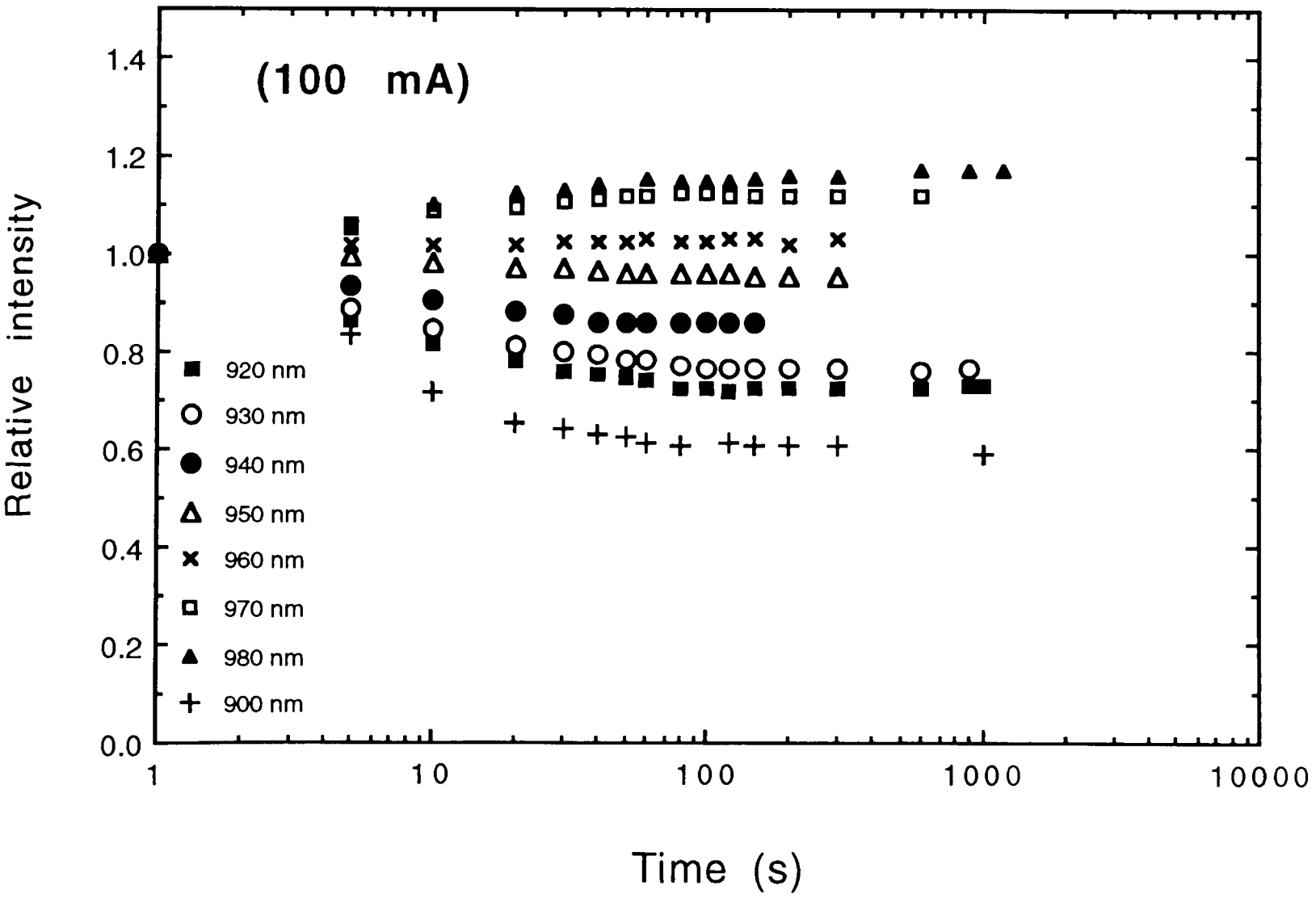

(10 mA)
Relative intensity
1.8
1.6
1.4
1.2
1.0
0.8
0.6
0.4
0.2
0.0
860 nm
900 nm
920 nm
1
10
100
1000
10000

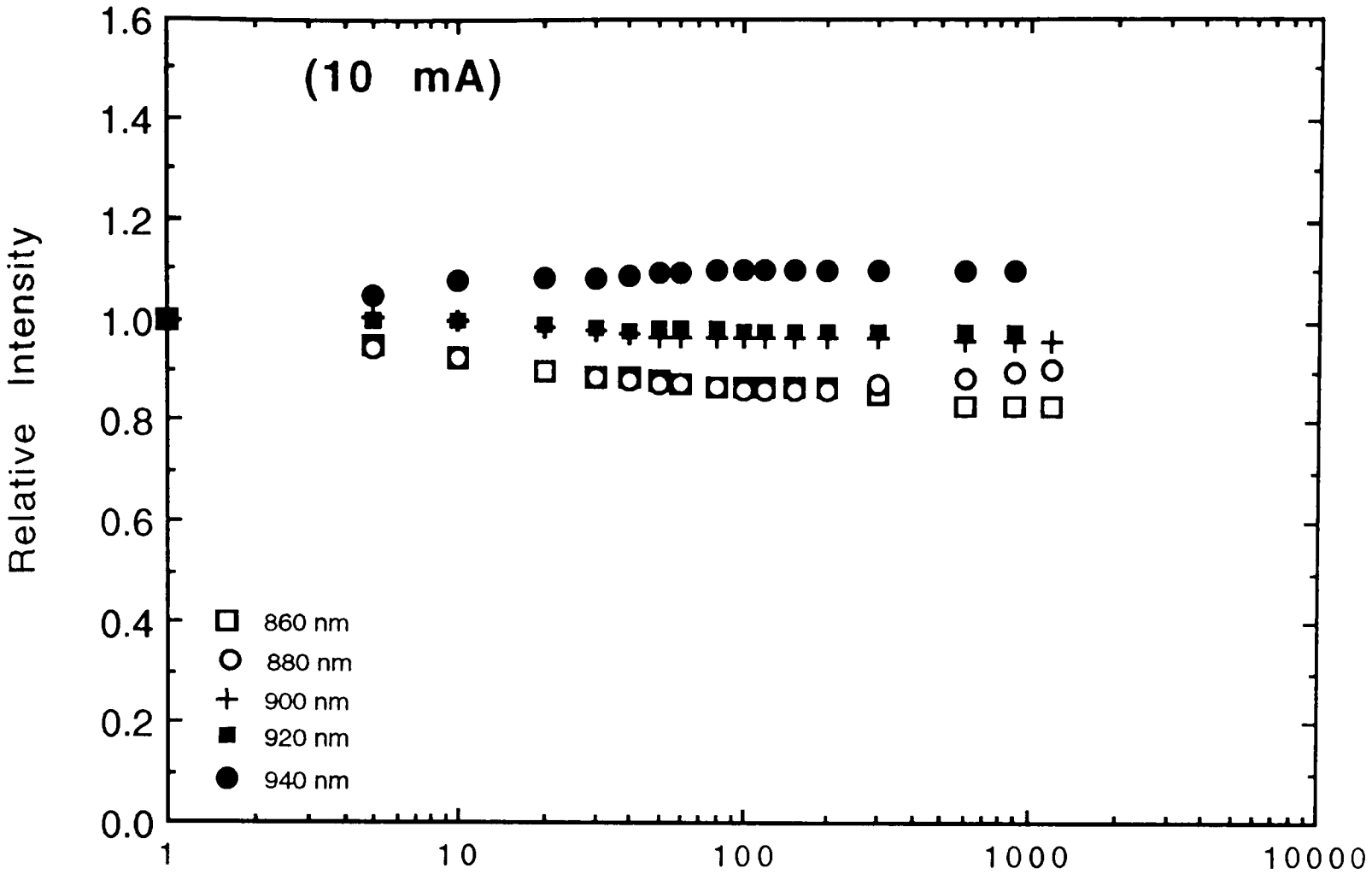

(50 mA)
Relative intensity
1.8
1.6
1.4
1.2
1.0
0.8
0.6
0.4
0.2
0.0
860 nm
900 nm
940 nm
1
10
100
1000
10000

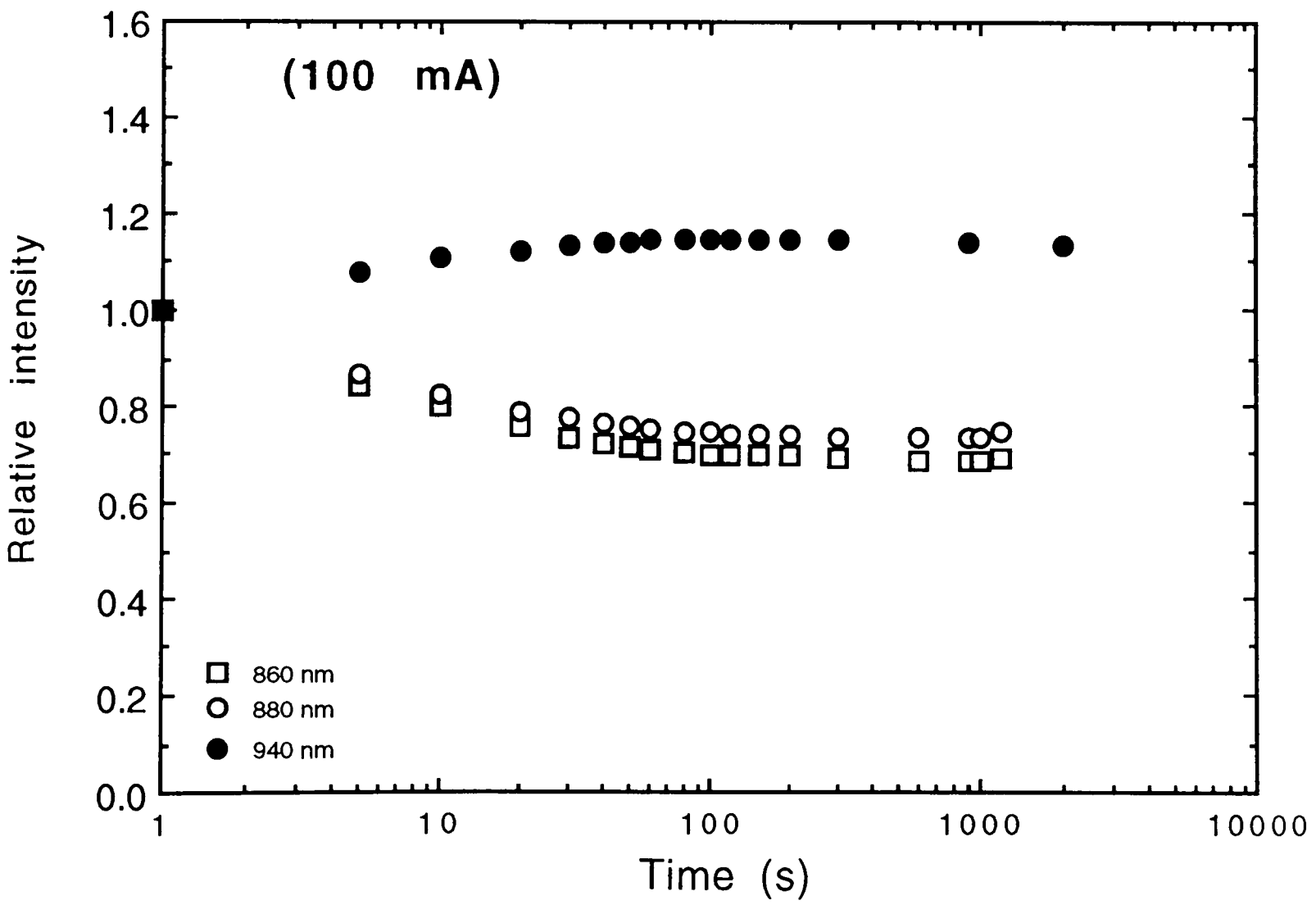

(100 mA)
Relative intensity
1.8
1.6
1.4
1.2
1.0
0.8
0.6
0.4
0.2
0.0
860 nm
900 nm
940 nm
1
10
100
1000
10000
Time (s)

(c) TSUS 5402


(10 mA)
Relative intensity
1.4
1.2
1.0
0.8
0.6
0.4
0.2
0.0
930 nm
950 nm
1
10
100
1000
10000


(100 mA)
Relative intensity
1.4
1.2
1.0
0.8
0.6
0.4
0.2
0.0
920 nm
930 nm
940 nm
950 nm
960 nm
970 nm
980 nm
900 nm
1
10
100
1000
10000
Time (s)


(d) TEMT 484
(10 mA)
Relative Intensity
1.6
1.4
1.2
1.0
0.8
0.6
0.4
0.2
0.0
1
10
100
1000
10000
860 nm
880 nm
900 nm
920 nm
940 nm


(100 mA)
Relative intensity
1.6
1.4
1.2
1.0
0.8
0.6
0.4
0.2
0.0
1
10
100
1000
10000
860 nm
880 nm
940 nm
Time (s)

the suitability of the TEMT 484 diodes for IRSL is clear. Later work by the author on the bleaching of the feldspar IRSL signal confirmed this judgment (see section 5.2.4). A redesigned module ("Mk IV") based on these diodes is described in the following section.

2.4 THE SHUTTERED DIODE ARRAY - "Mk IV"

Despite the TEMT 484 being the most suitable diode of those tested in respect of power and wavelength stability, because of the wavelength dependence of the photodiode the problem of power drift during the initial stages of a long illumination remained. It was therefore necessary to introduce a shutter to control sample illumination rather than switching the diodes. The use of a fast electronic shutter (Melles Griot, Ilex electronic shutter, 48 V, action time 3 msec) meant no significant loss of timing performance while permitting a warm-up delay, typically of about 20 minutes at 50 mA (see Fig.2.4.1), to allow the array beam intensity and spectrum to equilibrate.

The 880 Δ 80 nm emitter TEMT 484 was selected from those tested as the most suitable on the basis of resistance to spectral and intensity shifts, adequate radiant power and a relatively narrow beam cone. The latter characteristic permitted the diode rings to be sufficiently distant from the sample disc to allow the insertion of a light guide and so improve collection of luminescence. An additional advantage, possible because of the electrically inert resin package, was contact close-packing of diodes, enabling compact assembly of the diode rings.

The diode module and its inclusion in a TL glow oven assembly are shown in Spooner *et al* (1990), Figs. 2 and 3. Some aspects only of the Mk IV performance will be discussed here as this module and its general performance are fully described in

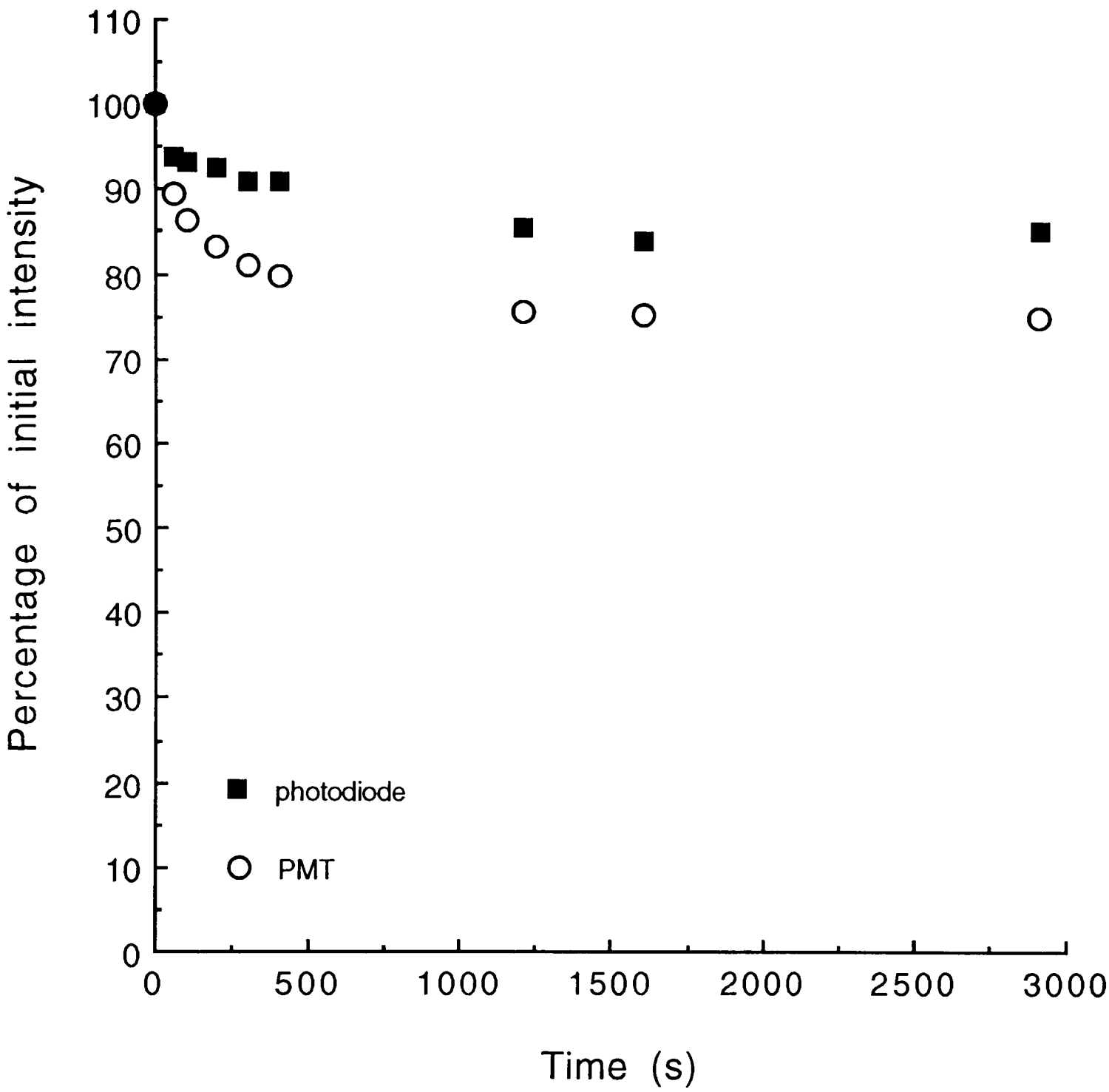


Fig. 2.4.1 The output beam intensity of the MK IV module following switch-on, as monitored both by the module internal photodiode and by an EMI 9635Q PMT with a 2 mm Schott glass edge cut RG 830 filter.

Spooner *et al* (1990) and Spooner and Franks (1990), and due reference can be made.

Following discussion with another practitioner, illumination uniformity from individual diodes was measured to confirm the accuracy of the manufacturers specifications for typical radiation intensity variation from optical axis. Measurement involved moving a 1 mm^2 silicon photodiode in a grid pattern normal to the optical axis of a clamped LED and so acquiring a beam "footprint". Results confirmed manufacturers data, important as the narrow (8° cone ½ angle) beam was essential to optimisation of the diode-sample distance designed into the Mk IV module.

Knowledge of the IR radiant energy from this array incident on a sample disc is not necessary for dating applications - all that is needed is a means of quantifying (arbitrary units) the relative IR intensity delivered by the array to permit setting and adjustment of the diode current so as to supply a reproducible illumination. This requirement is filled by a photodiode (Siemens # BPW-34) attached inside the module so as to monitor IR reflections from the back surface of the closed shutter. Temperature dependent changes of the photodiode sensitivity are small (0.05 %/°C) and further minimized by mounting the photodiode on a thermocouple-controlled Peltier effect heat pump (Radio Spares, Peltier mini-module, cat # 618-718). This monitoring provided the basic IR illumination control used throughout this work.

A refinement was absolute calibration of the IR flux received by the sample disc. Considering the illumination as the sum of 24 independent diverging beams intersecting the disc from a range of zenith angles and directions and with points of intersection of the emission axes of each diode with the disc unknown precisely, it was not possible to accurately calculate the power incident on the disc. Earlier, to obtain a relative power measurement a large area silicon photodiode (Radio Spares, cat# 303-674) was

incorporated into a purpose-built mount which could be reproducibly positioned on the TL glow oven heater plate. The photodiode active area (circular) was 100 mm^2 and with suitable XYZ spacers it could be positioned under the diode array in a position closely replicating that of a sample disc. Its principal value was as a monitor of diode array performance, a schematic diagram is shown in Spooner *et al* (1990), Fig.4. However, conversion of photodiode output (arbitrary units) to power (mW/cm^2) required a specific calibration factor to be determined for this photodiode and filter geometry. To this end a known power Ar-ion laser beam (5.4 mW/cm^2, measured by radiometer, Molectron model PR-20) was directed at normal incidence onto the mounted photodiode through the 4 ND filters (2 ND Schott glass and 2 ND Kodak Wratten) required to attenuate practical OSL beam powers to measurable intensities. Infrared power delivered to the sample was then found from:

$$IR\ (mW/cm^2) = [5.4(mW/cm^2) * M50(\lambda)/M50(514nm) * R(514nm)/R(\lambda) * ND(514nm)/(ND(\lambda)eff)]$$

where M50 = meter readings, (arbitrary units for meter scale 50)
R = photodiode spectral response to 514 nm and IR light respectively
ND(514nm) = filter attenuation factor for normally incident 514 nm light
ND(λ)eff = filter attenuation factor for IR, at mean incidence angles from diode rings and allowing for the greater beam path length through filters due to incident beam obliquity.

The photodiode spectral response data came from Radio Spares data sheet 303-674, and the filter transmissivities were measured using a Shimadzu UV-240 spectrophotometer. Evaluation of the above expression gave:

$$IR\ (mW/cm^2) = 0.0011 * M50$$

For typical operating currents this indicated powers at the sample of ≈ 20 mW/cm^2.

			1	Wavelength		2	3	4	emperature coefficients	
Diode	Manufacturer	Power (manufacturer)	Cone 1/2 angle	Peak wavelength (nm)	Measured FWHM (nm)	spectral shift (nm)	spectral shift (nm)	ntensity change	Power	wavelength
TEMT 8850	Three-Five Systems Ltd	50 mW/SR at 100mA	15°	880	68	7	12	10.9	-	-
TEMT 484	Three-Five Systems Ltd	100mW/SR at 100mA	8°	880	72	7	7	6	-0.53%	-
SFH 481-1	Siemens	10-20 mW/SR at 100mA	15°	880	86	8	14	14.3	-0.50%	0.25 nm/°C
LED 55C	GE/RCA	5.4 mW at 100 mA	15°	940	40	6	-	19.4	-	0.28 nm/°C
LED 55CF	GE/RCA	5.4 mW at 100 mA	38°	940	40	7	-	15.5	-	0.28 nm/°C
CQX 19	Telefunken	20 mW at 250 mA	40°	950	40	5	-	12	-	-
TSUS 5402	Telefunken	15 mW at 100 mA	25°	950	59	7	8	7.2	-0.80% per °C from 25°C	-
IN 6266	GE/RCA	0.25 mW at 100mA	20°	940	40	5	-	11.6	-	0.28 nm/°C

1.Manufacturer's data
2.Shift in peak wavelength at 50 mA between 2 seconds and 30 minutes after switch on
3.Shift in peak wavelength at 100 mA between 2 seconds and 30 minutes after switch on
4.Intensity change at 50 mA between 2 seconds and 30 minutes

Table 2.3.1 Some characteristics of various IR LEDs (after Spooner and Franks, 1990).

Power was later remeasured when a Coherent radiometer (model 200/10) became available. Here the module was positioned above the radiometer detector head using spacers while a 1cm diameter aperture located so as to mimic a sample disc permitted only IR which would impinge on the disc position to pass to the radiometer active area. At an array current of 48 mA the total power received by the radiometer without the aperture in place was ≈ 91 mW, and with the aperture, 32 mW. This direct measurement agrees reasonably with the on-plate photodiode data and calculations based on the manufacturers radiant intensity data, as well as earlier direct power measurements (Molectron pyroelectric radiometer, model PR-20; however the Molectron had a small and recessed active area, preventing the above approach, and so only individual diodes were measurable - array power estimation was therefore less certain). The discrepancy with the photodiode data is attributed to errors in correction for the different effective path lengths in filter material of a normal incidence beam (known power laser beam) and the diverging IR beams incident at a range of angles from the two concentric diode rings.

The "Coherent" data was then used to correct the above calibration equation to its final form:

$$IR\ (mW/cm^2) = 0.0018 * M50$$

Some additional refinements for ease of use were also made: (i) quick and accurate sample positioning on the TL oven heater plate was enabled by use of a "tufnol" mask made to locate onto the plate while the sample disc was positioned. (ii) No filters were routinely incorporated in the PMT housing, but were held in a "quick change holder". This caused some loss of signal (≈ 8%) due to poorer collection solid angle but permitted filter changes without disturbing the PMT. A clamping ring attached to the module (following a suggestion by Questiaux) enabled the PMT, filter holder and diode module to be

manipulated as one unit, so increasing sample changeover speed and protecting the unfiltered PMT from inadvertent light exposure.

The performance of this module in practice was highly satisfactory, and further developmental work was deemed unnecessary.

2.5 THE AUTOMATED OPTICAL DATING SYSTEM - INTRODUCTION

The optical dating procedure is well suited to automation, as was noted by Huntley *et al* (1985), following which an automated sample changer for use with an Ar-ion laser was built and commissioned in 1987 (Godfrey-Smith, 1991).

Automated reading of IRSL was encouraged by early highly promising results using the Mk III and Mk IV modules, particularly for fine grain feldspathic materials. The critical advantage over TL and OSL, in the case of European silt and loess, was the much reduced residual signal level (see Spooner *et al*, 1990). However, the major practical difficulty to dating application of the modules was the operator time required for changing sample discs, exacerbated by positioning errors and samples damaged by repeated handling introducing scatter into the data. This led to a collaboration with Littlemore Scientific Engineering (Elsec), initiated by M.J. Aitken with the object of producing an automated sample changer on which a diode module could be mounted. The anticipated benefits were greatly accelerated throughput of samples while improving the quality of the dates produced by encouraging the use of larger numbers of discs and dose points and eliminating handling damage and pseudo-recuperation effects.

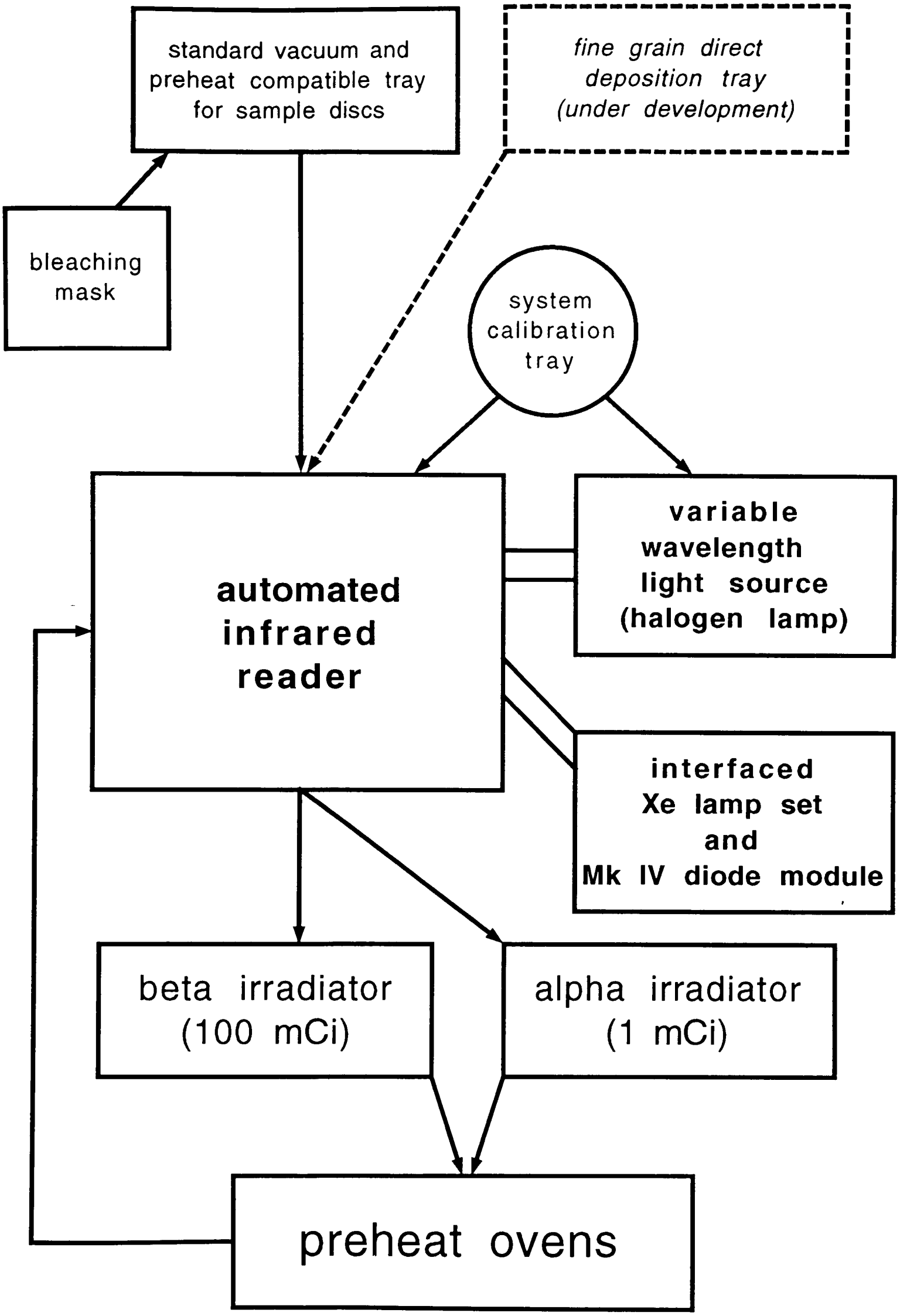


Fig. 2.6.1 The automated optical dating system

2.6 A SYSTEM OVERVIEW

This section gives an overview of the complete optical dating system designed by the author and built by W.D Hall (Elsec), based on the automated sample changer, then briefly describes the various elements of this system. The apparatus are commercially available from Elsec, and the reader is referred to the enclosed proprietary data sheets for system descriptions. The automated optical dating system, as at the time of writing, is shown in schematic form in Fig. 2.6.1.

The advantages of automation in the luminescence reading procedure itself are obvious and here the complete optical dating system was developed as a deliberate extension of this theme. Benefits of the system now included further great reduction of "hands on" operator time (potentially to zero for fine grains if direct deposition of the grains into recesses in purpose-built trays proves successful, so eliminating the need for discs as substrates), protection of the sample discs from damage (particularly necessary for fine grain work) and removal of cross-contamination possibilities, aided by rapid screening of sample trays for luminescent contaminants (for example, a 1 sec short exposure to each position requires ≈ 8 minutes only).

2.7 DESIGN CONSIDERATIONS

Design of the IRSL reader was constrained in the broadest sense by the intended overall function of the set, i.e. - isothermal IRSL only with no planned extension to TL capability as a future option. This limitation was imposed at the commencement of the

project to avoid compounding the anticipated complexities of constructing a novel optical dating reader with the incorporation of the technology of an automated TL reader. Within these guidelines specific design aspects were then addressed, principally

(1) - illumination module

(2) - sample tray design and capacity

(3) - inadvertent bleaching of adjacent samples during reading

(4) - temperature control

(5) - software considerations

Considering each in turn :

(1) Three IR diode module designs had been shown to be satisfactory at this time - the Mk III and Mk IV units described above and the TSUS 5402-based module of Poolton and Bailiff (1989). The latter design was rejected for reason of diode wavelength (950 nm) used, and the Mk IV on cost and complexity grounds due to its requirement of a fast electronic shutter. This left the Mk III type design. It was considered that microprocessor controlled timing would ensure the practicality of cold and hot mode operation and so overcome the troublesome diode warming effects encountered earlier. In addition the diodes would be "heat sunk" in an aluminium block in an attempt to further reduce these such problems (although measurements on single diodes showed only 30 % improvement). In most other respects (excepting Peltier type cooling of the monitoring photodiode) the diode module incorporated in the automated reader was a precise copy of the Mk III module. Luminescence collection efficiency was $\approx$ 3.14 times that of the Mk IV module, the latter losing detector solid angle due to the interposed shutter.

(2) Sample tray design was governed by ease of construction and control which dictated two stepper motors giving X-Y movement (G.C.W.S Wheeler and E.T. Hall, pers.

comms. 1989). A square tray offered the maximum number of sample disc positions possible for any given linear translational constraint imposed on an X-Y grid, and an 8 × 8 array (64 sample discs) was then chosen as a compromise between compactness and the perceived upper limit on the number of discs needed for a sound growth curve. Trays were of 6.25 mm thick aluminium plate, 188×188 mm, and black anodised to suppress scattered stimulating light. Screw-on black anodised lids could be attached, and for additional protection against inadvertent bleaching of the samples each lid carried a recessed neoprene "O" ring. Recesses for discs were milled 2.5 mm into the tray, giving some protection to the discs and particularly to lower the discs below the plane of the tray top and so shield the samples from scattered stimulating light in the readers. The trays could withstand indefinite annealing at 250°C.

(3) "Spillover" of stimulating light from the disc under illumination to adjacent samples was countered by precise machining of the sample trays and tray stage so as to permit the tray to traverse beneath the stimulation beam with only a very narrow gap between the surface of the tray and the underside of the reader compartment. Recessing the discs (see above) and matt black colouring of the trays and all internal surfaces of the reader compartment further prevented bleaching to the extent that no detectable depletion of IRSL from samples adjacent to the target position was observed following 12 hours exposure (pers. comm. Jun Xie, 1990).

(4) Three elements of the system were identified as being temperature sensitive and so needing controlled temperature. These were the monitoring photodiode, the IR diode array and the sample itself (IRSL decay rate varying ≈ 1 %/°C @ 20°C). Enclosure of the reader unit inside a temperature controlled box was dismissed as too expensive and inconvenient, so each temperature sensitive component was individually considered.

Peltier type cooling ensured temperature stability of the monitoring photodiode, air conditioning maintained laboratory temperature adequately for diode array stability, and the sample temperature was controlled by a preset (20°C) large water-cooled Peltier type unit mounted underneath the sample tray stage.

(5) Software initially was written to test the reader design feasibility. Following successful trials a software structure was established whereby one program, "OSL", operated the hardware and controlled data acquisition and an independent data analysis program, "PLATO", provided offline analysis with graphical and numerical output. A subsidiary program permits conversion of data from the Elsec file format into ascii code, so enabling data export. A third program, "AGE", performs age evaluation using the palaeodose evaluated from "PLATO" (or elsewhere) and user-input dosimetric data (currently in preparation in collaboration with M.J. Aitken). A software overview is given in Appendix E, the listing is proprietary.

A feature worked into both the data acquisition and analysis programs was flexibility, given the debate on all stages of palaeodose estimation. An outline of some key options follows. The period over which luminescence is measured can be subdivided into a maximum of 16383 channels, of variable duration with minimum period 10 msec. This permits user selection of the integration periods of interest, especially greater time resolution of the shine curves in the early stages of the decay. Normalization factors can be either read from a pre-measured "short exposure" file or inserted by the user. Background subtraction is possible by either the "subtraction technique" (Aitken and Xie, 1992) or by user inserted data. Growth curve fitting is currently performed both by linear fitting and exponential fitting using a program authored by B.W. Smith (Smith, 1983). Future incorporation of additional curve fitting algorithms is planned for.

2.8 SYSTEM PERIPHERALS

Following are brief descriptions of some of the various elements of the complete system (see Fig. 2.6.1).

Interface with pre-existing illumination sources. The automated IRSL reader was positioned in proximity to both the Mk IV diode module and the Xe lamp set to permit interchanging either with the Elsec diode module. As sample illumination from both these sources was controlled by fast electronic shutter, this required interfacing the Elsec reader with the shutters so that diode activation signals were converted to shutter opening and holding voltages. Appendix F shows the circuit diagram of the shutter driver by which this was accomplished. In addition each alternative light source required a purpose-built adaptor and spacer ring to optimise illumination and luminescence collection geometry.

Monitoring of reader performance is done using a "calibration tray", which is of the same dimensions as a sample tray but incorporates various item to permit convenient assessments of relative beam power, detector efficiency and non-luminescent background levels. Relative beam power is measured using a large area silicon photodiode (Radio Spares cat# 303-674) embedded in the tray so as to present to the illuminator an aspect analogous to that of a sample disc, with the beam being attenuated to measurable intensities by a 0.5 mm thick $\approx$ 4 ND Schott glass filter. (Conversion of arbitrary meter units to mW/cm^2 was done by comparing the luminescence decay rates induced from loess samples by the Mk IV module and the Elsec set. At 48.1 mA, after warm-up, the ratio of the mean decays over the first 5 sec was Elsec/MkIV = 1.002 ± 0.012, and the calibration equation determined as $mW/cm^2 = 9.3 \times 10^{-3} \times M50$, where M50 = calibration tray photodiode output measured by "Xe set meter 1"). A second measure of

relative beam power (suitable for green light stimulation but not IR) is provided by a 10 mm ϕ OG 530 Schott glass disc (see Appendix A). Non-luminescent background measurements can reproducibly be made using various constant-reflectivity targets recessed into the tray in sample disc positions: clean 9.7 mm ϕ stainless steel disc, clean 9.7 mm ϕ aluminium disc, 10 mm ϕ ground glass diffuser disc and a black anodised vacant position. Detector performance may be monitored by a "Facey" source (plastic scintillator incorporating ^{14}C, (Bailiff, 1980) embedded in the tray (a typical countrate for the Oxford set using an EMI 9235 PMT and 2 mm Schott BG 39 filter was 39.94 ± 0.04 kcps).

The compatible alpha and beta irradiators are described in the enclosed Elsec literature, some details of the selection of a 100 mCi ceramic type $^{90}Sr/^{90}Y$ beta source are in Appendix B.

An accessory for direct deposition of fine grains is undergoing trials. This consists of a grid arrangement of 64 three cm lengths of stainless steel tube, individually "O" ring sealed at their bases, which can be clamped onto a purpose-built tray. Evaporation of a fine grain suspension in methanol from these tubes produces a uniform deposit of fine grains in the tray apertures. This procedure eliminates the need for sample discs and should permit precisely mass normalized aliquots of optimum thickness for alpha irradiation to be produced, as almost all grains placed into the tubes should settle to the tray surface. A 2 ml aliquot of suspension of concentration 1 mg grains/1 ml fluid conveniently deposits a 10 μm thick solid layer over a 10 mm diameter sample disc area. The "bleaching mask" accessory consists of a grid of apertures corresponding to alternate positions on a standard sample tray, in each of which a 25.4 mm ϕ filter can be sealed. The halogen lamp based variable wavelength light source will be described elsewhere.

CHAPTER 3 FELDSPAR LUMINESCENCE CHARACTERISTICS

3.1 INTRODUCTION

Early promising dating results using IRSL indicated, in line with the original work by Hütt *et al* (1988), that at least for the sample dated (an alluvium layer constrained by Romano-British occupation layers, Spooner *et al*, 1990) in addition to being dose-dependent the signal was sufficiently bleachable to be fully reset in nature and possessed adequate stability over the time range considered (2,000 a). However, that the IRSL was sufficiently stable for dating generally could not be assumed given its origin from minerals of the diverse feldspar group, for which numerous cases of fading have been documented. Furthermore the low photon energy adequate to stimulate luminescence raised the possibility that the traps were too shallow to retain trapped charge over longer timescales without thermal "leakage" at ambient temperatures. Consequently, as IR-emitting diodes provided a convenient measurement technology and the basics of an optical dating methodology preexisted (Smith *et al*, 1986), signal stability became the fundamental question of concern for dating. This question had already been highlighted as critical in feldspar OSL dating using green light for stimulation (as well as other wavelengths for stimulation (Spooner and Questiaux, 1989), and also TL) and consequently it was appropriate to make a thorough investigation of feldspar signal stability on a mineral-specific basis. At the same time in the hope that there might be measurement conditions under which a stable signal was measured and unstable signals were excluded, a comprehensive study of feldspar luminescence characteristics was made.

In the first place a pilot study using identified feldspars from the RLAHA mineral

collection was undertaken to investigate the possibility that short-term (anomalous) fading was present in IRSL (and OSL) but as yet unreported. The IRSL of three samples, one each of orthoclase (Z6), sanidine (Z15) and labradorite (BA#6), was measured as a function of storage duration at room temperature. Results were in accord with previous TL fading studies by others as orthoclase showed no fading whereas the sanidine and labradorite faded, the latter rapidly, in agreement with work by Wintle (1974) using this same sample. Sanidine constitutes a fading species which may possess high concentrations of potassium and a specific gravity < 2.58, and so not be removable by density separation from the high potassium fraction.

As short-term anomalous fading was detected in the luminescence stimulated by both IR and green light this raised potentially severe problems for dating using this (< 2.58 gcm^{-3}) fraction. The more comprehensive investigation was then commenced to define further the fading behaviour of the high potassium feldspars and also to extend to the high sodic feldspars and plagioclase. The approach was to obtain samples of feldspar minerals representative of the more common feldspar compositions, determine the luminescence sensitivities (for both TL and optical stimulation), emission spectra and source traps of the optical dating signals then to survey the suite of samples for anomalous fading behaviour; the latter is reported in chapter 4. It was anticipated that the detection of significant anomalous fading in some of the feldspars would permit subsequent work aimed at characterizing and, optimistically, determining efficient means of removing this fading.

The present chapter describes the characterization of the set of feldspar samples. The first section introduces the samples and presents scanning electron microscope (SEM) and x-ray diffraction (XRD) analyses performed for mineralogical identification,

composition analysis and purity assessment. The next section presents data on the relative luminescence sensitivities of the samples as measured by IRSL, OSL and TL. This is followed by IRSL emission spectra measurements made using various optical filter combinations. Results of bleaching the feldspar TL by prolonged exposure to IR and 514.5 nm illumination are then presented in an attempt to identify the source TL glow peaks of the optical dating signals, and possibly to identify a single source peak for later kinetic analysis. Finally the thermal activation characteristic curves of the TL sensitivity in the < 180°C region of the glow-curves of each of the feldspars are given.

3.2 THE FELDSPAR SAMPLES

The feldspar group of minerals can be chemically described as alumino-silicates with the majority of the species represented on the compositional ternary system $KAlSi_3O_8$-$NaAlSi_3O_8$-$CaAl_2Si_2O_8$. However, classification of a feldspar involves determining not only the chemical composition but also the crystallographic system. This is dependent on the temperature of crystallization and subsequent thermal history, and leads to four series of the alkali feldspars (high-albite-high-sanidine, high-albite-sanidine, low-albite-orthoclase and low-albite-microcline) and high, low and intermediate temperature series for plagioclase.

For luminescence dating in practice this structural complexity of the feldspar group is not accounted for in the methods used for mineral separation (effectively only density separation and only for coarse grains). For example the commonly separated high potassium fraction, specific gravity < 2.58, can contain high temperature structural forms (sanidine), a lower temperature form (orthoclase) and the lowest temperature form

(microcline) in the same sample. Consequently even a strong correlation between structural form and fading would lack applicability save as a possible blanket rejection criterion for samples identified (for example by XRD) as containing fading species. As the intent here was the practical circumvention of fading the emphasis was on acquiring feldspar samples representing the more abundant species found in detrital deposits, so scarcity in nature led to the exclusion of barium feldspars and anorthite from this study.

Wherever possible care was taken to obtain single crystals which appeared uniform visually. These were prepared as ≈ 200 μm slices ("Isomet" low speed saw, from Buehler, Lake Bluff, Illinois, USA 60044). Samples obtained from the Natural History Museum were provided as 100 μm thin sections. The remaining samples, either too small and fragile for slicing or obviously of mixed phase, were crushed in an agate mortar. Repetitions of gentle crushing then sieving converted up to 45% of the initial sample mass to 90-180 μm grains. For mixed phase samples this mode of presentation gives greater disc-to-disc uniformity than slices, although slices are preferred where possible as they eliminate any erroneous interpretation of grain loss as signal loss. In either case, for luminescence measurements the prepared samples were attached to 9.7 mm diameter stainless steel discs by silicone oil. The portions of sample for microanalysis were embedded in resin, polished and coated with carbon.

Sample composition was determined using a wavelength dispersive X-ray analysis system (WDS) attached to a Cameca SU30 scanning electron microscope (SEM). Concentrations of elements P, Si, Ti, Al, Fe, Mg, Ca, Mn, Ba, Na and K were measured and are tabulated in Appendix G. The molecular percentages of orthoclase (Or), albite (Ab) and anorthite (An) were also calculated. For mixed phase samples, the fractional volume of the minor phase was estimated and the composition also measured. In all cases

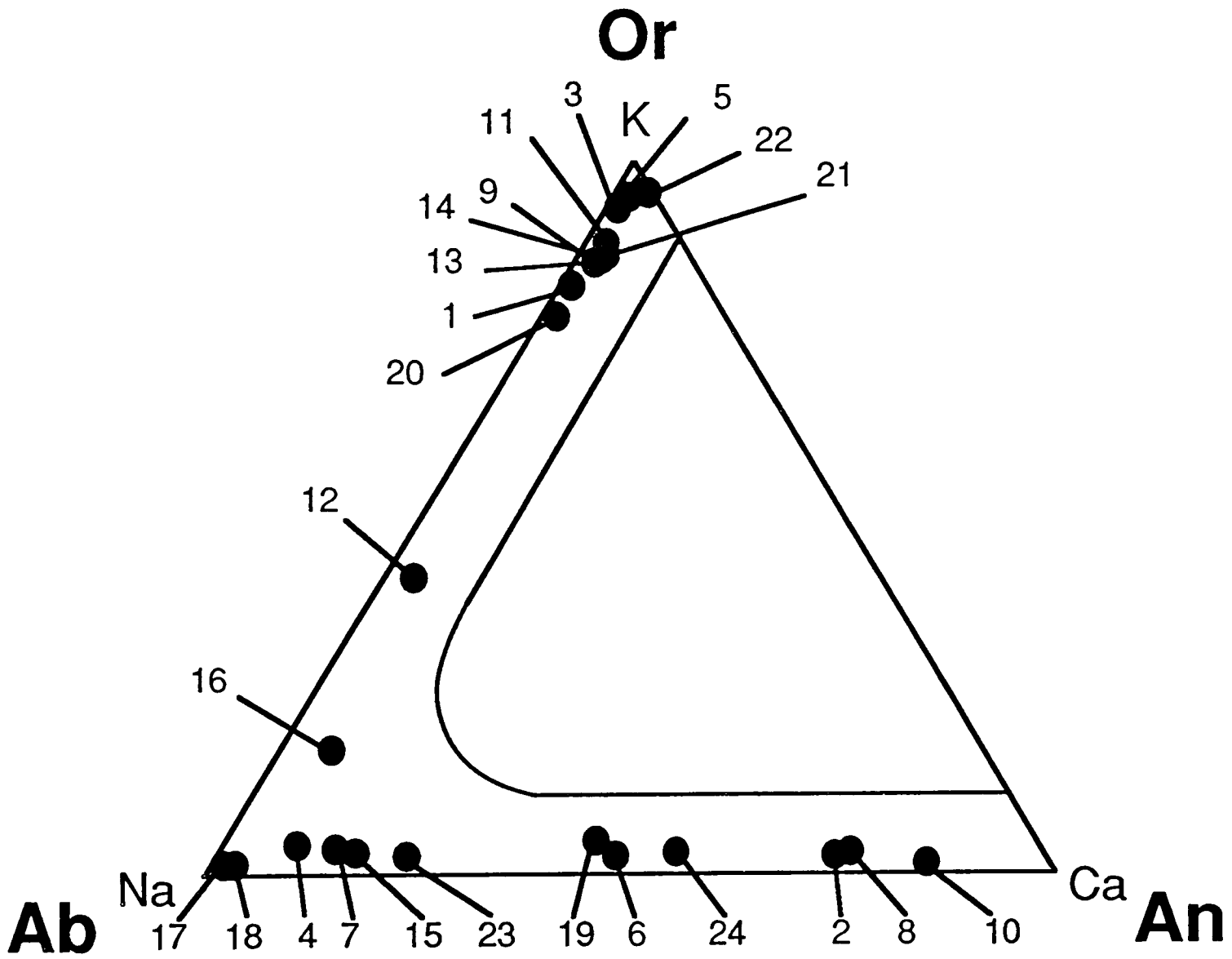


Fig.3.2.1 The feldspar samples, positioned on the ternary diagram from their Ab : Or : An molecular percentage ratios. Also shown are the respective index numbers as in Table 3.2.1.

REFERENCE		MINERAL	ORIGIN	COMPOSITION			MINOR PHASE		PRESENTATION
				Ab	Or	An	Fractional vol.	Composition	
1	_	Adularia	St Gothard, Switzerland	19.3	80.5	0.2	_	_	90- 180μm grains
2	#25	Bytownite	Silesia, Germany	26.5	0	73.5	0.001	9.2:2.1:88.7	90- 180μm grains
3	Z5	Microcline	_	9.4	90.6	0	0.01	99.6:0.4:0.0	75- 125μm grains
4	#17	Oligoclase	Norway	89.8	1	9.1	0.001	11.9:88.0:0.1	90- 180μm grains
5	no.3062	Microcline	Hadam Neck, Connecticut, U.S.A.	7.3	92.6	0.1	0.0001	99.2:0.7:0.1	90- 180μm grains
6	#23	Labradorite	St Paul Island, Canada	51.5	1.5	47	0.00001	0.1:0.1:99.8	90- 180μm grains
7	#18	Oligoclase	Sweden	85.2	1	13.8	0.001	15.5:84.2:0.3	90- 180μm grains
8	#26	Bytownite	Crystal Bay, Minnesota, U.S.A.	25.7	0.3	74	_	_	90- 180μm grains
9	Z15	Sanidine	_	13.9 to 52.9	85.8 to 42.6	0.3 to 4.5	_	_	90- 180μm grains
10	Z4	Bytownite	_	15.9	0.1	84	0.0001	31.5:0.5:68.0	90- 180μm grains
11	Z6	Orthoclase	_	11.4	88.3	0.3	0.01	92.3:0.2:7.5	90- 180μm grains
12	Patmos	Sanidine	Patmos, Greece	56.2	40.1	3.7	_	_	90- 180μm grains
13	Dup.(C)	Microcline	Pennsylvania, U.S.A.	13	86.9	0.1	0.001	98.5:0.3:1.2	100μm slices
14	Z11	Microcline	_	12.6	87	0.4	0.0001	96.8:1.0:2.2	200μm slices
15	Dup.(A)	Albite	Sacheuga mines, Zimbabwe	83.7	0.6	15.7	_	_	100μm slices
16	1947, 199(2)	Anorthoclase	Mt Kenya, Kenya	78.1	15.7	6.2	_	_	100μm slices
17	_	Albite	Alps, France	99.2	0.4	0.4	_	_	90- 180μm grains
18	Amelia	Albite	Amelia, Virginia, U.S.A.	98.3	0.8	0.9	_	_	90- 180μm grains
19	BA#6	Labradorite	_	52.4	1	46.1	_	Mixed phase	90- 180μm grains
20	Z9N	Microcline	_	20.7	79.2	0.1	0.001	93.0:0.0:7.0	200μm slices
21	Z9	Microcline	_	13.6	86	0.4	0.01	98.7:0.3:1.0	200μm slices
22	_	Orthoclase	Madagascar	1.8	98.2	0	_	_	200μm slices
23	Dup.(B)	Oligoclase	Sweden	78.2	0.8	21	_	_	100μm slices
24	Dup.(D)	Labradorite	Labrador, Canada	44.6	1.5	53.9	_	_	100μm slices

Table 3.2.1 The feldspar samples and their sources, along with the mode of sample presentation in each case. Details of the minor phases are also included.

the minor phase constituted ≤ 1% of crystal volume, and so the preparations would ensure reasonable disc to disc reproducibility (TL/mg). Also, although any extreme sensitivity contrasts between phases were undetectable with the apparatus available, the minor phase in most cases was ≤ 0.1% of crystal volume and so luminescence contributions were presumed insignificant.

Analysis conditions were : accelerating voltage 20 kV; beam current 20 nA; beam diameters ranging from 5 μm to 30 μm; detection limits of ≈ 0.05 wght.%; data was corrected by ZAF procedures via the program "PAP" developed at the Office National de l'Etude et de la Recherche Aérospatiales by J.L. Pouchou and F. Pichoir.

X-ray diffraction (XRD) analyses were performed on powdered portions of each sample to confirm crystallographic identifications, particularly amongst the alkali feldspars, this being necessary as the similar composition and density can be exhibited by orthoclase, microcline and sanidine.

Table 3.2.1 gives some details of the samples and their positions in the feldspar ternary system are shown in Fig. 3.2.1

3.3 LUMINESCENCE SENSITIVITIES

Luminescence measurements were made using a Risφ automated TL glow oven for the TL (Bøtter-Jensen, 1988), an infrared emitting diode array (Spooner *et al*, 1990) for infrared stimulated luminescence, and an Ar-ion laser set (Smith *et al*, 1986) for green light stimulation. Fig. 2 of Spooner (1992) shows the optical filters used and the corresponding transmission spectra, along with the excitation wavelengths, and gives the type of photomultiplier tubes (PMT) for each case. Irradiations, pre-treatments and the

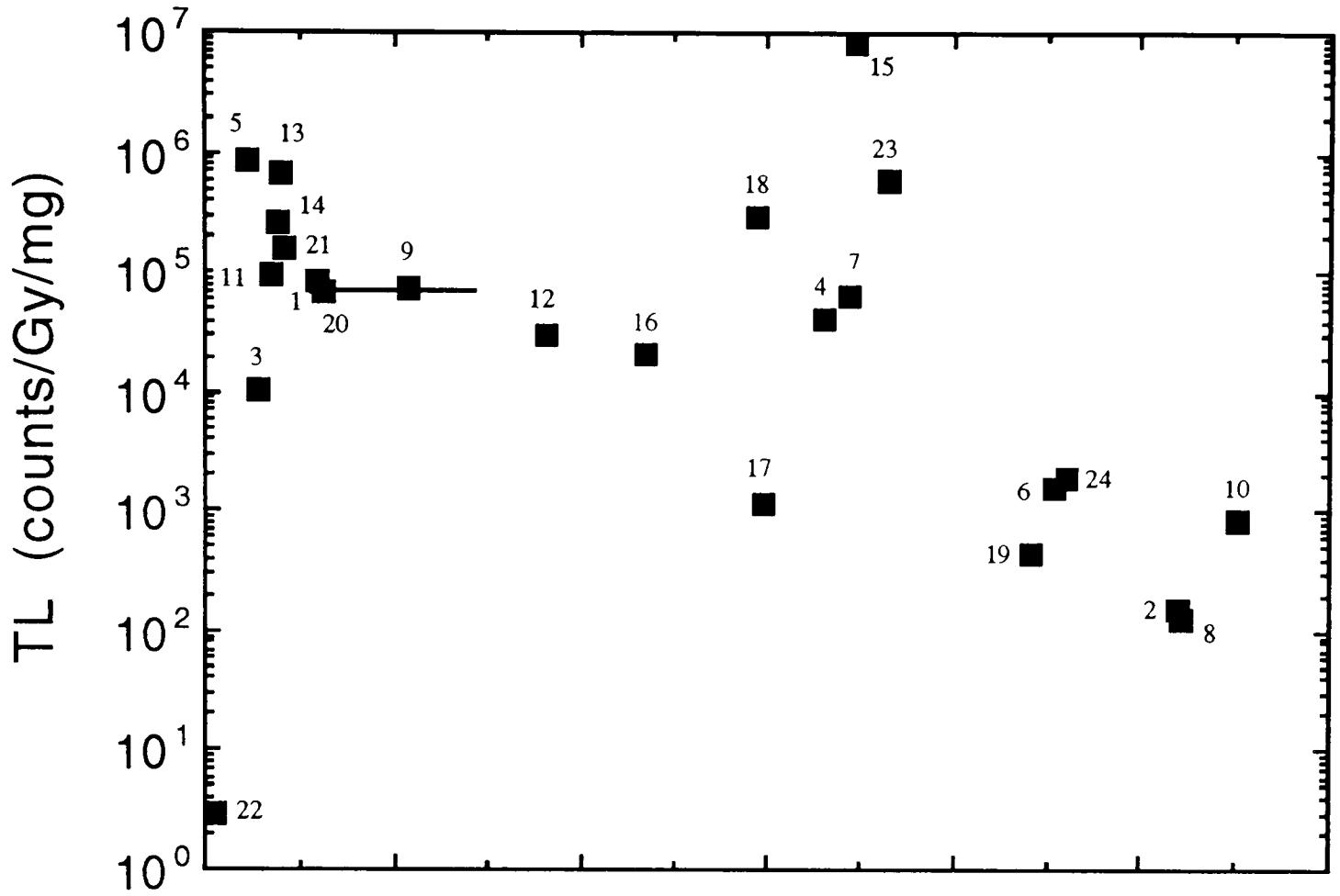


Fig.3.3.1 The TL sensitivities of the feldspars.
Data plotted are the mass normalised TL/Gy (integrated from 264°C to 550°C) Vs feldspar composition. Doses were 1 Gy $^{90}Sr/^{90}Y$ beta irradiation in all cases. TL measurements were made with a Risø automated TL glow oven (EMI 9635Q PMT with a Corning 7-59 and HA3 filters). Heating rate was 5°C/s to 550°C maximum with reheats subtracted. No preheats were given and no allowance has been made for sample optical transparency.

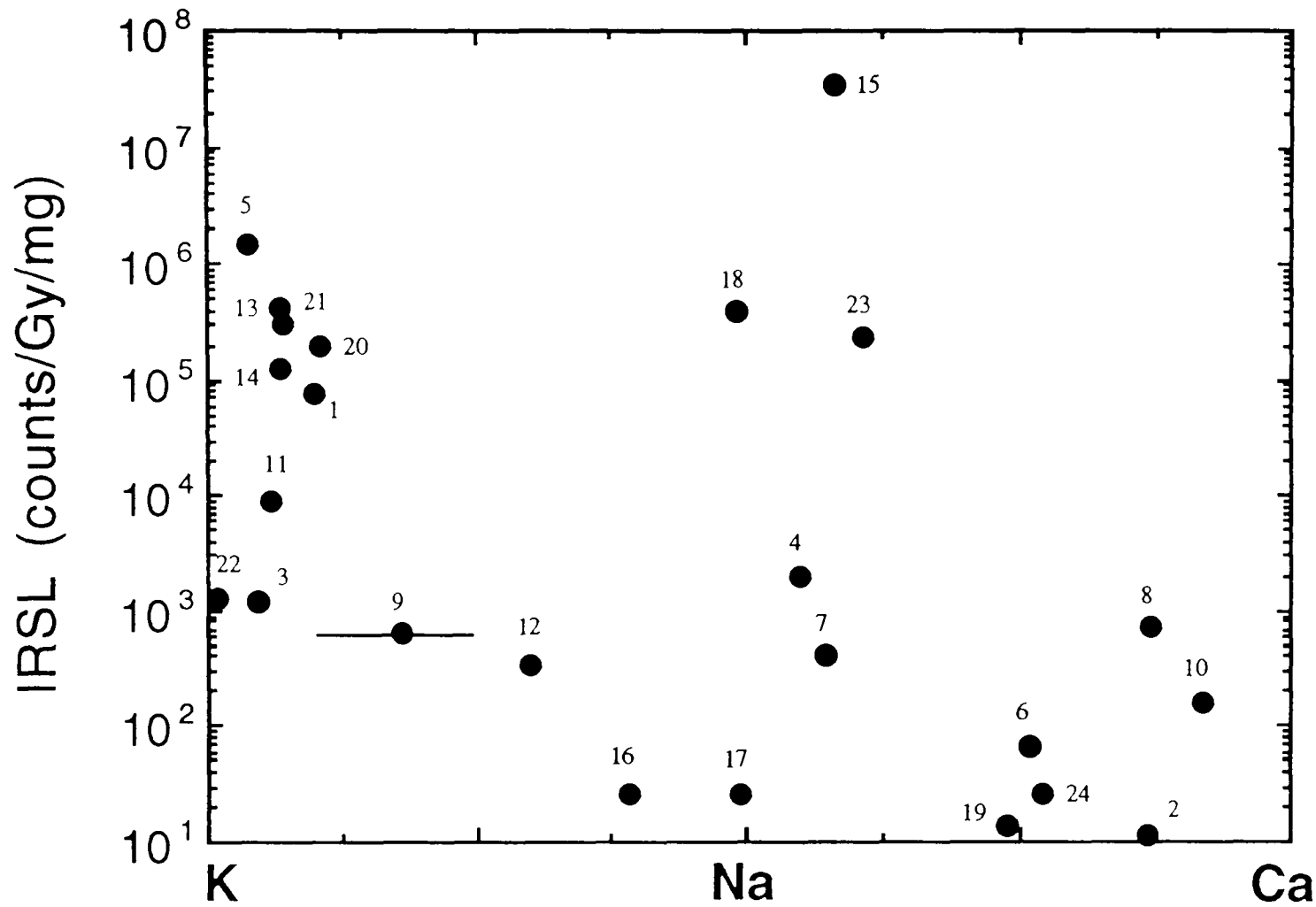


Fig.3.3.2 Luminescence sensitivities of the feldspars under optical stimulation by 880 Δ 80 nm IR. Data plotted are the mass normalized luminescence per gray measured following a 100 Gy ^{90}Sr-^{90}Y beta irradiation then preheat of 160°C for 1 hour. Total exposure energies were 54 J, with emissions detected using an EMI 9635Q PMT with one Schott 2 mm BG39 filter. No allowance has been made for sample optical transparency.

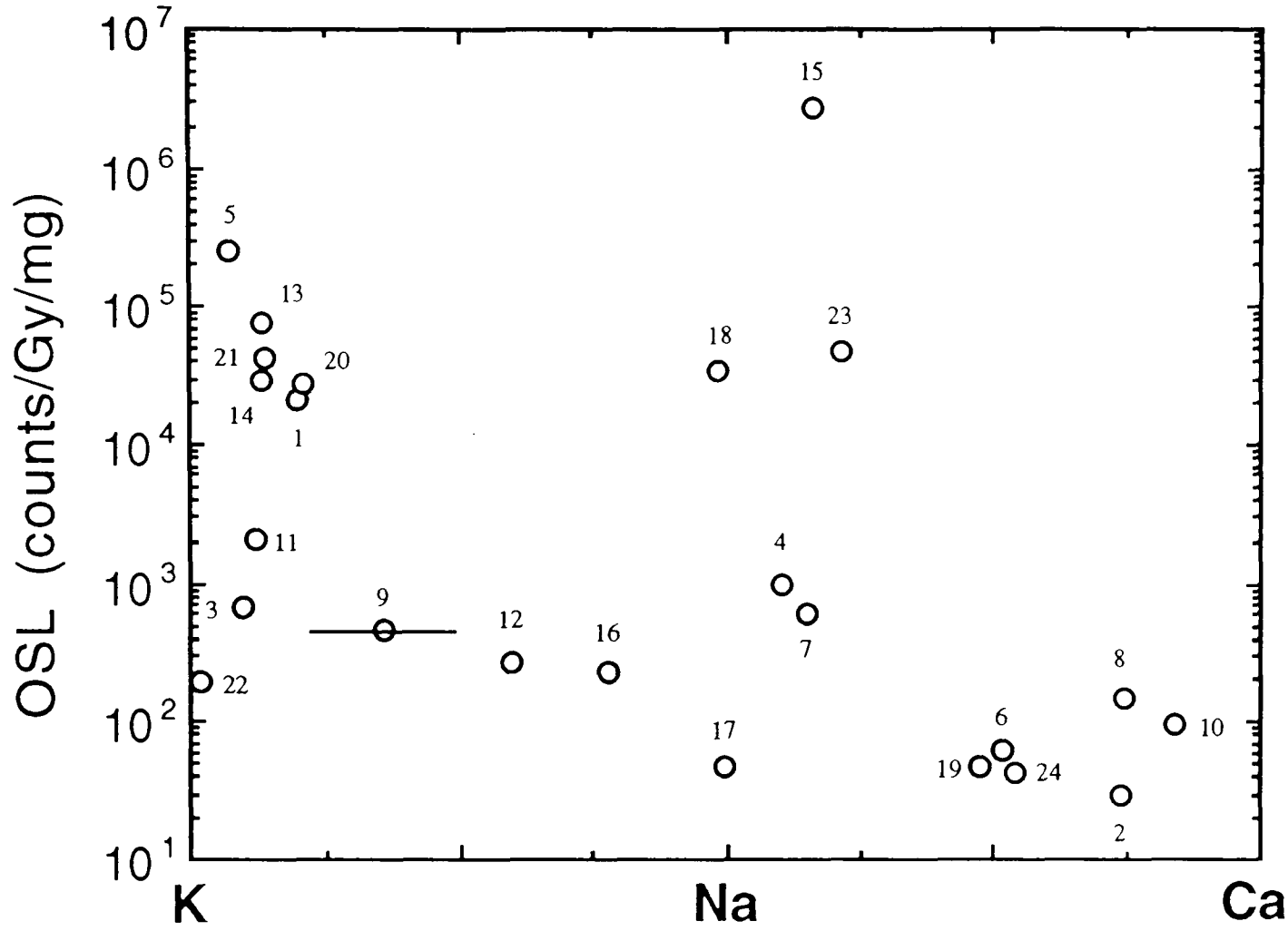


Fig.3.3.3 Luminescence sensitivities of the feldspars under optical stimulation by 514.5 nm light. Data plotted are the mass normalized luminescence per gray measured following a 100 Gy $^{90}Sr/^{90}Y$ beta irradiation then preheat of 160°C for 1 hour. Total exposure energies were 22.5 J, with emissions detected using an EMI 9235Q with Corning 7-59 (16 mm) and Schott BG39 (0.5 mm) filters. No allowance has been made for sample optical transparency.

FELDSPAR	TL Σ(264°C - 550°C) (Counts/Gy/mg)	IRSL (1st 10 mJ) (Counts/Gy/mg)	OSL (1st 10 mJ) (Counts/Gy/mg)	IRSL (Long exposure) (Counts/Gy/mg)	OSL (Long exposure) (Counts/Gy/mg)
5. No. 3062 microcline	857751	11401.8	7326.3	1496954	254570
22. orthoclase	3	0.0	1.3	1297	199
3. Z5 microcline	10311	8.2	14.6	1215	687
11. Z6 orthoclase	96691	75.5	93.3	9240	2140
21. Z9 microcline	155826	1748.4	1266.7	301120	42024
14. Z11 microcline	258484	955.3	1330.3	124695	29343
13. Dup(C) microcline	675309	2537.5	1561.4	427377	77875
1. adularia	81063	634.1	271.0	78016	21543
20. Z9N microcline	67920	1274.8	864.2	201314	28051
9. Z15 sanidine	71947	3.2	47.2	624	453
12. Patmos sanidine	31241	1.9	2.1	333	273
16. 1947,199(2) anorthoclase	20526	0.0	0.1	26	234
17. albite	1190	0.0	0.2	25	47
18. Amelia albite	288492	6000.0	4792.1	385293	35394
15. Dup(A) albite	8500000	252000.0	110000.0	35370305	2778714
4. 17 oligoclase	41182	28.8	24.8	1992	1001
7. 18 oligoclase	66747	5.3	9.0	404	597
23. Dup(B) oligoclase	578667	4870.7	5717.3	239932	48236
19. BA6 labradorite	449	0.2	0.1	14	49
6. 23 labradorite	1546	0.4	0.6	67	64
24. Dup(D) labradorite	1938	0.4	0.1	26	43
2. 25 bytownite	150	0.1	0.1	11	30
8. 26 bytownite	131	3.7	2.5	722	148
10. Z4 bytownite	867	2.2	3.1	156	97

Table 3.3.1 The normalised luminescence for each of the feldspar samples. See text and Figs.3.3.1-3 captions for experimental details. The long exposure data corresponds to that shown in Fig.3.5.3.1, and the TL and short exposure data to that in Figs.3.3.1-3. The backgrounds subtracted from the long exposure data are calculated from electronic noise plus scatter off clean target discs and may be slightly under estimated.

luminescence measurement procedures are outlined in the captions to Figs. 3.3.1 and 3.3.2.

The sensitivities of the samples under optical stimulation were measured, along with TL sensitivities for comparison. Fig. 3.3.1 shows TL light sum per gray for the high temperature TL (approximating that glow curve region stable over archaeological timescales).

Fig. 3.3.2 and Fig. 3.3.3 show luminescence resulting from 10 mJ exposures to infrared and green light (note that this form of representation on the feldspar composition does not include information on trace element concentrations, the presence or abundance of intergrown minor phases, structural state, degree of structural disorder (Goedicke, pers. comm. 1990) or thermal history - all of which may be relevant to both luminescence sensitivity and anomalous fading behaviour). Data are uncorrected for detector spectral response. The normalised luminescence data are given in Table 3.3.1, along with similarly normalised data measured during long exposures to 514.5 nm light and 880 Δ 80 nm IR, although the latter data correspond to the long exposure shine curves shown in Fig.3.5.3.1.

3.3.1 DISCUSSION

The luminescence seen in each case follows a general trend, most clearly shown in the case of TL, in that the brightest samples are the high potassium and high sodium feldspars, with a rapid decrease in sensitivity as calcium content increases across the plagioclase series. Superimposed upon this trend is considerable variation in sensitivity at any given composition. The apparent systematic variation in luminescence intensity with composition is in accord with TL sensitivity data by Akber (1986), Akber and Prescott (1987) and Huntley *et al.* (1988) and the OSL intensities observed by Huntley

et al. (1989) when 514.5 nm or 632.8 nm illumination was used.

Luminescence was detected from feldspars representing all compositional regimes, but not from all individual samples (IRSL was not always detected, probably due to low emission levels rather than real absence of signal), and the general correlation between sensitivity and major element composition has some notable exceptions; possible causes may include crystal structural state, thermal history and trace element concentrations. Work to assess the latter would be desirable, with initial emphasis on high sodic feldspars - as these exhibit the most extreme range of sensitivities under optical stimulation (varying, for infrared stimulation, from no signal detected following 100 Gy beta dose to a 5 mg aliquot of sample 17, to ≈ 100,000 photon counts/Gy/mg for the first 10 mJ of exposure for sample 15). However, even the most sensitive sample studied (sample 15) has, assuming 100% luminescence efficiency, a maximum trapped charge concentration of ≈ 5×10^{6} (counts/Gy/mg) × 10^{3} (Gy) × 2.5×10^{3} (mg/cm^{3}) × 10^{3} (detector quantum efficiency) ≈ 10^{16} charges/cm^{3}, corresponding to a weight for weight concentration of about 1 ppm, the remainder may have correspondingly lower concentrations. As a large suite of elemental impurities are typically present at ppm concentrations, an unambiguous correlation of luminescence intensity with any particular elemental impurity seems optimistic. Furthermore there is strong possibility that the luminescence defects may either be complex clusters of impurities and so not amenable to identification by bulk compositional analysis techniques, or indeed be structural defects such as broken bonds, voids or dislocations and so not be detectable at all by such means. Finally, there is the possibility that the observed luminescence represents only a small, luminescing, fraction of a much larger charge population untrapped during measurement, the remainder of which undergoes non-luminescent recombination. The relative magnitudes of the observed

signal may therefore hold no straightforward correlation with the true magnitudes of the defect concentrations present. Additional data would be required from techniques such as ESR or thermally stimulated conductivity (TSC) to investigate this possibility.

Finally, it may be noted that following heating to 550°C for the TL measurements, no OSL signal was detected from any sample regardless of stimulation wavelength used or emission bands monitored. This result suggests that optical dating may not in general be able to exploit the work by Guerin and Valladas (1980), utilizing the apparent non-fading of high temperature (≈ 600°C - 700°C) TL peaks in volcanic plagioclase to date successfully lava flows in the Massif Central, France, as there appear to be no generally occurring glow peaks at temperatures higher than 550°C capable of optical excitation, at least by the wavelengths used here.

3.4 IRSL EMISSION SPECTRA

3.4.1 INTRODUCTION

TL emission spectra of various feldspars have been reported by workers such as Pasternack and Levy (1978), Akber and Prescott (1985), Akber (1986), Huntley *et al* (1988), Kirsh and Townsend (1991) and Dalal *et al* (1991). Recently feldspar emission spectra measured under optical stimulation have also been reported by, for example, Huntley *et al* (1989), Huntley *et al* (1991), Jungner and Huntley (1991) and Bailiff and Poolton (1991). This section presents the IRSL emission spectra of the feldspars in this study. Stimulation was by IR wavelengths only (880 ∆ 80 nm), as the full sensitive range of the PMT photocathode was then available for luminescence detection, and also as IR

is the preferred stimulation waveband for feldspathic materials (primarily because of greater certainty of pre-burial zeroing, better signal/noise ratio and technical simplicity). Three principal reasons motivated this work.

First, with reference to the fading measurements made later in the course of this work (chapter 4): emission spectra resolution between fading and non-fading signals might be feasible - either because different fading behaviours are exhibited by different emission bands in the same mineral or because some emission bands may be dominated by emissions from fading or non-fading minerals, so permitting spectral rejection or selection. Regardless of emission spectra published for other feldspar samples it was necessary to determine the emission spectra of this particular set of samples to permit interpretation, from a spectral perspective, of fading measurements made using these samples.

A second reason for measuring the emission spectra of these samples concerned the intended application of kinetic analysis methods. The methods applicable generally assume the detector spectral response to be constant, so if the luminescence exhibits more than one emission waveband these methods are not necessarily reliable.

Thirdly, the work of Akber (1986) and Akber and Prescott (1985) gave rise to the hypothesis (Spooner and Questiaux, 1989) that differences between the IRSL emission spectra may permit discrimination between feldspar species, or at least enable choice of optical filters to bias the detected emissions towards a chosen group of the feldspars (such as high potassic or high sodic). This hypothesis assumed the IRSL and TL emission spectra to be congruent; it was used as a working hypothesis in that study (Spooner and Questiaux, 1989) directed at breaching the "100 ka" barrier rather than circumventing short term fading (based on the working assumption, probably simplistic, that the two are separate phenomena).

Results of an initial spectral study on these feldspars are given in Spooner (1992). A range of optical filters were used in conjunction with optical stimulation. These were: for 514.5 nm stimulation, 5 mm Corning 7-51 + 1 mm Schott BG 39, and for infrared stimulation, 2 mm UG 11, 7-51 + 2 mm BG 39, 4 mm Corning 5-58 + 2 mm BG 39, 4 mm Corning 7-59 + 2 mm BG 39 and 2 mm Schott GG 475 + BG 39. Following approximate correction for detector spectral response, in general the occurrence and relative intensities of the various emissions from these samples agreed with the findings, using optical stimulation, of Huntley *et al.* (1989), Huntley *et al.* (1991), Jungner and Huntley (1991) and Bailiff and Poolton (1991) who show that K-feldspars emit most intense emission in a broad band centred at ≈ 400 nm, while the high-sodic feldspars and plagioclase exhibit a dominant emission peaking at ≈ 570 nm.

Although this correlation offered hope of spectral selection of either K-feldspars or sodic feldspars plus plagioclase (or sodic feldspars or plagioclase alone if appropriate density separation is also used), it was noted that all oligoclase (sodic) samples gave a very broad emission across the full spectral range observed, with especially intense UV emissions. More generally, samples possessing intense emissions at any given emission peak appeared to give significant emissions at other wavelengths also, making reliable spectral rejection of unwanted feldspar species seem impractical.

The depressing significance of these conclusions coupled with the preliminary nature of the study led to a more thorough remeasurement of the spectra, the details of which follow. The methodology closely parallels that of Jungner and Huntley (1991).

3.4.2 EXPERIMENTAL

Portions of each of the samples were mounted onto stainless steel discs and the "natural" luminescence drained by heating (5 K/s to 550°C with similar reheat). A Littlemore Sci. Eng. Co. beta irradiator (Type 733L) was then used to administer beta doses ranging from 3.3 Gy to 220 Gy, depending on sample sensitivity. Dosing was followed by ≈ 12 hour delay before preheating for 60 seconds at 220°C using a Risϕ automated TL reader. IRSL was measured using an Elsec automated optical dating system (Type 9010) and various optical filter combinations based on two "primary" filters - one Schott BG 40 (3 mm) and two Schott UG 11 (total 4 mm). These defined two waveband "envelopes" which were themselves subdivided by the addition of Schott edgecut colour glass filters, one at a time. The transmission spectra are shown in Fig. 3.4.2.1 and the measured fractional transmittance of the filter combinations, along with other details, are given in Table 3.4.2.1.

All luminescence measurements were made using short exposures (≈ 30 mJ). An initial normalization exposure was given with only the BG 40 filter present. Four filter combinations followed, then a second normalization exposure was performed. This routine was repeated until all filter combinations had been used. Data analysis consisted of first subtracting backgrounds (taken as the mean scatter off 10 blank discs), then correcting for signal "pile-up" (1 % / 100,000 counts), then correcting for signal depletion due to the repeated short exposures (using the interposed normalization exposures). Next the counts in each individual waveband were determined by sequential subtraction of adjacent wavebands from long wavelengths to short (this data is given in Appendix H). This was followed by normalization for sample mass and beta dose. Finally data were corrected for

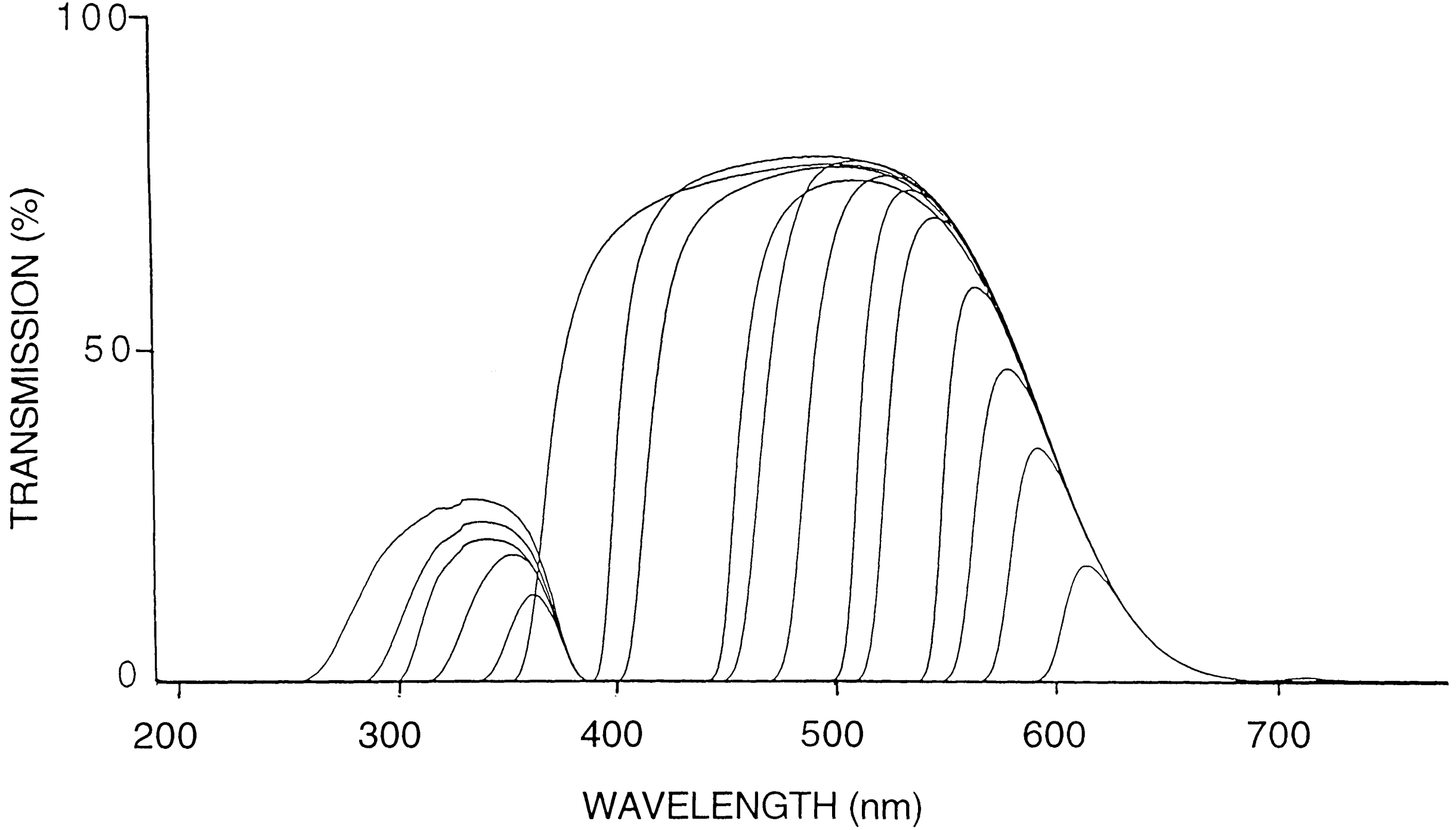


Fig. 3.4.2.1 The transmission spectra of the various filter combinations.

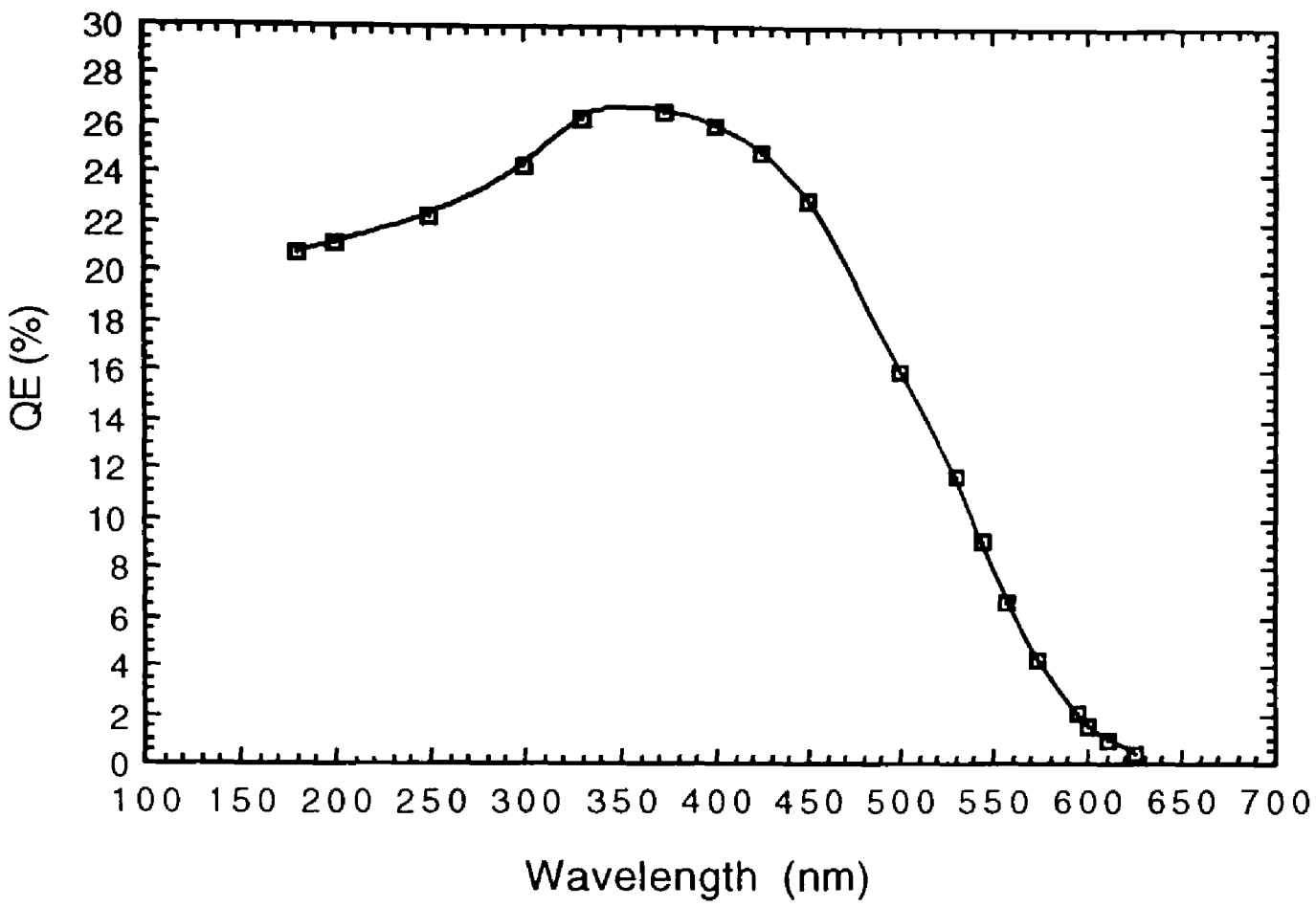


Fig.3.4.2.2 The quantum efficiency (manufacturers data) of the bialkali photocathode of the EMI 9635Q PMT used for the spectral measurements.

Optical filters	Midband wavelength (nm)	FWHM (nm)	Fractional transmittance	PMT QE	1/(QE*trans.)
2*UG11	294	23	0.329	0.240	12.66
2*UG11+WG 305	310	10	0.307	0.250	13.03
2*UG11+WG 320	322	22	0.218	0.260	17.64
2*UG11+WG 335	341	22	0.203	0.270	18.24
2*UG11+WG 360	360	25	0.137	0.270	27.03
BG40+GG 375	386	28	0.640	0.268	5.83
BG40+GG 400	410	19	0.808	0.258	4.80
BG39+GG 400	412	18	0.763	0.255	5.14
BG40+GG 420	437	36	0.713	0.240	5.84
BG40+GG 455	460	10	0.693	0.218	6.62
BG40+GG 475	476	15	0.783	0.193	6.62
BG40+GG 495	497	28	0.738	0.162	8.36
BG40+OG 515	517	12	0.694	0.136	10.60
BG40+OG 530	536	28	0.662	0.103	14.67
BG40+OG 550	558	15	0.620	0.067	24.07
BG40+OG 570	572	18	0.482	0.043	48.25
BG40+OG 590	594	28	0.311	0.021	153.12
BG40+RG 610	618	33	0.206	0.006	809.06

Table 3.4.2.1 Details of the filter combinations, quantum efficiency of the PMT (see also Fig.3.4.2.2) and the detector spectral response factors evaluated for the midpoint of each waveband. Fractional transmittance refers to the half peak transmittance value.

detector spectral response (see Fig. 3.4.2.2 for the PMT quantum efficiency and Table 3.4.2.1 for correction factors) and then divided by the waveband FWHM.

3.4.3 RESULTS AND DISCUSSION

The IRSL spectra are presented in Fig. 3.4.3.1 (a)-(c) grouped along broad compositional lines according to potassic, sodic and plagioclase classification, and in Fig. 3.4.3.2 (a)-(f) according to luminescence intensity of the most prominent emission peak in each case. It must be noted that only short exposure data is presented here and that the relative intensities may vary as a shine down proceeds, ie, the decay curve forms under optical stimulation show some variations between feldspars (see section 3.5). Generally three distinct emission peaks are seen, the well known "potassium feldspar" peak at ≈ 410 nm and the "plagioclase" peak at ≈ 570 nm. Microcline is seen to have a broad range of emissions, though blue/UV wavelengths are dominant. Also prominent is a strong peak in the UV at ≈ 320 nm, previously reported by Jungner and Huntley (1991) and Bailiff and Poolton (1991). Generally the findings are in accord with the IRSL emission spectra of Bailiff and Poolton (1991). The range of sensitivities seen in Fig. 3.4.3.2 are in agreement with data presented in section 3.3, and attention is again drawn to the lack of correlation between emission intensity and composition. The presence of some 570 nm emission in the high potassic samples and some 410 nm emission in the sodic and plagioclase samples does not disprove the hypothesis that the 410 nm emission peak is specific to potassium feldspars whereas the 570 nm emission is specific to sodic and plagioclase feldspars (Prescott, pers. comm. 1989). This finding is explicable if the intergrown minor phases have greater sensitivity than the matrix phase, and that each of

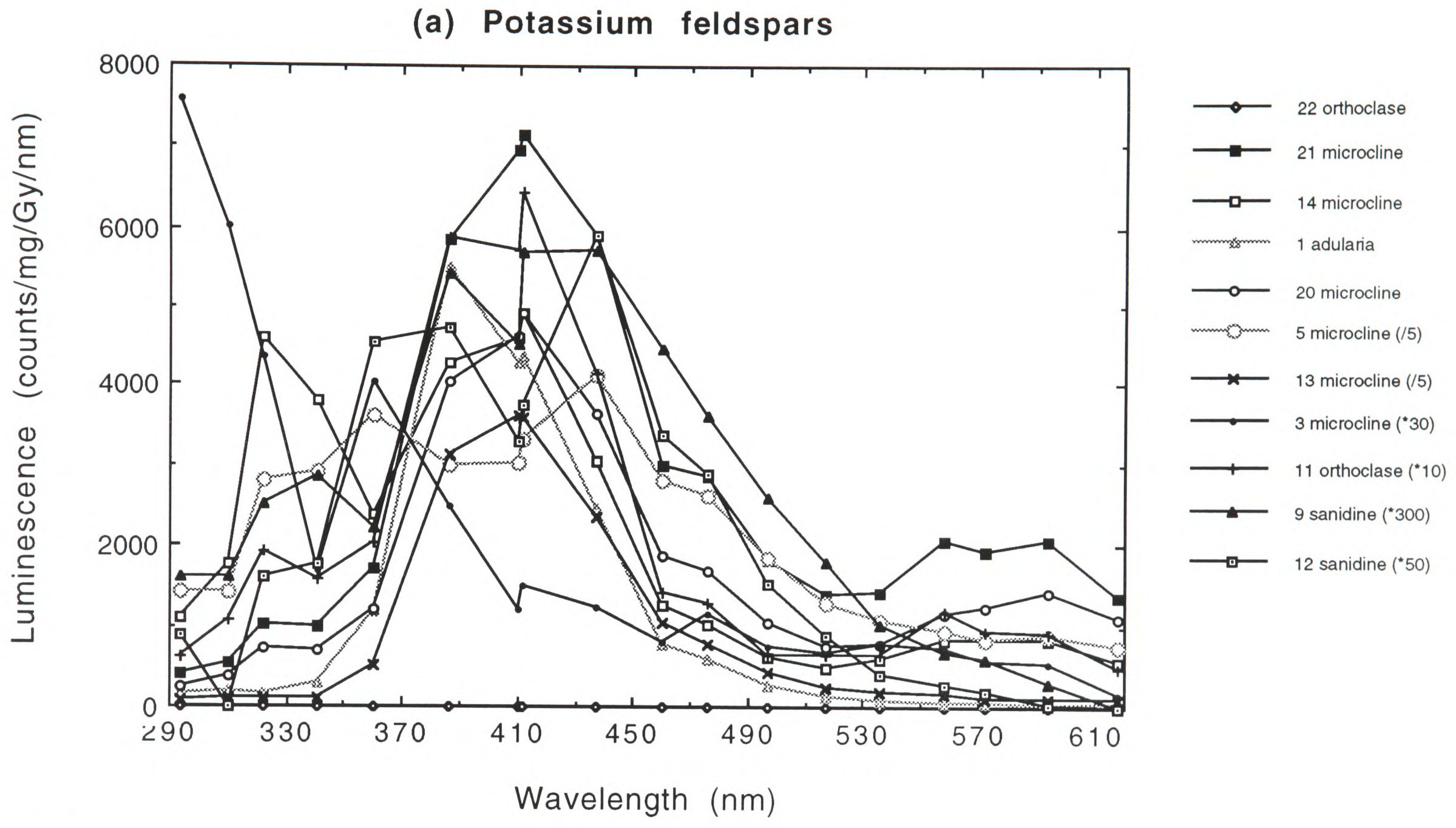
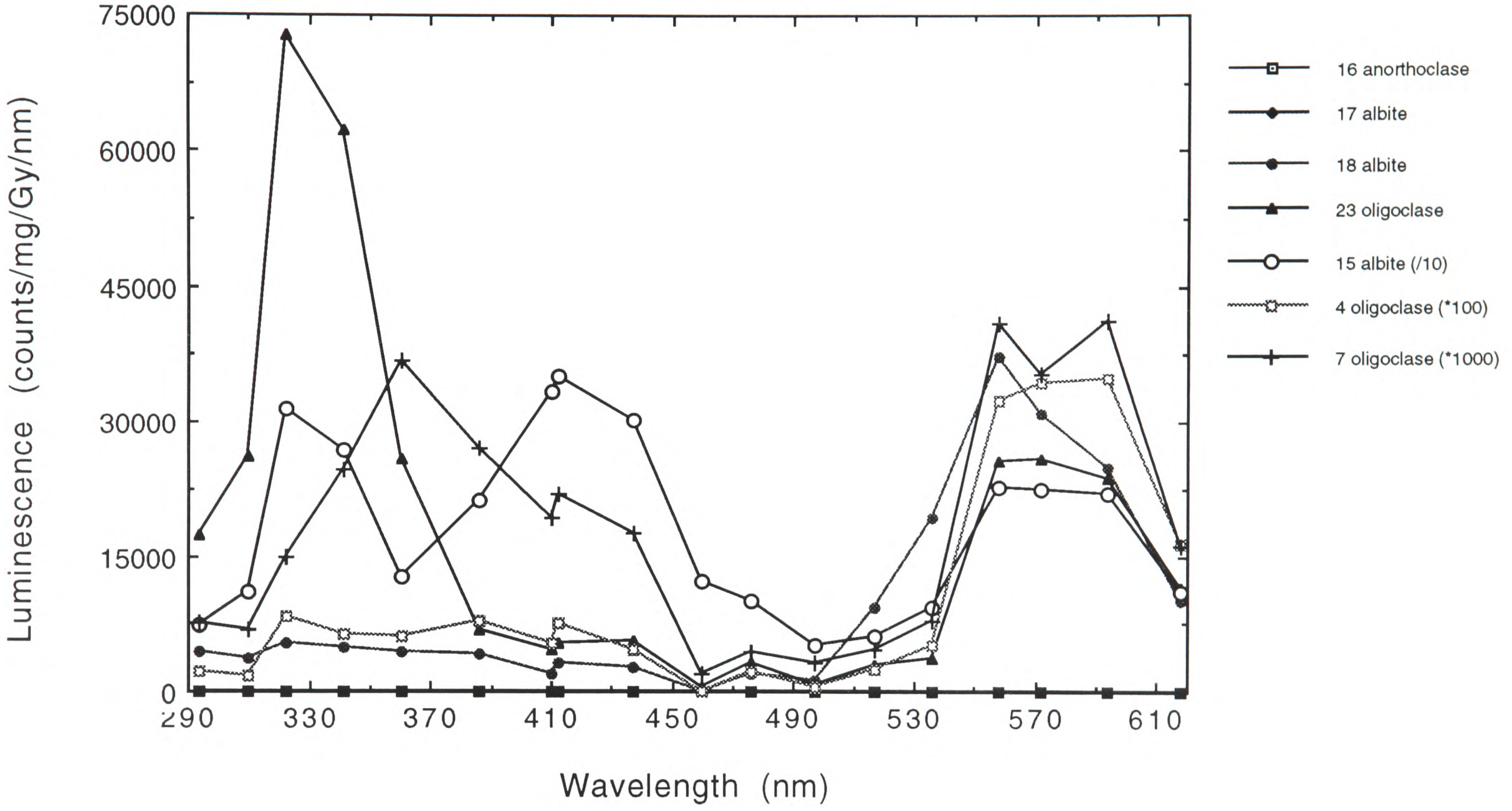
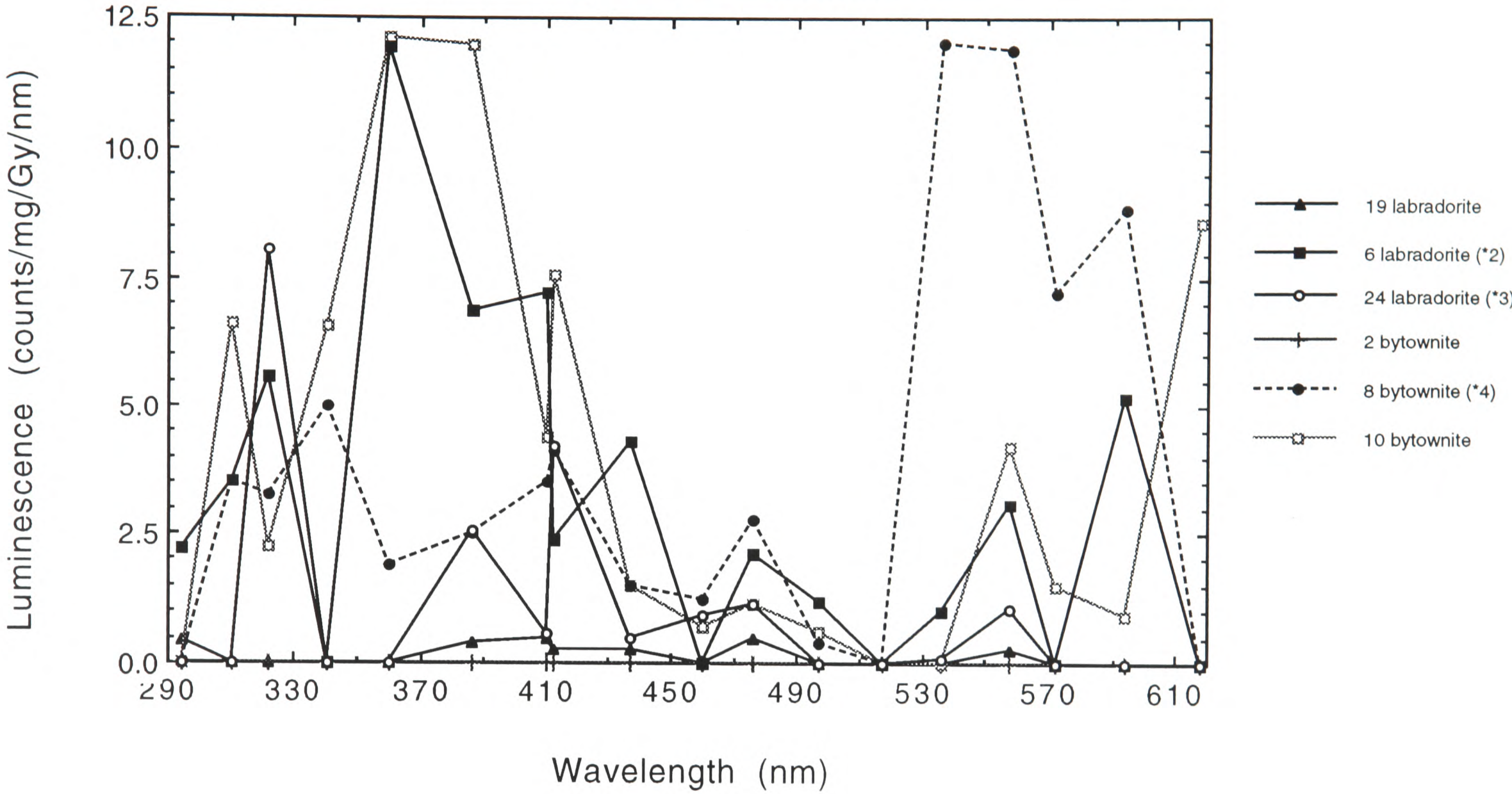


Fig.3.4.3.1.(a)-(c) The IRSL emission spectra grouped according to composition. All spectra are corrected for the spectral response of the PMT and the transmissivities of the various filter combinations. Note that some spectra have been scaled, the scaling factors are given in the legend.

(b) Sodic feldspars



(c) Plagioclase feldspars



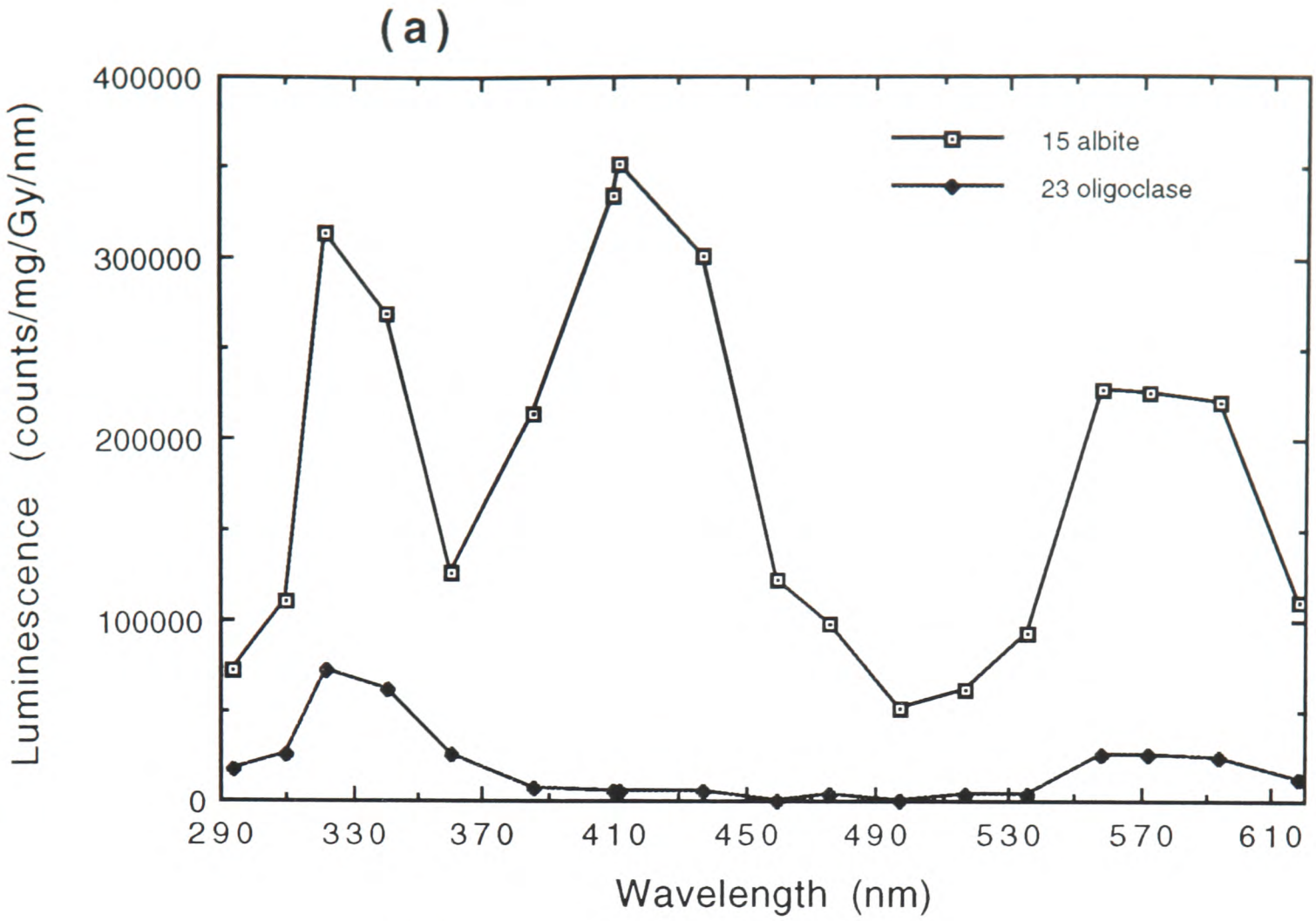
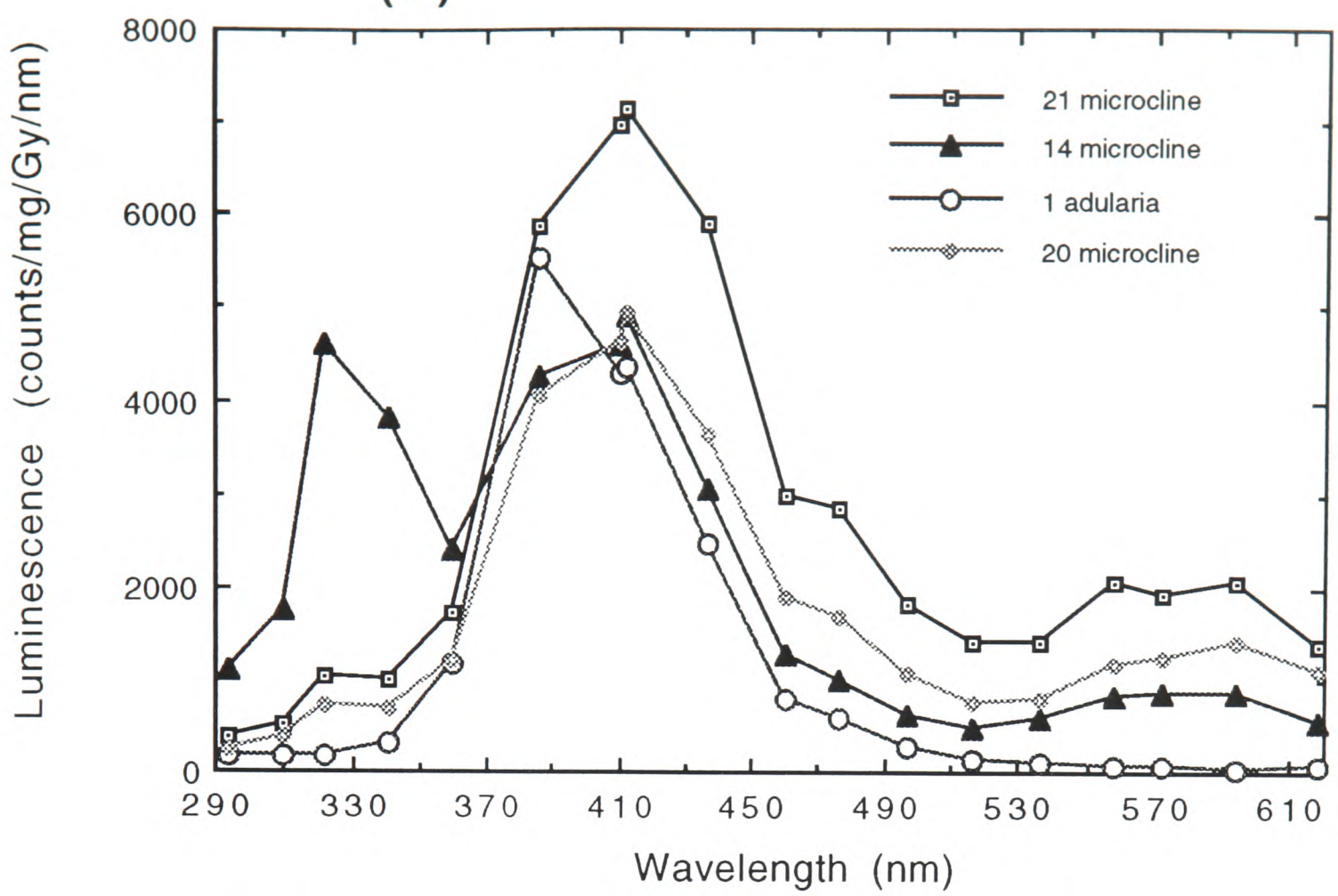
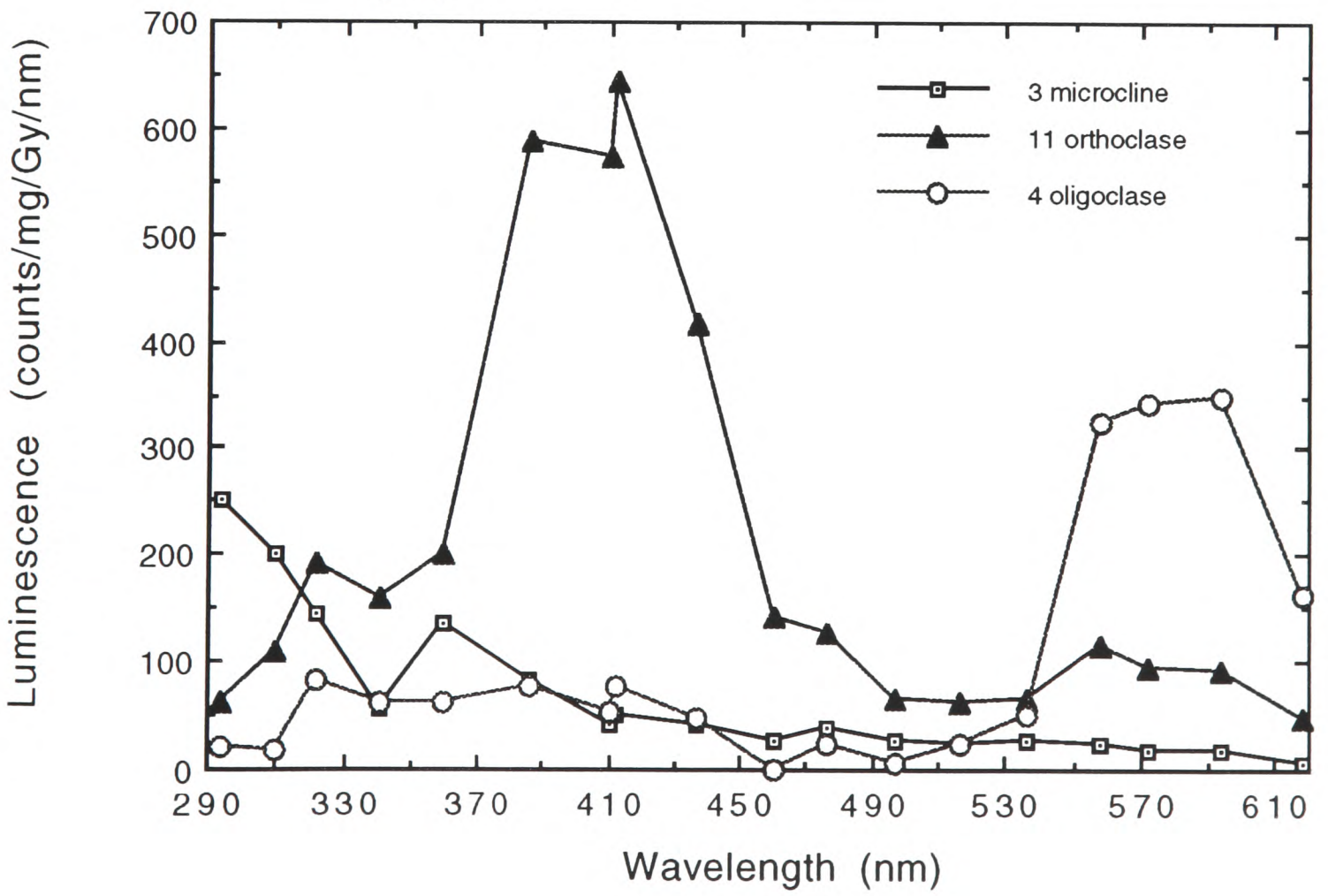


Fig.3.4.3.2.(a)-(f) IRSL emission spectra grouped according to luminescence intensity of the most prominent emission peak. All spectra are corrected for the spectral response of the PMT and the transmissivities of the filter combinations. Note that each successive graph displays a sensitivity range one order of magnitude less than the preceding graph.

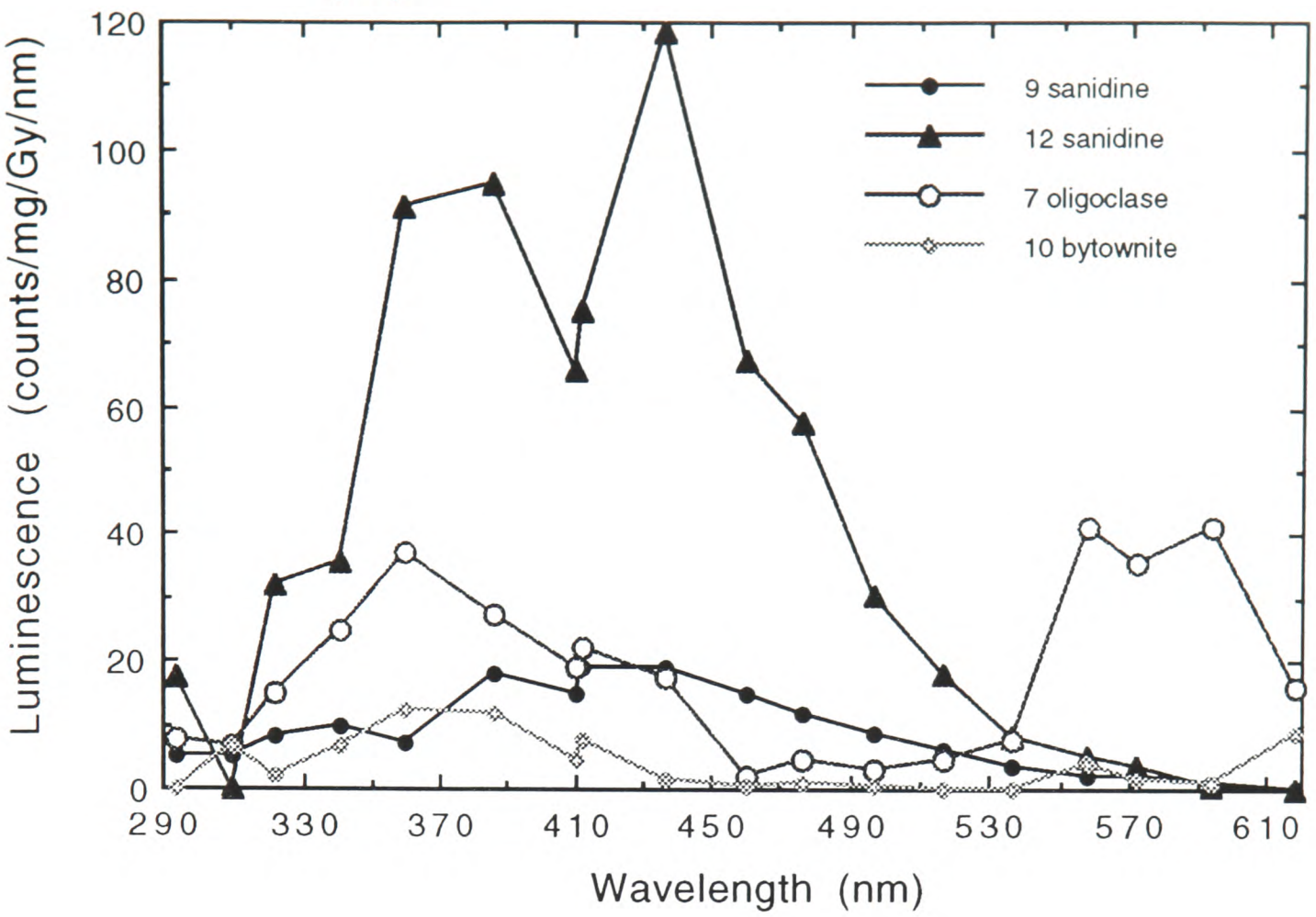
(c)


8000
6000
4000
2000
0
Luminescence (counts/mg/Gy/nm)
290
330
370
410
450
490
530
570
610
Wavelength (nm)
21 microcline
14 microcline
1 adularia
20 microcline

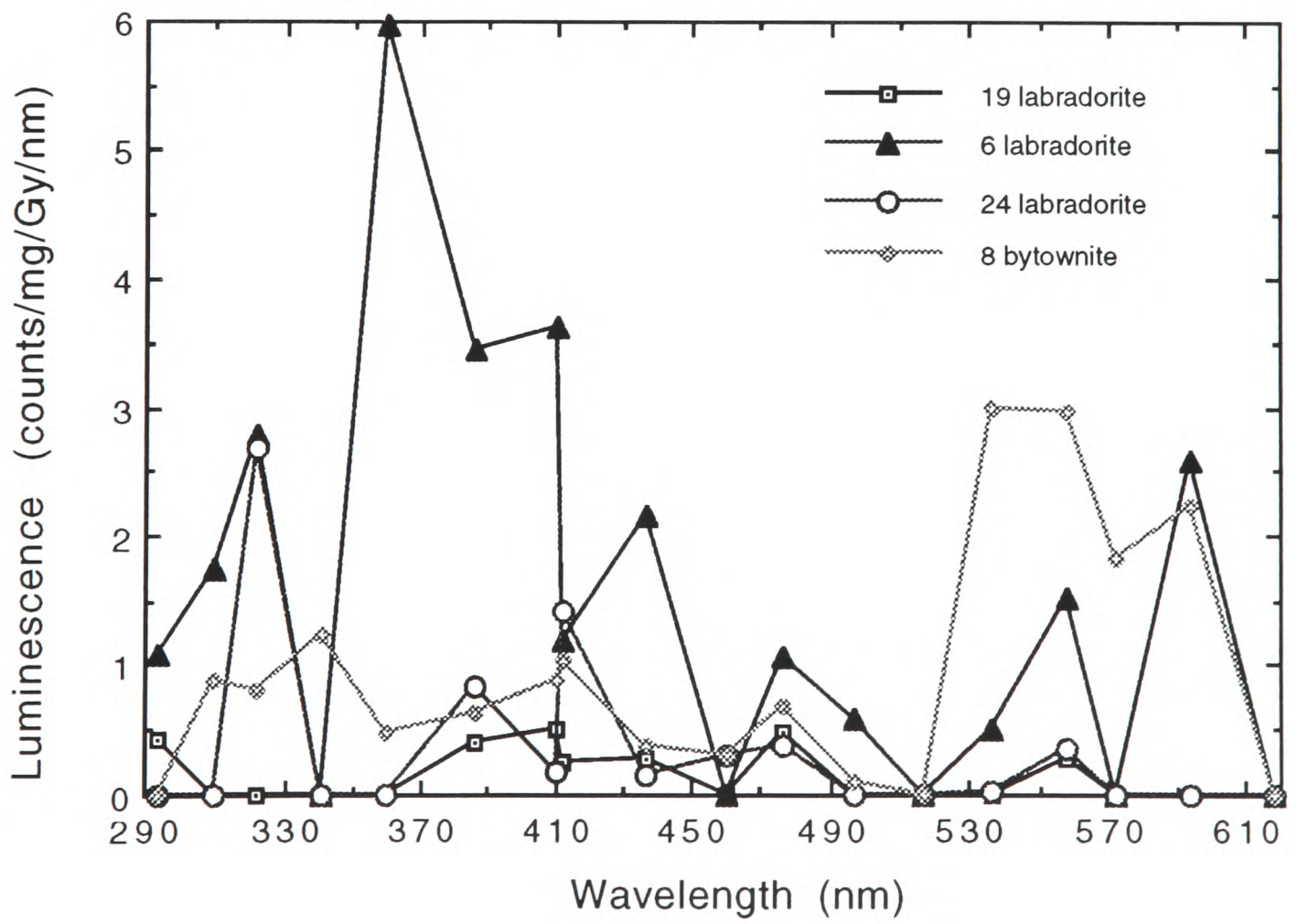
(d)


700
600
500
400
300
200
100
0
Luminescence (counts/mg/Gy/nm)
290
330
370
410
450
490
530
570
610
Wavelength (nm)
3 microcline
11 orthoclase
4 oligoclase

(e)


Luminescence (counts/mg/Gy/nm)
120
100
80
60
40
20
0
290
330
370
410
450
490
530
570
610
Wavelength (nm)
9 sanidine
12 sanidine
7 oligoclase
10 bytownite

(f)


Luminescence (counts/mg/Gy/nm)
6
5
4
3
2
1
0
290
330
370
410
450
490
530
570
610
Wavelength (nm)
19 labradorite
6 labradorite
24 labradorite
8 bytownite

the compositional phases of a perthitic grain emit the characteristic emission of that species.

However, the general pattern of behaviour is in accord with the earlier findings, supporting the hypothesis that practical clear-cut discrimination between feldspar grains on the basis of their IRSL emission spectra is not possible, though it must be emphasised that the characteristic wavebands of the potassic and sodic feldspars are most prominent in their respective categories (presumably due to dominance of the luminescence by the contribution from the matrix phase in each case) and do support the notion of biasing the detected signal towards one or other compositional grouping.

3.4.4 RELEVANCE TO FADING

With respect to the circumvention of fading it must be noted that OSL or IRSL data such as presented here represent a "snapshot" of the emission spectra in time and so give no information on whether fading proceeds uniformly across the emission spectrum or affects certain emission bands only. Consequently, although the absence or otherwise of fading of any specific emission peak is not immediately apparent, deductions can be made from the relative intensities of the uncorrected count data (Appendix H) in conjunction with the proportion of the total signal seen to fade. Such analysis reveals no specific waveband immune to fade or specifically prone to fade. Additionally, these measurements indicate there are only three IRSL emission peaks available for study with the detection systems currently employed in luminescence dating and so circumvention of fading by emission selection relies on at least one of these emission peaks not fading. Given the findings of Balescu *et al* (1991) and hypothesis of Balescu and Lamothe (1992)

and Wintle and Duller (1991), supported by dating evidence, that UV emissions systematically give incorrect (low) ages for high potassium feldspars at least, due to self-absorption of the luminescence within the grains, the emission peak at 320 nm is precluded from use in coarse grain studies regardless of its fading behaviour. Fine grain IRSL dates using these emission wavelengths have also given low ages (Spooner and Questiaux, 1989), though apparently through the unknown long term fading mechanism rather than internal absorption of signal. The possibility that the 320 nm emission of younger fine grain samples may not exhibit fading is not eliminated by these results. Considering the other principal emission peaks, in both cases the fading by naturally abundant species such as oligoclase, sanidine and microcline (see Chapter. 4) coupled with their spectra and occasional extremely high sensitivity precludes relying on either the 410 nm or 570 nm emissions as reliably non-fading in all circumstances.

In summary, although systematic variations in emission intensity appear to occur across the feldspar ternary system, they are not well enough defined to permit differentiation between feldspar species. However, emission wavelength appears to be characteristic along broad compositional lines and so offers stronger possibilities for discrimination between broad compositional regions of the feldspar ternary systems. Having said this it should be taken into account that mixed phase grains may possess emission peaks characteristic of their various phases and so apparently not follow the simple pattern alluded to. Nevertheless it seems likely to be possible with a polymineral sample (fine or coarse grain) to bias towards either high potassium or plagioclase feldspars by filter choice, at least when infrared excitation wavelengths are employed, though it must be emphasised that neither compositional regime nor emission wavelength or intensity offers specific advantages in the circumvention of fading.

3.5 BLEACHING OF FELDSPAR LUMINESCENCE

3.5.1 INTRODUCTION

Glow curves from each feldspar were measured following bleaching by 514.5 nm and 880 ± 80 nm illumination in an attempt to characterise the feldspar samples further. Additionally, if only certain TL peaks were bleached by these wavelengths, it raised the possibility of stimulation-wavelength resolution between fading and non-fading signals, and furthermore, following the work of Templer (1986b), that correlations may exist with fading which enable identification of localised transition effects and so lead to effective preheat or optical wash treatments. The question of whether fading and non-fading feldspars show different bleaching behaviour is more fully addressed in Chapter 5. A final aim was the identification of suitable samples for kinetic studies (on the ≈ 330°C and ≈ 380°C TL peaks) to investigate the thermal stability of these probable IRSL source traps, and incidentally, to assess claims (Aitken and Xie, 1991) for the general elimination of feldspar IRSL by various preheats.

These measurements were intended primarily as an aid to interpretation of the fading work (see Chapter 4) and so do not constitute a comprehensive time-resolved or multi-wavelength study. They do however comprise the first study made of the bleaching of a comprehensive suite of feldspars by the two wavebands principally used in optical dating, along with recording of the stimulated luminescence emitted during the bleaching. Indeed, with the exception of Robertson *et al* (1991), there are no published studies on the bleaching behaviour of known composition feldspars, and therefore the complete data

set is shown (see Fig. 3.5.3.1).

3.5.2 EXPERIMENTAL

The procedure to measure the response of the samples to 514.5 nm and 880 ∆ 80 nm illumination was :

(1) thermally drain the "natural" TL by heating to 550°C at 5 K/s with reheating for background.

(2) normalization dose (3 Gy - 60 Gy depending on sample sensitivity), followed by an on-plate preheat of 1 minute at 220°C then TL measurement as per (1)

(3) dose (3 Gy - 60 Gy), then on-plate preheat for 1 minute at 220°C

(4) IR long exposure (1800 s, totalling ≈ 54 J)

(5) 514.5 nm short exposure (1 s, totalling ≈ 12.5 mJ)

(6) measurement of the residual TL, as per (1)

(7) normalization as per (2)

(8) dose and preheat as per (3)

(9) 514.5 nm long exposure (1800 s, totalling ≈ 22.5 J)

(10) IR short exposure (1 s, totalling ≈ 30 mJ)

(11) measurement of the residual TL, as per (1)

(12) normalization as per (2)

The stimulated luminescence measurements were made using an Elsec Type 9010 Optical Dating reader for IRSL (EMI 9235 PMT with 2 mm Schott BG39 filter) and a modified Elsec Type 9010 reader attached to an Ar-ion laser for 514.5 nm OSL (EMI 9635 PMT with 2 mm Schott BG39 and 5 mm Corning 7-51 filters). TL measurements

and preheats were performed on a Risϕ automated TL glow oven, with an EMI 9635 PMT and Corning 7-59 and HA3 filters, (Oxford "Risϕ 2"). Quantitative comparisons between the light sums measured under optical stimulation and those of the TL removed by the corresponding illumination are precluded by the different emission wavebands monitored in each case.

3.5.3 RESULTS AND DISCUSSION

The TL data is presented to show first the dosed and preheated "natural" glow curves (step 2) overlain by the residual glow curves from the respective bleaches, and then the natural glow curves overlain by glow curves representing the TL removed or transferred by the bleaches. These latter data were obtained by subtraction of the residual glow curves from the naturals, following Questiaux (pers. comm. 1989). Sensitivity changes induced by the repeated dose-heat cycles were assessed from the ratios of integrals of the prominent TL peaks from runs (2), (7) and (12) and concluded to be insignificant, consequently no corrections for sensitization were made.

Inspection of the natural and residual TL glow curves shown in Fig. 3.5.3.1 encourages a number of generalizations:

1) All the feldspars show significant bleaching of the high temperature TL (> ≈ 250°C). Although no distinct trends related to composition are apparent, the high calcic samples may be the most resistant to bleaching.

2) There is no characteristic "source peak" for either the OSL or IRSL, with bleaching by both wavelengths affecting all peaks to varying extents.

3) The glow curves of the K-feldspars appear to have the most complex structures, and

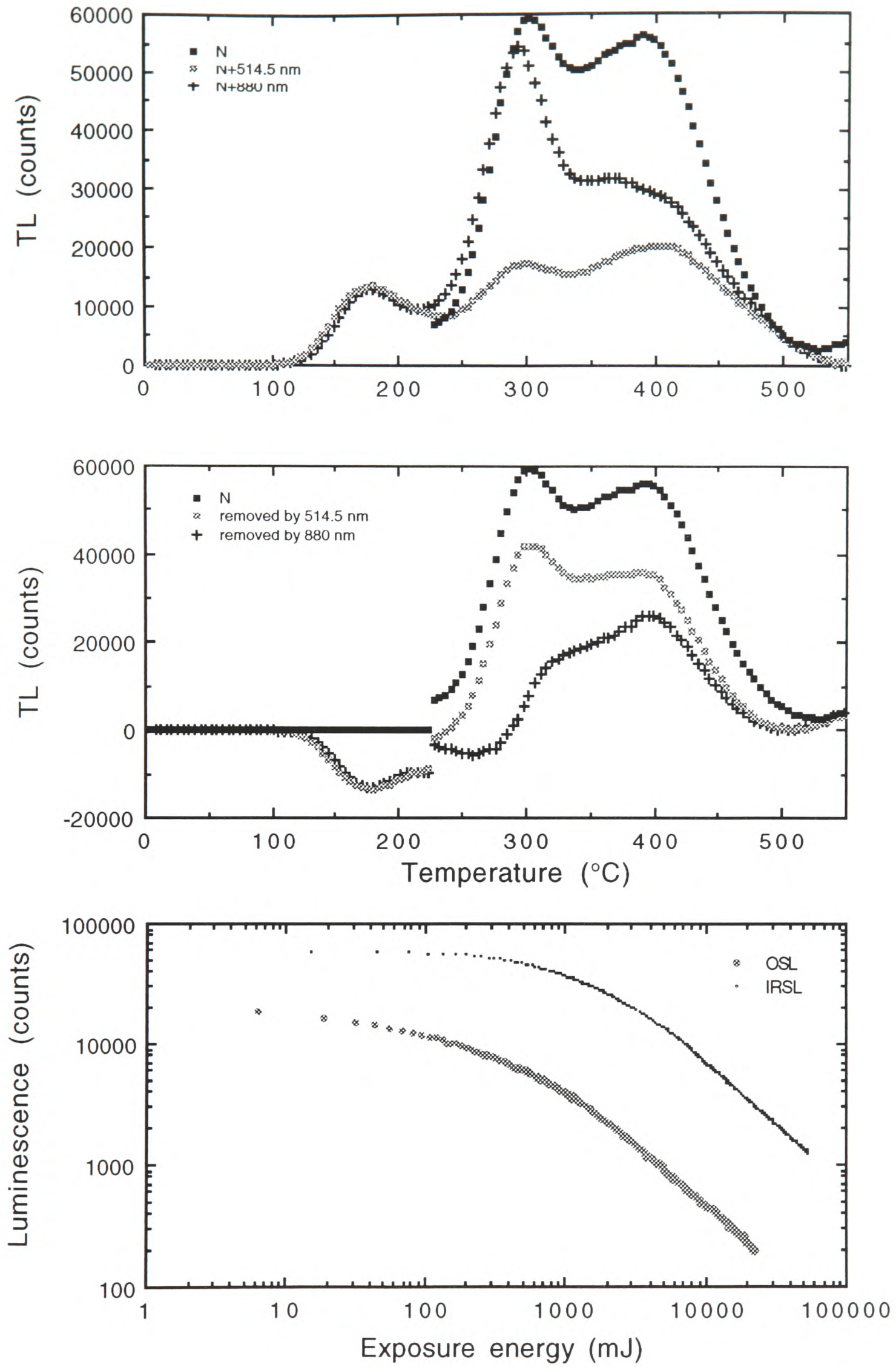
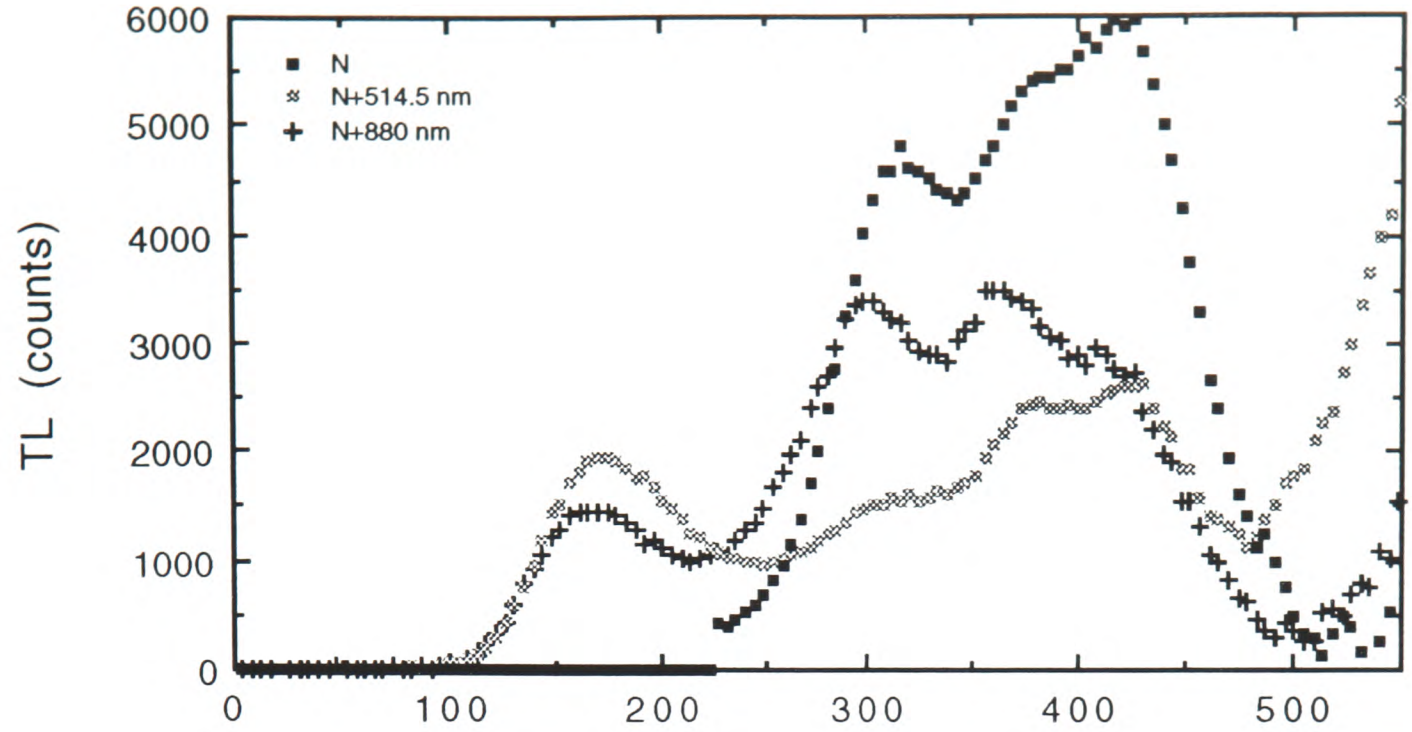
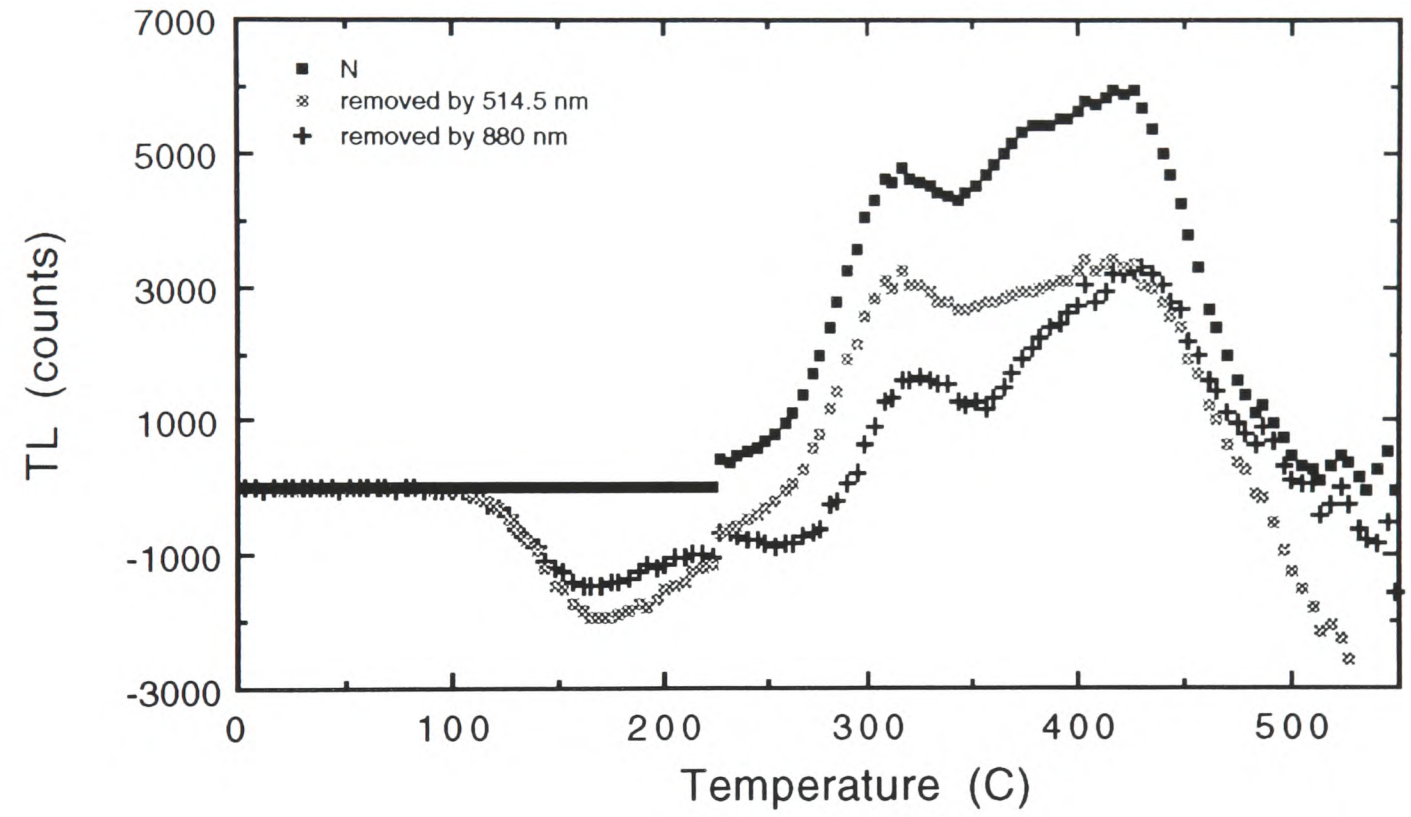
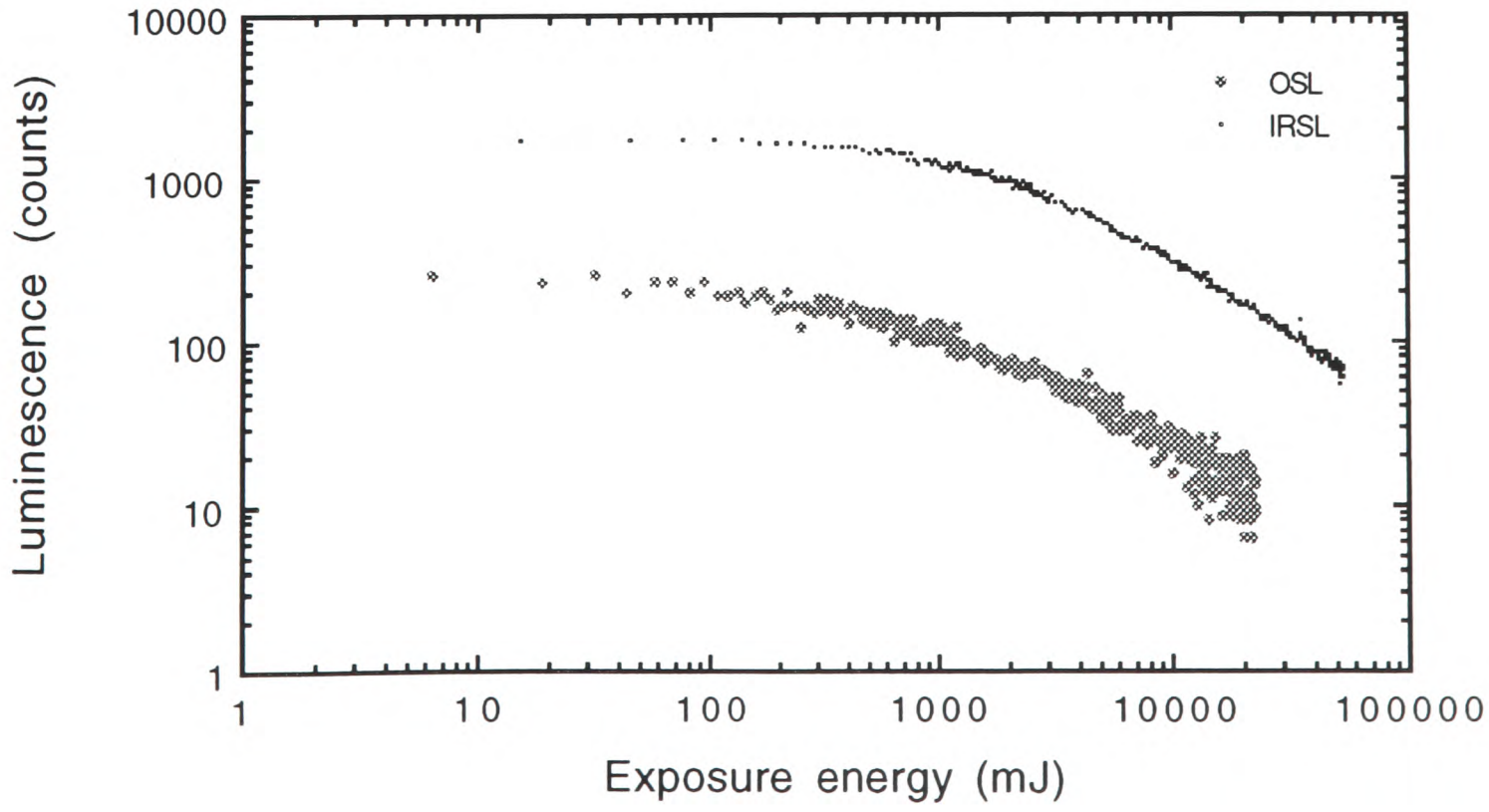


Fig.3.5.3.1 The bleaching of the feldspar TL by IR and green light, and the corresponding stimulated luminescence emitted during this bleaching. TL plotted are counts/channel and IRSL and OSL are counts/second; see section 3.5.2 for experimental details.

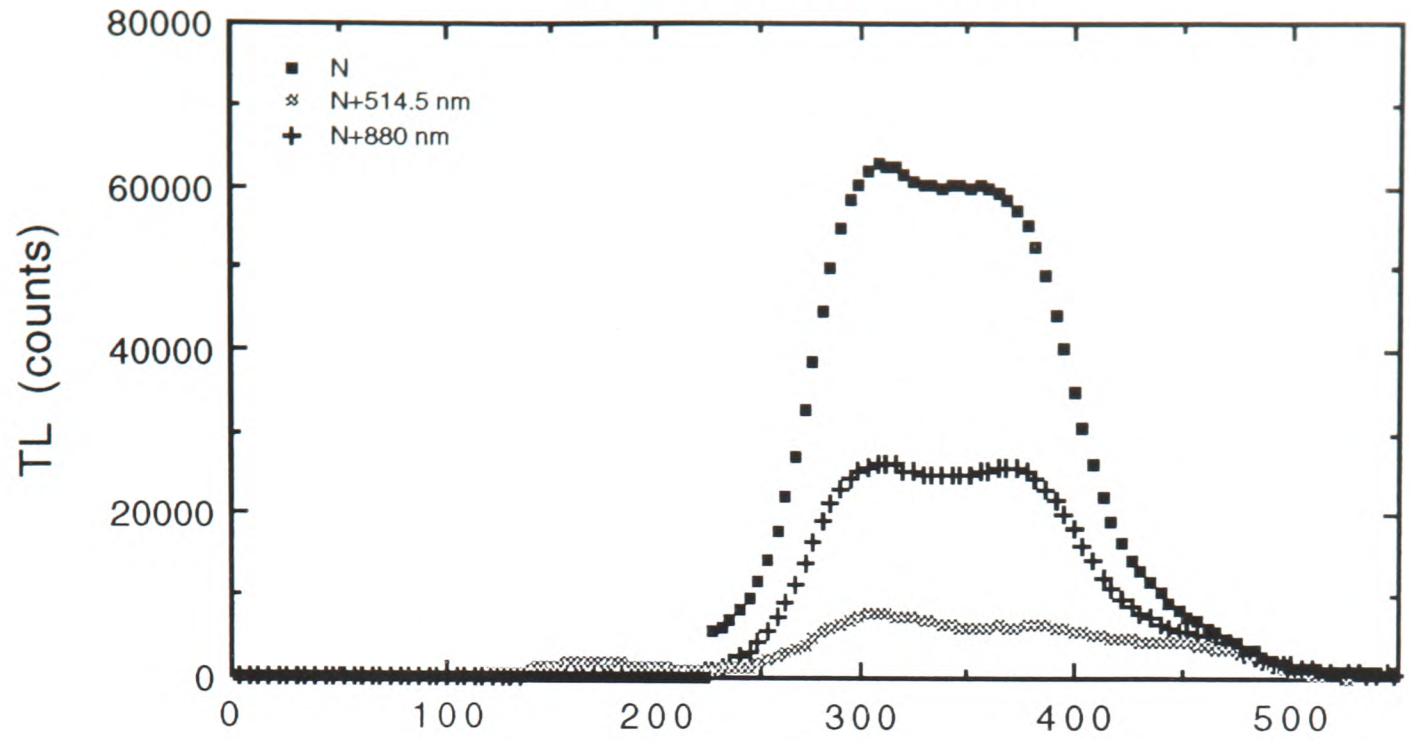
22. orthoclase

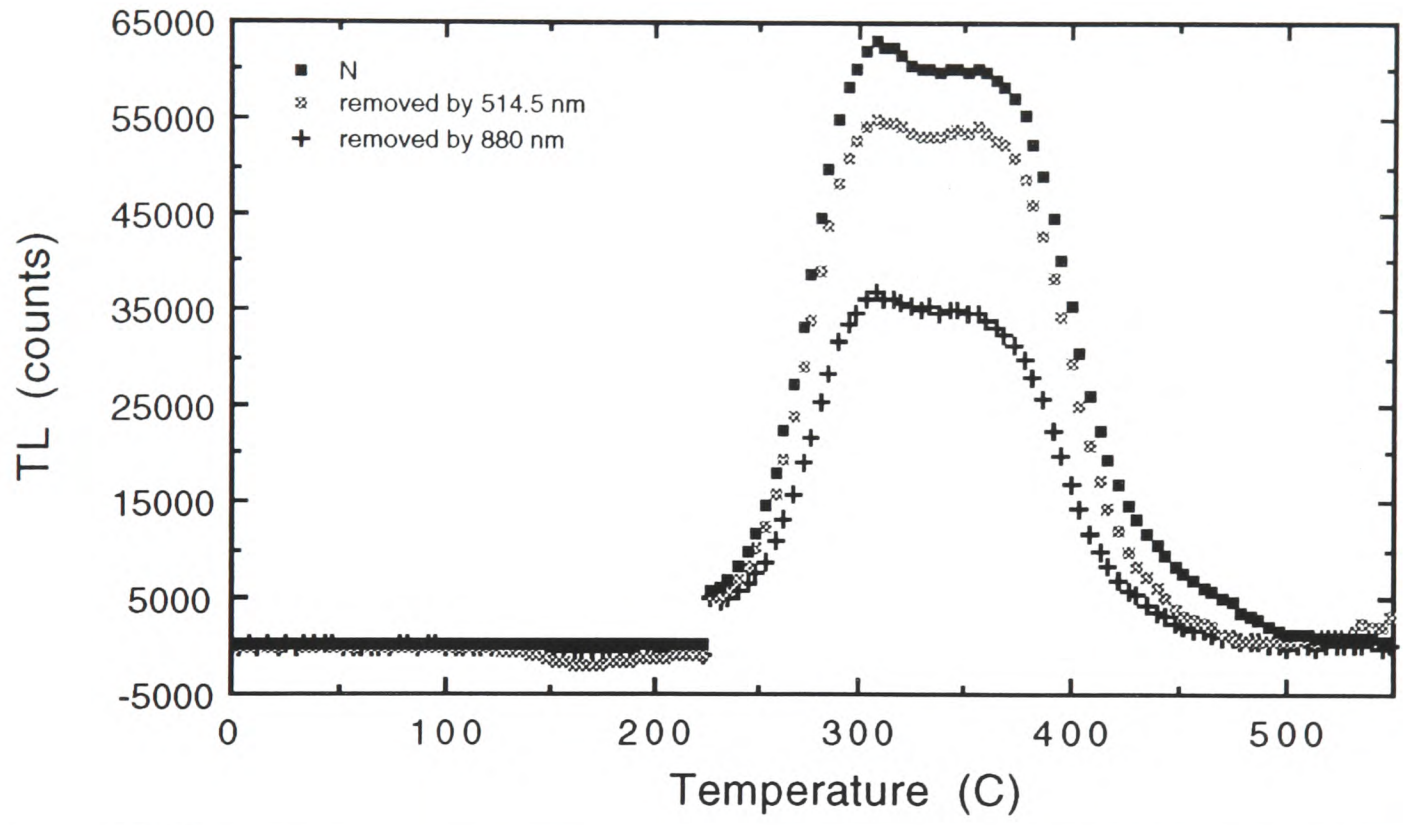


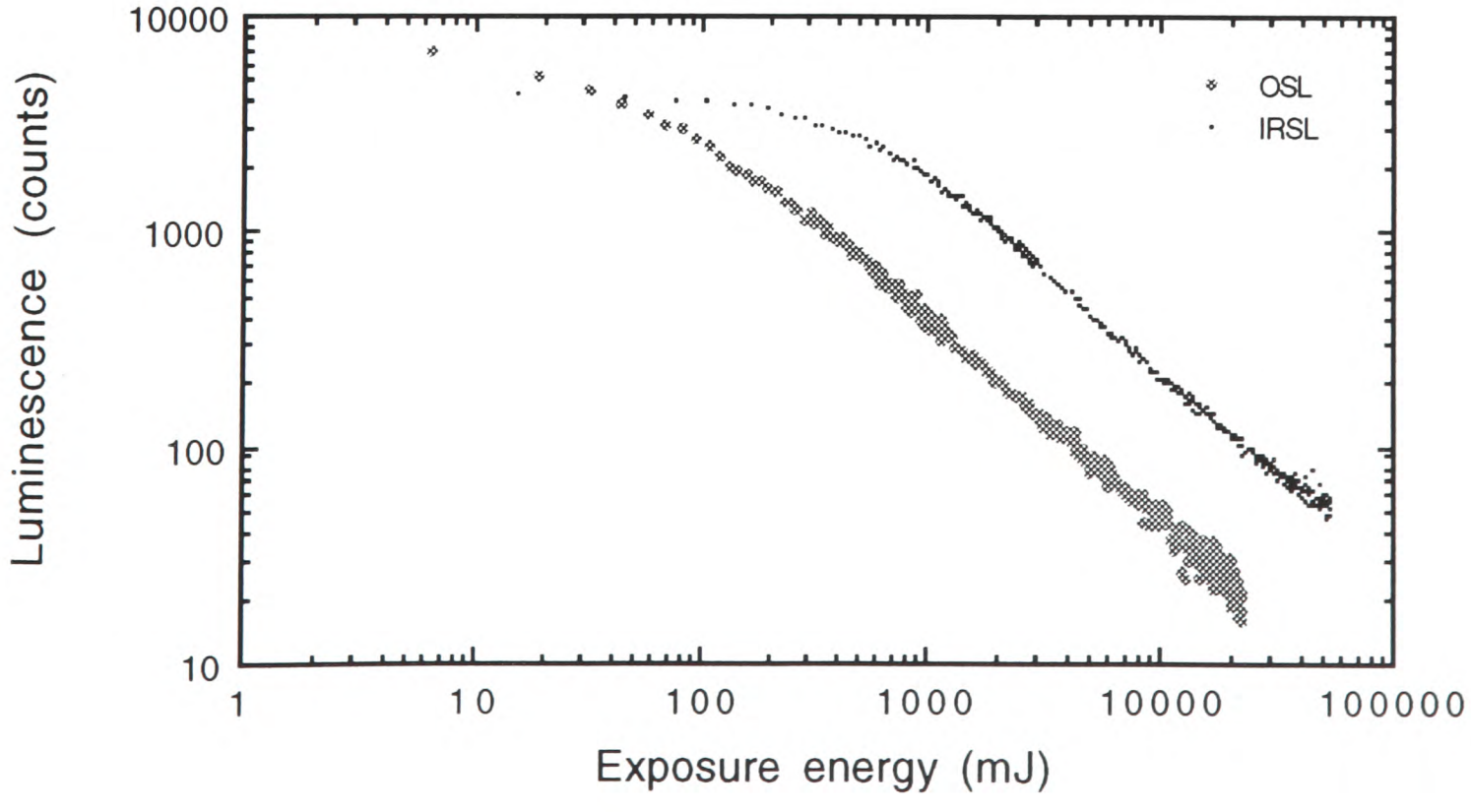




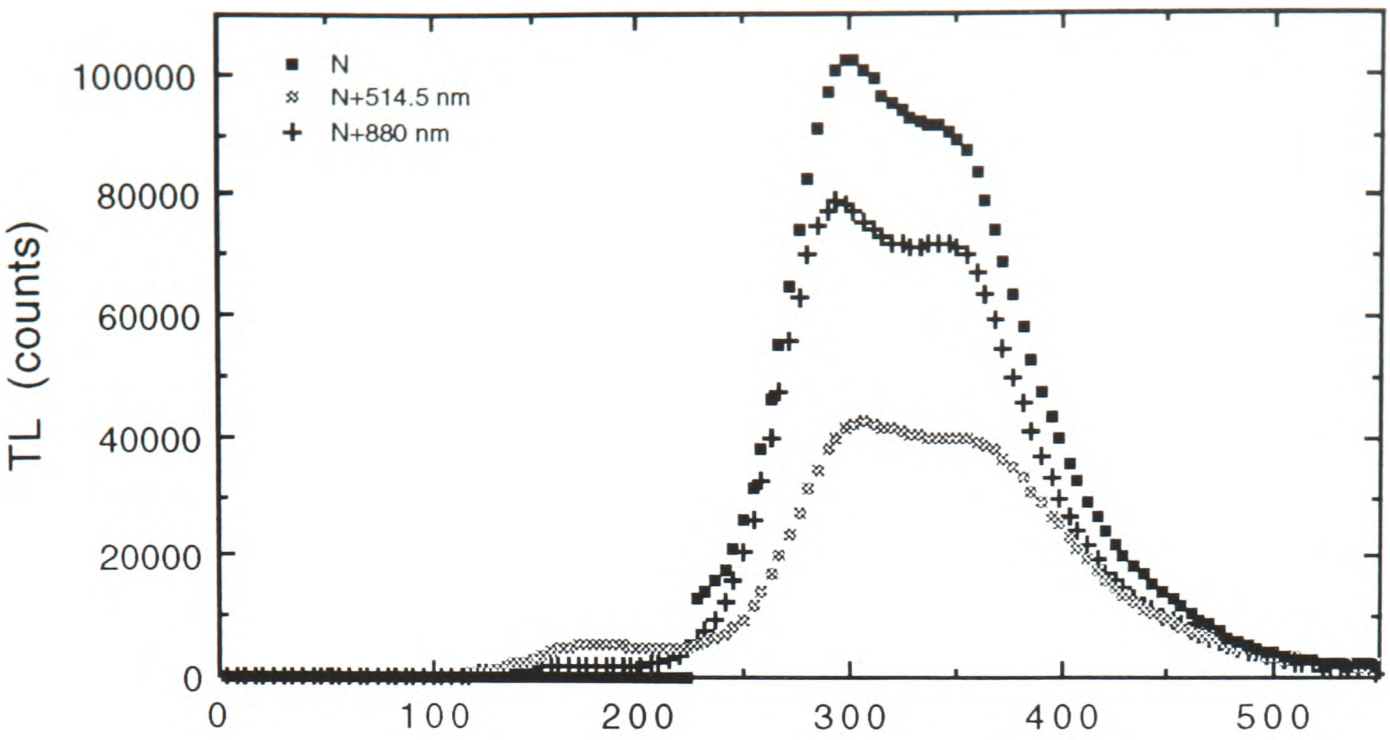
3. Z5 microcline

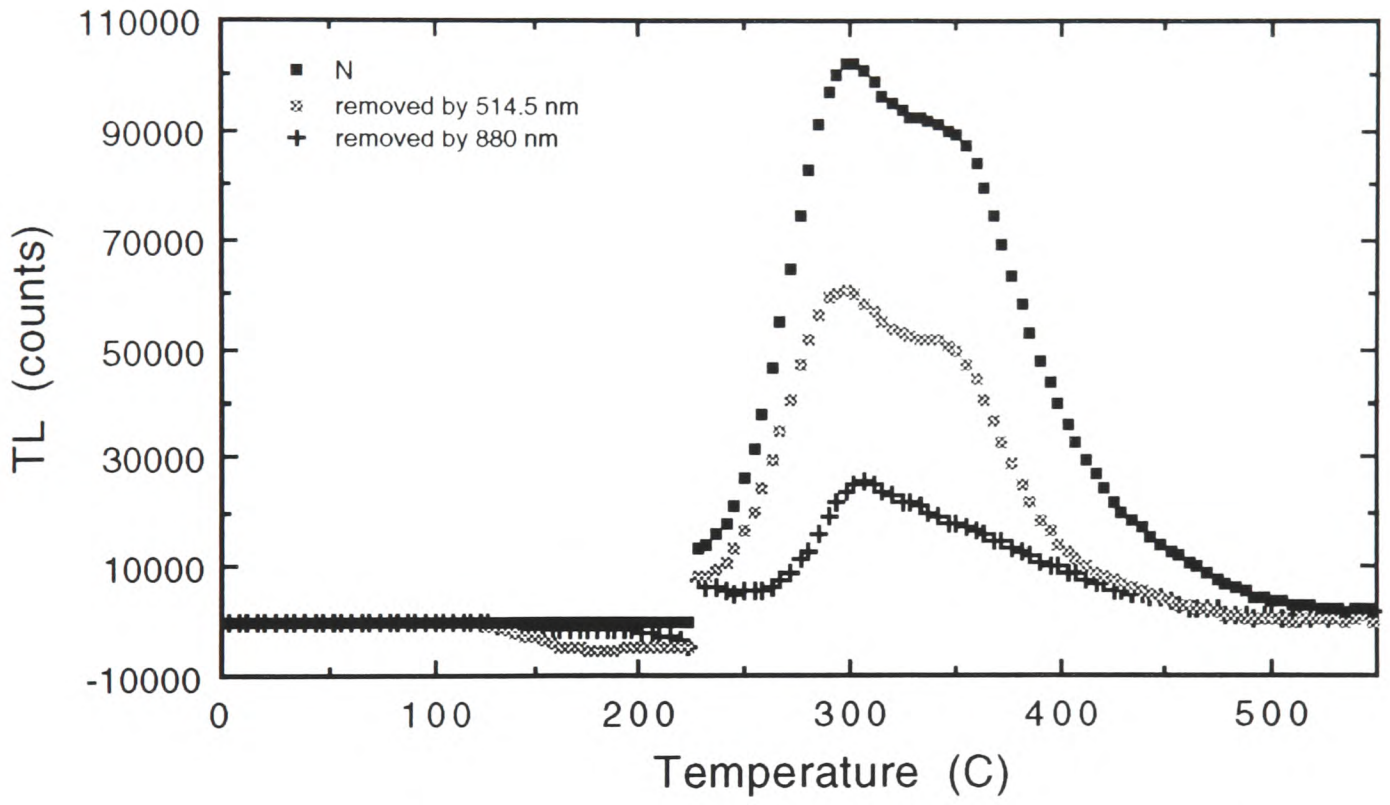


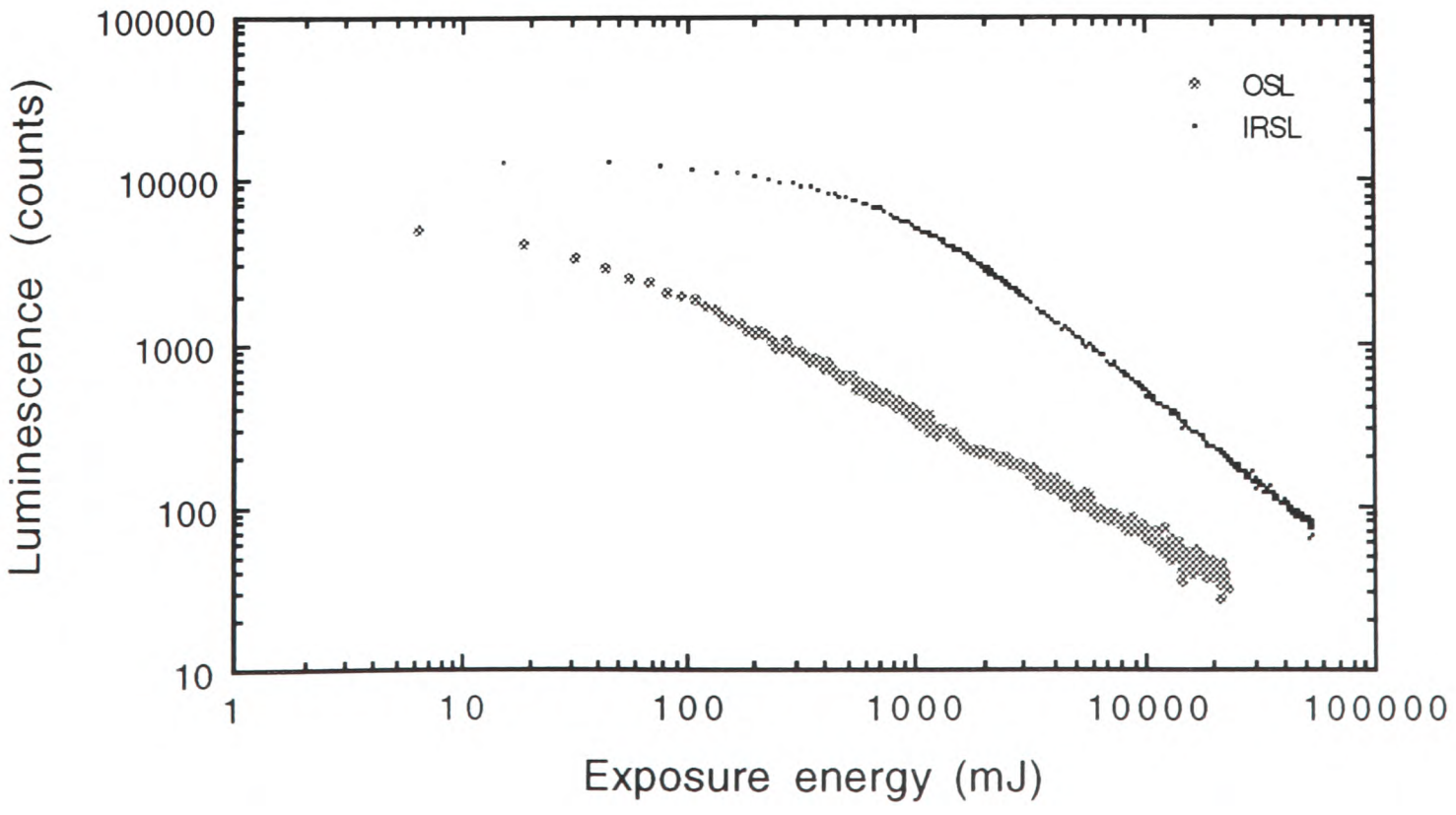




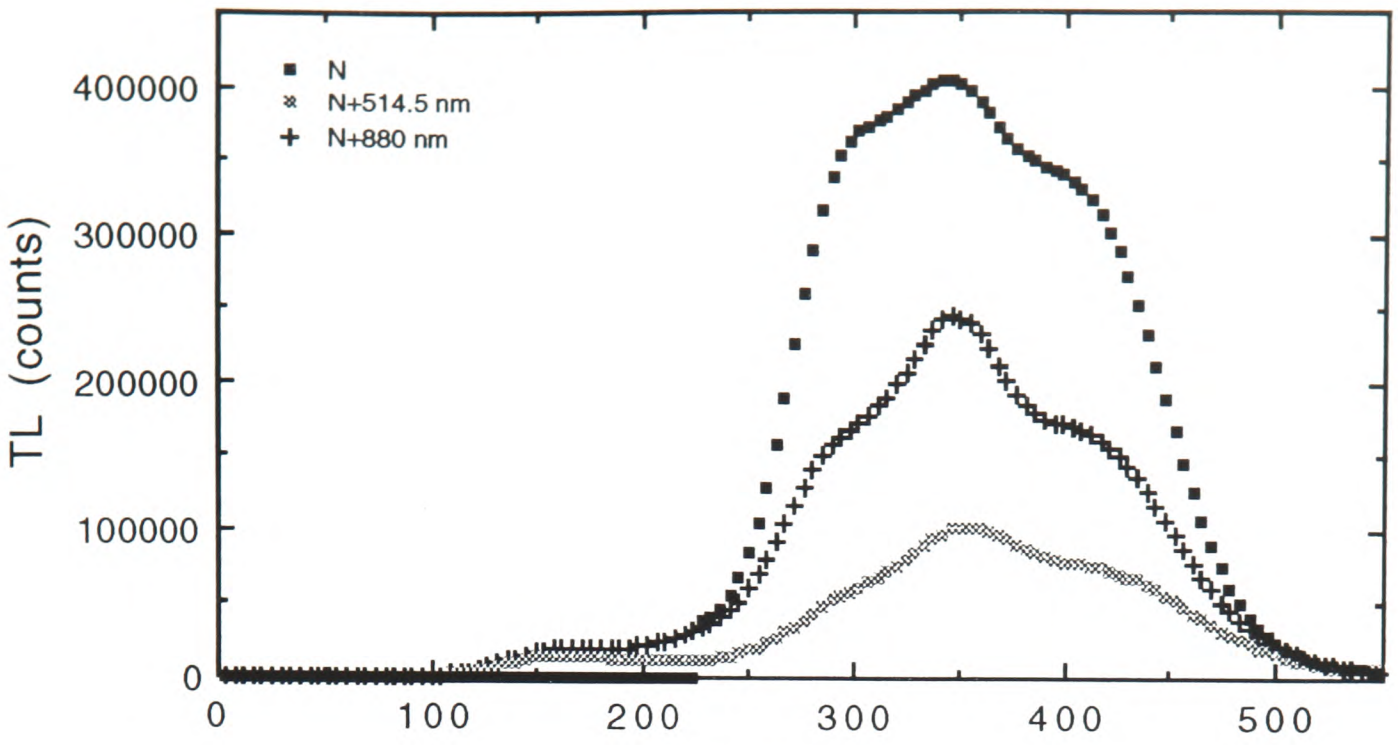
11. Z6 orthoclase

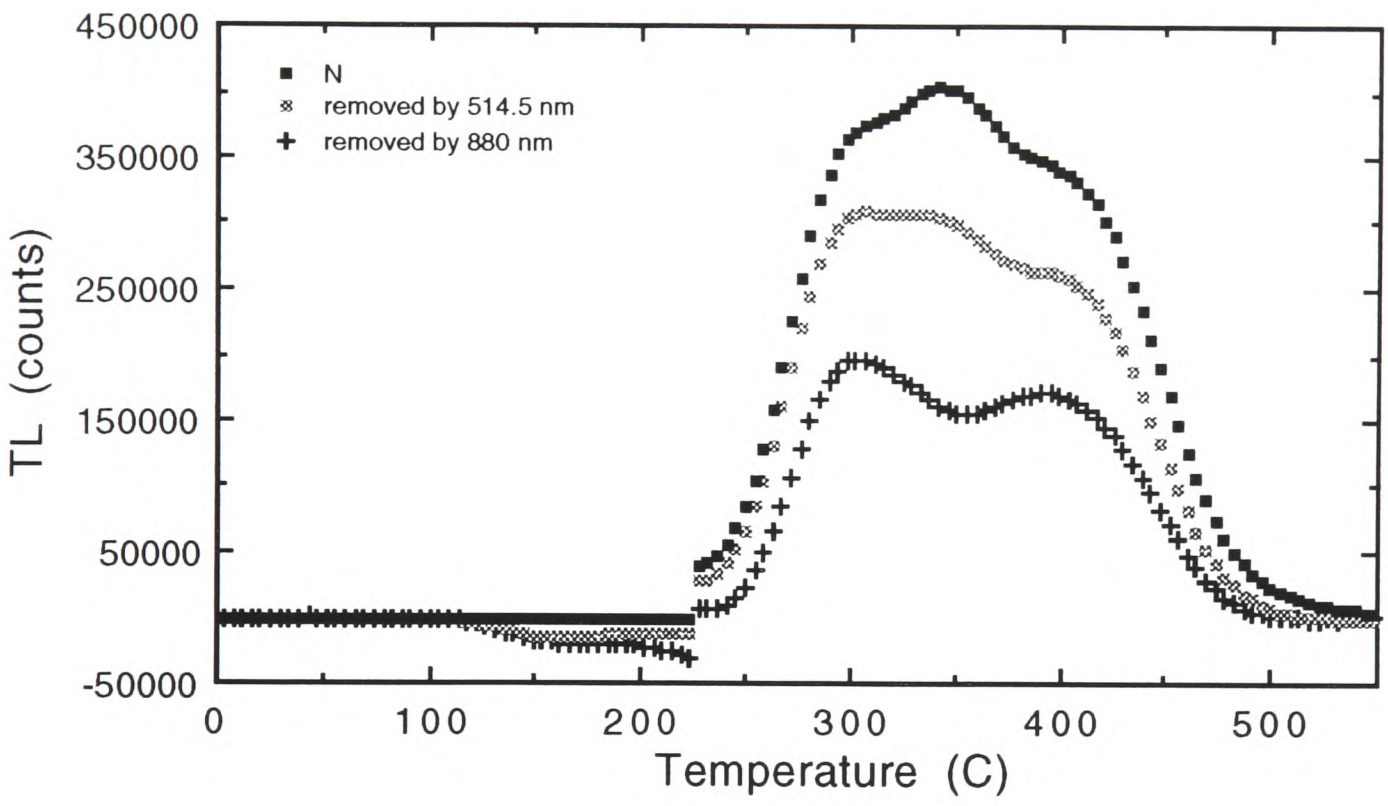


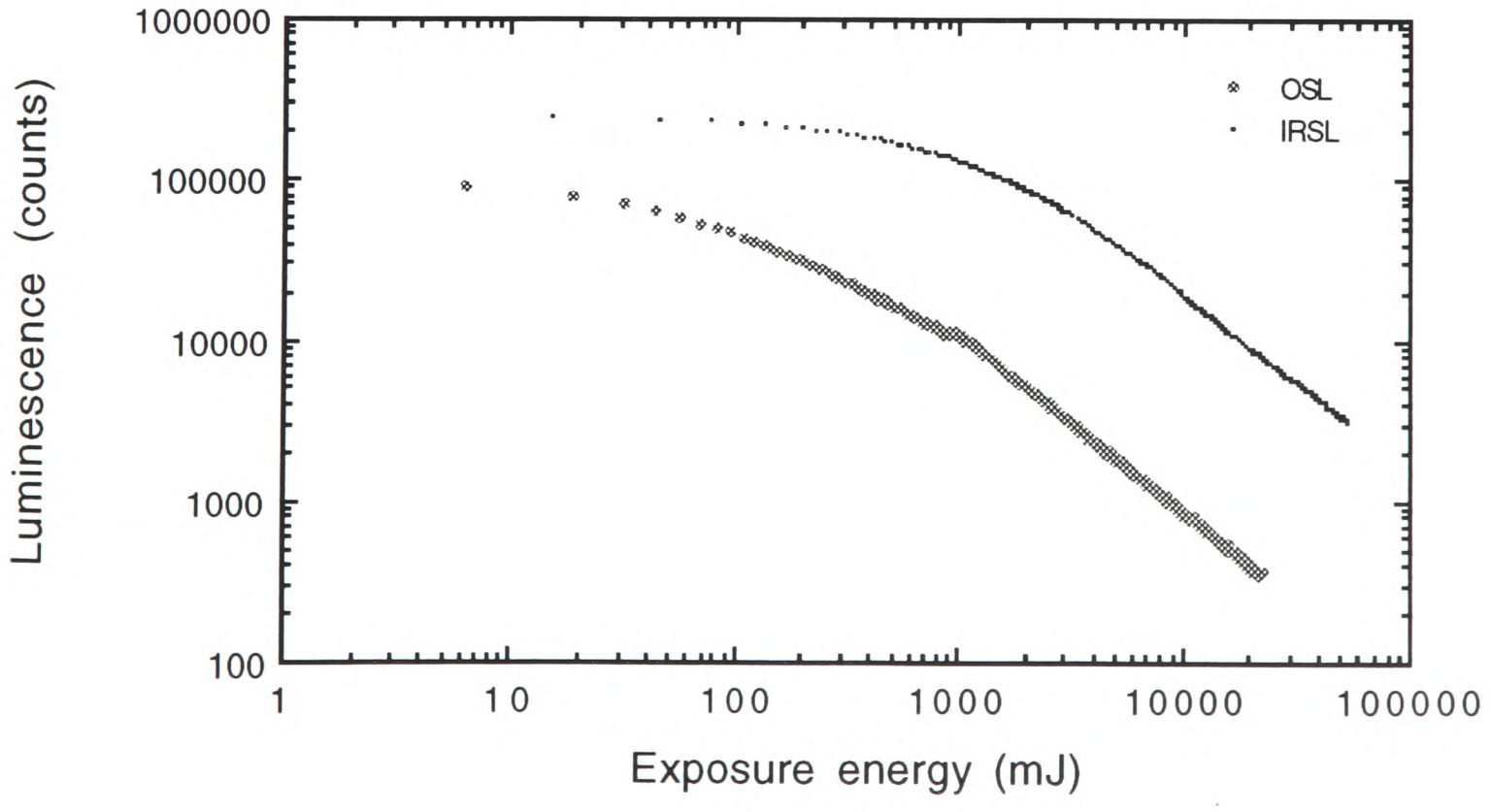




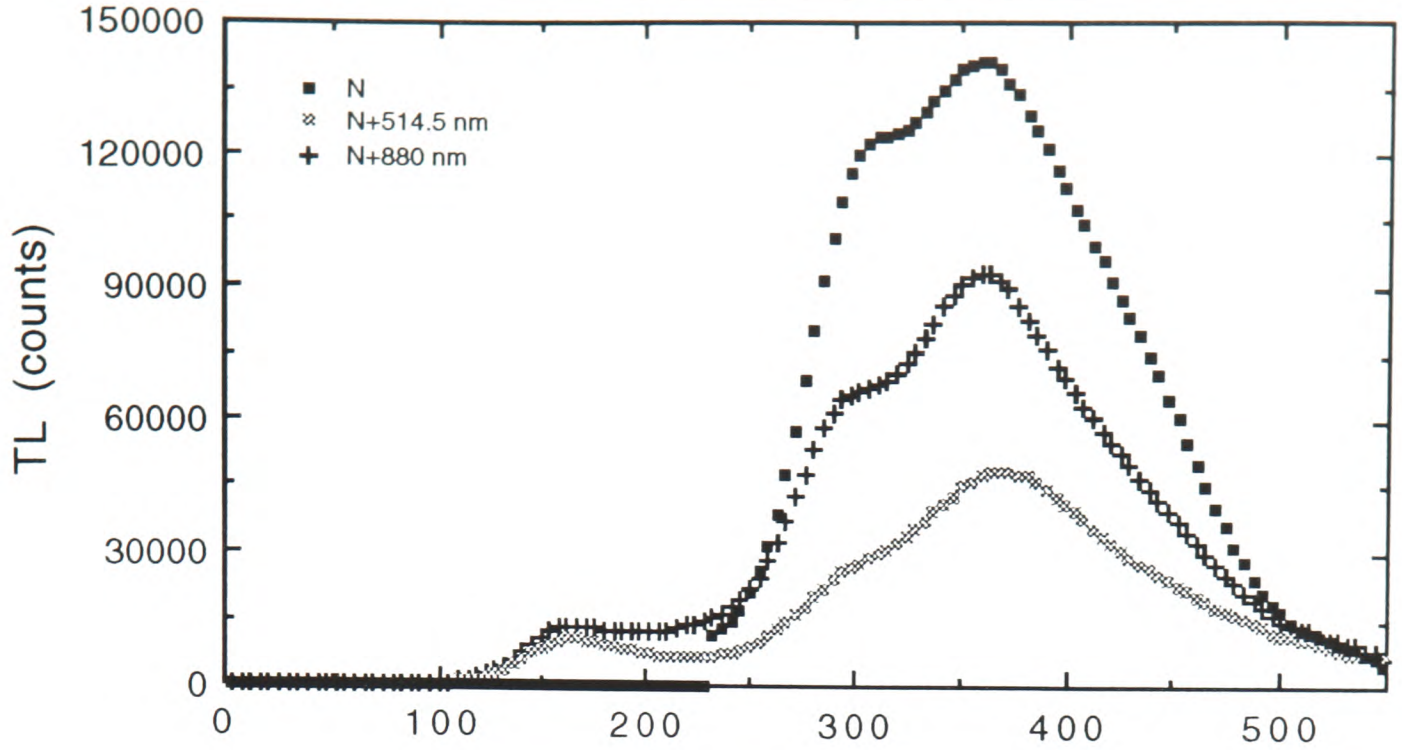
21. Z9 microcline

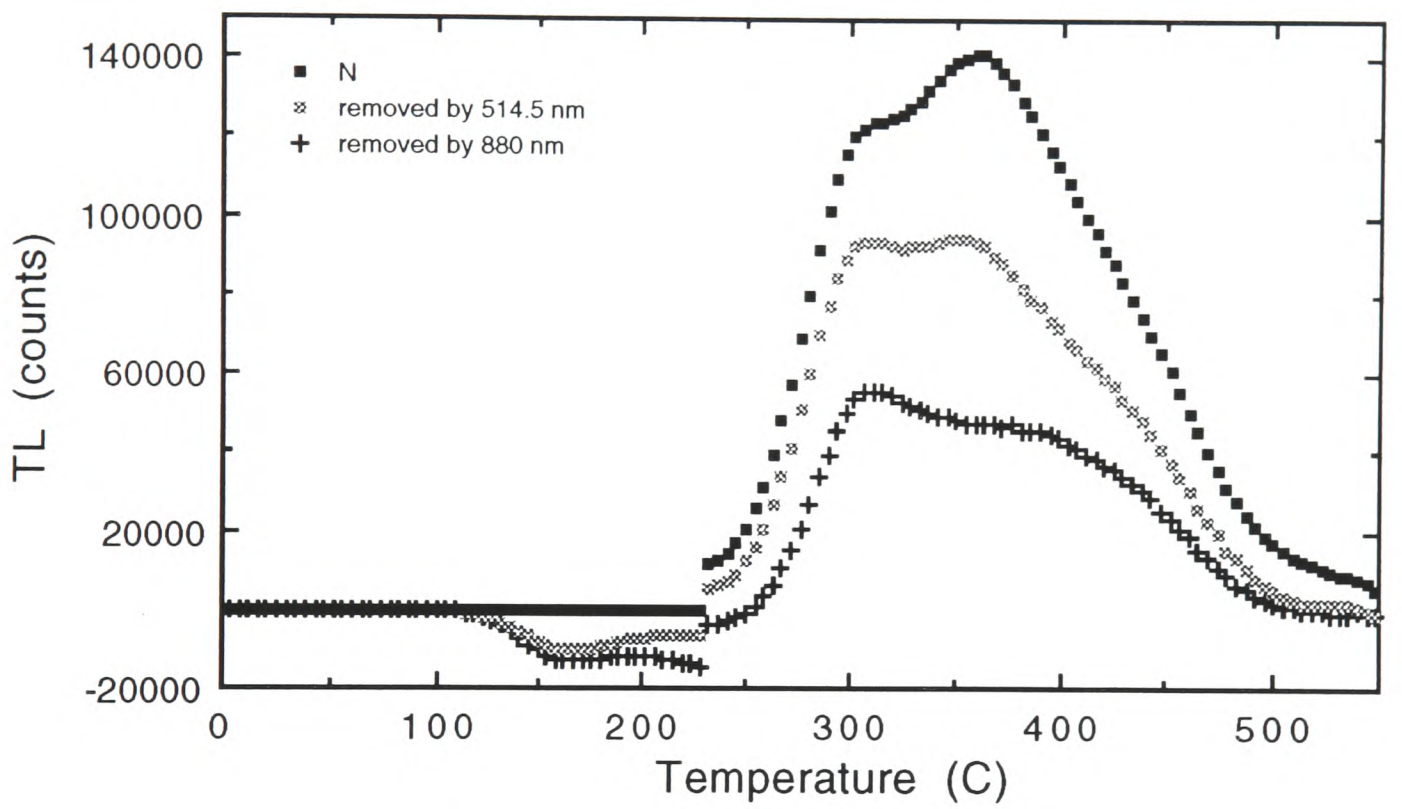


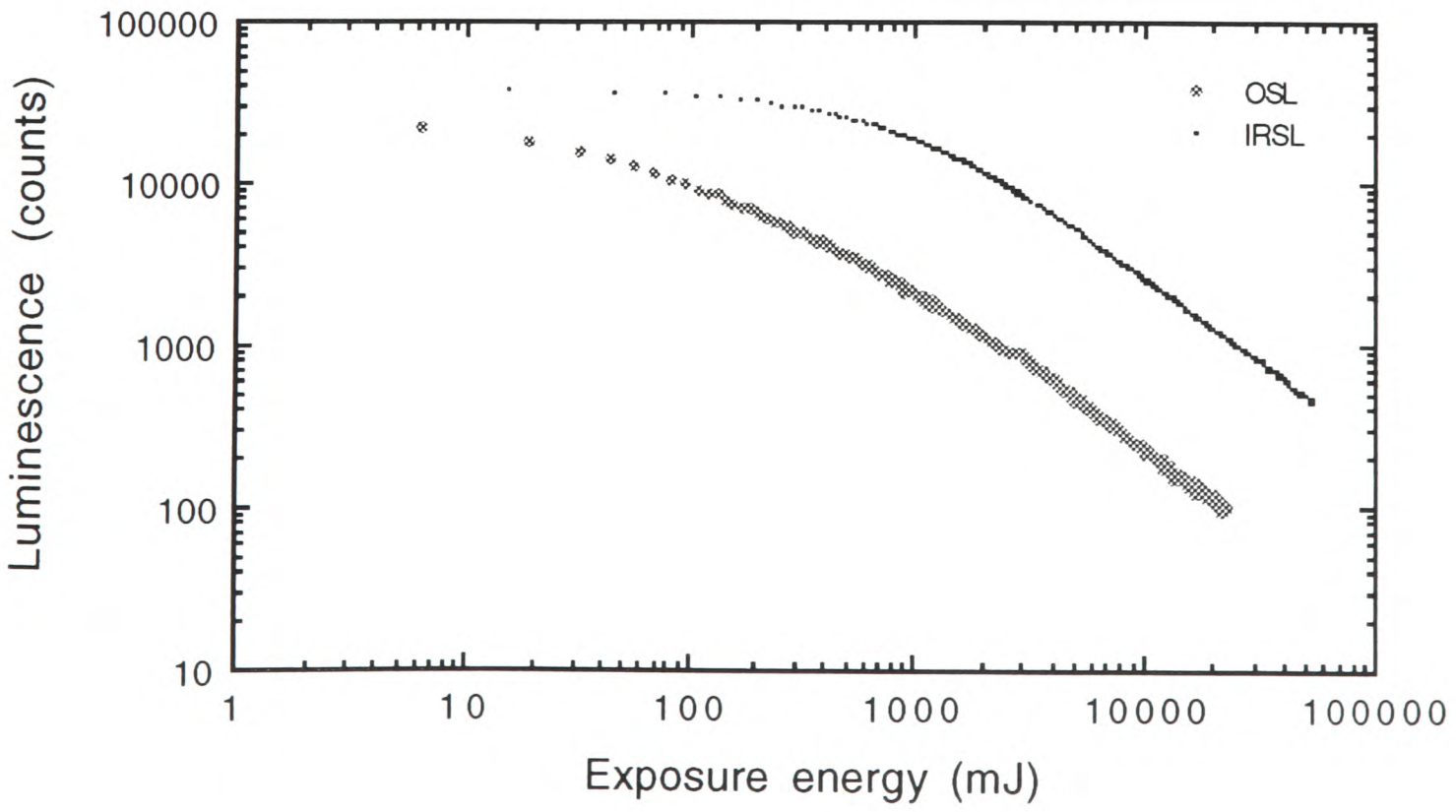




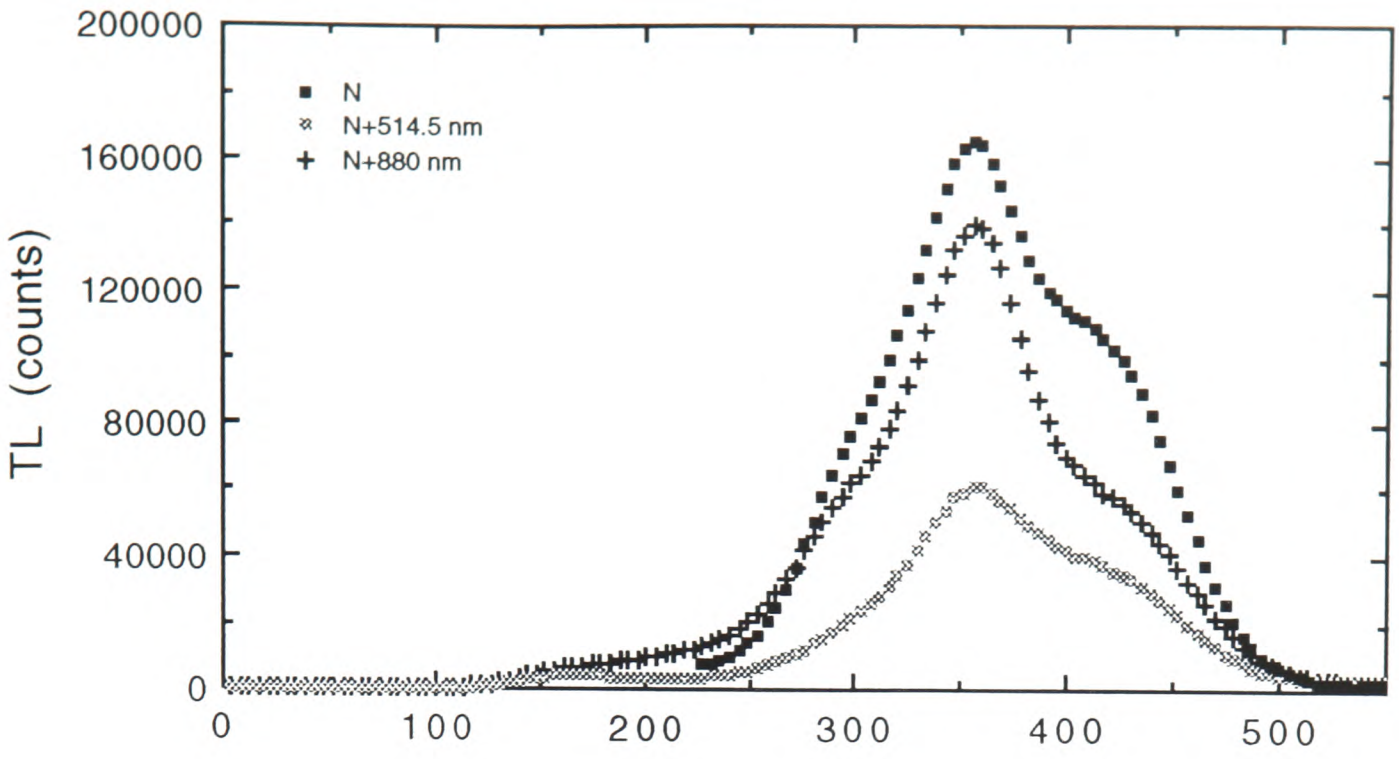
14. Z11 microcline

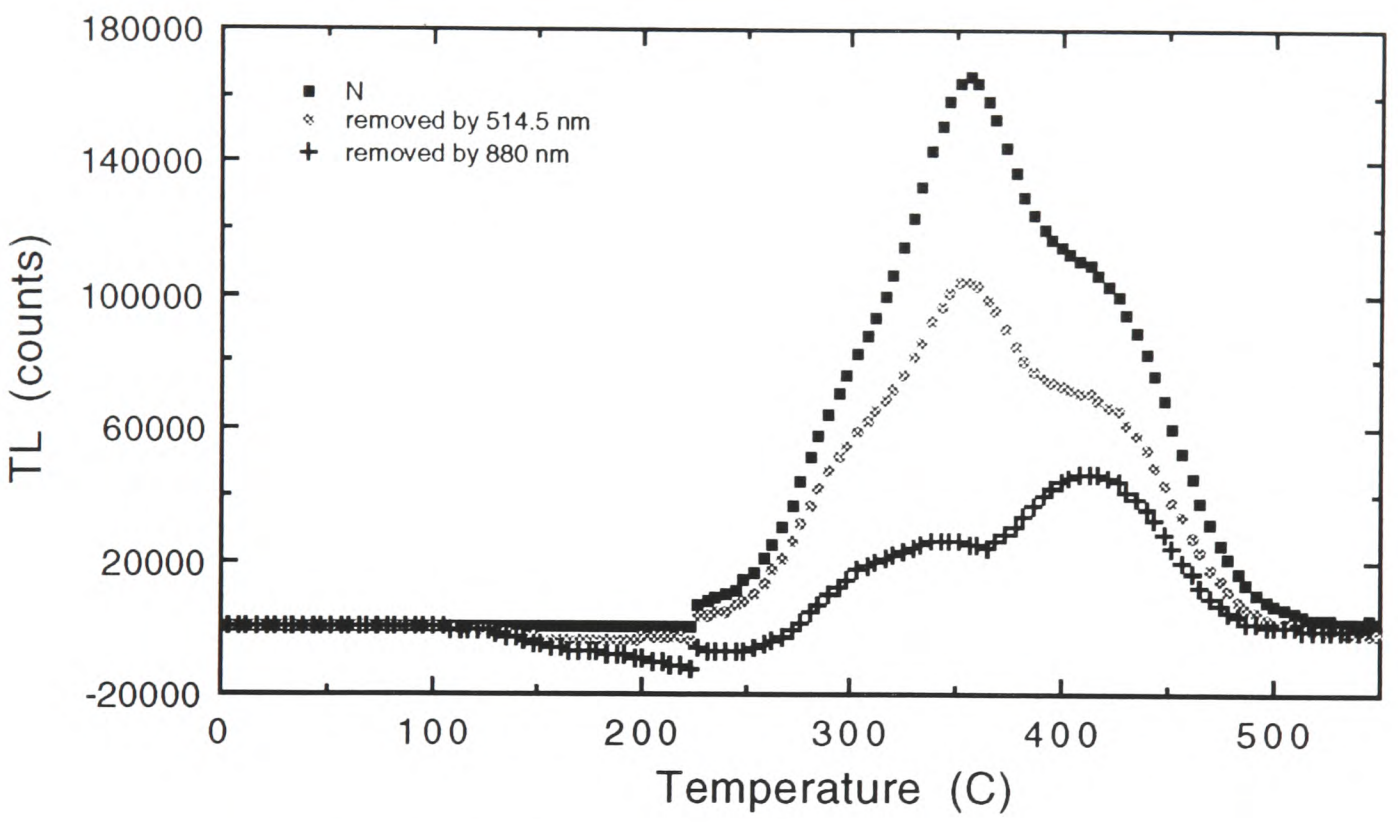


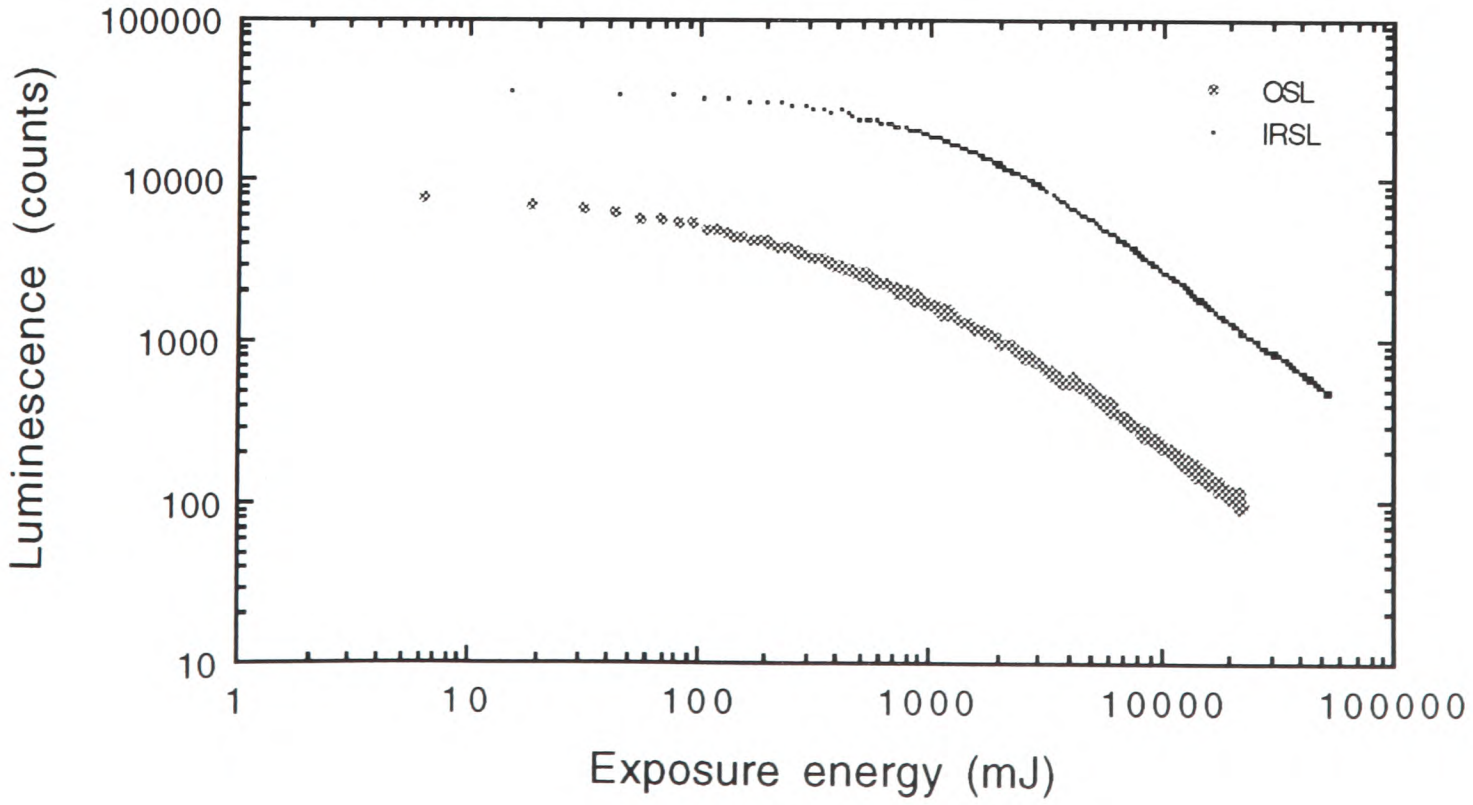




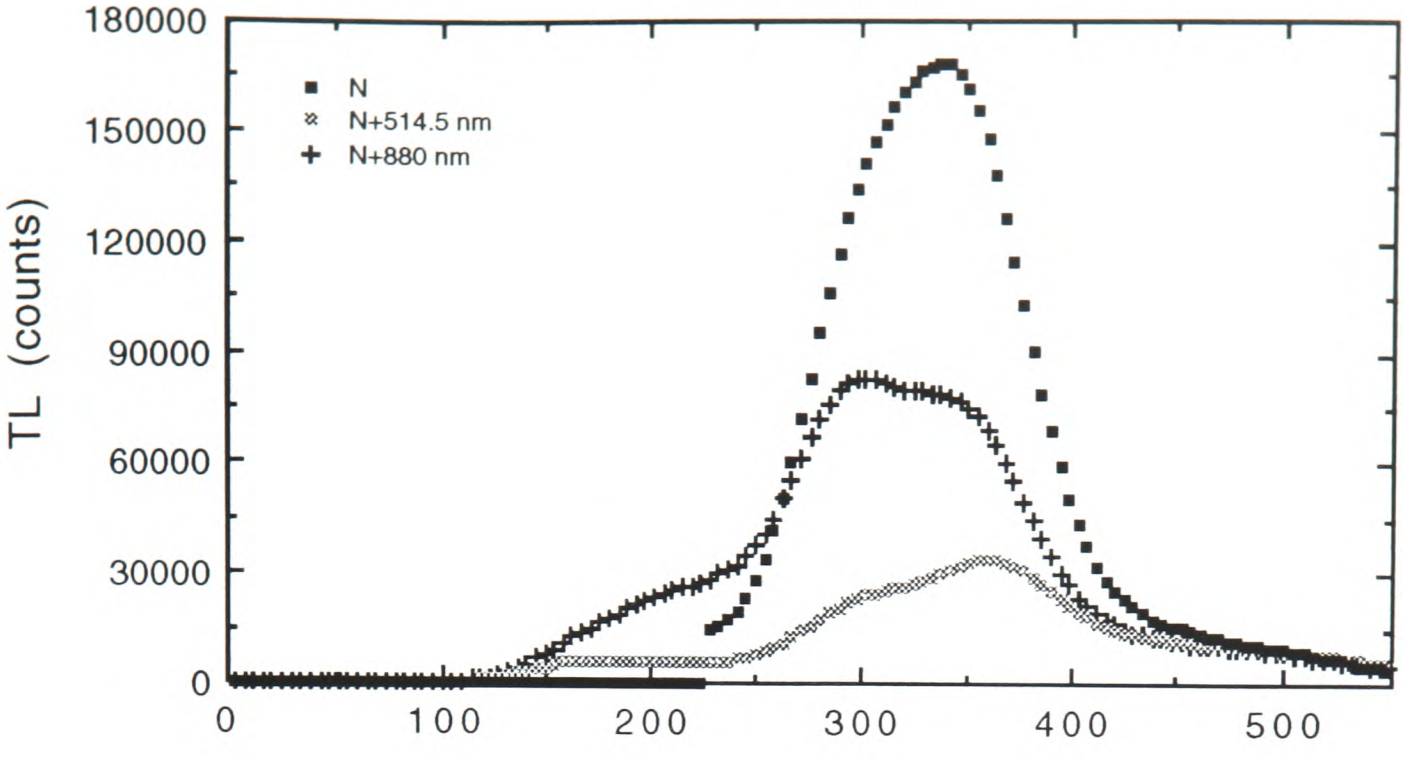
13. Dup(C) microcline

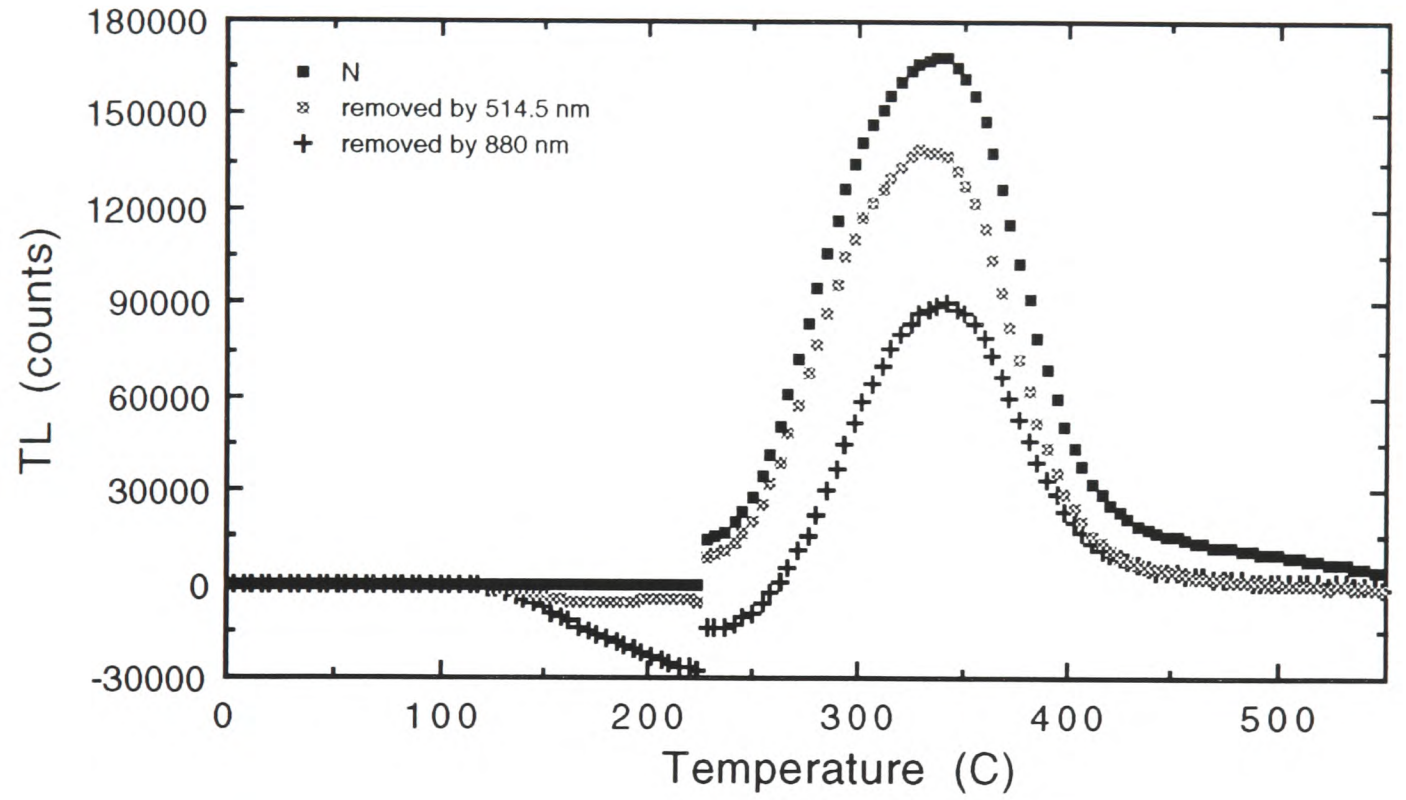


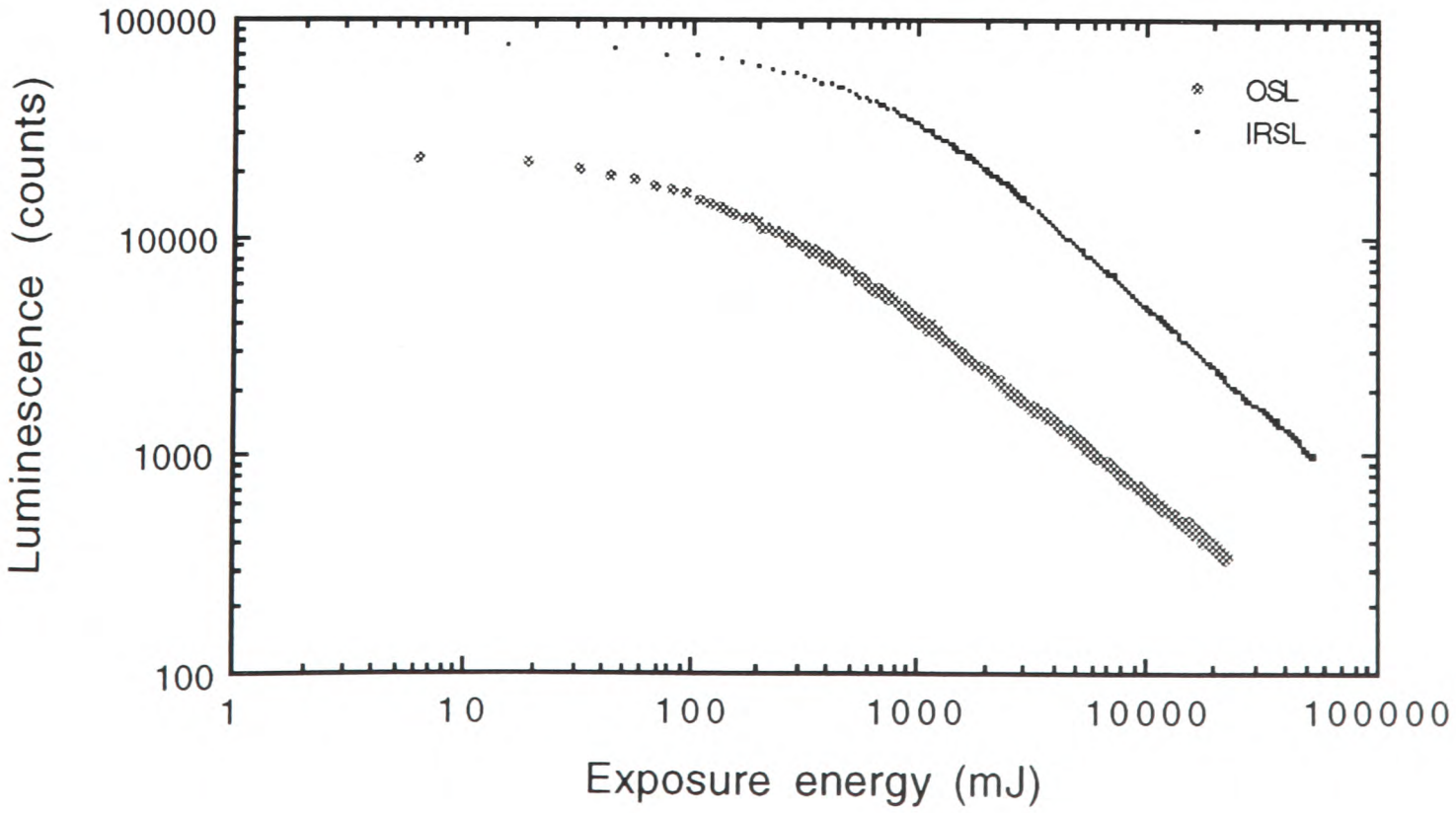




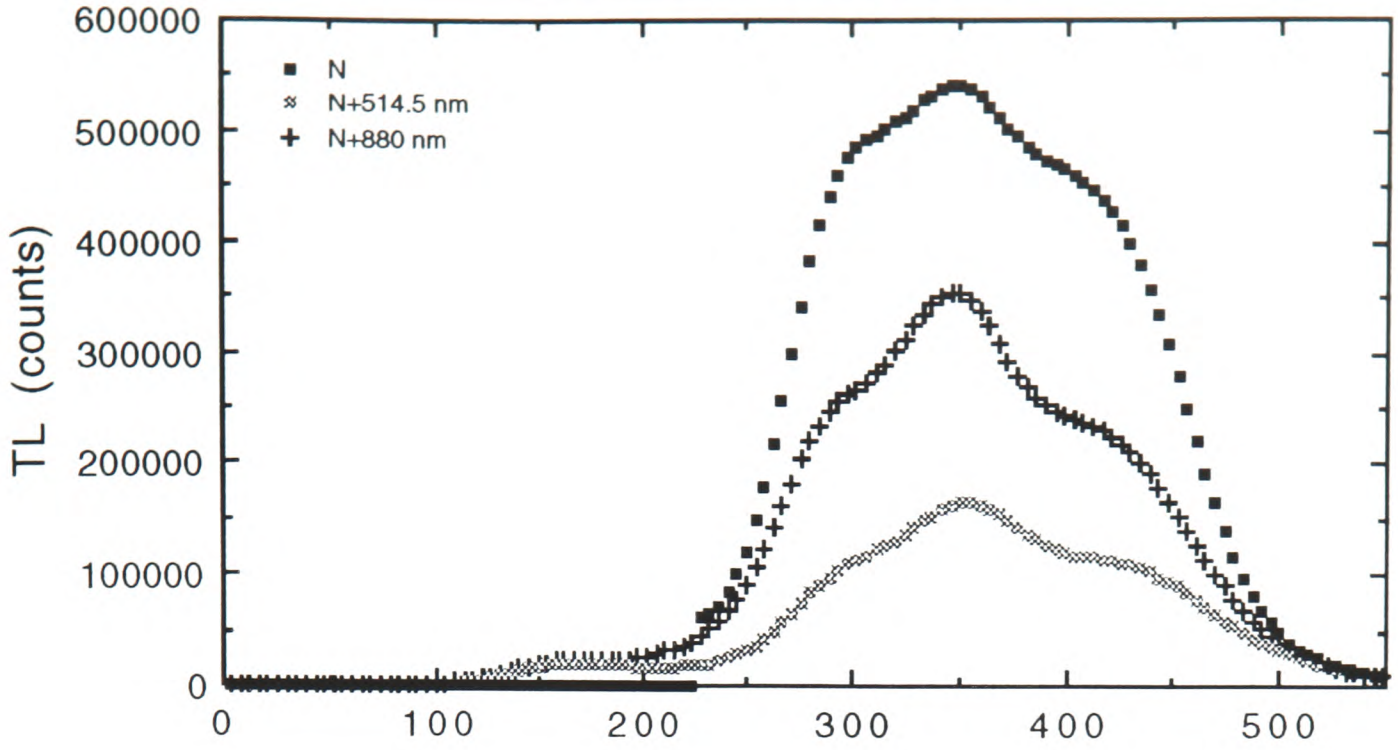
1. adularia

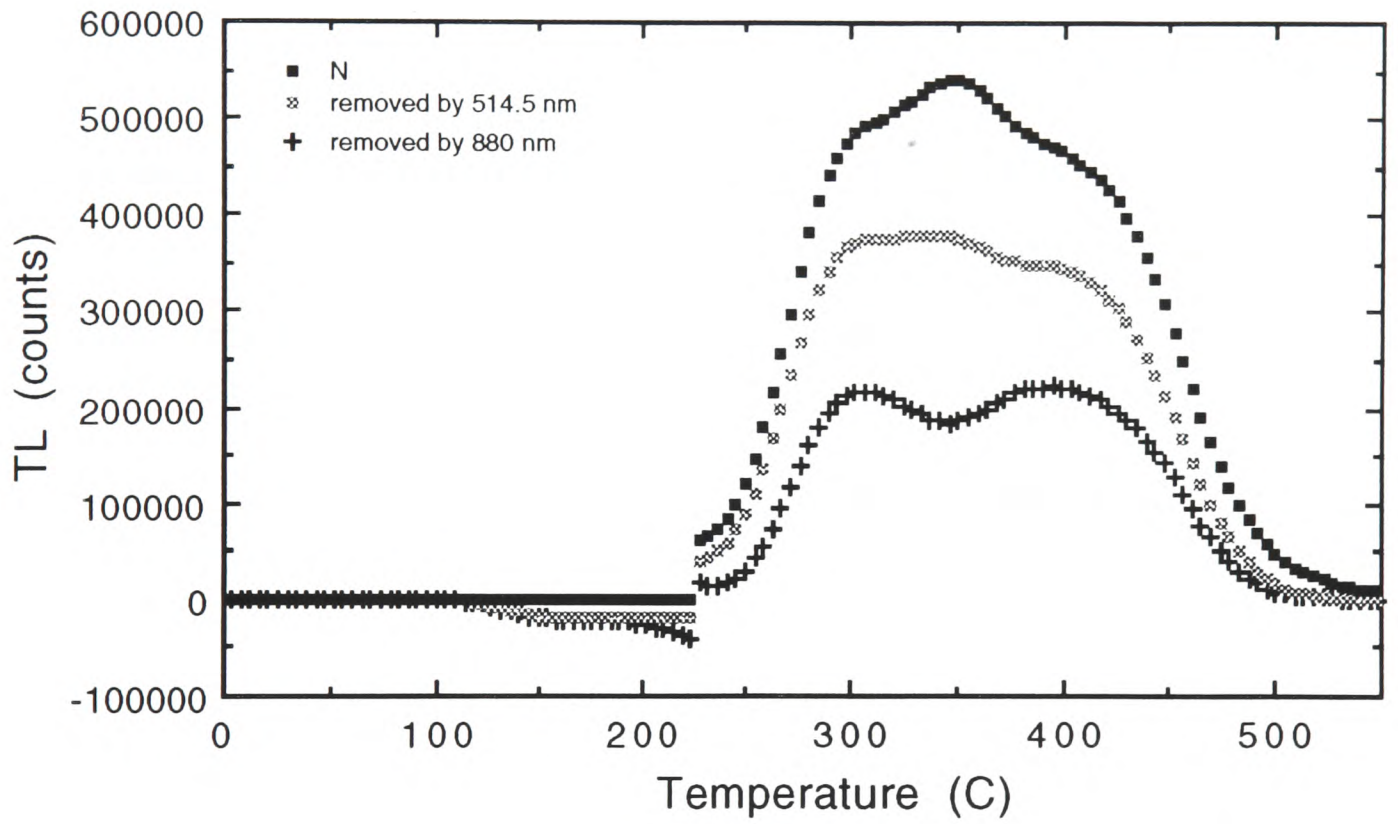

N
N+514.5 nm
N+880 nm
TL (counts)
180000
150000
120000
90000
60000
30000
0
0
100
200
300
400
500

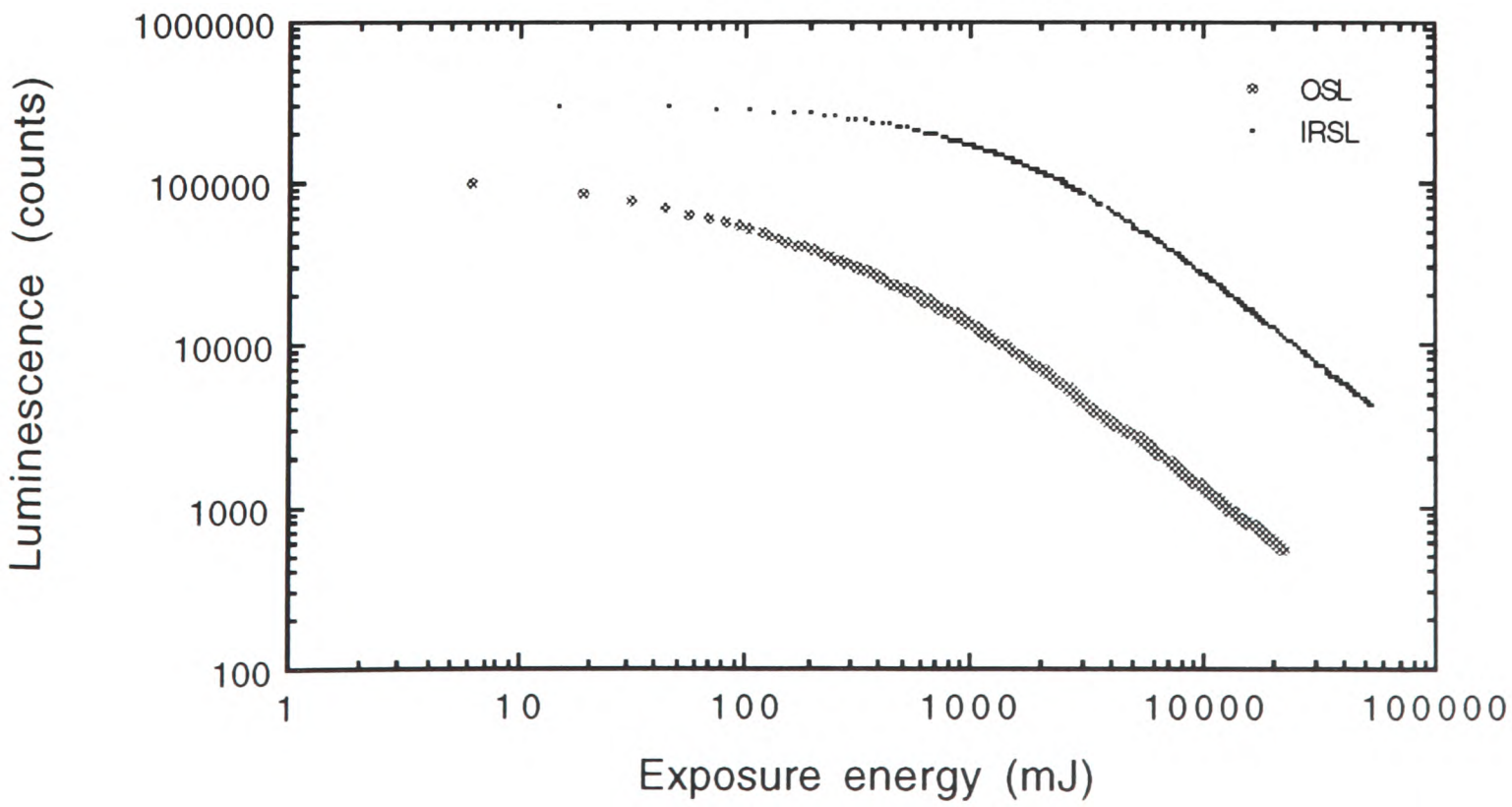

N
removed by 514.5 nm
removed by 880 nm
TL (counts)
180000
150000
120000
90000
60000
30000
0
-30000
0
100
200
300
400
500
Temperature (C)


OSL
IRSL
Luminescence (counts)
100000
10000
1000
100
1
10
100
1000
10000
100000
Exposure energy (mJ)

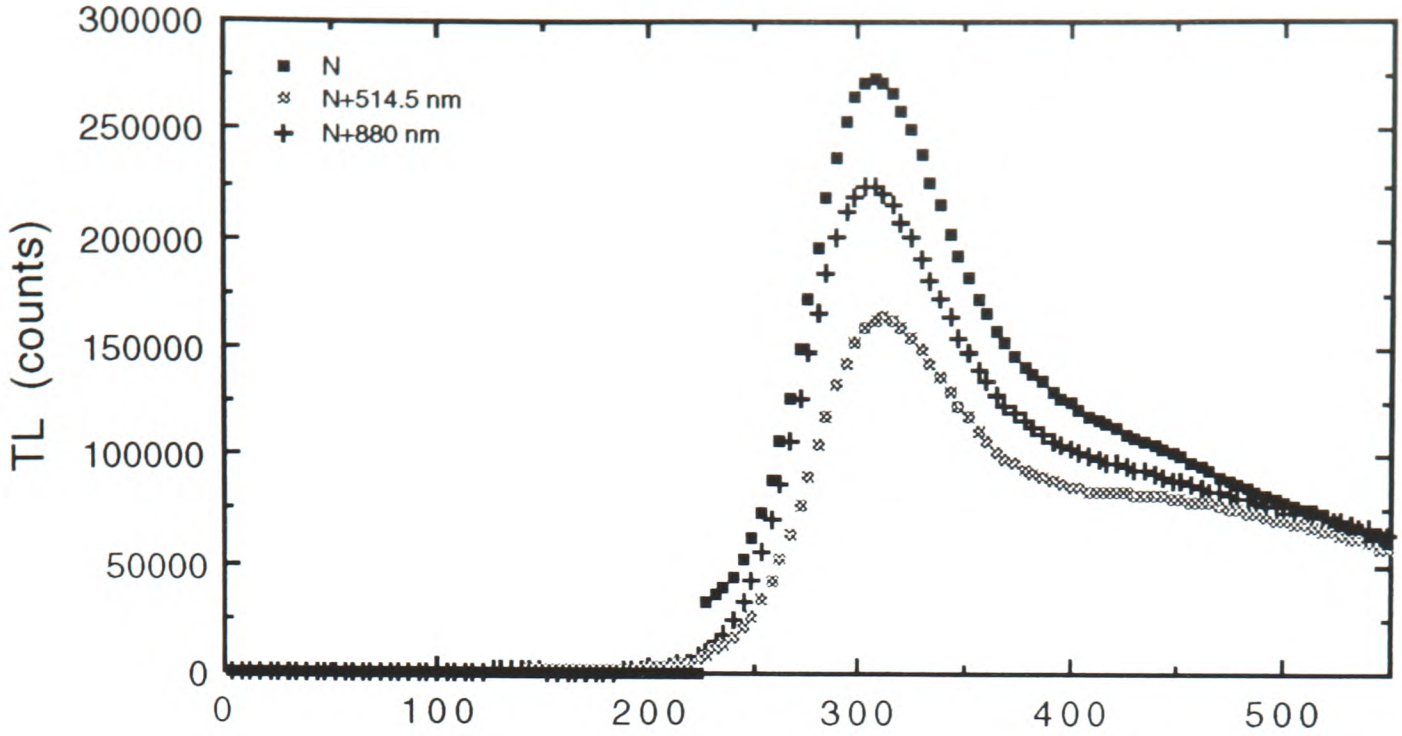
20. Z9n microcline

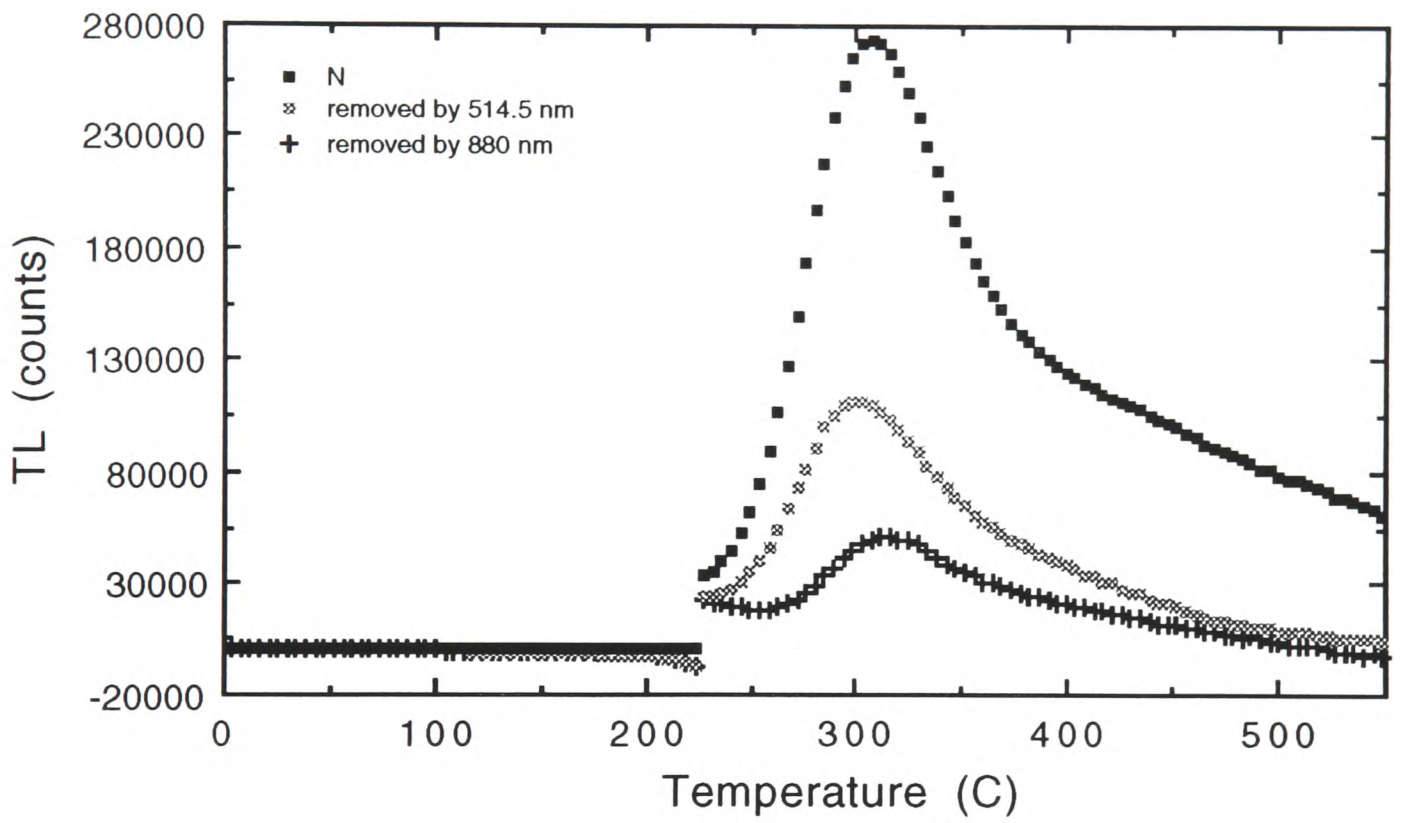


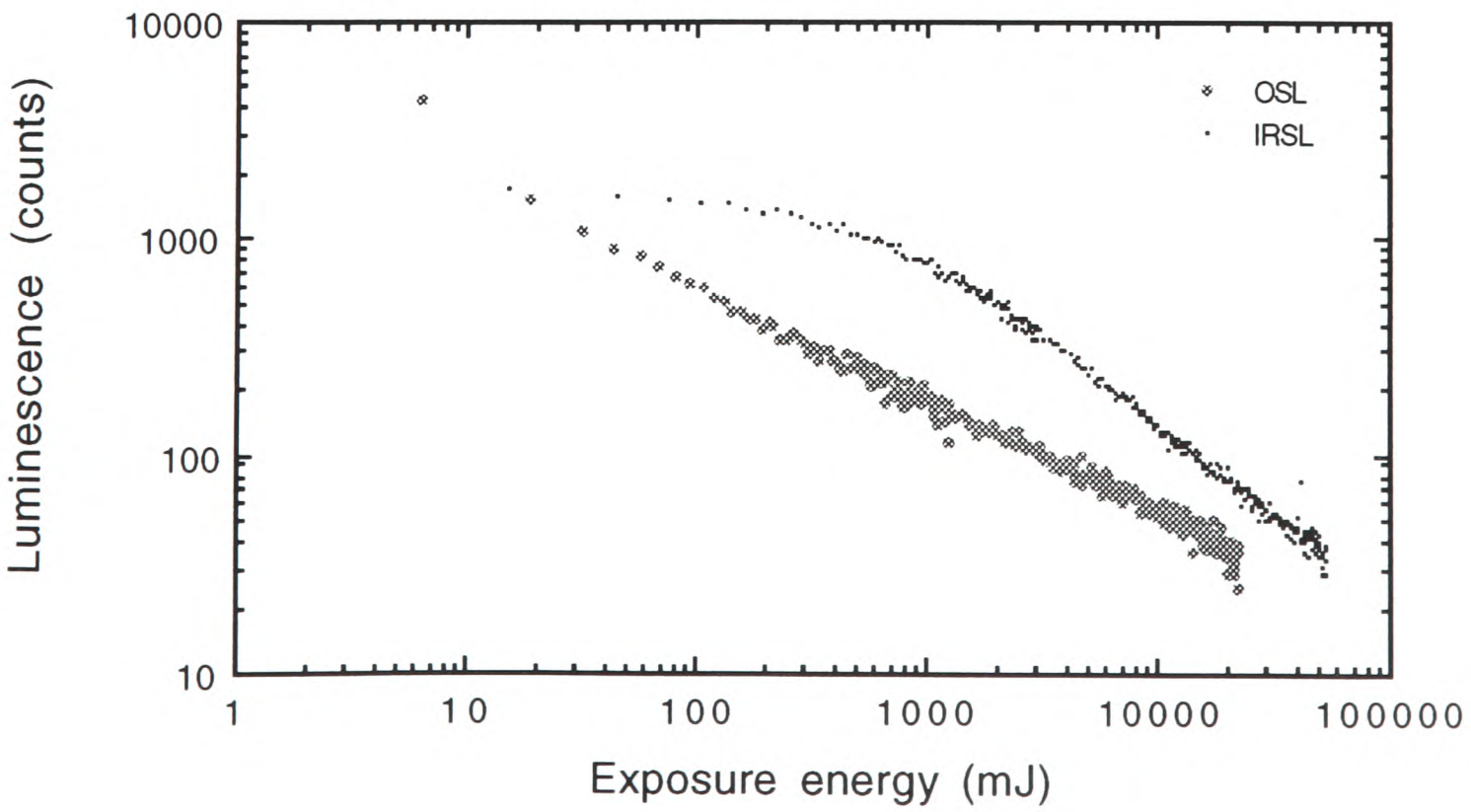




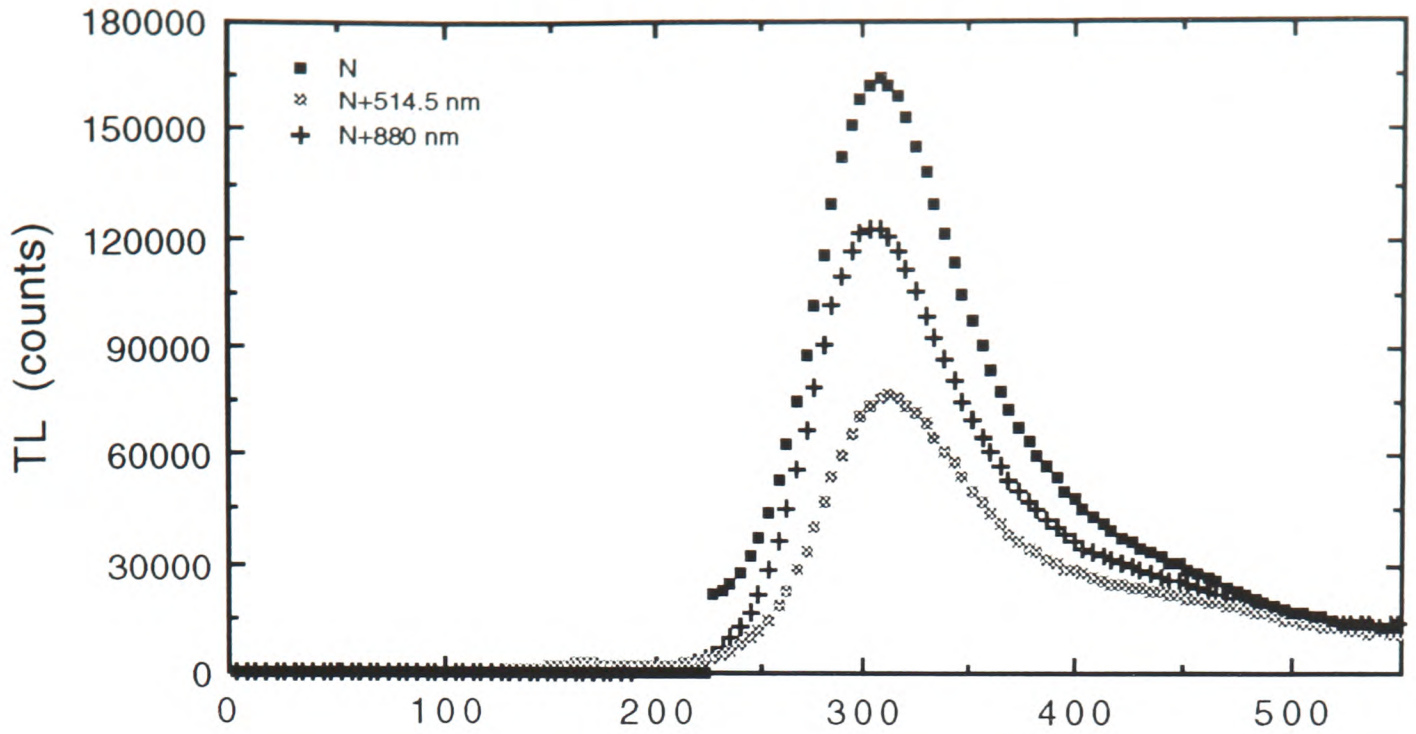
9. Z15 sanidine

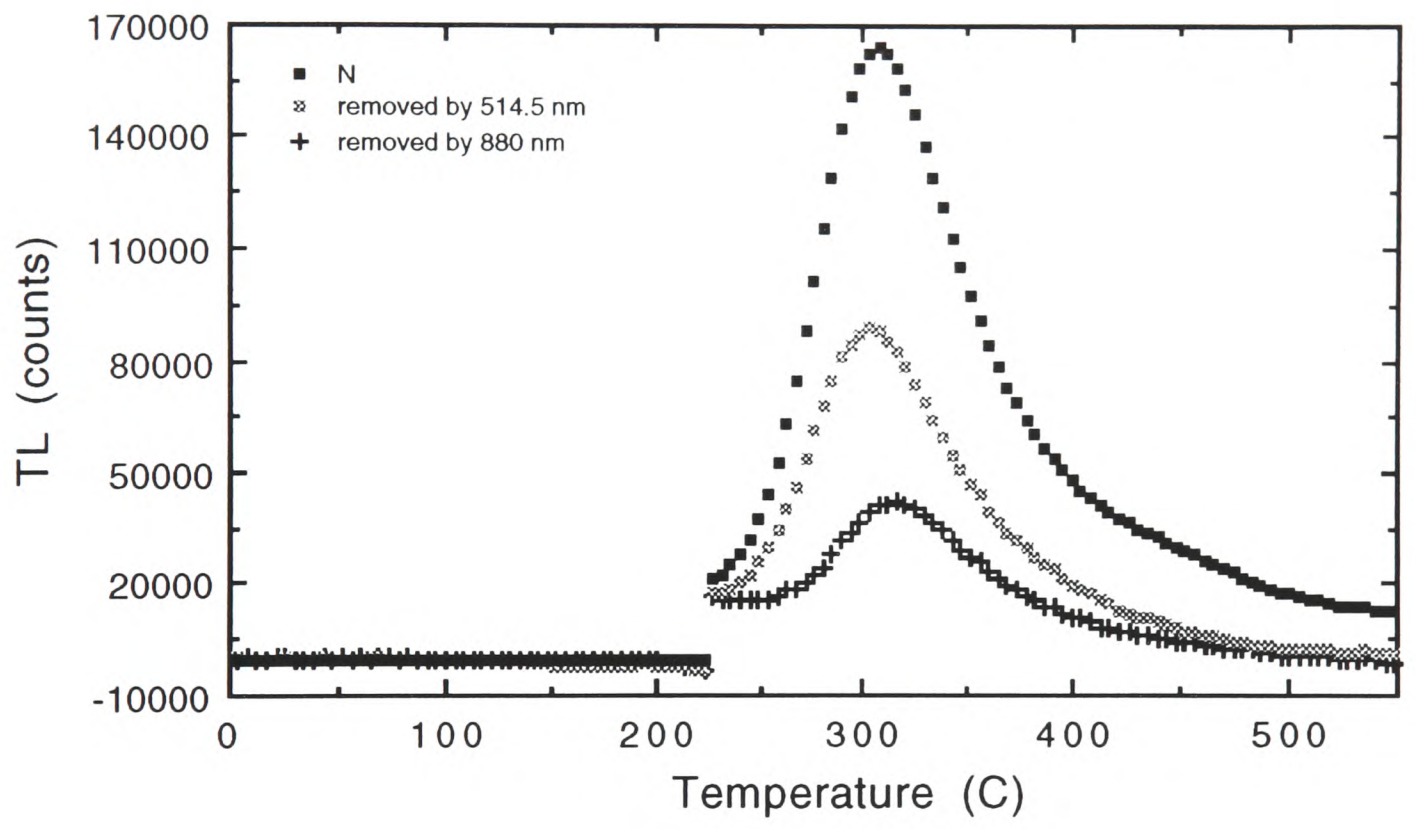


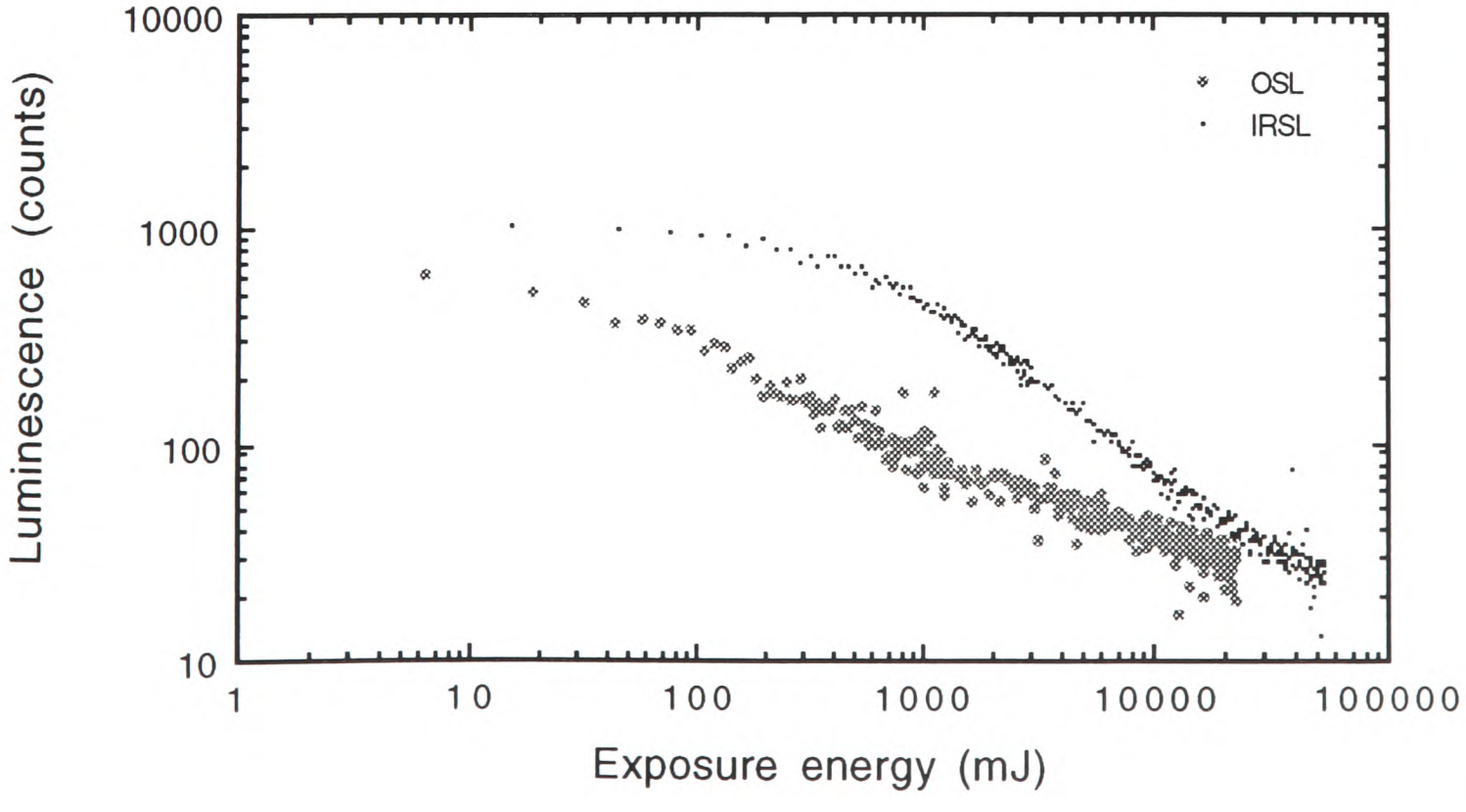




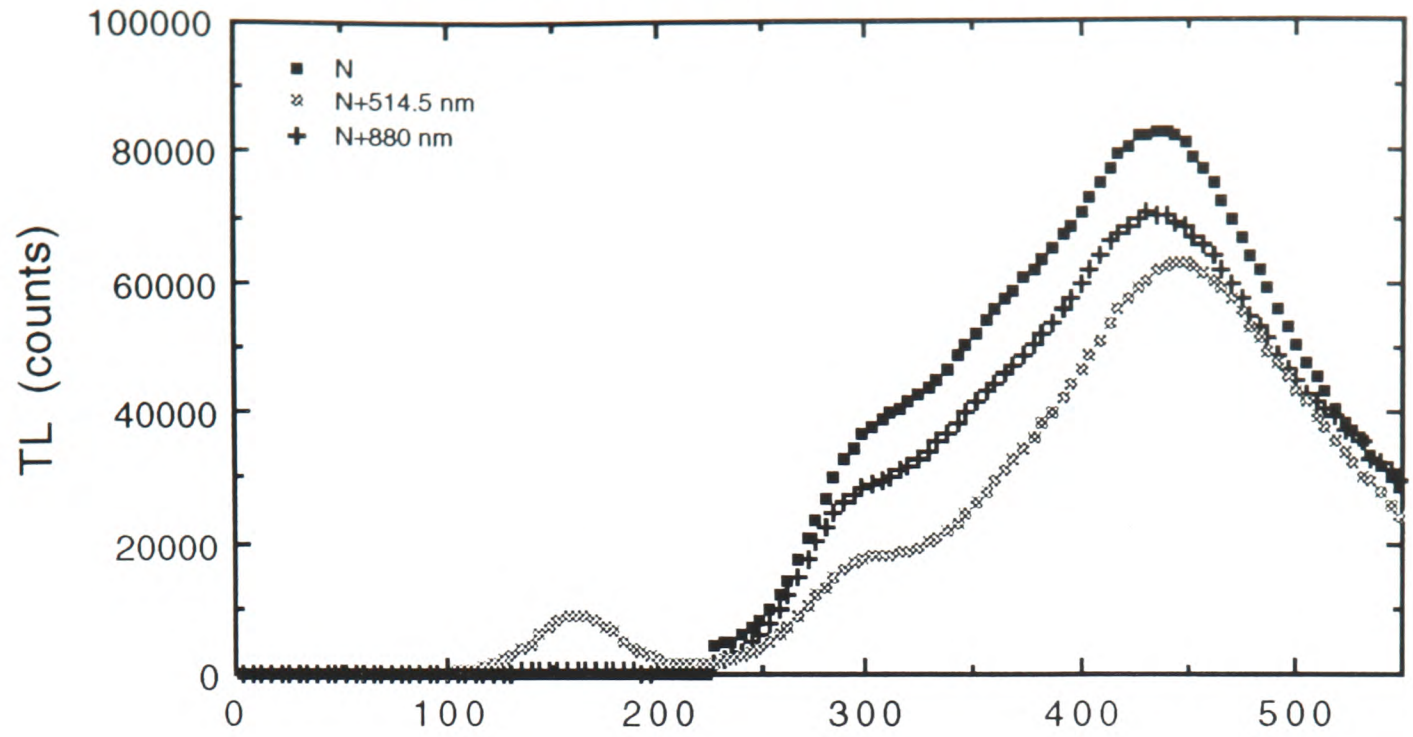
12. patmos sanidine

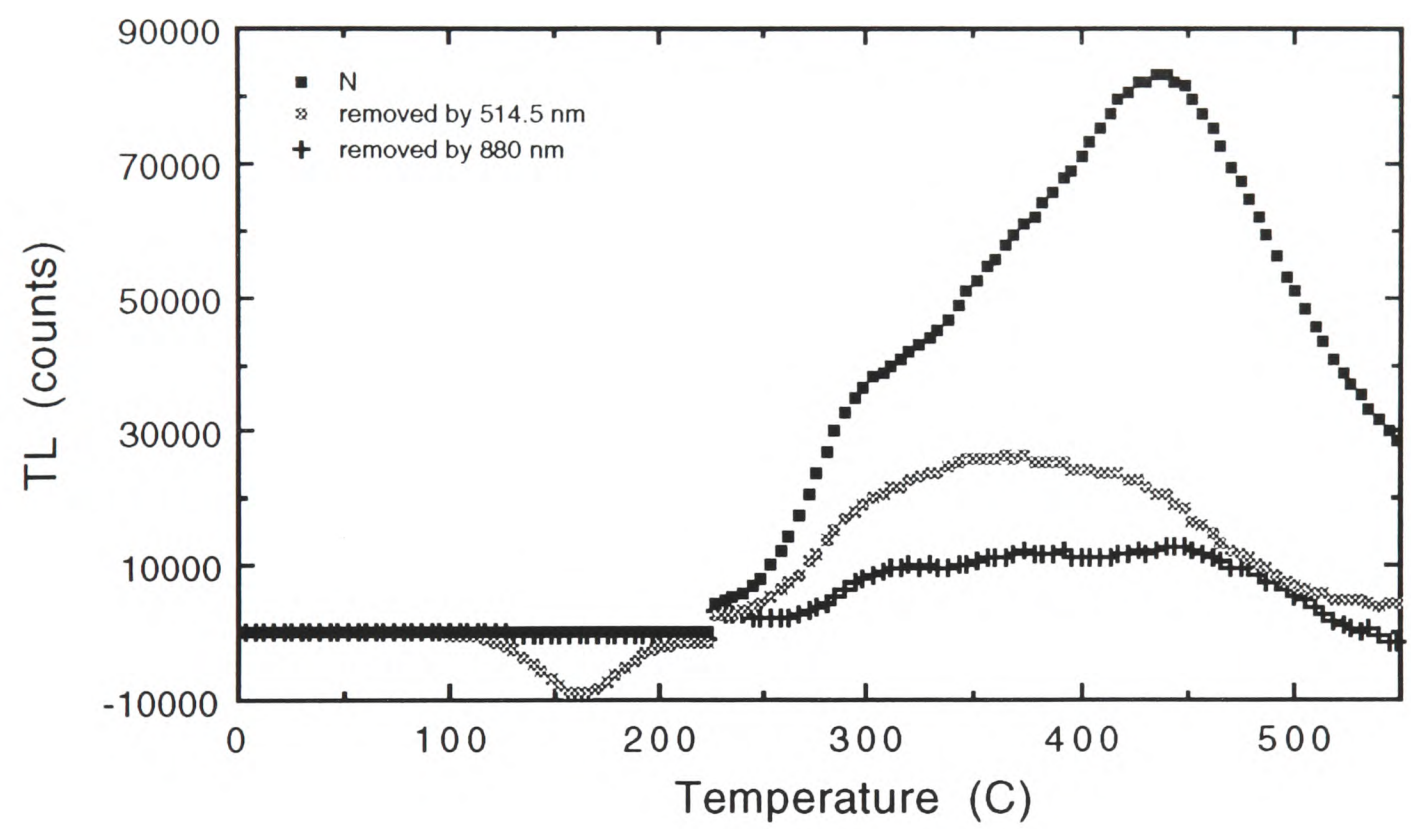


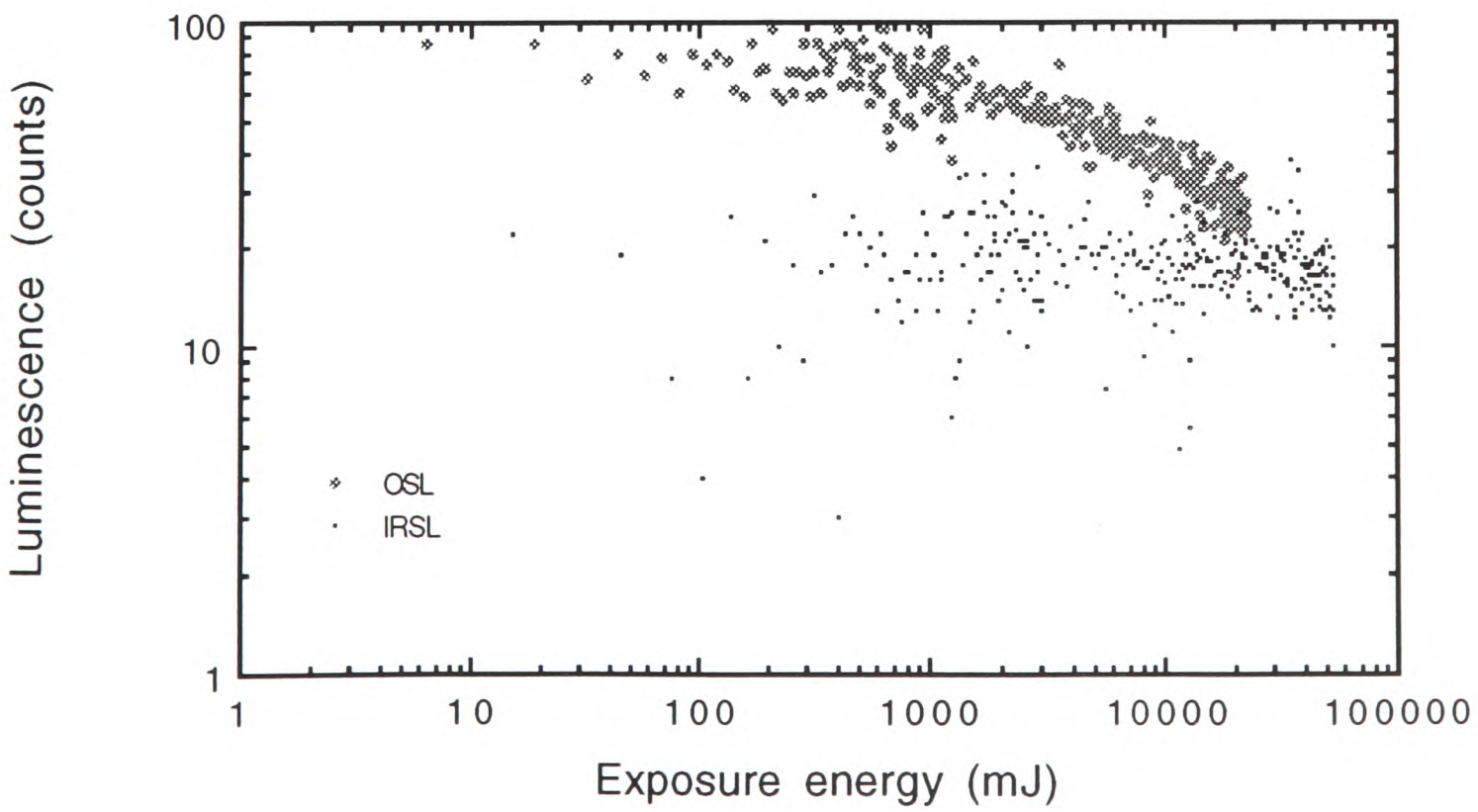




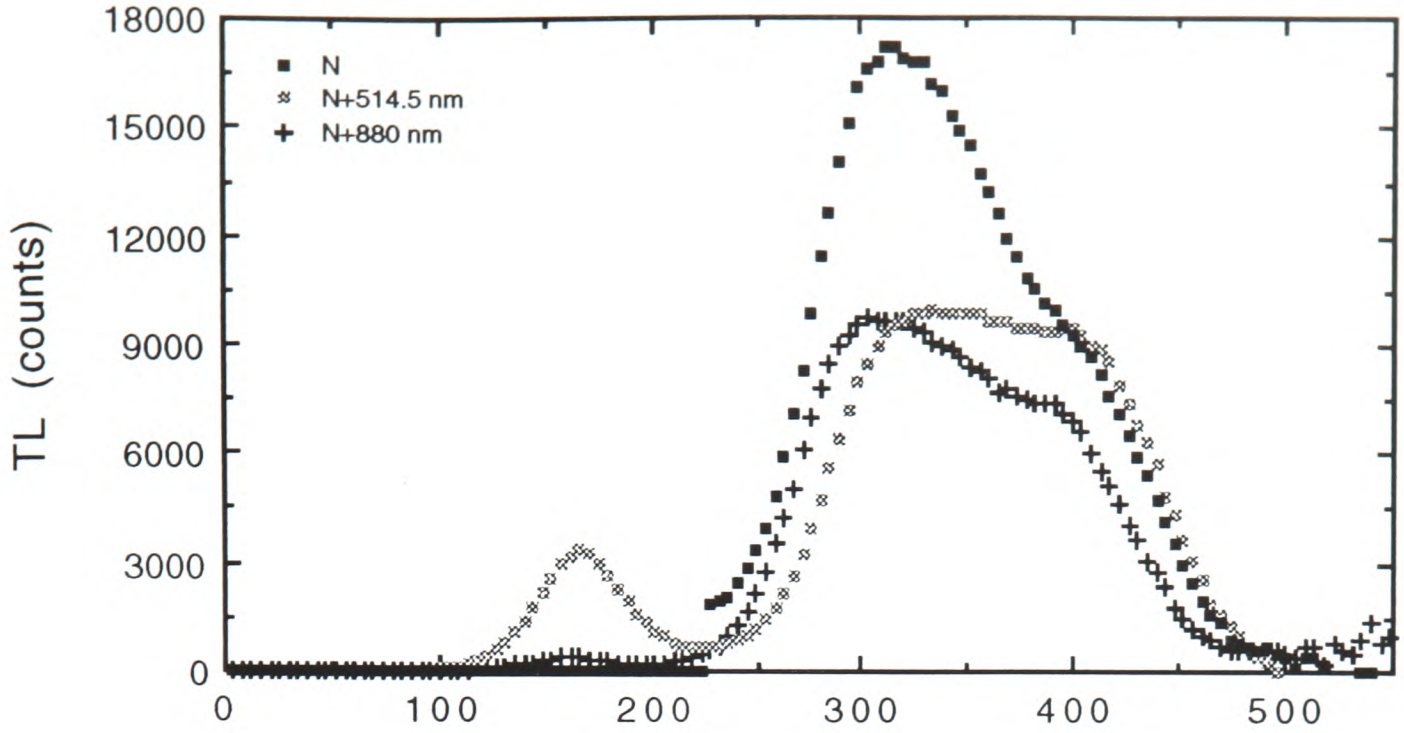
16. 1947,199(2) anorthoclase

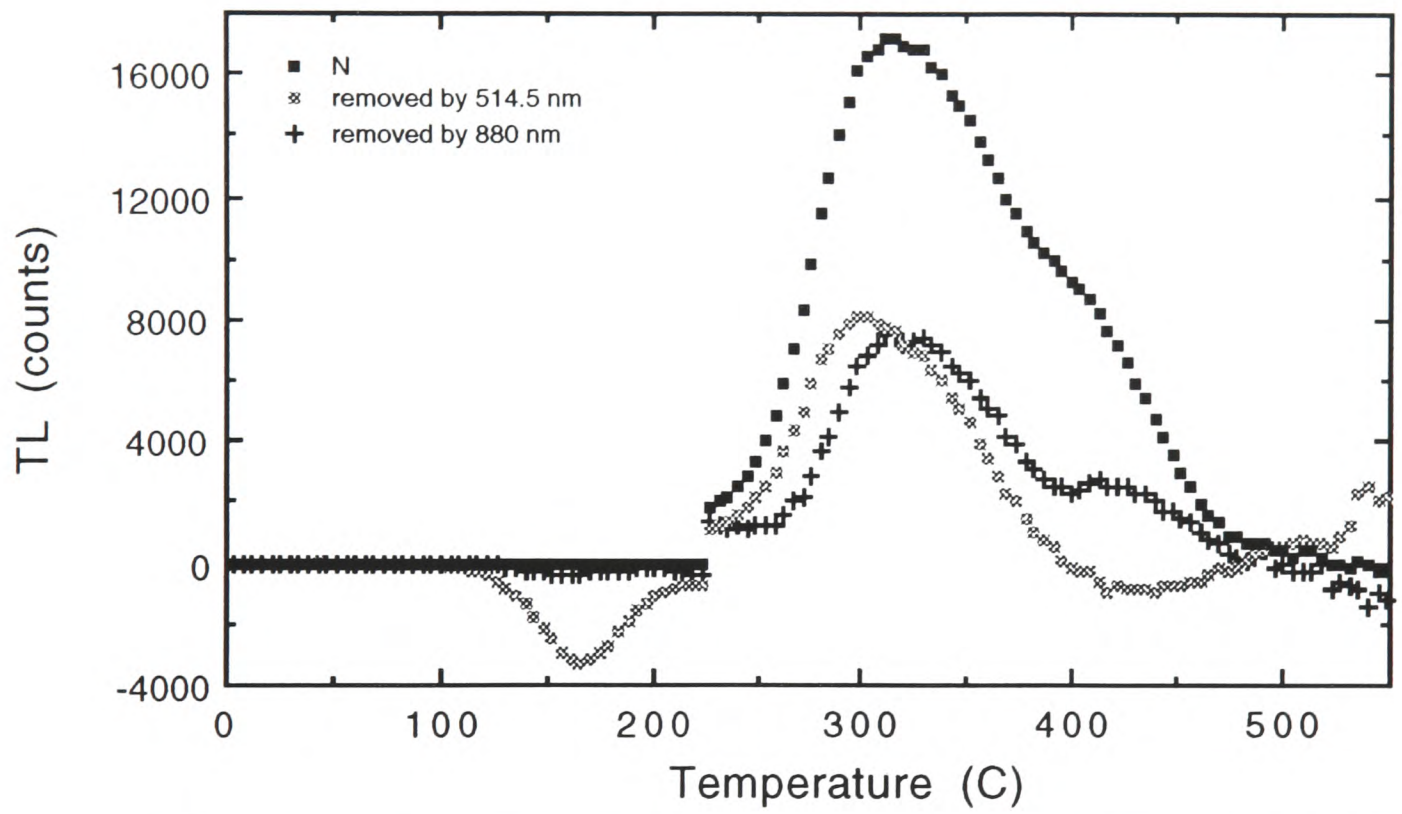


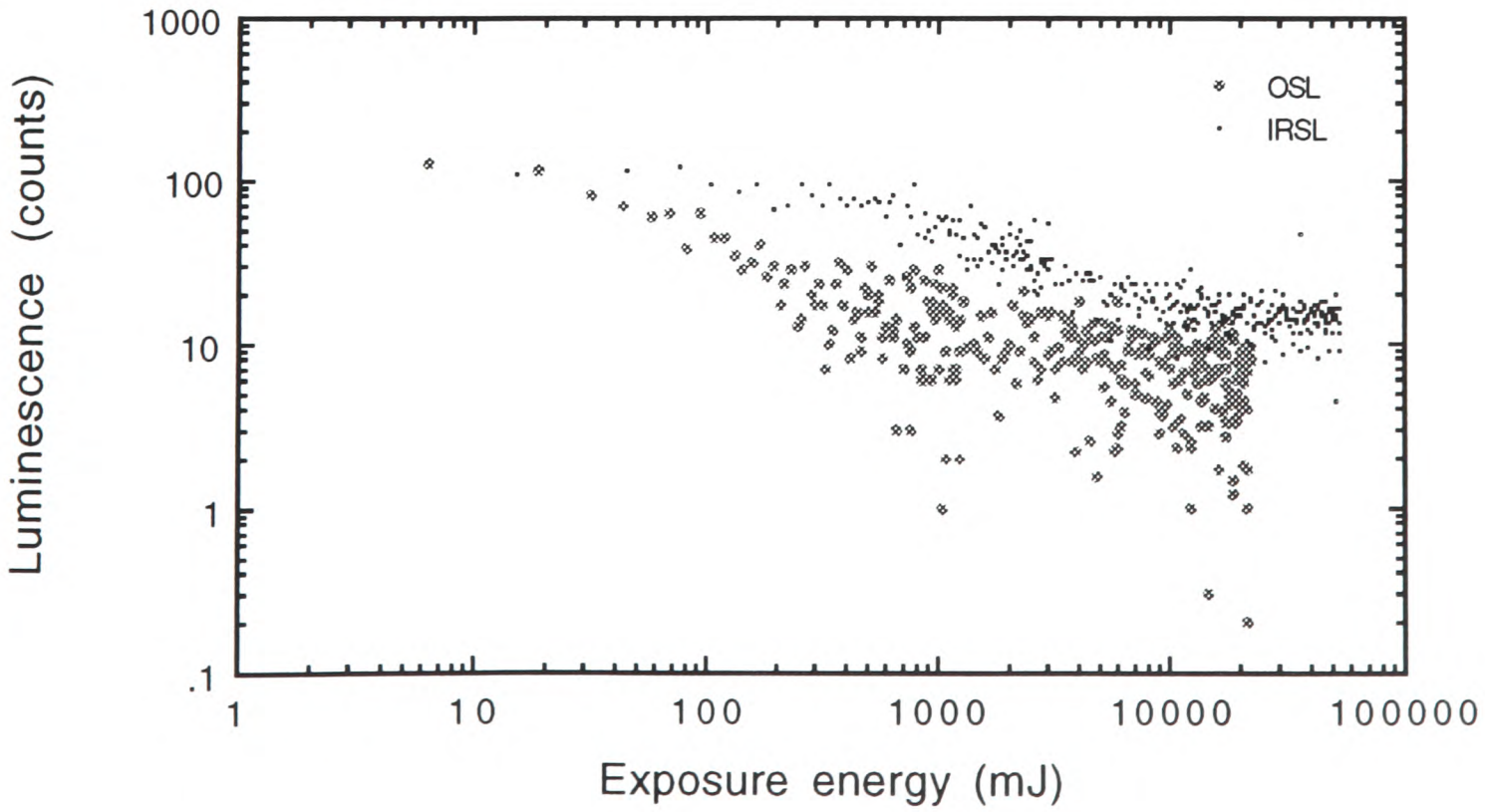




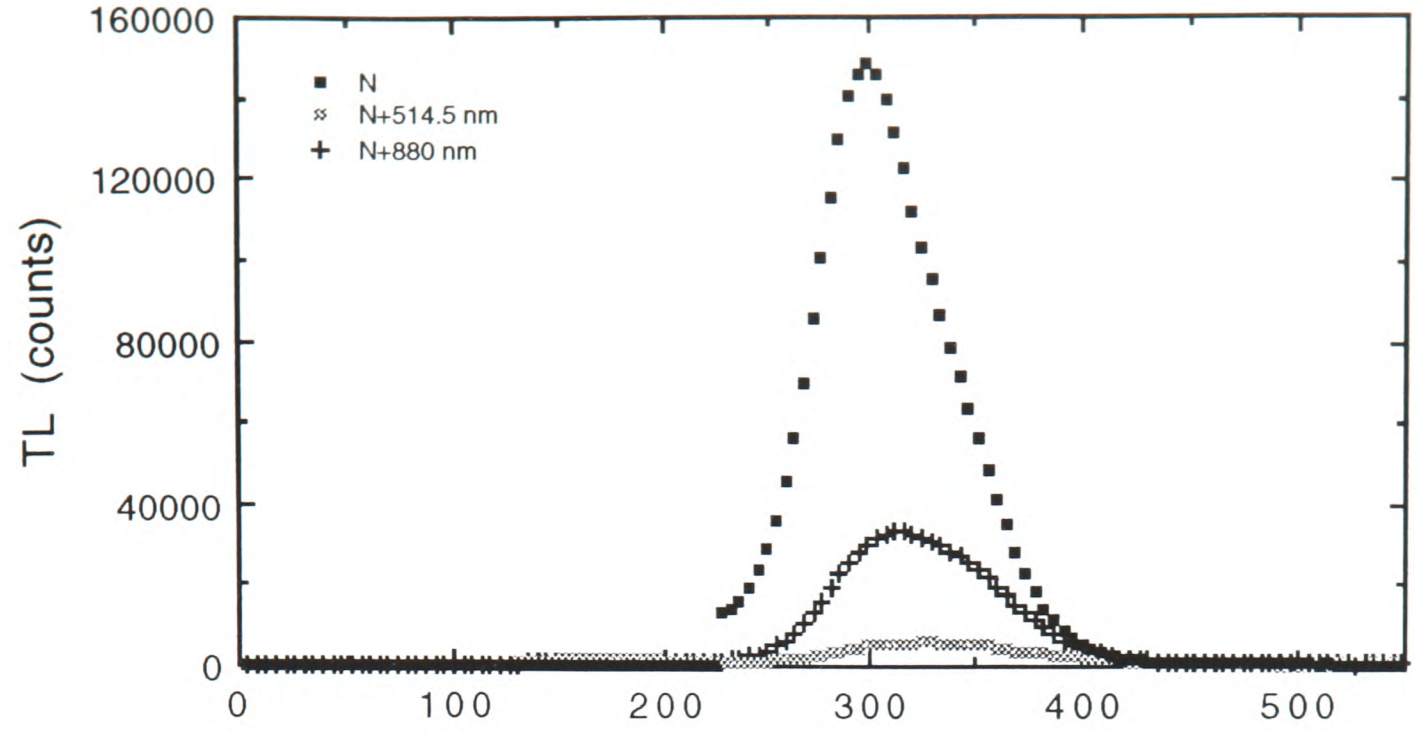
17. albite

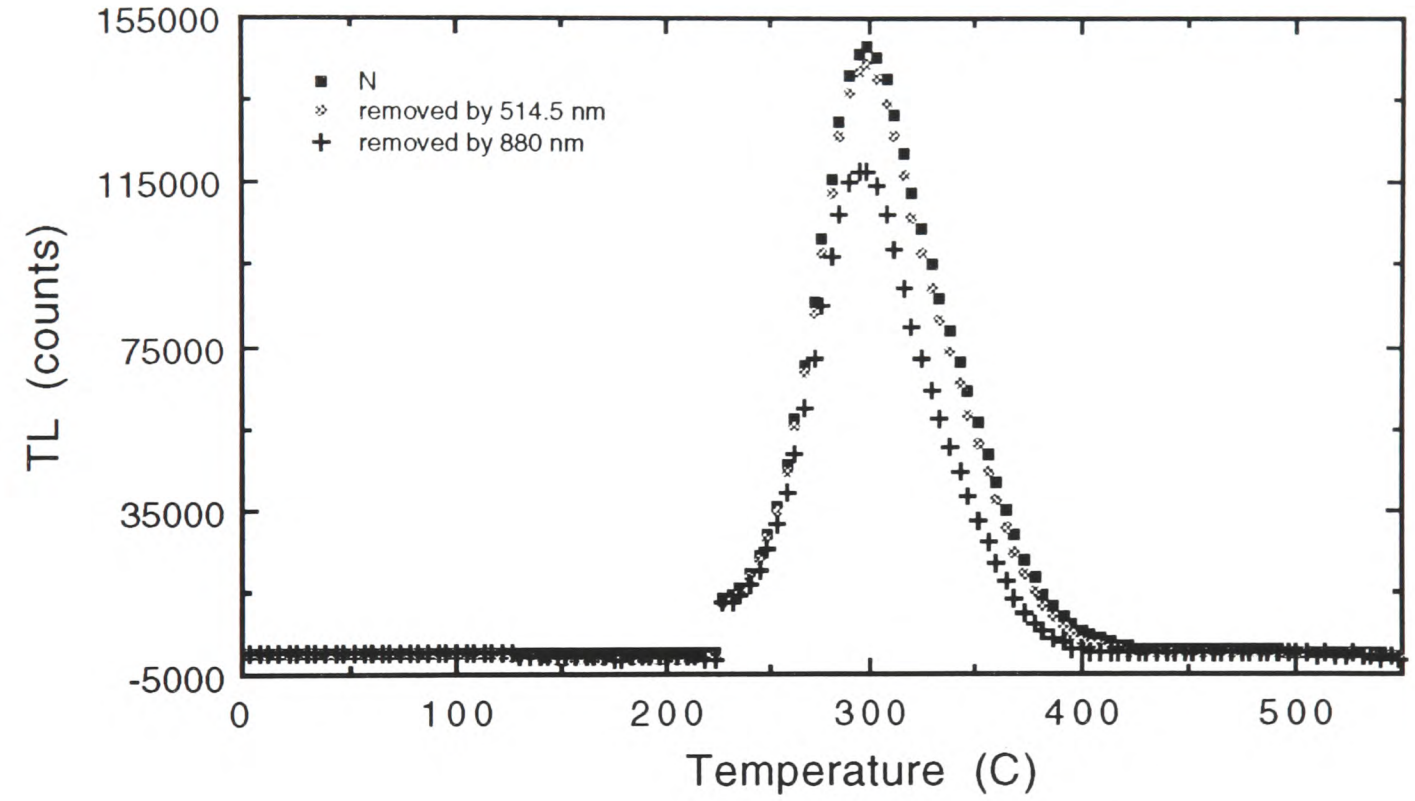

N
N+514.5 nm
N+880 nm
TL (counts)
18000
15000
12000
9000
6000
3000
0
0
100
200
300
400
500

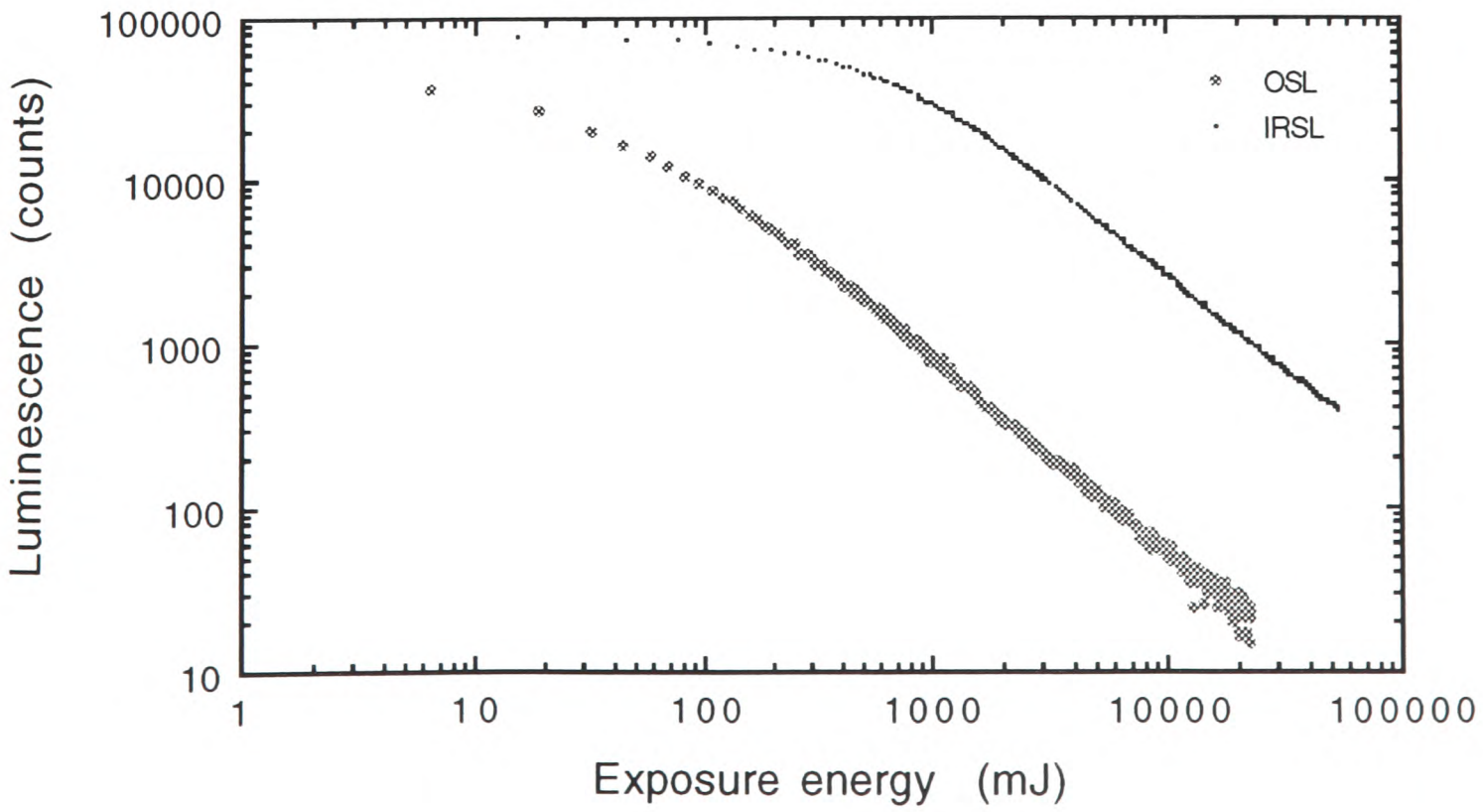

N
removed by 514.5 nm
removed by 880 nm
TL (counts)
16000
12000
8000
4000
0
-4000
0
100
200
300
400
500
Temperature (C)


OSL
IRSL
Luminescence (counts)
1000
100
10
1
.1
1
10
100
1000
10000
100000
Exposure energy (mJ)

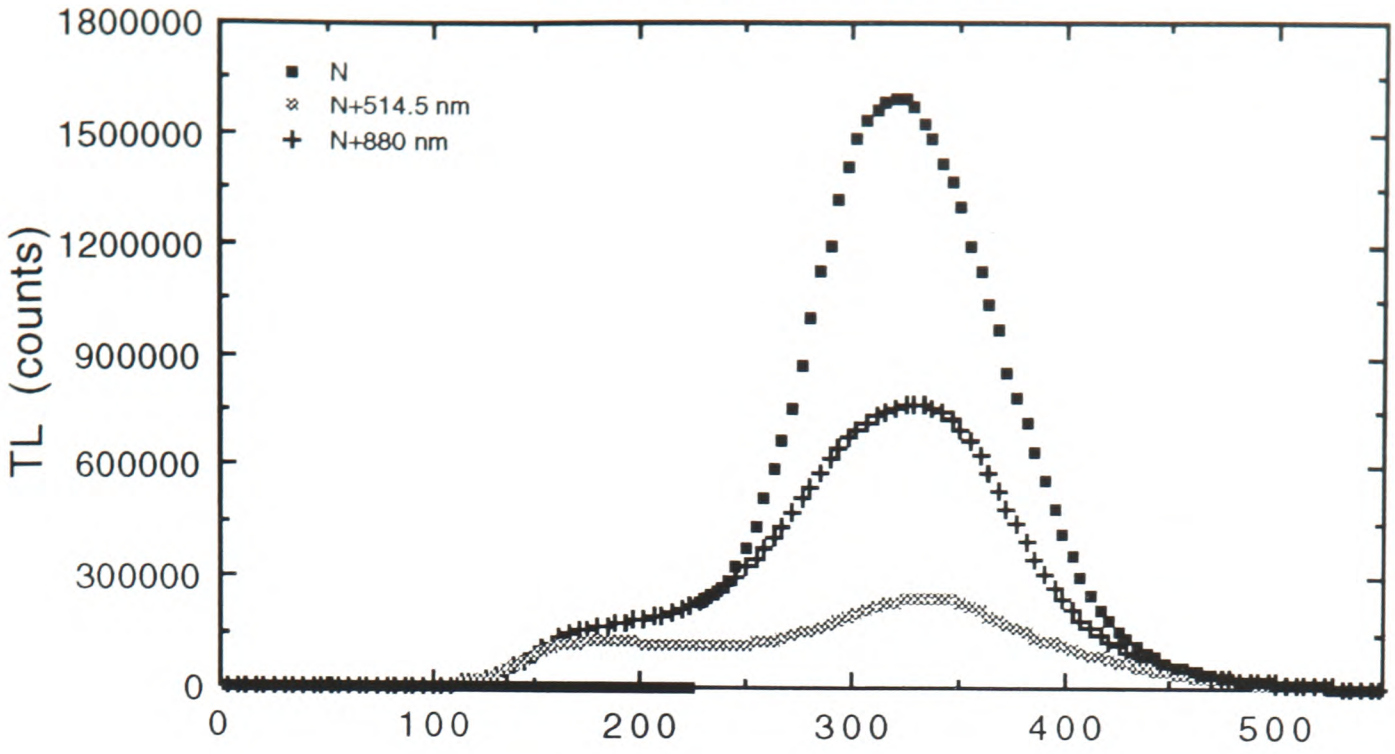
18. Amelia albite

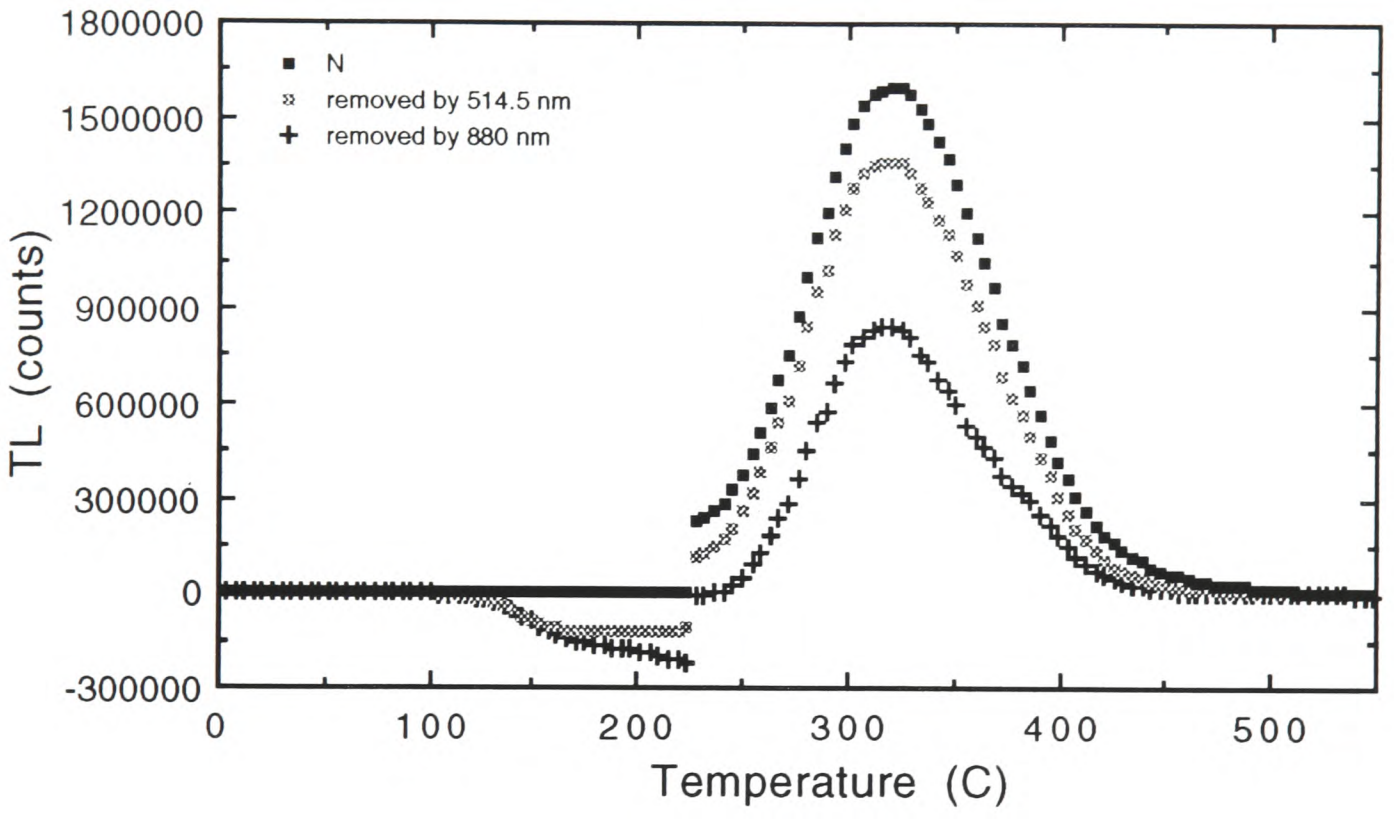


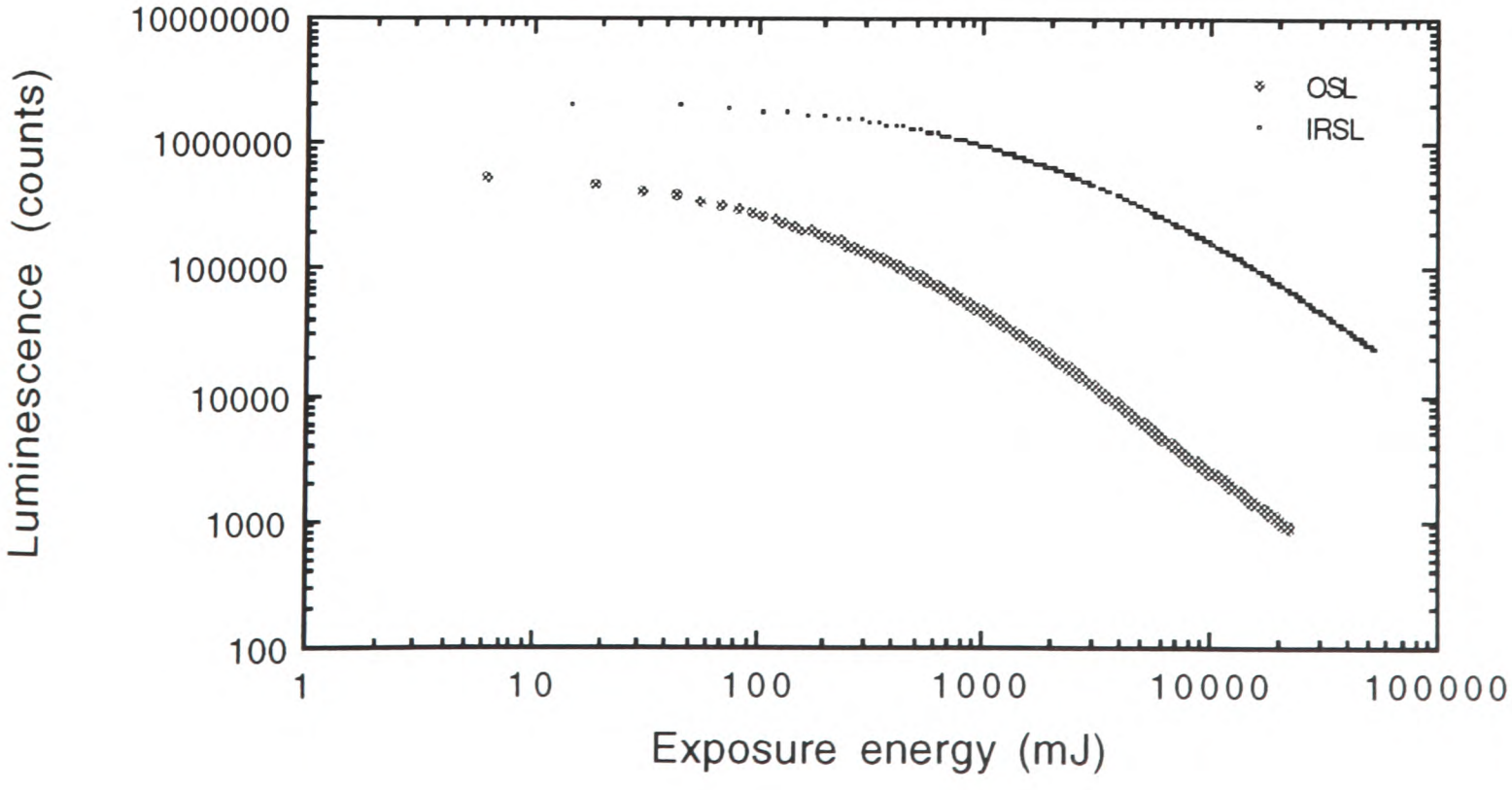




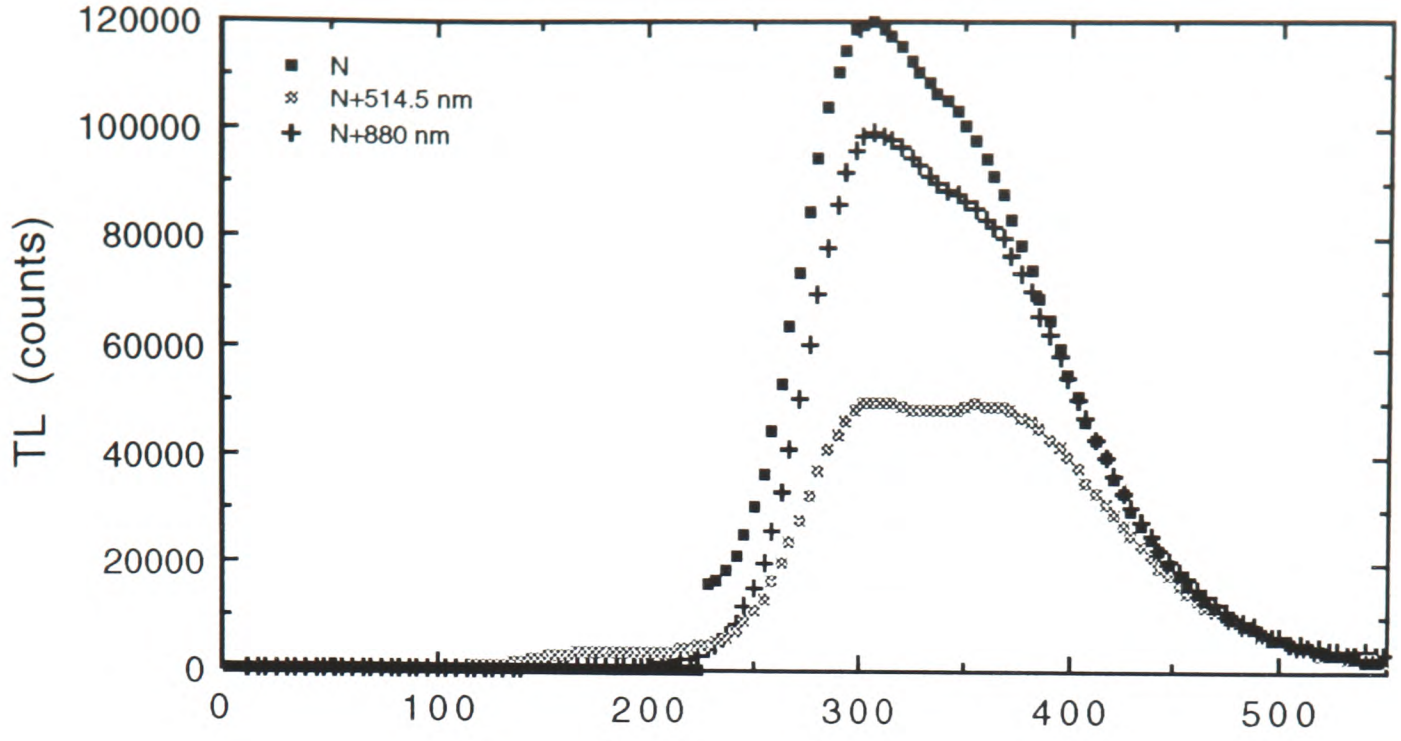
15. Dup(A) albite

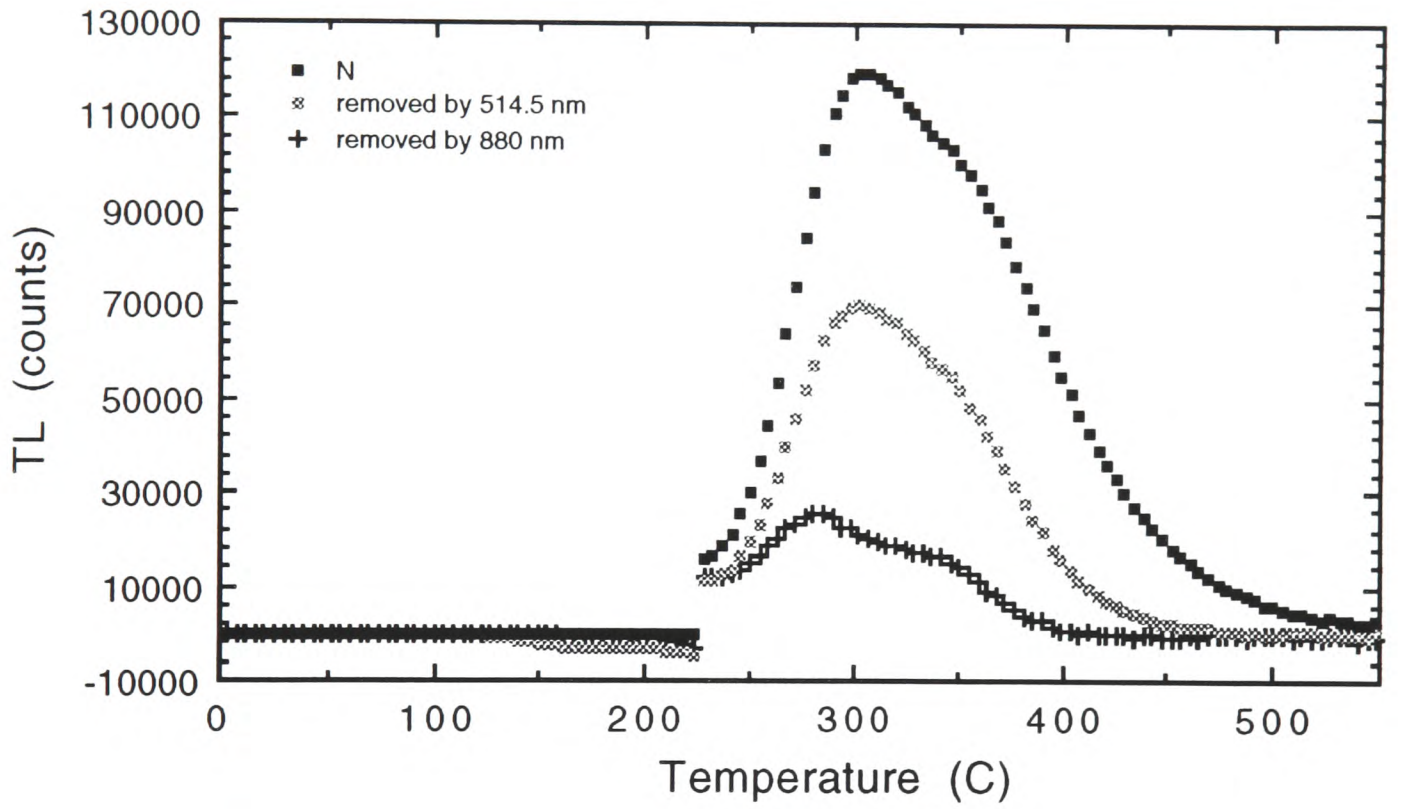


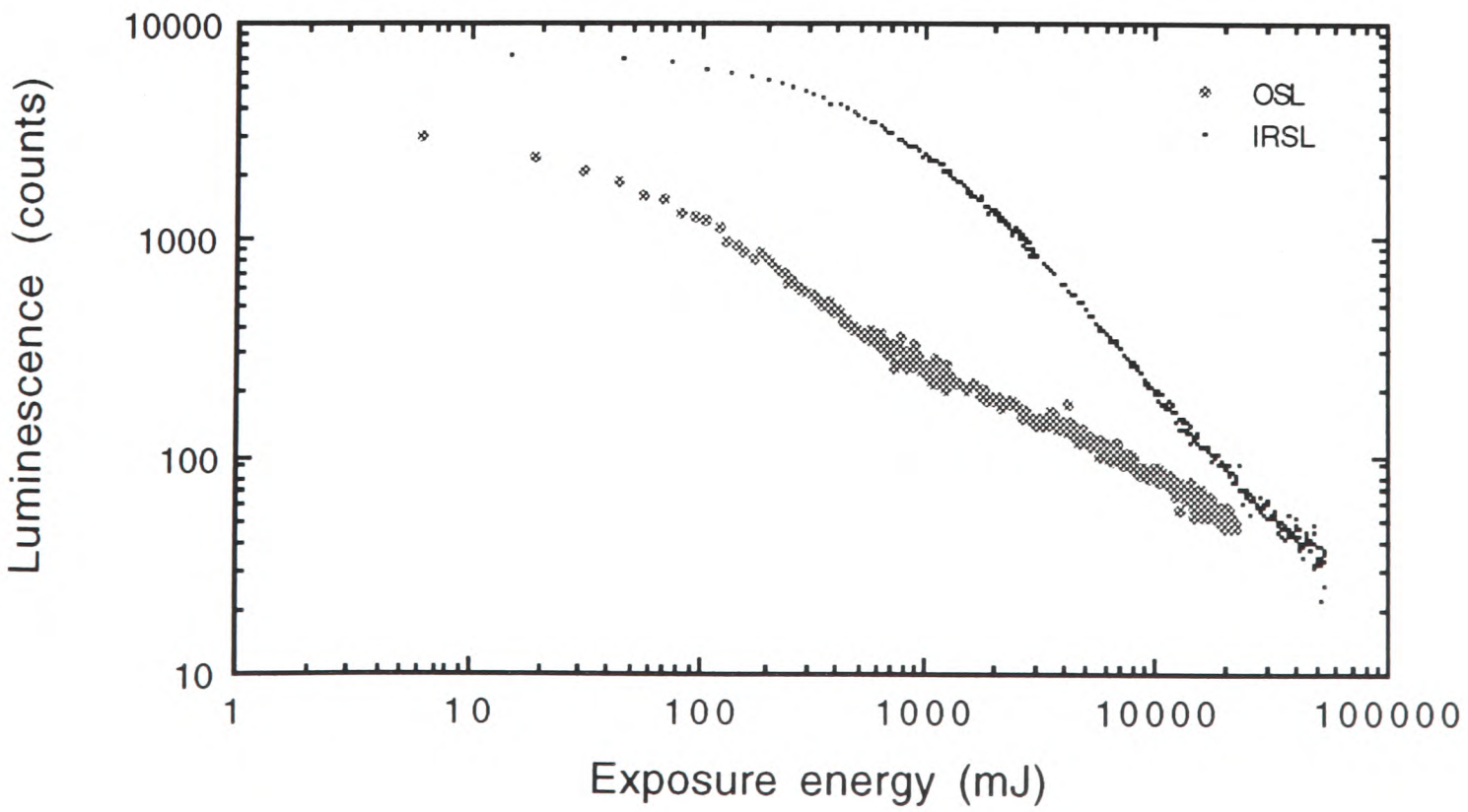




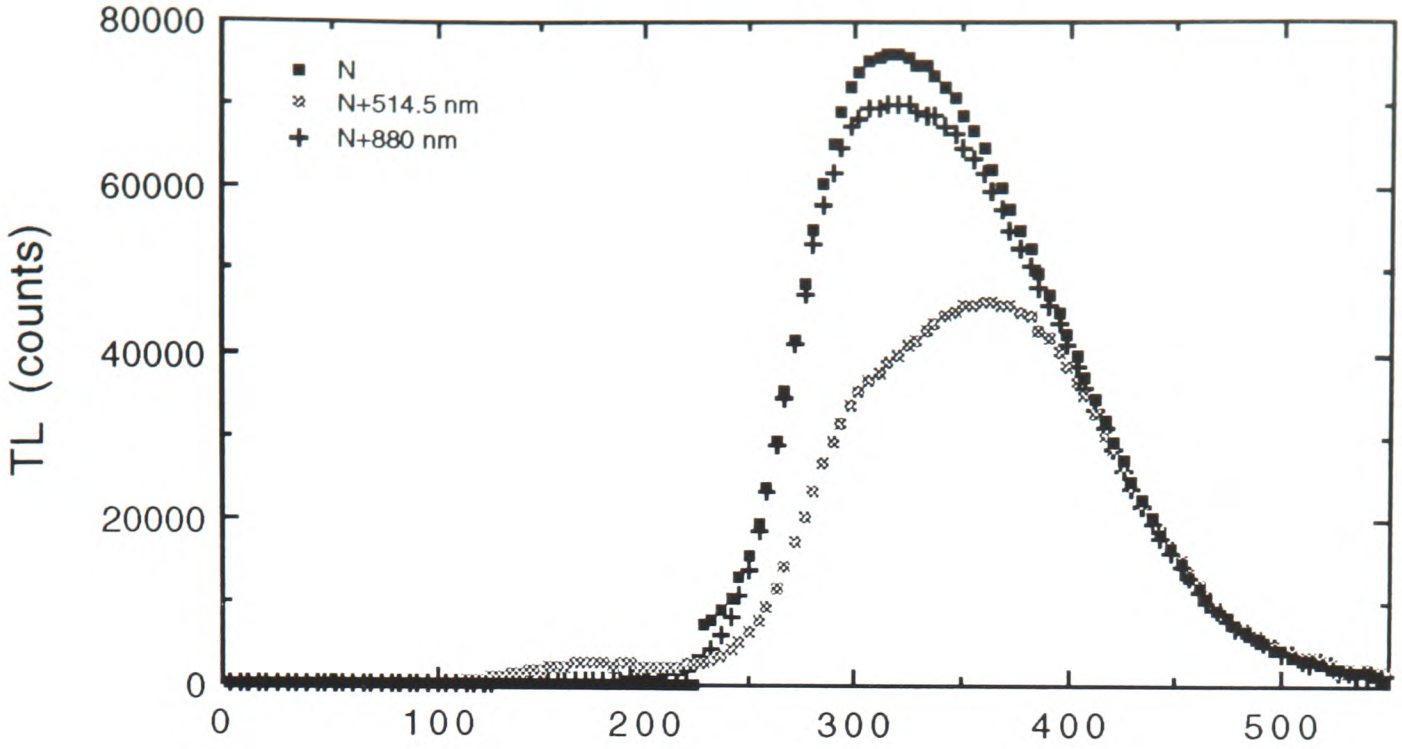
4. 17 oligoclase

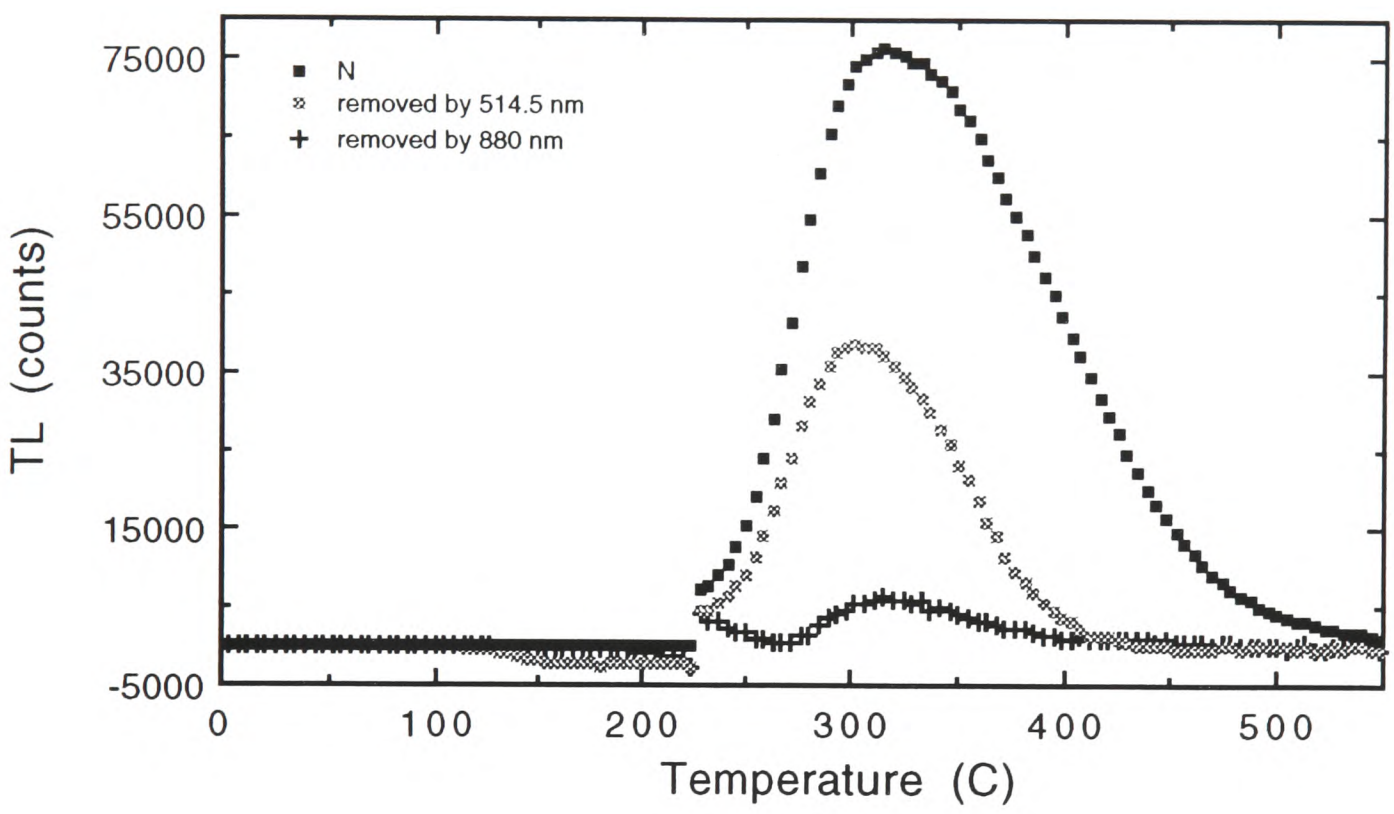


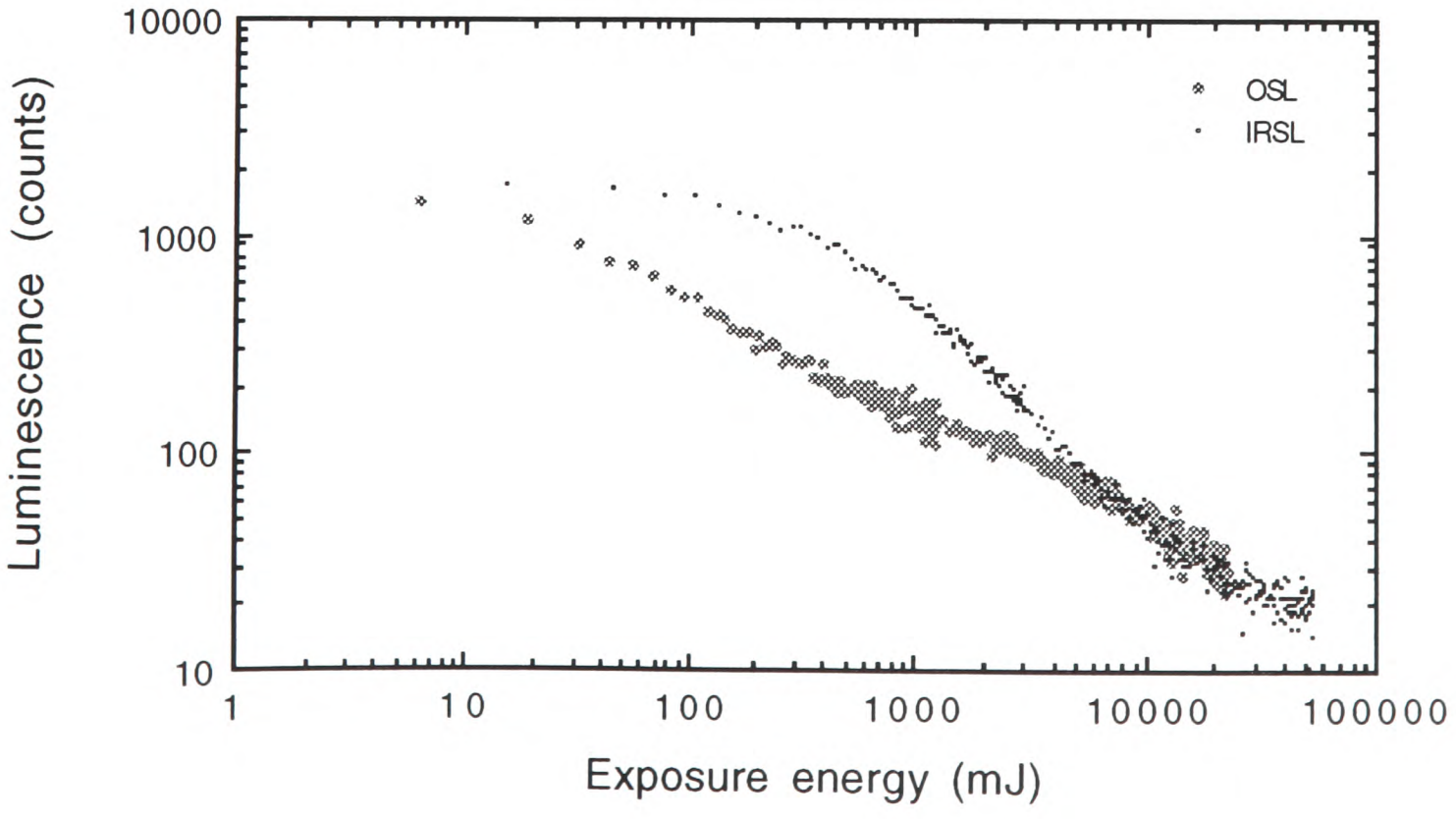




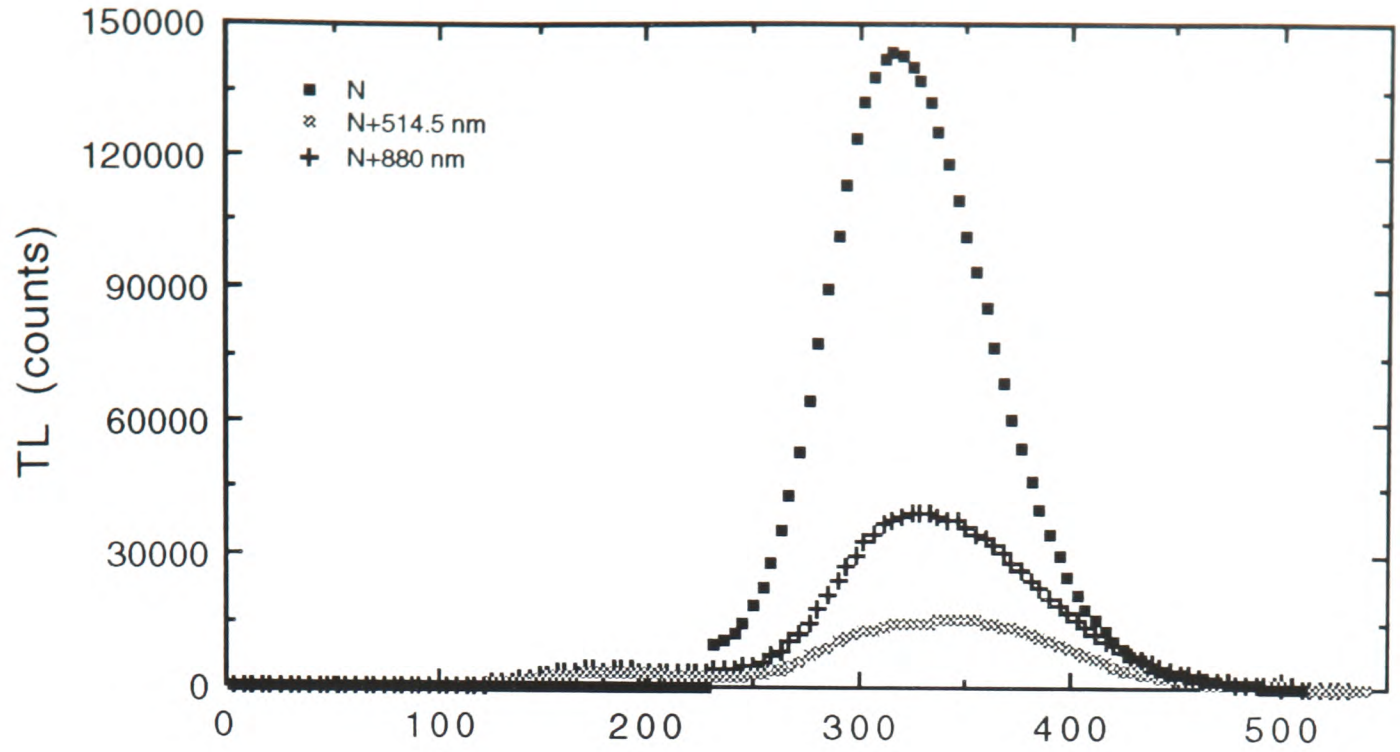
7. 18 oligoclase

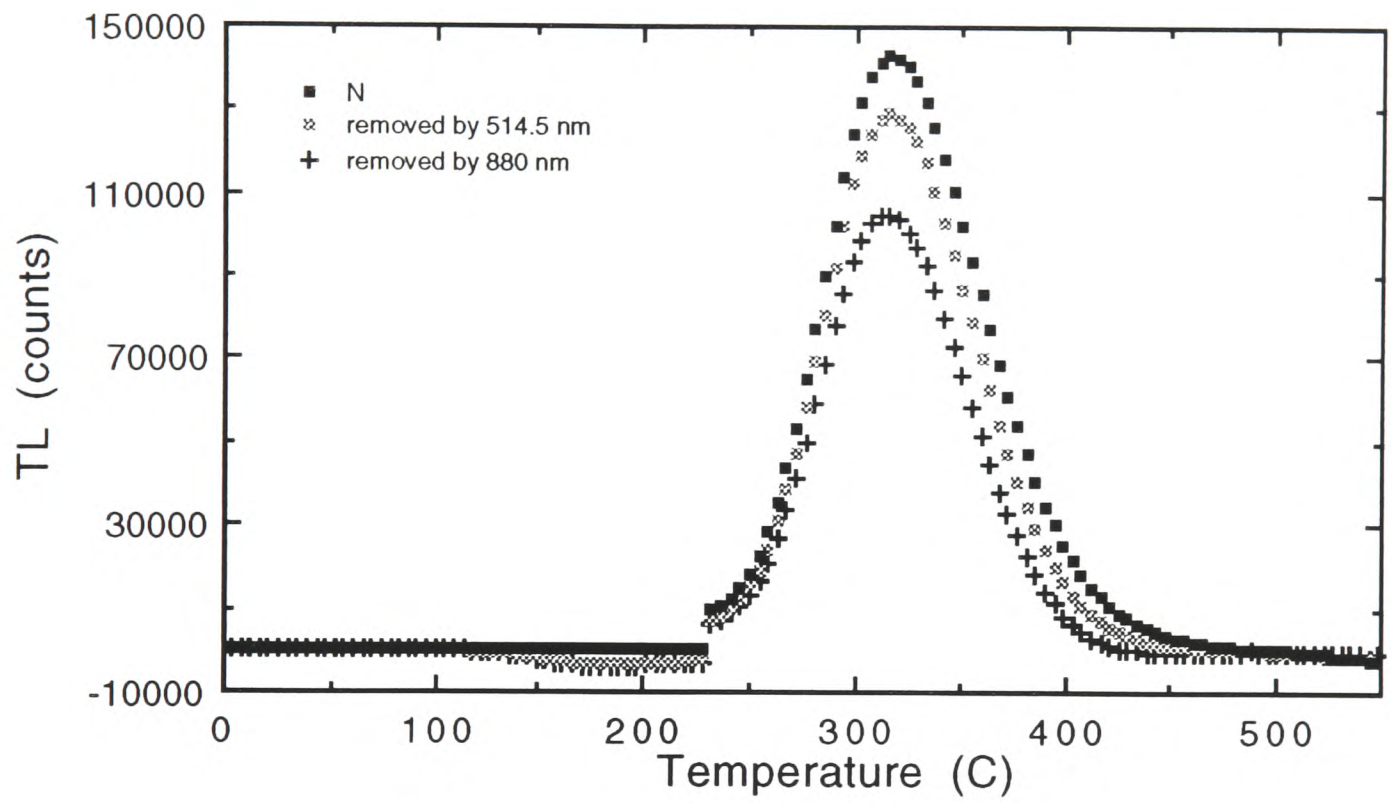


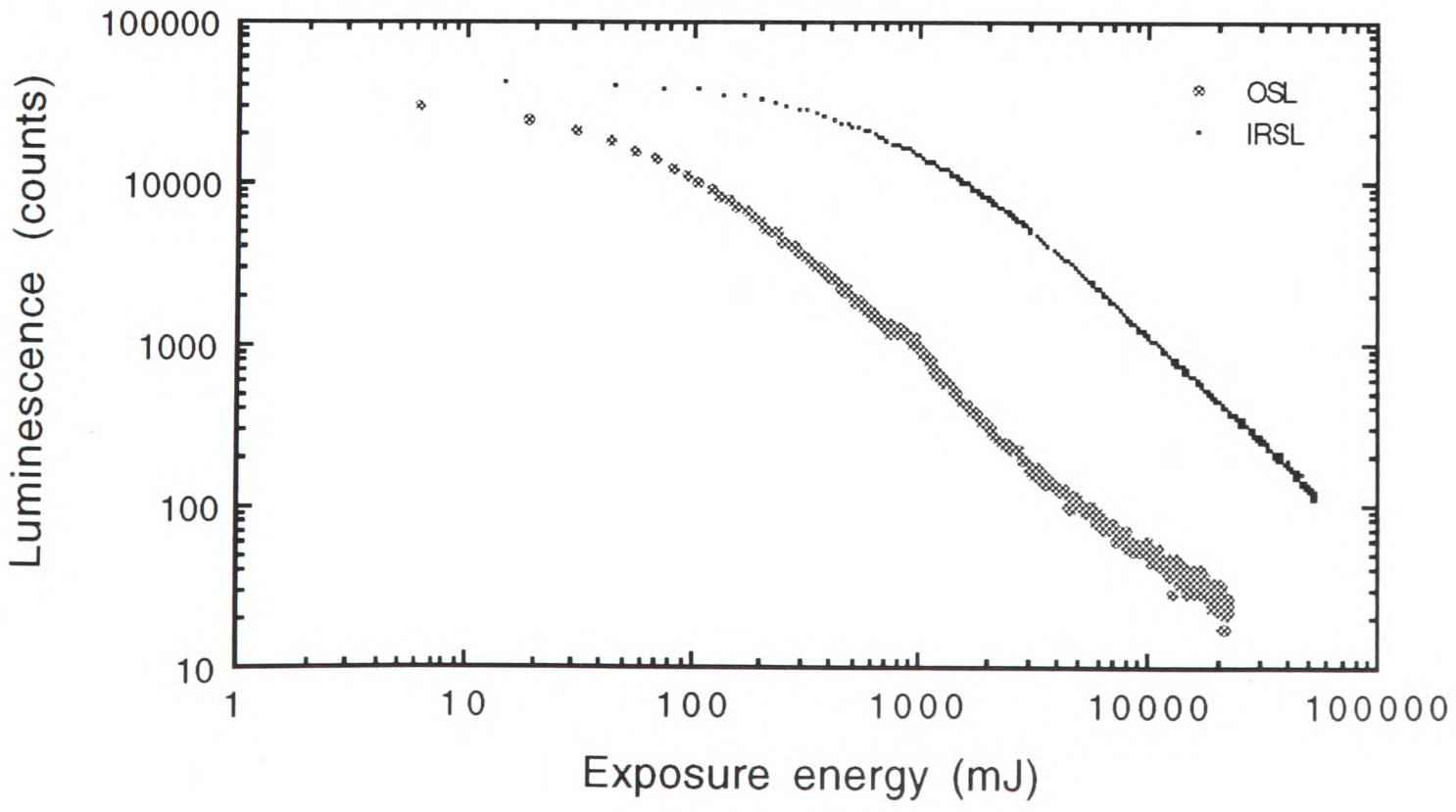




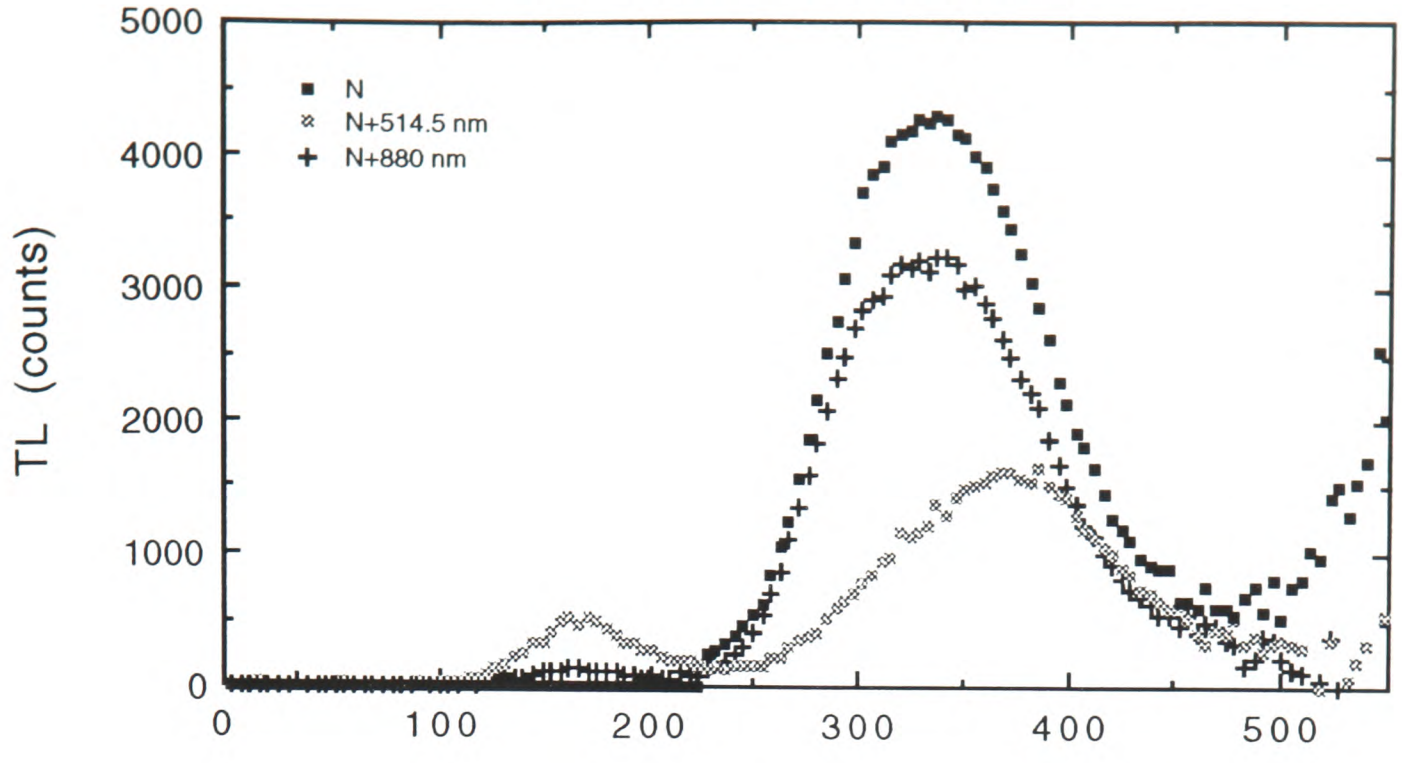
23. Dup(B) oligoclase

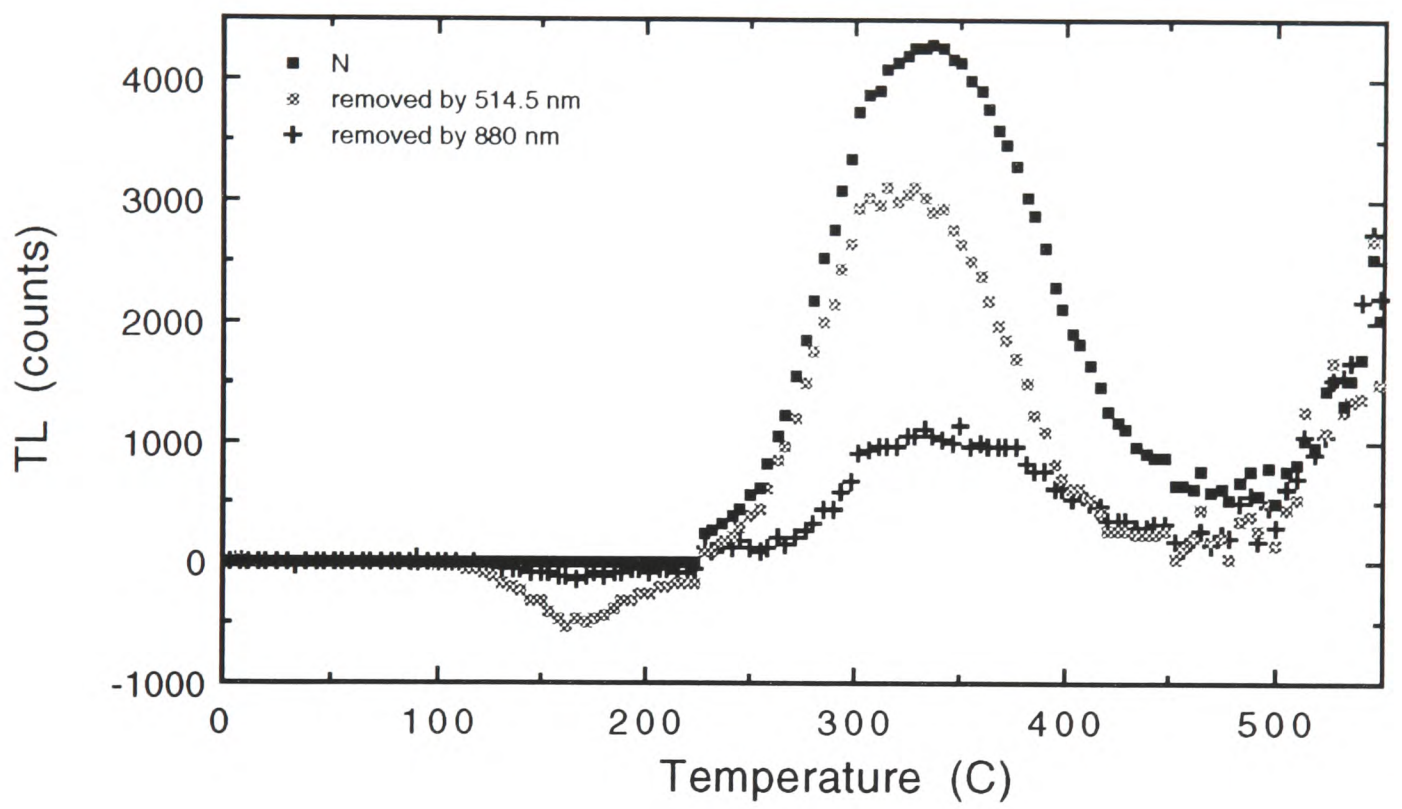


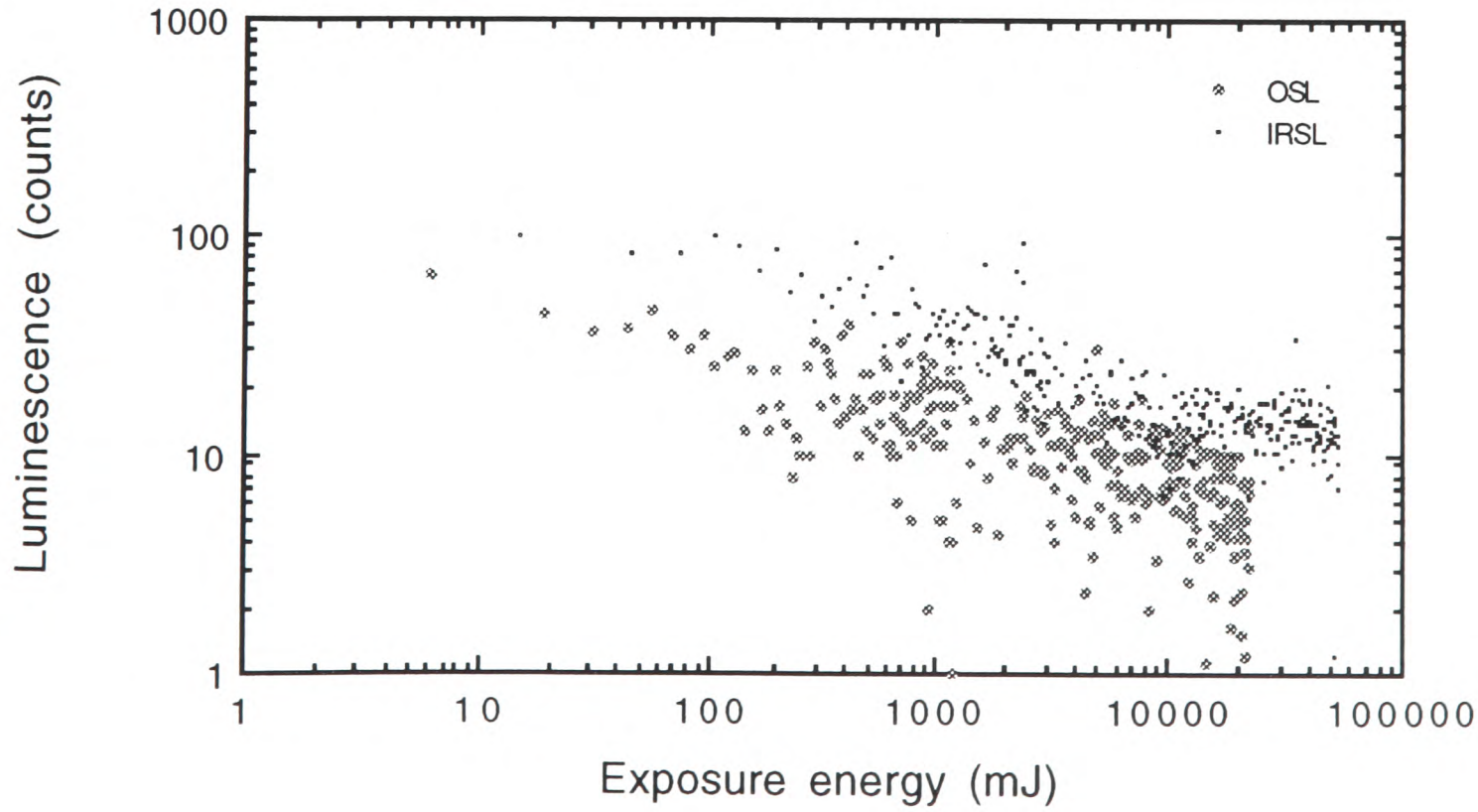




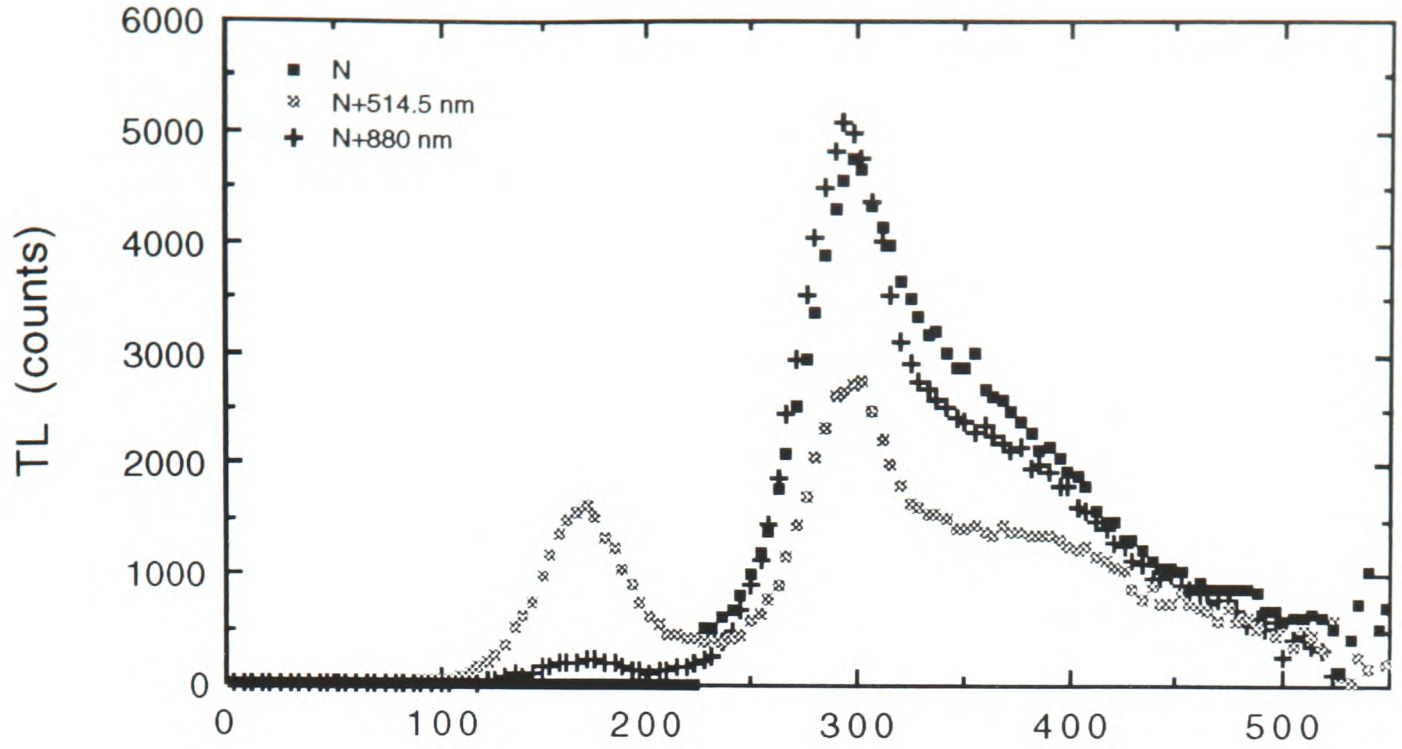
19. BA6 labradorite

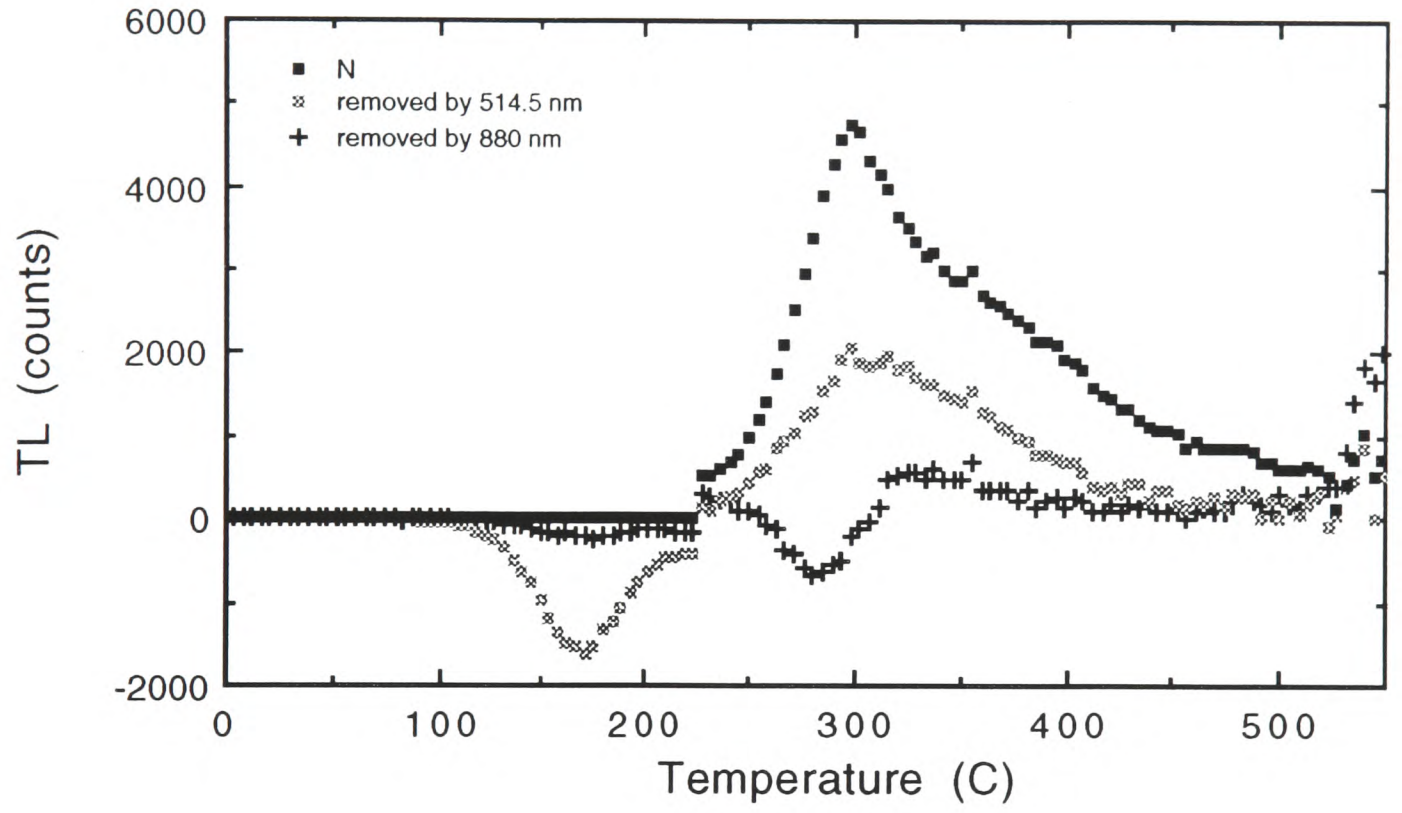


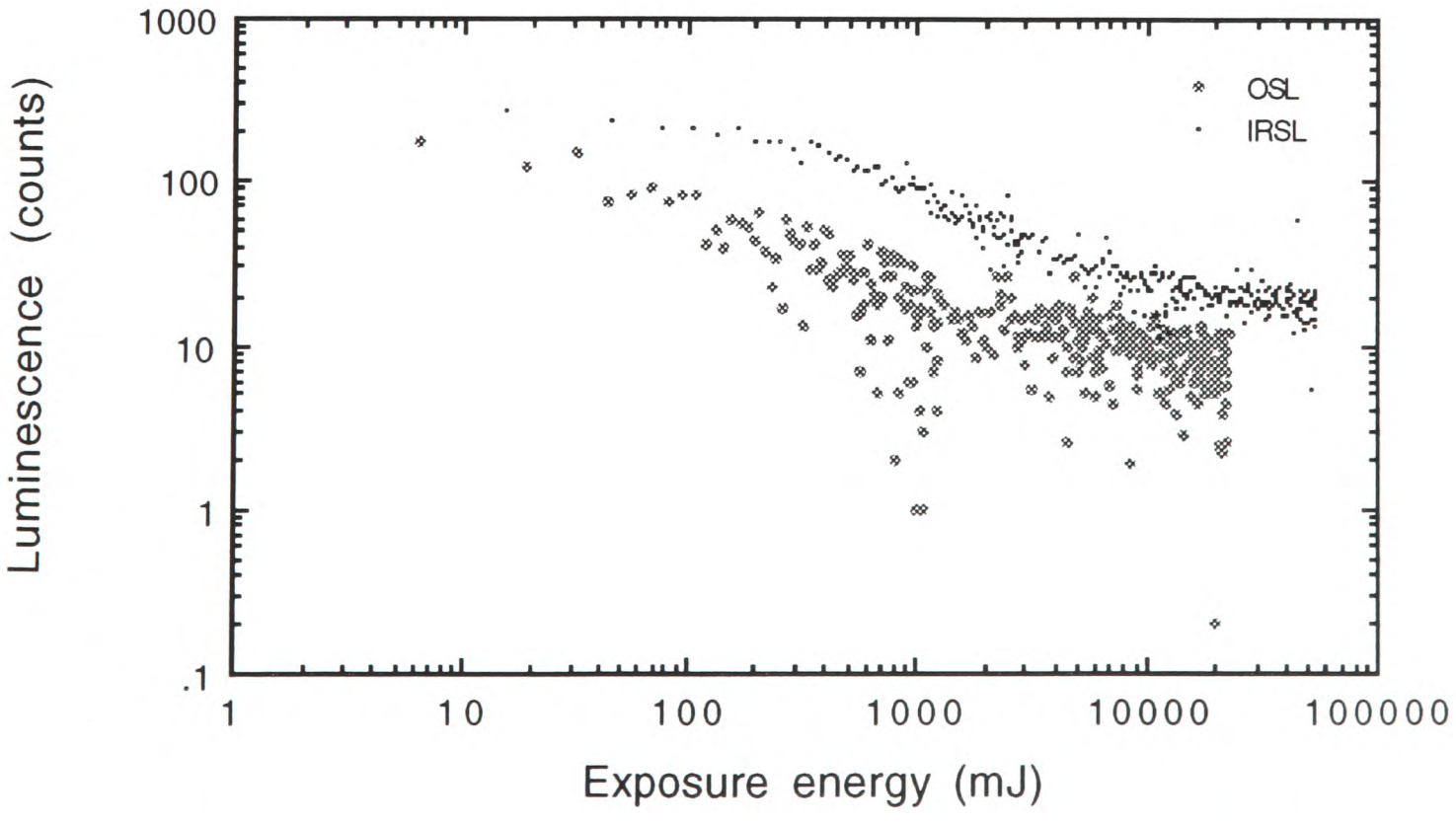




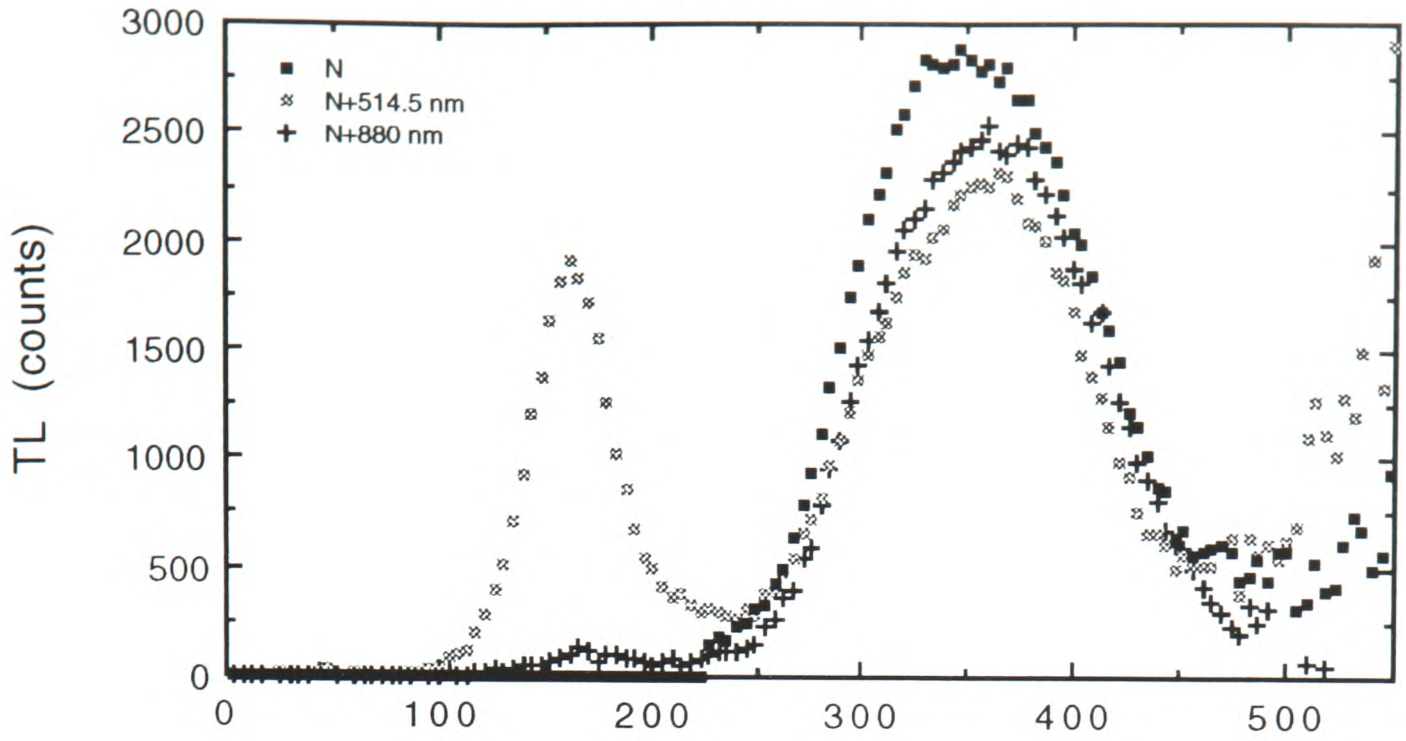
6. 23 labradorite

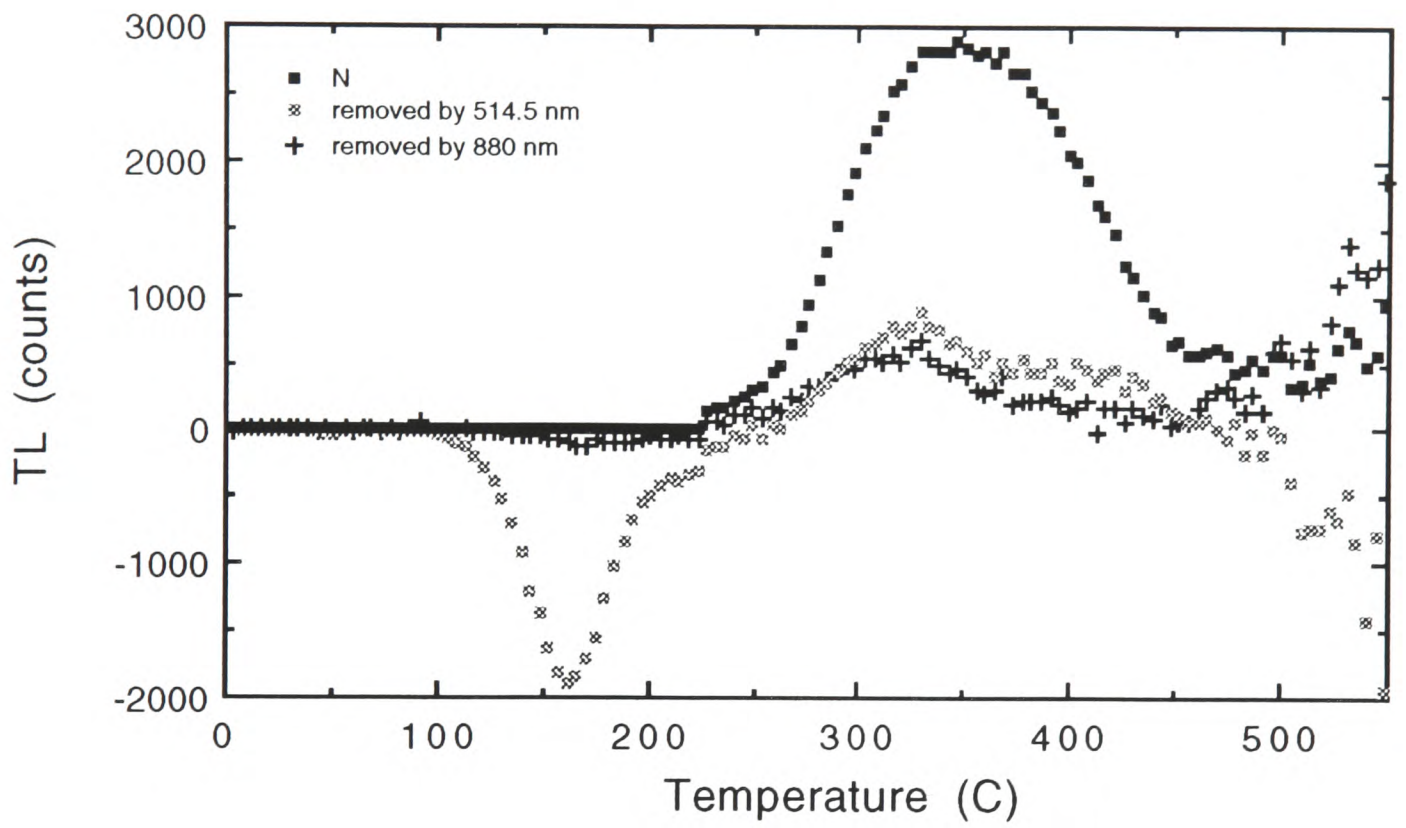


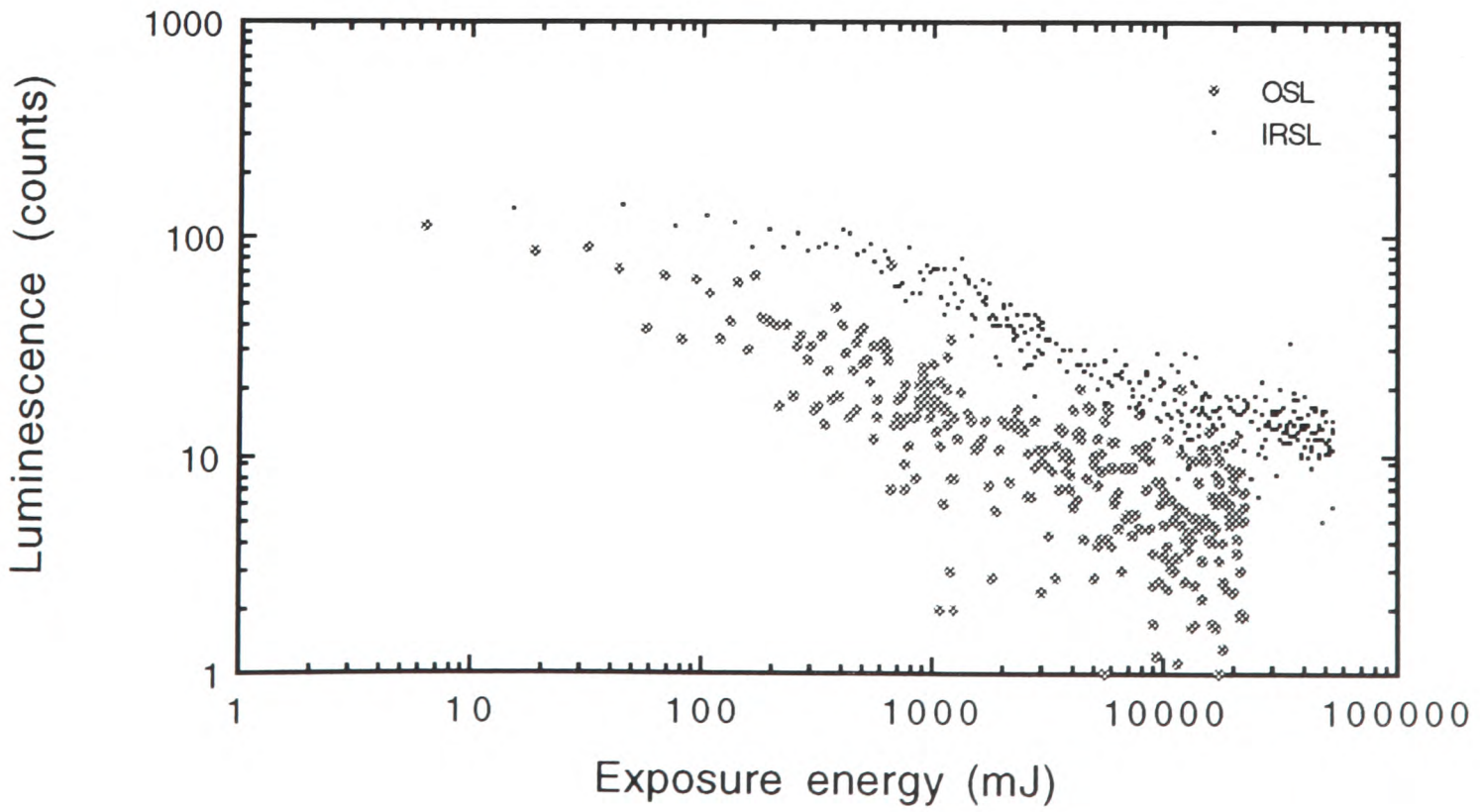




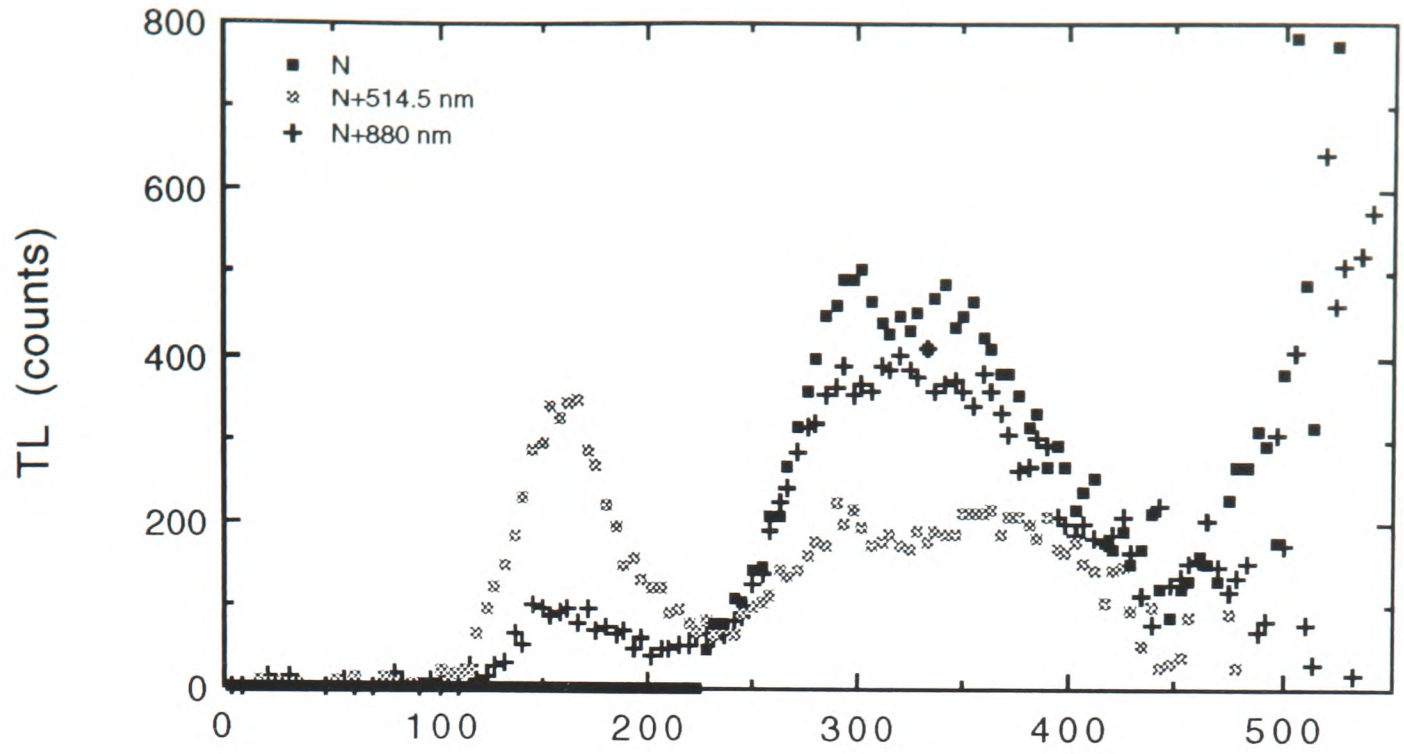
24. Dup(D) labradorite

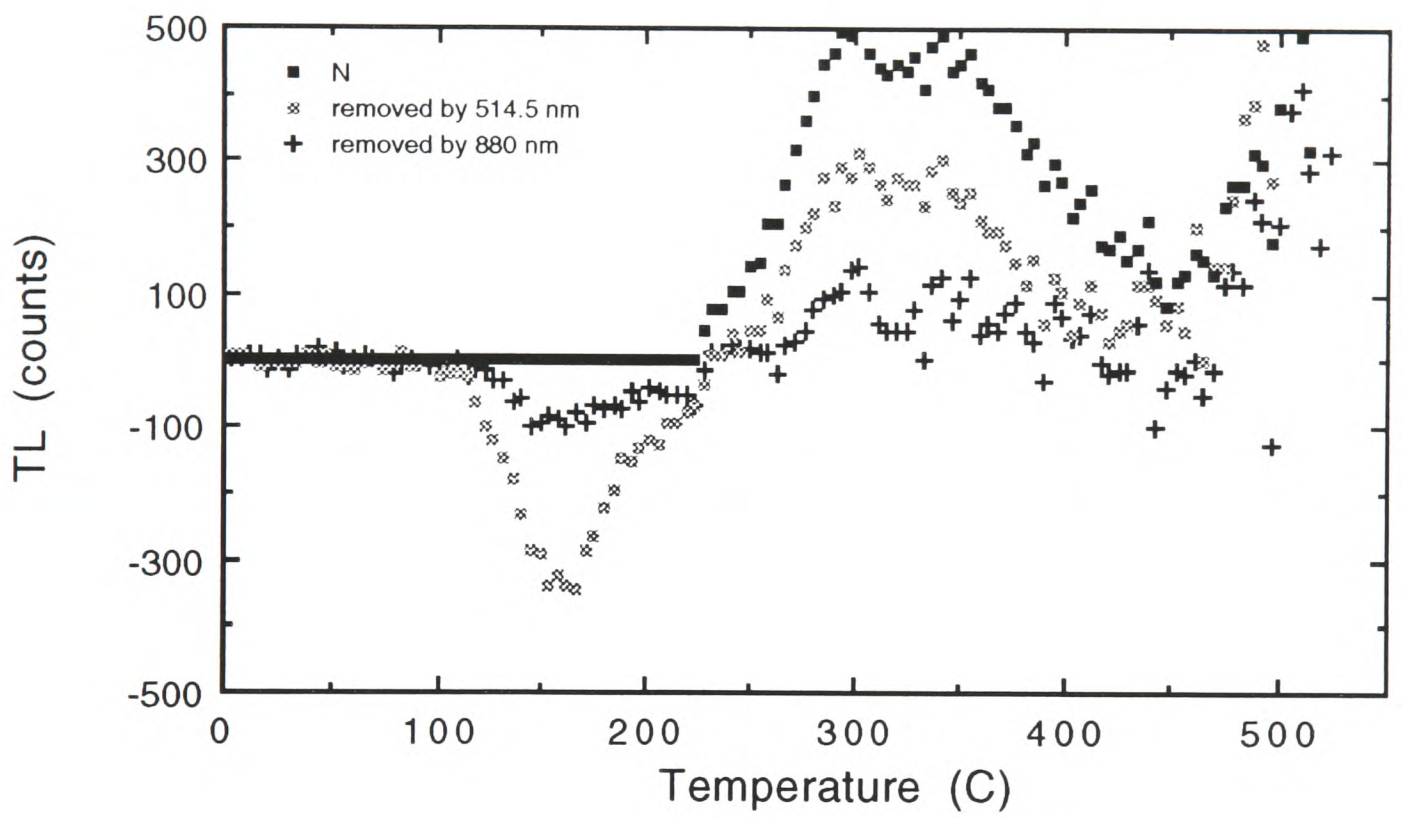


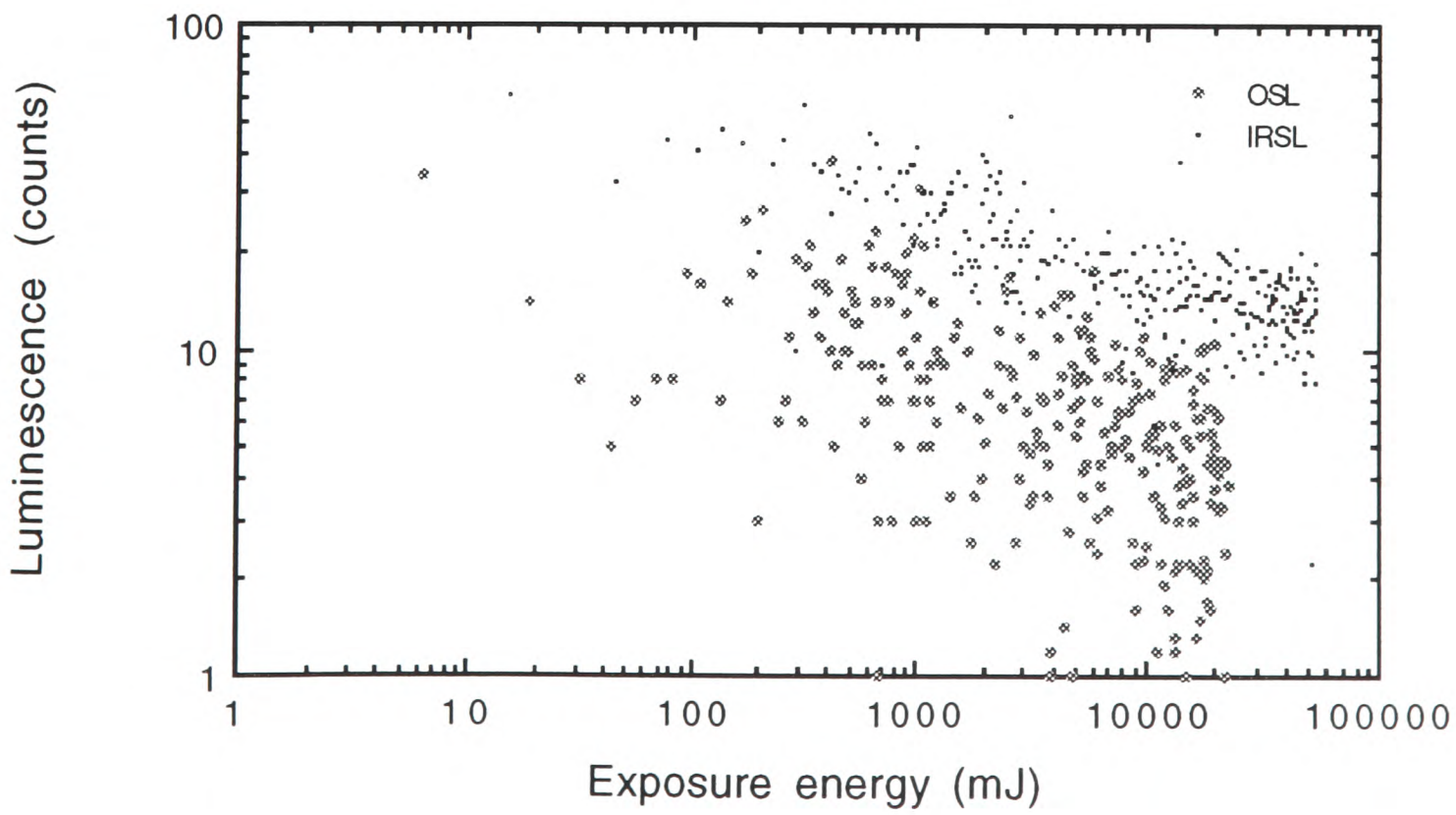




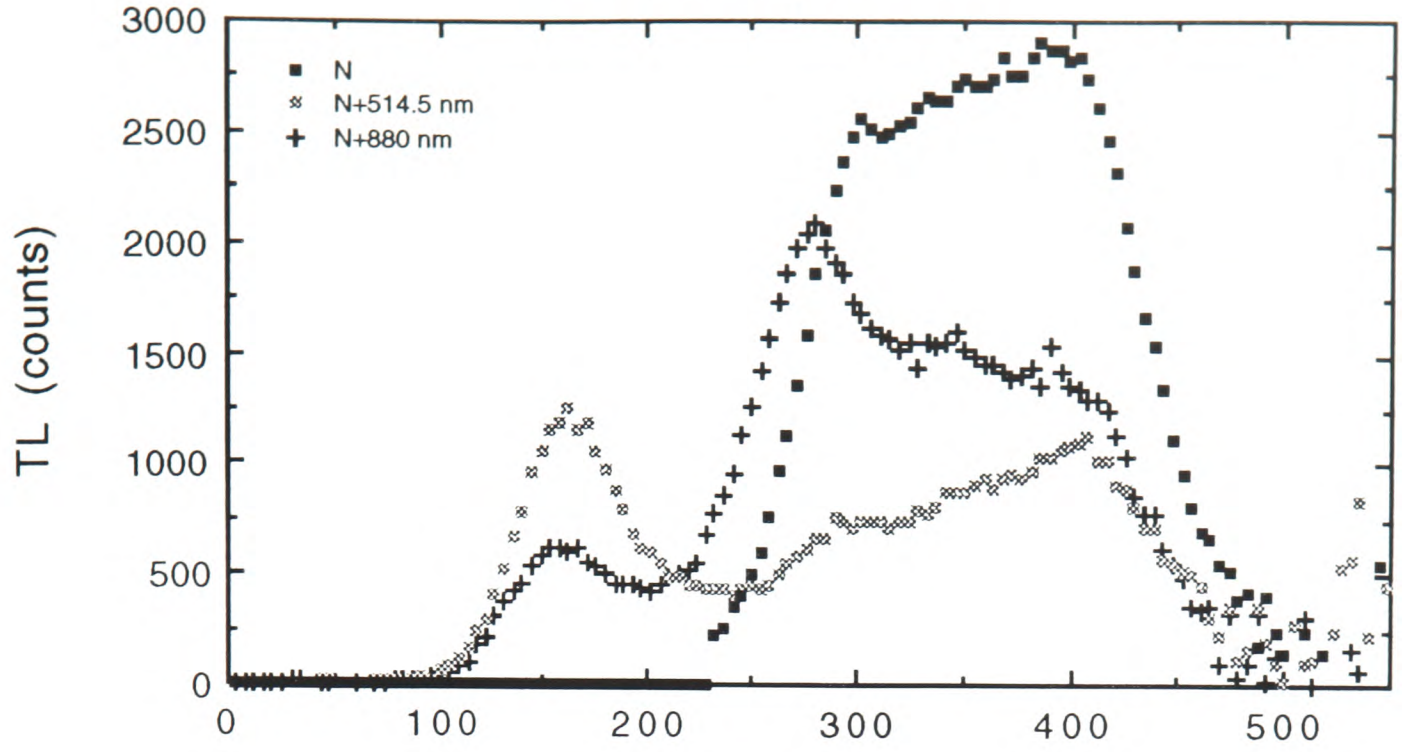
2. 25 bytownite

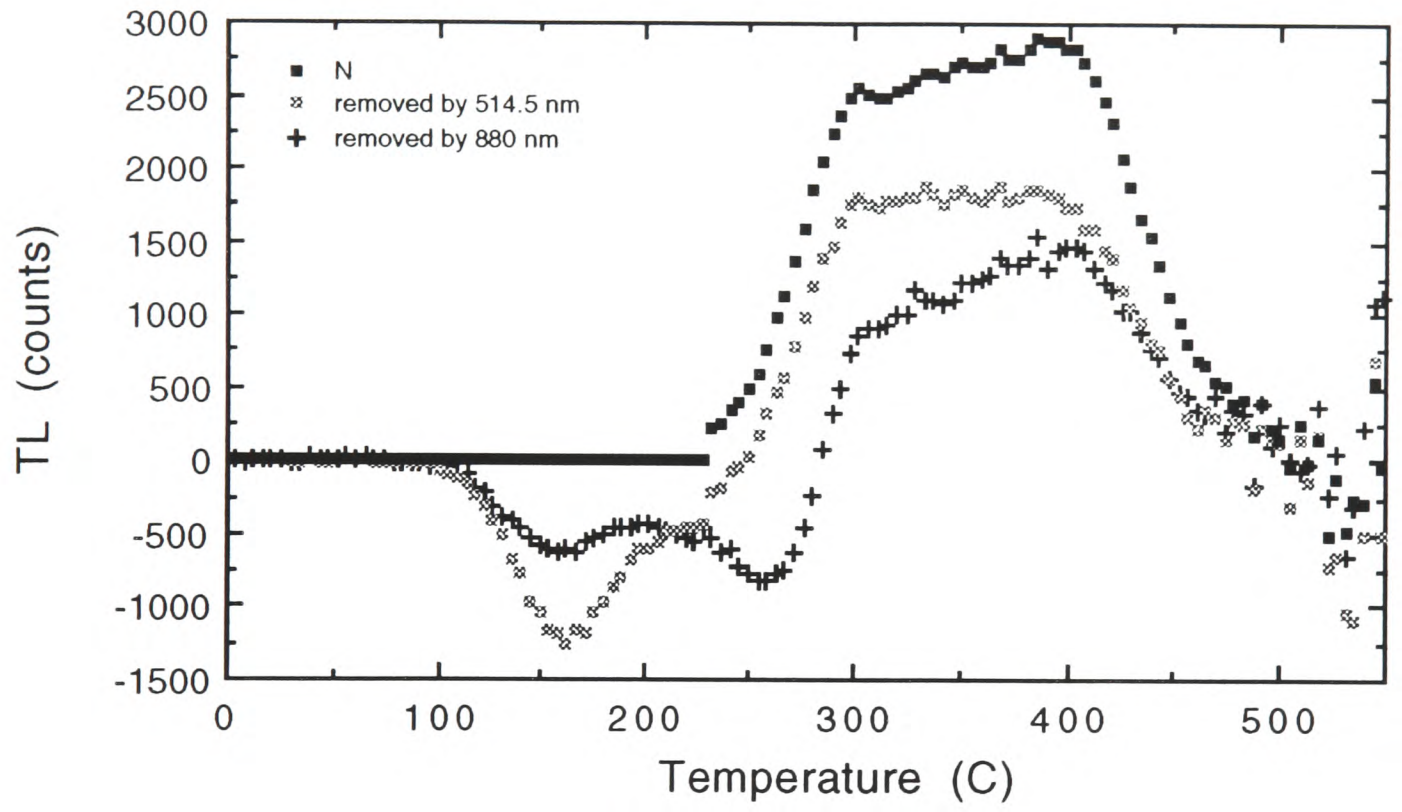


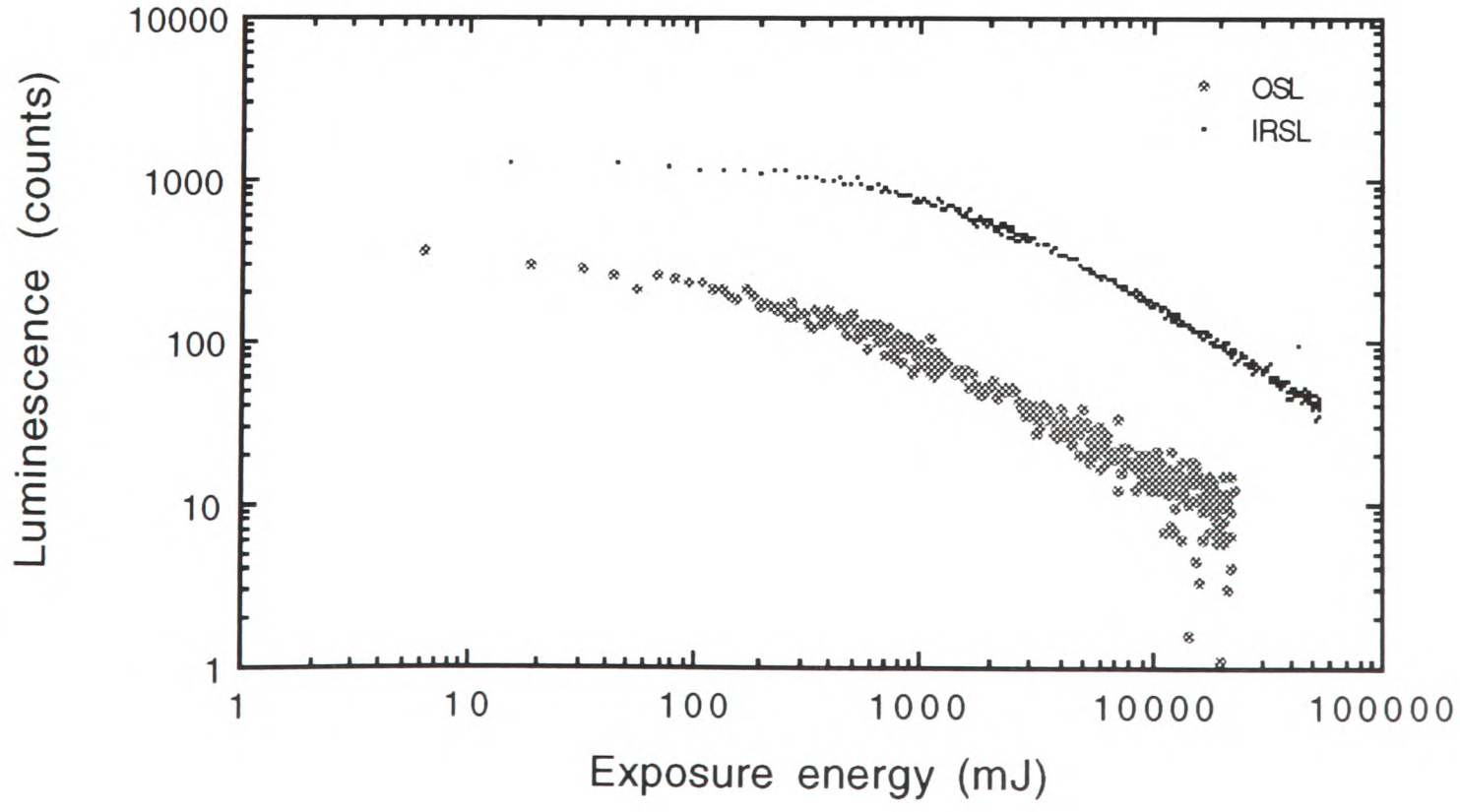




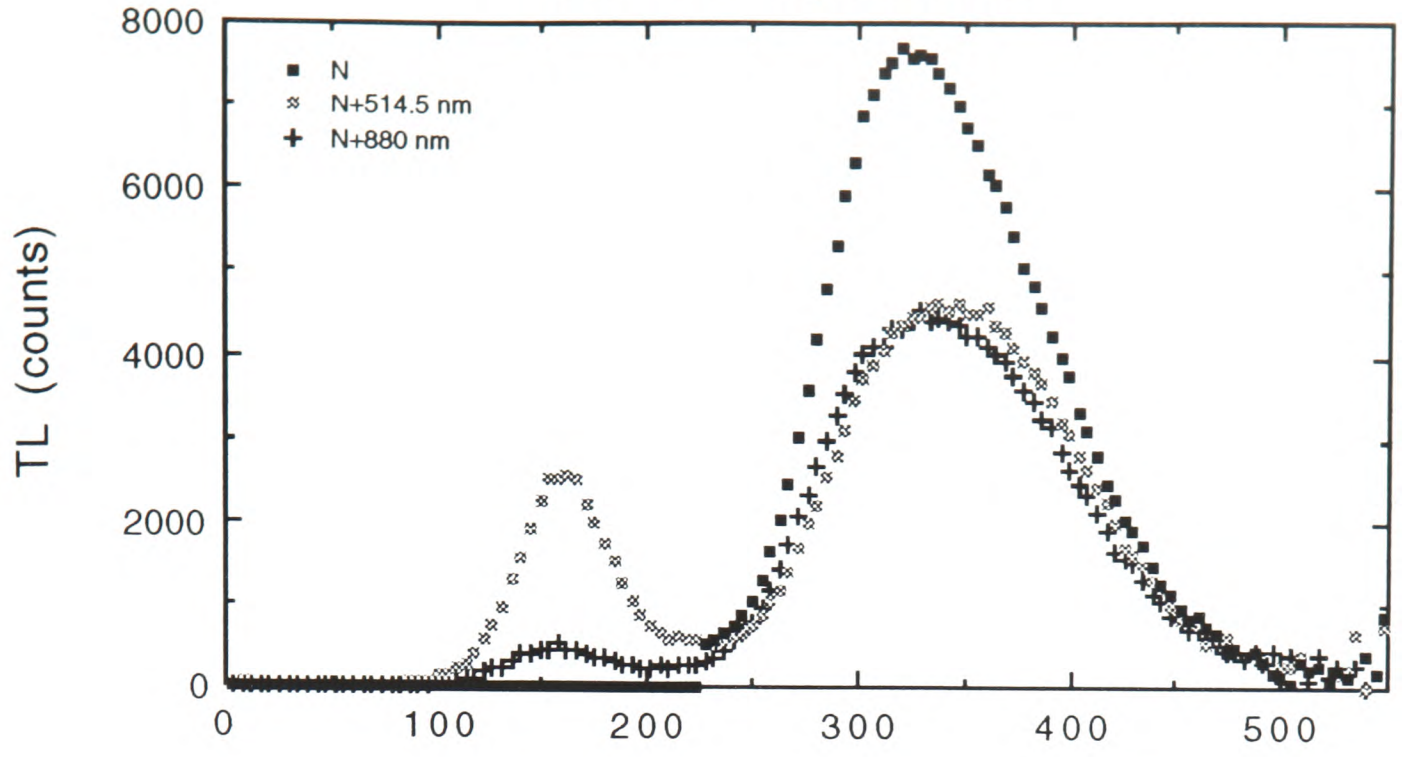
8. 26 bytownite

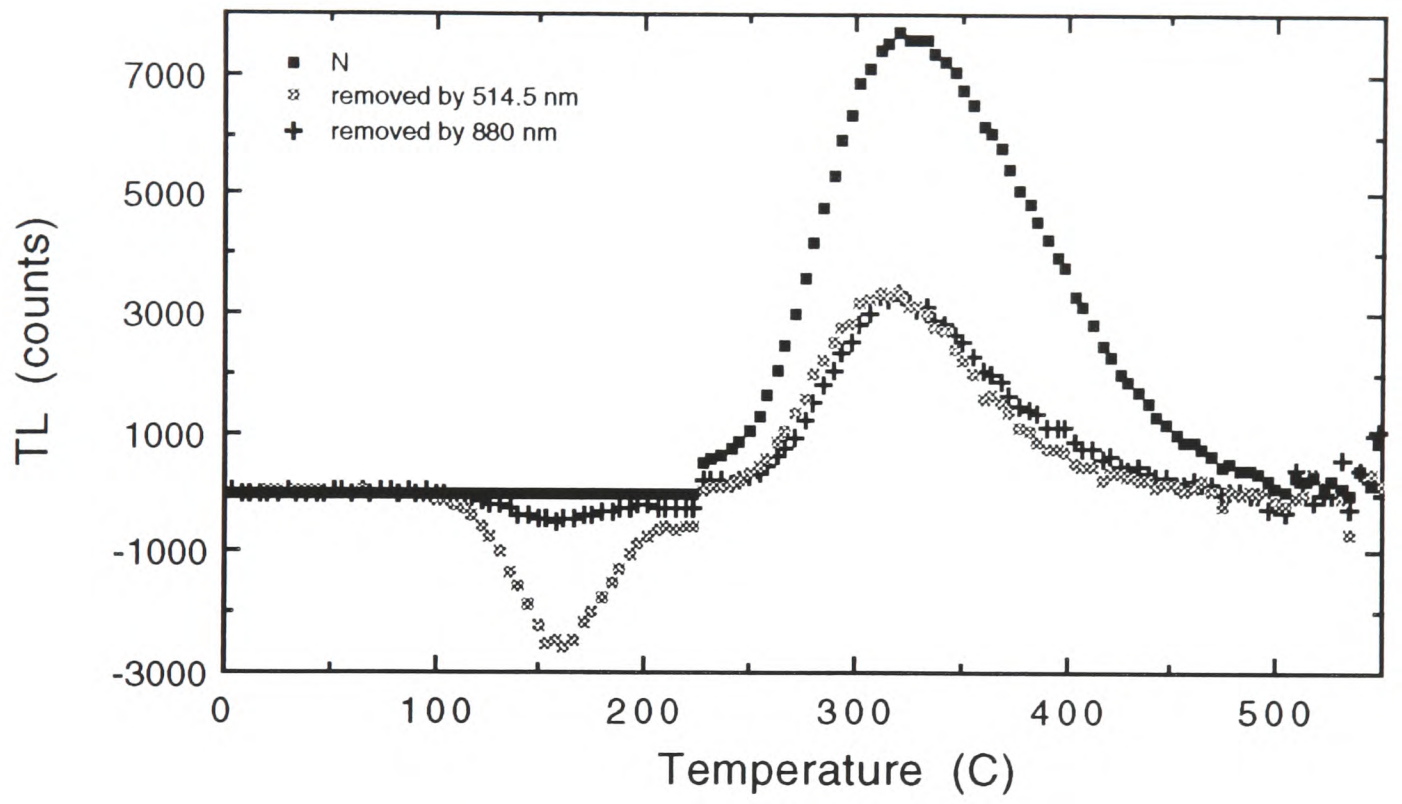


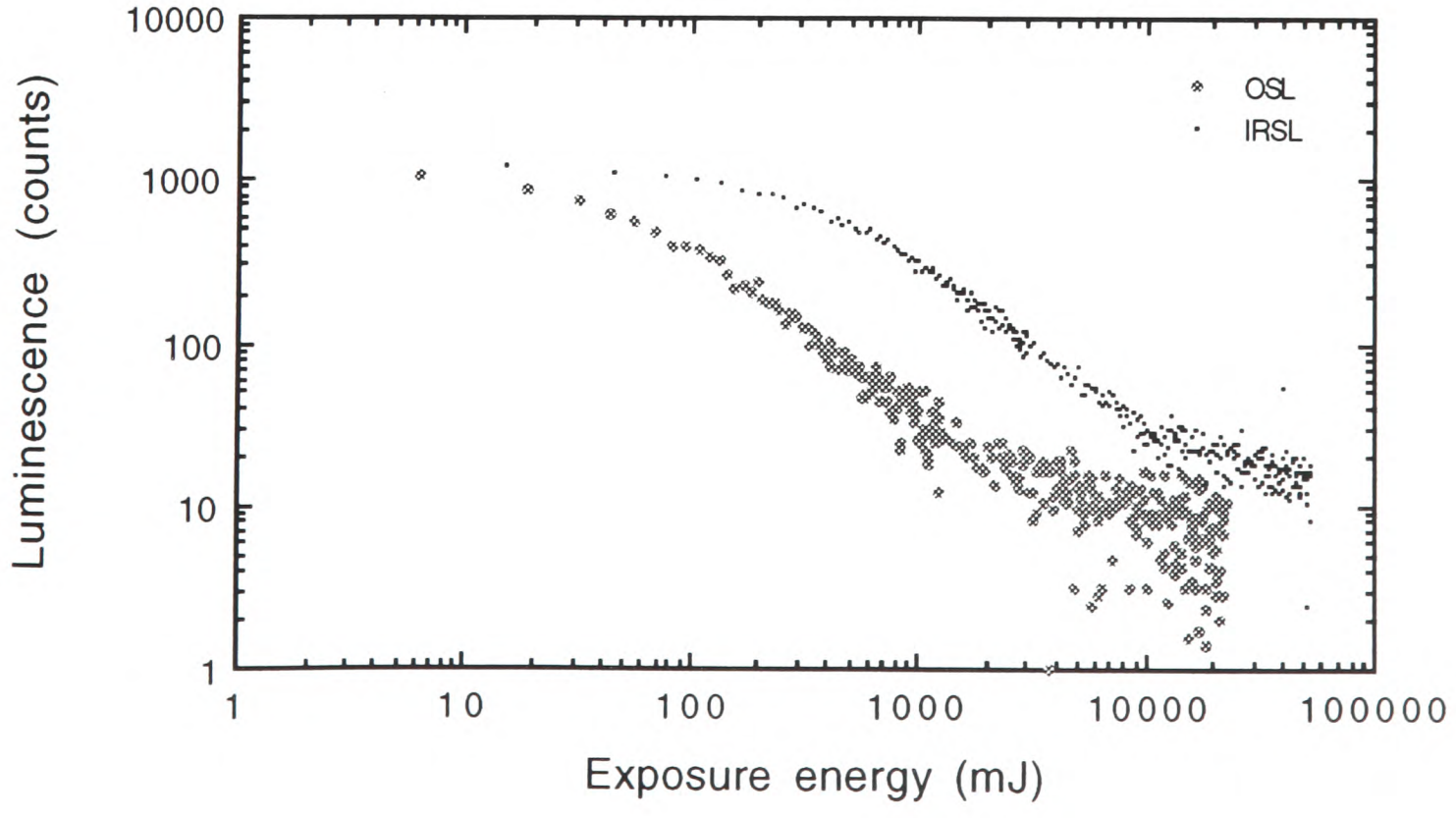




10. Z4 bytownite







FELDSPAR	Natural TL peaks			TL peaks observed after 514.5 nm exposure (22.5 J)			TL peaks observed after 880 nm exposure (54 J)		
	280-330 (C°)	330-400 (C°)	> 400 (C°)	280-330 (C°)	330-400 (C°)	> 400 (C°)	280-330 (C°)	330-400 (C°)	> 400 (C°)
5. No. 3062 microcline	305	390		305	390		305	390	
22. orthoclase	315	380	420	300	380	420	295	360	410
3. Z5 microcline	310	370	460	310	380	460	310	380	460
11. Z6 orthoclase	300	360		300	370		295	350	
21. Z9 microcline	295	345	410	295	350	430	290	345	420
14. Z11 microcline	300	360	460	300	370	460	290	360	460
13. Dup(C) microcline	300	360	430	300	360	440	300	360	440
1. adularia	300	340	460	300	360	460	300	350	460
20. Z9N microcline	300	350	425	300	350	430	300	350	430
9. Z15 sanidine	310		450	310		450	310		450
12. Patmos sanidine	310		450	310		450	310		450
16. 1947,199(2) anorthoclase	300	360	435	300	360	440	300	360	430
17. albite	310	360	405	320	350	405	300	350	400
18. Amelia albite	300			310	350		310	350	
15. Dup(A) albite	320				335	440	325		440
4. 17 oligoclase	305	370		305	370		305	370	
7. 18 oligoclase	315			315	360		315		
23. Dup(B) oligoclase	315				340		330		
19. BA6 labradorite	300	340			370		300	340	
6. 23 labradorite	300	340	460	300	390	460	300	390	460
24. Dup(D) labradorite		350			360			360	
2. 25 bytownite	300	350		295	360		295	350	
8. 26 bytownite	300	300-400			300-400		280	300-410	
10. Z4 bytownite	320				340		325		

Table 3.5.3.1 The approximate T_{max} values for the TL glow peaks observed before and after bleaching by 880 ▵ 80 nm IR (54 J total deposited energy) or 514.5 nm light (22.5 J total deposited energy). TL measurement was at 5 K/s. The TL peaks were identified by their visual prominence, hence there is an element of judgement in the assigned temperatures.

FELDSPAR	IRSL : Initial countrate Io (cps)	IRSL : final countrate If (cps)	Residual reached If / Io (%)	Fractional initial decay 2nd/1st sec	Initial decay rate (% / mJ)	Energy for 50 % depletion (mJ)	Energy for 90 % depletion (mJ)	IRSL (cps) after OSL	(IRSL after OSL)/Io (%)
5. No. 3062 microcline	59181 ±243	1218.7 ± 35	2.1	0.964 ± 0.006	0.12	1600	14000	864 ± 30	1.5
22. orthoclase	1724 ± 42	61.1 ± 8	3.5	0.974 ± 0.034	0.09	2500	18000	67 ± 11	3.9
3. Z5 microcline	4330 ± 66	48.3 ± 7	1.1	0.914 ± 0.022	0.29	780	5500	65 ± 11	1.5
11. Z6 orthoclase	13079 ± 114	67.8 ± 8	0.5	0.866 ± 0.013	0.45	720	4000	31 ± 10	0.2
21. Z9 microcline	244088 ± 494	3082.6 ± 56	1.3	0.910 ± 0.003	0.30	1170	8000	864 ± 30	0.4
14. Z11 microcline	38789 ± 197	443.1 ± 21	1.1	0.887 ± 0.007	0.38	930	6500	211 ± 17	0.5
13. Dup(C) microcline	35549 ± 189	465.1 ± 22	1.3	0.919 ± 0.008	0.27	1140	8000	204 ± 16	0.6
1. adularia	76010 ± 276	970.5 ± 31	1.3	0.879 ± 0.005	0.40	810	6000	427 ± 22	0.6
20. Z9N microcline	303239 ± 551	4178.1 ± 65	1.4	0.919 ± 0.003	0.27	1290	9000	1283 ± 37	0.4
9. Z15 sanidine	1685 ± 41	29 ± 5	1.7	0.875 ± 0.036	0.42	810	7500	19 ± 9	1.1
12. Patmos sanidine	1060 ± 33	27.5 ± 5	2.6	0.878 ± 0.045	0.41	750	7000	6 ± 8	0.6
16. 1947,199(2) anorthoclase	22 ± 5	10 ± 3	45.5	1.000 ± 0.292	0.00	-	-	1 ± 8	4.6
17. albite	110 ± 10	9.1 ± 3	8.3	0.773 ± 0.144	0.76	700	-	11 ± 9	10.0
18. Amelia albite	76906 ± 277	388.7 ± 20	0.5	0.877 ± 0.005	0.41	690	4000	75 ± 11	0.1
15. Dup(A) albite	2066084 ± 1437	23644.5 ± 154	1.1	0.870 ± 0.001	0.43	840	8000	16374 ± 128	0.8
4. 17 oligoclase	7121 ± 84	25.1 ± 5	0.4	0.824 ± 0.018	0.59	570	3500	19 ± 9	0.3
7. 18 oligoclase	1718 ± 41	14.6 ± 4	0.9	0.817 ± 0.036	0.61	510	2700	14 ± 9	0.8
23. Dup(B) oligoclase	43324 ± 208	108.9 ± 10	0.3	0.819 ± 0.007	0.60	570	3300	86 ± 12	0.2
19. BA6 labradorite	101 ± 10	7 ± 3	6.9	0.911 ± 0.144	0.30	70	-	8 ± 9	7.9
6. 23 labradorite	269 ± 16	13.3 ± 4	4.9	0.732 ± 0.094	0.89	510	5500	0 ± 8	0.0
24. Dup(D) labradorite	137 ± 12	5.9 ±2	4.3	0.847 ± 0.126	0.51	800	30000	0 ± 8	0.0
2. 25 bytownite	61 ± 8	7.8 ± 3	12.8	0.770 ± 0.194	0.77	1000	-	4 ± 8	6.6
8. 26 bytownite	1268 ± 36	39.2 ± 6	3.1	0.929 ± 0.040	0.24	1470	15000	17 ± 9	1.3
10. Z4 bytownite	1253 ± 35	8.1 ± 3	0.7	0.777 ± 0.043	0.74	390	2500	3 ± 8	0.2

Table 3.5.3.2 Some aspects of the IRSL signals for each of the feldspars. IR power at the sample was ≈ 30 mW/cm^2, and an exposure time of 1800 seconds gave a cumulative deposited energy of 54 J. Sample temperature was maintained at 20°C. The initial decay rates are calculated as (1-(2nd second counts / 1st second counts))/mJ. Errors assigned are from counting statistics only. The final two columns represent the IRSL signal remaining after an exposure to 22.5 J of 514.5 nm light.

FELDSPAR	OSL : initial countrate Io (cps)	OSL : final countrate If (cps)	Residual reached Io / If (%)	Fractional initial decay 2nd/1st sec	Initial decay rate (% / mJ)	Energy for 50 % depletion (mJ)	Energy for 90 % depletion (mJ)	OSL (cps) after IRSL	(OSL after IRSL)/Io (%)
5. No. 3062 microcline	18235 ± 135	198.2 ± 14	1.1	0.891 ± 0.011	0.87	200	2400	3000 ± 56	16.5
22. orthoclase	259 ± 16	13.5 ± 4	5.2	0.927 ± 0.090	0.58	700	8000	1105 ± 35	426.6
3. Z5 microcline	6777 ± 82	20.2 ± 4	0.3	0.786 ± 0.018	1.71	64	580	335 ± 21	4.9
11. Z6 orthoclase	4959 ± 70	32 ± 6	0.7	0.819 ± 0.021	1.45	69	663	254 ± 18	5.1
21. Z9 microcline	92039 ± 303	358.2 ± 19	0.4	0.865 ± 0.005	1.08	104	2000	4600 ± 68	5.0
14. Z11 microcline	22566 ± 150	101.1 ± 10	0.5	0.816 ± 0.010	1.47	75	900	1773 ± 43	7.9
13. Dup(C) microcline	7549 ± 87	95.4 ± 10	1.3	0.917 ± 0.017	0.66	244	3000	1105 ± 35	14.6
1. adularia	23740 ± 154	346.1 ± 19	1.5	0.936 ± 0.009	0.51	200	2000	3613 ± 61	15.2
20. Z9N microcline	97840 ± 313	552 ± 23	0.6	0.874 ± 0.005	1.01	125	1400	5520 ± 75	5.6
9. Z15 sanidine	4337 ± 66	38 ± 6	0.9	0.352 ± 0.030	5.18	<12	188	3252 ± 58	75.0
12. Patmos sanidine	613 ± 25	32 ± 6	5.2	0.847 ± 0.060	1.22	100	3000	49 ± 12	8.0
16. 1947,199(2) anorthoclase	86 ± 9	27.2 ± 5	31.6	0.989 ± 0.152	0.09	6000	-	51 ± 12	59.3
17. albite	129 ± 11	9.5 ± 3	7.4	0.915 ± 0.127	0.68	60	1500	11 ± 10	8.5
18. Amelia albite	37061 ± 193	20.8 ± 5	0.1	0.718 ± 0.008	2.26	44	263	1384 ± 38	3.7
15. Dup(A) albite	536031 ± 732	883.3 ± 30	0.2	0.881 ± 0.002	0.95	113	863	20353 ± 43	3.8
4. 17 oligoclase	2966 ± 54	46.9 ± 7	1.6	0.824 ± 0.027	1.41	75	450	146 ± 15	4.9
7. 18 oligoclase	1423 ± 38	28.8 ± 5	2.0	0.843 ± 0.039	1.26	65	1100	144 ± 15	10.1
23. Dup(B) oligoclase	30074 ± 173	26.9 ± 5	0.1	0.836 ± 0.009	1.31	68	350	879 ± 31	2.9
19. BA6 labradorite	68 ± 8	13.1 ± 4	19.3	0.662 ± 0.192	2.70	90	12000	15 ± 10	22.1
6. 23 labradorite	172 ± 13	11.7 ± 3	6.8	0.715 ± 0.118	2.28	63	1400	41 ± 11	23.8
24. Dup(D) labradorite	114 ± 11	6.8 ± 3	6.0	0.772 ± 0.142	1.82	60	1700	7 ± 10	6.1
2. 25 bytownite	34 ± 6	3.8 ± 2	11.2	0.412 ± 0.318	4.70	100	-	11 ± 11	32.4
8. 26 bytownite	359 ± 19	12.2 ± 3	3.4	0.822 ± 0.079	1.42	170	3000	47 ± 12	13.1
10. Z4 bytownite	1090 ± 33	10.4 ± 3	1.0	0.794 ± 0.046	1.65	65	350	26 ± 11	2.4

Table 3.5.3.3 Some aspects of the OSL signals for each of the feldspars. The 514.5 nm beam power at the sample was ≈ 12.5 mW/cm^2, and an exposure time of 1800 seconds gave a cumulative deposited energy of 22.5 J. Sample temperature was maintained at 20°C. The initial decay rates are calculated as (1-(2nd second counts / 1st second counts))/mJ. Errors assigned are from counting statistics only. The final two columns represent the OSL signal remaining after an exposure to 54 J of 880 ▵ 80 nm IR. Points of interest are the increased signal from 22. orthoclase, assumed to result from phototransfer to preferentially green-bleached TL peaks, and the inefficient removal of green stimulable signal from 9. Z15 sanidine by the prolonged IR exposure.

in particular have bleachable TL (including by IR) at glow curve temperatures exceeding 400°C.

4) There appears to be a range of bleachabilities even amongst samples of similar compositions.

5) The highly calcic species (labradorite and bytownite) display an apparently characteristic major PTTL peak at 160°C under 514.5 nm stimulation, with relatively less prominent IR transferred TL peaks.

These findings agree generally with those of Robertson *et al*, (1991) where TL of all samples studied (six alkali feldspars and an oligoclase) was bleached to varying extents, with rapid reductions observed in the oligoclase and Amelia albite TL. The oligoclase TL peak at 280°C was the only feldspar peak seen to show rapid selective bleaching similar to that of the 325°C TL peak in quartz. However, a result conflicting with the present study was reported for the anorthoclase, which was found by Robertson *et al* (1991) to have the most rapid bleaching. This sample was also known to fade and so led them to speculate that susceptibility to bleaching may possibly be of use as a diagnostic tool to detect fading.

Table 3.5.3.1 gives the T_{max} values for the identifiable TL peaks observed before and after bleaching. Although the "characteristic" feldspar peak at 280°C is seen in all samples, this observation must be qualified as some of these peaks are the remnants of lower temperature peaks which survived the preheat. The glow curves presented in Appendix I generally enable discrimination between "real" and remnant 280°C peaks. Considering possible manifestation of higher order kinetic effects: Amelia albite shows residual TL having a T_{max} displaced to a slightly higher temperature, (though either higher order kinetics or to a spectrum of trap energies giving rise to a spectrum of bleachabilities

are possible explanations).

An inspection of the glow curves (see Fig. 3.5.3.1) representing charge moved by the illuminations confirms that all samples undergo some bleaching at both wavelengths. Furthermore the existence of low temperature PTTL peaks in all samples demonstrates the retrapping of the charge untrapped by bleaching from the high temperature TL donor traps (and so supports the accepted description of feldspar kinetics as not first order). As a corollary, the prompt luminescence emitted during such bleaching - the OSL or IRSL - is assumed to also originate from these donor traps and so possess the same stability as the source TL glow peaks - this assumption is used in chapter 5 in concluding IRSL signal thermal stability by linkage to stable (kinetically determined) TL peaks. (However it is recognised that the depletion of a TL peak under a given illumination does not necessarily mean that detectable luminescence is simultaneously being emitted). It is noteworthy that in some samples, and especially in the variously bleached "naturals" shown in Appendix I, bleaching reveals subtle glow curve structure by "optical peak stripping".

The bleached glow curves and corresponding shine curves shown here lead directly to the postulate that the optically stimulable traps comprise at least two variants of a similar trapping centre. One variant, "green stimulable only", lacks the characteristic IR bleachability attributed by Hütt *et al* (1988) to an excited state in the trap. A second variant possesses this characteristic and so can be bleached by both green and IR wavelengths. That both wavelengths reduce TL at the same glow peaks suggests that the differences between the subsets of trap types do not result in a detectable alteration to the "primary" trap parameters, that is, the trapping state E and s values appear the same for each type of trap, when TL is measured at 5 K/s. Evidence supporting this interpretation

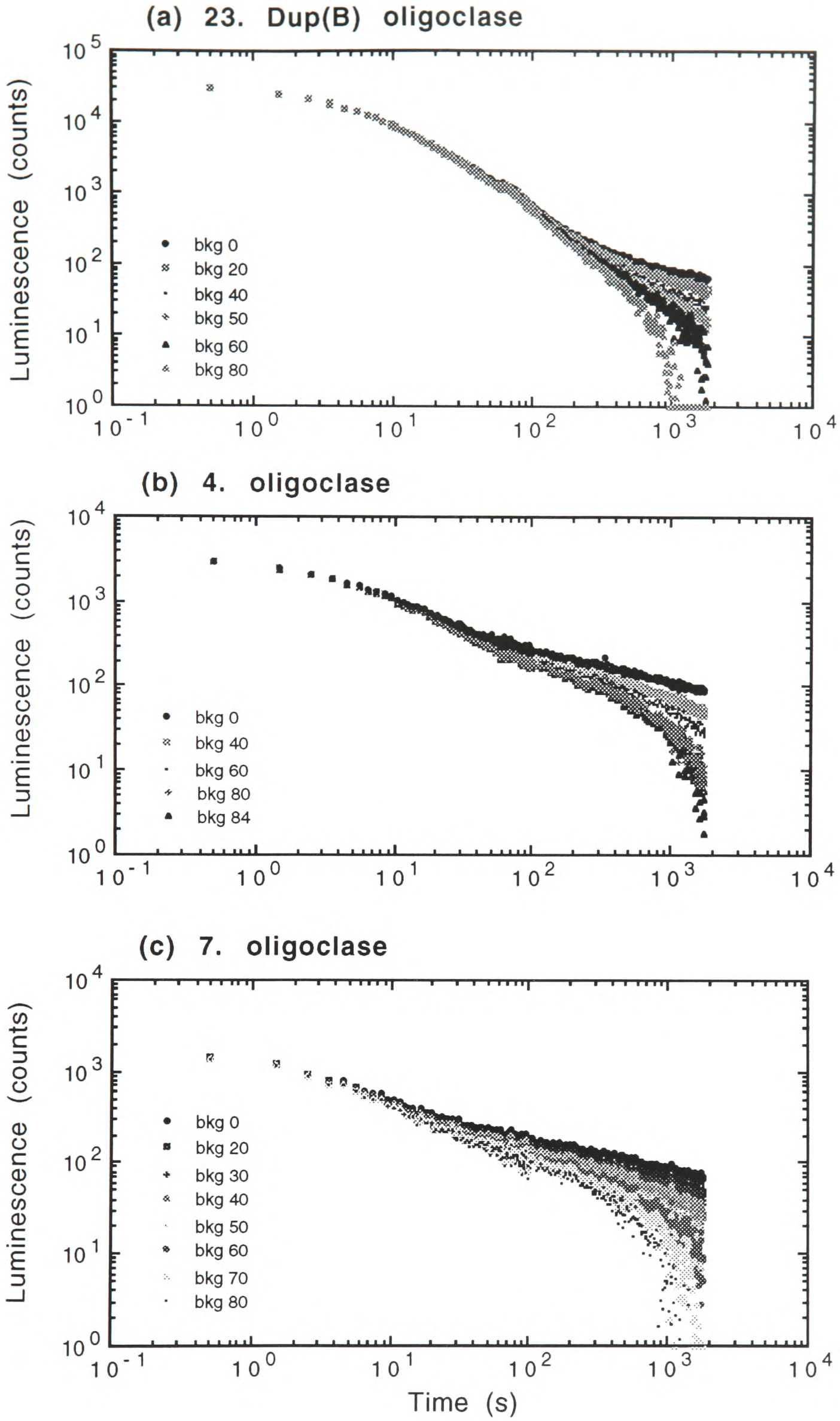


Fig.3.5.3.2 The families of IRSL shine curves resulting from the subtraction of various background values from the IRSL data for each oligoclase in an attempt to remove the sigmoidal flex apparent in the shine curves. Data plotted are counts/second.

is that in cases where significant IRSL is observed the final countrates reached (see Tables 3.5.3.2 and 3.5.3.3) appear too small for continued IR illumination to cause significant further reduction of the TL to the residual levels seen following the 514.5 nm exposure, and a significantly greater proportion of the green stimulable signal survives IR exposure than the converse. The question of the existence of two subsets of similar trap types is further investigated in Chapter 5 (having relevance to the kinetics of these peaks and also possibly to their fading behaviour).

It is notable that in all cases there is a substantially greater light sum from IRSL than from OSL; this is attributed to attenuation by the much more restrictive filtering in the latter case, but nonetheless highlights the signal/noise ratio advantage of IRSL over OSL.

The stimulated luminescence data are presented as recorded, with the only modification being the subtraction of background values determined as the mean countrate measured during illumination of ten clean stainless steel discs. As the subtraction of an inadequate background will result in a sigmoidal distortion of the shine curve (R.H. Templer, pers. comm. 1992), various backgrounds ranging from zero to the entire final countrate were subtracted from each of the three oligoclase samples to test the influence of this effect here. The oligoclase were selected as all three showed distinctly sigmoidal IRSL shine curves before any background subtractions were made. However Fig.3.5.3.2 shows that in all cases no assumed value of the subtracted background eliminated the sigmoidal flex of the shine curve. Consequently the interpretation given here for these cases of this curve form is that generally, as the primary luminescence source traps become depleted, contributions from less easily bleached traps and the combined effects of thermal and optical untrapping from shallow phototransfer peaks become increasingly

dominant. Sigmoidal shine curve forms are presumably observed when these latter sources of charge play significant retrapping roles and have thermal lifetimes at ambient temperatures or bleaching susceptibilities which combine to give a greater lifetime than possessed by the source traps under the conditions of measurement.

3.5.3.1 INITIAL DECAY RATES

Tables 3.5.3.2 and 3.5.3.3 show data quantifying aspects of the stimulated luminescence behaviour for both stimulation wavelengths.

The initial decay rates (IDR) are significantly greater for OSL than for IRSL, in agreement with the relative bleaching efficiencies of these wavebands (see section 5.2.3). However, the decay rates tabulated here may not represent "true" decay rates, as they are dependent on various factors affecting the transmission of stimulation photons into the volume of the sample material. These include :

(1) sample aspect and reflectivity with respect to the stimulation light

(2) distribution of sample on the disc, given that non-uniform illumination beam intensity profiles will result in a range of effective beam powers.

(3) the effective optical transmissivity of the sample material, (depending on the mean particle size and distribution of sizes as well as the optical transmittance).

(4) shadowing and beam scattering effects from adjacent grains.

For example, the K-feldspars illustrate the range of IDR observed, from 0.09 % / mJ to 0.45 % / mJ for IRSL and 0.51 % / mJ to 1.71 % / mJ for OSL. Overlapping the range for feldspar OSL is the range for quartz OSL (ie, 0.44 % / mJ to 0.60 % / mJ for five natural samples and from 0.55 % / mJ to 0.61 % /mJ for the same five samples,

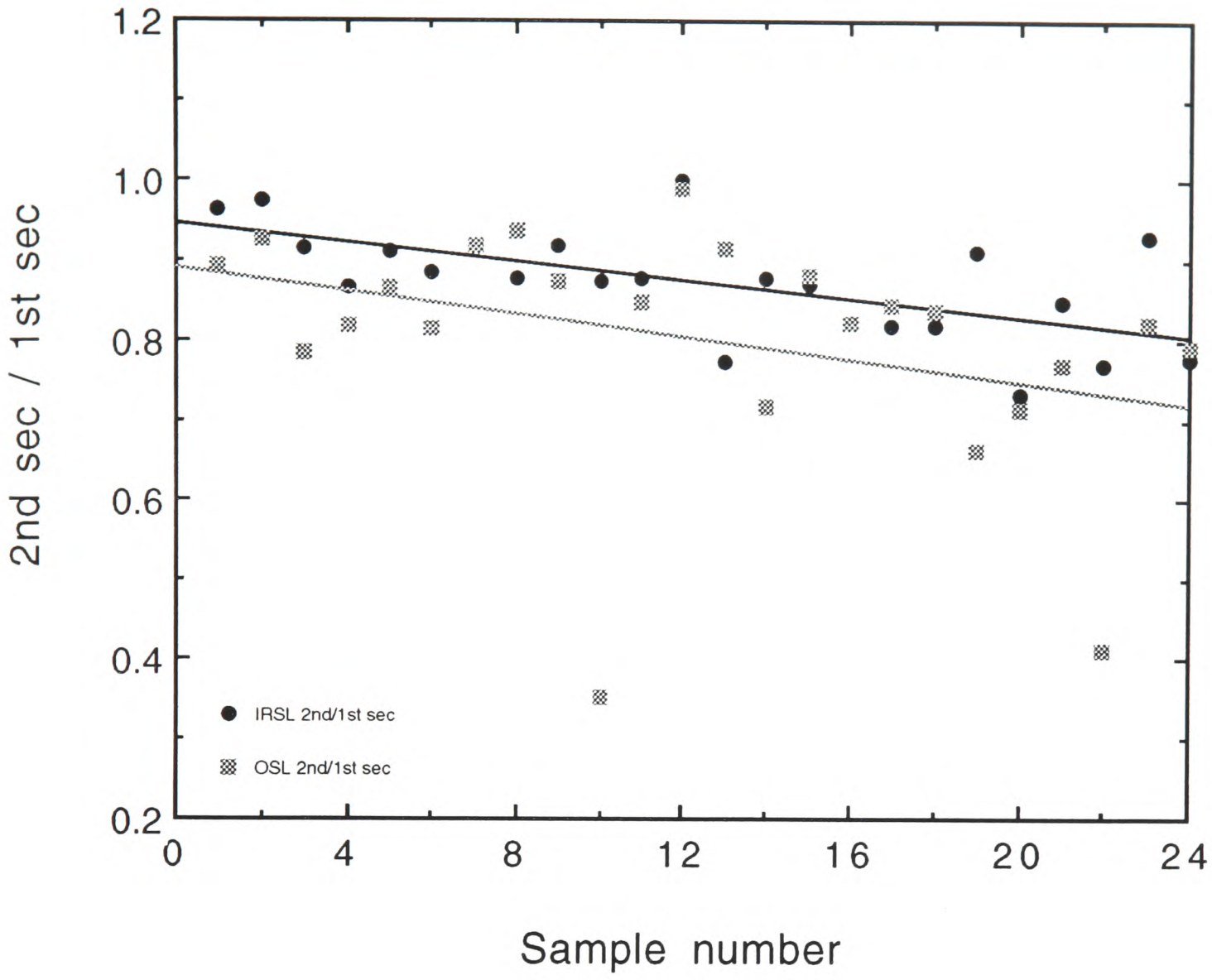


Fig.3.5.3.1.1 The initial decay rates for each of the feldspar samples (plotted against the sample numbers assigned in Table 3.2.1) under exposure to 514.5 nm light and IR illumination. Powers at the sample were ≈ 12.5 mW/cm^2 of 514.5 nm light and ≈ 30 mW/cm^2 of IR. Sample temperatures were 20°C.

natural+120 Gy portions). The IDR, and other curve-shape based parameters, should therefore not be regarded as characteristic and precisely definable for a given mineral species. Further complications in defining the initial decay rate arise from any sample-to-sample variation and higher order kinetic effects (the latter may lead to some dependence of this parameter on the distribution of trapped charge populations). Some indication of this is suggested in Fig.5.8.4.2.2.1.(a)-(c). The IDR data are plotted in Fig.3.5.3.1.1 against the catalogue numbers assigned to them earlier (see Table 3.2.1). Both the OSL and IRSL show indications of increasing initial decay rates as sample composition varies from potassic through sodic to calcic, though again there is overwhelming scatter superimposed on the trend lines.

3.5.3.2 ABSENCE OF PEAK-SPECIFIC BLEACHING

To clarify further whether peak-specific bleaching occurred under either the IR or 514.5 nm exposures, ratios were plotted of the TL removed by the IR exposure with the "natural" TL (see Fig.3.5.3.2.1) and the ratios of the TL removed by the two bleaches are similarly compared in Fig.3.5.3.2.2.

Fig.3.5.3.2.1 shows that bleaching proceeds uniformly across the glow curves in general, (though in some cases it seems likely that the 360°C peak in K-feldspar resists bleaching by IR more strongly than the remainder of the glow curve, this behaviour is not ubiquitous). Negative values of the ratio occur where TL peak growth by phototransfer exceeds reduction of the natural by bleaching, resulting in a residual TL level greater than that of the natural.

There is a possibility that the ratio trends downwards in many samples above ≈

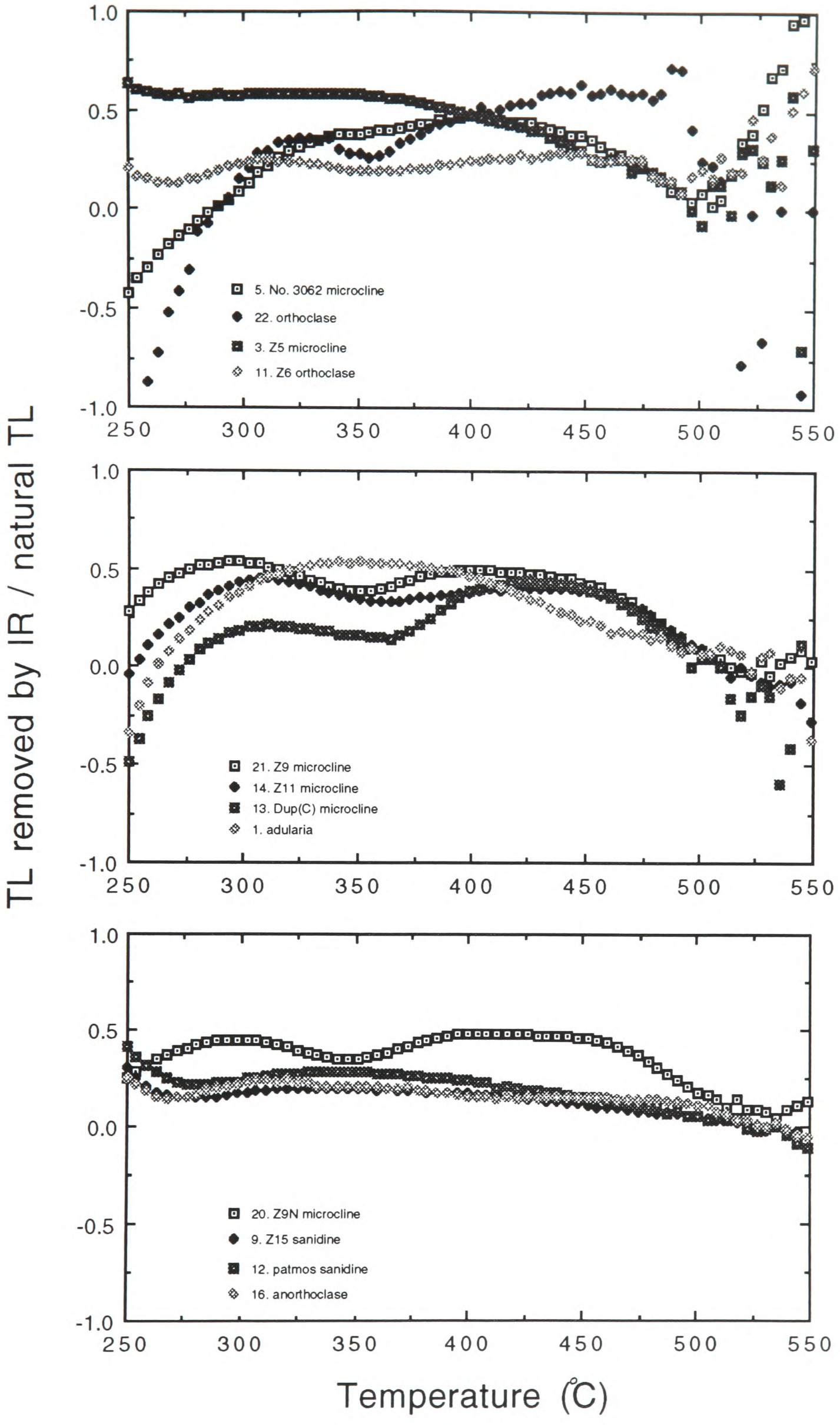
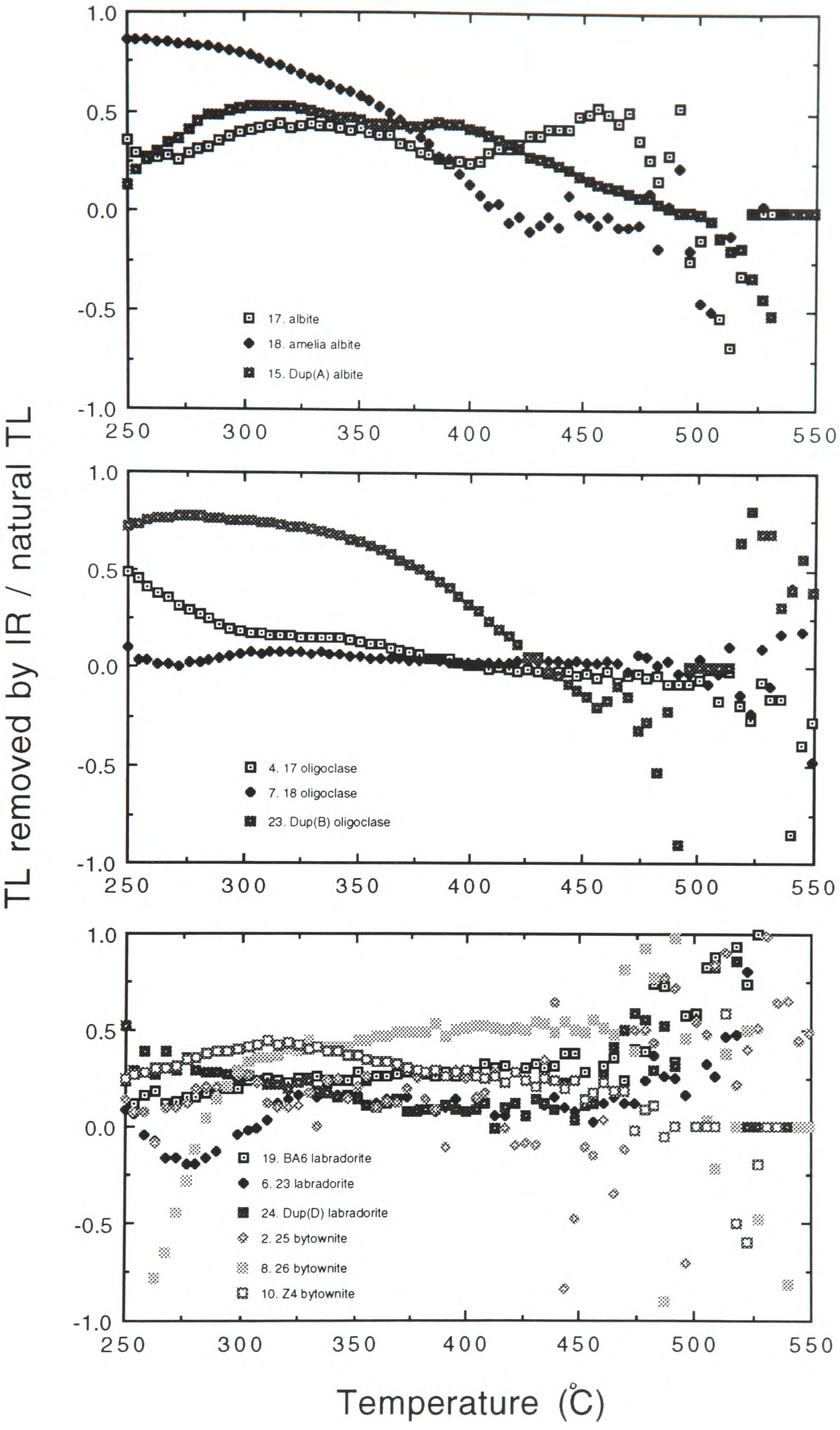


Fig.3.5.3.2.1 The ratio of TL removed by IR exposure to that of the natural TL. The negative values, particularly at temperatures < 300°C, indicate where phototransferred TL in the bleached glow curves exceeds the natural TL.


TL removed by IR / natural TL
1.0
0.5
0.0
-0.5
-1.0
250
300
350
400
450
500
550
17. albite
18. amelia albite
15. Dup(A) albite
4. 17 oligoclase
7. 18 oligoclase
23. Dup(B) oligoclase
19. BA6 labradorite
6. 23 labradorite
24. Dup(D) labradorite
2. 25 bytownite
8. 26 bytownite
10. Z4 bytownite
Temperature (°C)

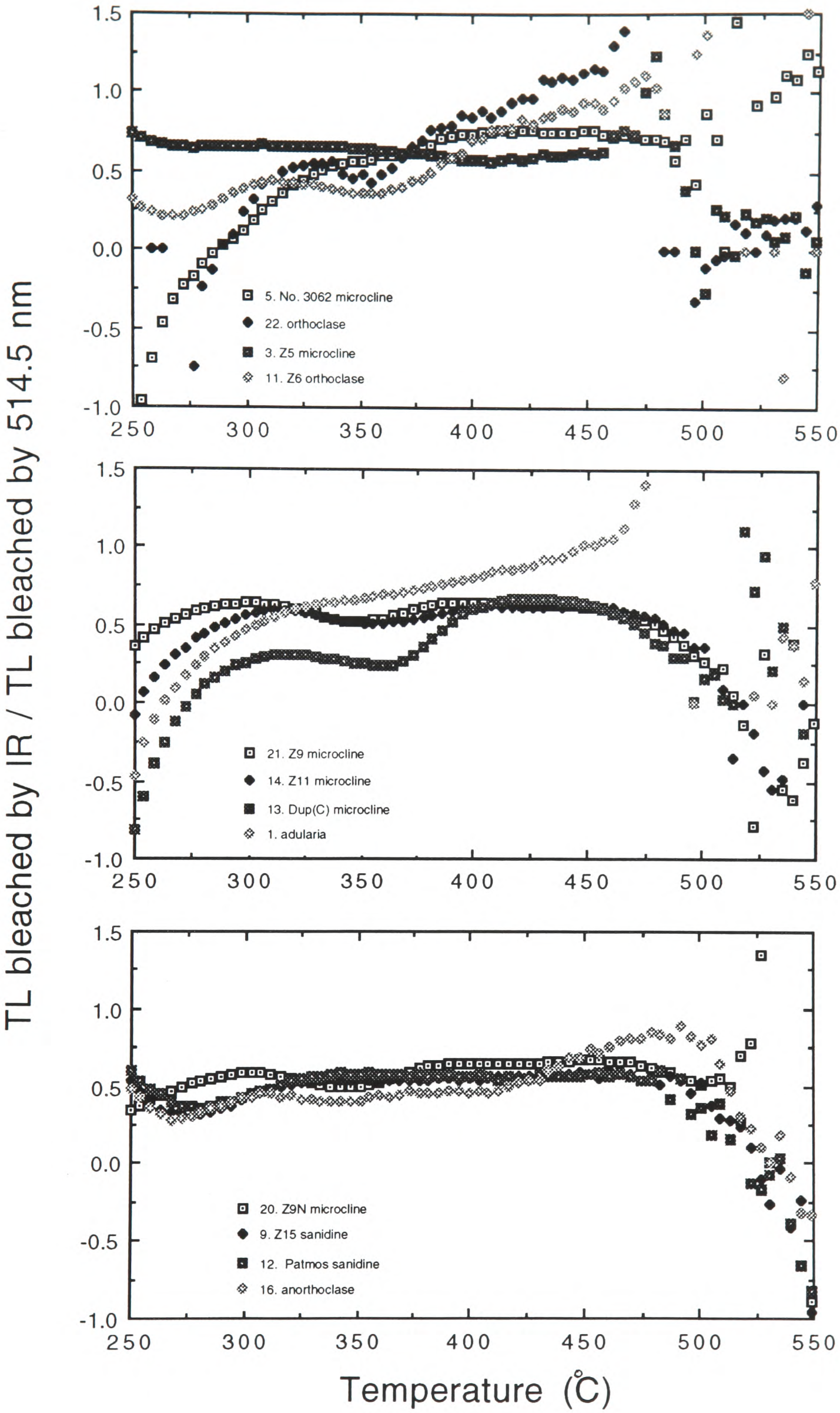
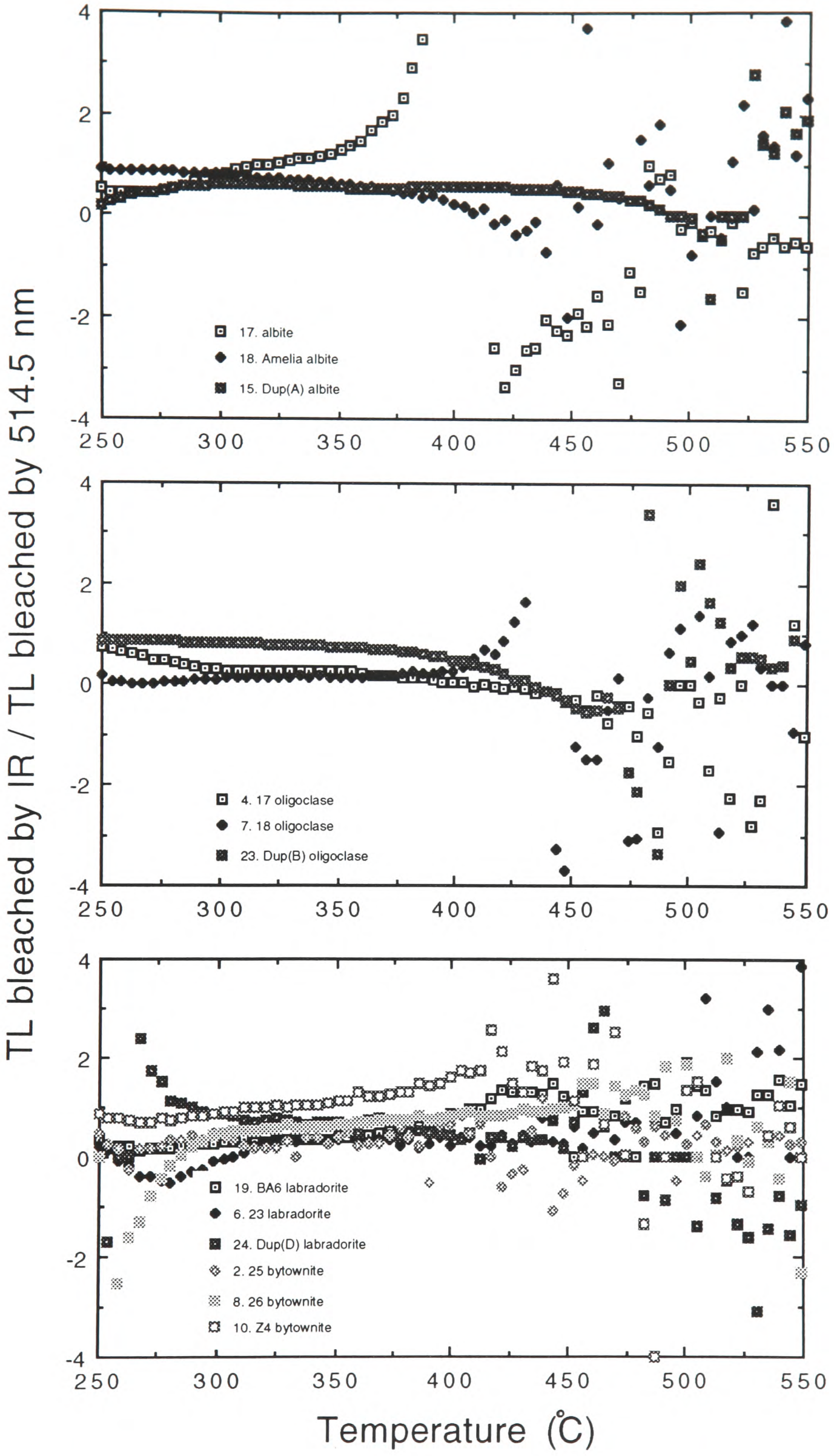


Fig.3.5.3.2.2 The ratio of TL removed by IR exposure to that removed by 514.5 nm exposure. The negative values, particularly at temperatures < 300°C, indicate where phototransferred TL in the bleached glow curves exceeds the natural TL.


TL bleached by IR / TL bleached by 514.5 nm
4
2
0
-2
-4
250
300
350
400
450
500
550
17. albite
18. Amelia albite
15. Dup(A) albite
4. 17 oligoclase
7. 18 oligoclase
23. Dup(B) oligoclase
19. BA6 labradorite
6. 23 labradorite
24. Dup(D) labradorite
2. 25 bytownite
8. 26 bytownite
10. Z4 bytownite
Temperature (℃)

450°C, indicating increasing resistance to IR bleaching at these temperatures. An interesting inference stems from the observation that for samples 3, 4, 9, 12, 15, 18, and 23 the ratio is trending downwards from at most ≈ 300°C, and for samples 18 and 23 the drop is particularly pronounced. As these two samples possess broad ATL peaks (the "complete" glow curve above room temperature, as shown in Appendix I), of which the higher temperature TL is simply a remnant surviving the preheat, the decreasing ratio is interpreted as indicating a broad band of trap energies, with the deeper traps (at higher glow curve temperatures) having a lower susceptibility to bleaching.

The ratios of the bleached TL are shown in Fig.3.5.3.2.2 to help identify any peaks displaying preferential response to either wavelength. With the possible exception of the 360°C TL peak in K-feldspar (as mentioned above), both wavelengths appear generally to bleach the same peaks, though not necessarily to the same extents or with the same efficiencies. The obvious exceptions are the peaks at 300°C in sample 5 (microcline), 360°C in sample 13 (microcline) and sample 21 (microcline) and 280°C in sample 8 (bytownite).

3.5.3.3 RELEVANCE TO STABILITY

The apparent lack of a single source TL peak or well defined hierarchy of bleachability for stimulated luminescence from feldspars (unlike the case of the 325°C peak in quartz) rules out the practical possibility of resolving between fading and non-fading signals by selection of stimulation wavelength and TL peak monitored.

The ubiquity, in the K-feldspars, of IR bleachable TL peaks at glow curve temperatures exceeding 350°C leads to the conclusion that none of the preheats in use in

optical dating procedures will reliably remove the IRSL from a feldspathic sample. This finding is in complete agreement with an extensive study on the effects of preheating on the IRSL signal from European loess (Questiaux, pers. comm. 1992). The contrary observation by Aitken and Xie (1991) refers only to a single sample and evidently cannot be taken as the general rule.

Regardless of the precise source peaks of the IRSL, that there are IR bleachable peaks at glow curve temperatures of ≈ 400°C strongly suggests that the IRSL originating from these peaks can be expected to be thermally stable over lifetimes greater than those over which dose saturation would curtail application of optical dating. To confirm this deduction it is necessary to directly measure the kinetic parameters of these peaks - this work is described in Chapter 5.

3.6 THERMAL ACTIVATION CHARACTERISTIC (TAC) CURVES

The search to find a luminescence characteristic correlated to fading behaviour led to the measurement of TAC curves for each of the feldspar samples. The speculation was that related mechanisms, ie, ion mobility or thermally activated hole movement, may be operant in both thermally activated sensitization and fading. Previously, TAC curves have only been reported by Bailiff (1987), who found 110°C TL peaks present in two samples of plagioclase studied (an albite and a labradorite), with the albite showing a maximum sensitization at 500°C, with Sn/So ≈ 20. However, no other reports of significant sensitization induced by repeated thermal cycling have been made (and indeed the absence of such behaviour has made possible the development of single-aliquot methods (Duller, 1991) which rely on limited sensitivity changes).

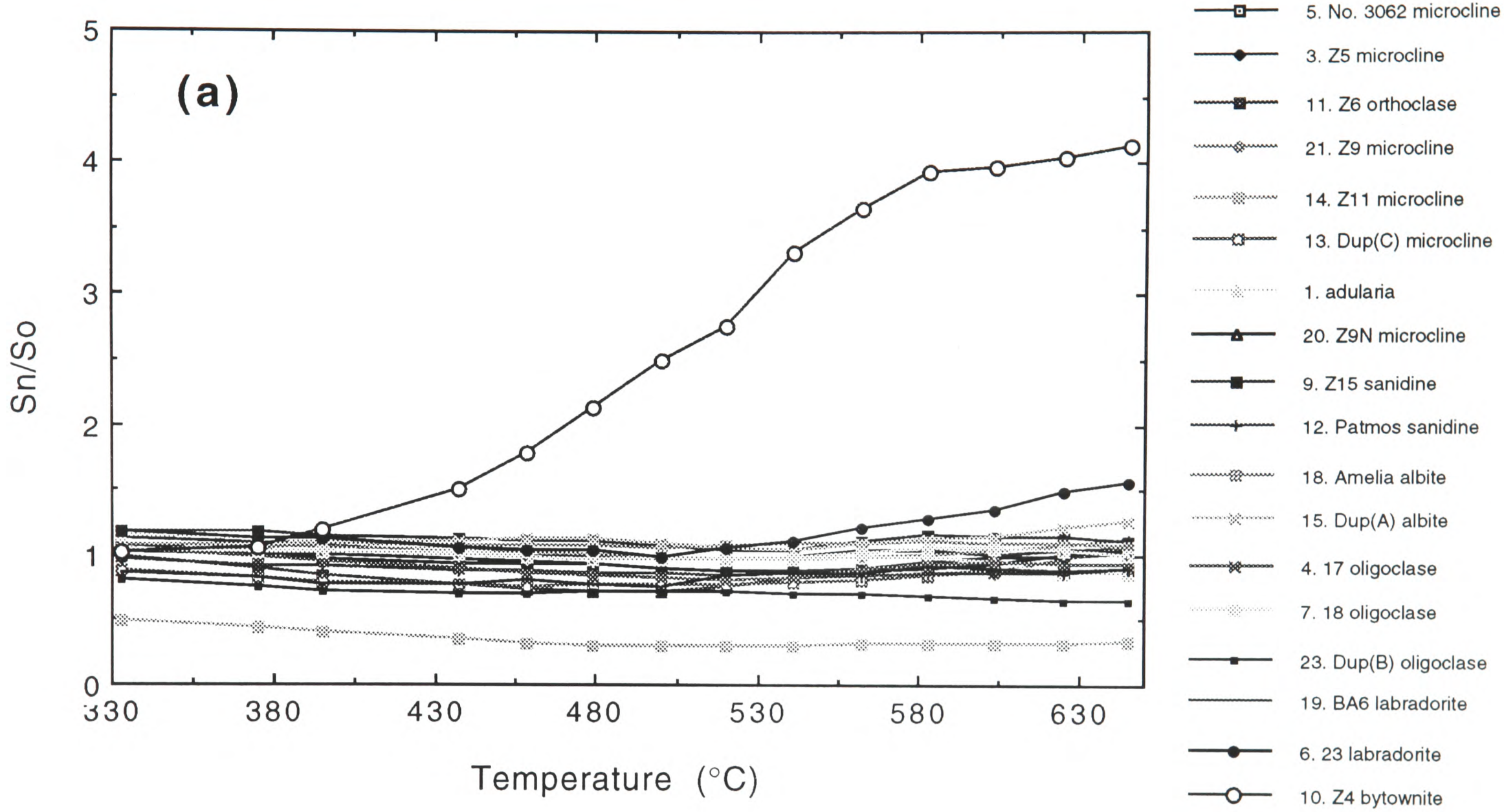
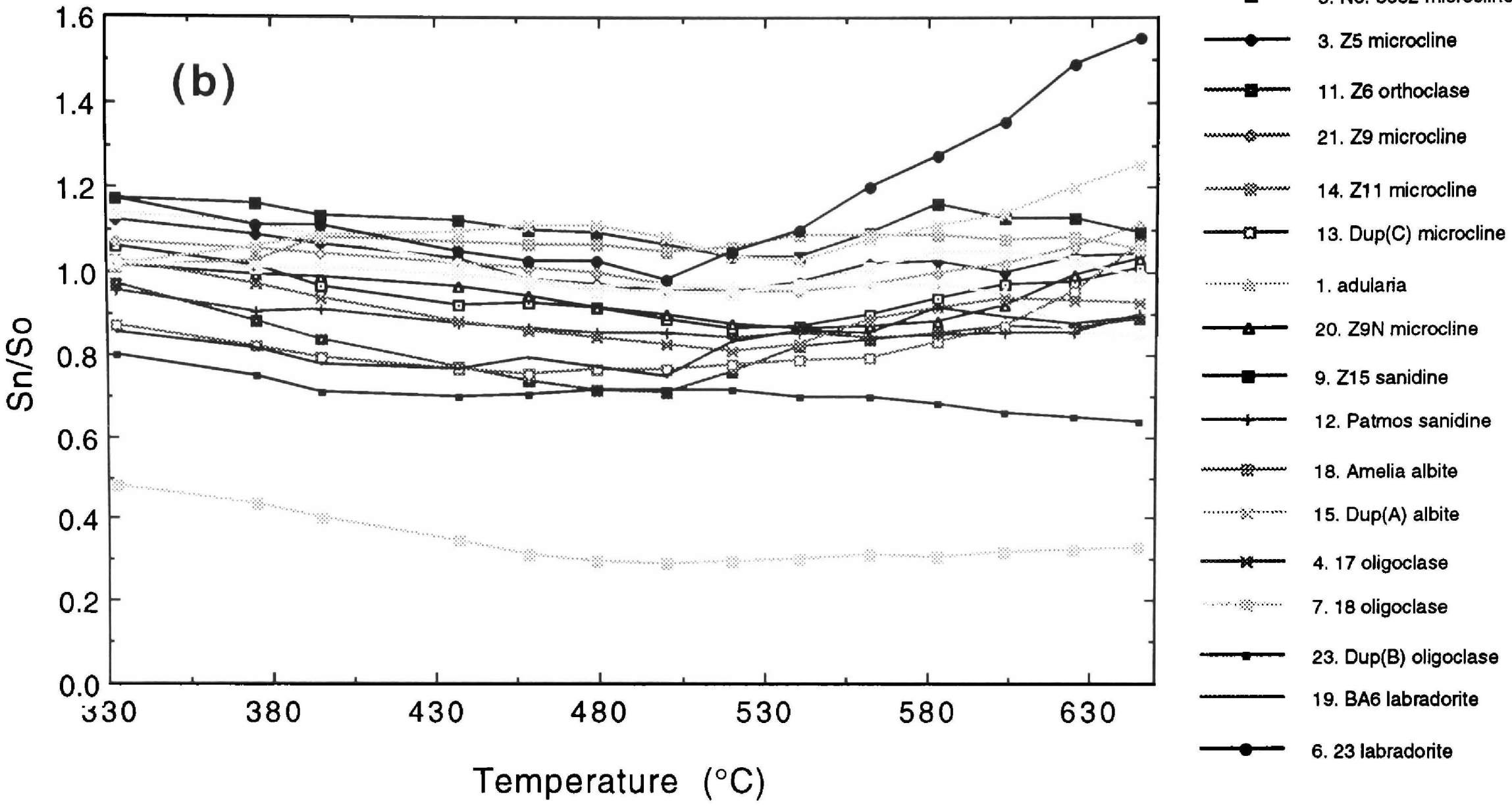


Fig.3.6.1 (a) The TAC curves of each sample; **(b)** the same data set but with sample 10. Z4 bytownite excluded.


(b)
Sn/So
1.6
1.4
1.2
1.0
0.8
0.6
0.4
0.2
0.0
330
380
430
480
530
580
630
Temperature (°C)
5. No. 3062 microcline
3. Z5 microcline
11. Z6 orthoclase
21. Z9 microcline
14. Z11 microcline
13. Dup(C) microcline
1. adularia
20. Z9N microcline
9. Z15 sanidine
12. Patmos sanidine
18. Amelia albite
15. Dup(A) albite
4. 17 oligoclase
7. 18 oligoclase
23. Dup(B) oligoclase
19. BA6 labradorite
6. 23 labradorite

"Natural" portions of each sample were attached to rhodium plated copper discs using silicone oil. Measurements were made using a Risϕ automated TL glow oven, with the procedure as follows:

(1) thermal wash (heat to 180°C at 5 K/s, stop at that temperature, no reheat)

(2) test doses of either ≈ 0.07 Gy or ≈ 0.7 Gy depending on sample TL sensitivity

(3) heat to 180°C at 5 K/s, with reheat, to measure TL - this value is S_o

(4) heat twice to the first activation temperature (333°C)

(5) test doses of either ≈ 0.07 Gy or ≈ 0.7 Gy depending on sample TL sensitivity

(6) heat to 180°C at 5 K/s, with reheat, to measure TL - this value is S_{333}

(7) heat twice to the next activation temperature (375°C)

(8) test doses of either ≈ 0.07 Gy or ≈ 0.7 Gy depending on sample TL sensitivity

(9) heat to 180°C at 5 K/s, with reheat, to measure TL - this value is S_{375}

(10) repeat steps (4)-(6) with successively higher activation temperatures until the final activation temperature (645°C).

The ratios S_{TEMP}/S_o are plotted for each activation temperature and so build the TAC curve (the TL in each case is that integrated in the region below 180°C). Fig.3.6.1(a),(b) show the TAC curves of each sample.

3.6.1 RESULTS AND DISCUSSION

Only five samples show sensitivity changes greater than 20 % of the initial sensitivity, and of these only two highly calcic samples (6. 23 labradorite and 10. Z4 bytownite) show significant increases. The sensitizations appear to be restricted to the ≈ 170°C TL peak in these two samples, but the other three samples (14. Z11 microcline, 15.

Dup(A) albite and 23. Dup(B) oligoclase) show uniform change across the entire glow curve temperature range monitored (0°C - 210°C). These findings apparently conflict with those of Bailiff (1987); possible explanations are: sample-to-sample variations, possible quartz contamination in Bailiff's samples, or that the early and complete saturation of the sensitization discussed by Bailiff (1987) did exist and had been activated in these samples before measurements commenced (however no evidence was found in the current work for the existence of such sensitization). The conclusion is that no correlation between fading and the magnitude of sensitization is apparent, and the most striking feature is the apparent absence of sensitization in most cases which is in accord with the common perception that the feldspar minerals are not greatly susceptible to sensitivity changes resulting from thermal cycling.

3.7 SUMMARY

Principal conclusions drawn from the studies described in this chapter are:

1) Luminescence sensitivities (TL, OSL and IRSL) vary greatly even within given feldspar species; the greatest range is seen in the high K and high Na samples.

2) IRSL emission spectra measured here in general parallel TL spectra published by others, and with prominent emission peaks at ≈ 330 nm, 410 nm and 570 nm (the relative proportions of which are species dependent).

3) Examples of feldspars of all species were found to bleach significantly under both IR and green light. No peak-specific bleaching correlating to feldspar species was seen

4) The feldspars studied here do not display significant thermal activation of the low temperature TL (temperatures < 200°).

CHAPTER 4 ANOMALOUS FADING OF FELDSPAR LUMINESCENCE

4.1 INTRODUCTION - AN OVERVIEW AND NOMENCLATURE

A variety of phenomena giving rise to age shortfalls have been reported in the literature at the time of writing. The principle purpose of this chapter (and the following) is to address some of these effects from the viewpoint of their impact on dating and investigate means of alleviating this impact.

Although a range of minerals exhibit fading, this thesis confines study to feldspathic materials, principally because of their widespread use for dating and on account of the specificity with which the luminescence can be stimulated from the feldspar minerals of a polymineral sample using IR stimulation (Spooner and Questiaux, 1989). The intent was to investigate the further possibility, opened by this mineral selectivity, that the signal from a single feldspar species may be free of fading altogether, or at the least fade via a mechanism permitting feasible isolation of a stable dating signal (analogous to the findings on zircon by Templer, (1986b)), and so permit reliable dating using some feldspar species.

In this section the types of age shortfall and effects to which these have been attributed are briefly introduced, along with some comments as to their generality, and finally an attempt is made to clarify nomenclature.

The various types of age underestimations are listed below, along with possible causes:

(1) "Anomalous" fading (Wintle, 1973, 1977), typically manifest as "overnight"

loss of artificially-induced TL during storage at room temperature, even from the 400°C-500°C region of the glow curve. Independent of sample grain size. This fading was found by Visocekas (1976, 1979, and 1985) to be explicable with a tunnelling model, and subsequently Templer (1986a,b) demonstrated that certain other cases, notably zircon and pumice, were well explained by the localised transition model. (A brief precis of attempts to circumvent this fading is given in Spooner, 1992).

(2) "Mid-term" fading (Xie and Aitken, 1991); this was introduced by Xie to explain dating results from a long loess section at Duanjapo, near Xian, China. A correction procedure based on a hypothesised athermal fading component comprising ≈ 40% of the TL and having a lifetime of ≈ 10^3-10^4 a was found to give dates in accord with expectation. This model is consistent with the localised transition model of anomalous fading (Templer, 1986a,b). General applicability presumably depends on local mineralogy.

(3) The "100 ka" limit effect (Debenham, 1985 and Wintle, 1985). This affects all old fine grain samples so far dated, and gives a practical age limitation of ≈ 50 ka for accurate dating. Postulated by Debenham (1985) as due to fading of luminescence centres.

(4) "Proportional" age shortfall such as reported by Dijkmans and Wintle (1989), Grün *et al* (1989), Balescu *et al* (1992) and Balescu and Lamothe, (1992). The latter works showed significantly greater ages from the use of blue transmitting filters (Corning 7-59) leading to a proposed explanation based on optical absorption of luminescence of UV wavelengths, by Wintle and Duller, (1991). This affects only coarse grain K-feldspars.

(5) Possible thermal instability of high temperature feldspar TL limiting the dating age range to less than the ultimate limit imposed by dose saturation (Hütt and Jaek, 1989), and named "long-term" fading by Mejdahl, (1988). Mejdahl (1988) studied "infinitely old"

alkali feldspars extracted from Tertiary sand, and found a range of lifetimes from 800-5400 ka, fitting saturating exponentials. He interpreted this as showing that lifetimes obtained for alkali feldspar by kinetic methods (Strickertsson, 1985) were overestimates, and that the luminescence underwent a long-term fading of the entire signal, reaching a dynamic equilibrium dependent on dose rate and ambient temperature in very old samples. Based on these data he then proposed a correction procedure. Although demonstrated by Mejdahl for only coarse grain alkali feldspars, thermal instability of this nature would affect all grain sizes. This effect sets an upper limit of ≈ 500 ka to the age range datable using the high-potassium alkali feldspars.

(6) Dose rate effects in potassium feldspars, manifest as enhanced trapping probabilities for the deeper (dating) traps during laboratory irradiation (Wintle and Packman (1988), and Mejdahl *et al* (1992)). This follows from the hypothesis that dose saturation reduces competition from the shallower traps not ordinarily significantly populated at the lower dose rates encountered in nature (typical natural dose rate ≈ 2 Gy/ka, compared to typical laboratory dose rate ≈ 2 Gy/minute; the dose rate used by Mejdahl *et al* (1992) was 70 Gy/minute). These dose rate effects are anticipated from potassium feldspar in particular (given the significance of the lower temperature TL peaks - see Appendix I), independent of grain size, and in principle can occur with any mineral having shallow traps.

(7) Weathering-induced changes to feldspar grains, presumably affecting fine-grains more than coarse grains.

(8) Systematic errors in the internal dose calculations for potassium feldspars.

(9) Age shortfall can also occur if the regeneration dating method is used, due to sensitivity increase during bleaching prior to regeneration. Conversely, age overestimation

can occur when there is a sensitivity decrease. (Wintle (1985), Rendell and Townsend, (1988), Li and Wintle, (1991), and Li (1992)).

The above age underestimations fall broadly into three categories: (A) methodological artifacts (4), (6), (8) and (9); (B) thermal fading (5); (C) "fadings" (1), (2), (3) and (7).

Considering prospects for dealing with each category:

(A) The methodological artifacts can in principle be dealt with: the fractional age shortfall attributed to self-absorption of the UV emissions within coarse grain potassium feldspar has been countered (Balescu and Lamothe, 1992) by selection of filters such that only visible emissions, which are not significantly self-absorbed, are measured. Alternatively, a smaller grain size (< 50 μm Wintle, pers. comm.,1992) can be used, or the coarse grain samples crushed down to below 50μm.

Promising results by Mejdahl *et al* (1992) have indicated that dose rate effects in potassium feldspars may be amenable to irradiation at elevated temperatures; work is in progress at Oxford (Questiaux, pers. comm. 1992) to assess independently the validity of this approach, as well as to establish whether or not it occurs at the more typical laboratory dose-rates of a few Gy/minute.

The regenerative method should be used with great circumspection, and preferably avoided.

Finally, a re-evaluation is required of the internal dose-rate contributions from the U and Th α-irradiation, K and particularly Rb (Questiaux, 1991).

(B) Thermal instability of the trapped charge from the high temperature (> 300°C) glow peaks for old samples is a fundamental problem (Hütt and Jaek, 1989), but can be corrected for, according to Mejdahl, (1988), but even so limits dating to samples of age

less than that at which dynamic equilibrium is approached. Accurate kinetic determinations should reveal this effect (see chapter 5).

(C) The "anomalous", "mid-term" and "100 ka limit long term" fadings. The latter two are the most difficult to define or deal with, as laboratory study is not feasible, and the precise cause of these effects remains unknown. Anomalous fading has a several possible causes, and different potential solutions; the detection and removal of anomalous fading are later considered at length. Weathering effects (though not strictly a "fading") are included here as they may contribute to both "mid-term" and "long-term" fadings, if not be the sole cause.

Regarding nomenclature: the above effects all contribute to age underestimations in various cases yet are necessarily not all aspects of the same phenomenon. It is therefore not correct to assign an "umbrella" term such as "anomalous" fading to cover all. The terms which are recommended for these effects are given below.

Methodological effects are subdivided into optical self-absorption (4), competition during dosing (6) and dosimetric considerations (8). "Apparent fading" suitably describes these effects.

The use of "long term" fading to describe the apparent thermal instability (5) is considered too ambiguous, and "thermal instability" will be used here. This follows from general usage of "long term" fading as referring to that identified by Debenham (1985) for fine grain samples.

The term "anomalous fading" is retained, despite the later suggestion of "fading" (Clark and Templer, 1988), only as a convenience (noting that strictly this fading is not "anomalous", but may in some cases be predictable from correctly measured kinetics - see section 4.2.4). Anomalous fading is taken as referring to loss of luminescence observable

over laboratory timescales from the high temperature region of the glow curve (here defined as that TL surviving a preheat of 60 seconds at 220°C). "Mid-term" and "long term" fading are taken to refer to the effects first described by Xie and Aitken (1991) and Debenham (1985) respectively. These are possibly mediated by similar mechanisms to the short term anomalous fading observed in the laboratory, simply possessing a greater lifetime.

In this thesis effort was concentrated initially on identifying and attempting to circumvent anomalous fading, in response to the generality of the problem - anomalous fading can affect any dating using feldspathic materials regardless of the age range. Thermal instability of feldspar luminescence was also investigated at a later stage (see chapter 5).

Although the stability of feldspar luminescence for long range dating remained uncertain, the original work (IR stimulation of K-feldspar) by Hütt *et al* (1988) had reported a thermal trap depth of ≈ 2.0 eV and dating results which suggested effective thermal stability. This conclusion was supported by Spooner and Questiaux (1989) where extended IR bleaching removed 60% of the natural TL (at 320°C temperature abscissa) of an old loess sample (220-320 ka, Lab. ref. 722t1, from Achenheim, France). Glow curve shape changes extended to 400°C, the inference being that such dominance of the TL was unlikely from the residual of a thermally unstable trap or a trap strongly afflicted by non-thermal decay, at these glow curve temperatures.

4.2 ANOMALOUS FADING

4.2.1 INTRODUCTION AND PRELIMINARY RESULTS

However, neither of the results of the final paragraph (previous section) excluded the possibility that anomalous fading was present in IRSL (and OSL) of other samples but as yet unreported, although this situation was not of great significance if routinely used thermal prefading treatments adopted by various laboratories (i.e., ≈ 3 days at 125°C (Templer, 1985), 2 -4 weeks at 75 - 80°C (Stoneham and Winter, 1988), and 8 days at 75°C (Berger, 1988)) removed the fading component effectively in all cases. This optimistic approach followed from the work of Templer (1986a,b), in which the localised transition model was found to describe the anomalous fading seen in zircon TL. The prefading treatment demonstrated there had been extended with apparent success to the TL of feldspathic materials (Clark and Templer, (1988a,b), Stoneham and Winter (1988), and Bowman (1988)). However, it is noted here that those data were not for "pure" feldspar samples, but for maiolica in the latter two cases and polymineral fine grains from a zircon-rich province for the former. Contrary evidence, for the existence of tunnelling in the feldspars microcline and albite, was reported by Kirsh *et al* 1989 and 1990. Although the data of Kirsh *et al* 1989 and 1990 was also explicable as phototransferred TL, tunnelling could not be ruled out. Consequently the use of thermal pretreatments had not been unambiguously validated for feldspar minerals and fading via quantum mechanical tunnelling (Visocekas *et al.*, 1976; Visocekas 1979, 1985) could not be disregarded for the feldspar minerals: crucially as regards impact on dating the effects of such fading cannot be eliminated by laboratory procedures.

Therefore, to determine whether IRSL exhibited anomalous fading, and if so to test the efficacy of the thermal prefading treatments, a pilot study using identified feldspars from the RLAHA mineral collection was undertaken. Three samples were tested using IRSL, one each of orthoclase (Z6), sanidine (Z15) and labradorite (BA#6). The labradorite was known from the work of Wintle (1974) to show strong anomalous fading and the orthoclase was chosen as a presumably-stable high potassium feldspar. In anticipation of the detection of anomalous fading, possible mineral selectivity between fading and non-fading feldspar species was simultaneously tested as the mineral species chosen represented the significant compositional regions of the feldspar ternary system, omitting only albite.

Results were in accord with previous TL fading studies by others as orthoclase showed no fading whereas the sanidine and labradorite faded, the latter rapidly, in agreement with work by Wintle (1974) using this same sample. Sanidine constitutes a fading species which may possess high concentrations of potassium and a specific gravity < 2.58, and so not be removable by density separation from the high potassium fraction.

Principal conclusions were: anomalous fading similar to that seen in TL did occur in IRSL; the accepted thermal prefading routine (shown to be efficacious by Clark and Templer (1988a,b) as well as others) did not detectably accelerate fading in the labradorite tested; one of the two high-potassium feldspars faded significantly, indicating composition did not guarantee discrimination against fading.

These conclusions showed the need to define further the fading behaviour of the feldspar minerals, as previous assumptions on the general validity of thermal prefading treatments appeared unjustified.

4.2.2 THE FADING SURVEY

Following the worrying fading behaviour described above, a "survey" was made using a suite of 24 museum samples of feldspar with the aim of more fully exploring the fading of these minerals. Samples were selected so as to represent the regions of the ternary diagram most relevant to dating. The identification and characterization of these samples is described in Chapter 3, and the procedures by which fading was monitored (using both IRSL and OSL) are described in Spooner (1992). Results are presented in this and the following sections.

The ultimate aim of this study was the circumvention of fading in the dating context, hence most effort was directed towards finding readily measurable characteristics that usefully correlated with the fading behaviours observed here. Possible diagnostic characteristics or means of circumvention include:

1. Mineral species, both composition and structure
2. Elevated temperature storage of various durations
3. Delay at ambient temperature
4. Emission wavelength
5. Stimulation wavelength
6. "Optical wash"
7. Bleaching resonance behaviour
8. Susceptibility to bleaching
9. Shine-curve shape changes
10. Short-shine pulse shape (ie, "build-up")
11. Phosphorescence decay form
12. Phototransfer TL
13. Thermal activation characteristic curves
14. TL glow peak FWHM
15. Heating-rate variations (effect on glow-curves)
16. Differences between of α, β and γ dosing effects

(Of these, only 11, 12 and 16 are not considered in this work).

Nineteen samples possessing sufficient luminescence sensitivity to enable statistically meaningful measurement were monitored for fading of both the IRSL and OSL. IRSL data are presented for each of these, and OSL data for a representative subset.

4.2.2.1 FADING OF IRSL AT 10°C AND 100°C

The methodology is detailed in Spooner (1992). All measurements were made on samples from which the NTL was previously erased by heating at 5 K/s to 550°C and reheating, then $^{90}Sr/^{90}Y$ β doses were administered according to sensitivity. Finally a preheat of 60 seconds at 220°C on-plate was given immediately following dosing and the normalization measurement made at 20°C 200 seconds after the cessation of the preheat. This preheat was chosen so as to erase all TL which might undergo detectable thermal decay at 10°C over a timescale of a few years (the adequacy of this preheat for this task was confirmed by kinetic measurements on the TL surviving this preheat, see section 4.2.5). IRSL emissions were observed through a transmission window of 360 nm to 585 nm (50 % transmission points) provided by a 2 mm Schott BG 39 filter.

The ratio of the integrated IRSL after storage time t=t to that at time t=200 is shown for each sample in Fig.4.2.2.1.1. Each data point represents an individual disc exposed for 300 seconds, this approach being used so as to ensure that if changes occur to the shine-curve shapes with storage time, the effect on the total light sum will be correctly measured (short exposure measurements unavoidably bias towards the initial, highly bleachable, portion of the shine curve). Furthermore, following the demonstration by Templer (1986b) of the removal of anomalous fading luminescence from zircon samples using an "optical wash" of 600 nm light, the additional possibility that exposure

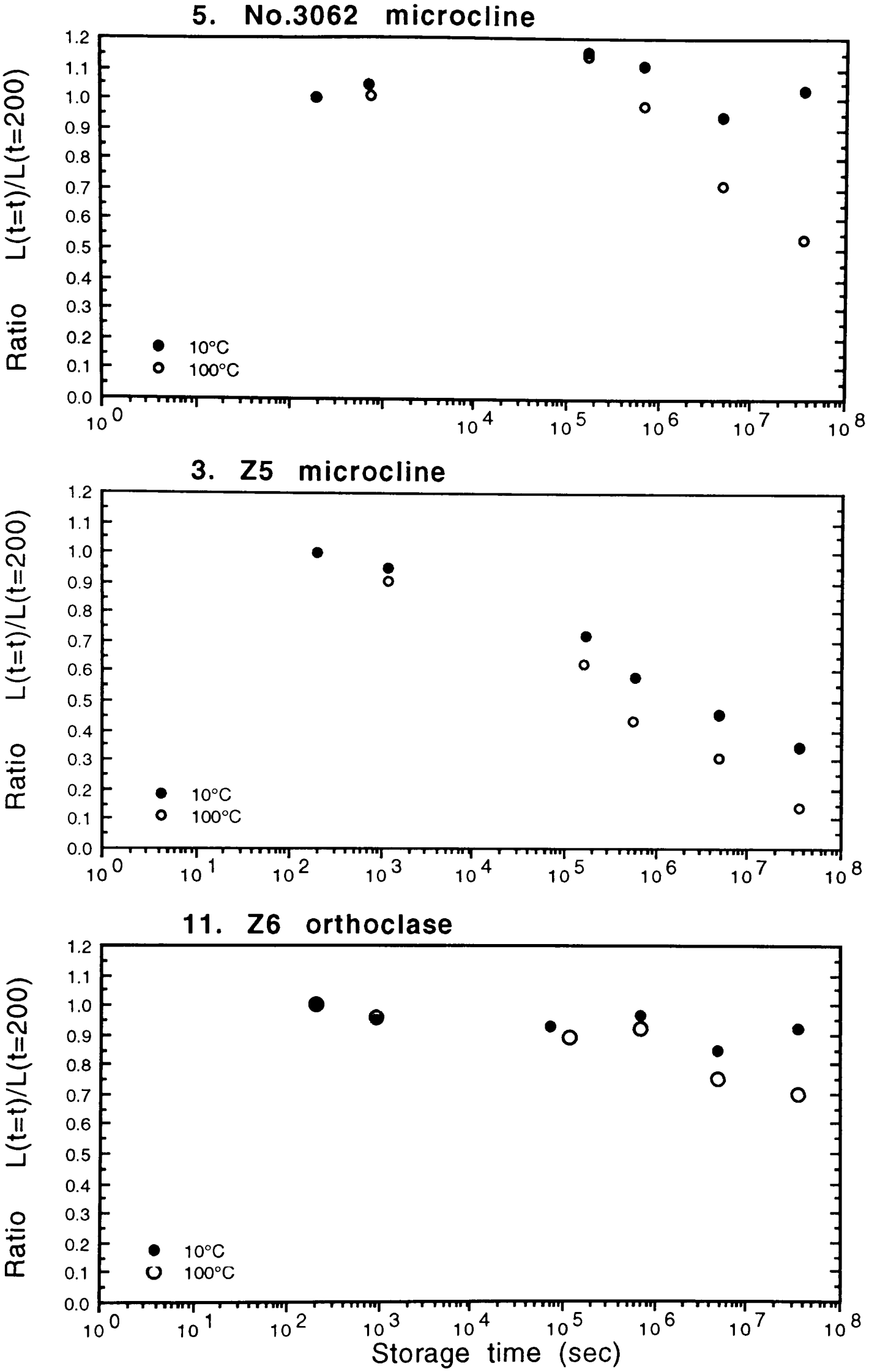
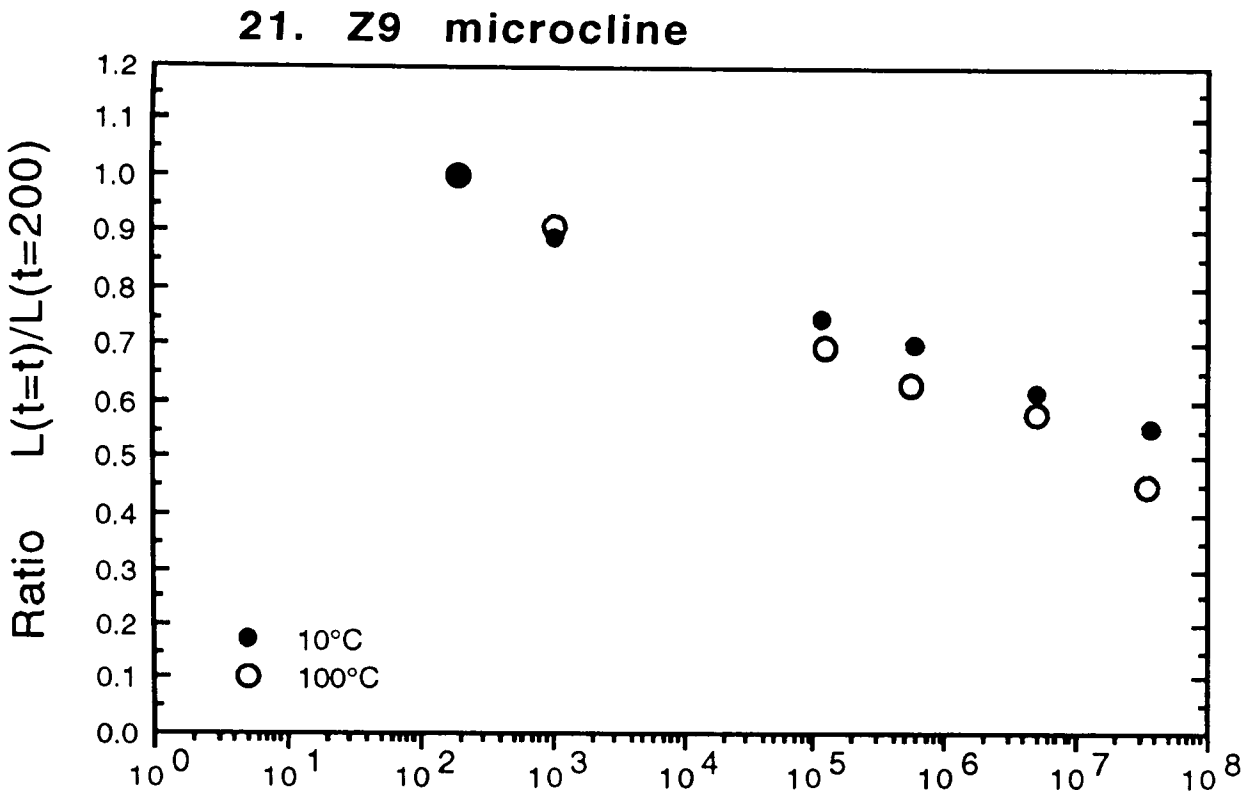
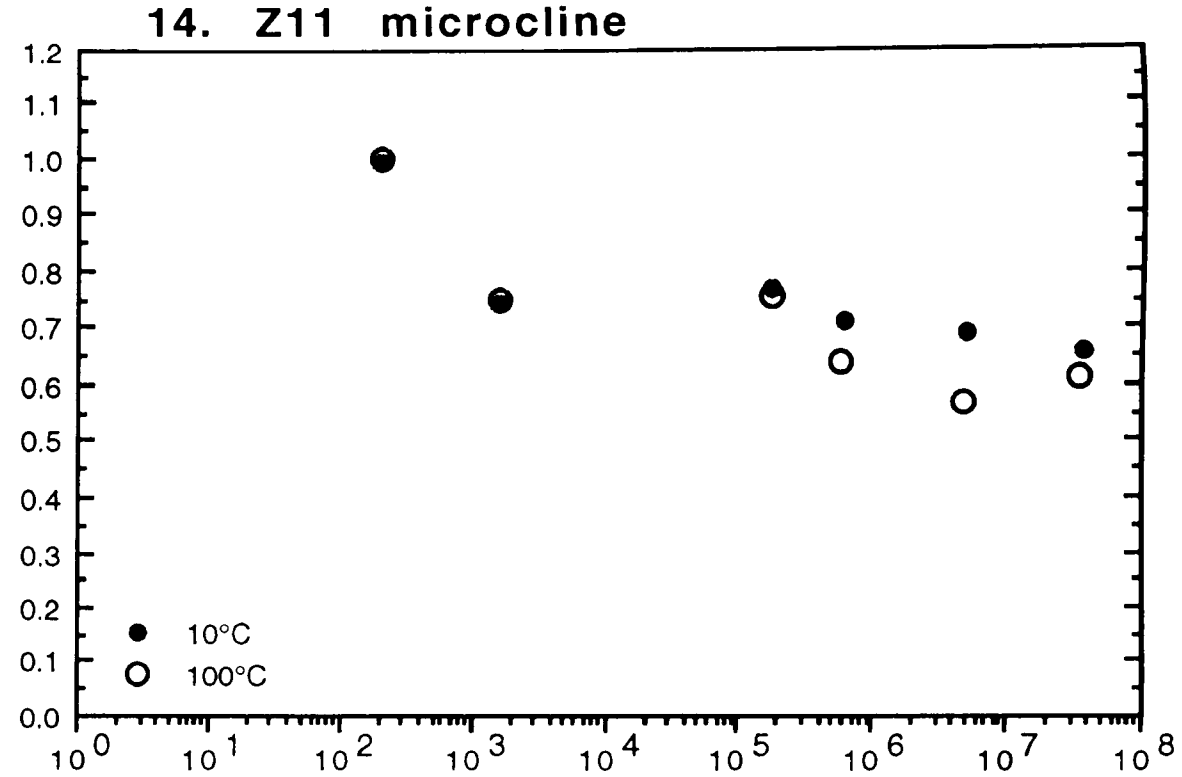
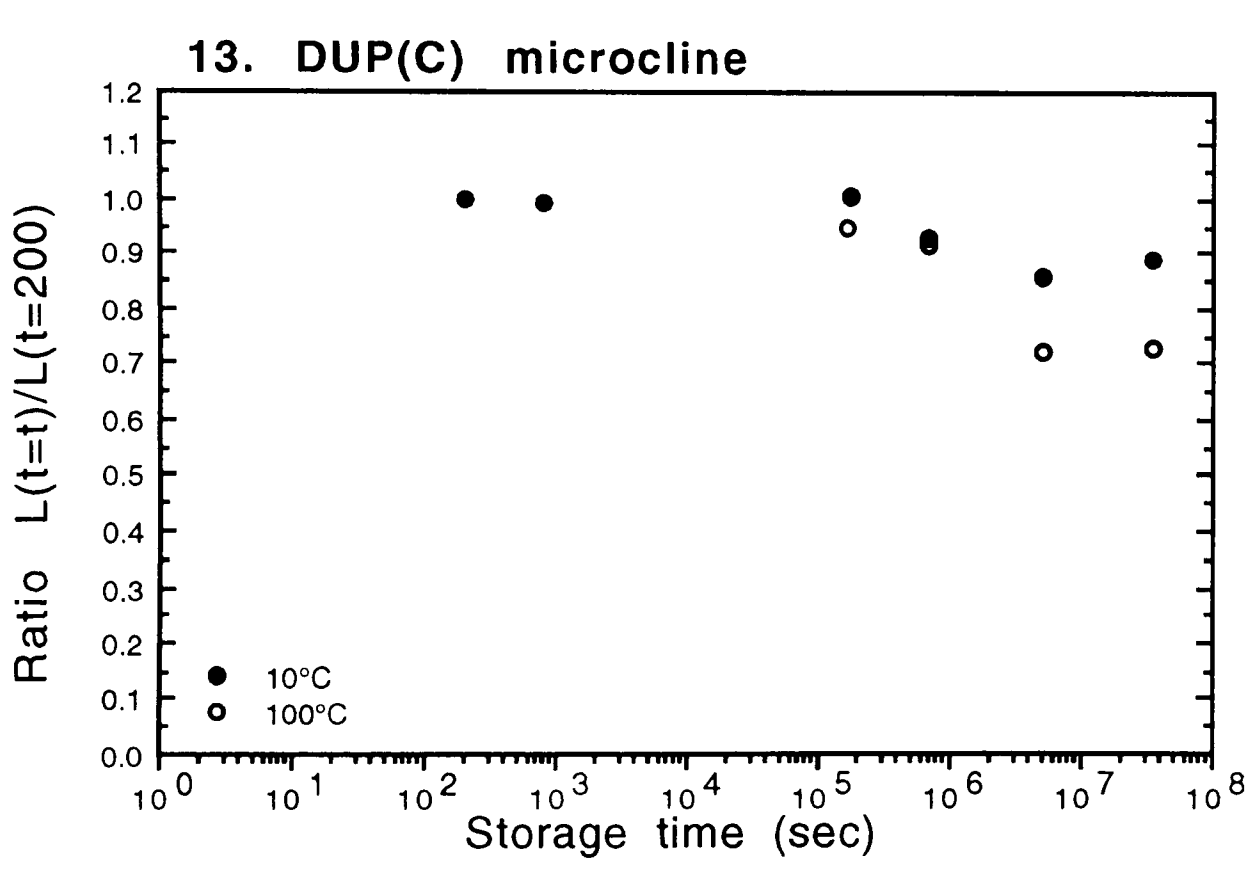
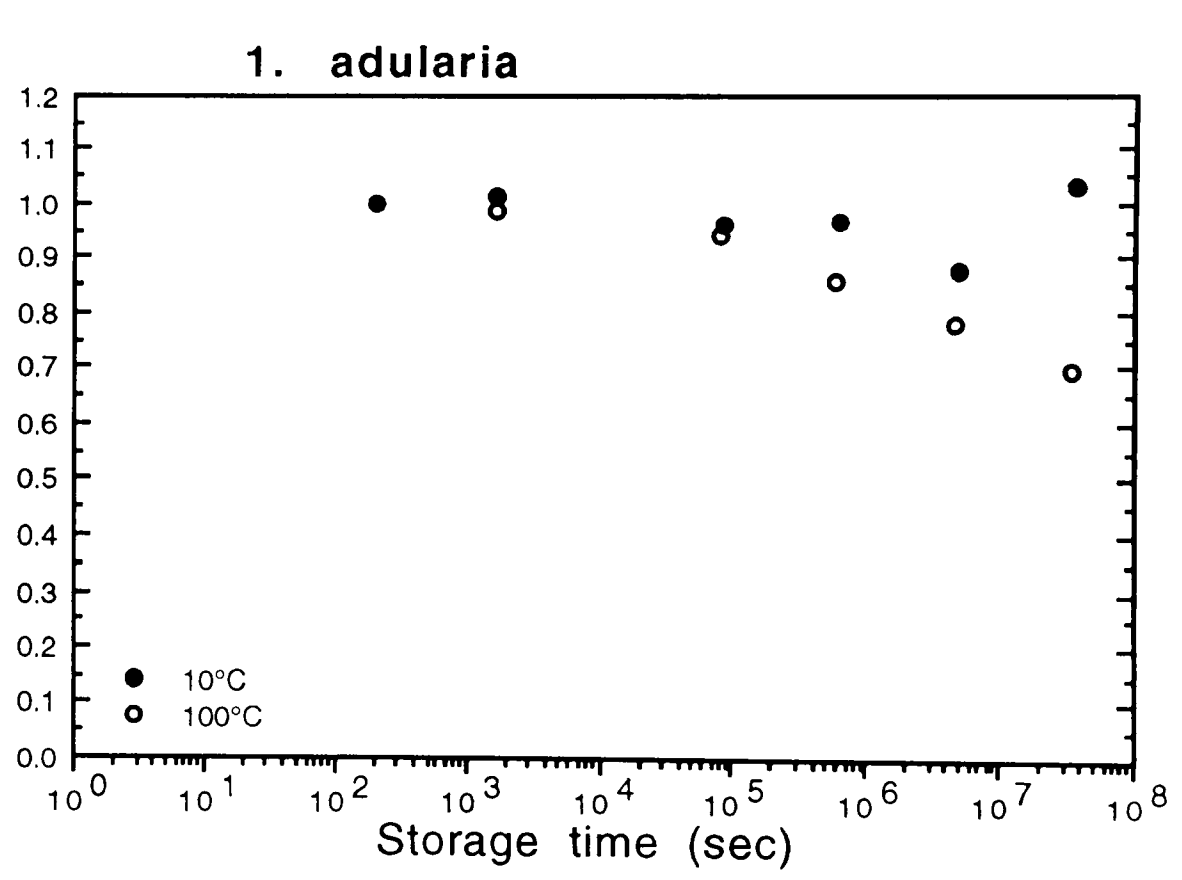


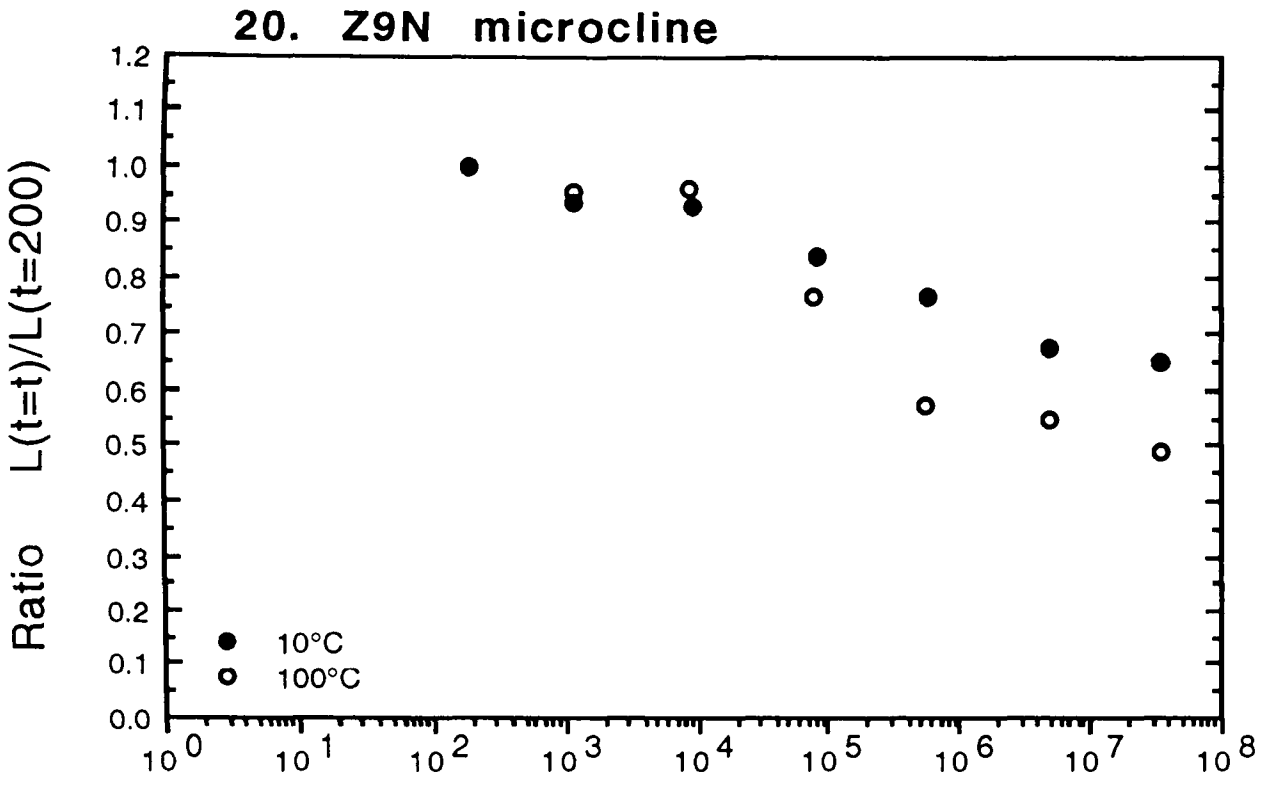
Fig.4.2.2.1.1 Fading of IRSL. The ratio of the integrated luminescence L at time t=200 seconds to that after storage time t=t is shown for each of the feldspars following various storage times at 10°C and 100°C. Measurements were made using an EMI 9635Q PMT (bialkali photocathode) with a 2 mm Schott BG39 filter. Exposure times were 300 seconds, with IR beam strength of ≈ 30 mW/cm^2. The routine is given in Spooner (1992).

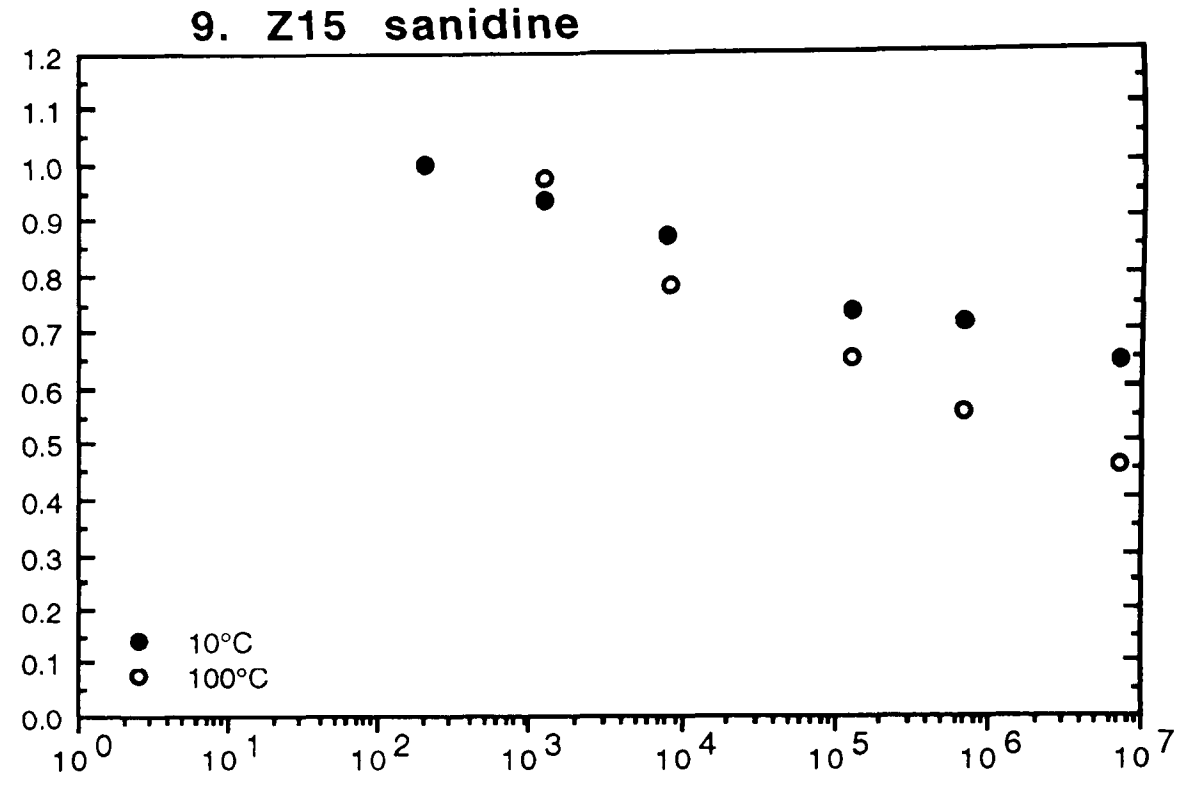

21. Z9 microcline
Ratio L(t=t)/L(t=200)
10°C
100°C

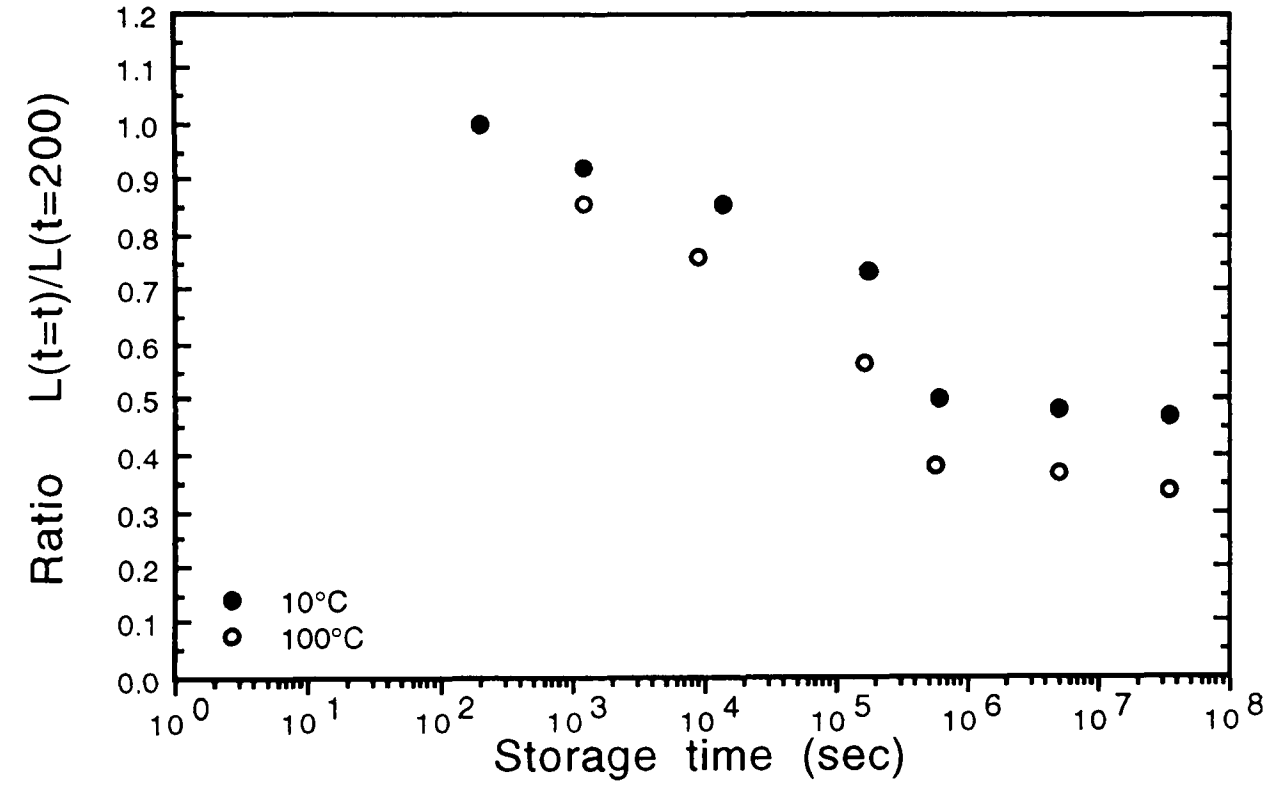

14. Z11 microcline
10°C
100°C

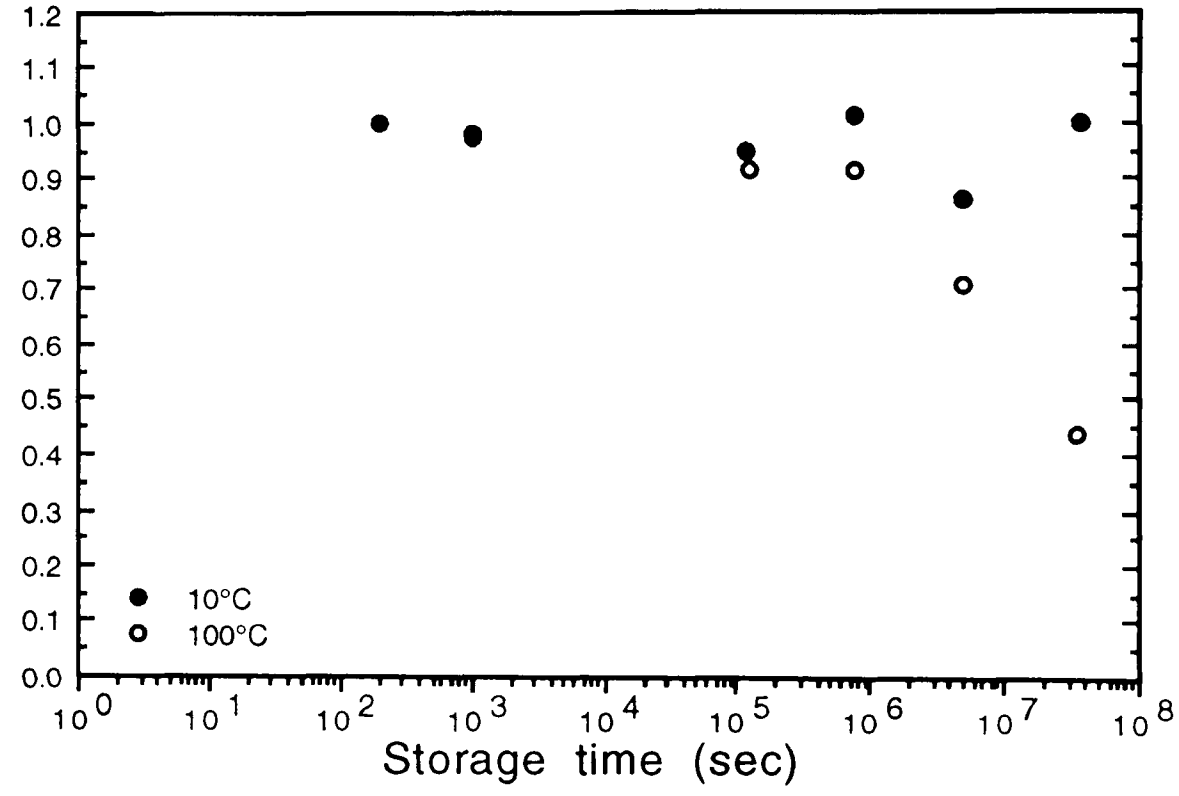

13. DUP(C) microcline
Ratio L(t=t)/L(t=200)
10°C
100°C
Storage time (sec)

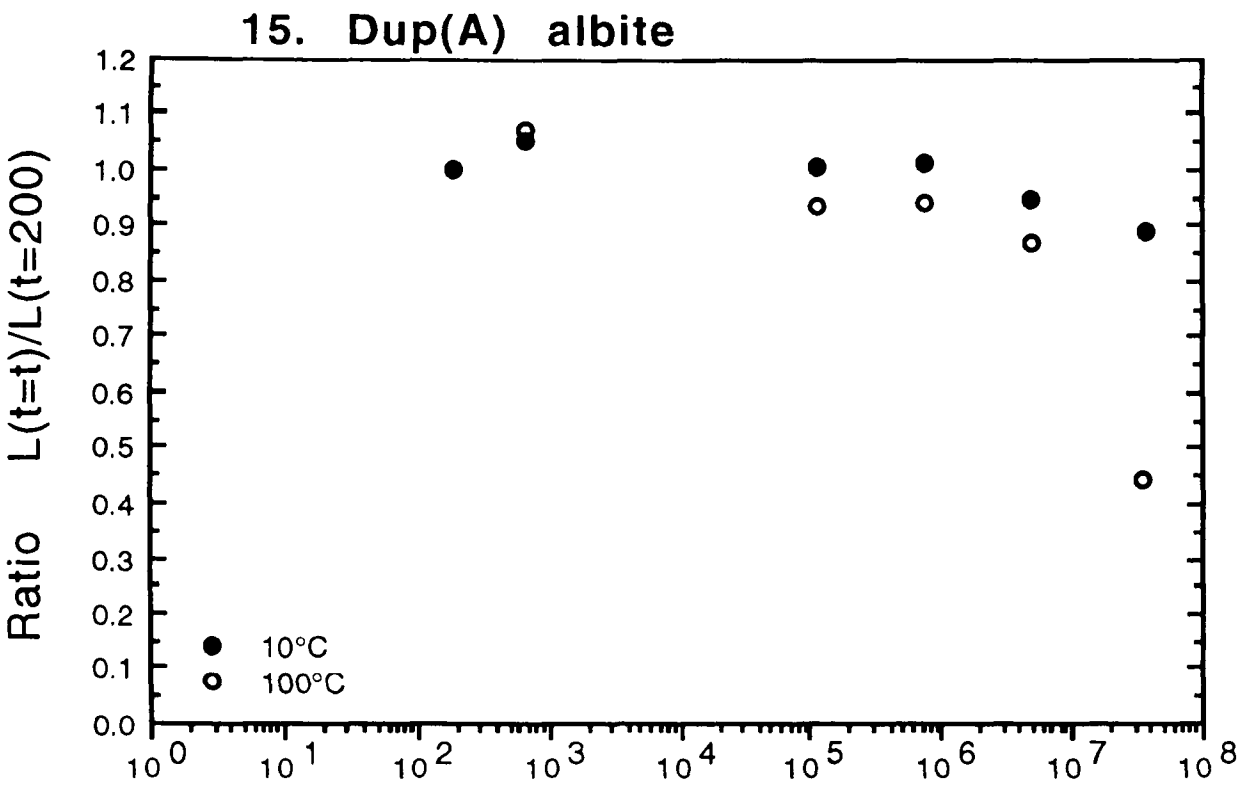

1. adularia
10°C
100°C
Storage time (sec)

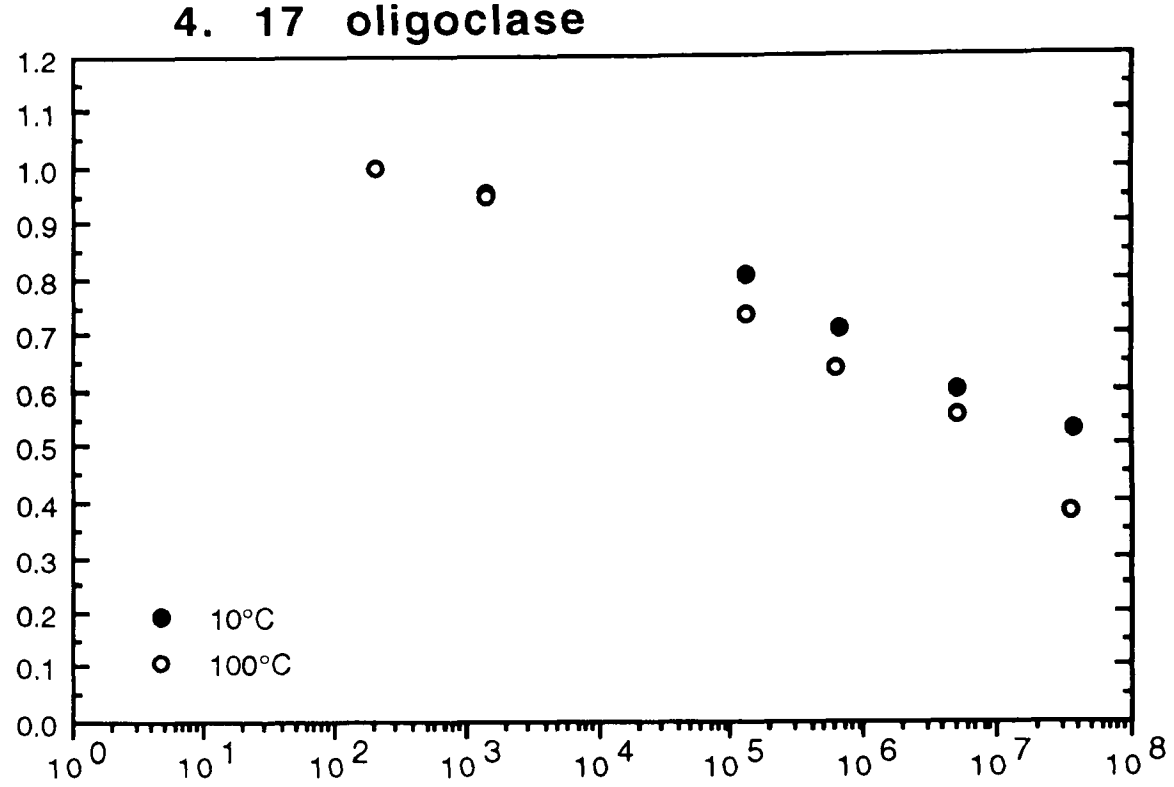

20. Z9N microcline
Ratio L(t=t)/L(t=200)
1.2
1.1
1.0
0.9
0.8
0.7
0.6
0.5
0.4
0.3
0.2
0.1
0.0
10°C
100°C
10^0 10^1 10^2 10^3 10^4 10^5 10^6 10^7 10^8

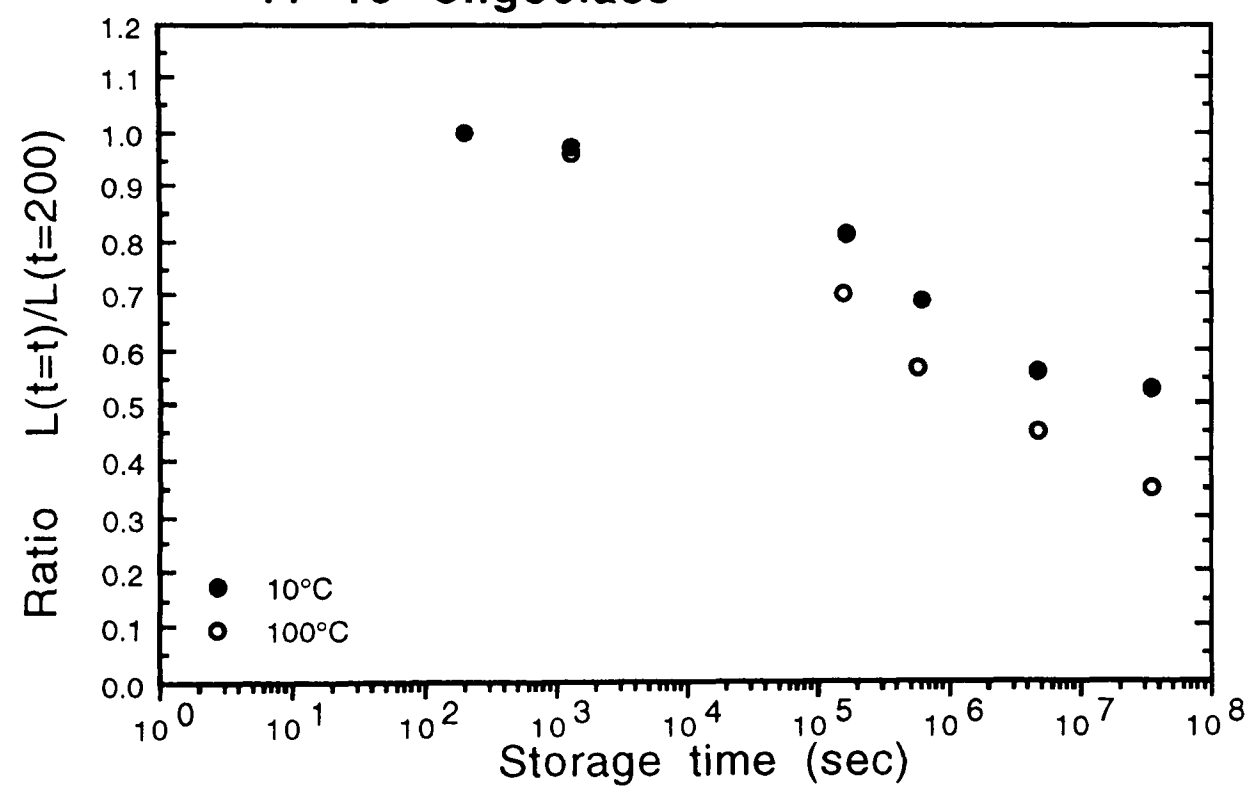

9. Z15 sanidine
1.2
1.1
1.0
0.9
0.8
0.7
0.6
0.5
0.4
0.3
0.2
0.1
0.0
10°C
100°C
10^0 10^1 10^2 10^3 10^4 10^5 10^6 10^7

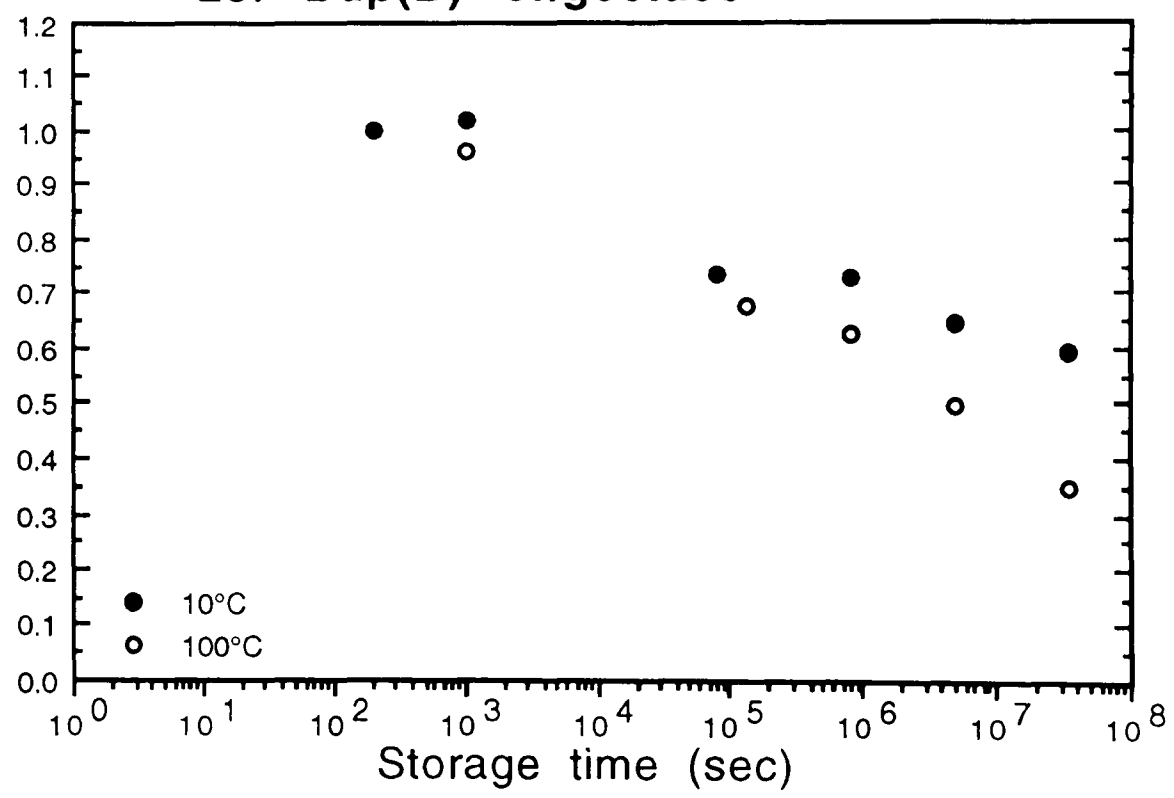

12. Patmos sanidine
Ratio L(t=t)/L(t=200)
1.2
1.1
1.0
0.9
0.8
0.7
0.6
0.5
0.4
0.3
0.2
0.1
0.0
10°C
100°C
10^0 10^1 10^2 10^3 10^4 10^5 10^6 10^7 10^8
Storage time (sec)

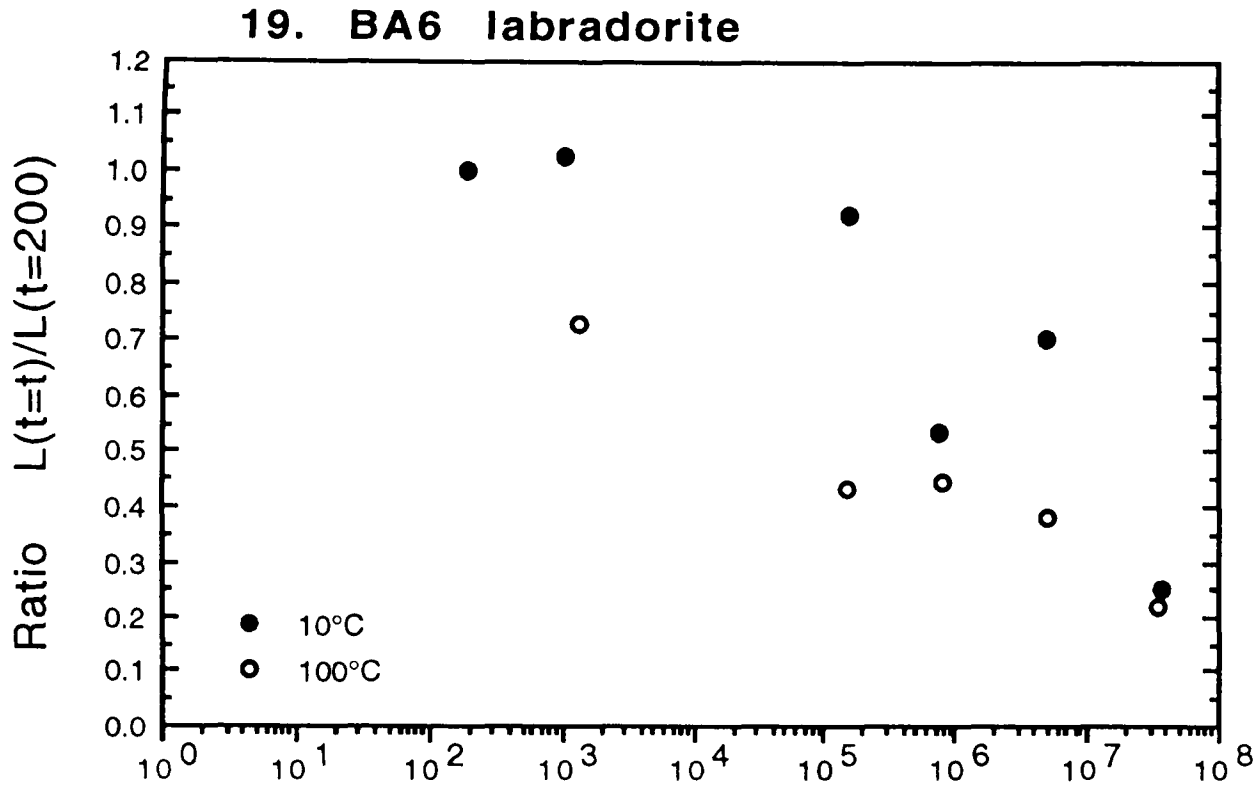

18. Amelia albite
1.2
1.1
1.0
0.9
0.8
0.7
0.6
0.5
0.4
0.3
0.2
0.1
0.0
10°C
100°C
10^0 10^1 10^2 10^3 10^4 10^5 10^6 10^7 10^8
Storage time (sec)

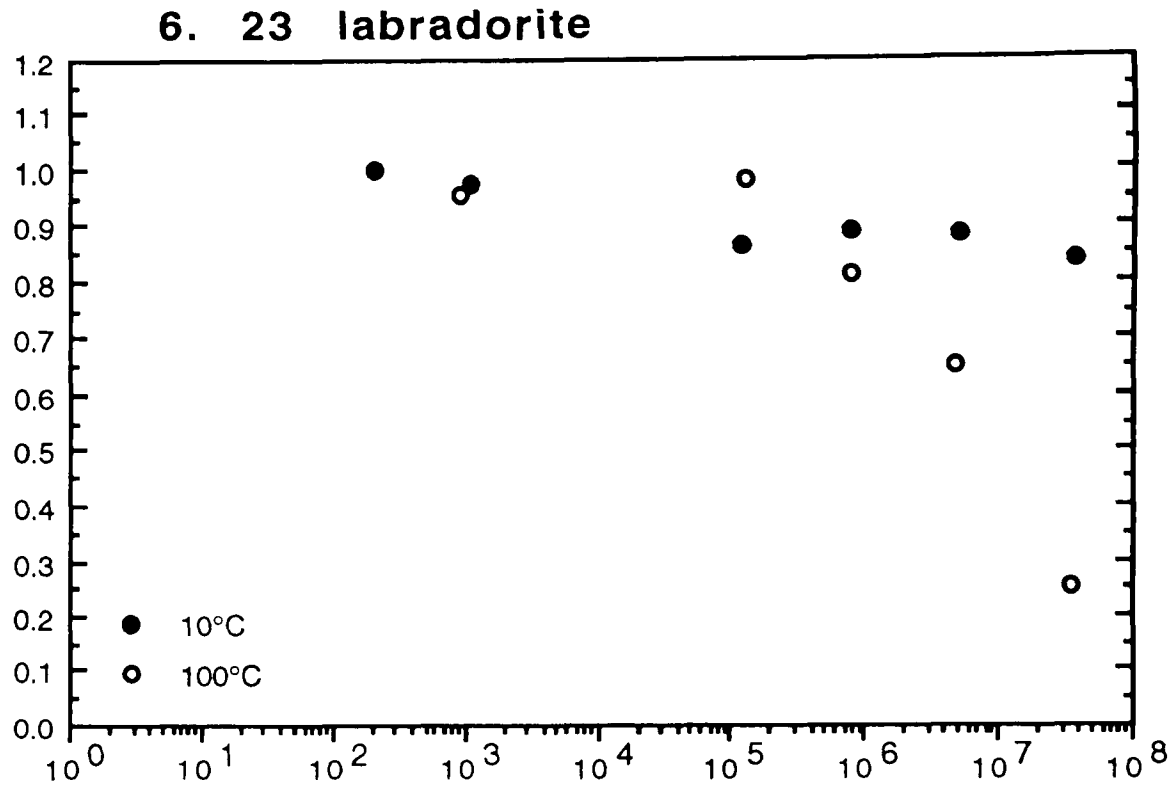

15. Dup(A) albite
Ratio L(t=t)/L(t=200)
1.2
1.1
1.0
0.9
0.8
0.7
0.6
0.5
0.4
0.3
0.2
0.1
0.0
10°C
100°C
10 0
10 1
10 2
10 3
10 4
10 5
10 6
10 7
10 8

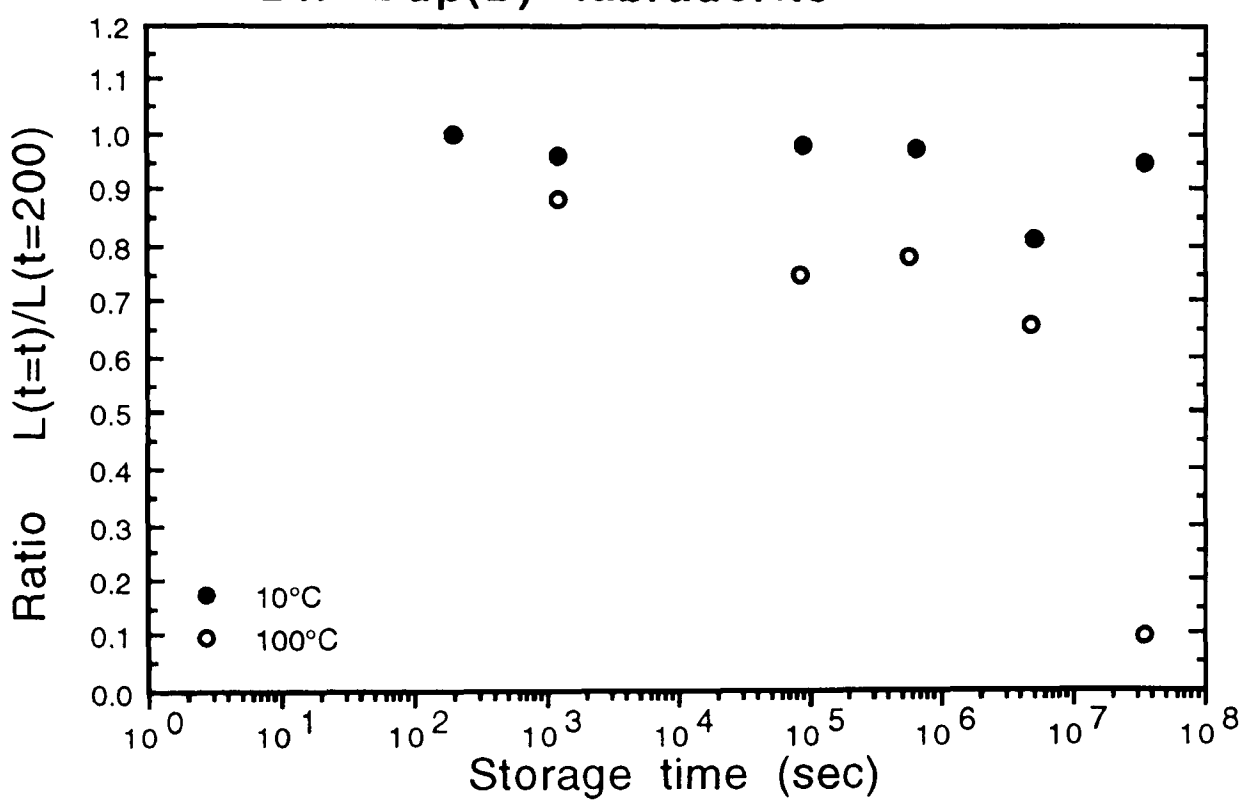

4. 17 oligoclase
1.2
1.1
1.0
0.9
0.8
0.7
0.6
0.5
0.4
0.3
0.2
0.1
0.0
10°C
100°C
10 0
10 1
10 2
10 3
10 4
10 5
10 6
10 7
10 8

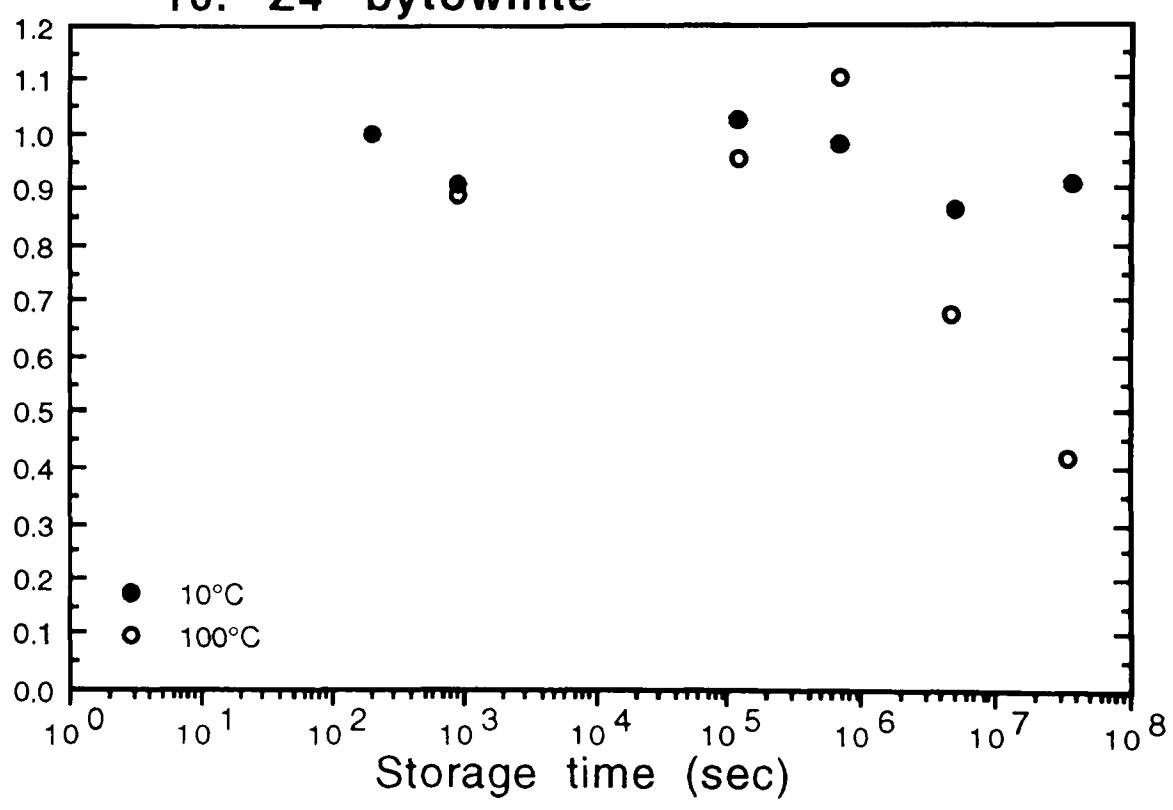

7. 18 oligoclase
Ratio L(t=t)/L(t=200)
1.2
1.1
1.0
0.9
0.8
0.7
0.6
0.5
0.4
0.3
0.2
0.1
0.0
10°C
100°C
10 0
10 1
10 2
10 3
10 4
10 5
10 6
10 7
10 8
Storage time (sec)


23. Dup(B) oligoclase
1.2
1.1
1.0
0.9
0.8
0.7
0.6
0.5
0.4
0.3
0.2
0.1
0.0
10°C
100°C
10 0
10 1
10 2
10 3
10 4
10 5
10 6
10 7
10 8
Storage time (sec)


19. BA6 labradorite
Ratio L(t=t)/L(t=200)
1.2
1.1
1.0
0.9
0.8
0.7
0.6
0.5
0.4
0.3
0.2
0.1
0.0
10°C
100°C
10 0
10 1
10 2
10 3
10 4
10 5
10 6
10 7
10 8


6. 23 labradorite
1.2
1.1
1.0
0.9
0.8
0.7
0.6
0.5
0.4
0.3
0.2
0.1
0.0
10°C
100°C
10 0
10 1
10 2
10 3
10 4
10 5
10 6
10 7
10 8


24. Dup(D) labradorite
Ratio L(t=t)/L(t=200)
1.2
1.1
1.0
0.9
0.8
0.7
0.6
0.5
0.4
0.3
0.2
0.1
0.0
10°C
100°C
10 0
10 1
10 2
10 3
10 4
10 5
10 6
10 7
10 8
Storage time (sec)


10. Z4 bytownite
1.2
1.1
1.0
0.9
0.8
0.7
0.6
0.5
0.4
0.3
0.2
0.1
0.0
10°C
100°C
10 0
10 1
10 2
10 3
10 4
10 5
10 6
10 7
10 8
Storage time (sec)

to IR would preferentially remove the anomalously fading component was simultaneously examined. However, ratios of IRSL shine-curves (i.e., the ratios of IRSL at successive points in the shine-down curve) after various storage durations revealed no detectable variation of this sort, hence it was concluded that IR was not preferentially bleaching the fading component. This result negated the possibility of using an IR optical wash in feldspar, or the attainment of a true palaeodose by using the later portions of the shine-curve of a fading sample.

Most notable is the occurrence of fading amongst high potassium microcline feldspars (in addition to sanidine), and its failure to either reach a stable remanent level or to be usefully accelerated by the elevated temperature storage used here. The usual presence in the light density fraction (< 2.58) of this feldspar species (and its frequent dominance) must be assumed, hence this finding dictates the necessity of actively monitoring such samples for anomalous fading and not simply relying on thermal pretreatments.

Principal conclusions are firstly that no mineral species or compositional regime of the feldspar ternary diagram are immune to fading (although there are individual samples that show no fading for 10°C storage), and secondly that elevated temperature storage does not eliminate anomalous fading effectively.

4.2.2.2 FADING OF OSL AT 10°C AND 100°C

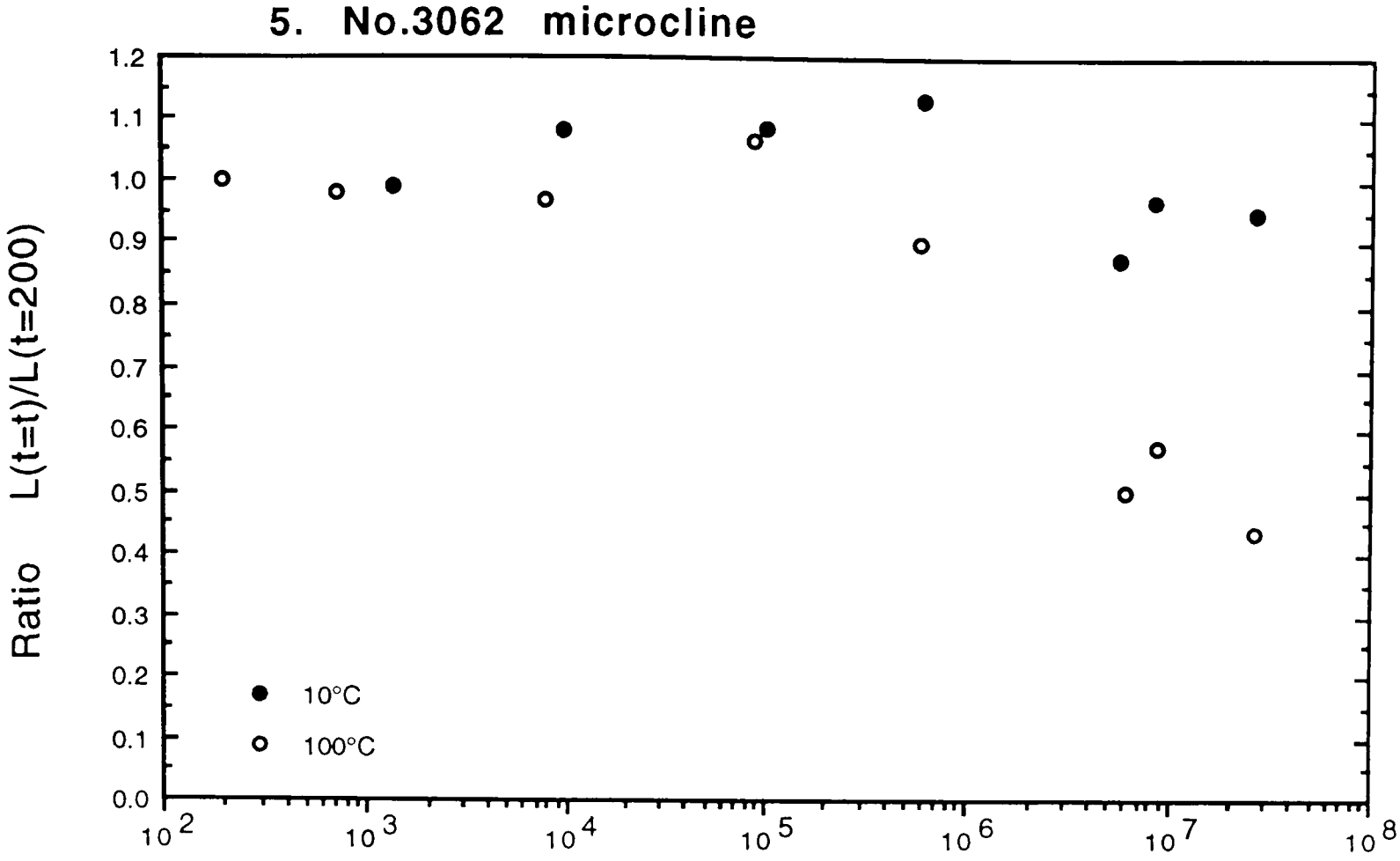
The OSL of each sample was also monitored, as for the IRSL, using repeated short exposures to 514.5 nm light from an Ar-ion laser, and incrementing the storage times. The detection window for emissions was 345 nm - 410 nm. Short exposure monitoring was

used for convenience although this approach entails two disadvantages - firstly, correction for depletion of the luminescence by the repeated short exposures, and secondly and more seriously, the vulnerability of such monitoring to exposure-energy dependent changes in the shine-curve shapes.

The measurement routine consisted of administering a $^{90}Sr/^{90}Y$ β dose, followed promptly by a preheat of 1 minute at 220°C on-plate. The normalization short exposures were of 0.5 mJ - 5 mJ, depending on the sample sensitivity, and the monitoring exposures were similar. Finally, a series of short exposures were given to similarly prepared discs of each sample to determine a depletion correction factor for each exposure to each sample, following which the TL was thermally drained (by heating at 5 K/s to 550°C) and background measurments made from the count-rates of these drained discs. Data from a subset of the samples monitored are presented in Fig.4.2.2.2.1, with the choice of samples selected largely based on the significance to dating of each mineral species; hence only one calcic plagioclase (19. BA6 labradorite) is included.

Results were generally in accord with those found when monitoring IRSL. Decay time constants for these samples are given in Table 4.2.2.4.2, along with those found from the decay of the IRSL (in Table 4.2.2.4.1). The general agreement between the decay rates measured under green and IR stimulation eliminates the optimistic possibility that an extended pre-measurement bleach with IR leaves a non-fading green-stimulable signal. There is an indication that the fading of OSL in some samples may proceed more rapidly than that of IRSL, but the evidence for such a difference is marginal given the measurement errors.

Principal conclusions were as for IRSL-monitored fading, with the additional point that green light does not have access to a non-fading portion of signal, so annulling hopes



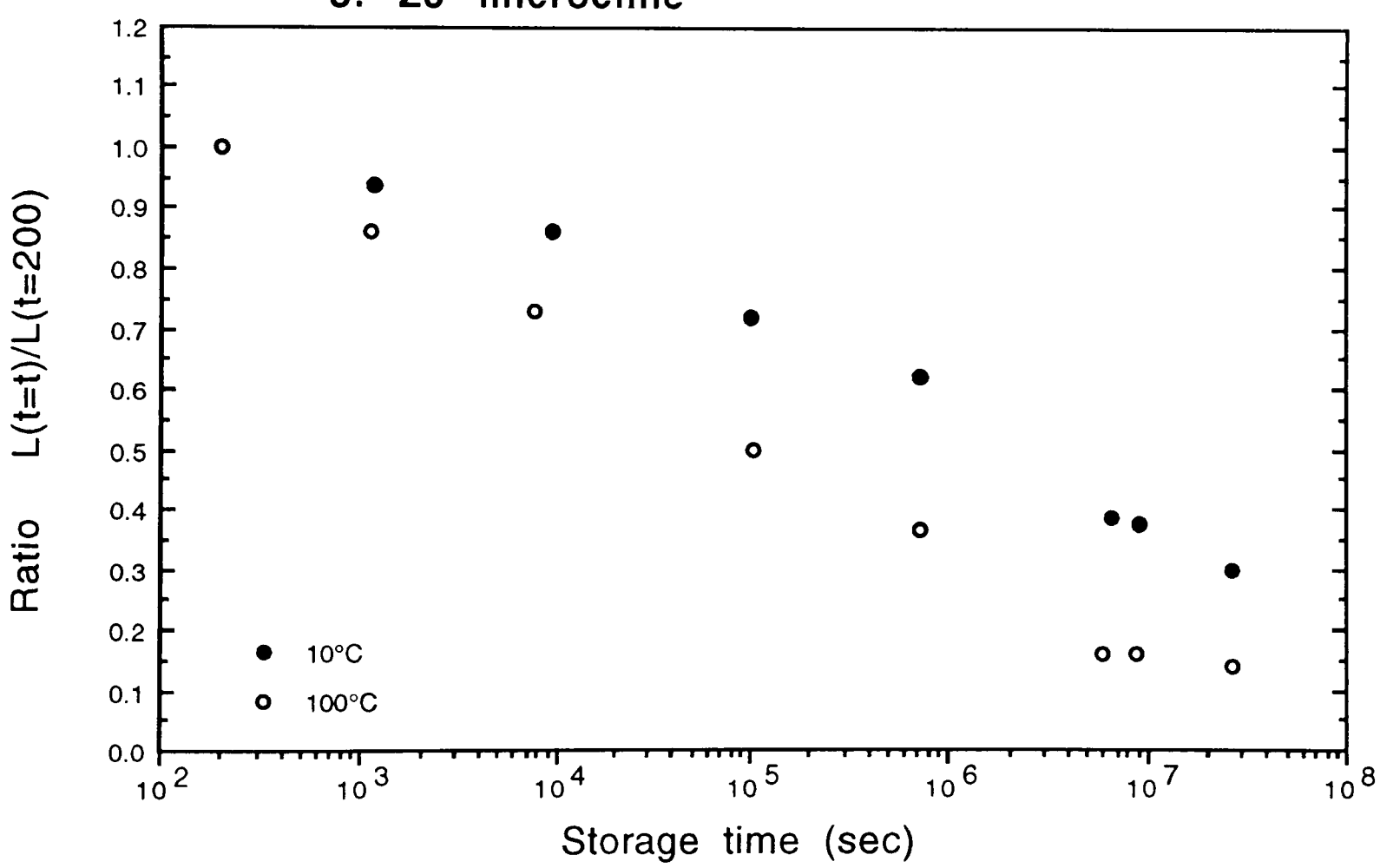
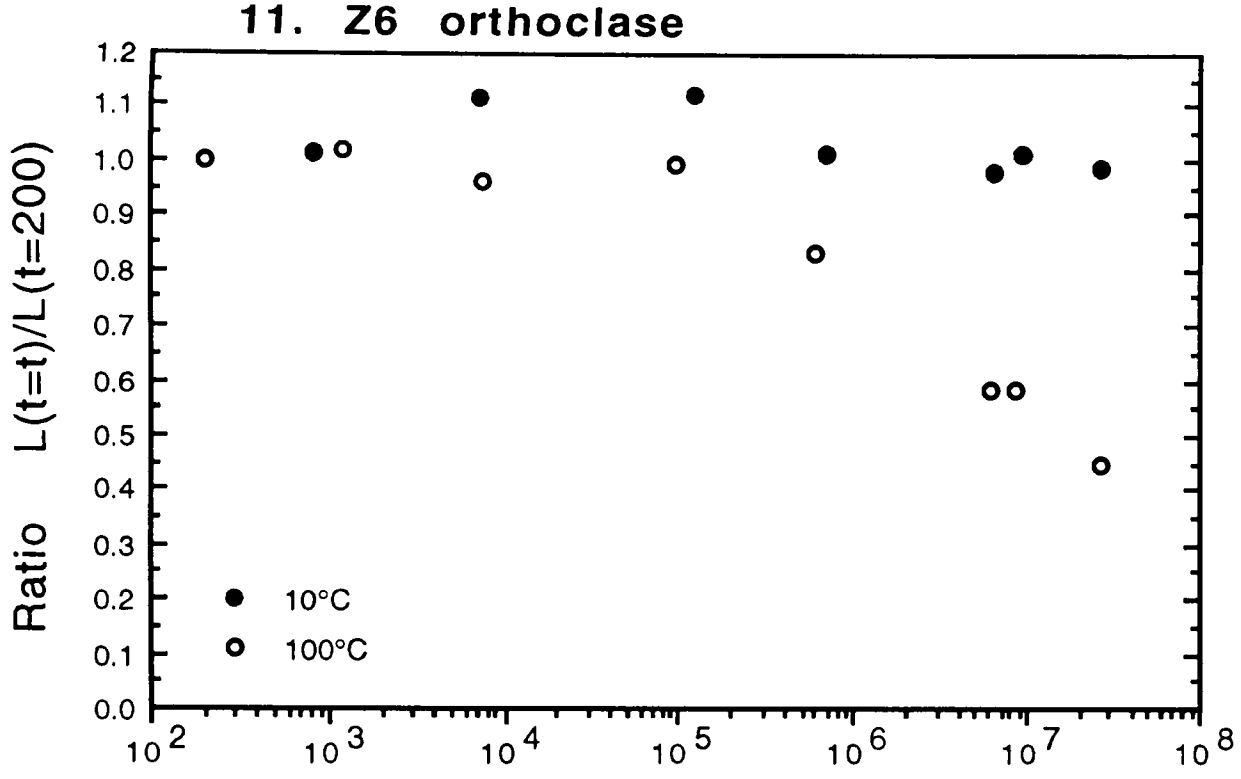
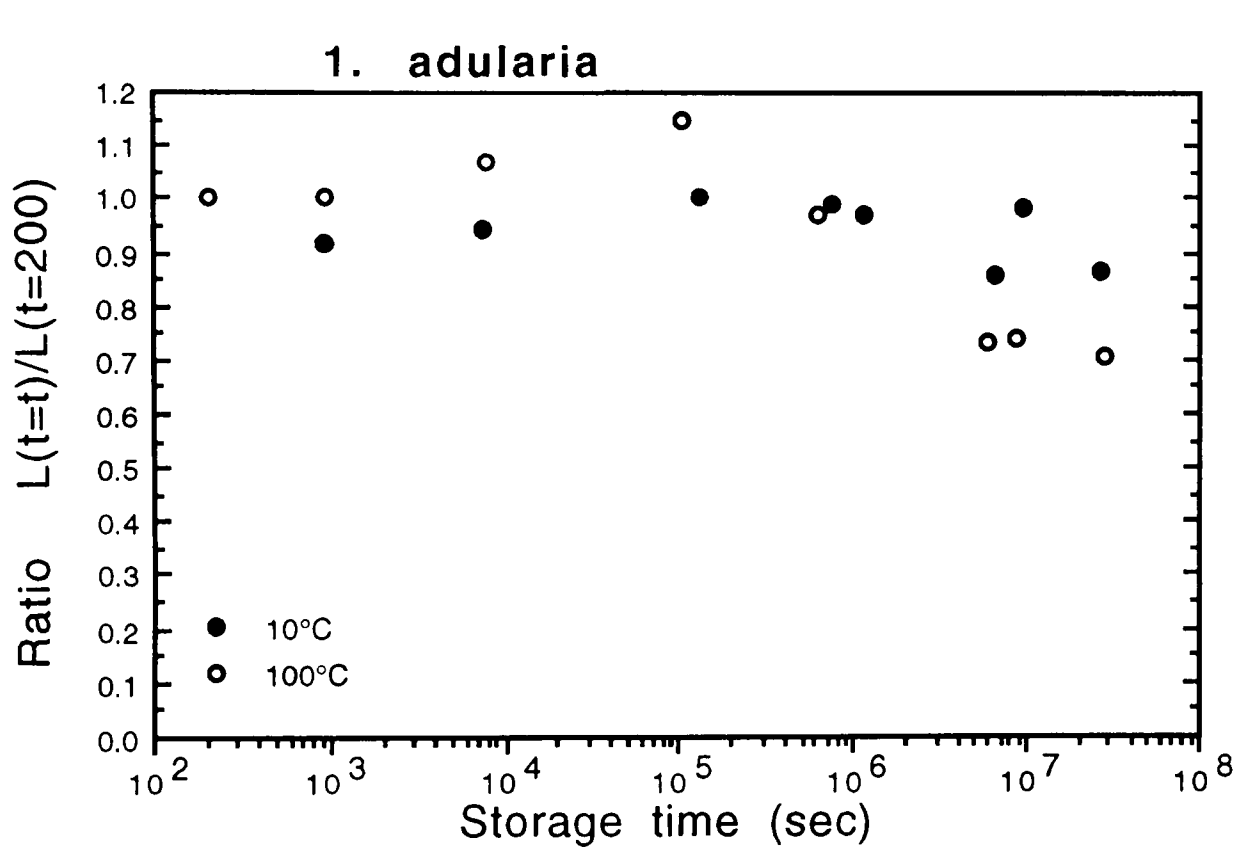
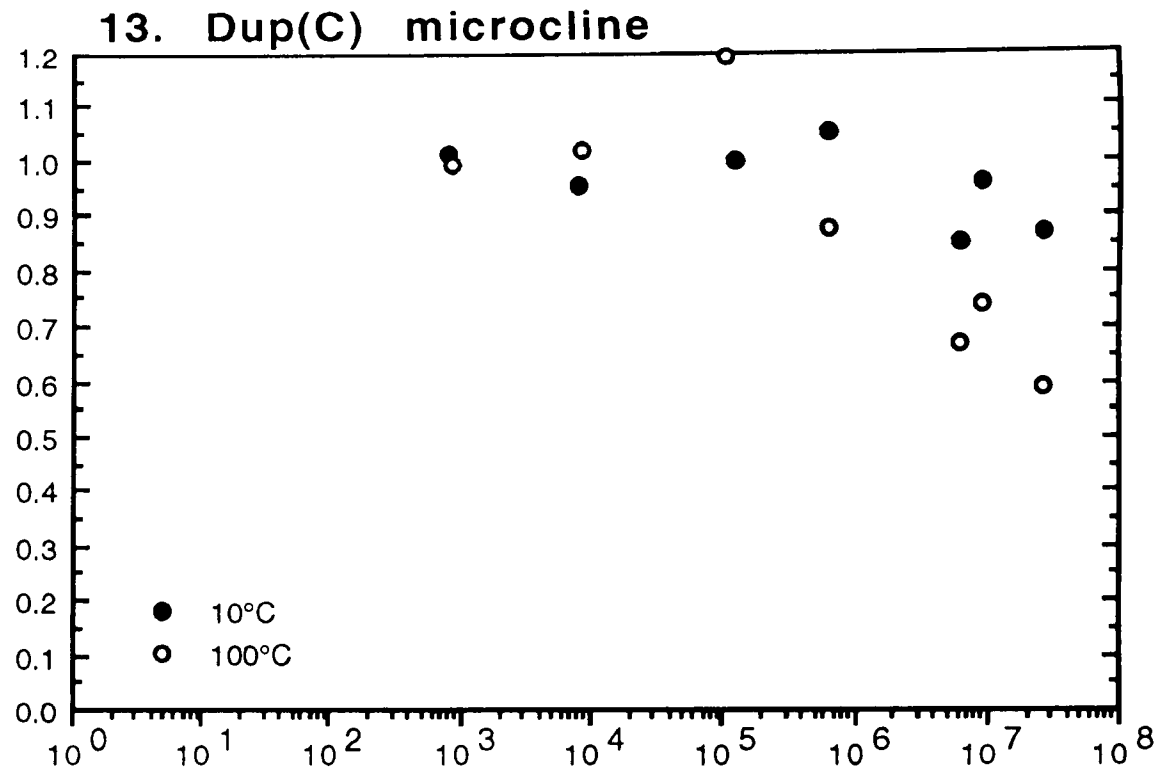
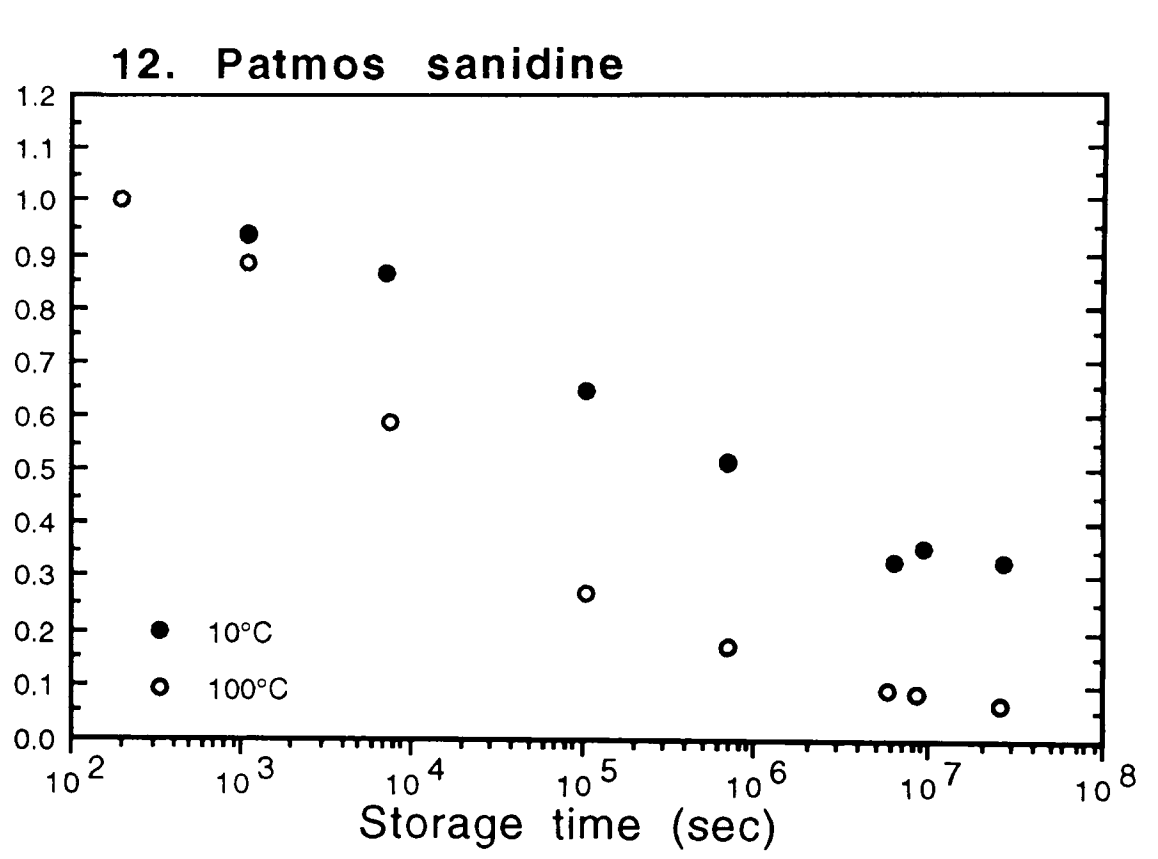


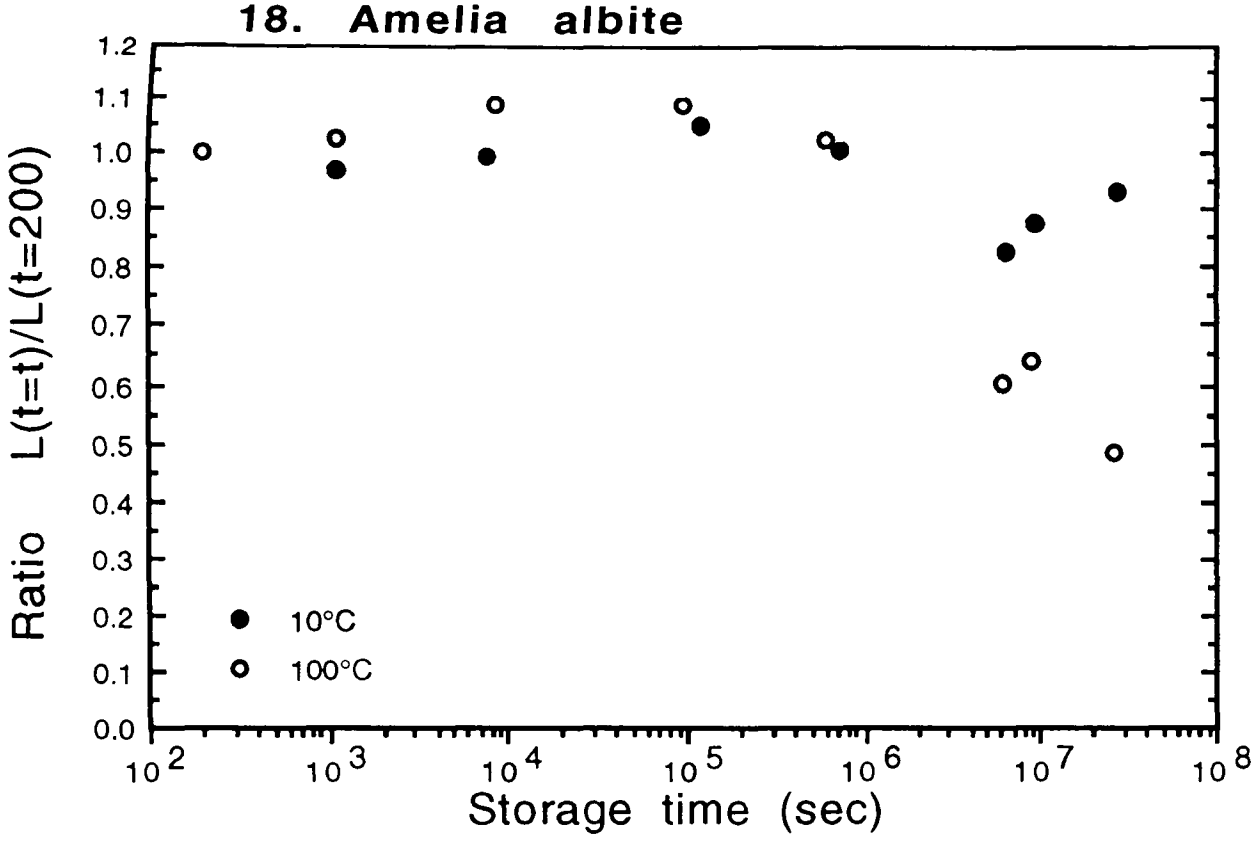
Fig.4.2.2.2.1 Fading of OSL from selected feldspars following various storage durations at 10°C and 100°C. Measurements were made using an EMI 9635Q PMT (bialkali photocathode) with 16 mm of Corning 7-59 and 1 mm Schott BG39 filter. Data plotted are the ratio of the normalization exposure countrate to that measured following storage. The measurement routine is described in Spooner (1992).

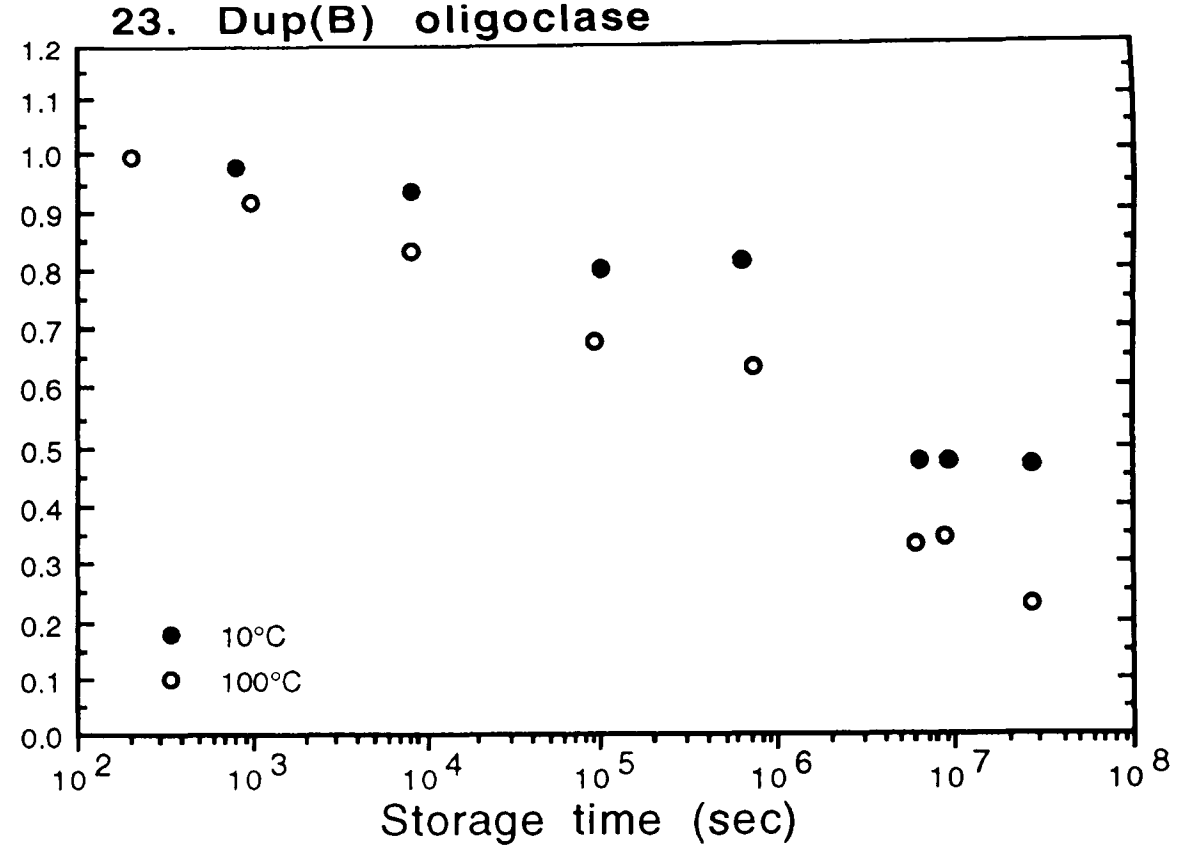

11. Z6 orthoclase
Ratio L(t=t)/L(t=200)
10°C
100°C

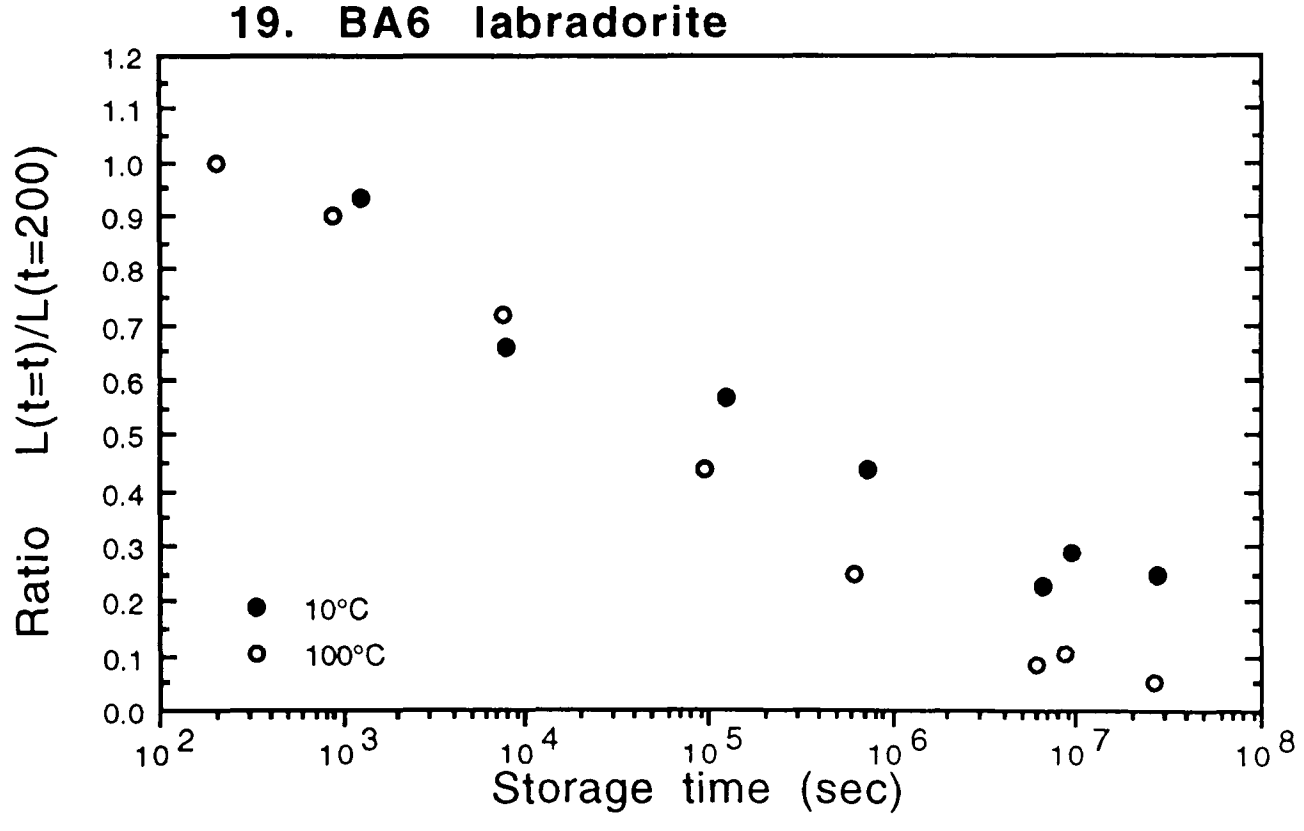

1. adularia
Ratio L(t=t)/L(t=200)
10°C
100°C
Storage time (sec)


13. Dup(C) microcline
10°C
100°C


12. Patmos sanidine
10°C
100°C
Storage time (sec)


18. Amelia albite
Ratio L(t=t)/L(t=200)
Storage time (sec)
10°C
100°C


23. Dup(B) oligoclase
Storage time (sec)
10°C
100°C


19. BA6 labradorite
Ratio L(t=t)/L(t=200)
Storage time (sec)
10°C
100°C

of stimulation-wavelength discrimination against fading (at any rate using green light). As for IRSL no major increases in fading rate were seen to result from elevated temperature storage (reduction in the OSL after the longer storage times at 100°C, as seen for 11. orthoclase and 5. microcline, is attributed to thermal draining of some of the OSL source-traps, seen as TL at ≤ 300°C).

4.2.2.3 FADING OF IRSL OF LABRADORITE AT 77 K

Although the preliminary work on BA6 labradorite had suggested an athermal fading mechanism (Spooner, 1992), the data for 19. BA6 labradorite given in Figs.4.2.2.1.1 and 4.2.2.2.1 suggested that the fading may be accelerated by storage at 100°C, compared to 10°C. Although this superficially conflicted with the report by Visocekas (1985) of tunnelling afterglow from this same sample at low temperatures which showed that athermal fading comprised at least a component of the fading seen, it left open the possibility that thermally assisted fading susceptible to removal by elevated temperature storage was present in this sample.

To test for the occurrence of thermal acceleration of anomalous fading in this labradorite, a further series of measurements were made (following discussion with I.K. Bailiff, 1990) monitoring the IRSL, but with the labradorite stored in liquid nitrogen (≈ -195.8°C). Results (not shown) demonstrated that although fading continued at -195.8°C the rate was significantly reduced. These findings are interpreted as showing that both thermal and athermal fading mechanisms are active in this sample, and consequently, although a preheat may reduce the significance of the fading component the reality of athermal behaviour ensures a preheat cannot eliminate it. This conclusion leaves open the

prospect that all the luminescence of this sample is unstable and will eventually fade - high temperature storage merely accelerating the process by making available the additional, thermally accessible, fading pathways.

4.2.2.4 DISCUSSION

Table 4.2.2.4.1 and Table 4.2.2.4.2 summarize results of the IRSL and (selected) OSL fading. As a convenient approximation, the tunnelling-type equation R = a - b*ln(t) was fitted to all data sets to give a reasonable quantification of the fading rate. Inspection of the data shown in Figs.4.2.2.1.1 and 4.2.2.2.1 suggests that this fading mechanism dominates, and that strong adherence to the localised transition form of fading is not seen. (Only data collected from samples stored at 10°C were analyzed, as the higher temperature storage (100°C) data includes an effectively indistinguishable "fading" due to thermal erosion of the TL which survived the preheat). The attribution of the observed fading of IRSL and OSL to an athermal tunnelling-type process is made, from these data, for two reasons: first is the "1/time" nature of the decay, which is characteristic of the tunnelling mechanism. It must however be borne in mind that the localised transition model, for appropriate E and S values, is also capable of giving rise to a similar form of remanent luminescence to that seen from tunnelling (Wheeler, 1990), with the consequence that definitive resolution between these two models is not feasible with typical experimental data collected at a constant temperature. Therefore while these data (from the 10°C storage) support either model, the additional information afforded by the storages at 100°C enable assignment of tunnelling as the dominant mechanism. This leads to the second reason: apparent thermal acceleration is not distinct for storage times less

than 1 month at 100°C, by which time the form of the decay curves are apparent and the "thermal acceleration" is almost certainly simply thermal drainage of some of the lower temperature TL traps contributing to the measured luminescence signals (thermal acceleration in TL is demonstrated in the following section).

The criterion for classification of samples as "fading" or "stable" was that the remanent luminescence must show a decrease at the 95% confidence level (based on scatter about the best-fit line) for the sample to be said to fade.

Superficially the data appear to suggest that tunnelling type fading is the dominant, if not the only, mechanism present. However it is possible that localised transition fading is also a significant portion of the fading component, but the storage temperatures were too low or storage durations too brief for this to become clearly apparent: the intrusion of thermal fading precludes significantly "stronger" preheats unless the TL is studied - this approach was taken for further work, using a range of storage temperatures as described for sanidine in the following sections.

The two mechanisms each offer different possibilities for control, and if tunnelling is unaccompanied by any other processes affecting the decay rate, precise laboratory monitoring of the fading over several decades of time should permit the accurate fitting of an equation of the form $R = a - b*\ln(t)$ to the remanent luminescence. However, this approach presupposes that the entire signal is susceptible to fading and that deviations from the "ln(t)" form for extrapolations of over an order of magnitude of time, as described by Wheeler (1990), do not occur. Finally, from the experience here, it would likely prove impractical to accomplish with high accuracy because of measurement errors in the monitoring of the fading.

The principal conclusions are that discrimination against anomalous fading is not

possible by choice of mineral species or density fraction, and that elevated temperature storage does not reliably remove the anomalously fading component. In no sample *which exhibited fading* was a stable residual level unambiguously achieved, and the absolute efficacy of preheat storage for eliminating anomalous fading luminescence from feldspars is disproved. However, apparently contrarily, the observed fading behaviours indicate partial success for preheating routines and lead to the recommendation that preheating in the dating of feldspathic materials remains a desirable element of the dating routine. This apparently contradictory recommendation follows from a consideration of typical sediment samples - as polymineral sediments (either coarse or fine grain) can contain a mixture of grains displaying fading or stable luminescence, elevated temperature storage will accelerate that component of the fading luminescence susceptible to such treatment, and the enforced storage duration will also permit athermal fading components to diminish in importance relative to the stable luminescence from other grains (if not from the fading grains themselves, given the implication from this work that stable remanent levels are not achieved ordinarily in feldspar samples displaying fading). Finally it must be emphasised that various feldspars, including examples of species commonly selected by density (coarse grains with densities < 2.58 gm/cm^3) for use in dating applications, were found not to fade detectably.

Table 4.2.2.4.1 Decay parameters for IRSL.

Sample	IRSL 10°C			
	a ± Δa	b ± Δb	Remanent IRSL after 2 months (%)	Classification
5. No.3062 microcline	1.052 ± 0.100	0.00035 ± 0.0080	105	stable
3. Z5 microcline	1.328 ± 0.044	0.0555 ± 0.0035	47	fades
11. Z6 orthoclase	1.024 ± 0.048	0.0078 ± 0.0039	90	stable
21. Z9 microcline	1.165 ± 0.021	0.0353 ± 0.0017	62	fades
14. Z11 microcline	1.019 ± 0.094	0.0219 ± 0.0075	68	fades
13. Dup(C) microcline	1.075 ± 0.049	0.0111 ± 0.0039	90	indeterminate
1. adularia	1.016 ± 0.071	0.0035 ± 0.0057	96	stable
20. Z9N microcline	1.170 ± 0.027	0.0302 ± 0.0023	70	fades
9. Z15 sanidine	1.180 ± 0.024	0.0348 ± 0.0022	64	fades
12. Patmos sanidine	1.276 ± 0.078	0.0494 ± 0.0064	51	fades
18. Amelia albite	1.002 ± 0.071	0.0030 ± 0.0057	96	stable
15. Dup(A) albite	1.090 ± 0.047	0.0090 ± 0.0038	95	stable
4. 17 oligoclase	1.237 ± 0.032	0.0401 ± 0.0025	62	fades
7. 18 oligoclase	1.258 ± 0.052	0.0422 ± 0.0042	61	fades
23. Dup(B) oligoclase	1.215 ± 0.053	0.0367 ± 0.0043	65	fades
19. BA6 labradorite	1.392 ± 0.202	0.0554 ± 0.0161	53	fades
6. 23 labradorite	1.059 ± 0.031	0.0128 ± 0.0024	86	fades
24. Dup(D) labradorite	1.037 ± 0.074	0.0078 ± 0.0060	92	indeterminate
10. Z4 bytownite	1.011 ± 0.074	0.0054 ± 0.0060	93	stable

Table 4.2.2.4.2 Decay parameters for OSL.

Sample	OSL 10°C			
	a ± Δa	b ± Δb	Remanent IRSL after 2 months (%)	Classification
5. No.3062 microcline	1.087 ± 0.094	0.0064 ± 0.0075	99	stable
3. Z5 microcline	1.382 ± 0.053	0.0615 ± 0.0042	43	fades
11. Z6 orthoclase	1.075 ± 0.061	0.0038 ± 0.0048	102	stable
21. Z9 microcline				
14. Z11 microcline				
13. Dup(C) microcline	0.964 ± 0.026	0.0009 ± 0.0011	95	stable
1. adularia	1.007 ± 0.061	0.0050 ± 0.0047	93	stable
20. Z9N microcline				
9. Z15 sanidine				
12. Patmos sanidine	1.369 ± 0.039	0.0628 ± 0.0031	40	fades
18. Amelia albite	1.074 ± 0.072	0.0097 ± 0.0057	92	stable
15. Dup(A) albite				
4. 17 oligoclase				
7. 18 oligoclase				
23. Dup(B) oligoclase	1.332 ± 0.088	0.0499 ± 0.0070	56	fades
19. BA6 labradorite	1.349 ± 0.061	0.0673 ± 0.0049	31	fades
6. 23 labradorite				
24. Dup(D) labradorite				
10. Z4 bytownite				

4.2.3 FADING OF TL IN SANIDINE

4.2.3.1 INTRODUCTION

The fading survey described above revealed a variety of fading behaviours amongst the feldspars. In some cases thermal acceleration suggestive of localised transition-mediated fading was seen, raising the hope for these samples that if a stable component of luminescence was present it could be isolated by a suitable preheat, so possibly enabling optical dating. To assess prospects for thermal removal of such fading (in these cases at least) the effect of elevated temperature storage on the fading rate and TL glow curves of two sanidines showing this type of fading was investigated. The sanidines 12. Patmos and 9. Z15 were tested; as similar results were obtained data is presented here for the Patmos sample only.

4.2.3.2 THERMAL ACCELERATION OF FADING IN 12. PATMOS SANIDINE

Glow curves shown in Fig.4.2.3.2.1 were measured from aliquots of sample stored at temperatures of 10°C, 100°C, 160°C and 220°C for durations of 1 day, 3 days, 1 week, 2 weeks, 5 weeks and 9 weeks. The fading measurements followed drainage of the NTL by heating to 550°C at 5 K/s then reheating, after which each aliquot received a dose of ≈ 500 Gy $^{90}Sr/^{90}Y$ β, a prompt preheat of 60 seconds at 220°C, then isothermal storage for various durations. TL was measured to 550 °C at a heating rate of 5 K/s using a Risφ automated TL reader with an EMI 9635Q PMT and Corning 7-59 and Chance-Pilkington

HA3 filters. Normalization factors were derived from the NTL which had been measured prior to the original added β dose; the light levels are directly comparable. Note the changes of scale of the TL intensity, and that the "no storage" unfaded glow curve is plotted with the 10°C data set only - the higher temperature storages reduce the TL intensities too drastically for the unfaded glow curve to be usefully overlain. Comparison of the glow curves show obvious thermal acceleration, most unambiguously in the glow curve region above 300°C for storage temperatures of 10°C and 100°C.

Fig.4.2.3.2.2 shows a subset of the data plotted according to storage duration. Thermal acceleration of the anomalous fading is clearly occurring in the higher temperature glow curve regions beyond the influence of "straightforward" thermal detrapping to the conduction band. Consequently this higher temperature TL region was analyzed for the presence of a stable remanent component, and also to examine further the localised transition-type behaviour. Fig.4.2.3.2.3(a) and (b) show TL integrated between 425°C and 450°C plotted for each storage temperature and duration (following Templer, 1985). The complex nature of the fading in this sample is clearly shown here, as at low storage temperatures the fading form is very close to logarithmic, whereas at the higher storage temperatures the character apparently changes to a form more in accord with the localised transition model; however a stable remanent level is not achieved even when the remanent level is < 3 % of the initial TL intensity, suggesting that such a level does not exist in this sample.

IRSL was also measured, using an Elsec automated optical dating reader (Type 9010) with an EMI 9235Q PMT with a 2 mm Schott BG 39 filter. Two short exposures ($\approx$ 30 mJ) were given, the first immediately following dosing and preheating (as a normalization measurement) and the second following each fading storage and just prior

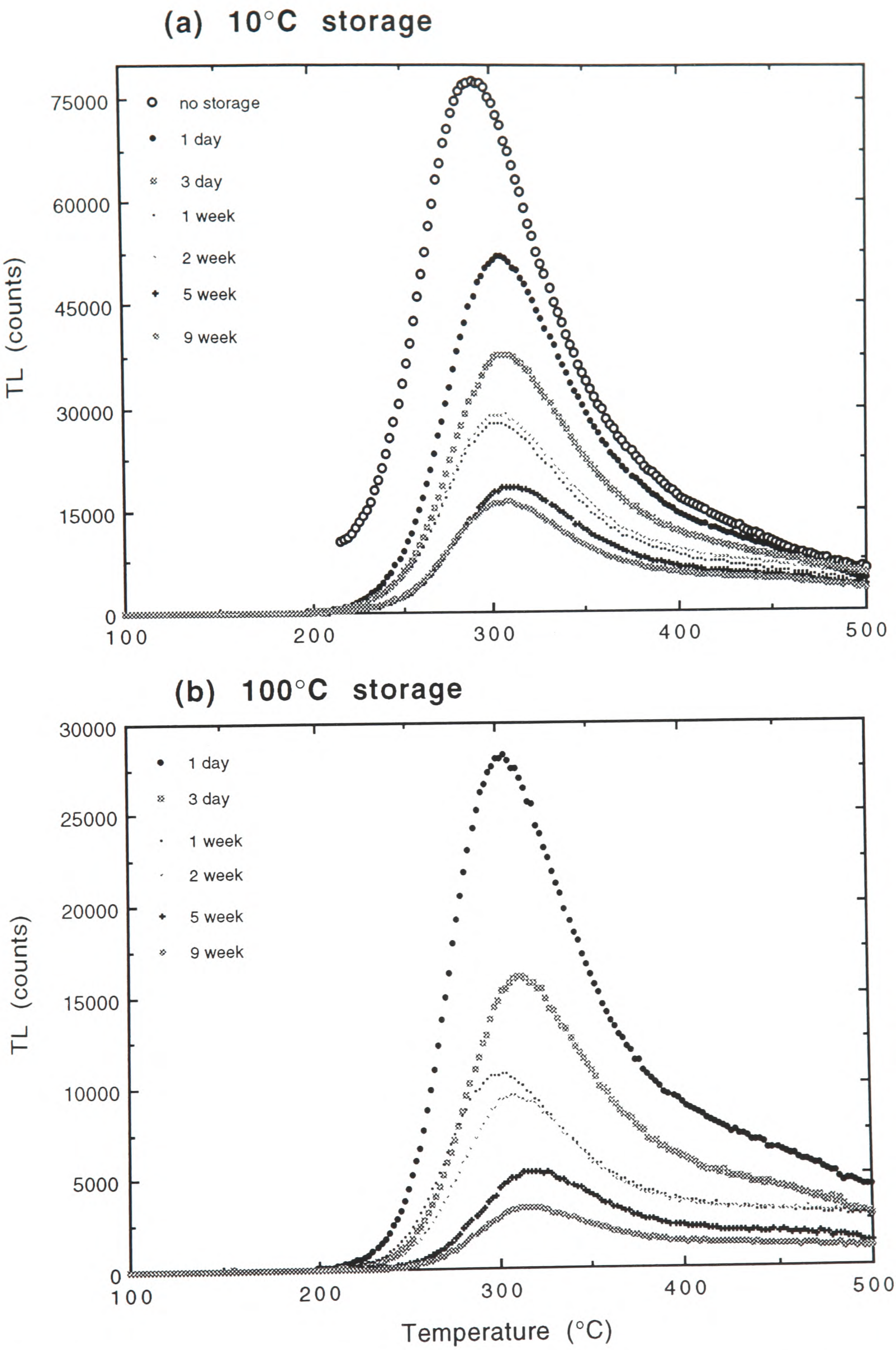
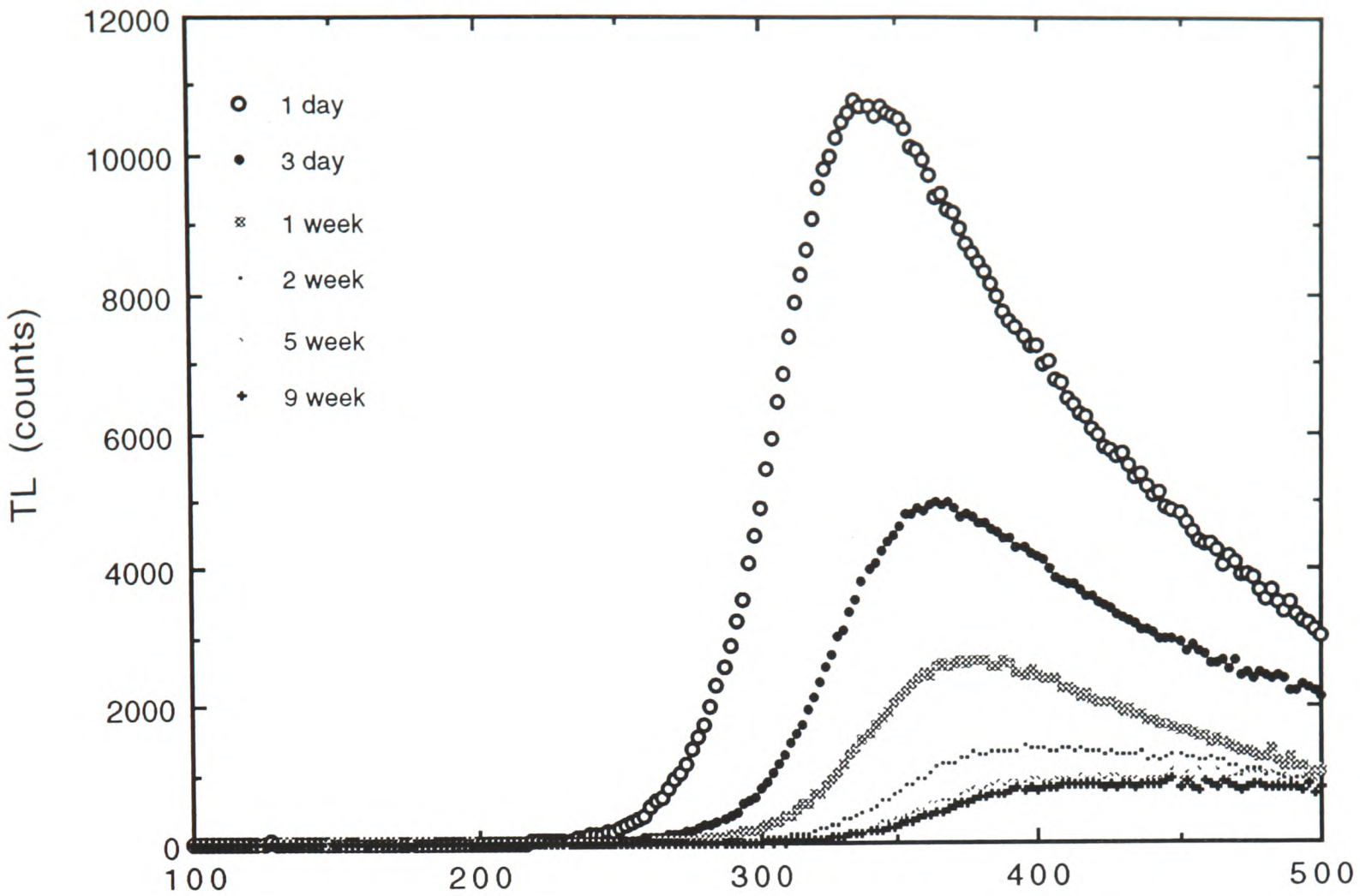
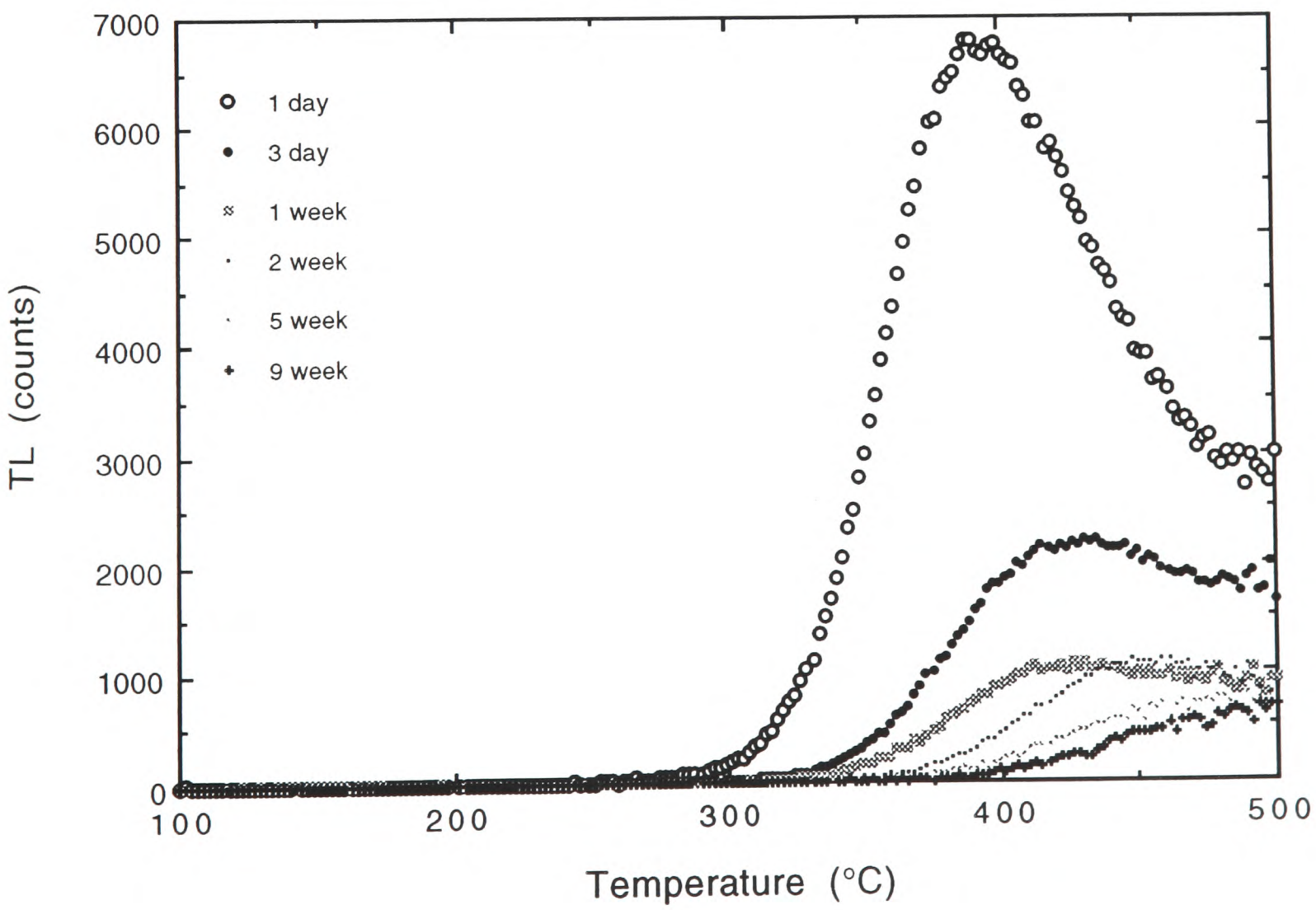


Fig.4.2.3.2.1.(a)-(d) Glow curves of 12. Patmos sanidine following various durations of isothermal storage, data (counts/2K) are plotted according to temperature of storage.

(c) 160°C storage



(d) 220°C storage



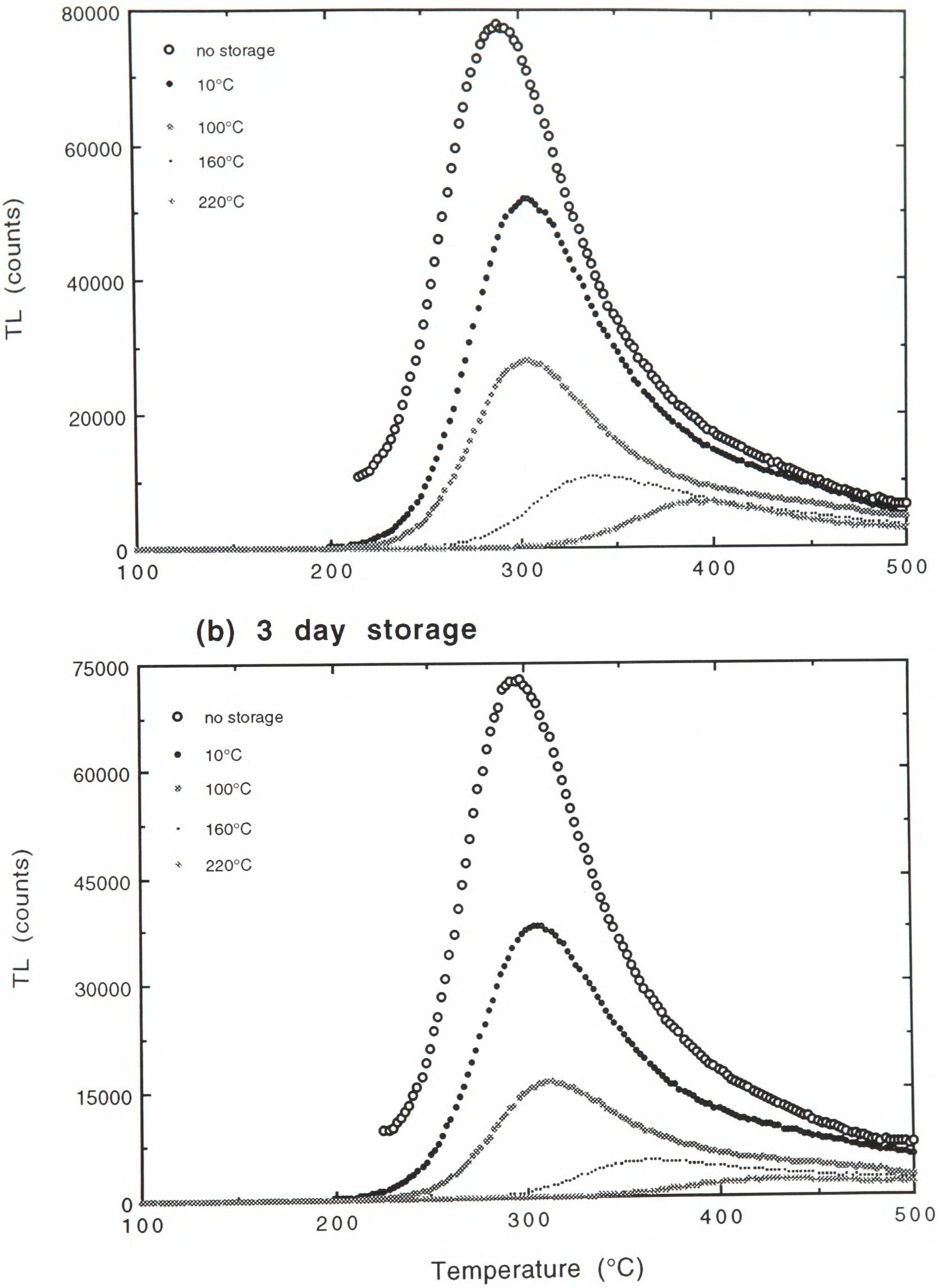
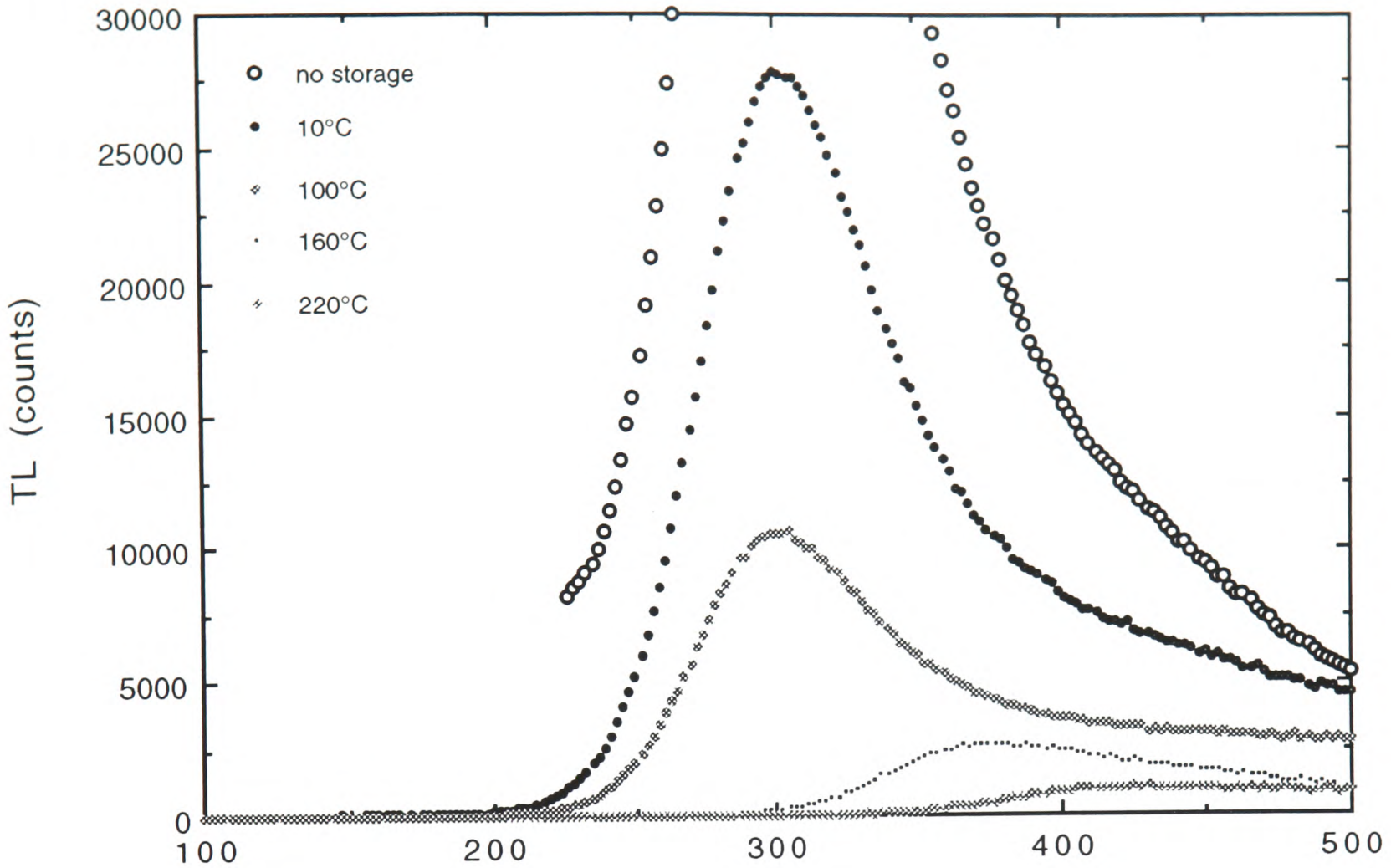
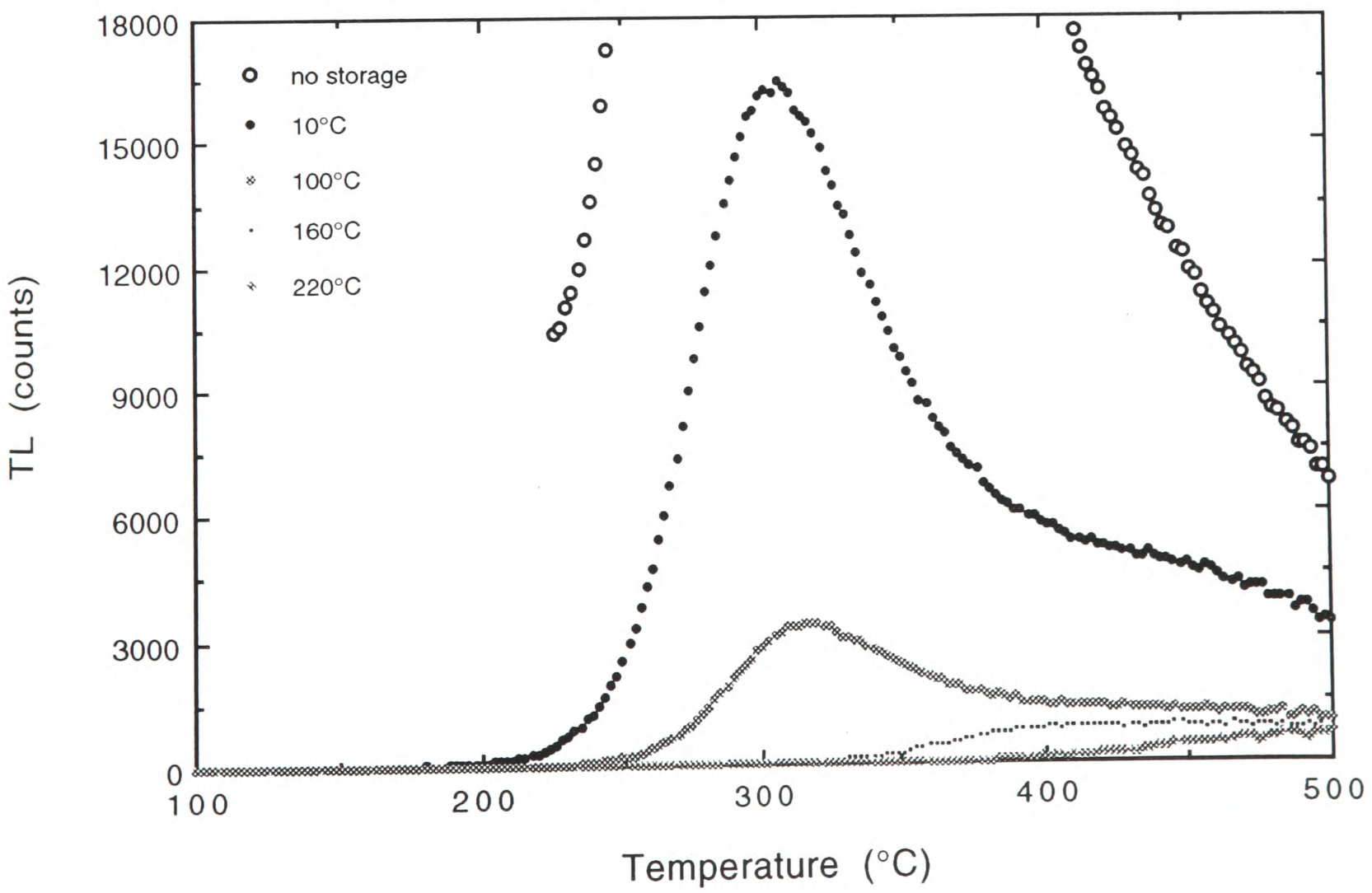


Fig.4.2.3.2.2.(a)-(d) Glow curves of 12. Patmos sanidine following the given storage durations at various temperatures. Note the temperature-dependent acceleration of fading, especially at glow curve temperatures greater than ≈ 400°C, where thermal detrapping to the conduction band is not significant.

(c) 1 week storage



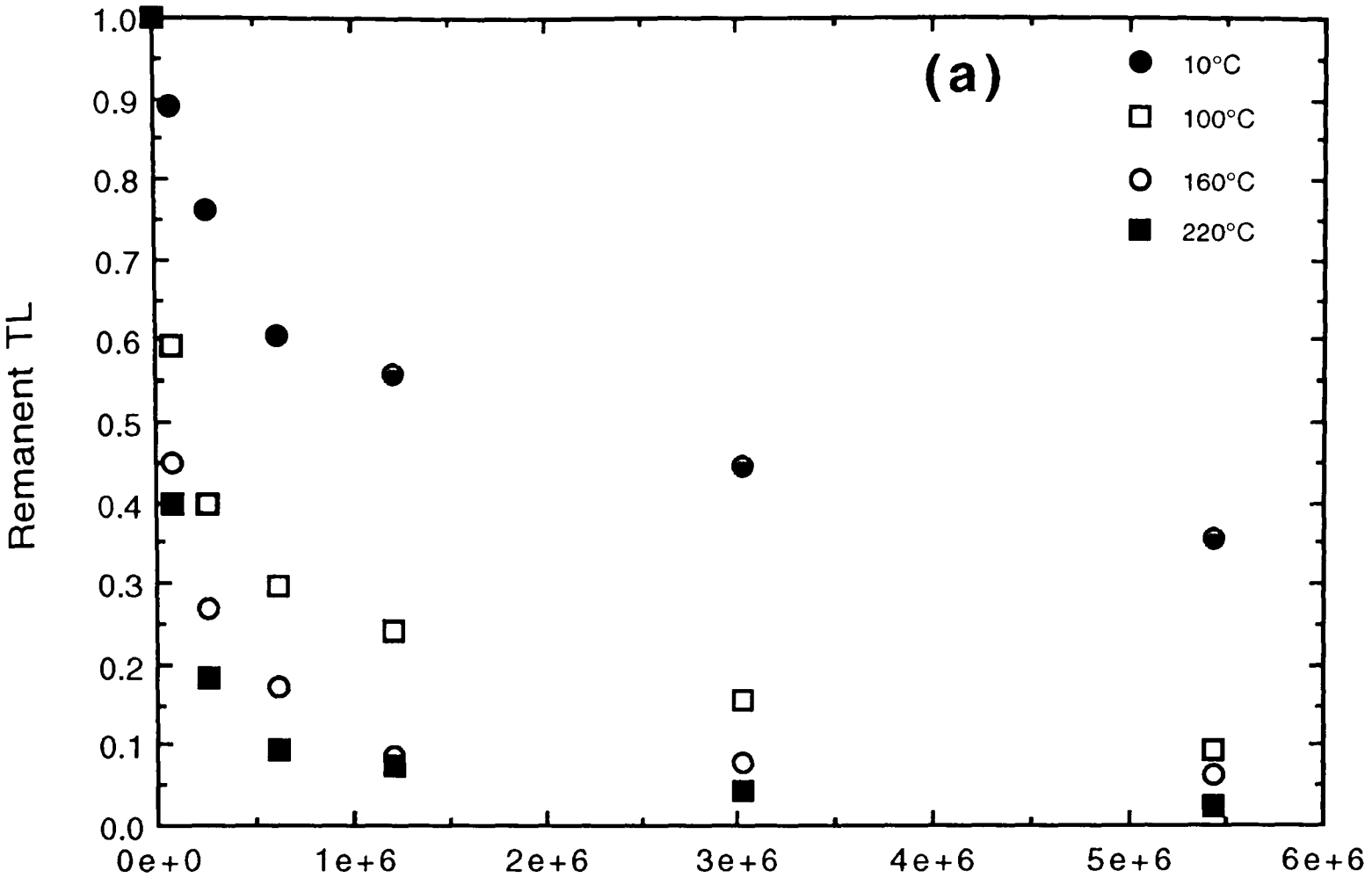
(d) 9 week storage



to TL measurements. Results suggested the IRSL decay was of similar form to that of the TL, but thermal erosion of the trapped charge populations contributing to this signal prevents unambiguous conclusions from being drawn, hence this data is not shown.

It must be noted that the use of long duration elevated temperature storage to assess elimination of the anomalously fading component is complicated if time-dependent sensitivity changes occur. If sensitization occurs, a false remanent level may result; conversely, desensitization could prevent recognition of an adequate preheat. The sanidines studied here showed indications, though not conclusive, of sensitization (defined as an increasing ratio of the TL sensitivity to a test dose following the fading measurements to that of the "NTL"). However even a worst case correction for sensitization did not reveal the Patmos sample to be showing "pure" tunnelling-type fading. Consequently it is inferred from the thermal acceleration evidence that localised transition type fading may be present in this sample, at least at and above ambient temperatures (though also bearing in mind the possible occurrence of thermally accelerated tunnelling as proposed by Huntley (1985)). This finding is consistent with the report by Tyler and McKeever (1988) of localised transition-type fading in an oligoclase (though admittedly their identification is not unequivocal). On the other hand measurements made on this same sample by R. Visocekas (1993) where the fading phosphorescence was studied at temperatures down to 77 K reveal relatively intense tunnelling phosphorescence, and so demonstrate that tunnelling is also operant. (Furthermore, comparison of the high temperature TL loss by fading with the phosphorescence detected showed significant thermal quenching of the signal; fortunately this phenomenon does not affect isothermal monitoring of the fading).

It was concluded that although thermal acceleration of fading in this sample does occur, there appears to be no stable component of remanent luminescence; ie, fading



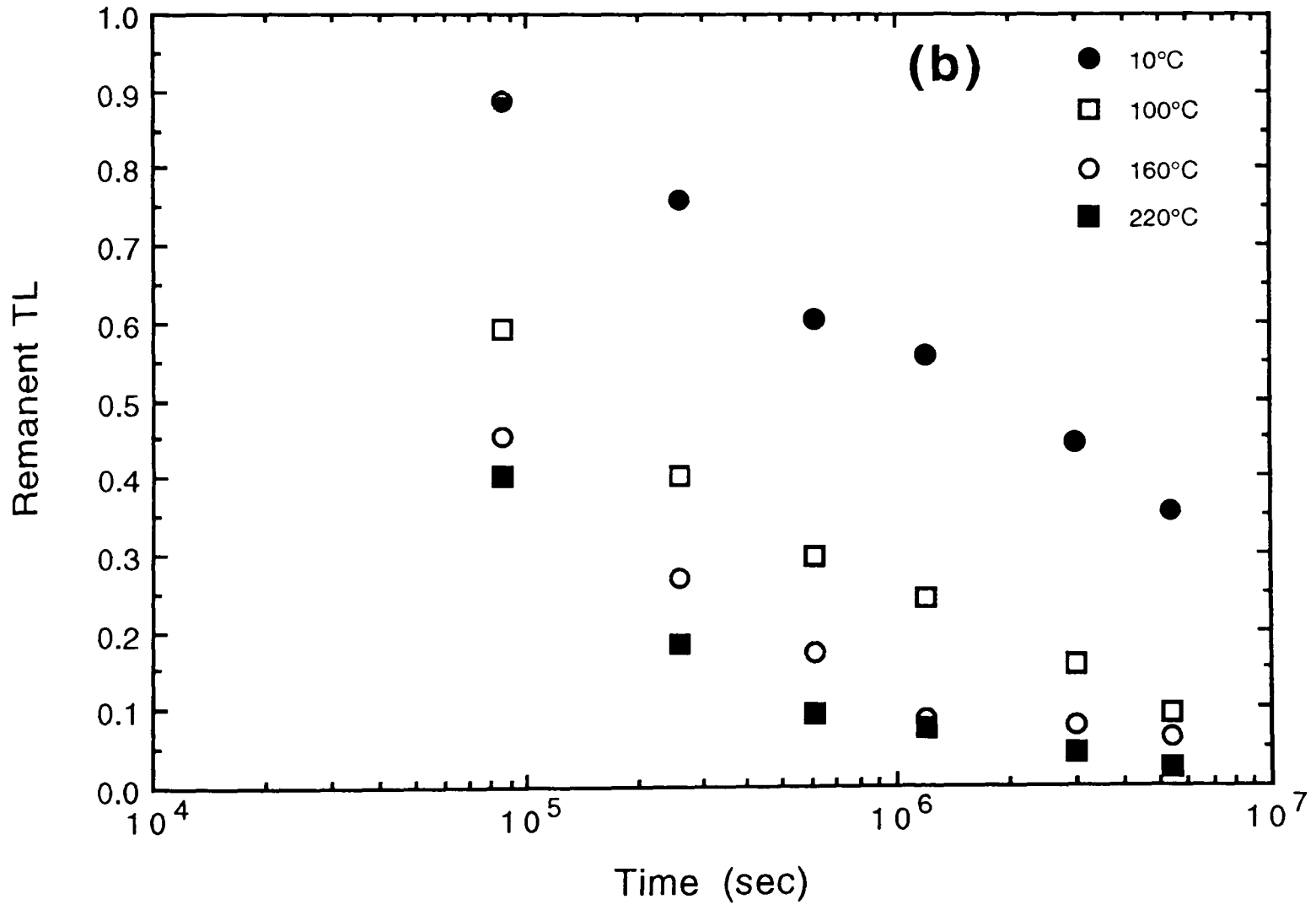


Fig.4.2.3.2.3 **(a)** The remanent TL integrated between 425°C and 450°C as a function of storage duration (seconds), **(b)**, the same data plotted against log(time) to reveal the logarithmic dependence of the fading with time at lower storage temperatures.

proceeds indefinitely. Tunnelling-type fading is also present and it is surmised that all the signal in this sample can fade by either route, and a consequence is that the "NTL" is simply a dynamic equilibrium level reached between environmental irradiation and fading. This conclusion was tested by dating 12. Patmos sanidine, as described below.

4.2.3.3 DATING OF 12. PATMOS SANIDINE

The sample 12. Patmos sanidine consisted of opaque pebbles (≈ 0.5 cm to 1 cm diameter, geologically determined age 8.9 Ma) of plutonic sanidine from the island of Patmos, Greece. Dating was performed using fine grains (4-11 μm) kindly drilled from the interior of a pebble under very low intensity red light by M. Winter and deposited on aluminium discs from acetone. TL measurements were made on the Risϕ reader as above. Glow curves for the NTL and various added β doses, along with an additive dose growth curve constructed from that data are shown in Figs.4.2.3.3.1 and 4.2.3.3.2).

The expected palaeodose (considering only the internal K + Rb dose contributions) for this sample is ≈ 8900 (ka) * 3.9 (% K) * 1.080 (Gy/ka/%K dry dose rate) * 0.85 (fraction of infinite matrix β dose received by a 7 mm diameter pebble) ≈ 32 kGy. The measured palaeodose is ≈ 17 Gy which at the calculated dose rate of ≈ 3.6 Gy/ka corresponds to an age of ≈ 4.7 ka, assuming no fading. Therefore the palaeodose calculated from the known sample age exceeds the measured value by a factor of ≈ 1,900, setting an upper limit for the "stable remanent" fraction of the TL measured immediately following laboratory irradiation as ≈ 0.0005. Furthermore, given the real situation in that the observed NTL is the fading remanent resulting from dose received over the last 4.7

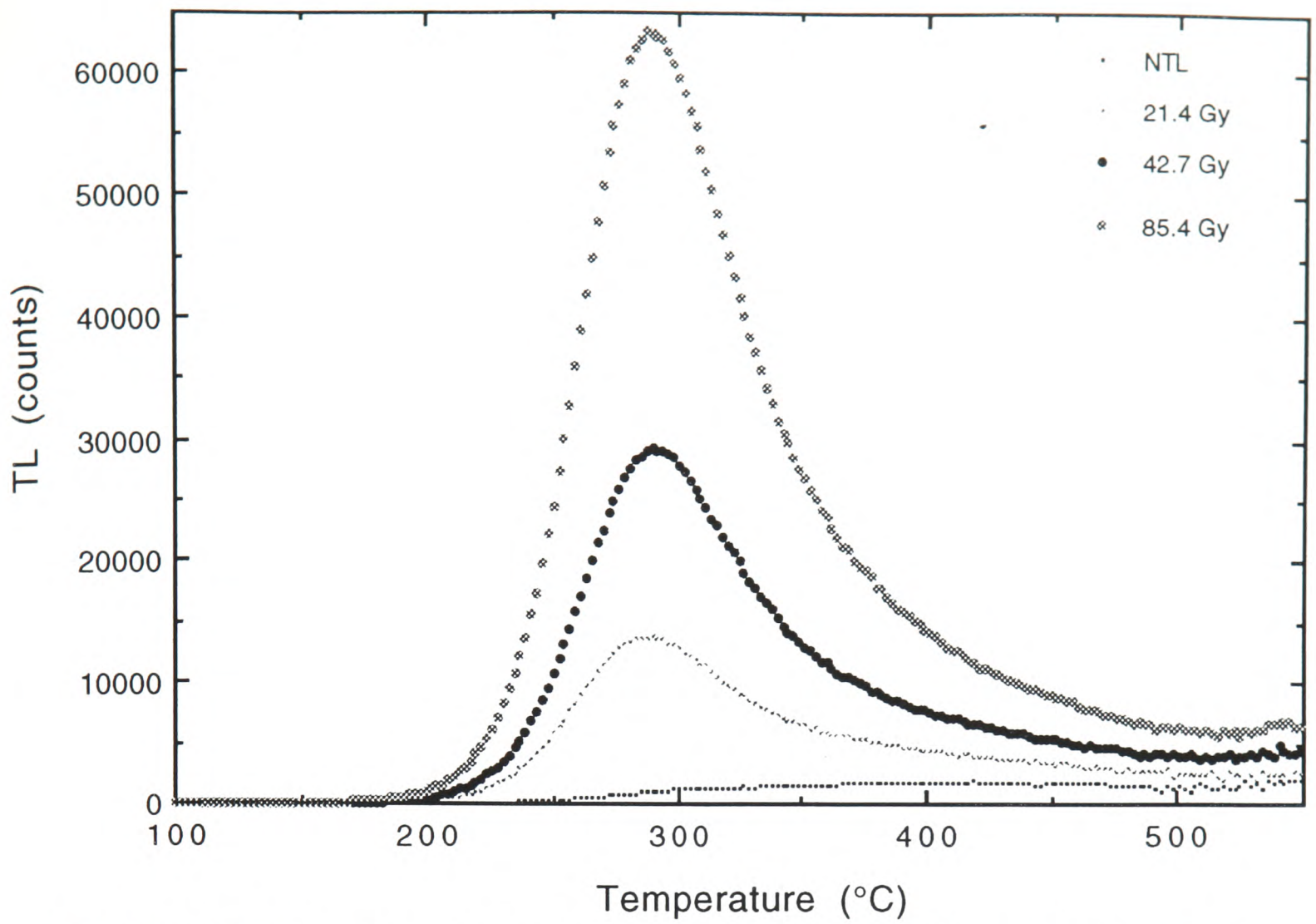


Fig.4.2.3.3.1 Natural and additive dose glow curves for 12. Patmos sanidine measured following a preheat of 60 seconds at 220°C. Data plotted are counts/2K.

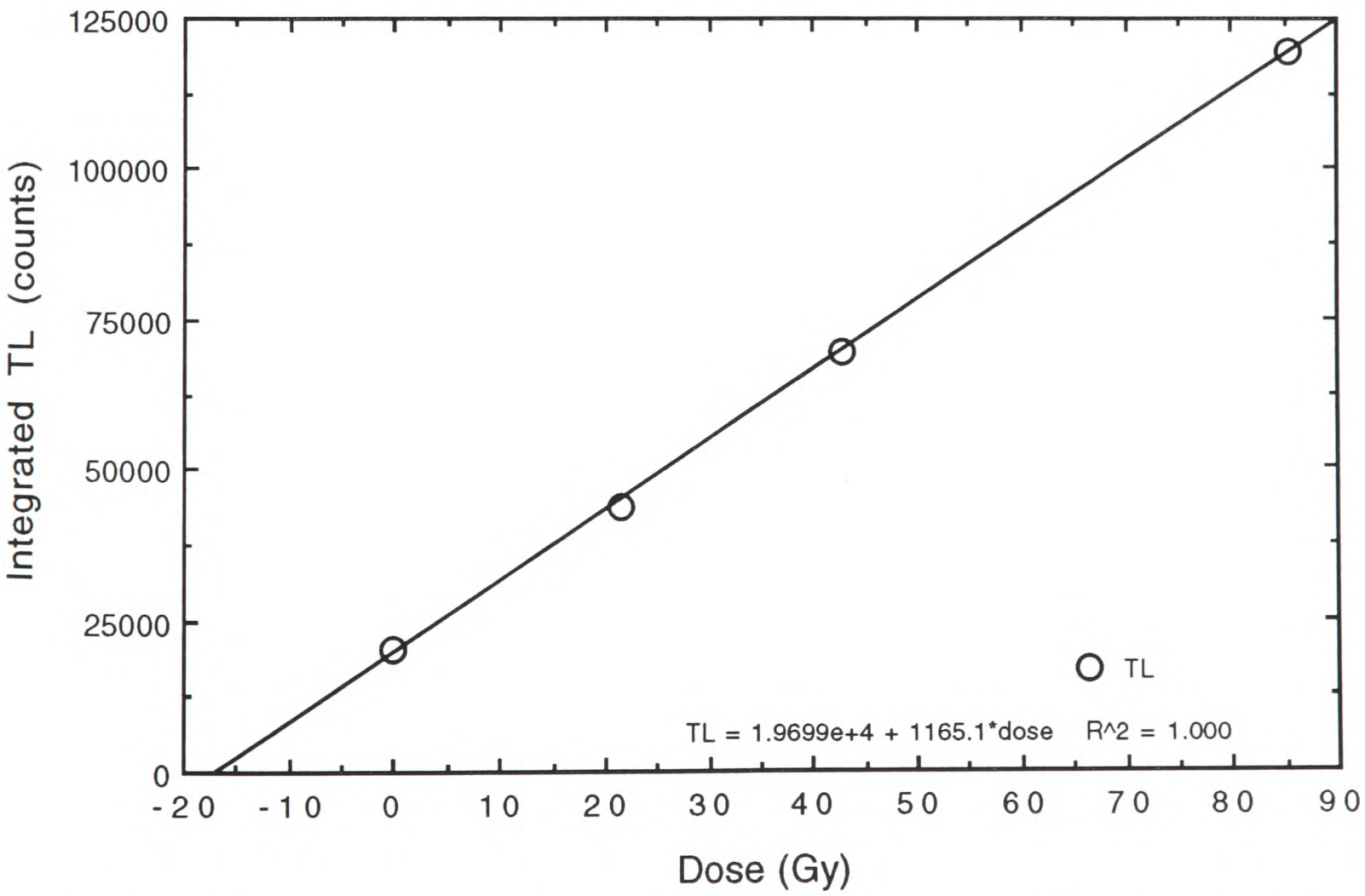


Fig.4.2.3.3.2 The additive dose growth curve for 12. Patmos sanidine; the linear fit shown (to TL integrated from 425°C to 450°C) gives a palaeodose of ≈ 17 Gy.

ka (at least), this is not inconsistent with the interpretation that the fading and induction of luminescence by the environmental radiation are in dynamic equilibrium, and that there is no stable component of the luminescence which can accrue with time, in this sample.

However it must be pointed out that the fading rate found for TL in the 425°C - 450°C temperature region is significantly greater than that found for the IRSL. If this fading rate (≈ 12.6 % / decade of time) is used instead, then effectively no contribution of TL to the observed NTL can be expected from doses received prior to ≈ 3 years ago, contradicting the above conclusion in favour of there being a stable TL fraction comprising just 0.05 % of the TL observed promptly after irradiation. Even if this latter picture is correct, all the preheats given were inadequate to eliminate the hypothetical 99.95 % of TL which is unstable; the strength of some of these preheats, ie, 9 weeks at 220°C, is such as to suggest that preheating is not a feasible means of isolating the stable signal in this sample (ignoring unexplored complications such as sensitivity changes during the preheats).

In summary, the conclusions given in section 4.2.3.2 are generally supported by the dating of this sanidine; although there is the possibility that a very small fraction of the TL does not fade, separation of this fraction by preheating does not appear feasible in this sample. Following these findings, a final attempt to isolate a fading signal susceptible to removal by elevated temperature storage was made using the novel approach of measuring the TL at very slow heating rates. Results are presented in the following sections.

4.2.4 A NEW APPROACH FOR INVESTIGATING LOCALISED TRANSITION FADING - THE METHOD OF VARIATION OF HEATING RATE

4.2.4.1 INTRODUCTION

This section describes an investigation into the use of variation of heating rate to probe thermally accessible sub-conduction band pathways between electron traps and spatially localised recombination centres. The aim was establishment of the applicability of this as a tool for the investigation of anomalous fading. It was anticipated that this work might lead to a method of studying and eliminating fading mediated by localised transitions, in the feldspar minerals.

The approach here follows the suggestion by Templer (pers. comm., 1990) that the fading TL component governed by the localised transition mechanism (Templer, 1986a, 1986b) may be manifest at slow heating rates as a previously unobserved TL peak appearing in the low temperature region of the glow curve. Isolation of such a TL peak would enable the application of kinetic techniques to determine its kinetic parameters - which should be those of the shared excited state required by this model. If this proved possible it would serve not only as confirmation of the localised transition model for this fading, but also, as a practical consequence for dating applications, allow the precise determination of the preheat conditions necessary to eliminate the fading component, leaving only stable luminescence.

That this fading-peak isolation may occur can be readily understood in terms of the effect of competing pathways available for charge passage between the electron and

hole traps. Consider the role in charge transport of the localised, sub-conduction band pathway : typical E and S values have been determined for zircon by Templer (1986a) as $E \approx 0.90 - 0.78$ eV (mean $E \approx 0.84$ eV) and $S \approx 3 \times 10^6$ s^{-1}. Although the low frequency factor effectively means that this transition is not favoured, the correspondingly low effective trap depth does permit the slow leakage of charge through this pathway from these traps at ambient temperatures. The entire trapped charge population having access to such pathways will typically undergo recombinations within about one month of storage at 20°C (Templer, 1985), so giving rise to the "anomalous" fading from otherwise apparently stable traps. The relationship between the trap E and S and the temperature at which the TL peak maximum (T_{max}) occurs is given by equation 4.2.4.1 (for the case of first order kinetics, which is applicable here. Indeed, as the electrons can only either self-retrap or recombine, this system is a nearly pure first order system).

Equation 4.2.4.1:

$$T_{max}^2 = \frac{\beta E}{kS} \exp\left(\frac{E}{kT_{max}}\right)$$

where T_{max} = TL peak maximum temperature (K)
E = trap depth (eV)
S = frequency factor (s^{-1})
β = heating rate (K/s)
k = Boltzmann's constant (eV/K)

At relatively high rates of heating, such as usual in TL glow curve measurements, (ie, typically in the range 1 K/s to 10 K/s), the TL peak resulting from conduction band transitions will occur at temperatures lower than if the charge untrapped via the localised route. For example, it can be shown from equation 4.2.4.1 that the TL peak corresponding to this localised transition will be observed at 306°C (for $E_{mean} = 0.84$ eV, $S \approx 3 \times 10^6$ s^{-1},

heating rate = 5 K/s). This T_{max} exceeds 285°C, which is that which would result from electron passage through the conduction band assuming a trap depth to the conduction band of 1.5 eV and S = 10^{13} s^{-1}. Therefore only the TL peak resulting from conduction band transitions will be observed. However if the heating rate is significantly reduced, the greater duration which the sample spends at elevated temperatures permits a significant fraction of the trapped charge to have access to the less probable localised pathway. For example, at a heating rate of 0.003 K/s and for the above trap parameters, the TL peak corresponding to recombinations via the localised pathway will have $T_{max} \approx 140°C$, compared to $T_{max} \approx 182°C$ for the corresponding TL peak arising from this same charge recombining via the conduction band, and so now be detectable.

The intent here was to reduce the heating rate sufficiently so that this "localised transition" peak appears. As a first step, a series of measurements were made on zircon, a mineral preferred to feldspar for testing this method as zircon exhibits fading which has been well studied (Templer, 1985, 1986a,b) and is characteristic of the localised transition mechanism. These measurements are reported below.

4.2.4.2 EXPERIMENTAL

The zircon sample used was 210f1, (Templer, 1985, 1986a), immediately available from "archival" material stored by Templer as coarse grains attached by silicone oil to rhodium plated copper discs. These prepared sample discs were used without any additional treatment except for thermally draining the "NTL" by heating at 5 K/s to 550°C in N_2 then repeat. Following thermal drainage artificial irradiations were administered as required, usually ≈ 200 Gy (600 seconds in slide 4 of the Oxford irradiator ß2000).

Irradiation was immediately followed by the "thermal wash" preheat introduced by Wheeler (1990) to erase lower temperature TL (determined as the minimum preheat necessary such that phosphorescence from thermal decay of TL from low temperature peaks was not observed at room temperature). This preheat was given on-plate in all cases and consisted of storage for 120 seconds at 175°C.

Given the possible occurrence of redder emissions resulting from recombinations via localised transition pathways (see Fig.4.2.4.1) two series of measurements were made, the first using restrictive blue/UV filtering (Corning 7-59 + 2 mm Schott BG39, passband 340-445 nm for 50% transmission), and the second using broader band filters (Corning 4-96 + HA3) with a redder passband, from 375-565 nm (50% transmission). Transmission spectra of both sets of filters are shown in Fig.4.2.4.2. Data were recorded using a multi-channel scaler card (EG&G Ortec, type ACE-MCS) hosted by a RM Nimbus VX computer.

Initial measurements were made using the blue/UV filters, as this combination was found to be particularly effective for suppressing the incandescence background during heating (for example, passing ≈ 3 cps at 300°C). However, use of the blue/UV passband filters did not show any significant "new" TL peak appearing as slower heating rates were used, a finding which led to repeat measurements using the broader and redder passband filters (4-96 + HA3). The possibility that repetition using the broader passband filters may show behaviour not observed from the blue/UV emissions followed from consideration of the emission spectra of this same zircon (210f1), as measured by Templer (1985). The emission spectrum, shown in Fig.4.2.4.2 overlain with the transmission spectra of the two filter sets, displays characteristic distinct emission peaks, attributed by Templer to recombinations at rare earth (specifically terbium) centres. As the localised transition

model presupposes the existence of at least one shared excited state "connecting" the electron and hole traps, it was hypothesised that some of the discrete excited levels of the recombination centres (terbium ions) necessary to give the observed line emission spectrum may also correspond to the "localised transition levels" of these recombination centres.

If this was the case, recombinations following passage of electrons to the recombination centres via such excited states may result in the emission of photons having energies characteristic of these ionic excited states, and a similar emission spectrum to that seen following conduction band transitions, but possibly with the crucial difference of the most energetic emission lines being absent. Indeed it is possible that none of the shared states result in emission of blue/UV photons, leaving the fading component an emission spectrum comprised of only the longer wavelength emission bands. It was this possibility that the use of the second set of optical filters was intended to address, as the passband now included the strong zircon emission bands at 490 nm and 550 nm, and so increased the chance of detecting a fading emission redder than that resulting from recombination via the conduction band. (The logical extension of this hypothesis was the use of no optical filters at all, to exploit the full sensitive range of the PMT photocathode, and preferably with a cooled, red sensitive PMT; however, time prevented this work here).

The glow curves measured using each set of filters are shown in Figs.4.2.4.3(a) and (b), (for comparison, some of the unpreheated glow curves measured for normalization purposes are shown in Fig.4.2.4.6). Inspection shows none of the optimistically anticipated discrete "anomalous" peaks (expected to have separated out from the remainder of the glow curve on the lower temperature side), but, significantly, does reveal a subtle systematic increase in the slope of the initial rise of the glow curves with

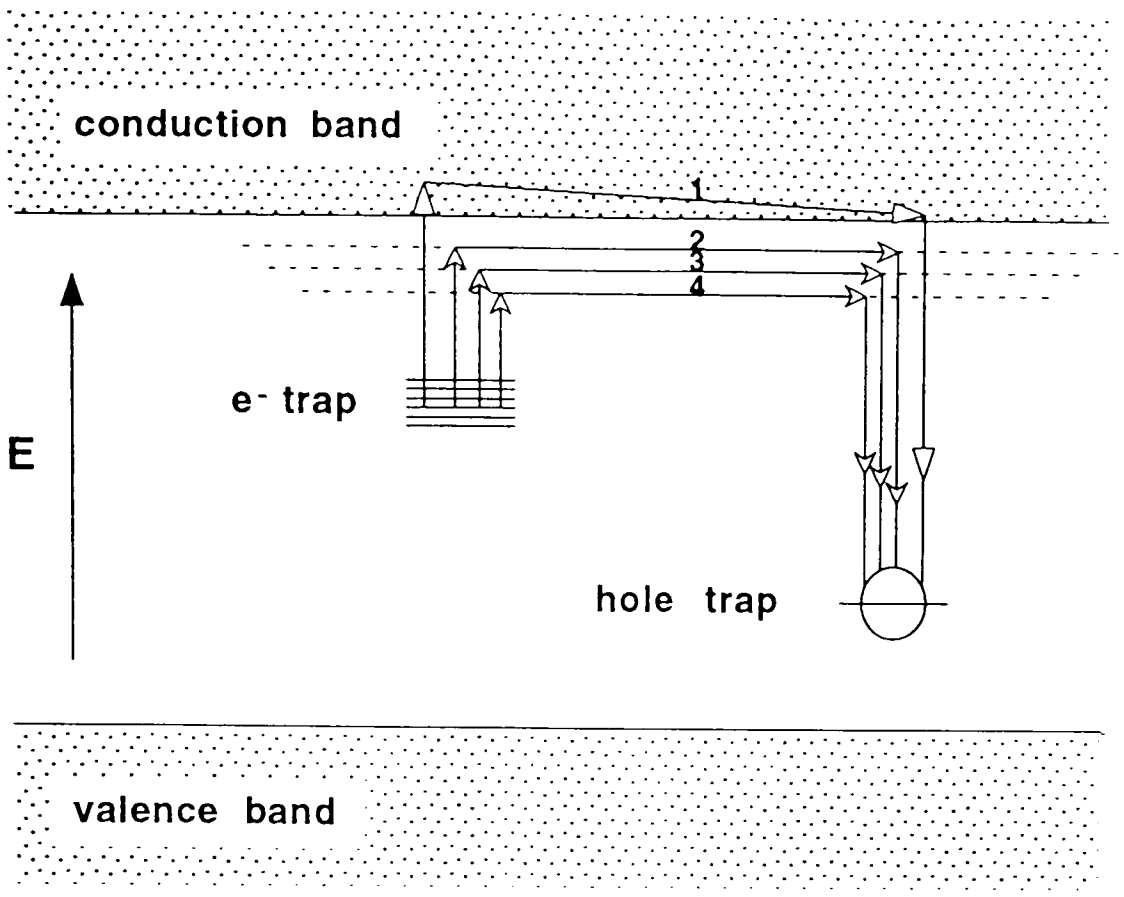


Fig.4.2.4.1 A simplified energy level diagram showing the electron trap-to-recombination centre pathway via the conduction band "1", along with three hypothetical sub-conduction band, localised, pathways "2", "3" and "4". The possibility that these localised pathways may correspond to excited states giving the line emissions characteristic of zircon TL was investigated using the two filter sets shown in Fig.4.2.4.2.

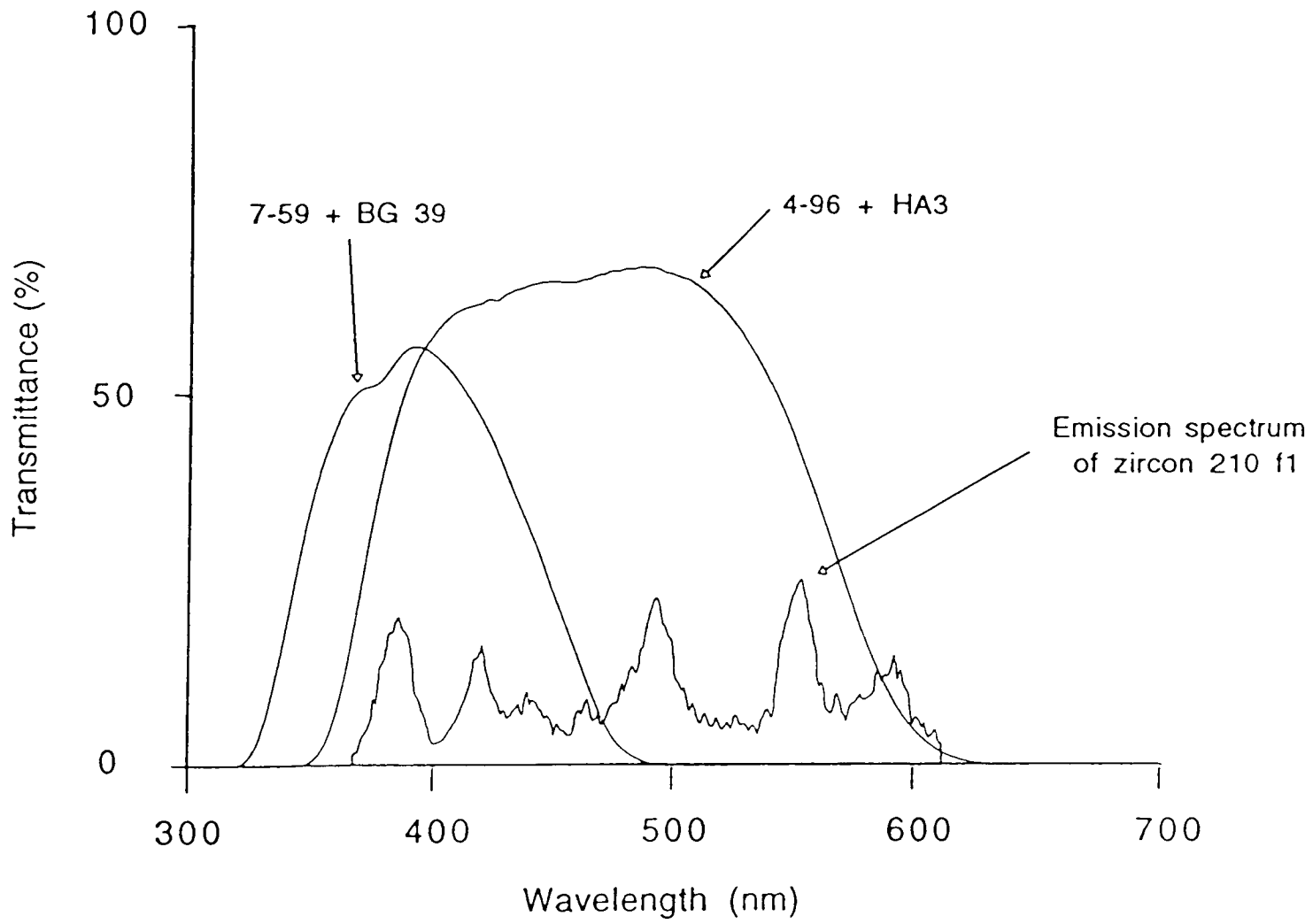


Fig.4.2.4.2 The two filter sets used for the heating rate variation study of zircon, overlain with the emission spectra of this same zircon sample (210f1) as measured by Templer (1985).

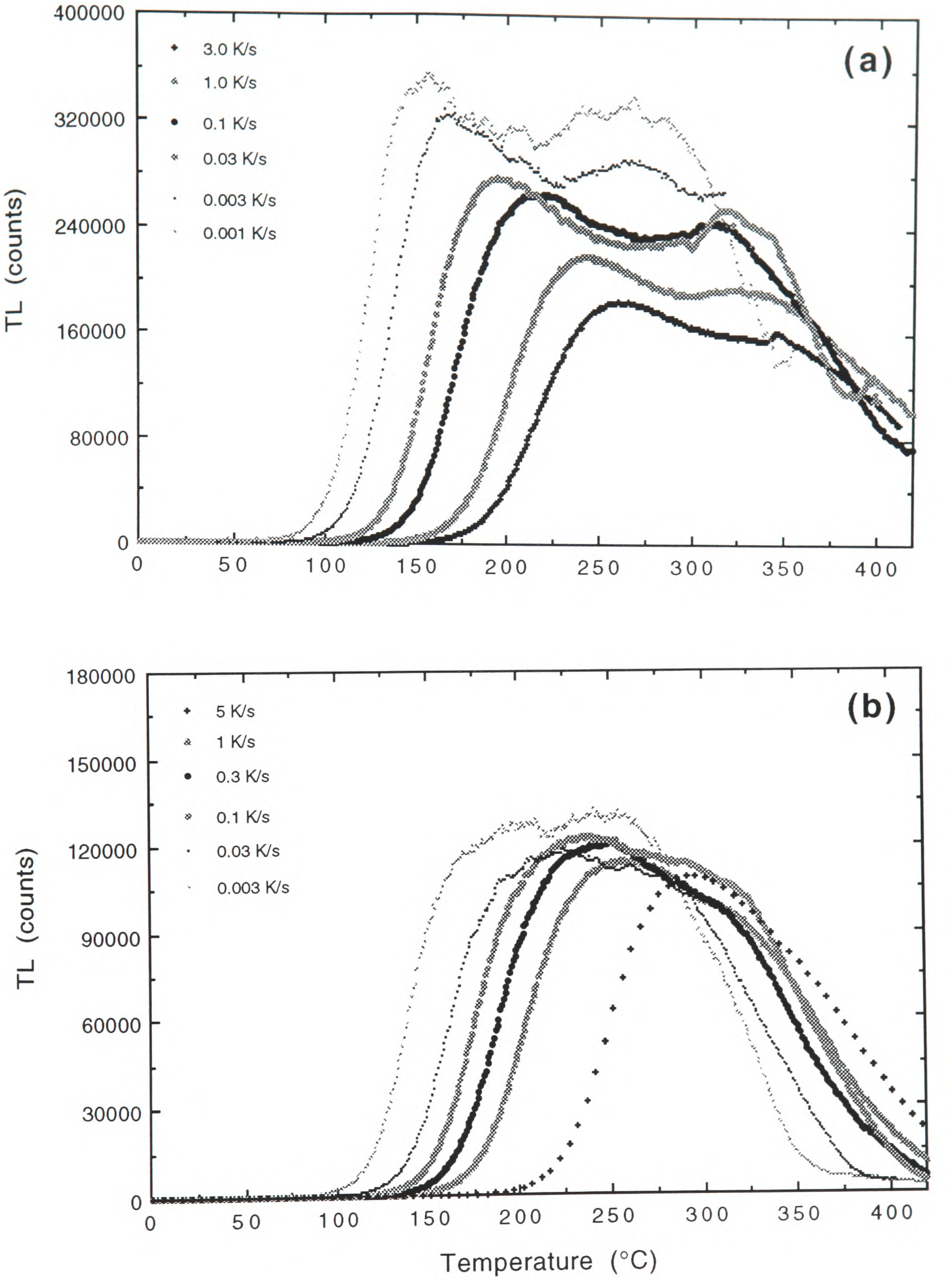


Fig.4.2.4.3 Zircon glow curves measured at the heating rates shown using either **(a)** Corning 4-96 + Chance-Pilkington HA3 filters, or **(b)** Corning 7-59 + Schott BG39 filters. Note the greater light sum from the broader bandpass filters (a). The fine structure on the "slowest" glow curves is probably due to ambient-temperature-dependent changes in the PMT dark count, and the excessive displacement of the 5 K/s glow curve in (b) towards higher temperatures results from thermal lag. Data plotted are counts/K.

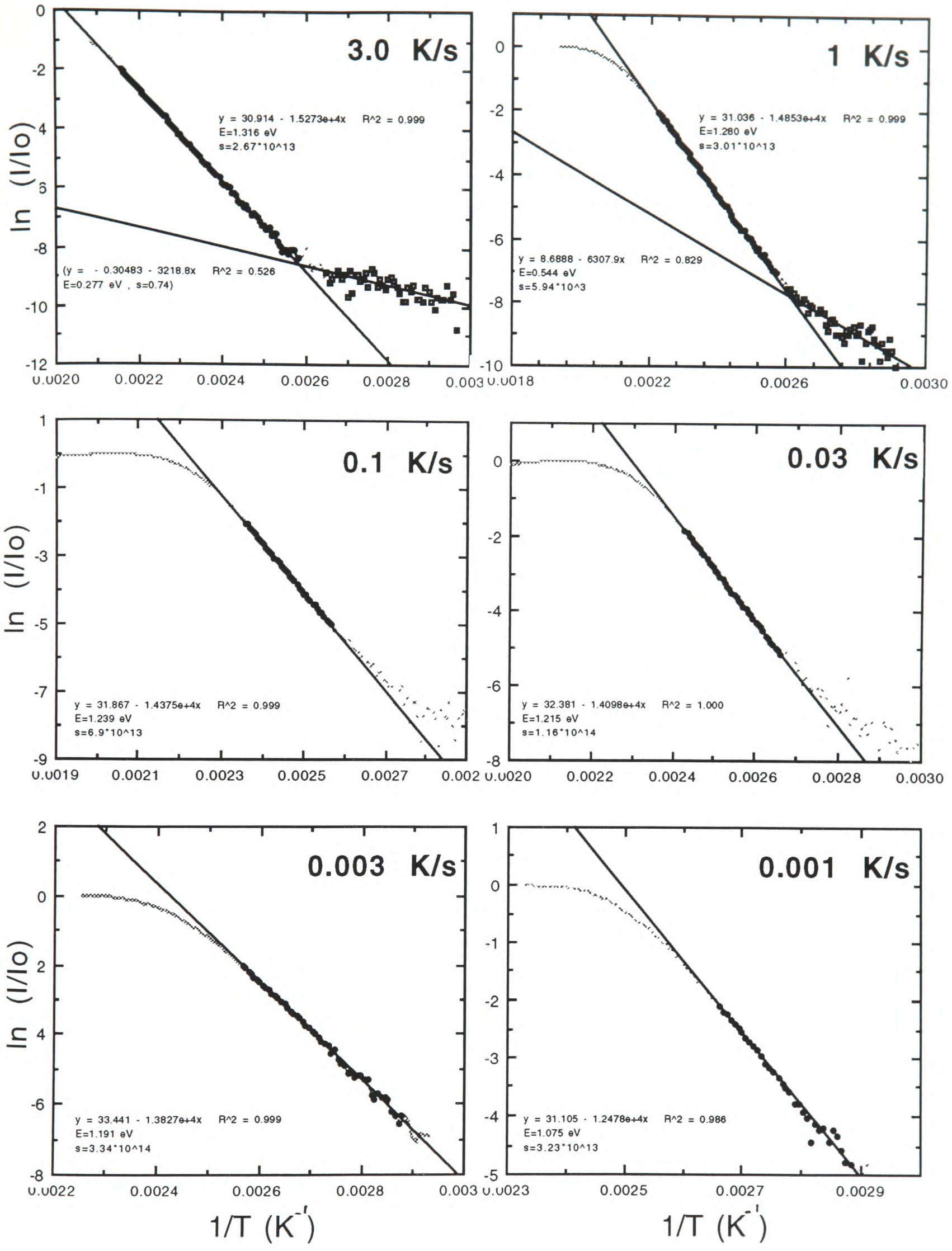


Fig.4.2.4.4 Initial rise plots for each of the zircon glow curves measured using Corning 4-96 + Chance-Pilkington HA3 filters. Note for the two fastest heating rates the appearance of a low intensity signal having low trap depths and frequency factors.

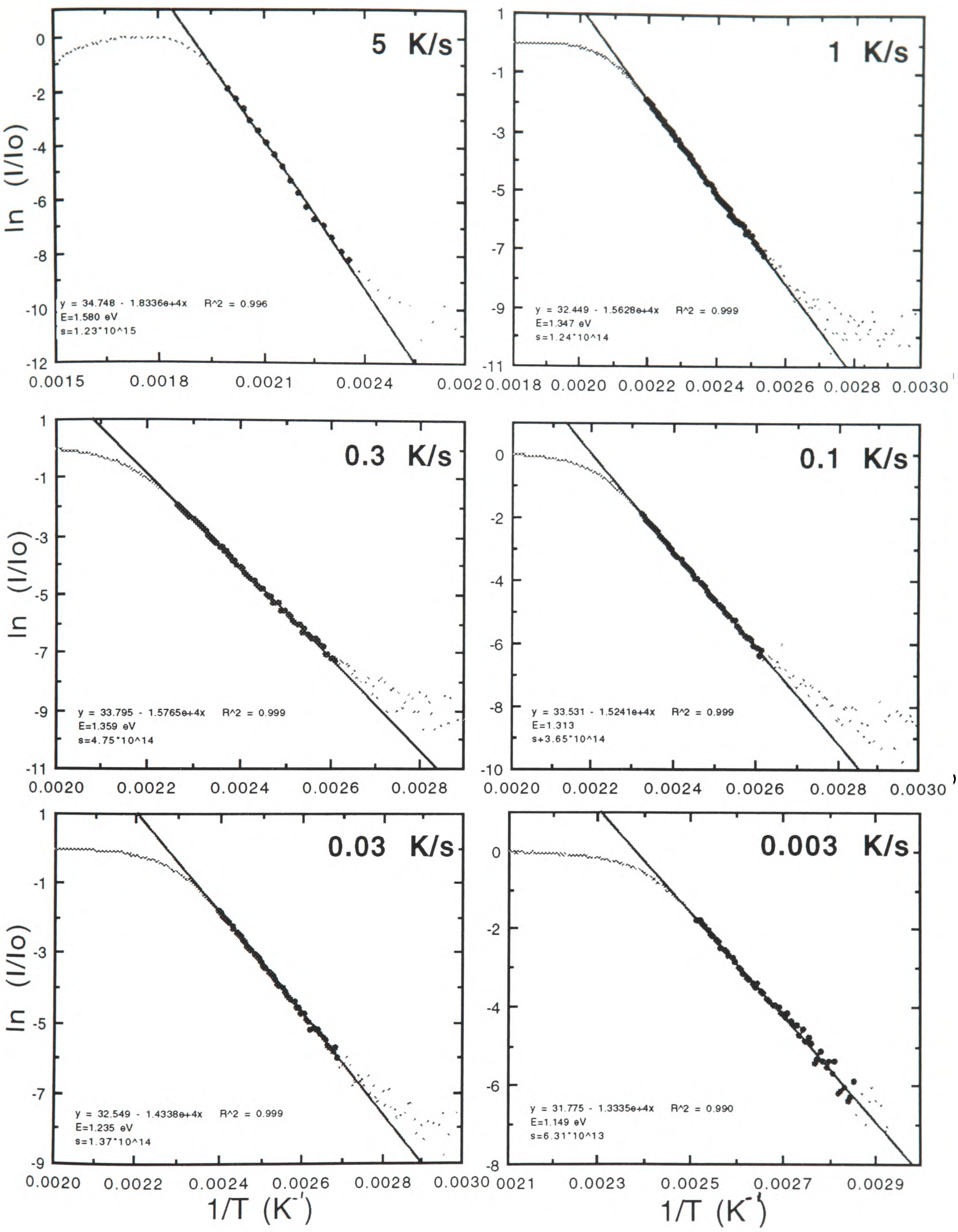


Fig.4.2.4.5 Initial rise plots for each of the zircon glow curves measured using Corning 7-59 and Schott BG39 filters.

decreasing heating rate. Initial rise analysis confirms this impression, (the corresponding initial rise plots are given in Figs.4.2.4.4) and the E values found are plotted in Fig.4.2.4.10. The E values should be interpreted in conjunction with Figure E12 (Templer, 1986b), where the initial rise method was used to measure zircon trap depths between room temperature and 350°C. Interpolating from Templer's data gives trap depths around 200°C of ≈ 1.3 eV, rising to ≈ 1.6 eV at 350°C. In the present work, TL surviving the thermal wash pretreatment does not occur significantly below 200°C when glowed at 5 K/s and the initial rise trap depth found from TL measured at 3 K/s is E ≈ 1.32 eV. This trap depth is consistent with the expectation of conduction band detrapping dominating at these faster heating rates, with the trap depths so determined relating truly to the trap depth below the conduction band. As the heating rate decreases, the trap depth is seen to monotonically decrease also, in accord with the predictions based on an increasing proportion of the electrons detrapping via the localised route. In addition, the frequency factor S also showed a decrease with decreasing heating rate, from ≈ 10^{11}-10^{8} s^{-1}, further supporting the interpretation that a kinetically different pathway is becoming increasingly dominant as heating rate decreases.

4.2.4.3 THE EFFECT OF ALPHA IRRADIATION

To investigate the effect on the TL glow curves (and trap parameters determined by the initial rise method) of the elevated temperature storage procedure recommended by Templer (1985) for removal of the fading component, the fading proportion of TL was measured by storing a dosed sample (210f1) on-plate at 125°C for 3 days (simultaneously recording the phosphorescence), and then measuring the remanent TL. Normalization

glows were made before and after this storage, and the normalization glow curves and remanent TL are shown in Fig.4.2.4.8(a), along with the TL lost during the storage period. The phosphorescence is shown in Fig.4.2.4.8(b); (attempts to fit the phosphorescence as the sum of the isothermal decay of a single TL peak plus a localised transition component (following Templer, 1986a) proved unsuccessful). The initial rise plots for glow curves measured at 1 K/s before and after the 3 day storage at 125°C are shown in Fig.4.2.4.7. Results are consistent with removal of the fading component by this storage.

However, the extent of fading in this sample in this work was found, surprisingly, to be significantly less than that measured by Templer (1985). The remanent level of TL at 380°C is ≈ 0.94, which is significantly greater than ≈ 0.70 found by Templer (1985) for this same sample. Given the same sample was used in both cases, the discrepancy was hypothesised to relate to the different experimental conditions between this work and that of Templer (1985). Here only coarse grains were used and ß irradiations performed, so both the grain size and radiation field differ from those used by Templer (fine grains and α irradiation). It had been considered prior to the commencement of these experiments that α and β irradiations should be equivalent for inducing fading TL, and although the natural radiation field experienced by zircon coarse grains is strongly dominated by the internal α dose, β irradiations were used here both for convenience and because of the availability of a higher dose rate β source. However, α and β irradiations are seemingly not equivalent, and a closer consideration of the localised transition mechanism leads to a possible explanation for this discrepancy, as discussed below.

The localised transition model attributes fading to the sub-conduction band passage of an electron to its paired recombination centre. Therefore, for this transition, and the consequent neutralization of the trapped electron to take place, there must also be a hole

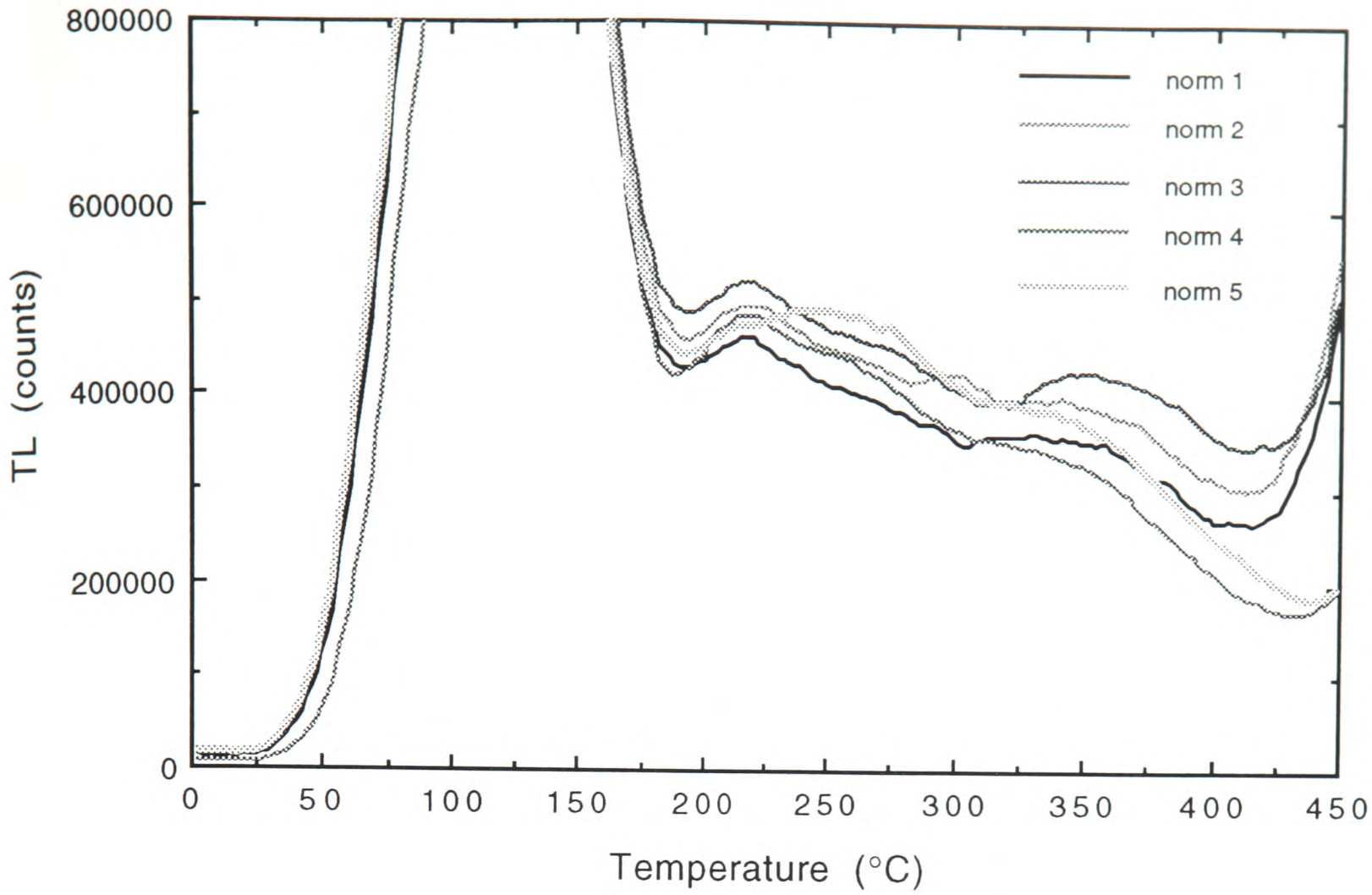


Fig.4.2.4.6 Zircon glow curves measured to enable normalization for sensitivity changes between successive dosing and glows. Note the slight sensitivity increase only.

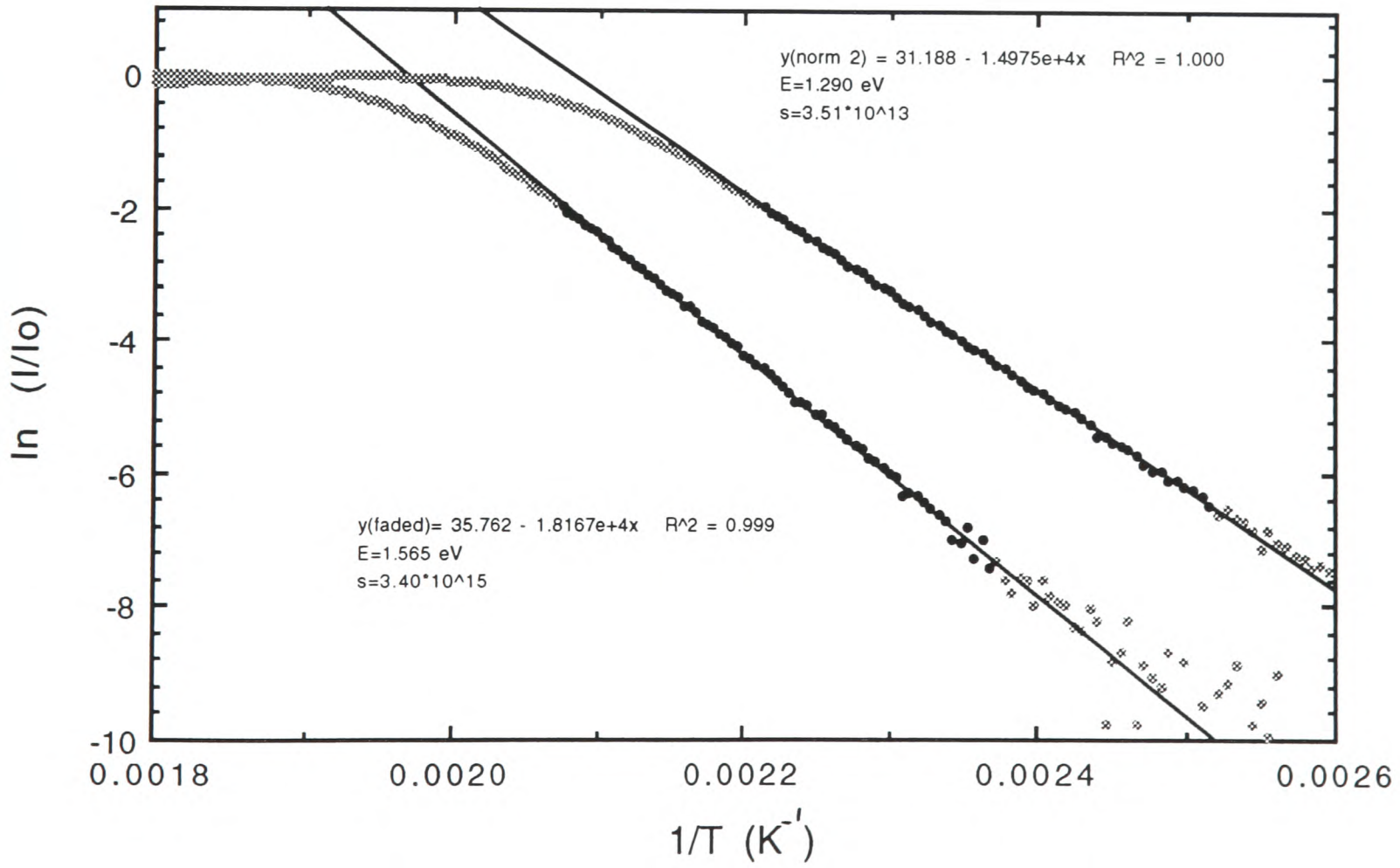
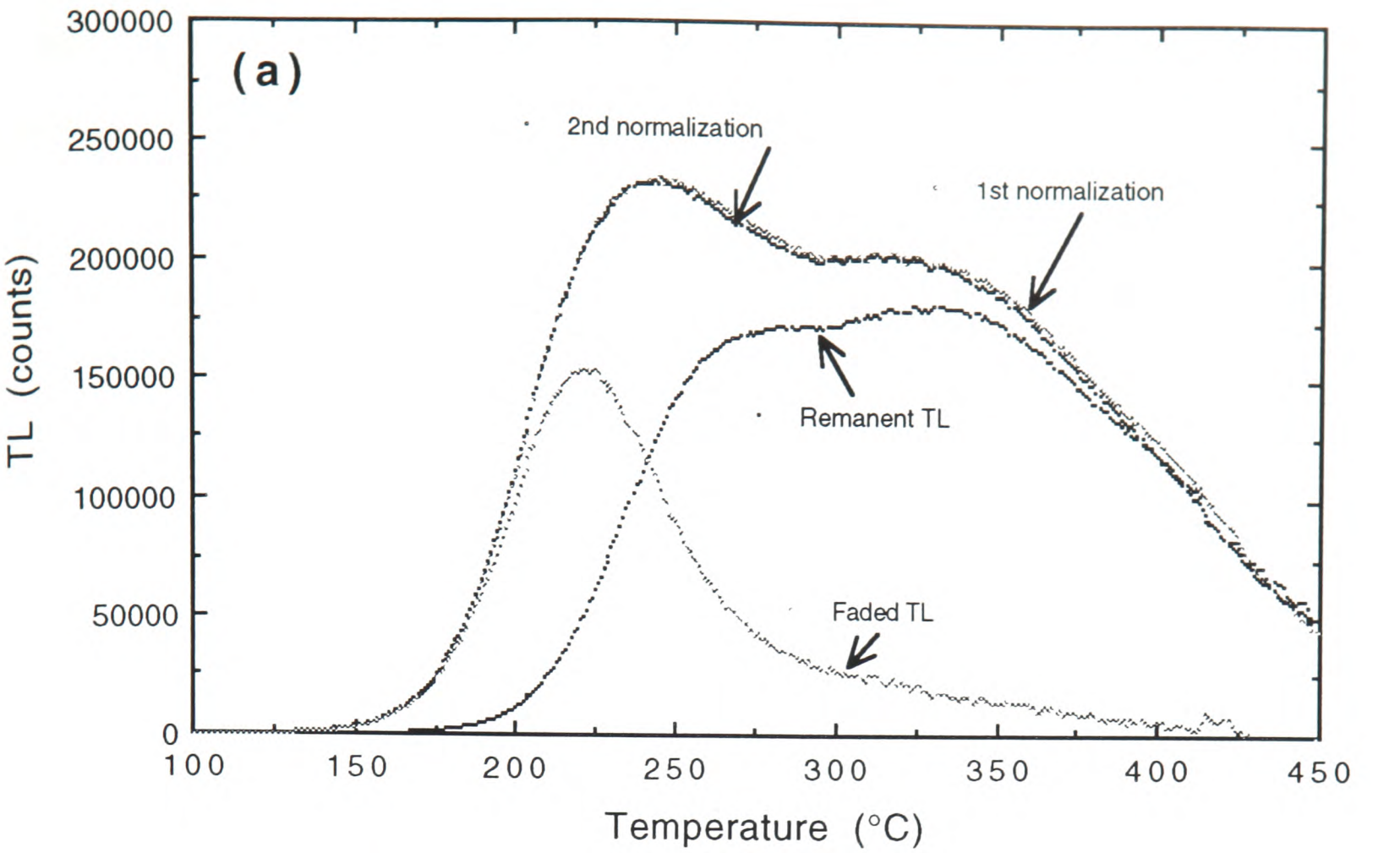


Fig.4.2.4.7 The initial rise plots for glow curves before and after elevated temperature storage for 3 days at 125°C, with otherwise the same conditions of dose, 120 second preheat at 175°C and measurement. "Norm 2" refers to data from the second normalization glow curve shown in Fig.4.2.4.8, whereas "faded" refers to data from the remanent TL in that same figure.



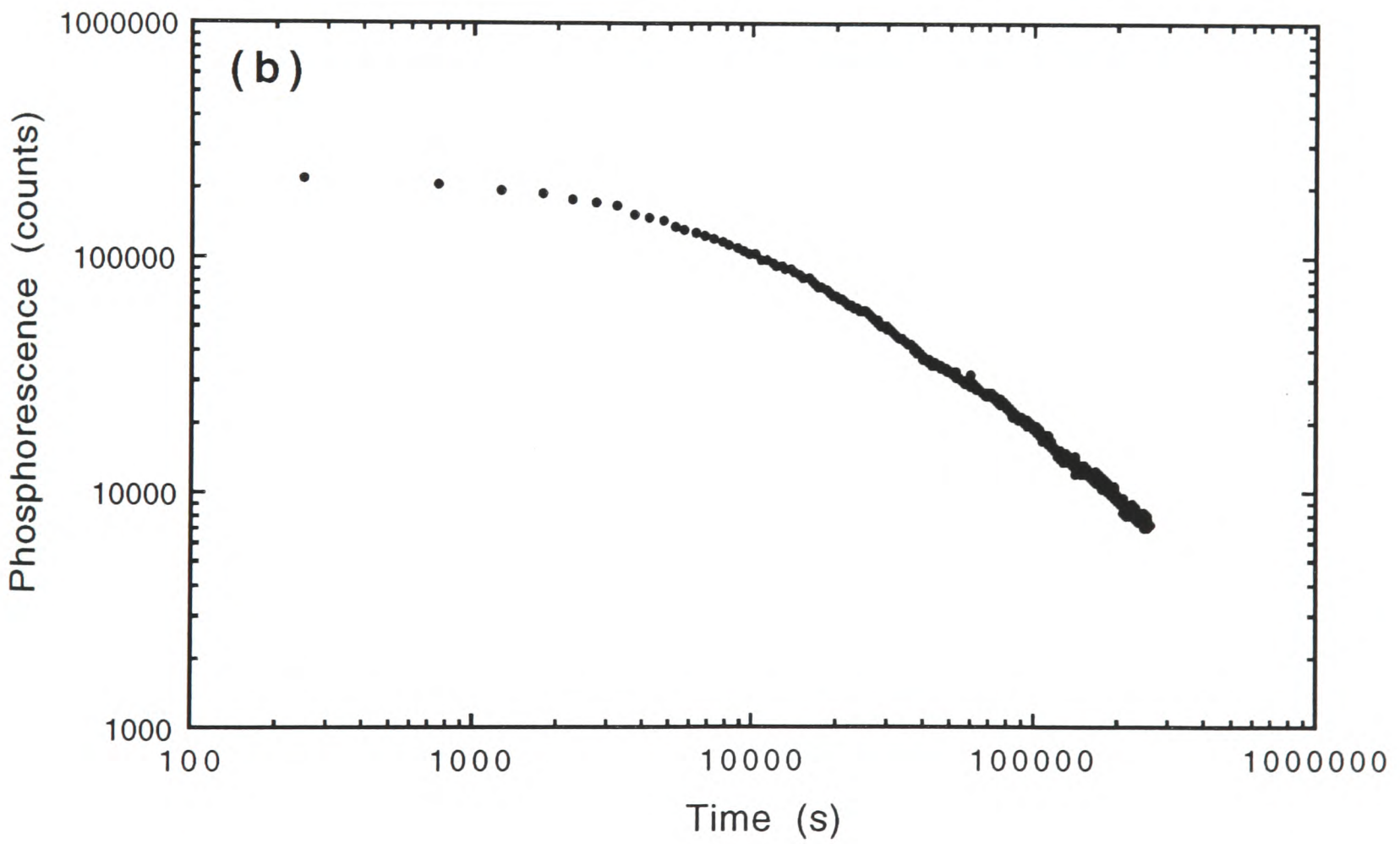


Fig.4.2.4.8 The remanent TL following 3 days storage at 125°C is shown in **(a)** overlain with normalization glow curves measured before and after the "faded TL" measurement. Also shown is the subtraction of the remanent TL from the 2nd normalization glow curve to display the TL lost during storage. **(b)** shows the phosphorescence emitted during this storage. Filters used were Corning 4-96 + Chance-Pilkington HA3 in all cases.

trapped at the corresponding recombination centre. Although the overall electrical neutrality of the crystal means equal numbers of electrons and holes in total are trapped, there is no requirement for these charges to be trapped together in pairs specifically in the paired trapping sites, as a homogenous distribution of both species of charge is expected (except following α irradiation). Therefore at trapped charge concentrations lower than saturation, electrons and holes may be trapped alone at either the electron or hole traps of a given trap pairing. In deep traps these "lone" charges will be effectively infinitely stable, as the only pathways available for detrapping are via the conduction or valence bands. Therefore occupancy by a lone charge of one or other of the trapping sites of a localised transition pairing does not mean that fading will occur.

Consider now the case of α irradiation - as the local dose in the α track is $\approx$ 60 kGy it is likely that the local ionization density is such that all vacant traps, both electron and hole, will be filled. Therefore all the paired defects capable of undergoing localised transition fading will possess both the charges required to do so, and the proportion of TL seen to fade following α irradiation will be a true measure of the proportion of such paired traps. In contrast, when ß doses are given, the much lower ionization density along the ß tracks means that the probability that both the electron and hole traps of a given pairing capable of localised transitions will be much lower. Consequently the proportion of stable remanent luminescence following β dosing will be greater than that following an equivalent α dose, provided the β dose does not approach the saturation dose level. (The above hypothesis may be simply test: a "growth" curve of the fraction of TL fading as a function of added ß dose should show an increase with increasing ß dose until the ß dose is approaching saturation. At these dose levels the fading fraction should equal the fading fraction seen following α dosing, as by this total ß dose all electron and hole traps

should be filled, and so the crystal now macroscopically approximates the microdosimetric conditions experienced in an α track).

It was now necessary to determine what effect the difference between α and β irradiations may have had on the assessment of the method of heating rate variations, and so to test whether the failure to observe a distinct "localised transition" peak appearing at slow heating rates was the result of the use of ß irradiation as implied above, two glow curves were measured following α irradiation. Heating rates used were 1 K/s and 0.003 K/s, and emissions were monitored as previously using the EMI 9635Q PMT and Corning 4-96 + Chance-Pilkington HA3 filters. Zircon 210f1 archived by R.H. Templer was again used, but this time as fine grains deposited on stainless steel discs. Following "NTL" erasure as previously, the sample received an α irradiation of 5000 seconds duration. Dosing was by an Elsec automated α irradiator Type 9022, containing a 1 mCi ^{241}Am foil and delivering a dose rate to fine grain quartz on aluminium of ≈ 7 Gy/minute, (D. Questiaux, June 1992); conversion for the α dose delivered to zircon on a stainless steel substrate (Aitken, 1985, page 307) then gives ≈ 580 * $(20.2/35.3)^{0.5}$ ≈ 440 Gy.

The glow curves are shown in Fig.4.2.4.9(a) and the corresponding initial rise plots in Fig.4.2.4.9(b). The behaviour appears similar to that seen following β dosing. There is a noticeably more pronounced low temperature peak following heating at 0.003 K/s than seen following similar heating after β irradiation, presumably as a consequence of the greater proportion of the charge now being trapped in paired traps and so now able to undergo localised transition recombinations. The E and S values found from these initial rise analyses are given in Table 4.2.4.1 and the E values are plotted in Fig.4.2.4.10 overlain with those measured from the β dosed samples. Both sets of values are in accord, supporting the interpretation implicit in the preceding discussion that the effects of α and

β irradiation are fundamentally the same in this case (zircon), differing only in the proportion of fading component induced by sub-saturation β doses.

4.2.4.4 RESULTS AND CONCLUSIONS

The kinetic parameters determined for each combination of heating rate, irradiation type and emission observed are given in Table 4.2.4.4.1. The kinetic evaluations were made under three assumptions: (1) first order kinetics apply; (2) there were no changes in TL emission spectrum with temperature as the glow curves were measured (Townsend and Kirsh, 1989); and (3) no thermal quenching occurred. Errors estimated for E were from curve fitting, for β from errors of timing between fixed temperatures, for T_{max} from the glow curve peaks and for frequency factor S using:

$$\frac{\Delta S}{S} = \sqrt{\left(\frac{\Delta E}{E}\right)^2 + \left(\frac{\Delta \beta}{\beta}\right)^2 + 2\left(\frac{\Delta T_{max}}{T_{max}}\right)^2} + \frac{1}{k}\cdot\frac{E}{T_{max}}\cdot\sqrt{\left(\frac{\Delta E}{E}\right)^2 + \left(\frac{\Delta T_{max}}{T_{max}}\right)^2}$$

It was concluded that although variation of heating rate did not give a "visually spectacular" revelation of a fading TL peak, the observed alterations to the initial rise kinetics were consistent with a decreasing proportion of recombinations proceeding via the conduction band as heating rate decreased, in favour of a sub-conduction band route having a lower E value (see Fig.4.2.4.10). This agrees with the predictions outlined above and arising from the localised transition model. Consequently, it was further concluded that the method of variation of heating rate was a valid means of analyzing fading samples and should prove successful if suitable localised transition routes were present.

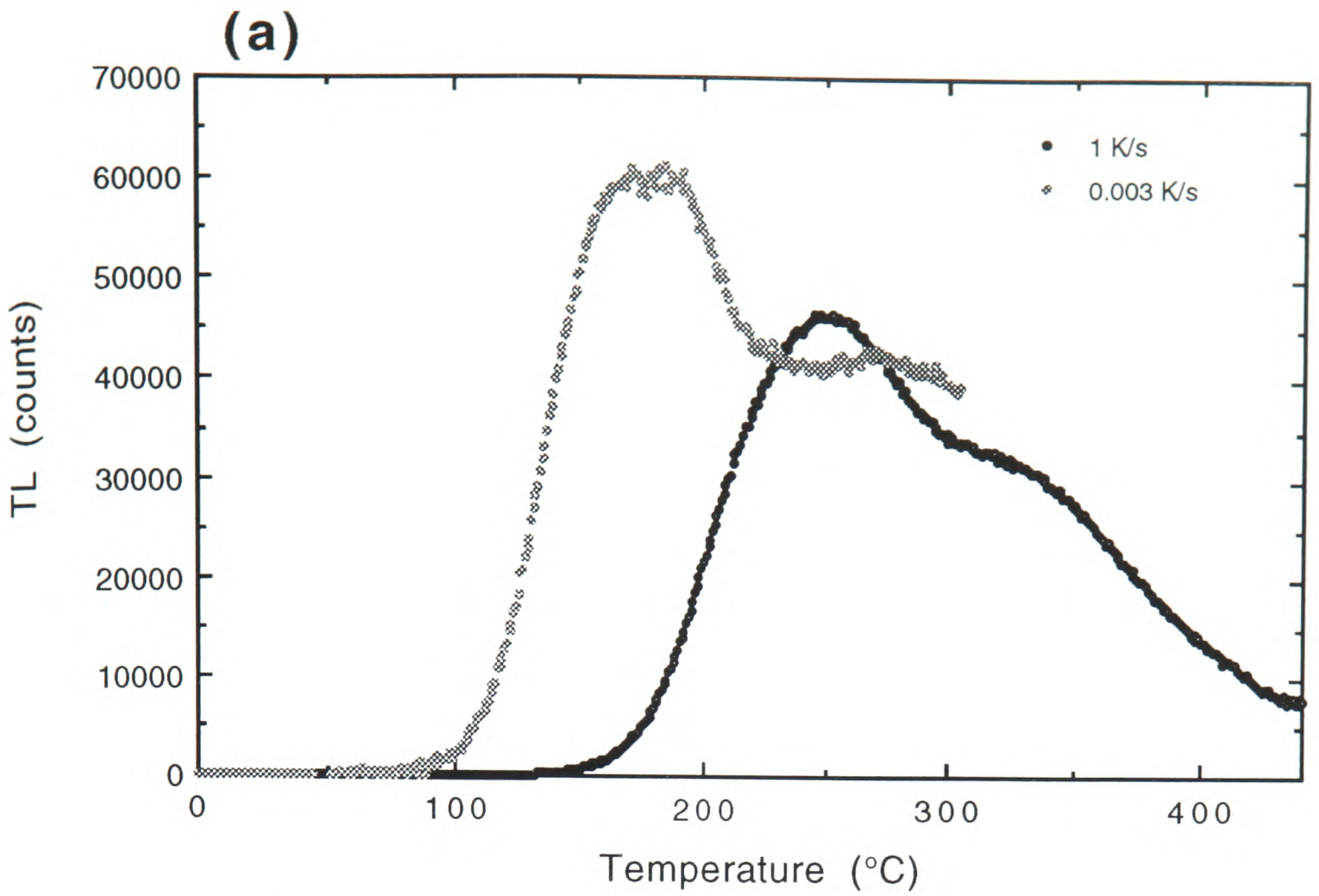


Fig.4.2.4.9 Zircon glow curves measured following α irradiation are shown in **(a)**, and the corresponding initial rise plots are given in **(b)**. Fine grain zircons on stainless steel discs were used, with the emissions being recorded at heating rates of 1 K/s and 0.003 K/s, and using Corning 4-96 + Chance-Pilkington HA3 filters. Note the similarity in behaviour to the β irradiated glow curves in Fig.4.2.4.3.

Table 4.2.4.4.1 The kinetic parameters for each combination of heating rate, irradiation type and emission observed.

FILTER	E±ΔE (2σ)	β (1σ) (±2%)	$T_m \pm \Delta T_m$		S	ΔS/S	$\tau_{20°C}$	
	eV	K/s	°C	K	s^{-1}		sec	ka
4-96 + HA3	1.316 ± 0.011	3.0	262 ± 2	535 ± 2	3.997 x10^{11}	0.51	1.08 x10^{11}	3.44
	1.280 ± 0.008	1.0	244 ± 2	517 ± 2	1.671 x10^{11}	0.47	6.23 x10^{10}	1.98
	1.239 ± 0.009	0.1	218 ± 2	491 ± 2	3.116 x10^{10}	0.50	6.59 x10^{10}	2.09
	1.215 ± 0.008	0.03	196 ± 2	469 ± 2	2.191 x10^{10}	0.49	3.62 x10^{10}	1.15
	1.191 ± 0.003	0.003	167 ± 2	440 ± 2	9.399 x10^{9}	0.86	3.26 x10^{10}	1.03
	1.075 ± 0.050	0.001	156 ± 2	429 ± 2	2.887 x10^{8}	1.16	1.07 x10^{10}	0.34
7-59 + BG39	1.580 ± 0.058	5	294 ± 2	567 ± 2	3.158 x10^{13}	1.09	4.77 x10^{13}	1512
	1.347 ± 0.010	1	256 ± 2	529 ± 2	3.806 x10^{11}	0.50	3.89 x10^{11}	12.3
	1.358 ± 0.012	0.3	246 ± 3	519 ± 3	2.703 x10^{11}	0.57	8.46 x10^{11}	26.8
	1.313 ± 0.010	0.1	238 ± 2	511 ± 2	5.202 x10^{10}	0.51	7.40 x10^{11}	23.4
	1.236 ± 0.013	0.03	224 ± 2	497 ± 2	5.958 x10^{9}	0.57	3.06 x10^{11}	9.70
	1.149 ± 0.032	0.003	204 ± 4	477 ± 4	2.429 x10^{8}	0.90	2.39 x10^{11}	7.58
Alphas 4-96 + HA3	1.284 ± 0.016	1.0	250 ± 2	523 ± 2	1.287 x10^{11}	0.61	9.48 x10^{10}	3.00
	1.072 ± 0.069	0.003	168 ± 2	441 ± 2	3.423 x10^{8}	1.35	8.04 x10^{9}	0.255
	1.072 ± 0.069	0.003	176 ± 3	449 ± 3	1.998 x10^{8}	1.34	1.38 x10^{10}	0.437

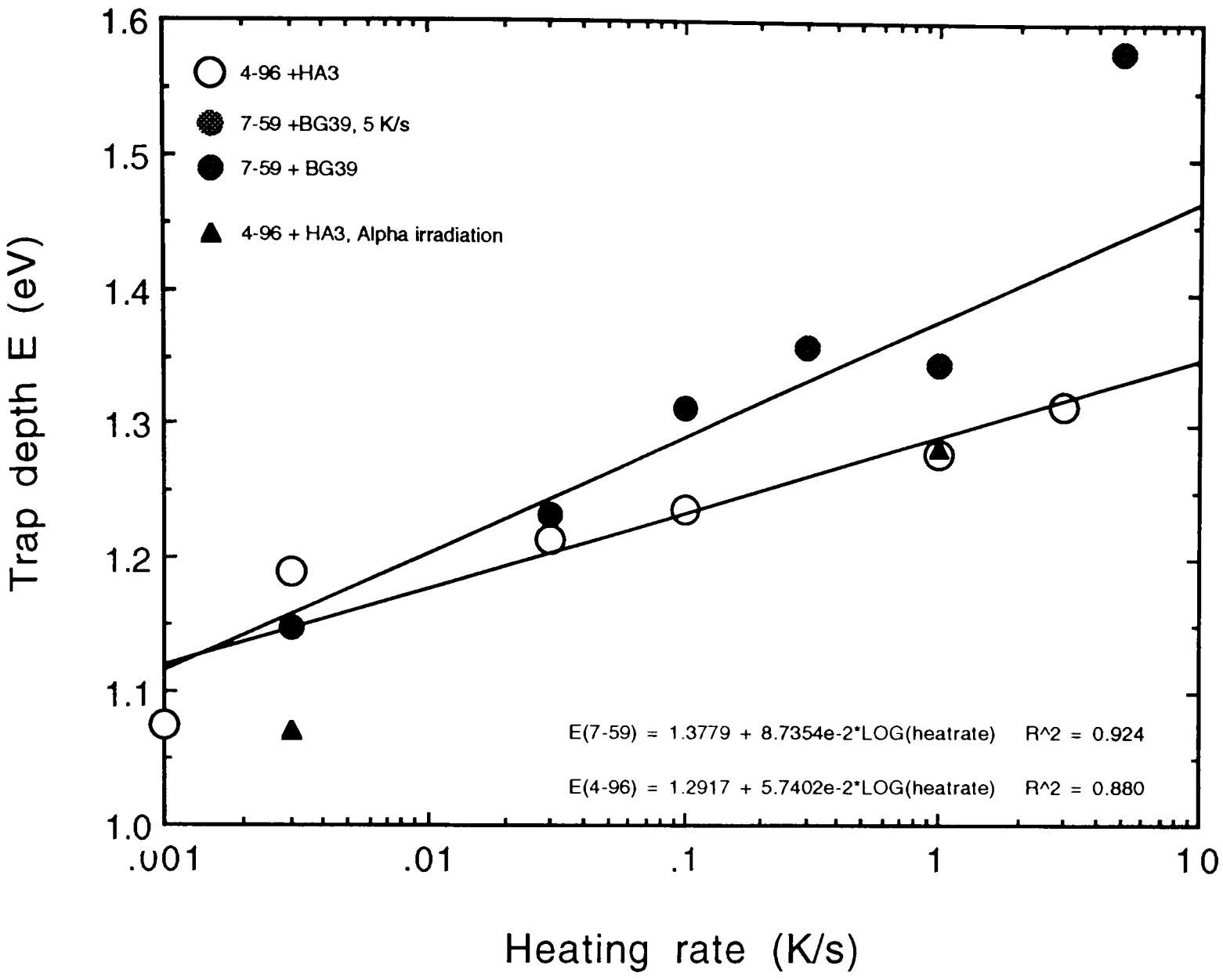


Fig.4.2.4.10 The trap depths found from the various combinations of heating rate and optical emissions are presented above. Irradiations were by $^{90}Sr/^{90}Y$ β unless otherwise indicated. The 5 K/s data is apparently aberrant, presumably due to the greater heating rate, and hence thermal lag effects. Otherwise there is good agreement between the various results, consistent with the slower heating rates revealing an increasing proportion of signal having lower E values appearing in the initial rise portion of the glow curve.

4.2.5 A SEARCH FOR LOCALISED TRANSITION-MEDIATED FADING IN FELDSPAR USING THE METHOD OF VARIATION OF HEATING RATE.

4.2.5.1 INTRODUCTION

Following successful trial of the method of variation of heating rates on zircon (see section 4.2.4), it was applied to feldspar to test the viability of the method as a means both of confirming the presence of localised transition-mediated fading in feldspathic samples and of determining the optimum preheat necessary to eliminate it.

Three samples, 9. Z15 sanidine, 12. Patmos sanidine and 23. Dup(B) oligoclase, were chosen for this study, using the criterion of apparent thermal acceleration of the observed fading; additionally, two samples measured as stable (see section 4.2.2.1) were included as controls (5. No.3062 microcline (high K) and 18. Amelia albite (high Na)). A secondary criterion required of each of these samples was high sensitivity, on account of the high background levels at the slower heating rates.

4.2.5.2 EXPERIMENTAL

The experimental procedure was broadly similar to that described for zircon (section 4.2.4): following dosing and prompt preheating (60 seconds at 220°C on-plate) the TL was measured in a nitrogen atmosphere (flow rate 0.5 litre / minute). Heating rates were 5, 1, 0.5, 0.05 and 0.005 K/s, obtained using a digital servo-control unit designed by M. Franks. Reheats were subtracted, a step especially important for the slower heating

rates as the integrated electronic noise alone (PMT dark count-rate ≈ 35 cps) was significant, in addition to the incandescence signal. TL was detected using an EMI 9635Q PMT with Corning 7-59 and Schott BG 39 filters and recorded using a multi-channel scaler card (EG&G Ortec, type ACE-MCS) hosted by a RM Nimbus VX computer. Counting time per channel was set so that the TL observed during each temperature increase of 1 K was acquired in discrete channels. The data plotted are counts/channel with the duration of each channel depending on heating rate, and so increasing from 0.2 seconds for a heating rate of 5 K/s to 200 seconds for 0.005 K/s heating rate.The filter combination was chosen from a range of UV/blue-pass filter combinations tested as having the highest signal:noise ratio at 300°C. Normalization factors were derived from the "NTL" measured prior to dosing.

4.2.5.3 RESULTS AND DISCUSSION

The families of glow curves measured for each sample are shown in Figs.4.2.5.3.1 - 4.2.5.3.5, (along with corresponding plots showing the data on which kinetic analysis were performed).

Only initial rise analysis was used to obtain kinetic values as the absence of separable and distinctive fading components (ie, "localised transition" TL peaks) precluded the application of kinetic techniques requiring distinct peaks. Kinetic analysis was consequently restricted to the rising edge of the glow curve complex; fortunately however, this was where fading via localised transitions was anticipated to be manifest, and initial rise analysis the most appropriate method for detection of this fading. The measured E and S values are given in Table 4.2.5.3.1. Corresponding lifetimes calculated for storage at

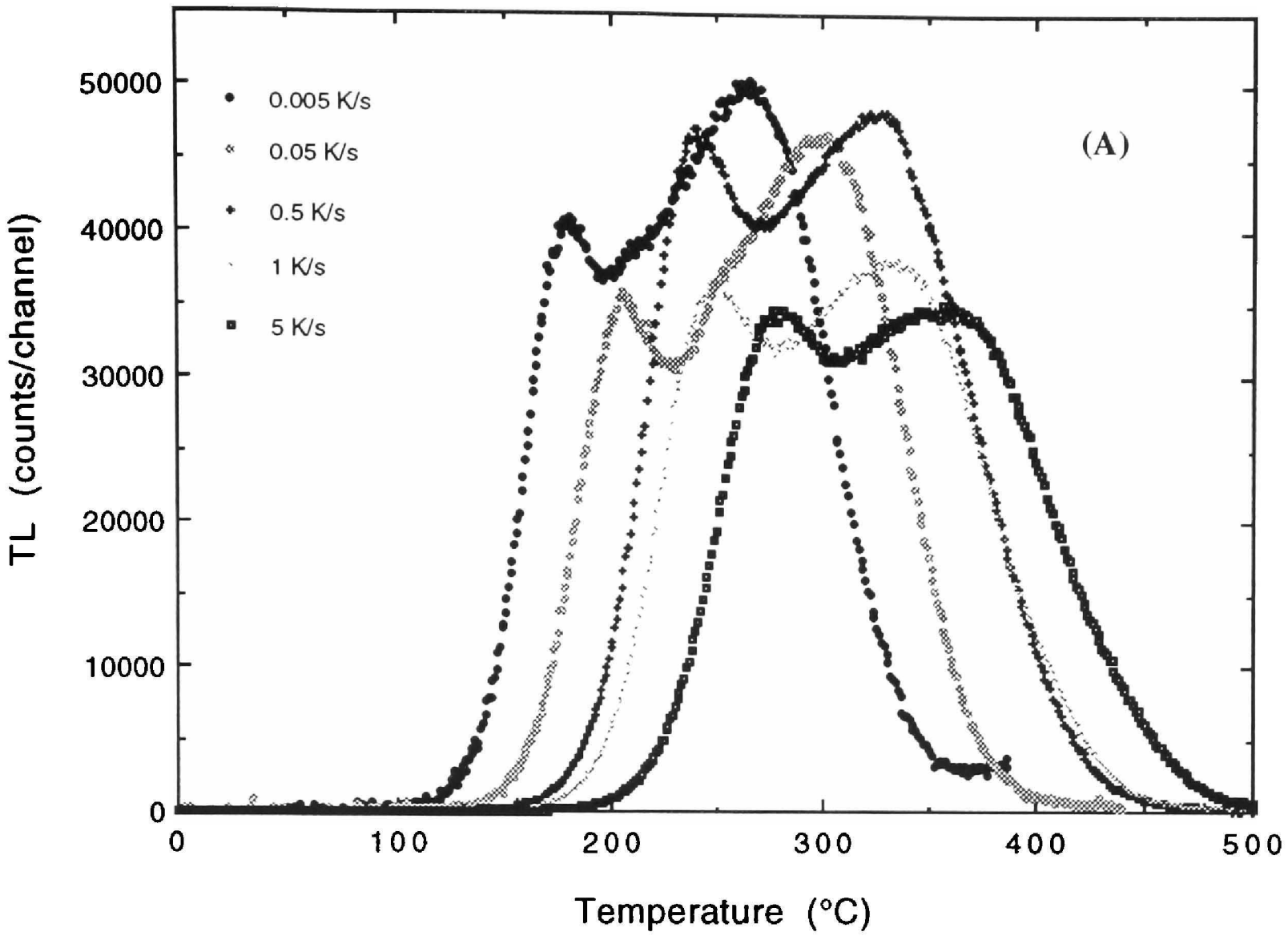


Fig.4.2.5.3.1(A) Glow curves for 5. No.3062 microcline measured at the heating rates shown, following a preheat of 60 seconds at 220°C. Data are counts/channel, where each channel represents 1K. Reheats are subtracted.

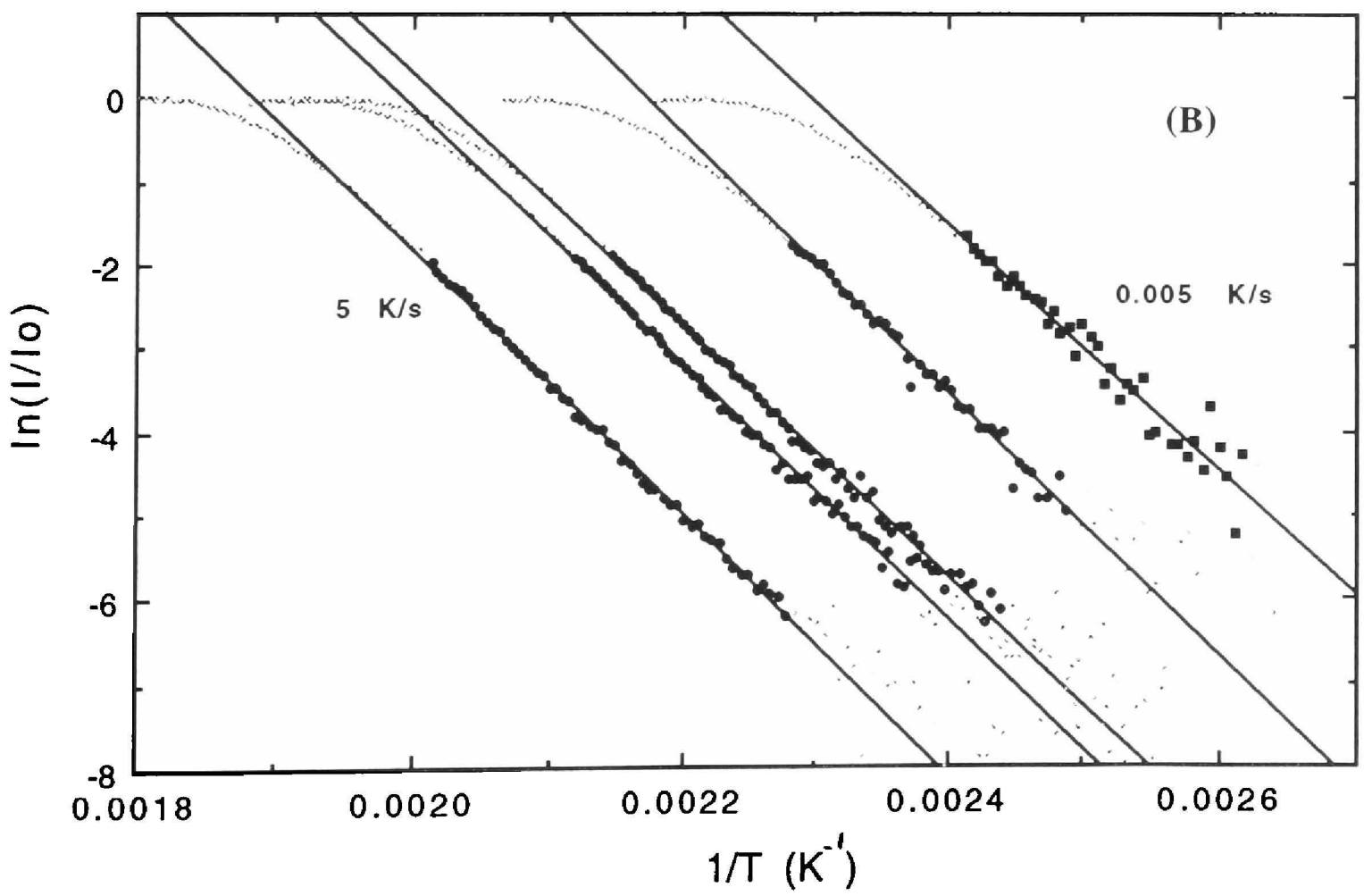


Fig.4.2.5.3.1(B) The initial rise portions of each glow curve, showing the (highlighted) data points on which initial rise analysis was performed. The relatively large scatter on the 0.005 K/s data set here and in the following Figures is a statistical consequence of subtraction of the greater electronic noise background at this slow heating rate.

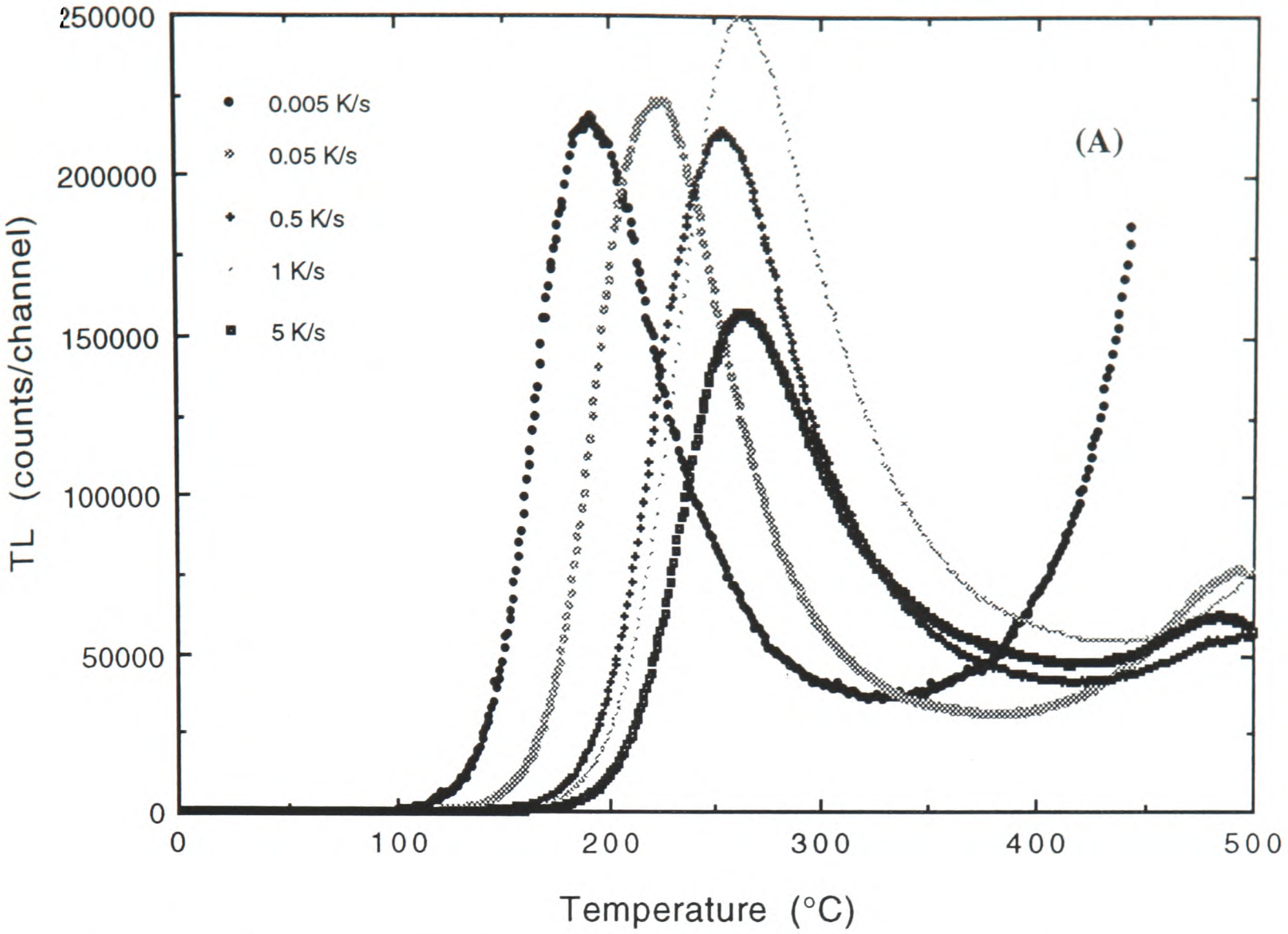


Fig.4.2.5.3.2(A) Glow curves for 9. Z15 sanidine measured at the heating rates shown, following a preheat of 60 seconds at 220°C. Data are counts/channel, where each channel represents 1K. Reheats are subtracted.

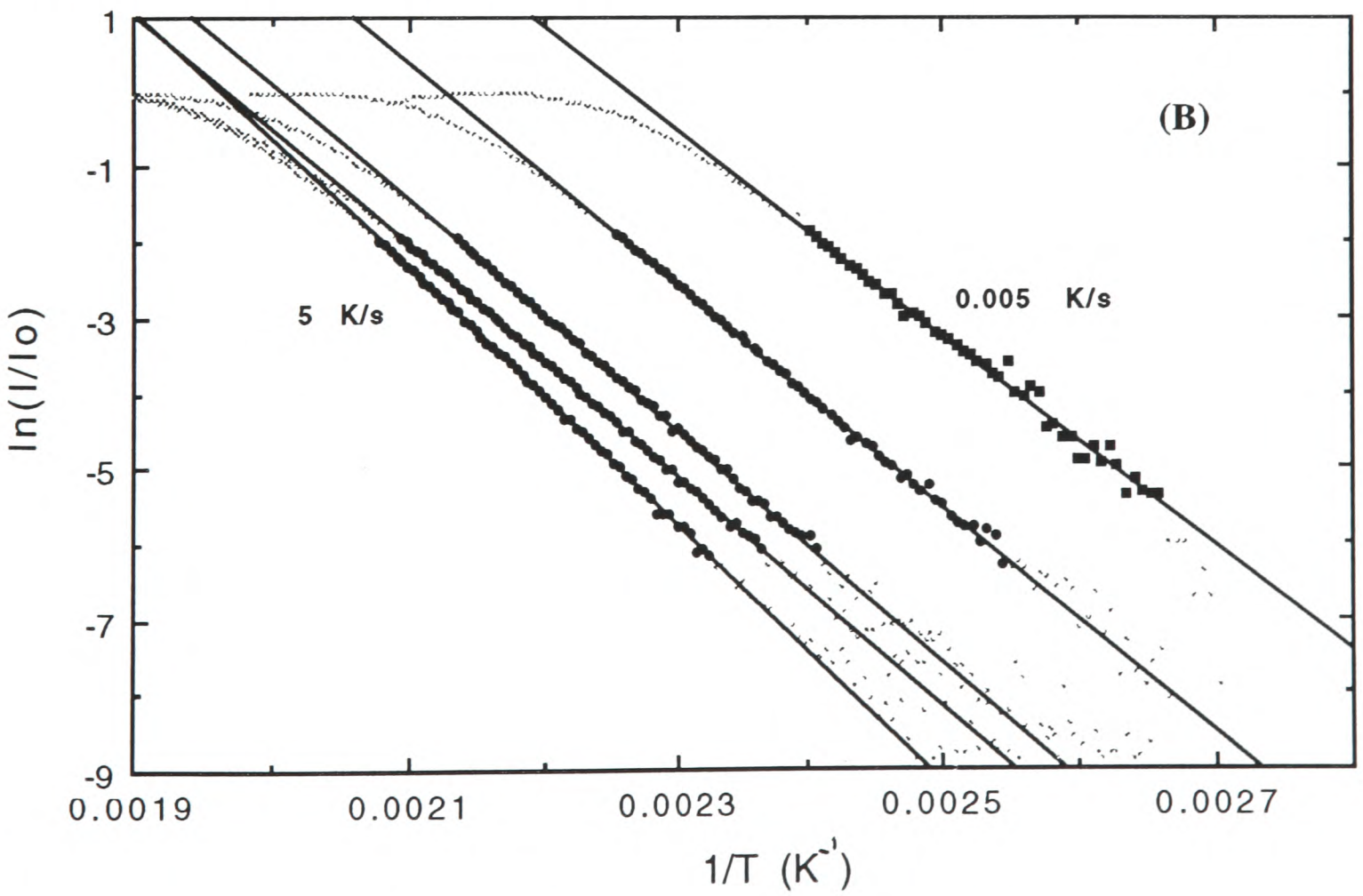


Fig.4.2.5.3.2(B) The initial rise portions of each glow curve, showing the (highlighted) data points on which initial rise analysis was performed.

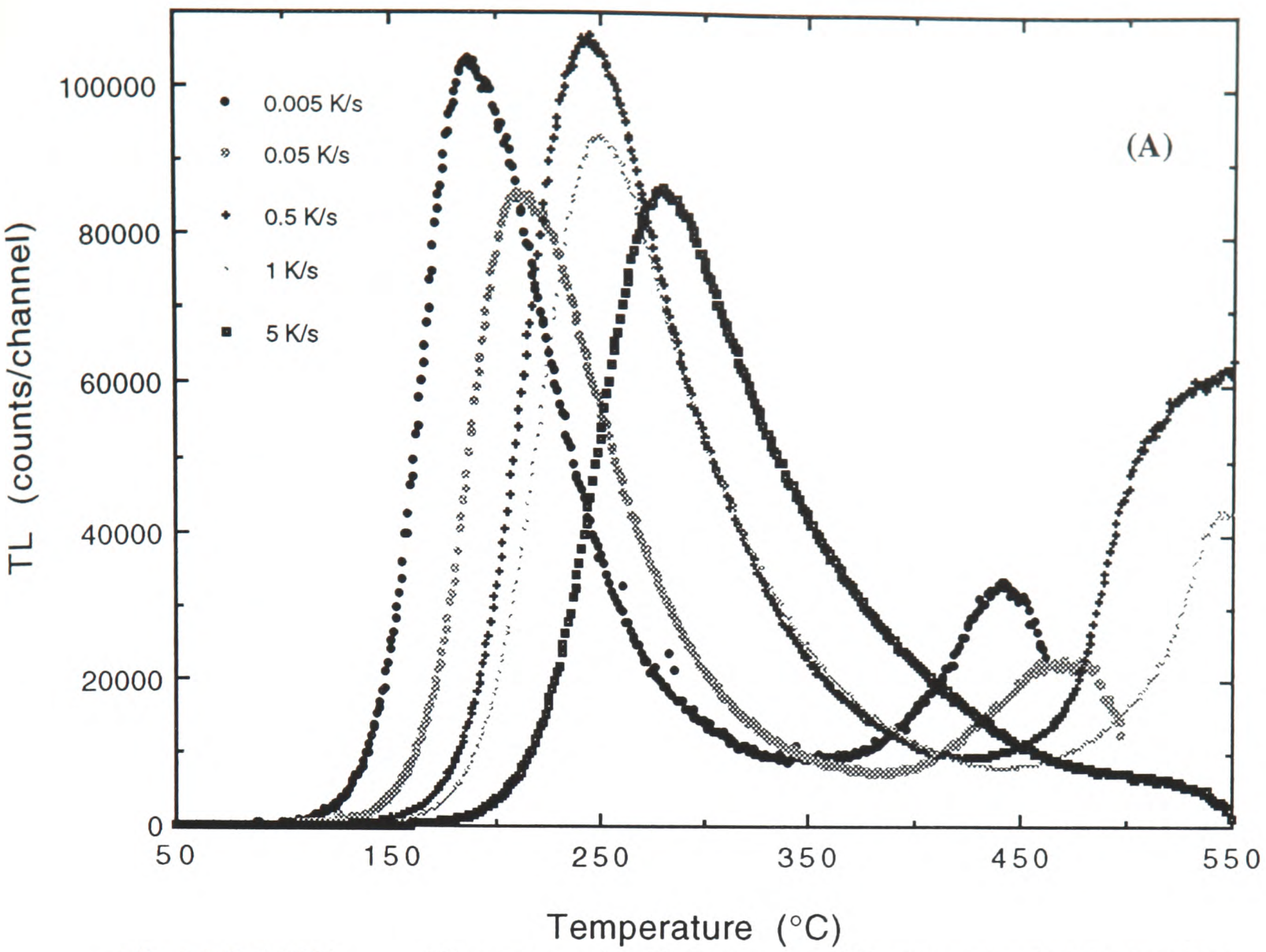


Fig.4.2.5.3.3(A) Glow curves for 12. Patmos sanidine measured at the heating rates shown, following a preheat of 60 seconds at 220°C. Data are counts/channel, where each channel represents 1K. Reheats are subtracted.

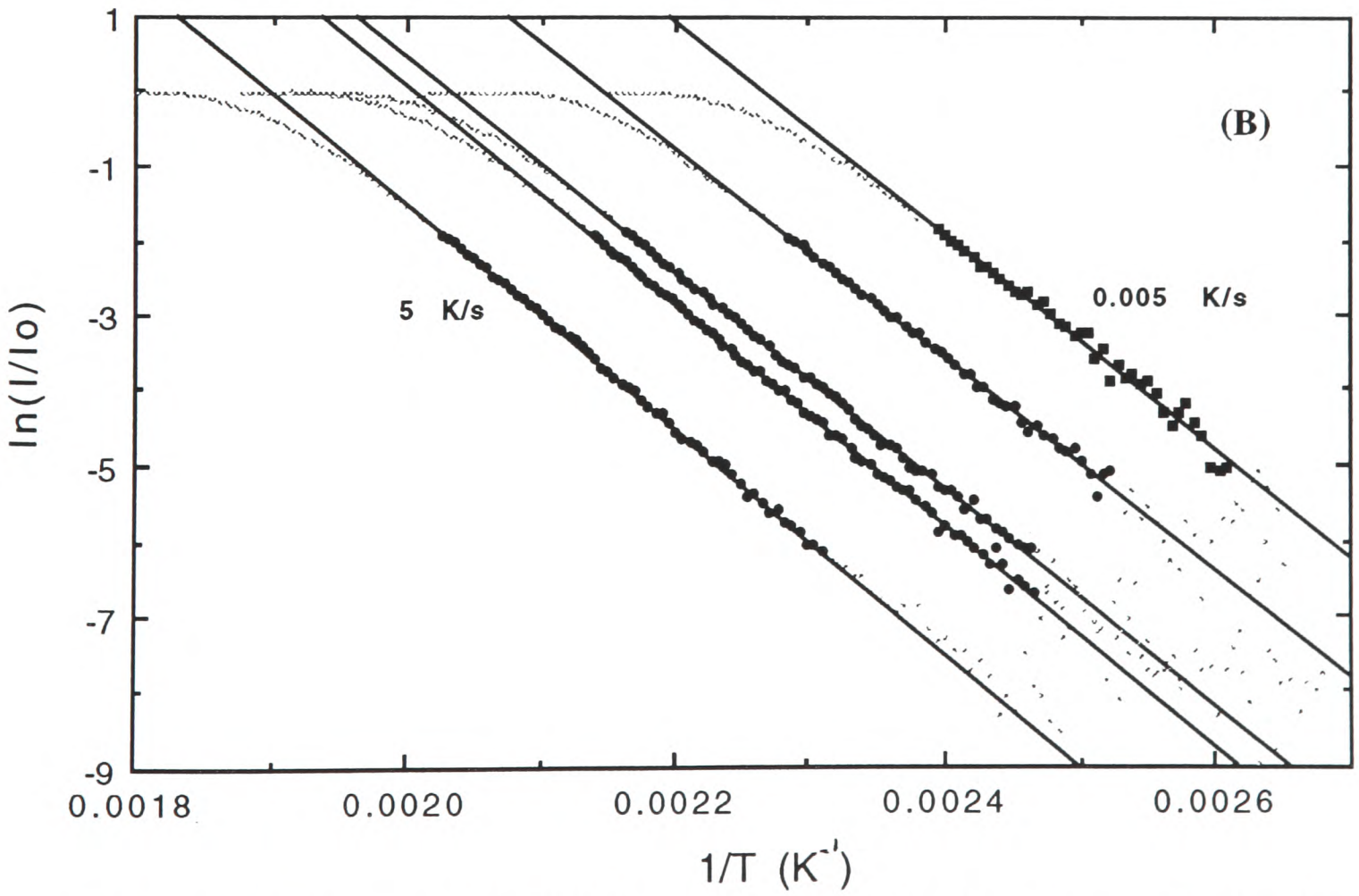


Fig.4.2.5.3.3(B) The initial rise portions of each glow curve, showing the (highlighted) data points on which initial rise analysis was performed.

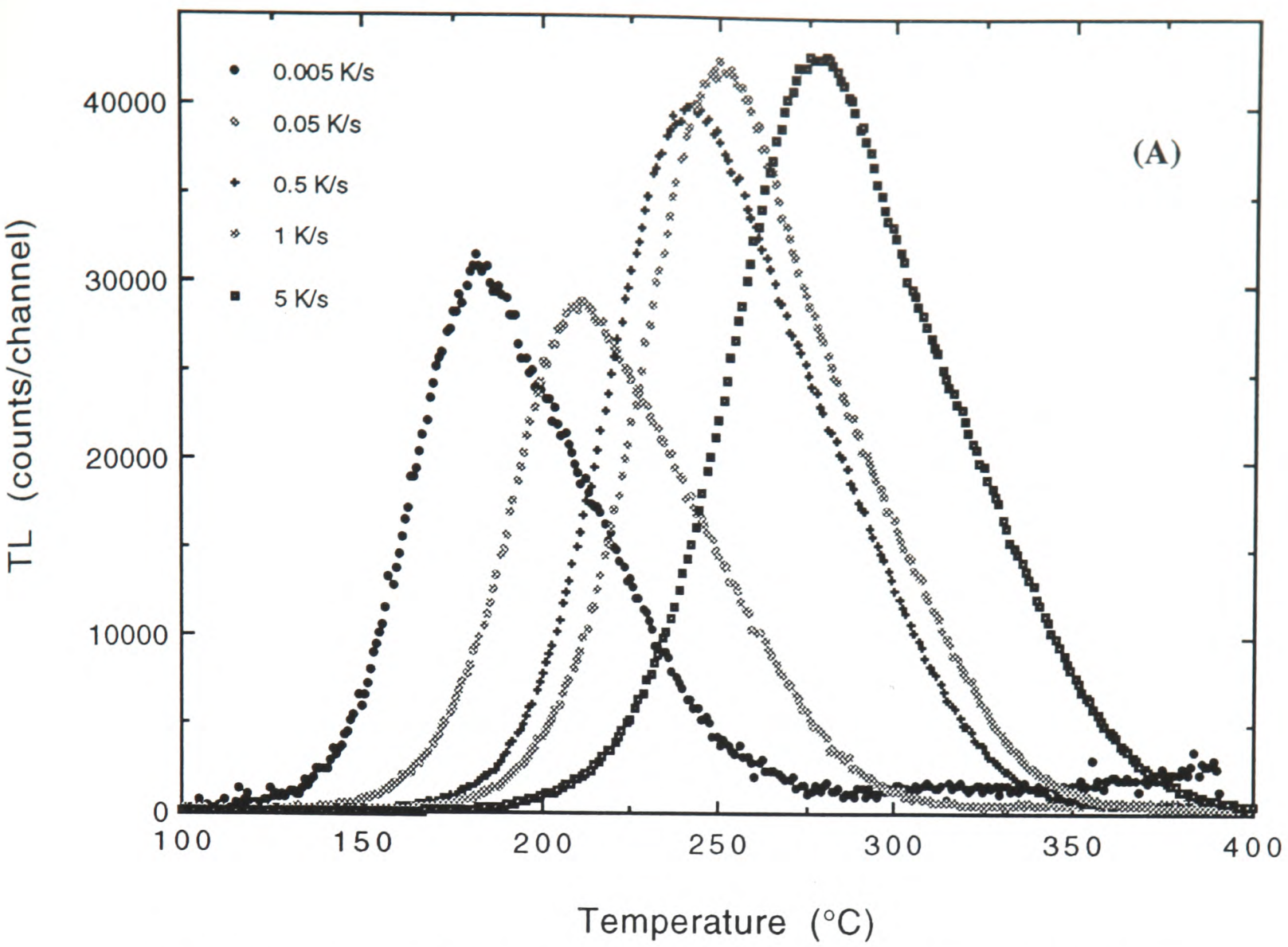


Fig.4.2.5.3.4(A) Glow curves for 18. Amelia albite measured at the heating rates shown, following a preheat of 60 seconds at 220°C. Data are counts/channel, where each channel represents 1K. Reheats are subtracted.

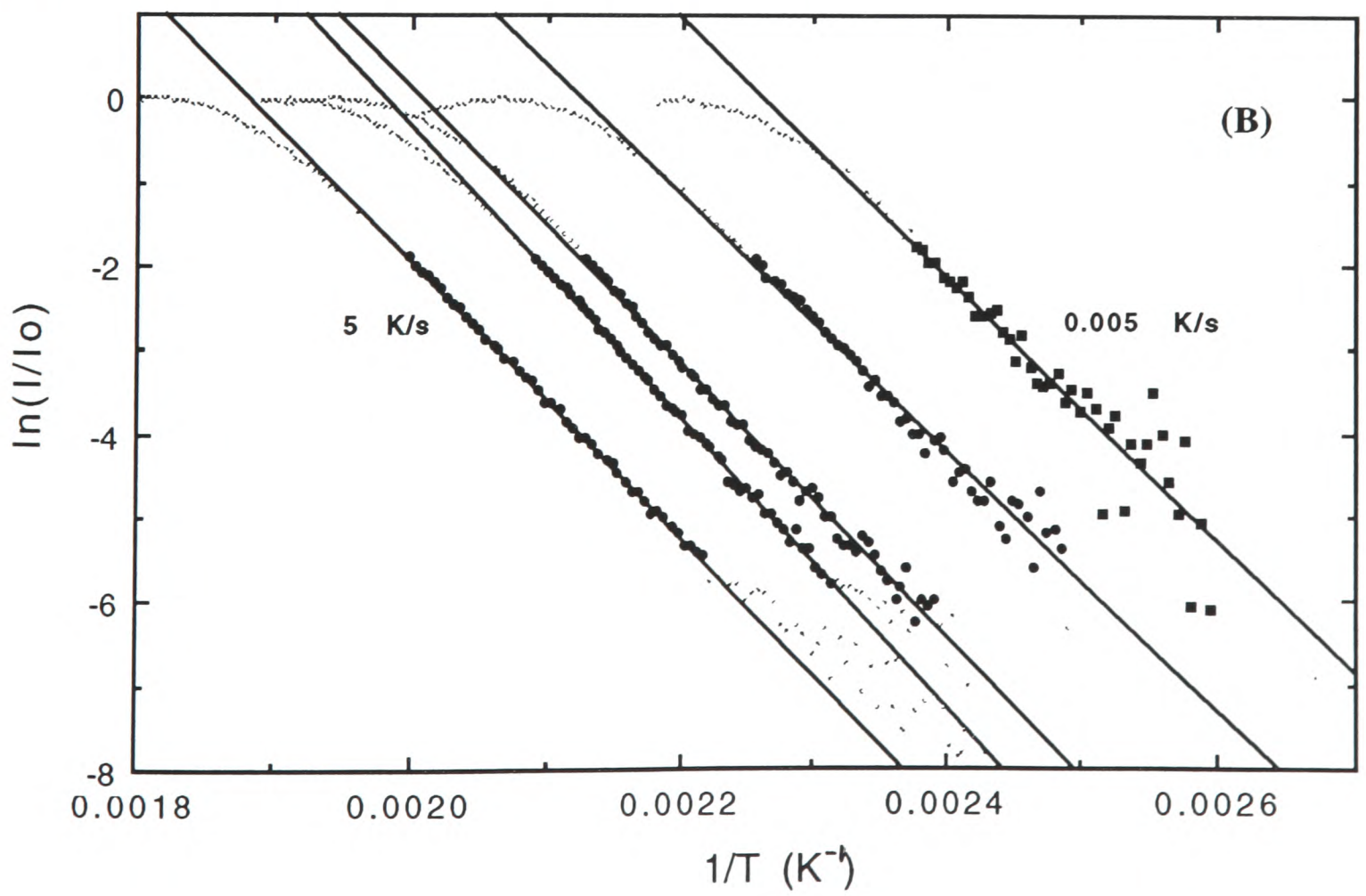


Fig.4.2.5.3.4(B) The initial rise portions of each glow curve, showing the (highlighted) data points on which initial rise analysis was performed.

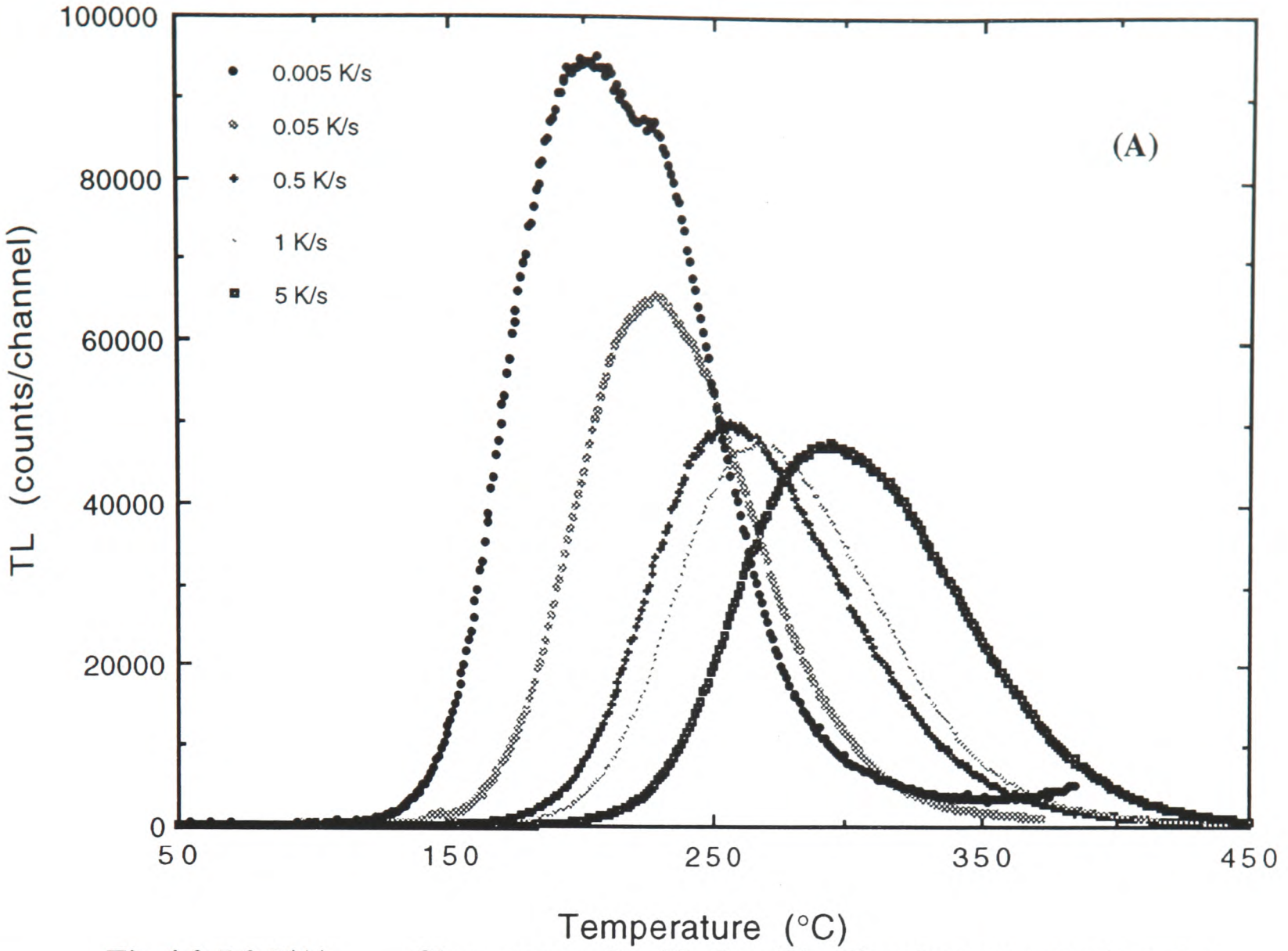


Fig.4.2.5.3.5(A) Glow curves for 23. Dup(B) oligoclase measured at the heating rates shown, following a preheat of 60 seconds at 220°C. Data are counts/channel, where each channel represents 1K. Reheats are subtracted.

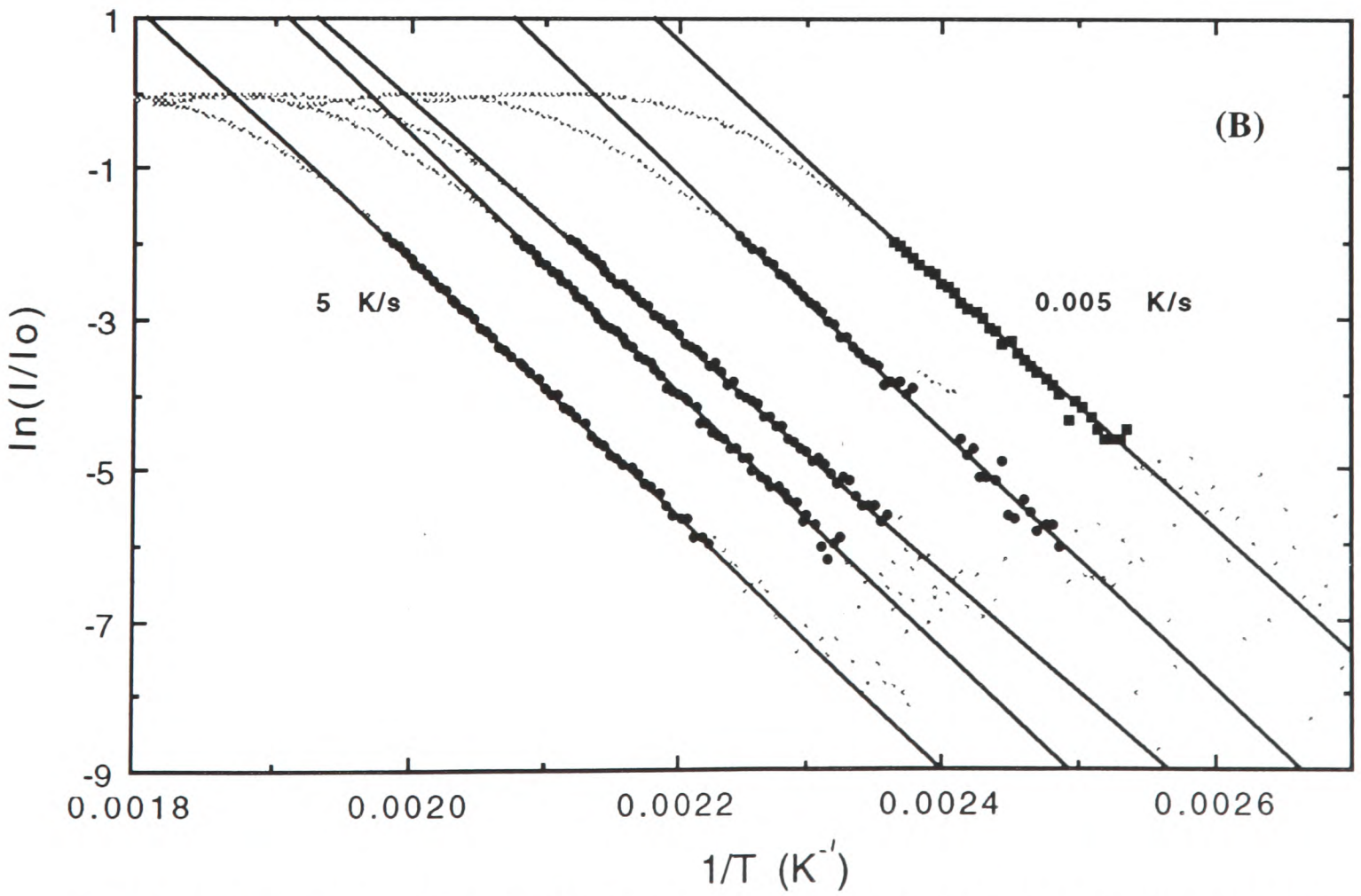


Fig.4.2.5.3.5(B) The initial rise portions of each glow curve, showing the (highlighted) data points on which initial rise analysis was performed.

20°C are also included, though their interpretation is less clear as the presumed mixture of conduction band and localised transition kinetics is irresolvable with this data set alone.

Note that the data obtained by heating at 5 K/s is included in Table 4.2.5.3.1 for completeness only, as the presence of a temperature gradient through the grains due to thermal lag is unavoidable at this heating rate. The TL is therefore the superposition of TL emitted at the range of temperatures through the grain, and the reliability of subsequent kinetic analysis is doubtful. Consequently conclusions on the utility of the method of heating rate variation are drawn only from the data collected at heating rates of 1 K/s - 0.005 K/s. Furthermore, although the data set does not permit accurate assessment of thermal quenching in these samples (as the small sample aliquots (≈ 1 mg each of microcline and albite) and necessary use of chips (oligoclase), as well as instrumental drift over the extended duration of measurements, were not conducive to precise normalization), the possible occurrence of thermal quenching (see sections 5.5.4 and 6.3.2) means the trap depths and lifetimes shown should be considered as lower limits.

Table 4.2.5.3.1 The kinetic parameters determined for each glow curve using the initial rise method.

Sample	Heating rate (K/s)	E ± ΔE (eV)	S (s^{-1})	ΔS/S	$\tau_{20°C}$ (s)	(ka)
5. No.3062 microcline	0.005	1.261 ± 0.104	4.40×10^{10}	1.64	1.1×10^{11}	3.5
	0.05	1.347 ± 0.055	5.40×10^{11}	1.16	2.7×10^{11}	8.5
	0.5	1.304 ± 0.024	1.85×10^{11}	0.75	1.4×10^{11}	4.5
	1.0	1.316 ± 0.032	3.19×10^{11}	0.85	1.3×10^{11}	4.2
	5.0	1.356 ± 0.019	6.51×10^{11}	0.64	3.2×10^{11}	10.0
9. Z15 sanidine	0.005	1.196 ± 0.035	3.35×10^{9}	0.94	1.1×10^{11}	3.5
	0.05	1.278 ± 0.013	2.89×10^{10}	0.57	3.2×10^{11}	10.3
	0.5	1.324 ± 0.009	1.34×10^{11}	0.48	4.3×10^{11}	13
	1.0	1.324 ± 0.006	1.68×10^{11}	0.41	3.5×10^{11}	11
	5.0	1.471 ± 0.009	1.88×10^{13}	0.48	1.0×10^{12}	33
12. Patmos sanidine	0.005	1.177 ± 0.035	2.69×10^{9}	0.95	6.4×10^{10}	2.0
	0.05	1.226 ± 0.024	1.88×10^{10}	0.77	6.4×10^{10}	2.0
	0.5	1.248 ± 0.016	3.31×10^{10}	0.61	8.6×10^{10}	2.7
	1.0	1.265 ± 0.008	8.74×10^{10}	0.46	6.4×10^{10}	2.0
	5.0	1.265 ± 0.013	8.06×10^{10}	0.54	7.0×10^{10}	2.2
18. Amelia albite	0.005	1.322 ± 0.087	1.61×10^{11}	1.49	3.3×10^{11}	10
	0.05	1.459 ± 0.048	6.02×10^{12}	1.08	2.0×10^{12}	64
	0.5	1.422 ± 0.029	2.54×10^{12}	0.82	1.1×10^{12}	35
	1.0	1.500 ± 0.020	1.80×10^{13}	0.68	3.4×10^{12}	108
	5.0	1.426 ± 0.015	3.17×10^{12}	0.58	1.0×10^{12}	33
23. Dup(B) oligoclase	0.005	1.438 ± 0.037	7.75×10^{11}	0.96	6.8×10^{12}	216
	0.05	1.478 ± 0.039	2.69×10^{12}	0.96	9.6×10^{12}	304
	0.5	1.382 ± 0.028	3.92×10^{11}	0.79	1.5×10^{12}	47
	1.0	1.477 ± 0.021	3.55×10^{12}	0.68	7.0×10^{12}	221
	5.0	1.464 ± 0.012	2.86×10^{12}	0.52	5.2×10^{12}	164

Peak shape factors (based on the parameters defined by Chen, 1969a,b, where μ = 0.42 for first order peaks, and μ = 0.52 for second order peaks)) for each glow curve were measured in an attempt to find a correlation between fading and changes in the glow curve shapes with heating rate; results are given in Table 4.2.5.3.2, where ω^* = FWHM, δ^* = upper wing of FWHM and $\mu^* = \delta^*/\omega^*$. Note that as the glow curves are apparently not "clean" single peaks free of satellites (and certainly not in the case of 5. No.3062 microcline), these shape factors are unsuitable for the derivation of trap parameters and are used only as a means of quantifying the overall glow curve shapes. Inspection of Table 4.2.5.3.2 reveals that although in each sample the glow curve FWHM decreases with decreasing heating rate, no apparent relationship exists between fading behaviour and shape factor. Consequently this approach was not pursued.

Table 4.2.5.3.2 Shape parameters for each sample and heating rate.

Sample	Heating rate (K/s)	ω^*	δ^*	$\mu^*=\delta^*/\omega^*$	$\Delta\mu^*$
5. No.3062 microcline	0.005	147	-	-	-
	0.05	157	-	-	-
	0.5	164	-	-	-
	1.0	168	-	-	-
	5.0	172	-	-	-
9. Z15 sanidine	0.005	74.6	44.8	0.601	0.043
	0.05	78.4	42.9	0.547	0.039
	0.5	87	54.1	0.622	0.045
	1.0	93.3	57.8	0.620	0.045
	5.0	98.9	61.6	0.623	0.045
12. Patmos sanidine	0.005	74.6	46.6	0.625	0.045
	0.05	80.2	54.1	0.675	0.049
	0.5	89.6	57.8	0.645	0.047
	1.0	93.3	61.6	0.660	0.048
	5.0	104.5	67.2	0.643	0.046
18. Amelia albite	0.005	58.2	38.1	0.655	0.033
	0.05	62.7	39.2	0.625	0.031
	0.5	61.6	38.1	0.619	0.031
	1.0	67.2	40.3	0.600	0.030
	5.0	73.4	42.5	0.579	0.029
23. Dup(B) oligoclase	0.005	86.8	50	0.576	0.029
	0.05	79.4	44.1	0.555	0.028
	0.5	86.8	51.5	0.593	0.030
	1.0	89.7	50	0.557	0.028
	5.0	97.1	57.4	0.591	0.030

Neither the control samples nor two of the three fading samples (12. Patmos sanidine and 23. Dup(B) oligoclase) show significant decreases of E and S with heating rate. The final sample, 9. Z15 sanidine, does show changes in these parameters commensurate with anomalous fading. However, the uniqueness of that sample precludes generalizing this result to other feldspars. (The OSL (514.5 nm stimulation) decay form is unique amongst those studied in that it obeys a power law after the first ≈ 10 mJ exposure; this sample was selected here solely on account of its exhibition of thermal acceleration of fading and extreme sensitivity to green light (data not shown) - both properties are explicable by the occurrence of localised transitions accessible to at least a component of the trapped charge population. The expectation was that Z15 sanidine may exhibit localised transition behaviour when analyzed by the method of heating rate variation and so provide a positive example of the detection of such fading in a feldspar mineral using this approach).

However, although the E and S values from Z15 sanidine do decrease in a manner consistent with expectation, the magnitude of the decreases is not greatly in excess of experimental error; given this sample is atypically strongly fading it is inferred that the identification of fading at all in less dramatically fading materials by this method must be problematic. Summarizing, failure to detect fading in 12. Patmos sanidine and 23. Dup(B) oligoclase shows the method of heating rate variation does not reliably provide useful information as to the existence or control of anomalous fading in the feldspar minerals.

However this work does indirectly assist in the building of a qualitative understanding of the fading processes occurring: given the success of the method of variation of heating rate when applied to zircon, where the fading at ambient temperatures

is predominantly via localised transitions, the null results using known fading feldspars imply that feldspar luminescence here is not necessarily fading via such a pathway, consistent with the conclusion of dominance by tunnelling-type fading reached earlier in this chapter, (though not completely ruling out the existence of localised transition pathways lacking suitable E^* and S^* values for detection by this method (where E* and S* are the activation energy and escape frequency factor of the localised transition pathway, (Templer, 1986a))).

In conclusion, while the method of variation of heating rate does indicate the presence of fading in those cases where localised transition pathways appear to play a prominent role, its inability to detect fading or even to separate a clearly identifiable fading component *from all samples exhibiting fading* prevents its use as a reliable diagnostic tool, and so relegates this method to the status of a useful tool for the investigation of fading mechanisms rather than one of significant practical value for the detection or treatment of fading in dating applications.

4.2.6 FADING MONITORING

4.2.6.1 INTRODUCTION

This section concludes the study on anomalous fading with an examination of possibilities for salvaging palaeodose estimates from samples exhibiting fading. In reiteration of the procedures useful if the fading mechanism can be unambiguously identified: fading via localised transitions alone can in principle be fully eliminated by a

suitable preheat, so enabling dating of the stable remanent luminescence component. Alternatively, if fading is solely via quantum mechanical tunnelling and the entire signal fades (necessarily at a rate sufficiently slow so as to allow significant accumulation of trapped charge over the time range dated), then although prospects are that dating is not feasible as the fading cannot be removed, it may in some cases appear possible to correct for such fading by extrapolation of the remanent luminescence function to the age of the sample. However, it has been shown by Wheeler (1990), that the remanent luminescence function may deviate from the ln(t) model after long times (based on Delbecq *et al* (1974)) and so make reliable extrapolation unsatisfactory, hence although a procedure for correction of "pure" tunnelling-type fading can be proposed, it is strongly recommended that such a procedure is not attempted and that the identification of tunnelling-type fading in a sample is rigorously regarded as a rejection criterion for dating that sample.

In either case, the fading must first be identified and the remanent luminescence levels measured. The next section describes a fading monitoring procedure for doing so by monitoring the remanent IRSL (or OSL) trapped charge population over storage periods of several months.

4.2.6.2 THE FADING MONITORING PROCEDURE

Outlined below is a procedure intended for the monitoring OSL or IRSL remanent levels with the aim of both detecting and characterizing fading within feasible laboratory timescales. The procedure is:

1) Drain the NTL (this step assumes no changes in fading behaviour result from NTL measurement)

2) Administer test dose (say ≈ palaeodose)

3) Prompt preheat (say 60 seconds at 220°C, as soon as possible following the dosing)

4) Short normalization exposure as soon as possible following the preheat; record the time elapsed between the cessation of the preheat and this exposure as t_0 (short exposure monitoring, for IRSL at least, is justified by the absence of change in the shape of the decay curves with exposure energy during long exposures; similar data was not collected for green stimulation)

5) Store at ≈ 10°C, (or preferably at the best-estimate of the environmental storage temperature experienced by the natural sample)

6) Throughout the storage period give incremental short exposures approximately logarithmically spaced in time (ie, at each of 15 minutes, 2 hours, 1 day, 1 week and 2 months following the normalization exposure; record these times as T_i)

7) Plot remanent luminescence, $L(T_i)/L(T_0)$, versus log(time).

Monitoring should be made concurrently on duplicate portions of sample undergoing storage at ≈ 100°C, in case thermally accelerable localised transition-type fading is present (note that care must be taken not to interpret thermal erosion of the IRSL or OSL over the longer storage times at raised temperature as fading).

Interpretation of monitoring involves comparison between the data collected following storage at ambient temperature and elevated temperature and some possible outcomes, along with suggested courses of action, are outlined below:

(A) No fading seen at either storage temperature : datable

(B) Fading thermally accelerable to a stable remanent level : conclude the only fading present is of the localised transition type: datable following suitable preheat

(C) Fading rate greater for elevated temperature storage but no remanent level reached :

not possible to determine mechanism: undatable

(D) Fading continues unaffected by storage temperature: only tunnelling-type (athermal) fading present; undatable.

At this juncture attention is drawn to the hazards of misleading presentation of fading monitoring data: remanent luminescence should be plotted versus log(storage time), not against a linear representation of storage time. An illustration of the potential of the linear representation to mislead is given in Fig.4.2.6.2.1; inspection of the same data set plotted in both ways appears to indicate a stable remanent level has been reached when linear plotting is used whereas the ln(time) plot shows fading continuing. Clearly, reliable detection of tunnelling-type fading requires ln(time) plotting of fading monitoring data.

Even so, experimental precision sets the limit to the detectable fading rate; for example, assuming that monitoring is performed over a period of 2 months (recommended as optimum duration in practice), this represents 5,259,600 s / 200 s ≈ 4.4 decades of time, hence if the measurement precision is ≈ 8 %, then fading rates of less than ≈ 1.8 % / decade will not be detectable. This has serious consequences for dating applications, as the required extrapolation to typical dating ages of interest, i.e., say ≈ 20 ka (given the doubts raised by Wheeler (1990) as to the rigorous validity of the assumption that long-timespan extrapolations can safely be made) is of the order of a further five decades of time; the cumulative fading which could pass the monitoring procedure undetected is therefore **4.4+(sample age/2 months)*fading rate**, and could so approach 15 %. As the dominant error source is day-to-day instrumental drift there is little likelihood of significant improvement in the precision available. Consequently the role of fading monitoring must be recognized as being restricted to the elimination of seriously fading samples from work programs, rather than as a fully reliable method for rejecting all cases

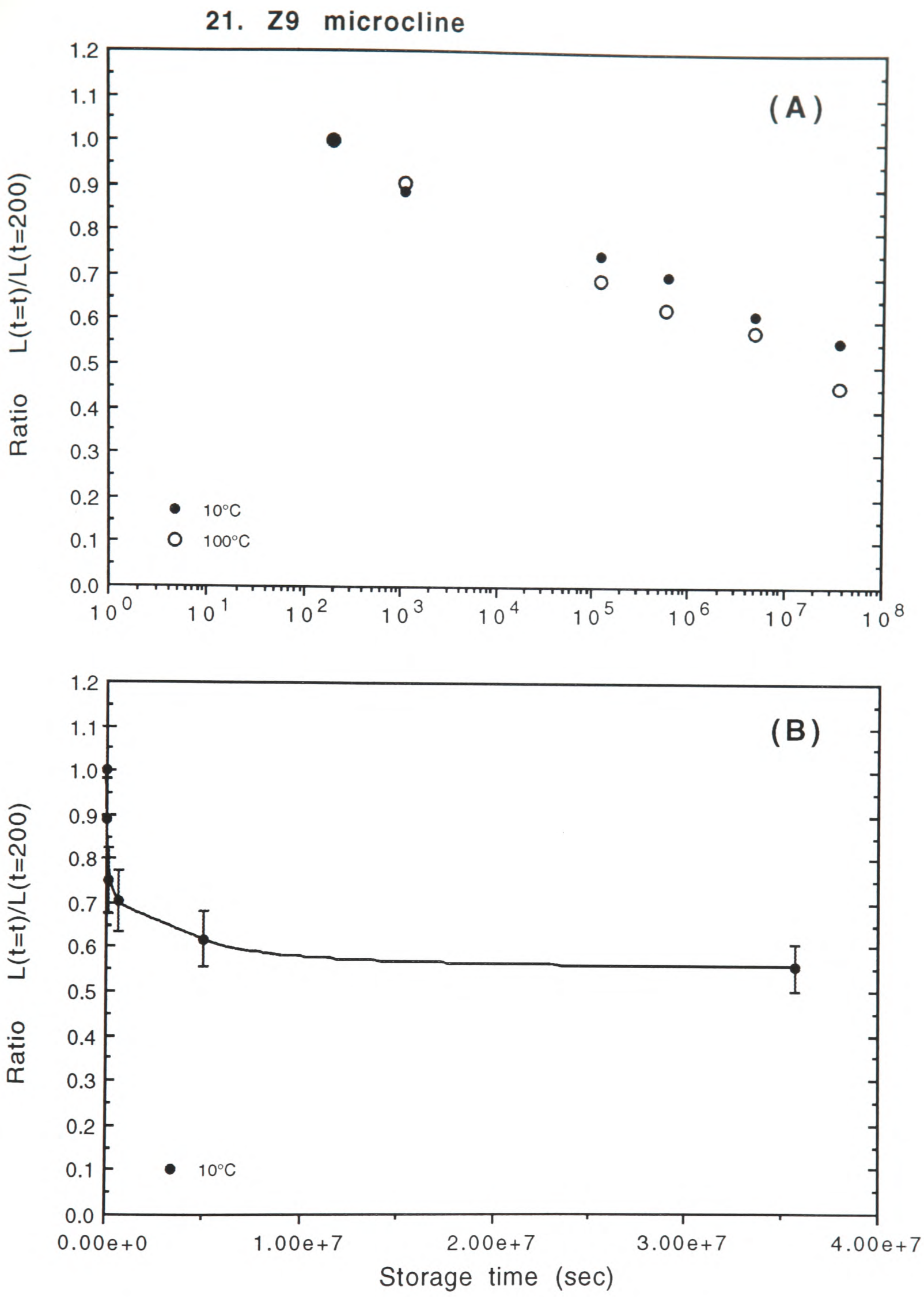


Fig.4.2.6.2.1 An illustration of the potentially misleading nature of linear time-representation of fading data. **(A)** shows the remanent IRSL data for sample 21. Z9 microcline plotted against log(time) as in Fig.4.2.2.1.1, and the same data for 10°C storage is replotted in **(B)** against linear(time). Within error limits (5 % here) the fading appears to have reached a stable remanent level in (B), whereas it is apparent from the log(time) plot that this is not truly the case.

of fading; and pessimistically, there exists the possibility that slowly fading samples will pass undetected through even the most rigorous monitoring procedure and give rise to slight age underestimates. Having said this, recent agreement has been reported by Visocekas, (1993) between the detection of fading phosphorescence at temperatures down to 77 K, emitted from a subset (six) of these same feldspar samples, and their identifications as fading or non-fading, given in section 4.2.2. This raises the possibility of a second means of testing for fading: monitoring the low temperature phosphorescence. Both methods would be favoured for certain cases, i.e., monitoring phosphorescence would be advantageous in cases where tunnelling fading is proceeding rapidly, or from sensitive samples, or where thermal quenching is present (Visocekas, 1993). On the other hand, signal/noise considerations may favour short exposure monitoring (IRSL or OSL) of the total trapped charge population, as described in section 4.2.2 for fainter samples.

Finally, attempts to salvage palaeodose data from fading samples requires unambiguous identification of the fading as "pure" localised transition fading; failing this, the determination of a valid preheating procedure is precluded. Furthermore, as the tunnelling fading component cannot be either removed or reliably corrected for, the detection of such fading must be taken as a rejection criterion.

4.2.7 SUMMARY

The preceding investigation into anomalous fading set successive goals as it evolved from a pilot study inspection of a small set of identified feldspars into a major effort aimed at firstly defining the occurrence of fading amongst the feldspar minerals and

secondly determining the fading mechanisms active with the ultimate goal (if possible) being a means of circumvention of anomalous fading in feldspathic materials.

With these goals in mind, some principal conclusions are:

1) Anomalous fading has been detected in TL, OSL and IRSL and is not restricted to any specific feldspar mineral or compositional regime of the feldspar ternary diagram;

2) Fading appears independent of stimulation wavelength;

3) Fading does not appear to be characteristic of any specific emission observed, and in a fading sample all emission wavebands appear to fade;

4) Although thermal acceleration of fading was seen, no stable remanent levels of luminescence were achieved; fading behaviour generally was consistent with dominance by a tunnelling-type fading mechanism capable of limited thermal acceleration but not of erasure by feasible elevated temperature storage;

5) Consequent to "(4)", the method of heating rate variations is of only limited utility due to the scarcity of feldspar minerals having dominant localised transition-type fading with kinetic parameters permitting effective use of that approach;

6) Correction for fading possible in principle only; in practice only samples in which the sole fading mechanism is tunnelling that does not deviate from the ln(t) form over the timespan dated are acceptable candidates for applying correction procedures. As these conditions are very unlikely to hold in reality, and, given additional sources of systematic error (such as erroneous identification of fading type), attempts at fading correction by extrapolation of the remanent luminescence line from laboratory monitoring timescales to the lifetime of the sample must be considered unsound, and discouraged;

7) Monitoring cannot detect all fading due to limitations of experimental precision.

In conclusion, the evidence shown here and elsewhere by others (Templer (1986a),

Visocekas (UK TL and ESR seminars, Dec. 1992)) reveals the complexity of the fading phenomenon and eliminates the optimistic picture in which the active fading mechanism in all samples can be determined and the fading reliably removed or corrected for. However, on the other hand there were some samples (and importantly, amongst the high-K species) which did not show any fading during 10°C storage for up to 13 months; from which it is concluded that some individual samples of species relevant to dating do not fade. Finally, the ability of fading monitoring to detect the presence of fading was strengthened by the results of the parallel study monitoring phosphorescence conducted by R. Visocekas.

CHAPTER 5 THERMAL STABILITY OF LUMINESCENCE FROM SELECTED FELDSPARS

5.1 INTRODUCTION

The preceding chapter briefly reviewed possible causes of age shortfall in the dating of feldspathic materials, then reported a detailed investigation of the anomalous fading of feldspar luminescence. From the latter it was concluded that anomalous fading cannot be either removed or reliably corrected for, making rejection of samples exhibiting fading the only prudent course of action. Following this philosophy, samples which do not exhibit anomalous fading in the laboratory monitoring procedure *may* then provide correct dates. However, a crucial assumption implicit in this argument is that the "stable" traps retain trapped charge throughout timescales of interest for dating. Verification of this assumption is essential to validation of dating using feldspathic materials, and its investigation is the subject of this chapter: the ultimate goal is the determination of the lifetime of an IRSL (or OSL) signal which survives "dating" preheats. This end was approached as a series of investigations: firstly, elucidation of the mechanism of IRSL production, to determine if it does involve a conduction band transition, (and incidentally confirming the essential veracity of the model proposed by Hütt *et al* (1988)); then determining the complete energetics of the IRSL source traps, using combined optical and TL techniques, and finally; comparing the findings with the "conventionally" determined trap parameters measured for a TL peak which survives a "dating" preheat and from which IRSL originates.

5.2 OPTICAL BLEACHING OF THE IRSL SIGNAL BY VARIOUS WAVEBANDS (MONITORED BY 880 ▲ 80 nm STIMULATION)

5.2.1 INTRODUCTION

The first stage in determining, by optical techniques, the energy structure of the IRSL source traps involved the measurement of the optical bleaching spectrum of the IRSL signal. If the model proposed by Hütt *et al* (1988) was correct, attributing the strong IRSL response to a "resonance" untrapping via excited states, then those excited states should be detectable through the presence of "resonances" in the bleaching spectrum. Importantly also, the bleaching spectrum should assist elucidation of the detrapping mechanism operant at shorter wavelengths and reveal if recombination is proceeding via the conduction band or otherwise.

While these experiments are similar in principle to that shown in FIG.5, Hütt *et al*, 1988, in which the bleaching action of 2.25 eV light on the optical response to 1.43 eV stimulation was monitored, in the present work the intent was specifically to map the optical response of the IRSL dating signal. Consequently, the stimulation (880 ▲ 80 nm) and detection wavelengths, and measurement apparatus used, were the same as used for dating. Therefore this work differs substantially in approach from the original work of Hütt *et al* (1988), and R. Clark (Oral presentation, UK TL seminars, Aberystwyth, 1991). Those workers selected a range of wavelengths from the output of xenon or halogen lamps by scanning monochromators, with the aim of mapping the excitation spectra of feldspars over as broad a range of stimulation wavelengths as possible, while necessarily being confined to the UV/blue wavelengths for emission detection. The stimulated luminescence

observed was then the superposition of contributions from all the various traps stimulated by any given excitation wavelength, with the consequence that those measurements were not optimal for obtaining information on specific trap types because of the interferences of other signals.

In contrast, as the specific purpose of this work was the measurement of the bleaching response of a specific trap or class of traps - those which give the IRSL dating signal, a different experimental procedure was followed in which the IRSL intensity was monitored between periods of bleaching by near-monochromatic light. A similar approach was taken by Bailiff and Poolton (1991) in measuring bleaching spectra for wavelengths between 450 nm and 1000 nm. That work supports the original model of Hütt *et al* (1988), concluding there exists an excited state ≈ 0.1 eV below the conduction band from which thermal detrapping to the conduction band occurs.

Reported below is the bleaching of the IRSL signal from five feldspars by twenty-eight wavebands ranging from ≈ 400 nm to ≈ 1065 nm. Bleaching illumination was provided by a 800 W halogen lamp, from which the filters (narrow band pass interference filters, ≈ 10 nm FWHM typically) selected near-monochromatic wavebands, the relatively dense coverage of the spectrum being intended to permit wavelength resolution of the expected resonance bleaching features. Samples were selected on the basis of composition and fading and non-fading behaviour as being a set representative of the feldspar ternary system and should therefore reveal any major-element or lattice-related differences, particularly through differences in any resonances found.

Additionally, to complete the study of fading described earlier (Chapter 4), these measurements also effectively constituted a comprehensive investigation of the procedure of optical washing (Templer, 1986b) as a means of selectively removing the anomalous

fading component. Justification for continuing an approach to fading based on the localised transition model, in spite of the previously described fading experiments appearing to eliminate that mechanism from any dominant role in fading, is the possibility that the storage times and temperatures used earlier may have been insufficient to enable efficient exploitation by thermal means of the hypothetical shared excited states (this follows if these states possess E^* approaching the thermal trap depth); however, these states may nevertheless be revealed by the occurrence of resonances in the bleaching spectrum. Templer (1986b) had shown that exposure to 600 nm light selectively removed the anomalously fading signal from zircon and interpreted this as a raising of the electrons to a shared excited state from which recombination was possible; a resonance bleaching at those wavelengths was predicted. Here, assuming the presence of localised transition type behaviour in some fading feldspars, "resonances" in the bleaching response spectra of these samples may indicate wavelengths at which bleaching of the fading component is proceeding via sub-conduction band localised levels in a manner analogous to that seen in zircon. The hope was that identification of such "resonant" wavelengths would permit development of a reliable optical wash treatment for feldspar.

Summarising, the principal aim in measuring the bleaching spectra of the IRSL signal was to enable better assessment of the long term trapping stability of the IRSL traps, from the trap energetics; intimately related was a second major aim - furthering understanding of the IRSL photo-eviction mechanism. An additional aim was testing the efficacy of optical washing as a means of eliminating anomalous fading in feldspar. Finally, and of practical relevance assuming the IRSL proved to be a dating signal, these measurements would also give insight into the environmental bleaching behaviour of the IRSL, and enable optimisation of sample preparation (ie, laboratory safelighting) and

measurement conditions.

5.2.2 EXPERIMENTAL

The five feldspar samples were prepared as described in section 3.3 and attached to stainless steel discs using silicone oil. Following draining of the "NTL" by heating to 550°C at 5 K/s and reheating, various $^{90}Sr/^{90}Y$ β doses of between ≈ 12 Gy and ≈ 200 Gy were given, depending on sample sensitivity. All samples then received a preheat of 60 seconds at 220°C using a Risφ automated TL reader was. Thirty-six discs of each sample were prepared; of these twenty-eight received measured exposures to the different test wavebands, interspersed with short exposures to 880 ∆ 80 nm IR to monitor the IRSL levels. The remaining eight discs were controls to account for run-to-run variations of the monitoring apparatus, bleaching (slight) by exposure to safelights, and particularly to allow correction for the cumulative trap depletion by the monitoring exposures.

IRSL monitoring was by an Elsec Optical Dating System Type 9010 with an EMI 9235Q PMT and 2 mm Schott BG39 filter. Exposures were of either 0.5 second or 1 second duration depending on sample sensitivity, chosen so as to optimise counting statistics without significantly depleting the signal.

The experimental procedure comprised an initial normalization exposure to each sample disc, after which the twenty-eight test filters (narrow band interference filters with typically 8 nm FWHM) were sealed over the discs and a timed exposure given. The filters were then removed to permit a short exposure measurement of the IRSL intensity, after which the filters were replaced and the cycle repeated. Logarithmically incrementing timed bleaches, interspersed with the monitoring exposures, were accumulated until cumulative

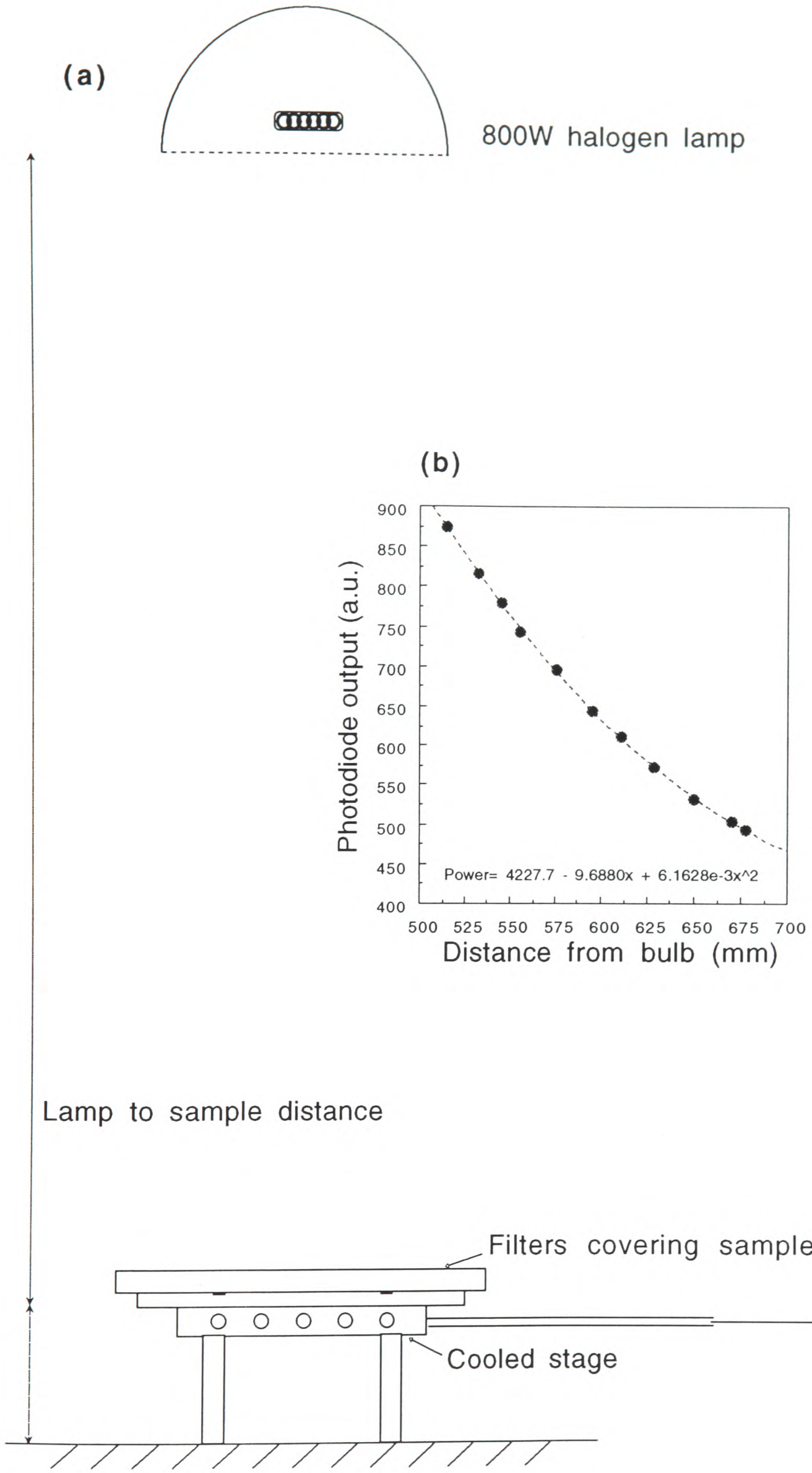


Fig.5.2.2.1.(a) The illumination apparatus based on a 800 W halogen lamp. Sample temperature was maintained at ≈ 10°C during bleaching; **(b)** the relationship of illumination intensity to sample-to-lamp distance.

exposure time totalled 8.5 hours. Residual TL was then measured for all discs using a Risϕ automated TL reader (with an EMI 9635Q PMT and Corning 7-59 and Chance-Pilkington HA3).

A schematic diagram of the arrangement of the 800 W halogen lamp and the water-cooled sample tray is shown in Fig.5.2.2.1. The inset, (b), shows the variation with distance of the power incident on the plane of the sample discs; this relationship was used to correct for the differing bulb to filter distances of the filters in the calibration procedure; additional correction factors accounted for the deviation of each disc position from the bulb-to-tray centre axis.

Data analysis for each sample disc/waveband consisted of subtracting the empty plate background, correcting for depletion (using the control discs) then normalizing using the initial (zero bleaching) short exposure IRSL intensity. This procedure gave the fractional IRSL residual as a function of bleaching duration. Direct absolute power calibrations for each filter, made using a Molectron PR-200 pyroelectric radiometer, were then used to convert cumulative exposure duration into cumulative exposure energy. The resulting IRSL residual values and cumulative exposure energies enabled the construction by interpolation of the decay curve for the IRSL signal under bleaching by that waveband.

5.2.3 IRSL DECAY CURVES FOR VARIOUS STIMULATION WAVEBANDS

The families of decay curves for each of the wavebands used are shown overlain for each feldspar in Fig.5.2.3.1.(a)-(e). Note that these decay curves are not equivalent to the shine curves stimulated by the various illuminations as those would contain, in

addition to the "IRSL", components of OSL originating from trap populations other than those giving rise to the IRSL. Data for bleaching by UV wavebands are excluded from presentation, as those filters possessed significant IR transmission windows in addition to their specified UV windows. However it must be noted that the trend in the UV was for *more* energy to be required to reduce the IRSL residual to a given level as bleaching photon energy increased, contrary to the expected effect resulting from unwanted simultaneous IR exposure leaking through the filters.

Comparison between the sets of decay curves for each sample reveals a striking similarity of response; only 9. Z15 sanidine deviates significantly from the general pattern - a not unexpected result as this sample was included on the likelihood that localised transition-type fading was present and that it may therefore exhibit bleaching "resonances". The apparent build-up of the residual IRSL intensity in this sample for small exposure times at shorter wavelengths is attributed to "resonant" bleaching via shared excited states the broad range of wavelengths over which this behaviour is observed is taken as evidence of a complicated structure to the distribution of these sub-conduction band levels, and no further analysis is attempted here (millisecond time-resolution short exposures on this sample revealed strong initial bleaching by 514.5 nm photons (65% signal reduction within the first second (5 mJ)) followed by a partial signal recovery if illumination was interrupted for several seconds). However, the precise connection of this behaviour to fading must be considered unproven as it is noted that sample 12. Patmos sanidine, while sharing similar fading behaviour, does not share a similar bleach response; additionally, 23. Dup(B) oligoclase fades but has a bleach response spectrum effectively indistinguishable from that of the stable microcline and albite samples.

Generally, the IRSL signal is most susceptible to bleaching by green/blue

wavelengths, and at these wavelengths the signal is effectively zeroed by exposures of ≈ 2 J/cm^2; corresponding to ≈ 5 minutes of clear day sunlight exposure (taking account of the wavelength region ≈ 400 nm to 800 nm). This estimation is very approximate, but serves to demonstrate the potentially rapid bleaching of the IRSL signal under natural illumination conditions. Furthermore, the bleaching response remains strong across the entire visible spectrum, even at redder wavelengths; this in conjunction with the resonant bleaching response in the near-IR ensures that the IRSL signal will bleach in virtually all natural contexts where a substantive illumination intensity is present. However, although these measurements by their nature simultaneously take into account the effects of phototransfer into the IRSL traps during bleaching, they can only do so for the near-monochromatic waveband used in each case. Consequently the effects of phototransfer expected during bleaching by natural sea-level sunlight (containing UV) are not included, though unlikely to be significantly different.

5.2.4 BLEACHING RESPONSE OF THE IRSL SIGNAL

To further interpret the bleaching response curves, the energies required to cause specified reductions to the intensity of the IRSL signal were measured for each waveband. Useful IRSL reductions were chosen to be of 10%, 50% and 90% and the necessary energies were determined from Fig.5.2.3.1.(a)-(e). Results are shown for each feldspar in Fig.5.2.4.1.(a)-(e), both as functions of stimulation wavelength and (insets) as functions of stimulation photon energy. In addition to supporting the observations stated above, this form of presentation permits more quantitative assessment of the untrapping processes giving rise to IRSL. The "peak" energies of each resonance along with the corresponding

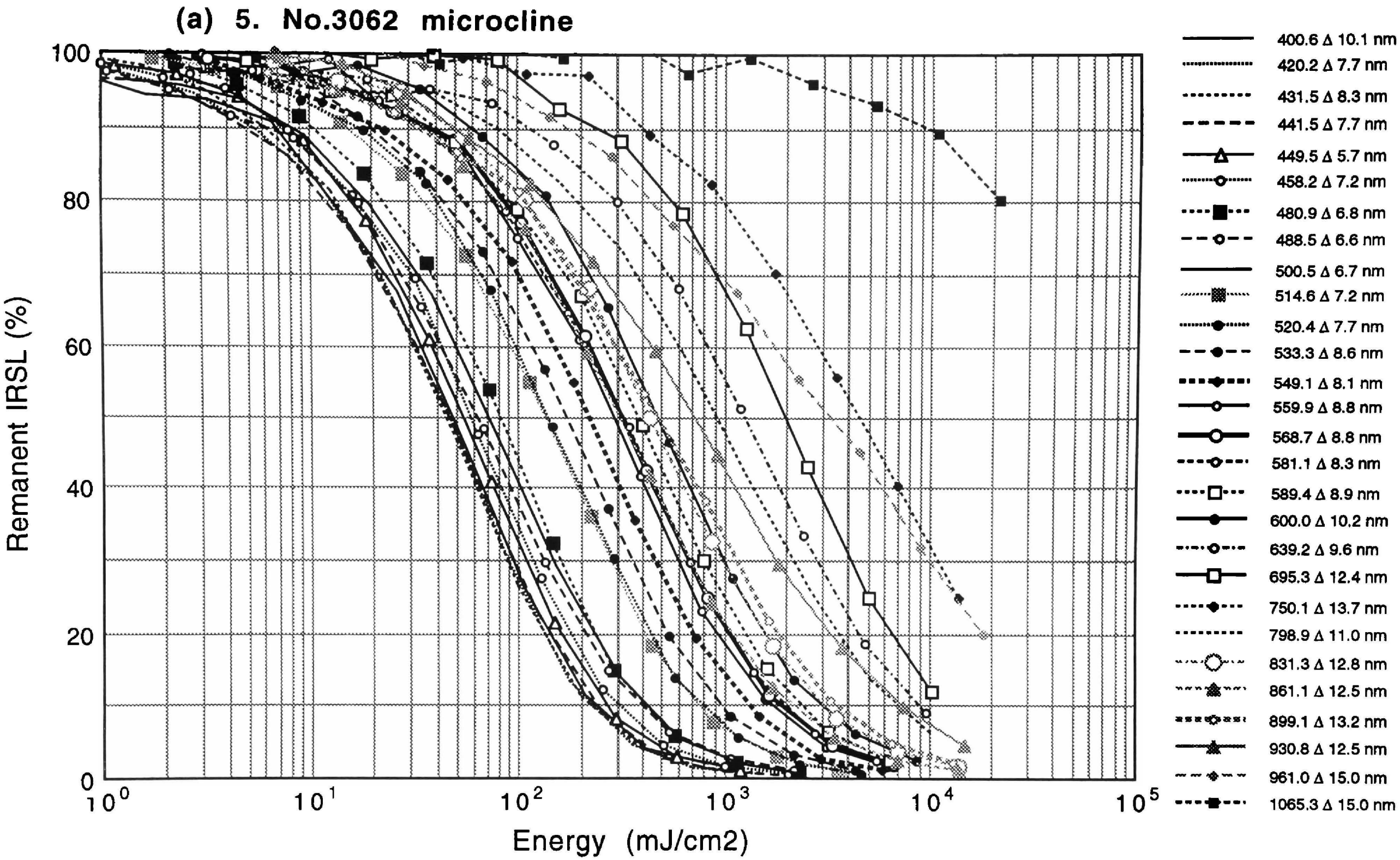
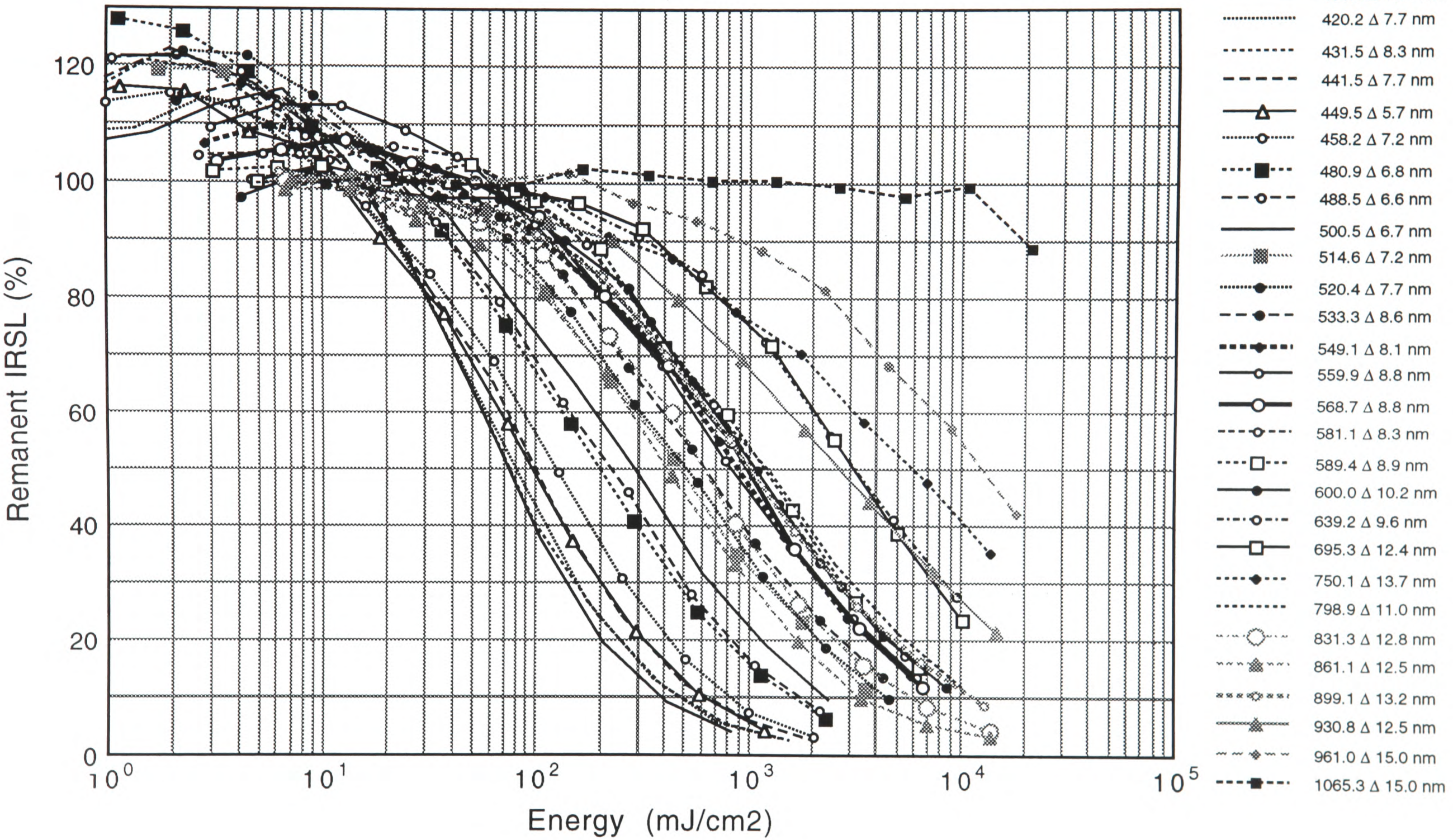
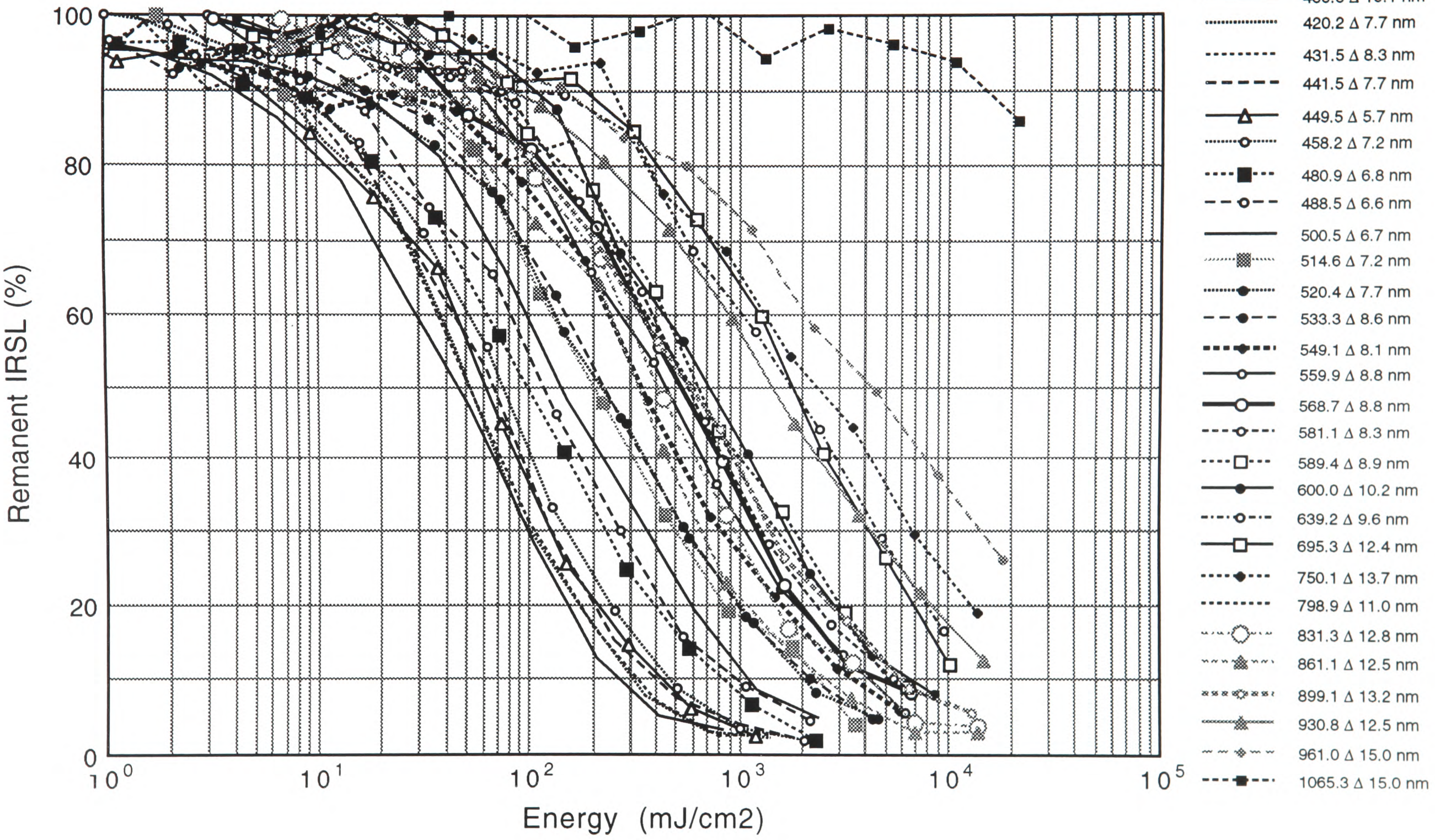


Fig.5.2.3.1.(a)-(e) Decay curves showing the bleaching of the 880 Δ 80 nm stimulated IRSL signal by various wavebands.

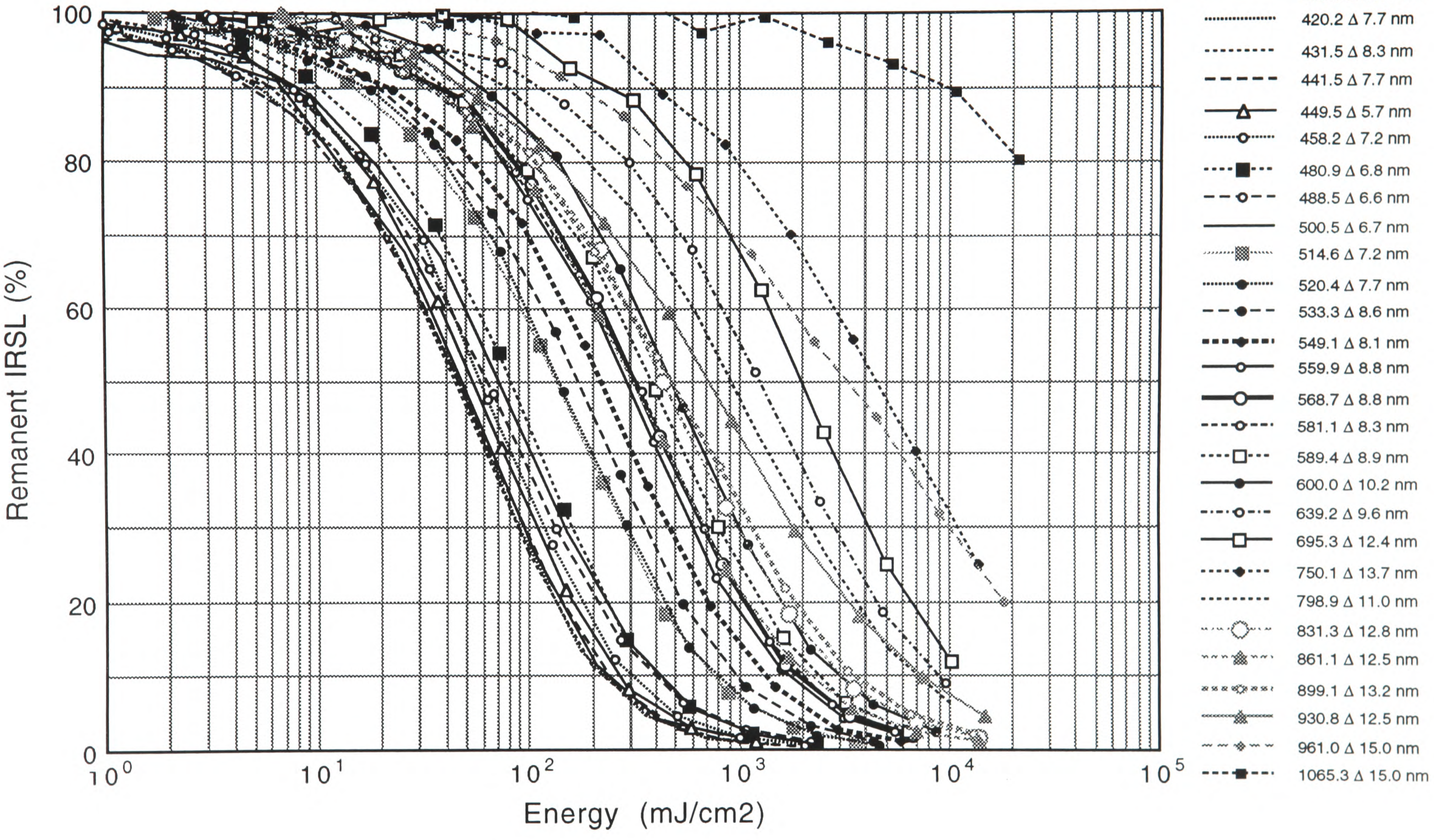
(b) 9. Z15 sanidine



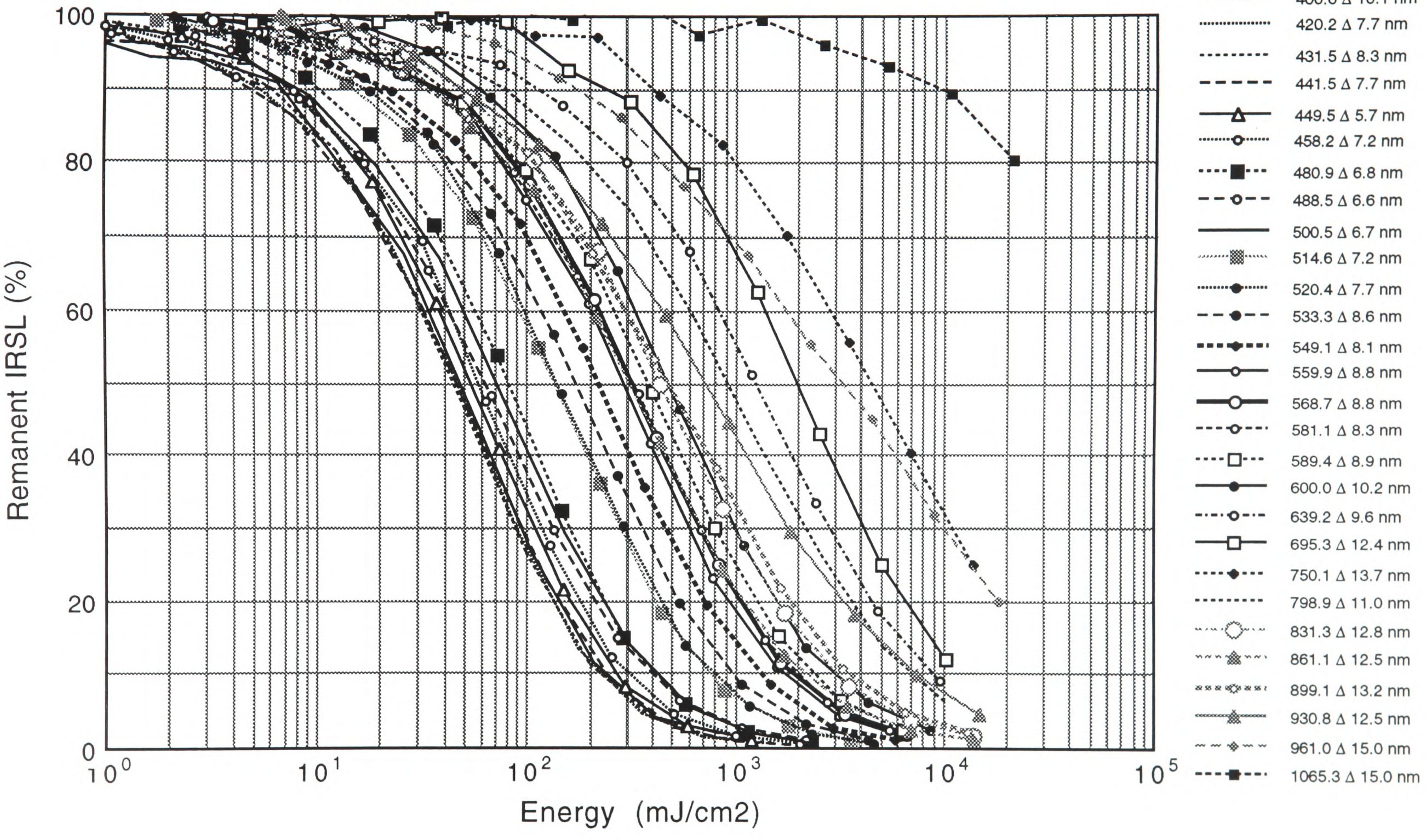
(c) 12. Patmos sanidine



(d) 18. Amelia albite



(e) 23. Dup(B) oligoclase



FWHM are given in Table 5.2.4.1.

Sample	Ground to excited state gap (eV)	Half-maxima points (eV)
5. No. 3062 microcline	1.44	1.37
		1.52
9. Z15 sanidine	1.44	1.39
		1.51
12. Patmos sanidine	1.45	1.37
		1.56
18. Amelia albite	1.43	1.32
		1.52
23. Dup(B) oligoclase	1.44	1.35
		1.52

Table 5.2.4.1 The energy required for the ground-to-excited state transition for each feldspar sample (assuming a model similar to that of Hütt *et al* (1988)). The half maxima points are the photon energies at which untrapping efficiency is half that at the resonance photon energy. Energies were measured from the 50 % IRSL residual curves shown in Fig.5.2.4.1.(a)-(e). Estimated errors are $\approx \pm 0.010$ eV on the ground-to-excited state energy, and on the half-maxima points.

The lower photon-energy wing of the FWHM is taken as being the best estimate of the excited state bandwidth, and the asymmetry of the resonance, showing broadening towards the higher photon-energy side, is attributed to the summation of bleaching by direct photoionization at those photon energies with that proceeding via the excited state, whereas on the lower photon-energy side the direct photoionization route is far less significant; consequently the energy range on that side relates more unambiguously to the bandwidth of the excited state.

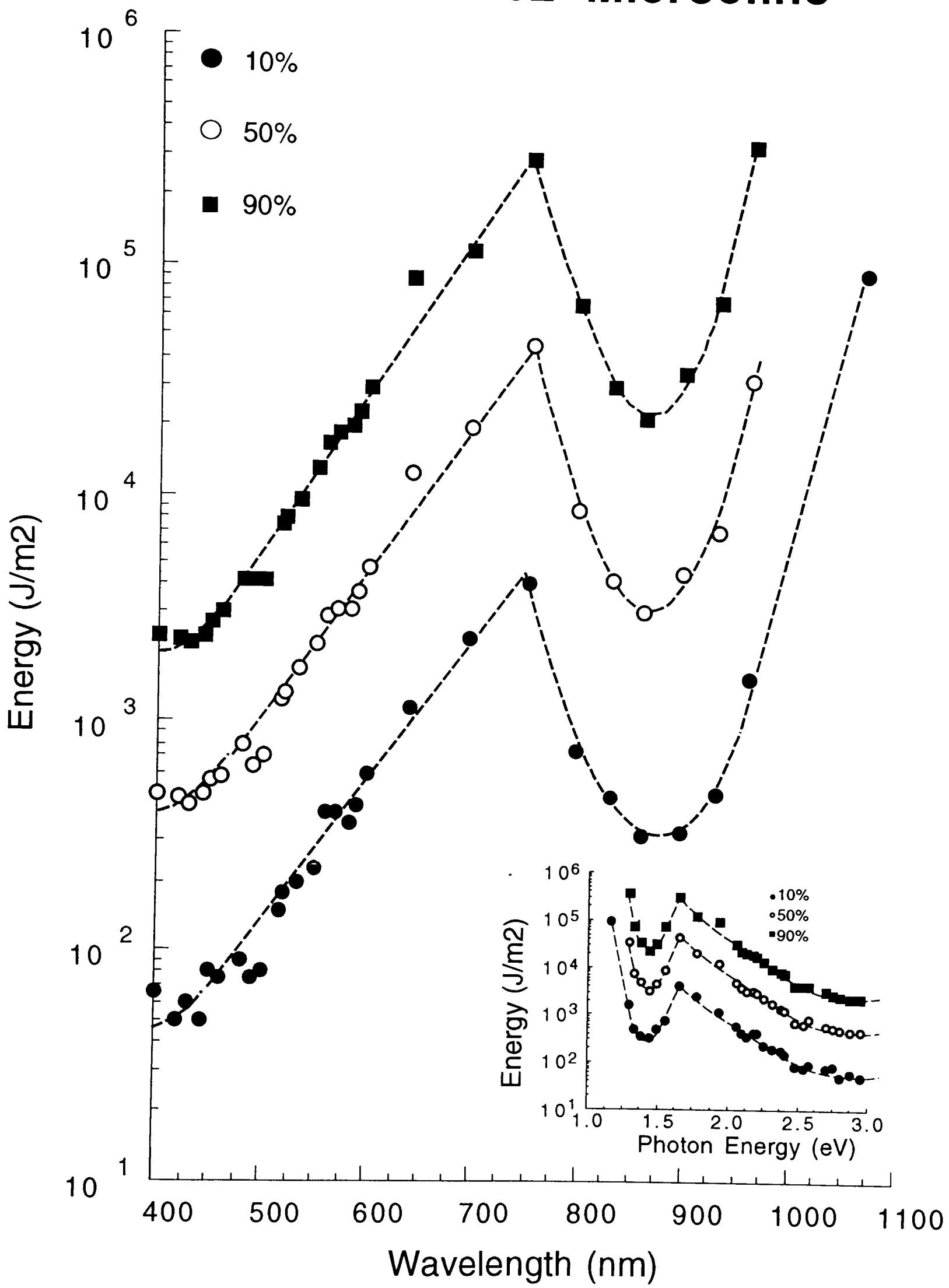
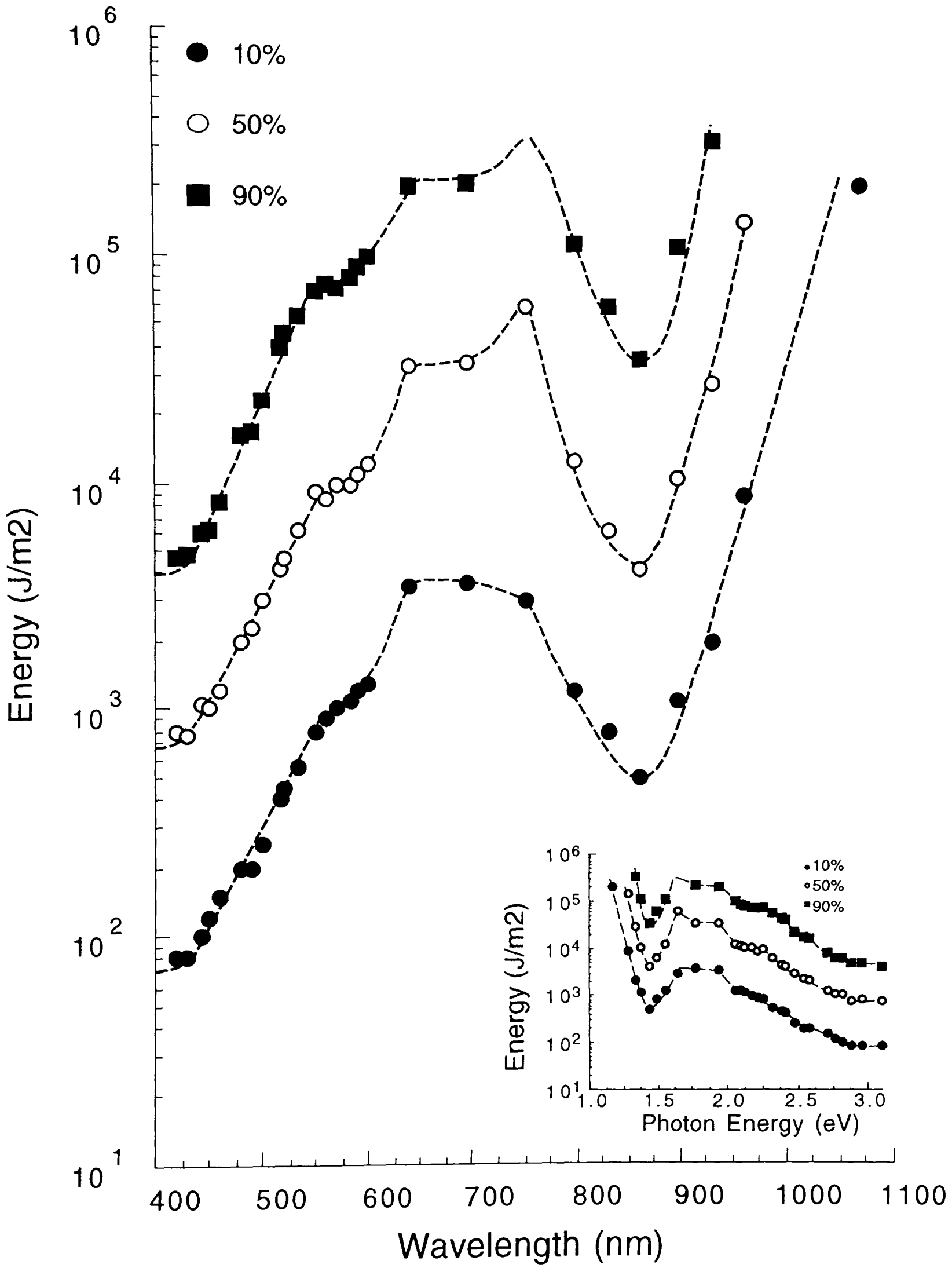
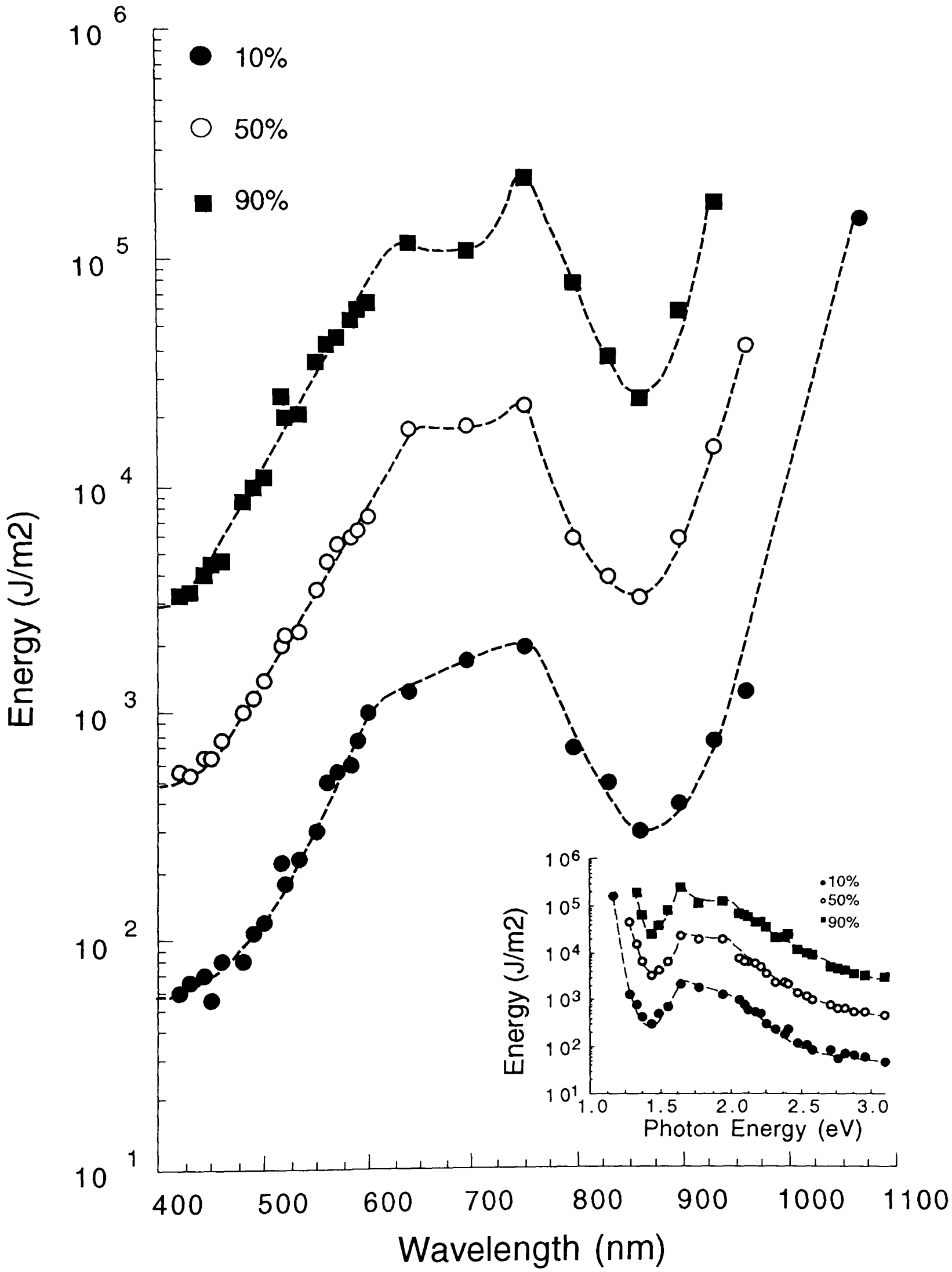


Fig.5.2.4.1.(a)-(e) The energy required at various wavelengths to reduce the IRSL signal to 10%, 50% or 90% of the initial level. The inset shows the data plotted against photon energy. Note the logarithmic scale of the energy axes.

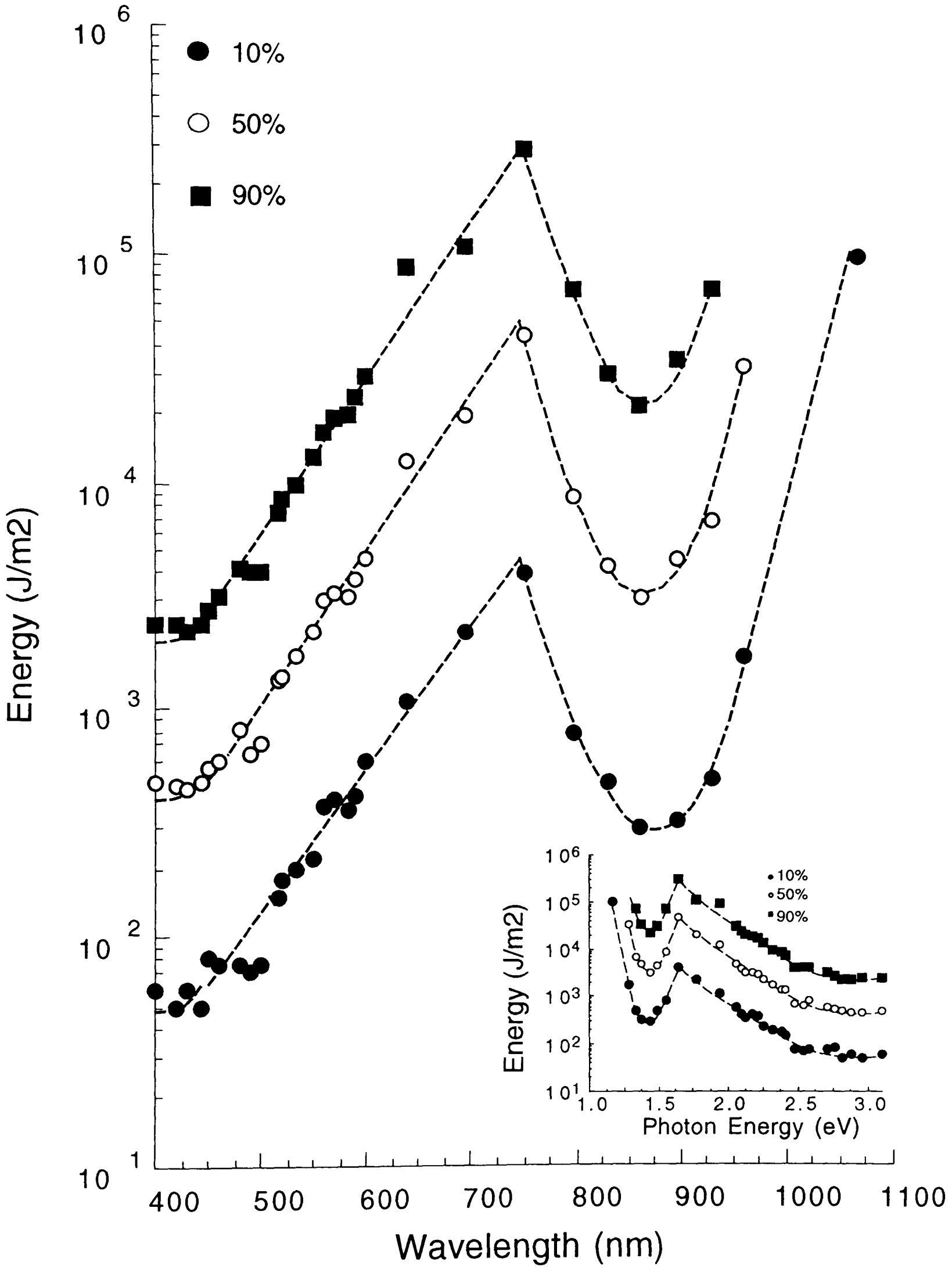
(b) **9. Z15 Sanidine**



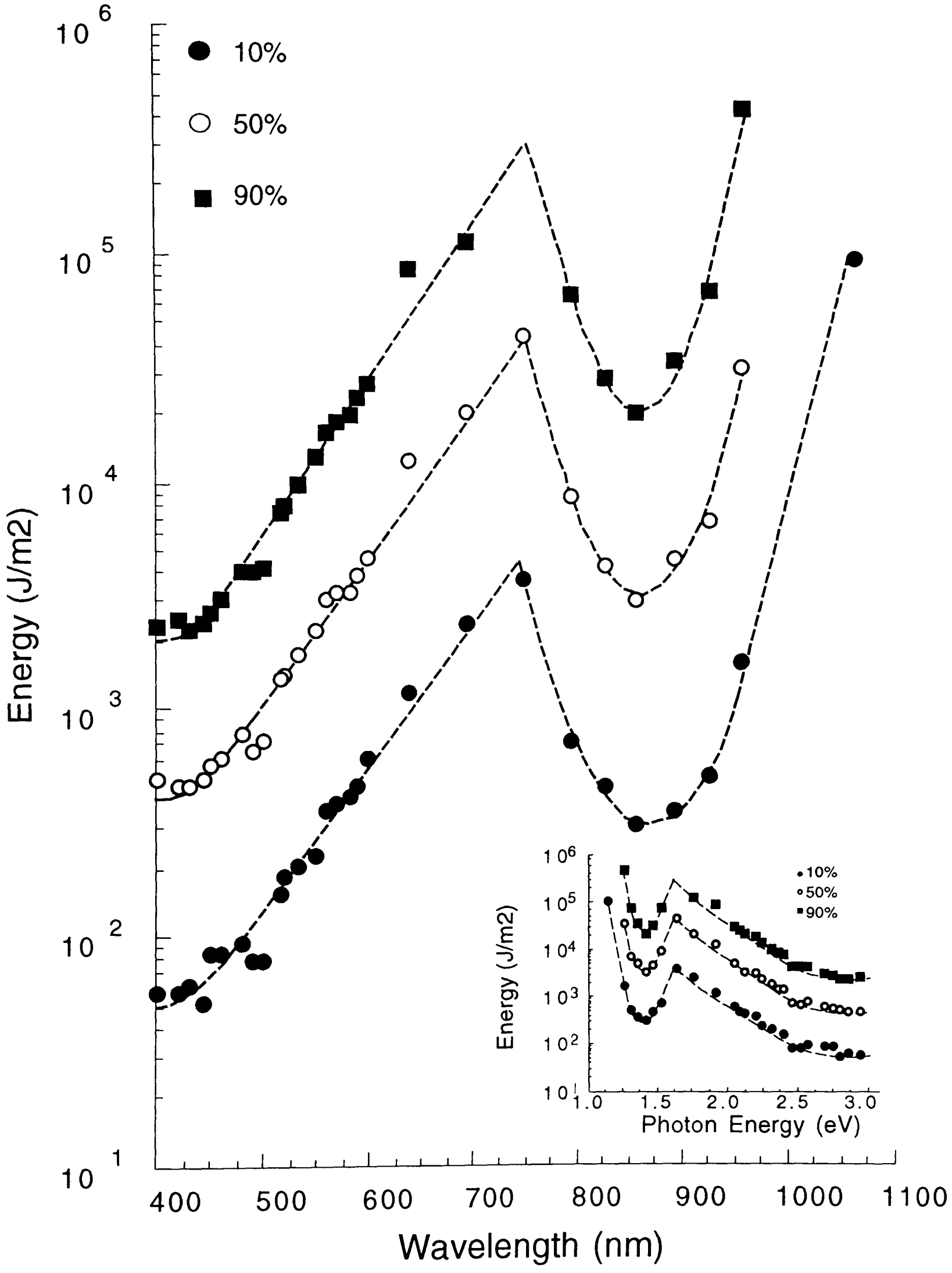
(c) 12. Patmos Sanidine



(d) 18. Amelia Albite



(e) 23. Dup (B) Oligoclase



The ground-to-excited state transition energy is seen to be the same for all samples regardless of composition or fading or non-fading behaviour, having an energy of ≈ 1.44 (± 0.01) eV which corresponds to a resonant wavelength of ≈ 861 ± 6 nm. This is in very good agreement with Hütt and Jaek (1989) in which the ground-to-excited state energy was found to be ≈ 1.43 eV (with the excited state to be ≈ 0.2 eV below the conduction band, and overall trap depths of ≈ 1.55 eV thermally and 2.25 eV optically).

5.2.5 DISCUSSION

The most remarkable feature of the bleach response curves is the apparent independence of their general form from influences attributable to the major-element compositions of the host lattices, and specifically, in the constancy of the ground-to-excited state energy gap. This latter is independent not only of sample composition but also of fading or non-fading behaviour. Additionally, although slight perturbations are seen to the bandwidths of the excited states from the different samples, the bandwidths themselves are more or less remarkably constant to a surprising degree.

These findings are explicable as being the result of the ground-to-excited state transitions of a single species of defect having a single excited state. Such a transition intrinsic to the defect will be minimally affected by the electronic environment of the crystal hosting the defect; consequently the transition energy will remain approximately constant and as a working hypothesis the IRSL source defect can be considered as a constant "unit" recurring throughout the feldspar series. The variety of feldspar luminescence behaviours observed then derive from the combination of this specific transition energy with the depth of the excited state below the conduction band, and

possibly with a range of escape frequency factors. The excited state depth below the conduction band will vary as it is influenced by the immediate electronic environment of the defect, and therefore not only by the major-element composition of the mineral through interactions with the host lattice, but also by the crystallographic system and the precise location of the defect within the lattice.

The general form of the bleach response curves is then interpreted as the superposition of two modes of detrapping: direct optical transition to the conduction band (photoionization) is the dominant mechanism and gives rise to the absorption edge characteristic of these plots (i.e., the near-exponential dependence of bleaching efficiency on photon energy - referred to as an Urbach absorption edge and described by Urbach's rule (Urbach, 1953):

$$\alpha(h\nu) = \alpha_0 \exp\left[\frac{-\gamma(h\nu - E_0)}{k_B T^*}\right]$$

Where α_o, E_o are material dependent, $\gamma \pm 0.5$ and T^* is the effective temperature (Hayes and Stoneham, 1985). Note that deviations from the exponential form of this equation will arise depending on the precise form of the density of states function for the conduction band of a given sample). Superimposed on the Urbach absorption edge is the evidence for the second mode of detrapping - a single resonance in the near-IR due to detrapping via the excited state pathway. The photon energy at the resonance wavelength is taken as being the optical energy required for the ground-to-excited state transition. Given that this is a bound state transition, that energy represents the "true" energy of the transition and would also be required of a phonon for the corresponding transition to be thermally activated.

The variety of IR bleachable peaks and their different behaviours in the various

feldspar minerals can readily be encompassed by this hypothesis, which additionally leads to several postulates: 1) excited state energy should be characteristic of a mineral due to the limited number of allowed electronic configurations in which the IRSL source defect can occur for a given crystallographic system and major-element composition. 2) IR bleachability of different TL peaks should vary as the different excited state depths (and the different S values?) lead to different electron residence times in the excited state before either thermal eviction or return to the ground state occur. 3) IRSL source traps must have thermal trap depths > 1.44 eV; bleaching of the low temperature TL peaks by IR wavelengths may occur, inefficiently, via direct transition to the conduction band by photoionization (and the possibility of IR stimulated sub-conduction band transitions cannot be excluded). 4) Speculatively, at LN temperatures resonant fluorescence should be observed under exposure to IR photons, with a lower and decreasing intensity seen at higher temperatures as the trapped charge is drained. The observation of this fluorescence would be strong proof of the veracity of the model of Hütt *et al* (1988).

A simple energy level diagram for the model described above is shown in Fig.5.3.4.1, and interpretation is as follows: at low photon energies (i.e., wavelengths >> 1000 nm) the photons lack the energy to raise trapped electrons efficiently to either the excited state or the conduction band and so bleaching does not occur. As photon energies increase, so the effects of increasing likelihood of direct transitions to the conduction band become apparent, albeit undramatically (i.e., bleaching by the 1065 nm waveband). At near-IR wavelengths the effects of direct transitions are greater, but the overwhelmingly dominant pathway is now via the excited state until photon energies become too great to give access to this level, (at ≈ 1.6 eV). Thereafter the direct transitions to the conduction band become completely dominant, with efficiency increasing near-exponentially across

most of the visible spectrum, until blue/UV wavelengths are reached.

The apparent levelling off of bleaching efficiency as UV wavelengths are reached is interpreted as being a real effect. An explanation can be proposed to account for this behaviour in terms of competition between bleaching and phototransfer of charge from other traps into the monitored traps. Such an explanation has recently been proposed by Robertson et al (0000) to account for an apparent bleaching "resonance" in the TL of a sanidine (Bailiff and Poolton (1989 and 1991) noted similar behaviour at UV wavelengths, using different samples, but attributed it to phototransfer from deep traps). An alternative explanation is that the greater photon energies at UV wavelengths permit increasingly efficient excitation of electrons from the valence band into the IRSL source traps. That this is possible comes from a consideration of the trap depths of the IRSL source traps in conjunction with the band gap of aluminosilicates: although the band gap is not precisely known, it is approximately 5 eV, and given the IRSL source traps have trap depths in excess of 1.5 eV (and maybe as much as 1.9 eV), then photon energies as low as $\approx$ 3.5 eV should be sufficient to excite valence band electrons into the deeper IRSL source traps.

Assuming this mechanism exists, potential consequences for IRSL dating must be considered. Fortunately, as only the deeper (IR bleachable) traps would be affected, then given the flux of visible and IR photons (capable of bleaching but incapable of excitation from the valence band) in natural bleaching spectra this effect should be overwhelmed by bleaching in the natural context. Its manifestation here is a consequence of the use of pseudo-monochromatic wavebands for stimulation, where the exclusion of visible and IR photons greatly reduces bleaching competition to the population of deep traps by direct excitation from the valence band. It is therefore inferred that this effect will be of

negligible significance to dating. Reported TL residuals observed from feldspars support this conclusion (i.e., Krϕnborg, 1983). The legitimacy of extrapolation from these results (given the samples were museum collection specimens) to natural sedimentary materials was demonstrated by excellent agreement with parallel work on the bleaching of the IRSL and OSL from natural loessic material performed by D.G. Questiaux (pers. comm. January, 1992).

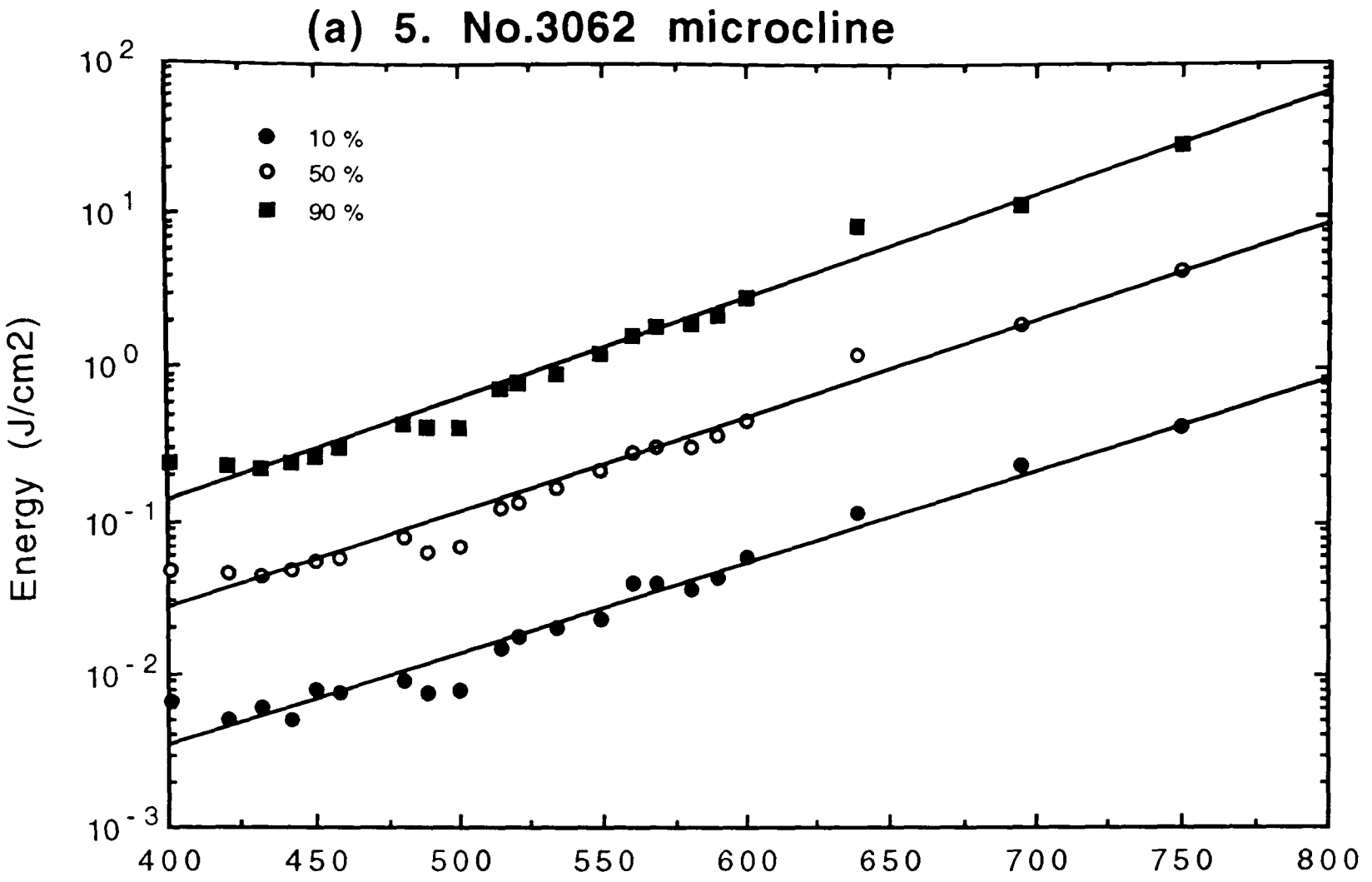
Fig.5.2.5.1.(a) and (b) show the bleaching response of 5. No.3062 microcline and 18. Amelia albite (chosen as being non-fading samples) over the wavelength range exclusive of the near-IR resonance. The bleaching responses in this wavelength range are well described by a function of the form $E = a * \exp(b\lambda)$, and the values found for the parameters a and b are given in Table 5.2.5.1. The near-exponential relation of these plots (with respect to photon energy) is entirely consistent with the Urbach rule (Urbach, 1953) and is taken as proof that shorter wavelengths are detrapping from the "IRSL" traps directly to the conduction band by photoionization (the relation of Mott and Gurney (1953) in which photon energy required to bleach is related to the thermal trap depth by $E_{optical}/E_{thermal} \approx \varepsilon_{high\ freq.}/\varepsilon_{static} > 1$ does not universally hold; indeed as the aluminosilicates are not highly ionic crystals, to which the Mott and Gurney relation pertains, such violation of that relation is not unexpected). Finally and significantly, the bleach response curves are effectively parallel over the range of signal reductions presented, indicating that bleaching is of one signal only, and that there are no "less bleachable" traps being probed by the IR stimulation as bleaching proceeds and lower regions of the shine curves reached. Note that these results confirm the essential veracity of the model of Hütt *et al* (1988) - discrepancies and "fine-structure" on the near-IR resonance in that work being due to mis-correction for the line spectrum of the xenon lamp light source used.

Sample	IRSL reduction (%)	a ($J.cm^{-1}$)	b (nm^{-1})
5. No. 3062 microcline	10	1.4×10^{-5}	0.0138
	50	8.4×10^{-5}	0.0144
	90	2.9×10^{-4}	0.0153
18. Amelia albite	10	1.4×10^{-5}	0.0137
	50	8.5×10^{-5}	0.0144
	90	3.1×10^{-4}	0.0153

Table 5.2.5.1 Energies required to cause the given reductions in IRSL from a microcline and an albite. Note the extremely similar values for corresponding reductions.

Regarding fading: the behaviour seen from 9. Z15 sanidine in Fig.5.2.4.1.(b) appears complex, but speculatively, it is hypothesised that there exists a range of optically accessible sub-conduction band pathways connecting electron and hole centres, and to which resonance excitation is possible by some of the visible wavelength photons used here. Indirect evidence that such a distribution of energy levels may be associated with the TL traps is drawn from the broad shapes of the TL glow curves of these two samples, in which there are no sharply defined glow peaks. However, regarding the potential use of optical washing as a means of alleviating fading, it must be noted that 9. Z15 sanidine was included for testing due to its uncharacteristic behaviour, hence generalisation from its bleaching response to that anticipated from other fading feldspars should not be made: the failure of the fading sample 23. Dup(B) oligoclase to show a response different in any way from that of the two stable control samples emphasises this point.

To summarize: the principal conclusion from these measurements is that the IRSL signal originates from only one defect type, possessing a ground-to-excited state transition energy of 1.44 ± 0.01 eV and having only one excited state. There is insufficient data here



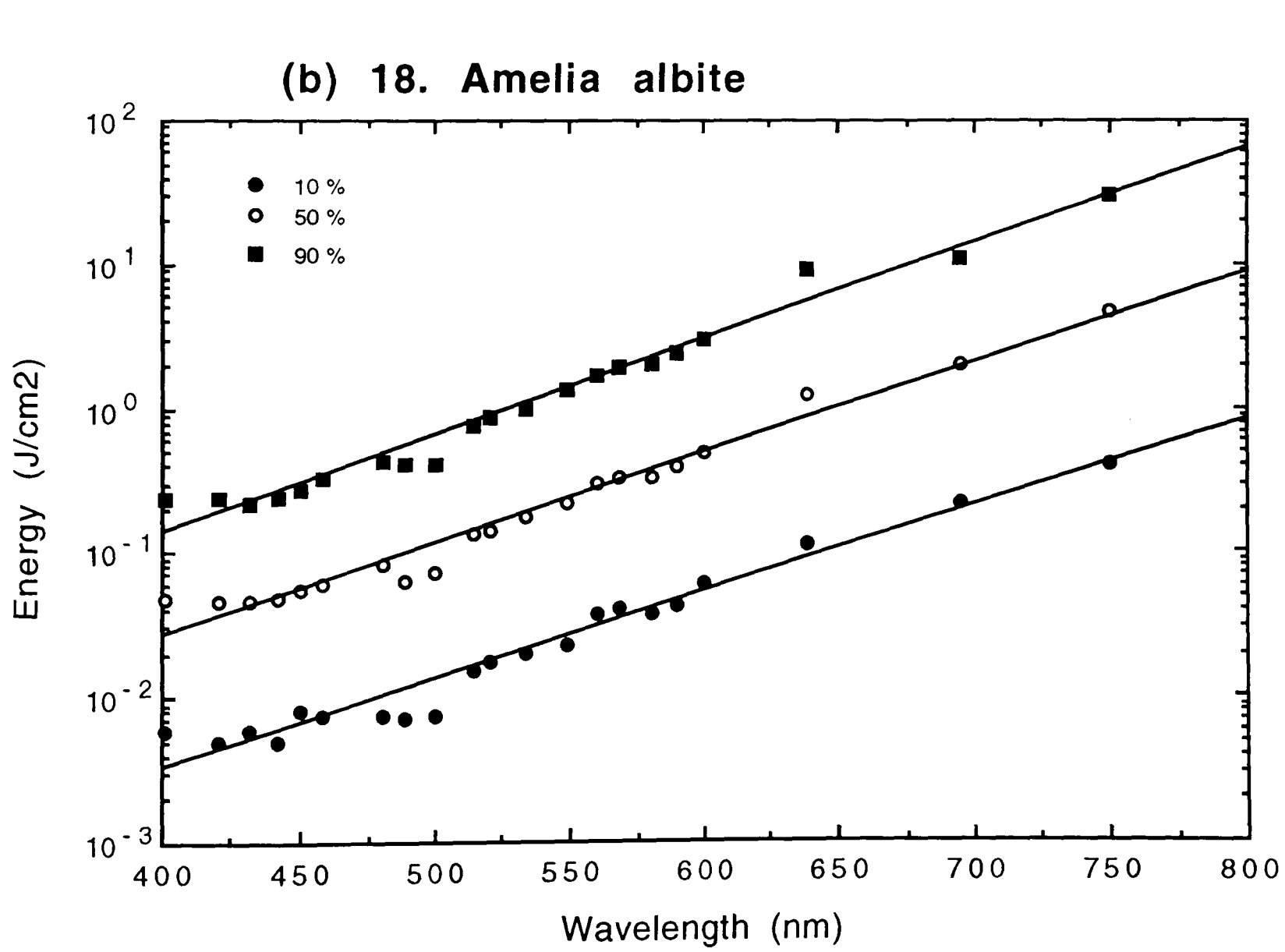


Fig.5.2.5.1.(a), (b) The bleaching of the IRSL signals from an albite and a microcline sample are shown above, to facilitate comparison of their forms in the visible spectrum for various progressions of bleaching.

to attempt to identify the "IRSL defect", and yet, to speculate on its possible identity, the observation of IRSL from all feldspar mineral species suggests that it is either a common structural defect (such as a stabilised broken Si-O bond) or based on an endemic substitutional impurity such as Mg^{++} substituting for Na^{+} or K^{+} (the V^{-} centre). However, as the most intense IRSL emissions appear to be from the high-sodic and high-potassic endpoints of the alkali series, i.e., the compositional regions of the ternary diagram in which there is highest degree of crystallinity, it is suggested that a structural cause is the more likely. Nevertheless, the variety of feldspar TL glow peaks seen to bleach under IR illumination (see section 3.5) appears to contradict this simple picture: resolution of this seeming paradox is made by the hypothesis of a variety of excited state depths below the conduction band, and possibly also a range of escape frequency factors. This then required testing by measurement of the excited state energies, as is described in section 5.3. Prior to that, a final bleaching study investigated bleaching of luminescence stimulated by photons too energetic to have access to the "IRSL" excited state pathway - i.e., bleaching of the 514.5 nm-OSL; a report of this work follows.

5.2.6 OPTICAL BLEACHING OF THE OSL FROM A MICROCLINE (MONITORED BY 514.5 nm STIMULATION)

5.2.6.1 INTRODUCTION

The preceding sections describe an investigation of the bleaching response of the IRSL signal by various near-monochromatic wavebands; here is reported a similar bleaching experiment but with the monitored luminescence being that stimulated by 514.5

nm light. The purpose was primarily to determine whether or not measuring the luminescence using photons having sufficient energy not to require the existence of the excited state pathway actually did result in the sampling of charge from traps lacking that pathway, in other words, are there "green only" bleachable traps in addition to the IRSL source traps. If this proved to be the case then the significance of also sampling from these traps during the optical dating measurement procedure would require assessment. The ultimate aim was to provide a physical basis for choice of stimulation wavelengths for optical dating applications.

The sample 5. No.3062 microcline was chosen for this study on account of its composition being representative of the high potassium feldspars (density < 2.58 g/cm^3), along with high sensitivity and non-fading luminescence.

5.2.6.2 EXPERIMENTAL

Measurements were much facilitated by the availability of 514.5 nm light from a 2W Coherent Ar-ion laser: using an optical beamline designed and built by the author the 514.5 nm line was selected, monitored, scrubbed of blue/UV plasma light and optically coupled to a modified Elsec Optical Dating System Type 9010 automated reader by a 3 mm ϕ glass fibre optic bundle (see Plates 5.2.6.1 and 5.2.6.2). Illumination for the monitoring short exposures was controlled by a fast Melles-Griot electronic shutter installed in the beamline. Due to the need to screen the EMI 9635Q PMT from scattered 514.5 nm photons, more restrictive optical filtering was required; for this a 5.1 mm Corning 7-51 and a 2 mm Schott BG39 filters were used. The bleaching, measurement and data analysis procedures were otherwise identical to those used when measuring the

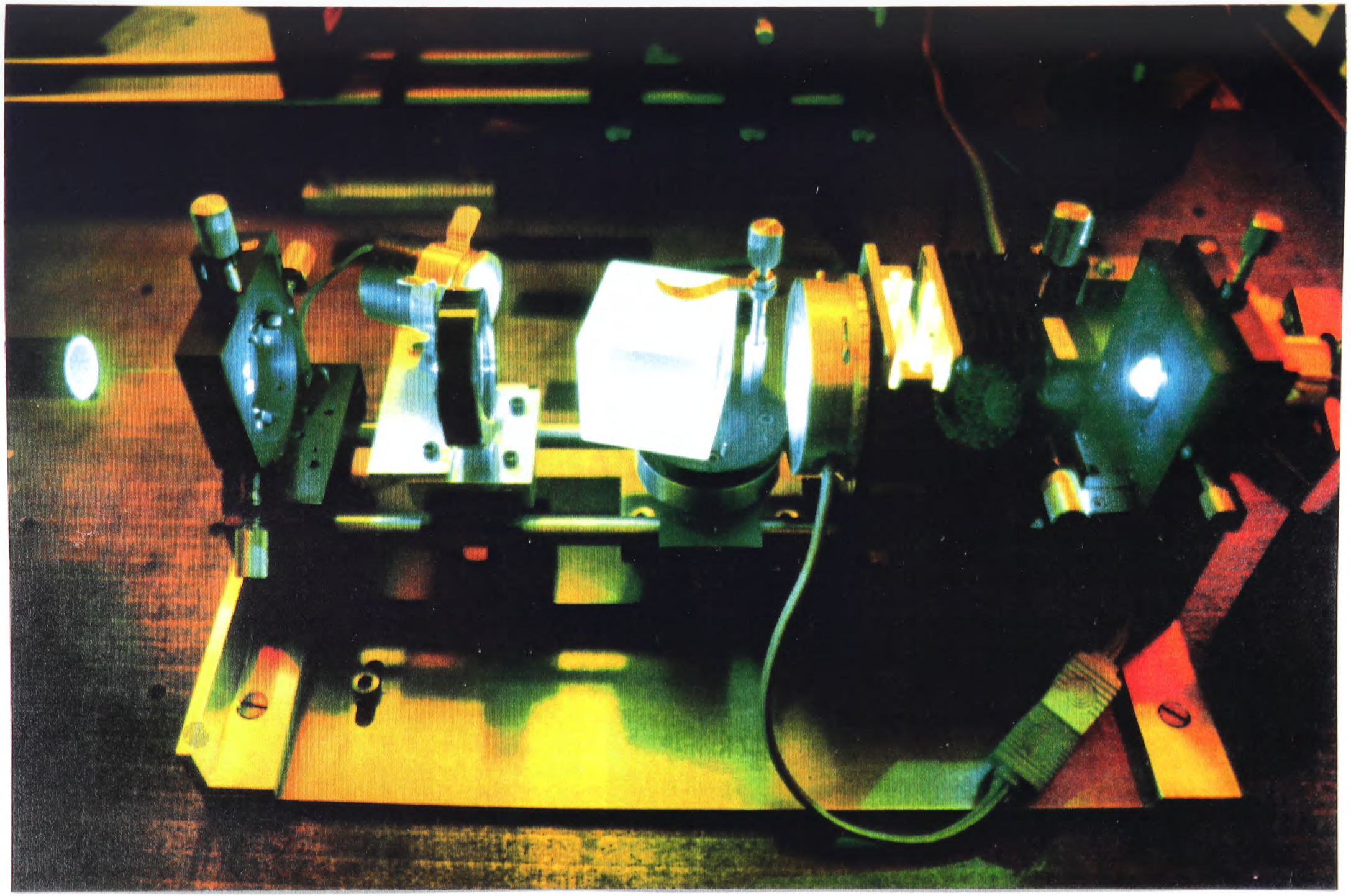


Plate 5.2.6.1 The beamline optical assembly interfacing the Ar - ion laser with a modified Elsec Optical Dating System Type 9010.
(see Plate 5.2.6.2. (a),(b))

a



b

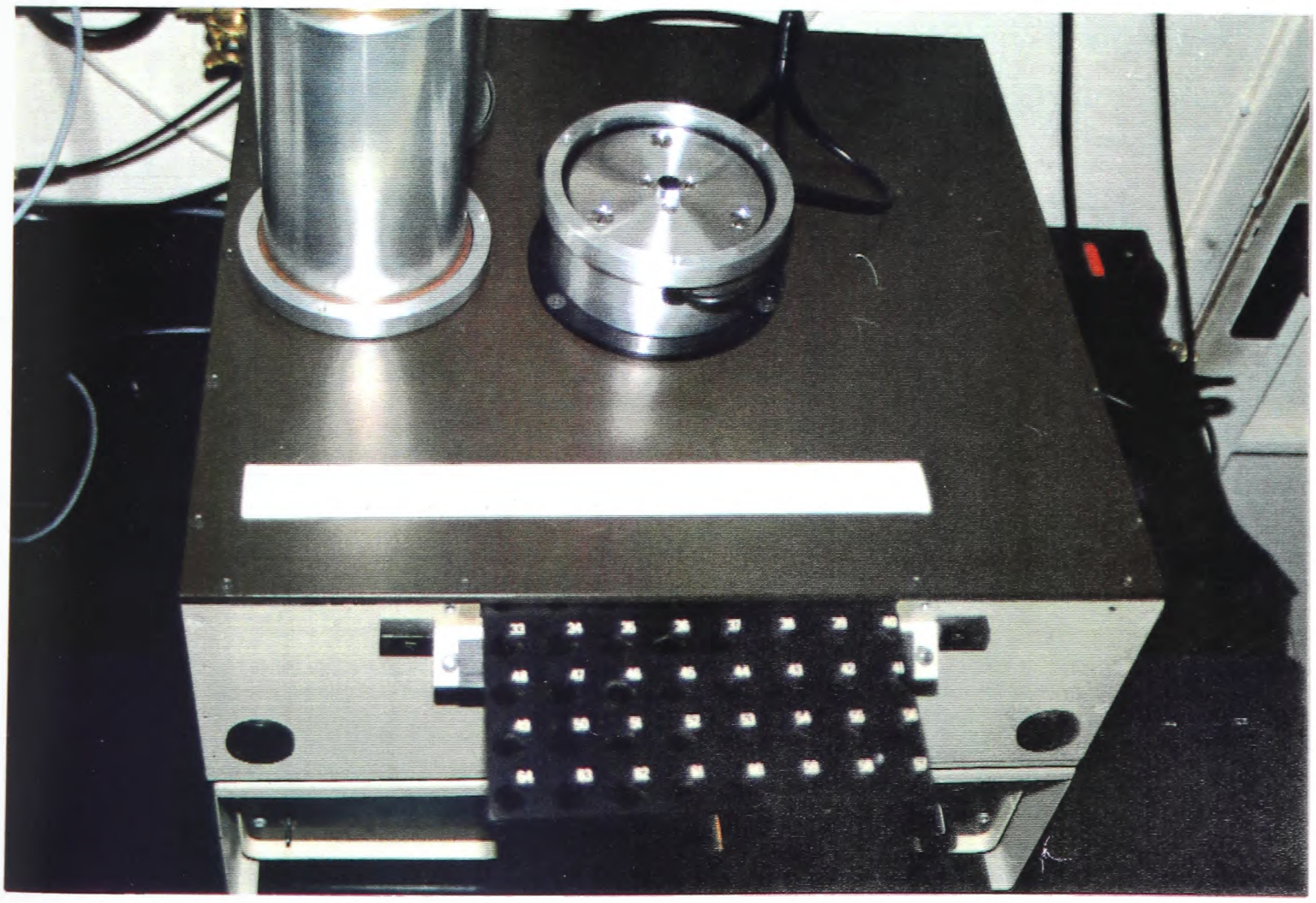


Plate 5.2.6.2 (a) The modified Elsec optical dating system type 9010. (b) a view of the illuminator assembly showing the trifurcated glass bundle, and light guide.

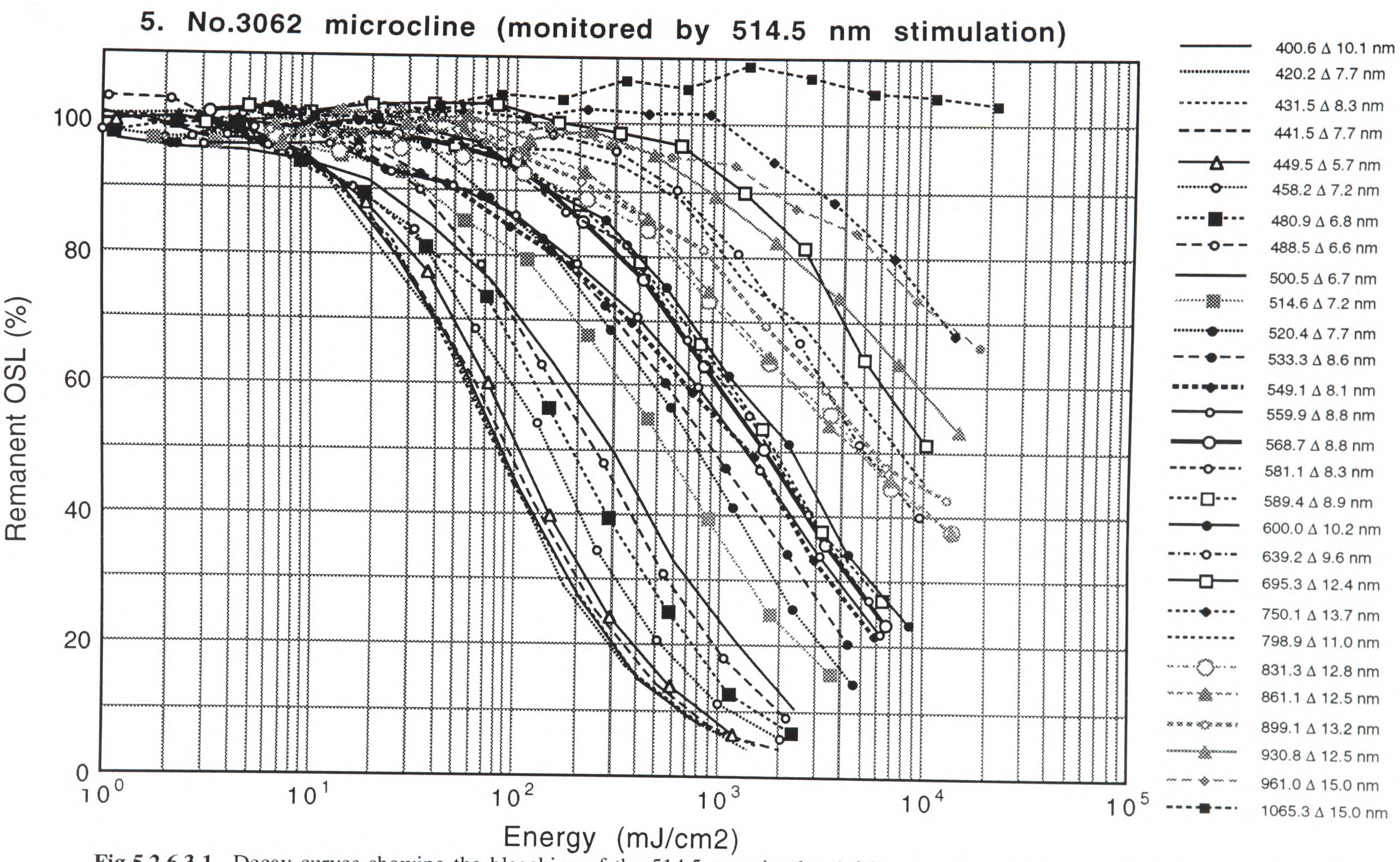


Fig.5.2.6.3.1 Decay curves showing the bleaching of the 514.5 nm stimulated OSL signal by various wavebands. Note the failure of any waveband to reduce the remanent OSL to zero. These data are directly comparable to Fig.5.2.3.1.(a).

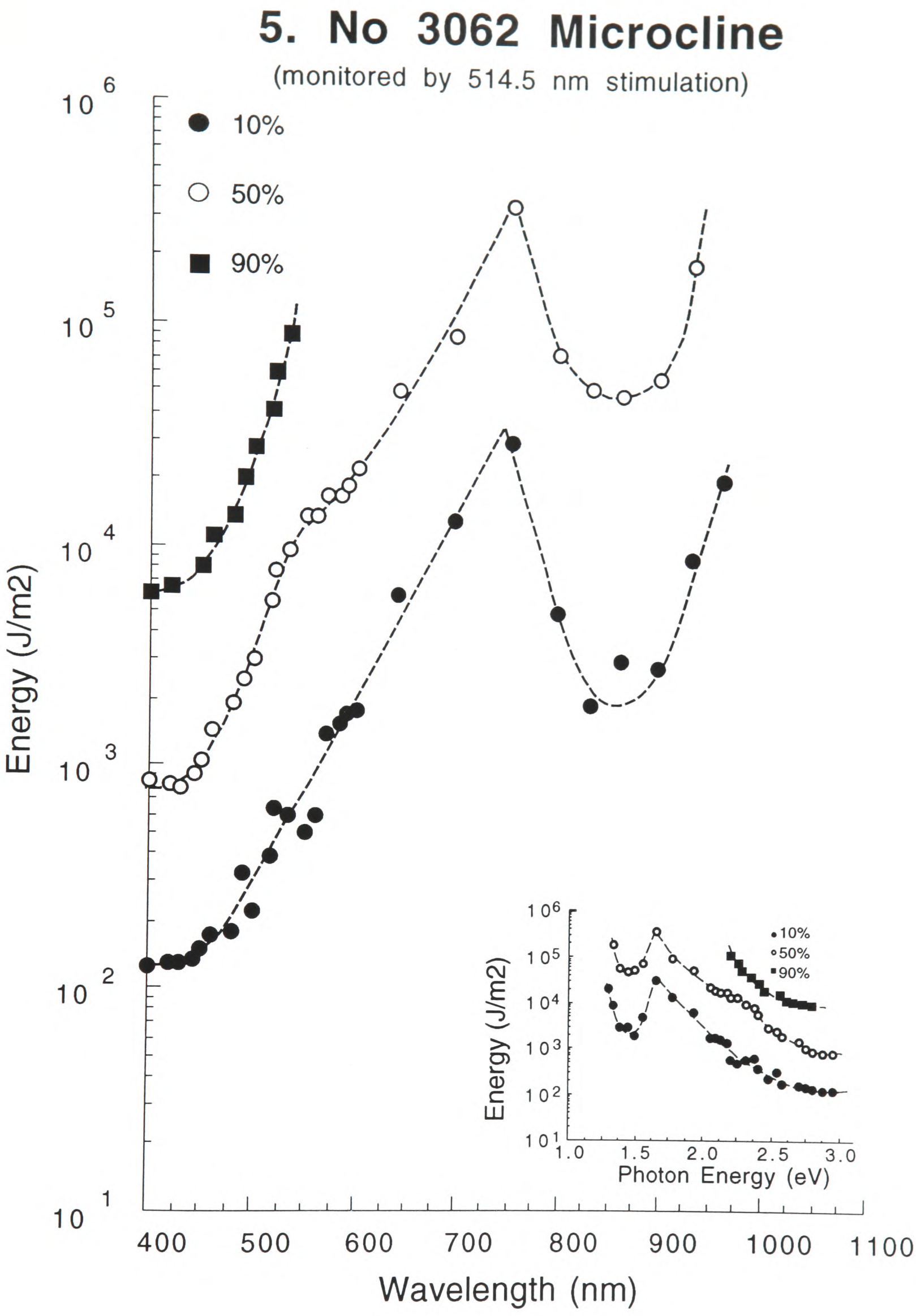


Fig.5.2.6.3.2 The energy required at various wavelengths to reduce the OSL signal to 10%, 50% or 90% of the initial level. The inset shows the data plotted against photon energy. These data are directly comparable with Fig.5.2.4.1.(a).

IRSL bleach response (see section 5.2).

5.2.6.3 RESULTS

The OSL decay curves resulting from illumination are shown in Fig.5.2.6.3.1 and the bleach response curves measured from these data for 10 %, 50 % and 90 % reductions of the OSL are shown in Fig.5.2.6.3.2. Both figures are directly comparable with those shown in section 5.2.4 resulting from IRSL monitoring.

5.2.6.4 OPTICAL BLEACHING OF MICROCLINE TL

An opportunity was offered by the above bleaching experiments to inspect and compare bleaching of the microcline TL by various wavebands. Simply, the TL residuals were measured for all wavebands used after all bleaching was complete for each of the five samples bleached; however, only a set of representative glow curves from 5. No.3062 microcline are presented, for reasons of brevity. The TL glow curves are shown in Fig.5.2.6.4.1; measurements were made using a Risϕ automated TL reader (with an EMI 9635Q PMT and Corning 7-59 and Chance-Pilkington HA3 filters), heating was at 5 K/s to 550°C with reheat, and normalisation was by factors derived from the "NTL" measured prior to the bleaching experiment; no corrections have been made for the different energies deposited in the various wavebands.

The question addressed by this work was which wavelengths bleach what, if any, regions of the TL glow curves, with particular emphasis on the effects of IR wavelengths. Previously, the significant extent to which prolonged exposure to IR (880 nm) bleached

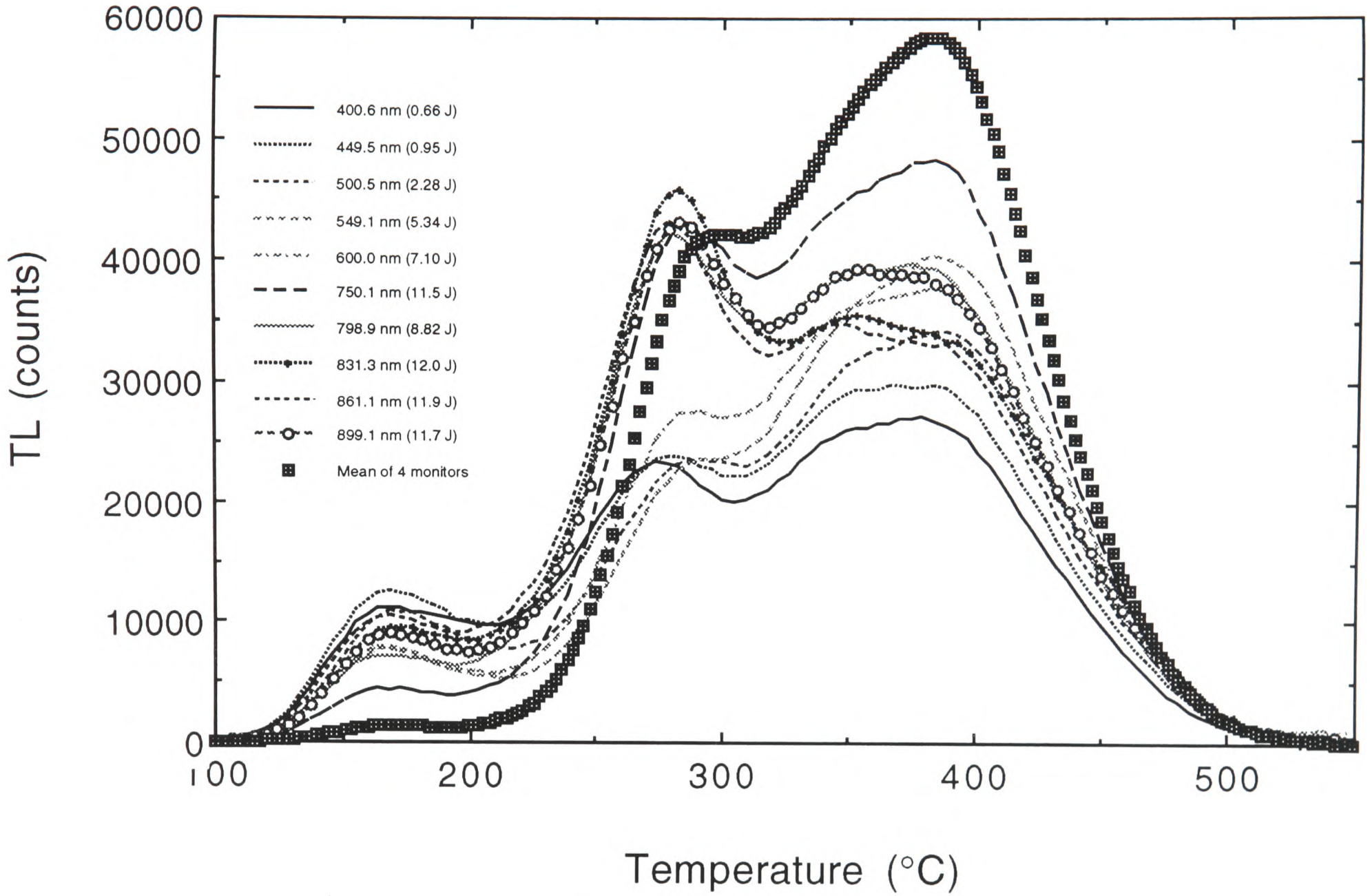


Fig.5.2.4.6.1 The remanent TL of sample 5. No.3062 microcline following exposure to a selection of the wavebands used to bleach the OSL (see Fig.5.2.6.3.1 for the respective bandwidths). The total energy deposited in each case is given in the legend. Second glow TL normalization only was used - no account has been taken of the differing total energies deposited in each waveband. Data plotted are counts/2K. Note that the TL peak seen at 160°C in the averaged glow curve of the four monitor discs is the result of phototransfer by the repeated 514.5 nm monitoring exposures.

the TL was first reported for both natural and additive-dose portions of a loessic sample from Achenheim, France, by Spooner and Questiaux, (1989), and was also a ubiquitous characteristic of the feldspar minerals studied here (see chapter 3). The contrary report by Bϕtter-Jensen *et al* (1991), in which it is stated that "a remarkable feature of OSL (i.r.) is that erasure of the signal by i.r. irradiation leaves the TL signal virtually unchanged" is not readily reconcilable with these results (although it is possible that major differences in samples or limited power or detection sensitivity of the prototype Risϕ reader/IR module combination account for this striking discrepancy).

Finally, attempts to assess the bleachabilities of the individual high temperature TL peaks from this data are complicated by phototransfer, however, some general conclusions can be drawn. The 380°C TL peak shows a trend of bleaching susceptibility with wavelength closely paralleling that of the IRSL signal. The least effective waveband is 750.1 ∆ 13.7 nm, with efficiency increasing monotonically towards shorter visible wavelengths; a "resonant" increase of bleaching efficiency appears in the near-IR. The behaviour of the 280°C TL peak shows competition between growth by phototransfer, presumably from the 380°C TL peak, and bleaching. The IR and redder visible wavebands appear not to bleach, but slight bleaching could be dominated by PTTL or masked by experimental scatter. All exposure wavebands induce PTTL growth at the 160°C TL peak, consistent with bleaching by all wavelengths involving detrapping to the conduction band.

5.2.6.5 DISCUSSION

The OSL decay curves for 5. No.3062 microcline shown in Fig.5.2.6.3.1 and the bleach response curves shown in Fig.5.2.6.3.2 show some important characteristics of the

OSL signal relevant to sediment dating. Firstly, comparison between the OSL and IRSL decay curves from the corresponding bleaching wavebands reveals the OSL signal resists bleaching more than the IRSL signal. Indeed, no given exposure wavelength or duration zeroed the OSL signal, whereas the IRSL can be apparently fully zeroed.

The explanation proposed to account for these results is that two populations (at least) exist - one bleachable by near-IR via the excited state, the other lacking this pathway and consequently only bleachable by direct photoeviction to the conduction band, presumably by photoionization.

Considering then Fig.5.2.6.3.2: the presence of the near-IR resonance in the early stages of bleaching (10 % reduction curve) shows that at least a fraction of the OSL signal is also that observed as IRSL; consequently the use of visible photons for stimulation is not specifically selecting a trapped charge population distinct from that giving rise to the IRSL. Comparison of the 10 % reduction curves for OSL and IRSL further reveals that although the resonance wavelength and strength are effectively indistinguishable, the energies required to bring about these levels of reduction are greater for the OSL, at blue wavelengths, by approximately threefold, rising monotonically to almost an order of magnitude by the red/IR boundary. The 50 % reduction curves show a bleaching energy discrepancy of similar form, but with additional features now apparent - not only is the resonance less intense, but there is also a distinct decrease in bleaching efficiency at shorter wavelengths (from $\approx$ 450 nm to $\approx$ 550 nm) before a return to the characteristic "IRSL" bleaching efficiency is seen at wavelengths > 550 nm. The trend of decreasing bleaching efficiency as the OSL signal is depleted continues, until 90 % depletion could no longer be achieved at wavelengths greater than $\approx$ 550 nm with the energies used in this experiment, showing that the "IR" bleachable signal has been erased

and that the remaining signal originated from the much harder to bleach "green only" trap population.

This finding is clearly significant to choice of optical dating strategies, for example: Bϕtter-Jensen *et al* (1991) proposed (previously suggested by Spooner and Questiaux, 1989) that green stimulation can be used following IRSL measurement to obtain both "green" and "IR" palaeodose estimates. However the results described in section 5.2.4 along with those shown above reveals this to be unsound for materials in which the resetting mechanism was optical bleaching, as the OSL component unbleachable by IR also resists bleaching by other wavelengths to an extent that makes depositional zeroing problematic. Also, this bleaching response must be considered in conjunction with the dominance of higher order kinetics in feldspar, strongly raising the question of whether this OSL signal can be fully zeroed under any bleaching conditions (Levy, 1982). It therefore seems that the "green only" traps effectively play the role of "hard" residual.

5.2.7 SUMMARY OF THE BLEACHING RESULTS

The remarkable similarity of the IRSL bleaching response curves, regardless of major-element composition or fading or non-fading behaviour, leads to the conclusion that there is only one "fundamental" class of defect giving rise to the IRSL signal, and that this defect has a characteristic ground-to-excited state transition energy of $\approx 1.44 \pm 0.01$ eV. Furthermore, the lack of distinct structure shown by the near-IR resonance reveals there is only one excited state associated with this defect. This defect is bleachable by visible wavelengths and in a manner consistent with the mechanism being photoionization to the conduction band. The absence of significant changes to the slopes of the energy Vs

wavelength plots as the IRSL source traps deplete from 10% to 90% indicate that no other "less bleachable" traps are being sampled by IR stimulation as, shinedown proceeds. Conversely, as bleaching of the OSL signal proceeds, after the longer wavelengths have erased the "IRSL" signal, they are incapable of efficiently bleaching the remaining luminescence (the "green only" traps) and so bleaching appears to slow or cease altogether. However, shorter wavelength stimulation (such as by the 514.5 nm Ar-ion laser line) will be capable of sampling from the "green only" population. The consequence for optical dating using these stimulation wavelengths is that the OSL signal will contain components of harder to bleach signal, of which the zeroing should not be expected under natural conditions on account of its practical unbleachability by wavelengths > 600 nm, intrinsically greater resistance to bleaching even at shorter wavelengths and, importantly, because the interactive kinetics characteristic of the feldspar minerals will ensure repeated retrapping and so prevent effective zeroing in finite bleaching times.

This interpretation dictates that shorter visible wavelengths should not be used to measure OSL for sediment dating applications on account of the unavoidable inclusion of inseparable components of harder-to-bleach signal, the zeroing of which in nature is problematic at best. The choice of stimulation wavelengths > 600 nm avoids sampling this harder to bleach component and so is the correct measurement strategy, at least from the considerations of depositional zeroing. Practical and technological convenience also supports the use of longer wavelengths for measurement, and, optimally, IR LED systems such as described in Chapter 2 to exploit the near-IR resonance.

In order to reconcile the great variety of IR-bleachable TL glow peaks with the predictions of the simple picture presented above, it was necessary to complete the description of the energetics of the IRSL source traps. This entailed measurement of the

depths below the conduction bands of the excited states of the same five feldspars. If there existed a range of excited state depths, and hence a range of total trap depths, then a variety of bleachabilities and different thermal untrapping characteristics, and consequently different TL glow curve forms, would be expected. Measurements of the excited state trap depths are described below.

5.3 TEMPERATURE DEPENDENCE OF THE IRSL SIGNAL

5.3.1 INTRODUCTION

In the original work of Hütt *et al* (1988) the mechanism governing IRSL was identified as thermally-assisted optical untrapping to the conduction band via two excited states reported as both being ≈ 0.8 eV below the conduction band and corresponding to the single ground state of an electron trap ≈ 2.0 eV deep thermally and ≈ 2.5 eV deep optically. Later work (Hütt and Jaek, 1989) revised the excited state depth value to ≈ 0.2 eV, and a thermal trap depth of ≈ 1.55 eV. The optical trap depths were then ≈ 2.25 eV for photoionization detrapping (direct to the conduction band) and 1.35 eV and 1.43 eV respectively for the two excited states. Bailiff and Poolton (1991) found values of ≈ 0.1 eV for the excited state depths from microcline, sanidine and albite, in reasonable accord with Hütt and Jaek (1989); likewise, Duller and Wintle (1991) found 0.15 ± 0.02 eV from Arrhenius analysis of IRSL from 50°C to 180°C. While section 5.2 shows that the ground-to-excited state energy is ≈ 1.44 ± 0.01 eV, in very close accord with Hütt *et al* (1988), and also disproves the existence of a broader resonance relating to the IRSL signal at ≈ 2.25 eV, those bleaching measurements do not give information on the depth below the

conduction band of the excited state. To complete the description of the trap energetics, this data was sought by measuring the dependence of the IRSL intensity on temperature. The thermo-optical bleach (TOB) analysis method applied by Hütt *et al* (1988) and Hütt and Jaek (1989) was not used here, and the excited state activation energies were instead obtained by Arrhenius analysis of the low temperature IRSL response, as described in the following sections.

5.3.2 EXPERIMENTAL

The same five samples for which the bleach response spectra were measured previously were used here. Samples were prepared as described in section 3.2, then attached to rhodium plated-copper discs using silicone oil. "NTL" was drained by heating to 550°C at 5 K/s then reheating; following this step were added $^{90}Sr/^{90}Y$ β doses of ≈ 70 Gy for 5. No.3062 microcline, ≈ 100 Gy for 18. Amelia albite and 23. Dup(B) oligoclase, and ≈ 200 Gy for 9. Z15 sanidine and 12. Patmos sanidine. All samples were measured following preheats of 60 seconds at 220°C using a Risφ automated TL reader.

IRSL measurement apparatus consisted of a multi-waveband light source based on a 1000 W xenon lamp (Spooner and Questiaux, 1989) used in conjunction with a cryostat stage built by R.H. Templer (Templer, 1985 and 1986b). The stimulation beam consisted of 861.1 ∆ 12.1 nm IR selected from the output of the xenon lamp using filters and directed onto the sample on the cryostat cold stage through a trifurcated glass fibre bundle. As the fibre bundle could not be sealed to sustain a high vacuum the oven chamber was evacuated (to ≈ 8×10^{-2} Torr) prior to use, but then brought to just above atmospheric pressure with dry nitrogen (flow rate of ≈ 600 ml /minute) for the

measurement process; the aim was to displace H_2O vapour from the system and prevent further diffusion of this vapour in. Although operating without vacuum limited the lowest temperature achievable to ≈ 100 K (primarily due to convection of heat to the sample stage by the N_2 gas), rather than the ≈ 80 K the cryostat set was capable of, in practice the limitation was not serious.

The measurement routine consisted of first giving a short exposure at ambient temperature, then lowering the temperature to its minimum and holding to permit thermal stabilization, followed by successive short exposures as the temperature was raised, each time allowing a pause for thermal equilibration before measurement. Heating was simply effected in the lower temperature regime by cessation of liquid nitrogen cooling, so permitting heat flow into the apparatus from the environment. Temperatures above ≈ 240 K were obtained using thermocouple-controlled servo heating. As relative response only was required for these experiments a precise calibration of the IR beam power was not made, however the beam intensity was believed to be approximately 5 mW/cm^2. Illumination of the samples was controlled by a fast electronic shutter (Melles-Griot, Ilex electronic shutter, action time ≈ 3 ms). Exposure times were of various durations depending on the sample sensitivities and temperature at which the measurement was made, with the aim being to accumulate sufficient counts at each temperature to achieve reasonable counting precision. Data was acquired using an EG&G Ortec MCS card (type ACE-MCS) hosted by a RM nimbus VX computer. Emissions were observed using an EMI 9635Q PMT with a 2 mm Schott BG 39 filter, so using the same emission detection waveband as used for the bleaching studies, and similar to that used in dating applications.

IRSL measurements on 5. No.3062 microcline were subsequently repeated following a preheat of 300 seconds at 260°C. Similar measurements were made using

green stimulation (516.3 ± 7.8 nm) from the same light source, however in this case the need to reject scattered stimulation photons restricted the detection waveband to the UV, (using Corning 7-51 and Schott BG39 filters).

5.3.3 RESULTS AND DISCUSSION

Analysis of the IRSL data consisted of subtraction of background, correction for depletion by the repeated short exposures and then normalization for duration of exposure. These data are shown as a function of temperature (°C) in Fig.5.3.3.1.(A),(B) to display both the effect of measurement temperature on the efficiency of IRSL production (as measured by short exposures), and also the composition-dependent variation in form of the low temperature response. The same data are replotted in Fig.5.3.3.2.(A) as a function of 1/T (K^{-1}). This mode of presentation highlights the similarity of responses of the two sanidines and the two high-sodic plagioclases (albite and oligoclase). Note that the data are not normalised for luminescence intensity.

The microcline displays a more complex structure, in which two components to the temperature response curve are apparent. As the choice of preheat (60 seconds at 220°C) had been made in order to leave the TL glow curves approximately equivalent to those expected in nature, both the 280°C and 380°C TL peaks were prominent in this microcline, hence the obvious interpretation is that the two components are associated with the 280°C and 380°C TL peaks respectively. However this was a significant finding in that it indicated IRSL was originating from two populations of traps in a single sample, with each trap type having different excited state depths, but, from the bleach response curves, each possessing the same ground-to-excited state transition energy. The

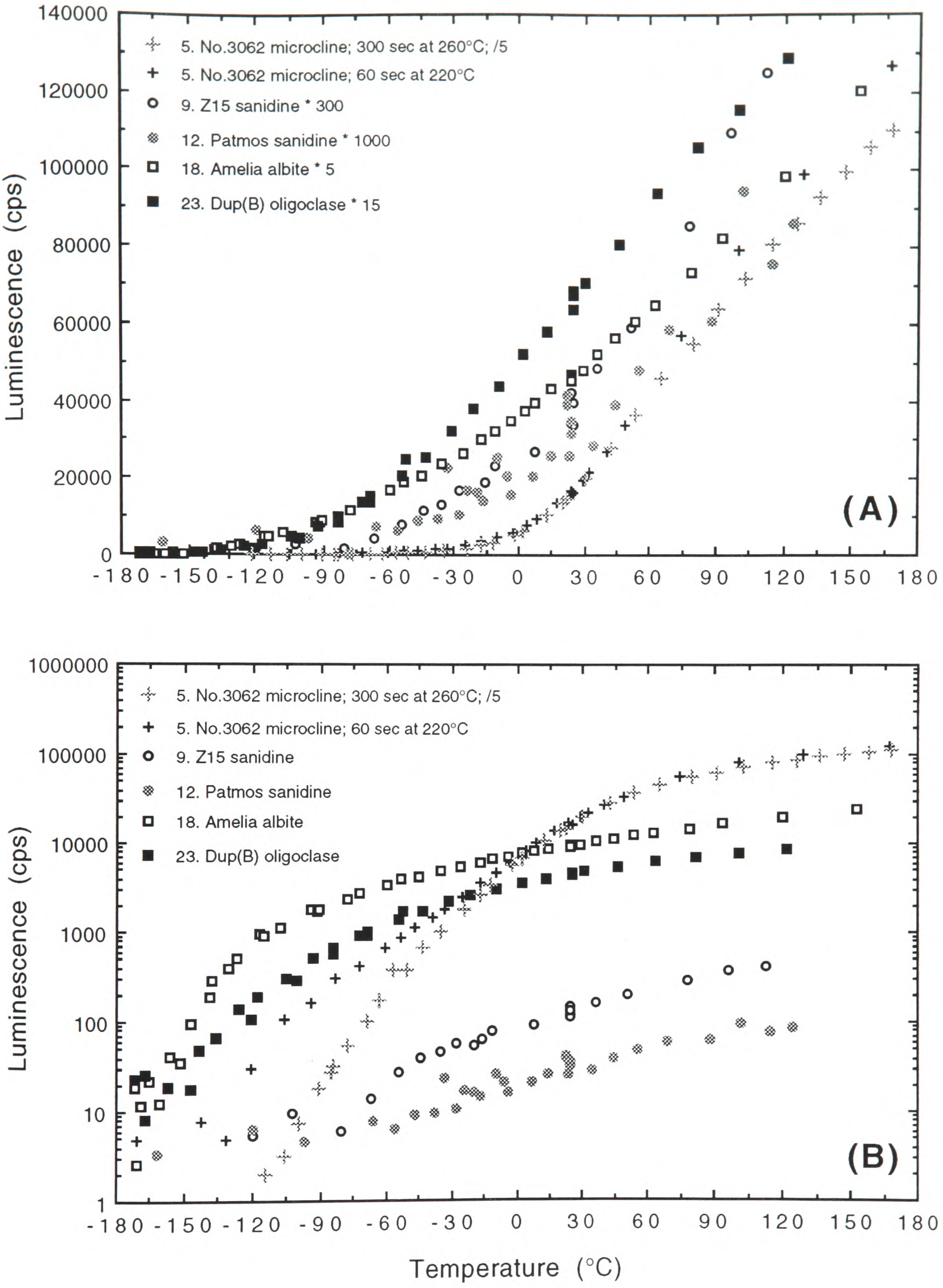
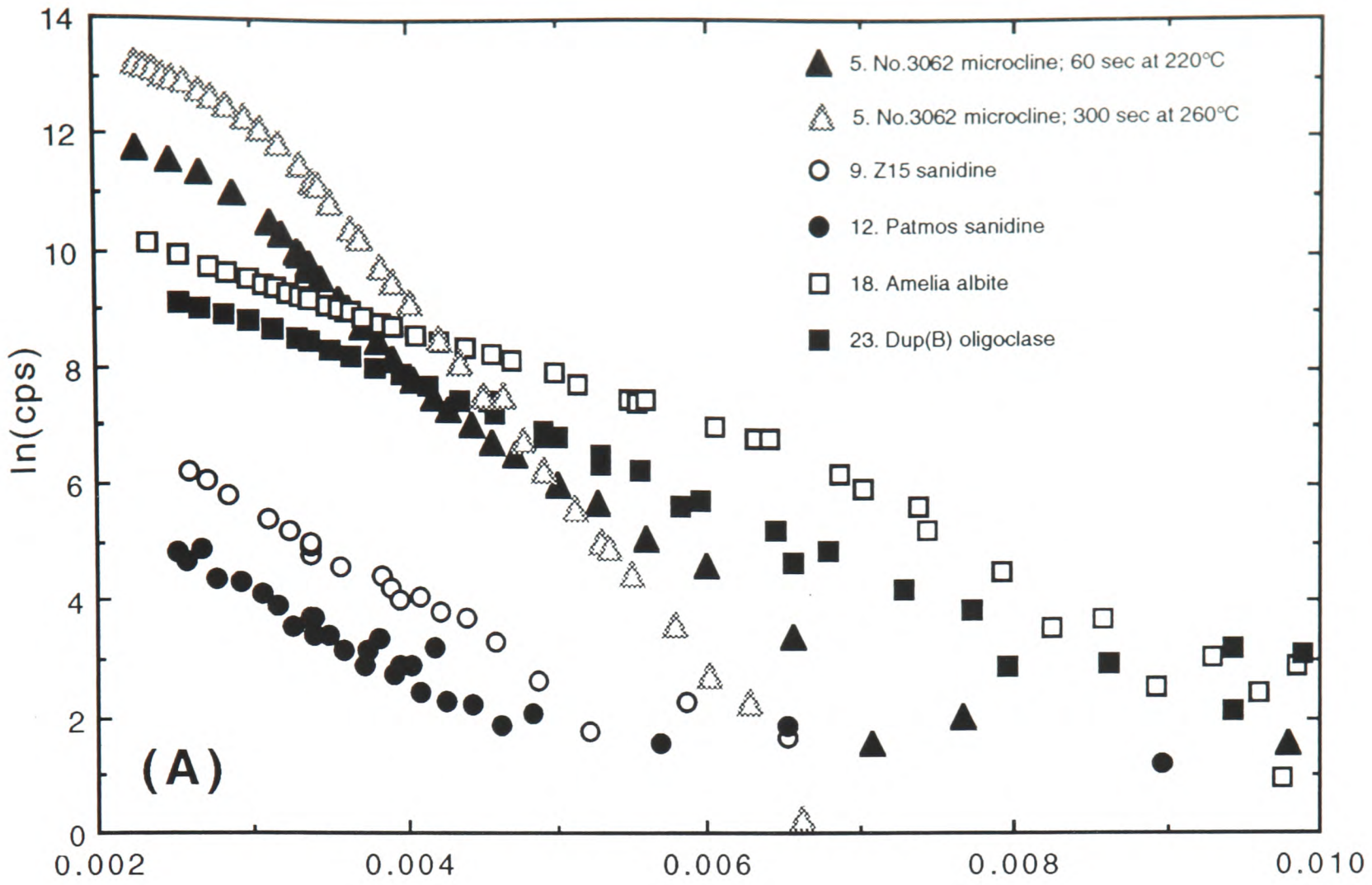


Fig.5.3.3.1.(A) The temperature dependence of the 861.1 ▵ 12.1 nm stimulated IRSL is shown for each of the feldspars. Data plotted are counts/second. Note for each sample that the IRSL is extinguishing at the lowest temperatures; **(B)** the data replotted so as to clarify behaviour at the lowest temperatures. Note the change in the microcline signal behaviour at the lowest temperatures following the more stringent preheat to remove the 280°C TL peak.



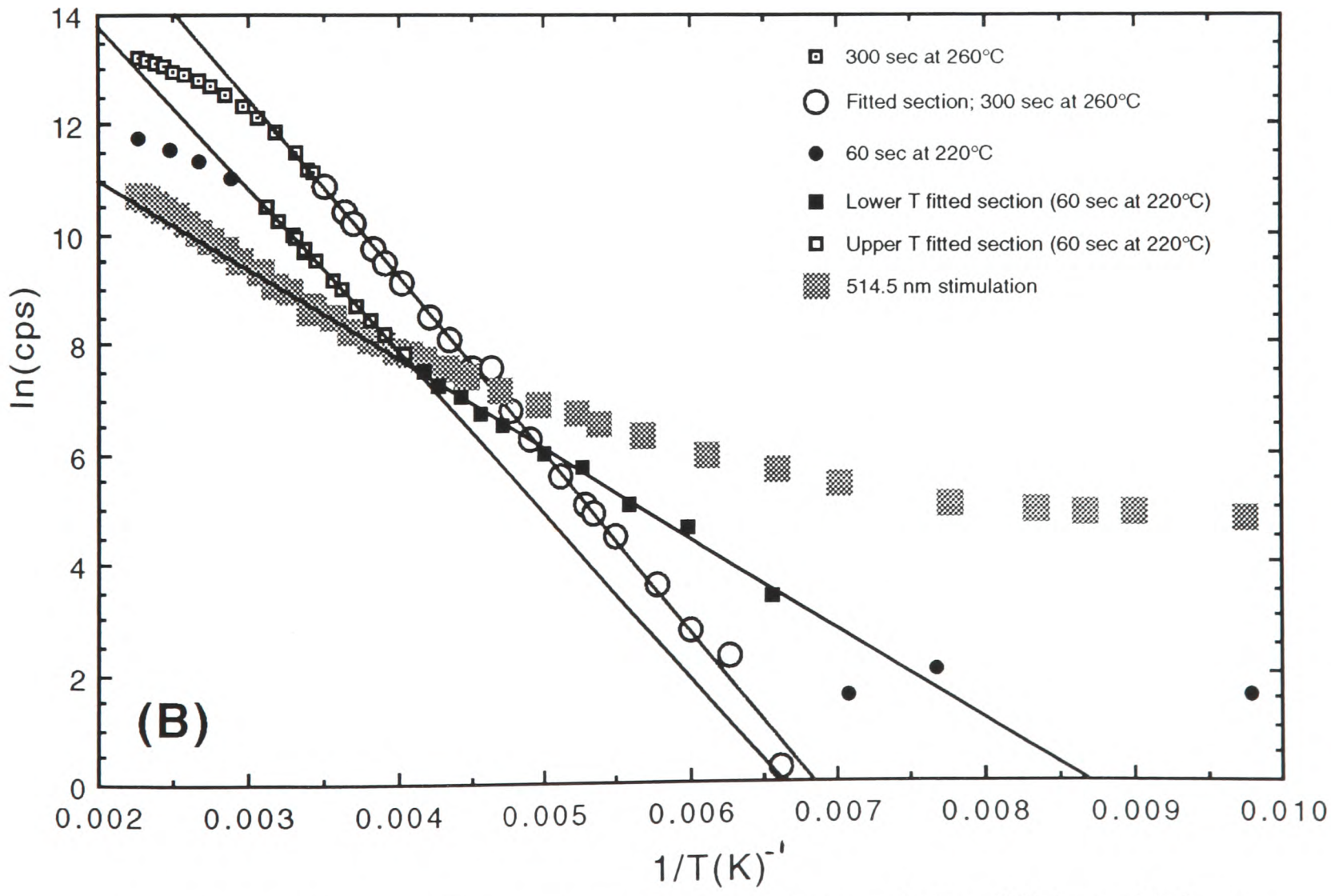
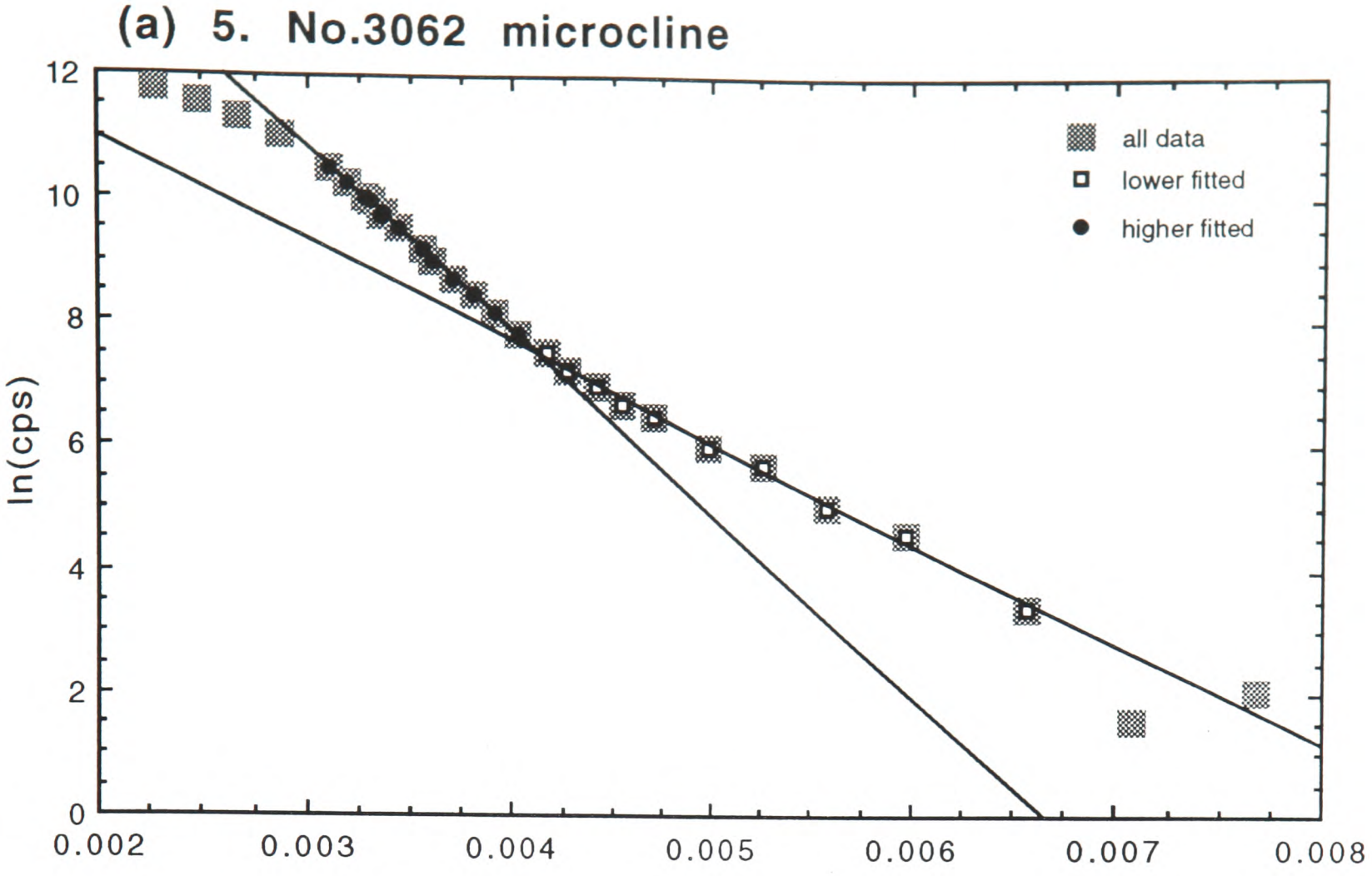


Fig.5.3.3.2.(A) The temperature dependence of the 861.1 ∆ 12.1 nm stimulated IRSL for each of the feldspars. Data plotted are counts/second; this mode of presentation highlights the relationship of response and major element composition.
(B) 5. No.3062 microcline: each IRSL temperature response curve is shown overlain by the portions analyzed to determine activation energies. Note the contrast in behaviour of the 514.5 nm stimulated signal to that of the IRSL signals, and also the IRSL signal behaviour following the more stringent preheat, to remove the 280°C TL peak.

measurements were therefore repeated, this time using portions of sample which had received preheats of 300 seconds at 260°C, adequate to completely eliminate the 280°C TL peak and so isolate the 330°C and 380°C TL peaks. Fig.5.3.3.2.(B) shows the IRSL data and the temperature ranges over which activation energy analyses were performed for 5. No.3062 microcline, following both preheats. Only one component is now seen, confirming the original attribution of TL peak to IRSL source. The excited state trap depth now found, 0.278 ± 0.004 eV, is hereafter regarded as the correct energy value for the 380°C TL peak excited state.

Also shown, overlain, in Fig.5.3.3.2.(B) are the OSL data for that microcline following a preheat of 300 seconds at 260°C. The low temperature response appears to be almost independent of temperature, with thermal dependence becoming more apparent at higher temperatures. These results are consistent with direct detrapping, by these 2.4 eV photons, to the conduction band from the ground state: at lowest temperatures there is no effective thermal assistance from the ground state, as the temperature is raised thermal assistance increases in a manner characterised precisely by the energy structure of the trap ground state.

Returning to IRSL behaviour: data obtained following 60 seconds preheat at 220°C is shown in Figs.5.3.3.3.(a)-(e) for each sample, with the analyzed sections of the response curves superimposed on the complete data sets. Arrhenius analysis was used to extract activation energies for each sample; the choice of the simple relation $I \alpha \exp(-E/kT)$ assumes that no other temperature dependent effects occur in the untrapping process (such as changing electron transport efficiency from the ground state to the excited state, or temperature dependence of the excited state frequency factor). Data in the lowest temperature range were excluded from the fittings due to greater scatter, resulting from



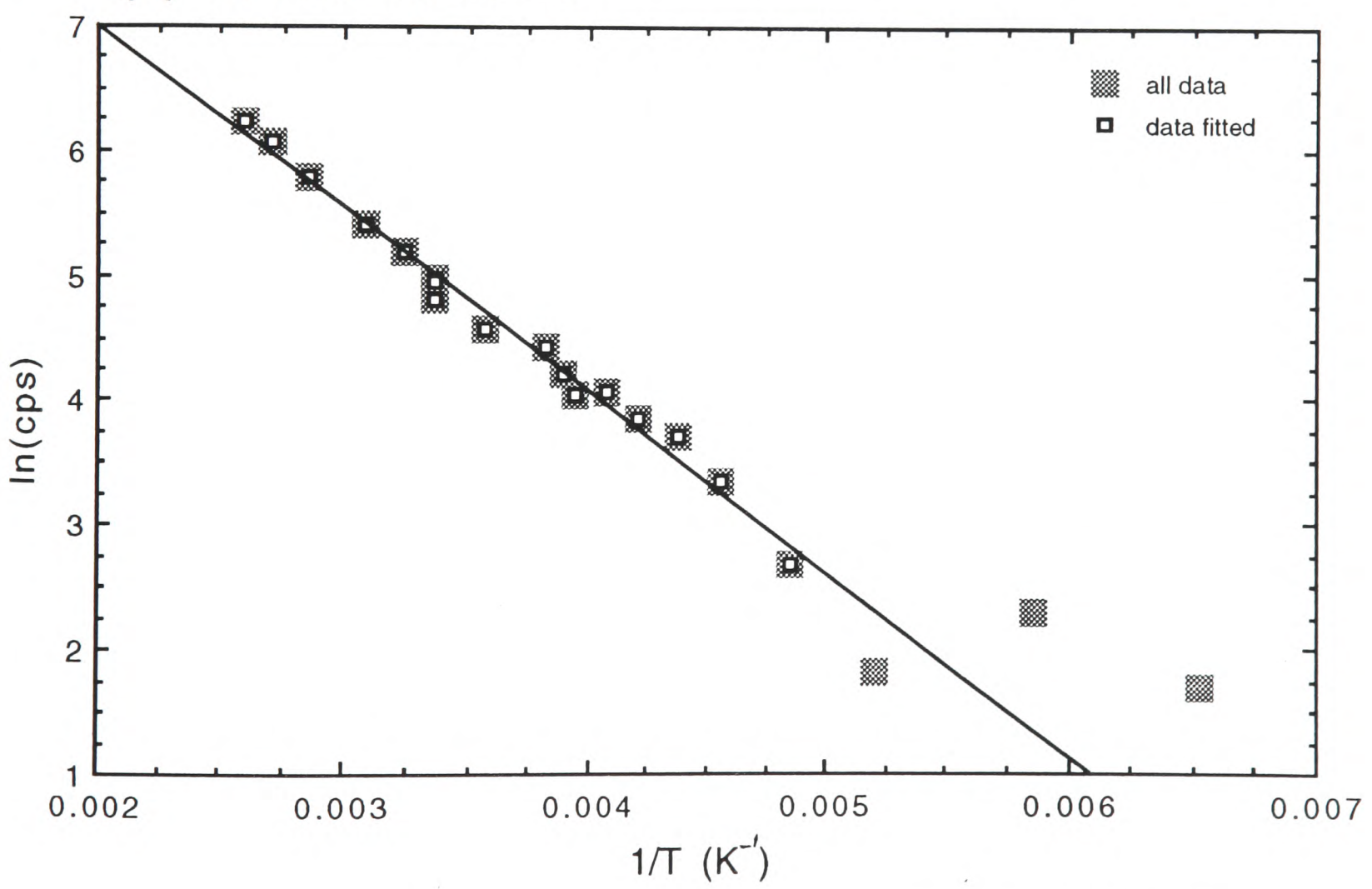
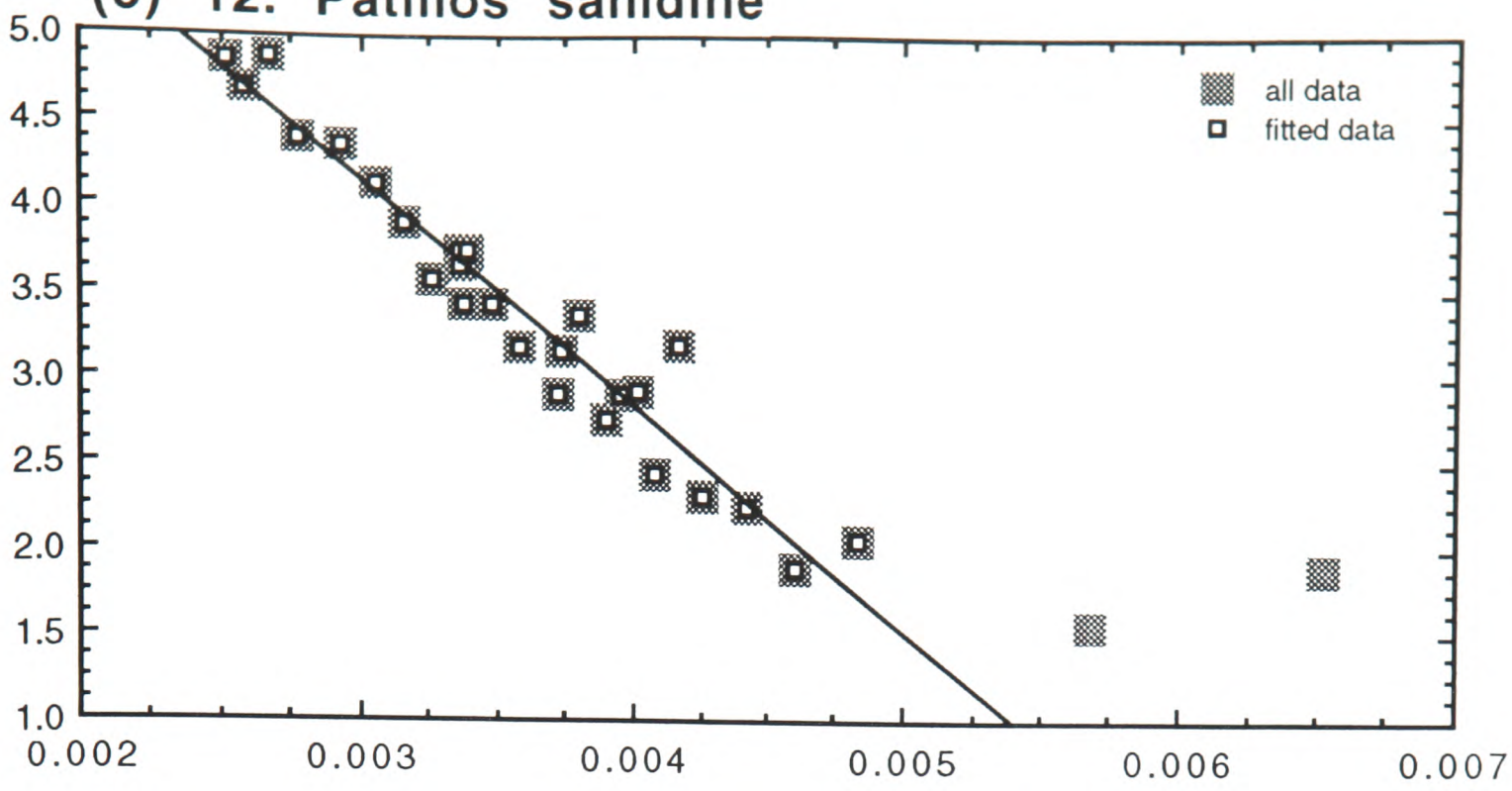
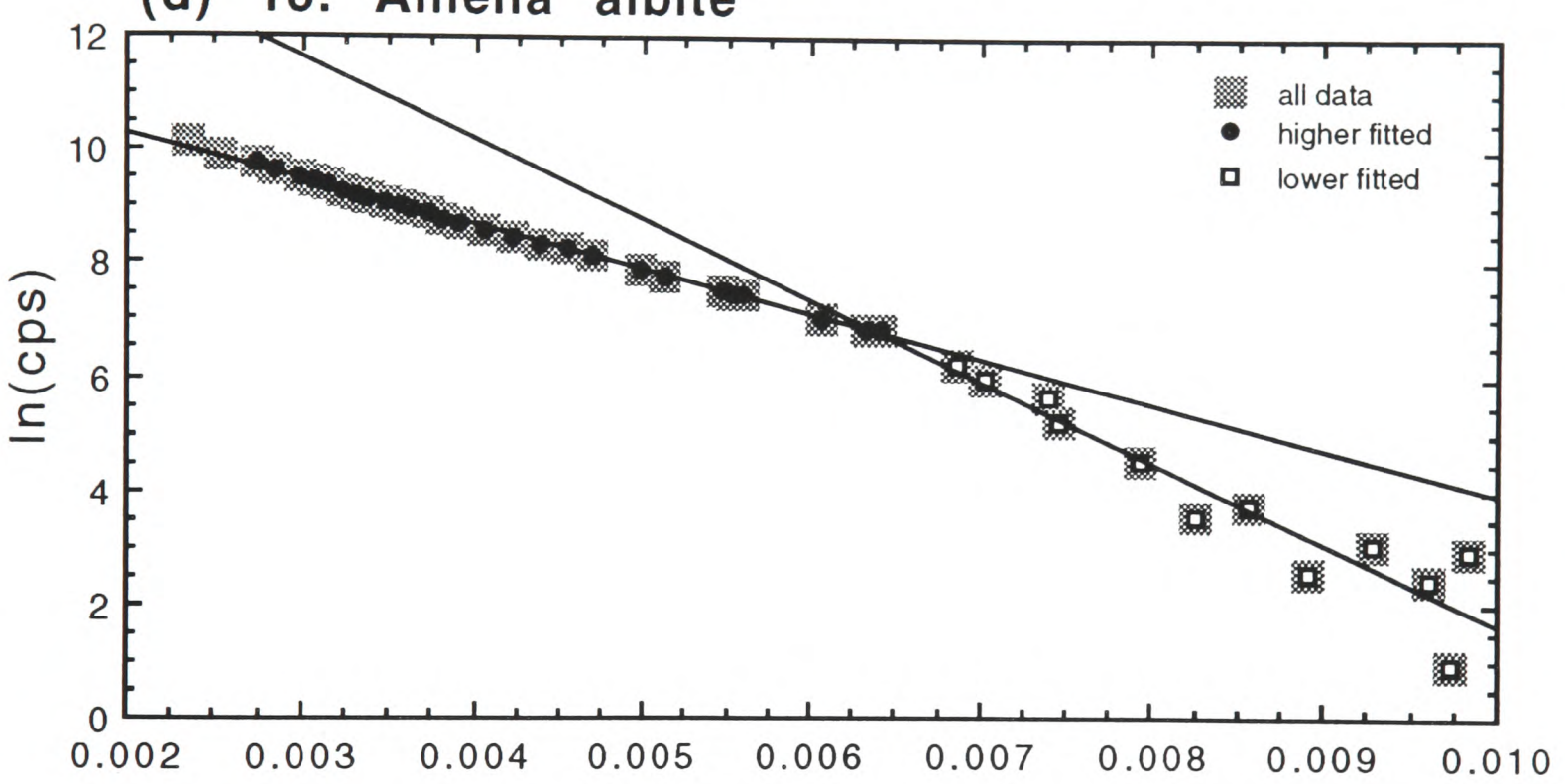
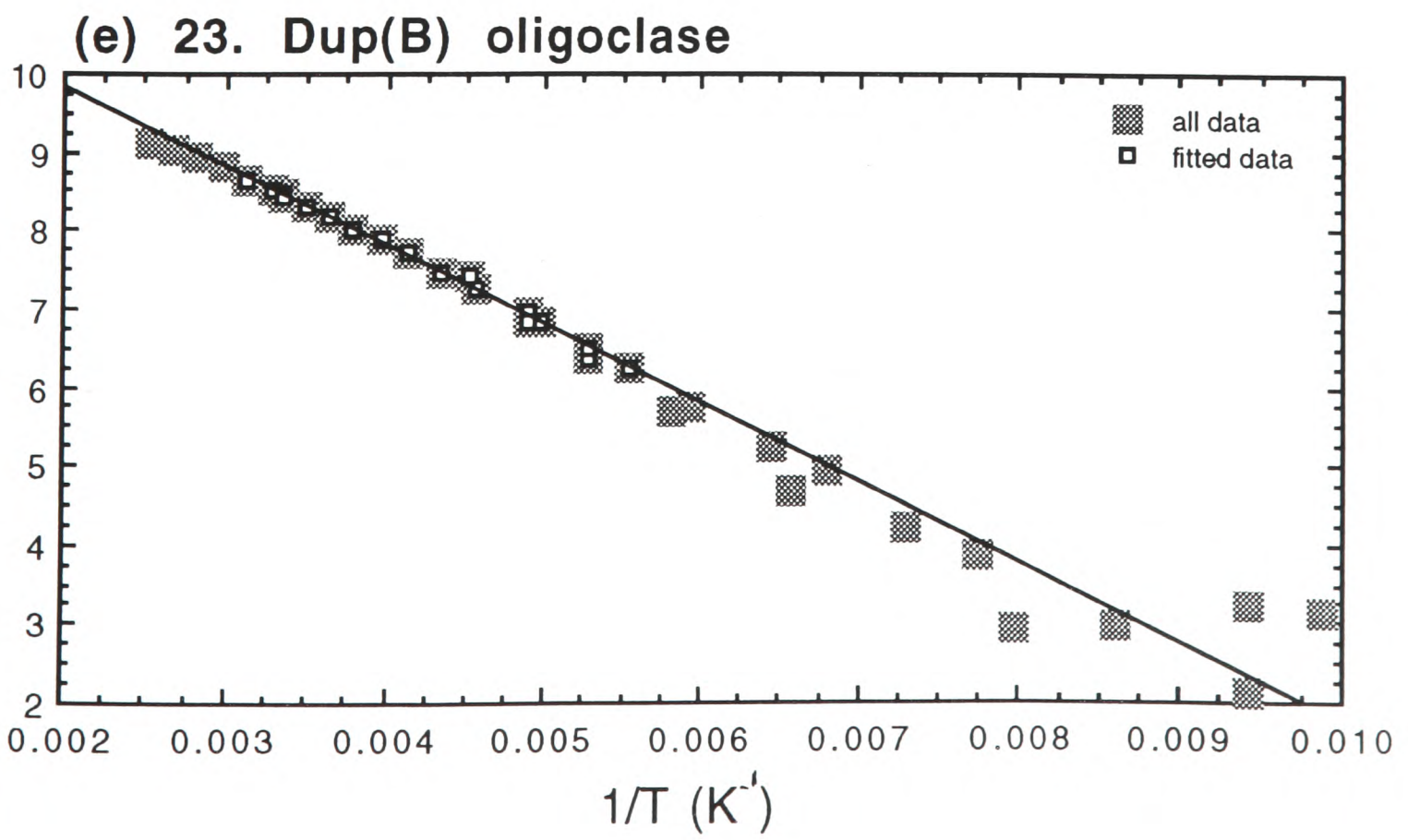


Fig.5.3.3.3.(a)-(e) The temperature response curves of each of the feldspars, measured using 861.1 ∆ 12.1 nm stimulation. The complete data sets (counts/second) are shown overlain by the portions from which the activation energies (see Table 5.3.3.1) were evaluated.


(c) 12. Patmos sanidine
all data
fitted data
5.0
4.5
4.0
3.5
3.0
2.5
2.0
1.5
1.0
0.002
0.003
0.004
0.005
0.006
0.007


(d) 18. Amelia albite
all data
higher fitted
lower fitted
ln(cps)
12
10
8
6
4
2
0
0.002
0.003
0.004
0.005
0.006
0.007
0.008
0.009
0.010


(e) 23. Dup(B) oligoclase
all data
fitted data
10
9
8
7
6
5
4
3
2
0.002
0.003
0.004
0.005
0.006
0.007
0.008
0.009
0.010
1/T (K-1)

the lower signal levels. Sublinearity at the highest temperatures was interpreted as due to "thermal saturation" of the excited state's effect: the mean phonon energy available to an electron in the excited state exceeding that required for thermal eviction, hence any electron reaching the excited state is then thermally untrapped. The thermal trap depths below the conduction band measured for each of the feldspars are given in Table 5.3.3.1.

Sample	Energy (eV) (2σ)
5. No.3062 microcline	0.155 ± 0.014 (lower T)
	0.255 ± 0.006 (higher T)
5. No.3062 microcline (300 second preheat at 300°C)	0.278 ± 0.004
9. Z15 sanidine	0.126 ± 0.007
12. Patmos sanidine	0.113 ± 0.012
18. Amelia albite	0.070 ± 0.002
23. Dup(B) oligoclase	0.087 ± 0.003

Table 5.3.3.1 The energies below the conduction band measured for the excited states of the various feldspars. Lower and higher T refers to differing components in the microcline, correlated to the prominent higher temperature TL peaks. Errors are from curve fitting only.

These results are in generally good agreement with those reported by Bailiff and Poolton (1991), in which the variation in IRSL was measured between 15°C and 150°C and thermal activation energies also evaluated from Arrhenius plots. Values found were 0.10, 0.09 and 0.08 eV (all ± 0.02 eV) for microcline, sanidine and albite respectively. The significant difference from the value tabulated above for microcline is possibly sample dependent: pulse annealing measurements reported in that same paper show the IRSL to be virtually extinguished by cut preheating to 350°C, it therefore seems likely that that sample lacked higher temperature IRSL source peaks. In contrast, 5. No.3062

microcline displays strong IRSL correlating with higher temperature peaks (> 380°C).

Finally, the possibility of a relation between the excited state trap depth and anomalous fading was eliminated: although Fig.5.3.3.2.(A) and Table 5.3.3.1 reveal three distinct classes of IRSL low-temperature response, the critical parameter appears to be major-element composition. For example, while the two (fading) sanidines show very similar behaviour, so also do the two high-sodic samples, albite and oligoclase. Yet here the oligoclase fades whereas the albite does not. It was concluded that neither the depths of the excited states of the IRSL source traps nor any observed features of the low temperature behaviour are related to anomalous fading in these samples.

5.3.4 SUMMARY

The preceding results confirm the validity of the model proposed by Hütt *et al*, (1988), though with the refinement of attributing the IR resonance to a single excited state $\approx 1.44 \pm \approx 0.01$ eV above the ground state, in close agreement with the value of 1.43 eV found for the upper excited state by Hütt *et al* (1988)) rather than the two originally identified by Hütt et al (1988), and also in agreement with a subsequent report by Bailiff and Poolton (1991). The depth of the excited state below the conduction band varies from sample to sample, with apparent dependence on the major-element composition, and also varies between the individual TL glow peaks of a given sample. A simplified schematic diagram of the generalised case is shown in Fig.5.3.4.1. Regarding fading, neither the trap energetics nor the bleach response curves show any reliable relationship to fading behaviour (noting that the fading sample 23. Dup(B) oligoclase is indistinguishable from stable controls for both these parameters).

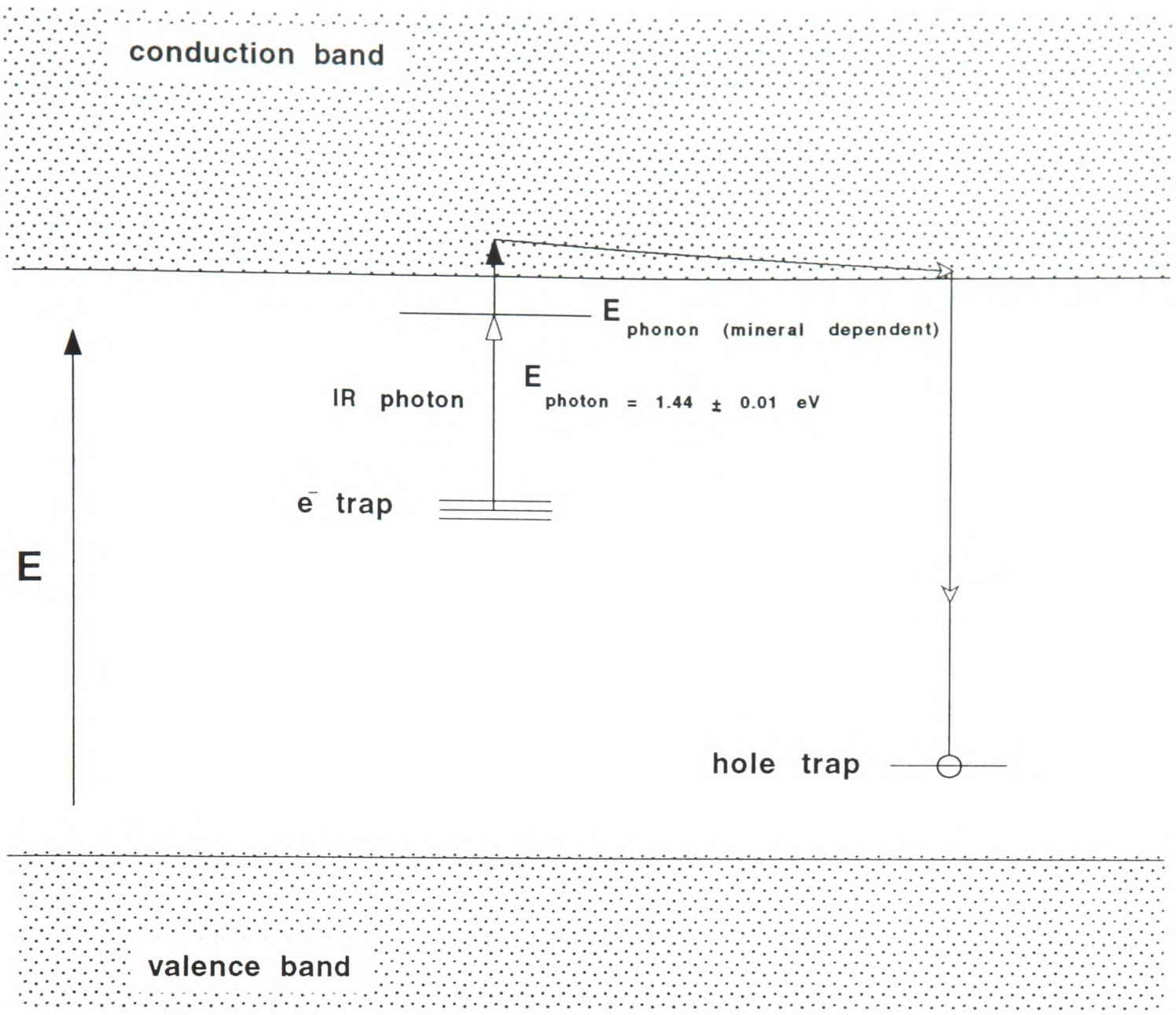


Fig.5.3.4.1 A model (after Hütt *et al* (1988)) for the IRSL mechanism. A band of energies are shown corresponding to the ground state of the electron trap, on account of later work (see section 5.5) indicating this to be the real situation. The excited state is shown as a single level for the sake of simplicity (the apparent bandwidths are given in Table 5.3.3.1); note that the depth below the conduction band of this state is dependent on the major element composition of the host crystal. Light sum data (see section 5.5.4) suggests the hole centres and electron traps are in spacial proximity, though quantification of this was not attempted here.

Having failed to find any correlation of fading either with the optical depths of the source traps or with the thermal depth below the conduction band of the excited state, it remained to eliminate two further possibilities: firstly that the untrapping was in reality a two-photon process rather than a photon-phonon process, and secondly that there existed more than one excited state level in a given sample, so permitting slow thermally activated "leakage" of charge from traps via shallower excited states or even by a "ladder" of metastable excited states. These investigations are described in chapter 6 and the following sections respectively. Following the latter a determination of the thermal trap depth of the IRSL source trap in one microcline feldspar is given.

5.4 DEPENDENCE OF THE IRSL ON PHOTON FLUX DENSITY

The IRSL mechanism in the feldspar minerals was believed to be a phonon assisted single photon process (Hütt, *et al* 1988), in which absorption of the photon raises the trapped electron from the trap ground state to a (bound) excited state from where the energy from phonon absorption completes the untrapping to the conduction band. However, an alternative model has been suggested (Godfrey-Smith *et al*, 1988) which requires two or more photons in the detrapping process - the first, as above, to raise the electron from the ground state to the excited state and the second to complete the detrapping to the conduction band, in place of the phonon absorption. Both alternatives are shown on a simplified energy level diagram in Fig.5.4.2.1, as "1" for the two-photon process and "2" for the phonon-assisted single photon mechanism.

It should be possible to distinguish between these models on the basis of rate of change of IRSL with photon flux. Simply, for the second mechanism requiring the

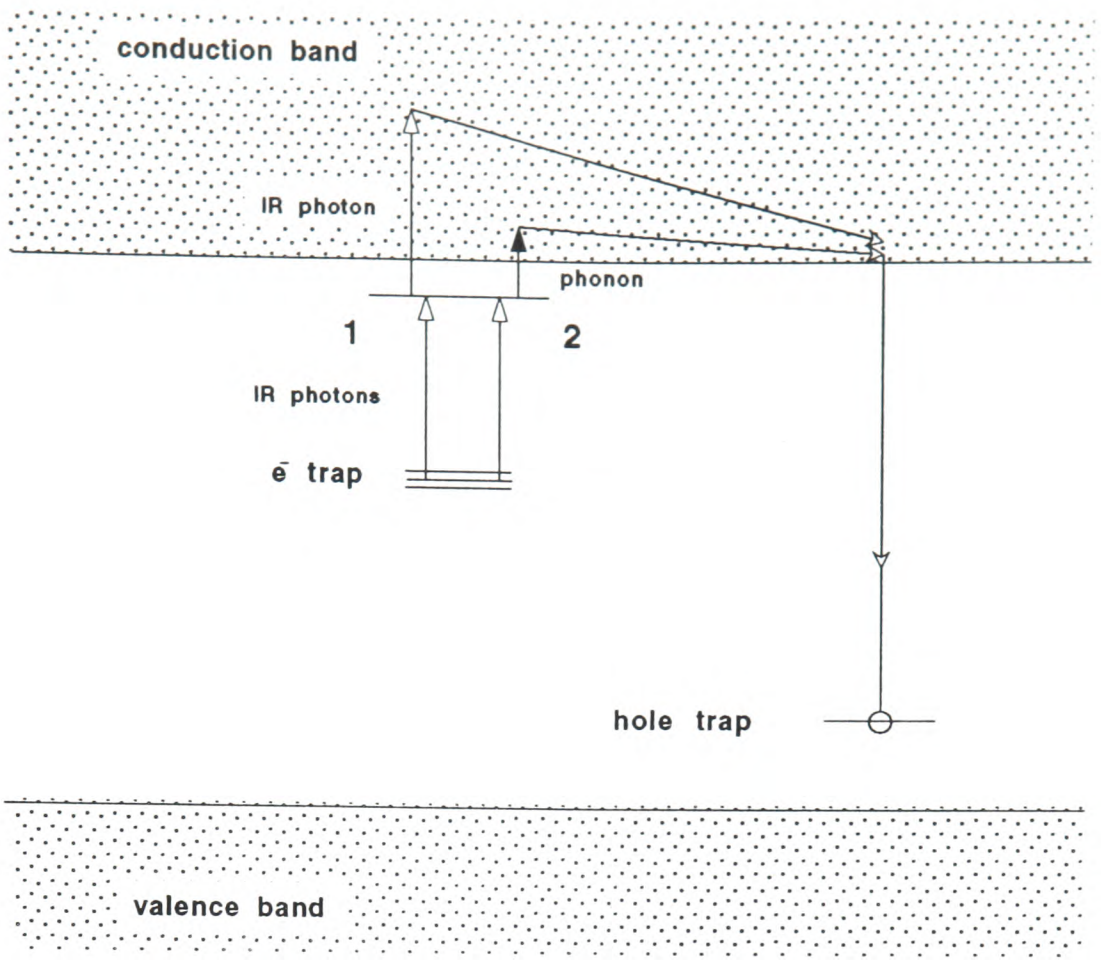


Fig.5.4.2.1 A simplified energy level diagram showing two possible competing modes for electron detrapping. Mode 1 represents a two photon process and mode 2 represents phonon assistance from the electron trap excited state to the conduction band.

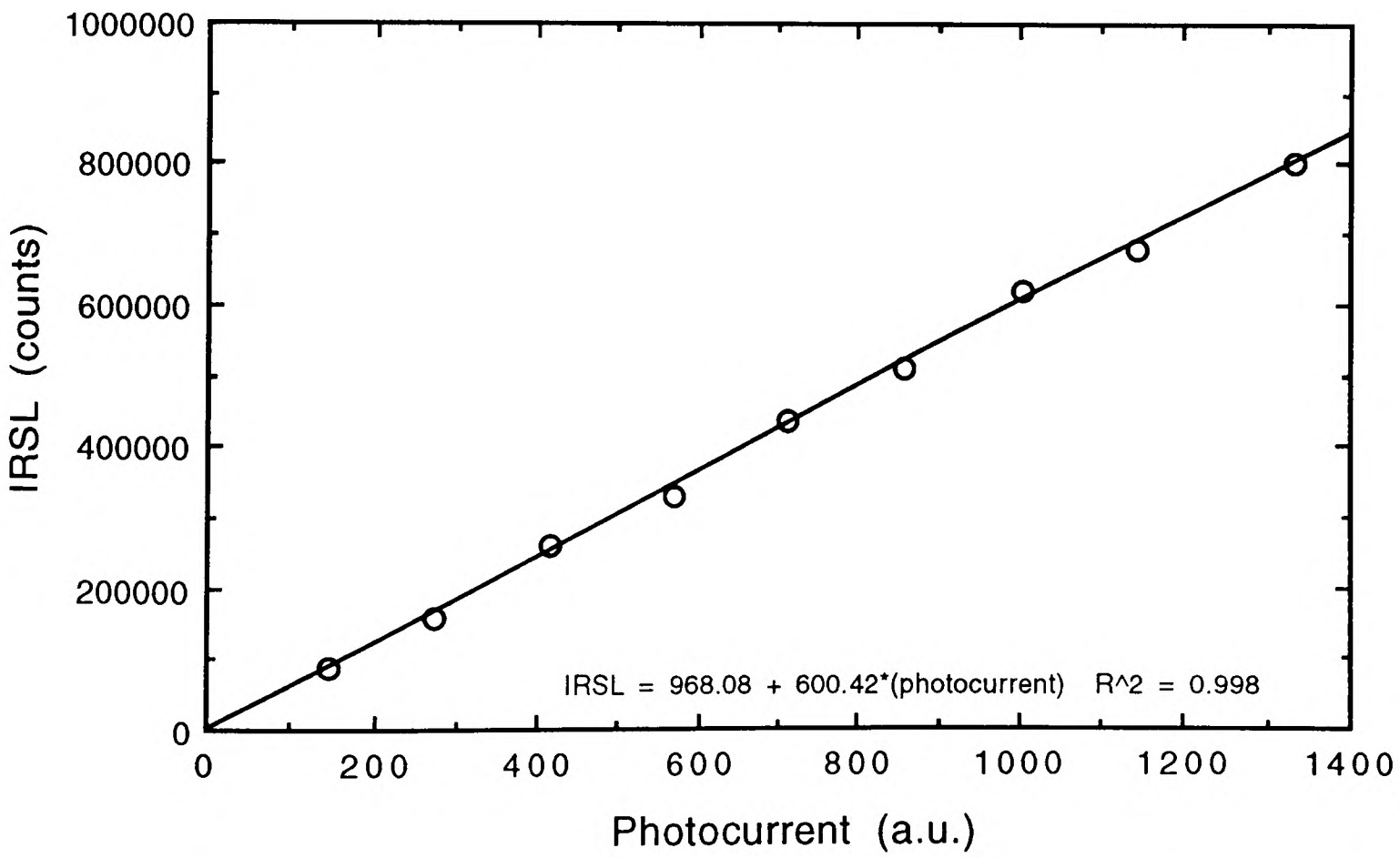


Fig.5.4.2.2 The dependence of the intensity of the IRSL from a microcline feldspar on the IR photon flux density. Photocurrent is directly proportional to the IR beam strength.

absorption of only one photon, the rate of IRSL production should be linearly proportional to the photon flux (ignoring depletion of the trapped charge population), whereas the first mechanism, requiring two related photon absorption steps, should show variation with the square of the photon flux. Below is described an experiment conducted to determine the form of the relation between IRSL intensity and photon flux.

5.4.1 EXPERIMENTAL

The sample used was 90-180 μm grains of microcline (5. No.3062 microcline) attached to the central 3 mm diameter of rhodium plated copper discs by silicone oil. Following drainage of the "NTL" by heating at 5 K/s to 550°C then reheating, a $^{90}Sr/^{90}Y$ beta dose of ≈ 160 Gy was given, and followed by an on-plate preheat in N_2 of 300 seconds at 260°C to eliminate all ATL peaks less thermally stable than the 360°C peak. All measurements were made using an Elsec automated reader (Type 9010) incorporating 880 ▵ 80 nm infrared LEDs, and with the sample temperature maintained at 20°C. IRSL was detected with an EMI 9235Q PMT (bialkali photocathode) and 4 mm Corning 7-59 + 2 mm Schott BG 39 filters.

The procedure consisted of giving short IR exposures (0.1 seconds) at various LED currents (ranging from 11.3 mA to 93 mA) and recording both the emitted IRSL and the photocurrent from the monitor silicon photodiode built into the Elsec reader. The diodes were used in cold mode with a sufficient delay between each exposure to ensure a similar LED output spectrum regardless of LED current. IRSL data were corrected for PMT dark current, pileup (1% / 100 kcps) and depletion, and are shown in Fig.5.4.2.2 plotted as a function of the photocurrent of the monitoring photodiode.

5.4.2 DISCUSSION

It is concluded from the linearity of the response of IRSL to photon flux (see Fig.5.4.2.2) that the detrapping process is a photon-phonon process, at any rate at the IR power levels used.

However, this conclusion includes the possibility that a small proportion of the electrons are evicted from the excited state to the conduction band by the absorption of a second photon, though implicitly this competing mode is undetectably insignificant. Support for this interpretation can be drawn from a consideration of the relative probabilities for the occurrence of each mode of detrapping. Simply, the effect of a two-photon process was not seen in the response curve as a flux-dependent deviation from linearity because the probability of detrapping via this mode is far lower than by the effectively competing mode of phonon absorption.

Assume the frequency factor S of the excited state to be a typical lattice vibration frequency factor of $\approx 10^{12}$ s^{-1} and the trap depth of the excited state to be $\approx$ 0.1 eV. The lifetime at 20°C in this excited state for an electron before detrapping to the conduction band is then $\approx$ 50 picoseconds. In comparison, the photon flux at 40 mW/cm^2 is $\approx$ 1.77×10^{17} 880 nm photons/second/cm^2 or $\approx$ 177 photons/second/0.1 nm^2 (where 0.1 nm^2 is assumed to be the absorption cross section of the trap excited state - it must be emphasised that this absorption cross section is an assumed value based only on the estimated geometrical cross section of an atomic scale defect). This means the residence time required for an electron to remain in the excited state long enough to detrap by absorbing a second photon is at least $\approx$ 5 ms. Clearly, as the phonon detrapping mode has a lifetime $\approx$ 10^8 times less than detrapping by absorption of a second photon it is

absolutely dominant at 20°C. Even reducing the temperature to increase electron residence time in the excited state by reducing the probability of phonon mode detrapping will not permit two-photon detrapping to be observed, as the excited state parameters assumed above require the temperature to be reduced to 52 K for lifetime before phonon absorption to be increased to 5 ms. However, it is inferred from the observed temperature dependence (see Fig.5.3.3.1) that at this temperature IRSL is not observed, presumably due to retrapping transitions back to the ground state occurring before either detrapping mechanism is effective.

In summary, there is very little likelihood of observing two-photon detrapping under these measurement conditions as the competing photon-phonon mode is overwhelmingly dominant, due to the much greater probability of phonon absorption in the excited state.

5.5 A KINETIC STUDY OF A MICROCLINE FELDSPAR

5.5.1 INTRODUCTION

Given the long-standing prominence of feldspathic materials in luminescence dating (for example Mejdahl and Winther-Nielsen (1982) and Mejdahl (1983)), few kinetic studies have been reported for feldspar minerals on the TL peaks usable as dating signals. The findings of Strickertsson (1985) and (1989), Mejdahl (1988) and (1989), Kirsh *et al* (1989) and (1990), and Sanderson *et al* (1989) are summarised in Table 5.5.1.1. Similarly, the lifetimes of the IRSL and OSL signals have received little attention, with the work of Hütt *et al* (1988) being the only published study. It was there claimed that the IRSL signal

was sufficiently stable for dating. The intention here then was to measure the trap parameters of TL peaks which appeared at sufficiently high glow curve temperatures to imply thermal stability and which were also associated with IRSL emission. Clearly then, the sample on which this work was to be performed should be stable, sensitive and of a mineral species abundant in sedimentary deposits.

Choice of sample was based on the previous characterisation work and measurements of fading behaviour (chapters 3 and 4). Fortunately, the high-potassium feldspars included the only sensitive non-fading samples consistently exhibiting TL peaks at glow curve temperatures exceeding ≈ 350°C, and so offered the possibility of being thermally stable (in agreement with published K-feldspar glow curves, i.e., Mejdahl and Winther-Nielsen, (1982) in which only a single broad peak at 360-400°C (heating rate 16°C/s) was seen to survive a preheat of 10 seconds at 290°C). Of the nine high-potassium samples measured, rarity (adularia), insensitivity, fading or perthitic nature ruled out all except 5. No.3062 microcline.

Selection and application of the kinetic methods used follows Chen and Kirsh (1981) and Kirsh (1992). The choice of kinetic methods must take into account that the TL of feldspar minerals not only obeys higher order kinetics but also appears to possess a band of trap depths centred on the mean trap depths of each TL peak. These characteristics effectively preclude reliable use of the isothermal decay method, nevertheless, a variant of that approach - ramping in steps at a very slow mean heating rate - was attempted here on an isolated microcline high-temperature TL peak; otherwise the isothermal decay method was not considered applicable. Another method also apparently unsuitable for application to the feldspars, or any other minerals having overlapping glow peaks, is the fractional glow method (Gobrecht and Hofman, (1966)).

Author	Sample type and origin	Mineral	Method	TL glow peak	E	S	b	$\tau_{(sec)}$	$\tau_{(ka)}$	Comments
Strickertsson, K (1985)	sediment 2.54-2.58 g.cm^{-3} (Denmark)	93% microcline 6% quartz	IR (fractional glow)	223°C peak 3 299°C " 4 384°C " 5 470°C " 6 (2.5°C/s)	1.48 ± 0.05 1.62 ± 0.05 1.65 ± 0.05 1.80 ± 0.05	5.1 x 10^{14} 8.9 x 10^{13} 2.8 x 10^{12} 1.3 x 10^{13}	1st order assumed	4.4 x 10^{11} 7.9 x 10^{14} 8.8 x 10^{16} 4.1 x 10^{20} @10°C	1.4 x 10^{1} 2.5 x 10^{4} 2.8 x 10^{6} 1.3 x 10^{10} @10°C	
Mejdahl, V (1988)	Tertiary sediments (Denmark)	alkali feldspar	equilibrium in "infinitely" old samples	280°C & 330°C (2°C/s)	-	-	-	2.5 x 10^{13} to 1.7 x 10^{14} @10°C	800-5400 @10°C	large variability; less for higher K
Mejdahl, V (1989)	Tertiary sediments (Denmark)	K-feldspar 11.4-13.1% K	equilibrium in "infinitely" old samples	230-260°C peak 3 300-350°C peak 4	- -	- -	- -	1.2 x 10^{13} 2.2 x 10^{13}	386 ± 44 711 ± 93	mean life decreases with increasing K content (internal absorption of signal???)
Strickertsson, K (1989)	Nordic sediments Nordic bedrock Scottish vitrified forts (44 samples)	K-feldspar	IR (fractional glow)	210°C peak 3 280°C " 4 350°C " 5 455°C " 6 (T_m from fractional glow)	1.48 ± 0.05 1.62 ± 0.05 1.65 ± 0.05 1.80 ± 0.05	5.1 x 10^{14} 8.9 x 10^{13} 2.8 x 10^{12} 1.3 x 10^{11}	1st order assumed	4.4 x 10^{11} 7.9 x 10^{14} 8.8 x 10^{16} 4.1 x 10^{20} @10°C	1.4 x 10^{1} 2.5 x 10^{4} 2.8 x 10^{6} 1.3 x 10^{10} @10°C	
	Tertiary sand	K-feldspar	IR (fractional glow)	225°C peak 3 295°C peak 4	1.28 1.57	1.1 x 10^{12} 9.6 x 10^{12}	1st order assumed	5.7 x 10^{10} 9.5 x 10^{14}	1.8 x 10^{0} 3.0 x 10^{4}	
	Cretaceous sand (as used by Mejdahl, 1989)			225°C peak 3 285°C peak 4	1.29 1.52	1.4 x 10^{12} 6.1 x 10^{12}		6.9 x 10^{10} 1.9 x 10^{14}	2.2 x 10^{0} 6.1 x 10^{3}	
Sanderson et al (1989)	Archaeological samples and pegmatitic microcline	K-feldspar	IR (fractional glow)	300-350°C 400°C	1.5-1.62 1.70-1.75	- -	1st order assumed	3.2 x 10^{12} to 3.2 x 10^{14} 3.2 x 10^{15} to 3.2 x 10^{16} @10-20°C	10^{2}-10^{4} 10^{5}-10^{6} @10-20°C	
Kirsh et al (1989)	Pre-Cambrian pegmatite (590±10)x10^{6} a	microcline	IR as input to Best-Fit program (BF data shown here for NTL)	170°C 234°C 274°C 309°C	1.20 ± 5-10% 1.32 " 1.46 " 1.52 "	1.5 x 10^{13} 3.7 x 10^{12} 7.8 x 10^{12} 3.5 x 10^{12}	1.6 2.0 1.4 2.4	1 x 10^{7} 4 x 10^{9} 4.3 x 10^{11} 1 x 10^{13} @20°C	3.2 x 10^{-4} 0.13 13.8 317 @20°C	lifetimes calculated by NAS from given data
Kirsh et al (1990)	Pre-Cambrian albitite rock ~6x10^{8} a	albite	IR as input to Best-Fit program (BF data shown here for NTL)	178°C 220°C 308°C 340°C 391°C	0.93 ± 5-10% 1.08 " 1.30 " 1.66 " 1.85 "	6.5 x 10^{9} x + $10^{0.5}$ 2.8 x 10^{10} " 4.3 x 10^{10} " 1.1 x 10^{13} " 2.5 x 10^{13} "	1.2 ± 0.3 1.1 ± " 0.8 ± " 1.5 ± " 2.0 ± "	1.5 x 10^{6} 1.4 x 10^{8} 1.6 x 10^{11} 1.5 x 10^{15} 2.6 x 10^{18} @20°C	4.9 x 10^{-5} 4.3 x 10^{-3} 5.2 x 10^{0} 4.7 x 10^{4} 8.3 x 10^{7} @20°C	lifetimes calculated by NAS from given data

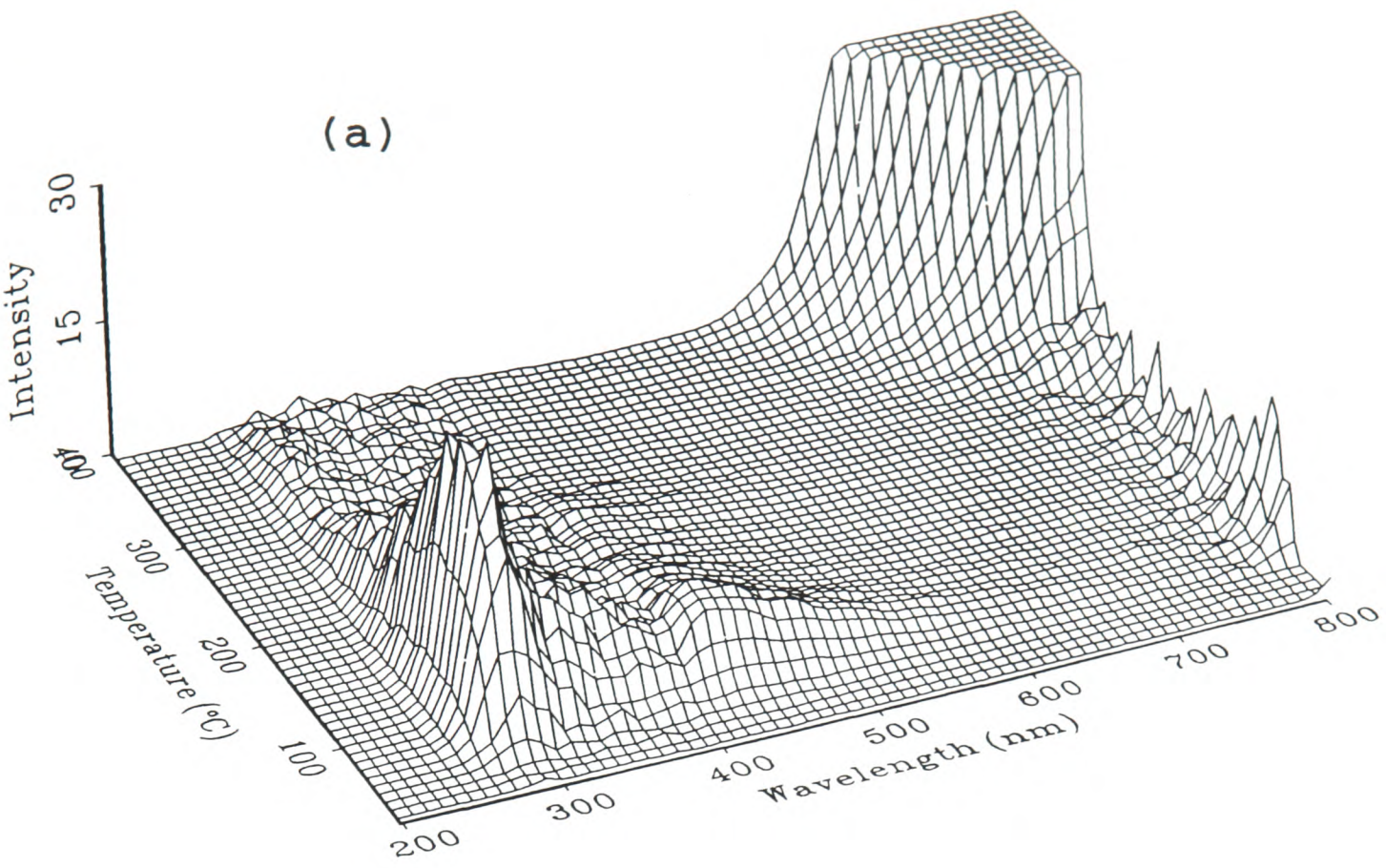
Table 5.5.1.1 A summary of results of kinetic analyses and stability assessments of various feldspathic samples published by others. Of note is the consensus that the high temperature TL (≥ 300°C) is more than adequately stable, thermally, for dating applications. Trap depths E are in electron volts (eV) and escape frequency factors S in s^{-1}.

Computer simulations by Kierstead and Levy, (1991) have shown that this method is only reliable for (1) single peak glow curves; or (2) glow curves containing peaks that do not overlap; or (3) the lowest temperature peak in multi-peak curves where the peaks are well separated. These restrictions are potentially highly significant, as the fractional glow method (a series of repeated initial rise measurements at successively higher temperatures) has been relied on in previous studies on feldspar kinetics (Strickertsson, 1985 and 1989, Sanderson *et al*, (1989)). In recognition of these caveats, results obtained using the fractional glow method cannot be treated as definitive, (whilst acknowledging that the data of both Strickertsson (1985 and 1989) and Sanderson *et al* (1989) have not been shown to be seriously in error).

Finally, the peak shift method of Hoogenstraaten may also be unreliable under certain conditions (Lewandowski and McKeever, (1991)) which may be encountered in feldspar minerals and lead to errors of up to 15% on E and 2 orders of magnitude on S.

Regarding other approaches, even studies on the lifetimes of "infinite" age feldspars by Mejdahl (1988 and 1989), intended to be free of the systematic errors associated with any kinetic method, must be regarded cautiously in view of the subsequent identification by Wintle and Duller (1991) of internal self-absorption of luminescence in high potassium feldspars, and the recognition here of the extremely high susceptibility to bleaching of the feldspar luminescence. Additionally, the possibility of undetected long-term tunnelling-type fading giving a laboratory-saturation-TL/NTL ratio greater than unity is raised by the findings presented in Chapter 4.

The method most relied on here is the initial rise method, particularly chosen for its insensitivity to kinetic order. However, even this method must be applied with caution as either thermal quenching or changes during TL measurement in the TL emission



(b)

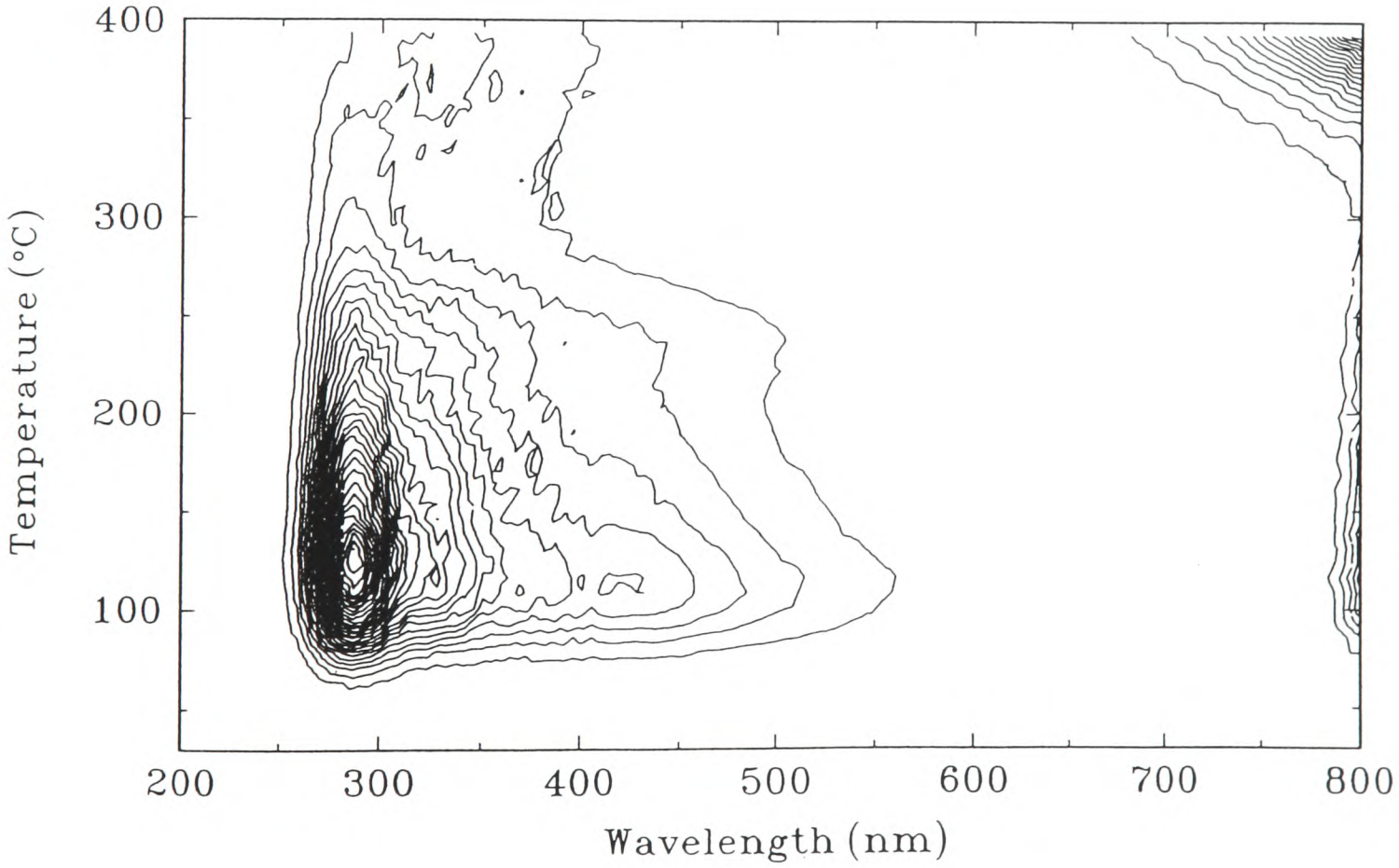


Fig.5.5.1.1.(a) The emission spectrum of 5. No.3062 microcline, measured promptly following an added $^{90}Sr/^{90}Y$ β dose of ≈ 100 Gy (no preheat given). The incandescence signal is seen rising at red wavelengths at temperatures ≥ 300°C; the temperature-independent "emission" at ≈ 800 nm is a system artifact. **(b)** A contour plot of the data set shown in (a); the relative intensity of the ≈ 280 nm emission is readily apparent, along with the constancy of emission wavelength.

spectrum will invalidate the results. Thermal quenching reduces the slope of the initial rise and hence the apparent trap depth, whereas changes in the emission spectrum may distort the shape of the glow peaks and so also introduce errors in the trap depth determinations. However, as the question here was that of the adequate thermal stability of feldspar luminescence, reasonable systematic underestimations of signal lifetimes are acceptable. Spectral stability was determined by measurement of the TL emission spectrum of 5. No.3062 microcline. The measurements were kindly performed by B.J. Luff of the University of Sussex, using a spectrometer based on two imaging photon detectors (Luff and Townsend, (1992)). Fig.5.5.1.1 shows the emission spectrum plotted (a) isometrically and (b) as a contour plot; there is no change in emission spectrum, hence this sample is spectrally stable to TL measurement and so is suitable for valid analysis by kinetic methods (assuming thermal quenching is not present).

Note that the kinetic tests provide information only on the stability of the electron traps with respect to thermal untrapping, and are insensible to other modes by which electrons may be lost from traps over timescales far shorter than predicted from the kinetics. Furthermore, no conclusions can be drawn regarding possible long-term fading of the hole centres, and so even if electron traps are truly stable, hole centre fading may still limit the dating time range to well below that expected (this is essentially the argument proposed by Debenham, (1985), to account for the 100 ka limit in fine grain materials).

The following sections describe the use of various preheating temperatures and durations to strip thermally successive TL peaks from the glow curve of a microcline feldspar sample, after which the attribution of the 380°C TL peak as a strong IRSL source is made. The isolation of this TL peak and its subsequent study by all applicable kinetic

methods follows; finally a comparison is made with the trap parameters measured for a sample of sedimentary Scandinavian K-feldspar (density < 2.58, provided by V. Mejdahl).

5.5.2 EXPERIMENTAL

Throughout this study TL measurements were performed using either a Risϕ automated TL reader or an Alldred TL set (controlled by a modified servo control unit which allowed choice of heating rates from ≈ 8 K/s to ≈ 0.0008 K/s). All measurements using the Risϕ system were made at a heating rate of 5 K/s in an N_2 atmosphere, with the emissions detected using an EMI 9635Q PMT with Corning 7-59 and Chance-Pilkington HA3 filters. Measurements performed with the Alldred system used an EMI 9635Q PMT with various filter combinations chosen to minimise the incandescence background at 300°C while not overly attenuating the luminescence signal. IRSL measurements were performed with an Elsec Optical Dating System Type 9010, with the emissions detected using an EMI 9235Q PMT with a 2 mm Schott BG39 filter.

The sample, 5. No.3062 microcline, was presented in the form of 90 - 180 μm grains attached by silicon oil to the central 3 mm ϕ area of rhodium plated copper discs. "NTL" was erased in each case by heating at 5 K/s to 550°C then reheating. Dosing was of $^{90}Sr/^{90}Y$ β irradiation, the magnitude of the dose varying from ≈ 20 Gy to ≈ 400 Gy depending on the experimental requirements; all preheats were performed using the Risϕ TL reader.

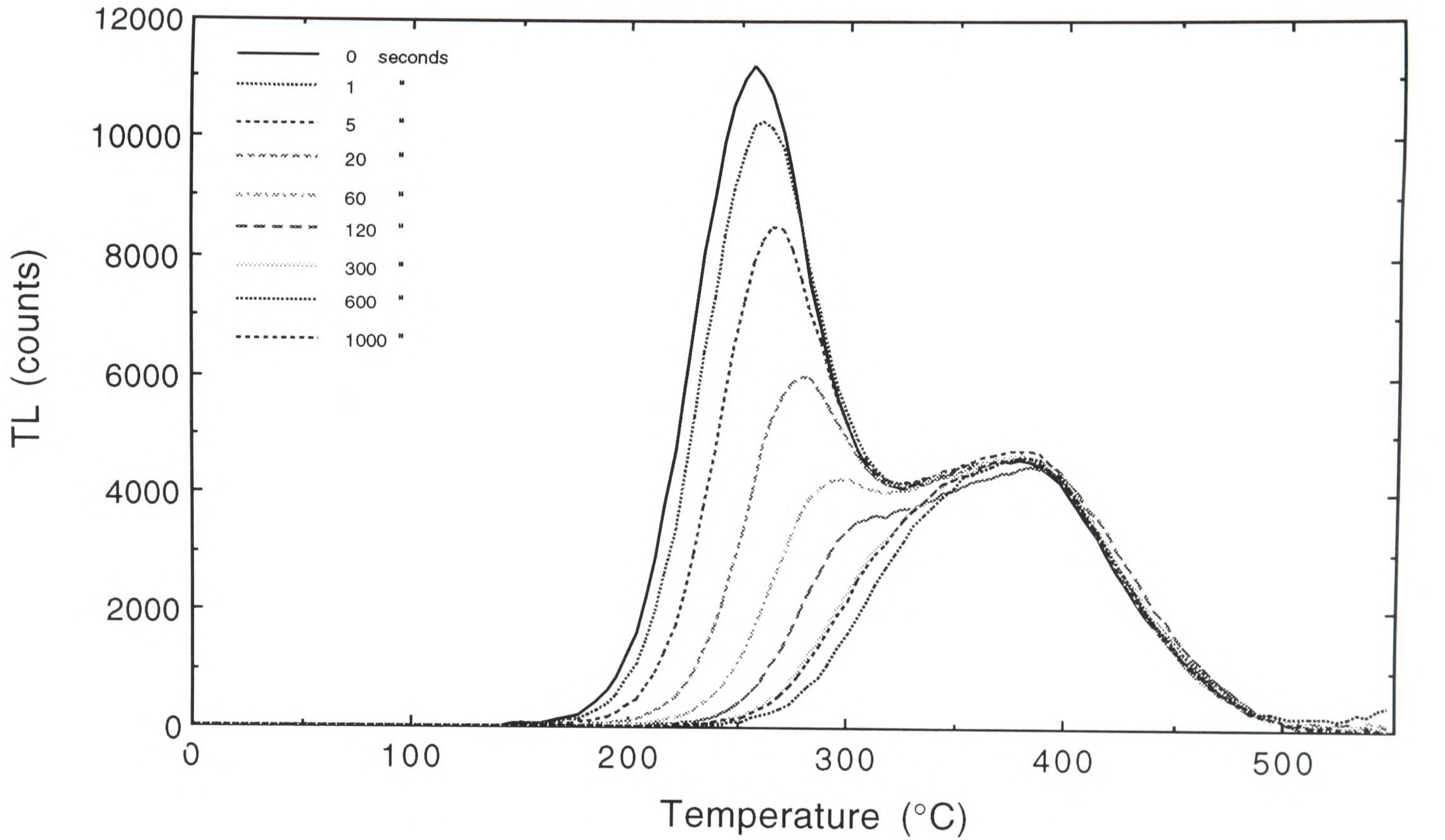


Fig.5.5.3.1 TL glow curves of 5. No.3062 microcline following various storage durations at 220°C. TL measurements were made at 5 K/s using a Risϕ automated TL reader; the data are second glow normalized.

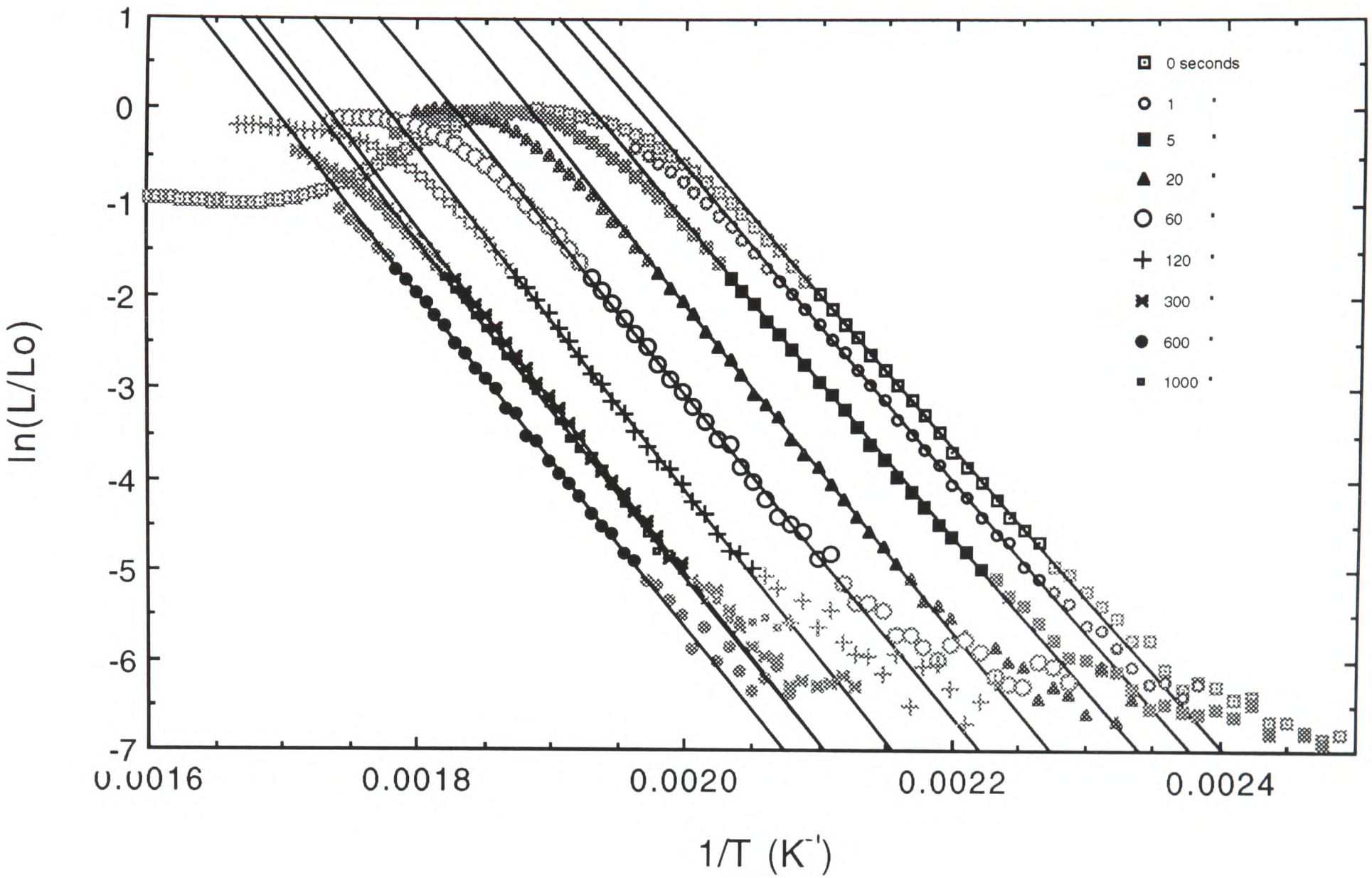


Fig.5.5.3.2 The initial rise portions of the TL glow curves of 5. No.3062 microcline following various storage durations at 220°C (see Fig.5.5.3.1) are shown overlain by the data fitted for initial rise analysis.

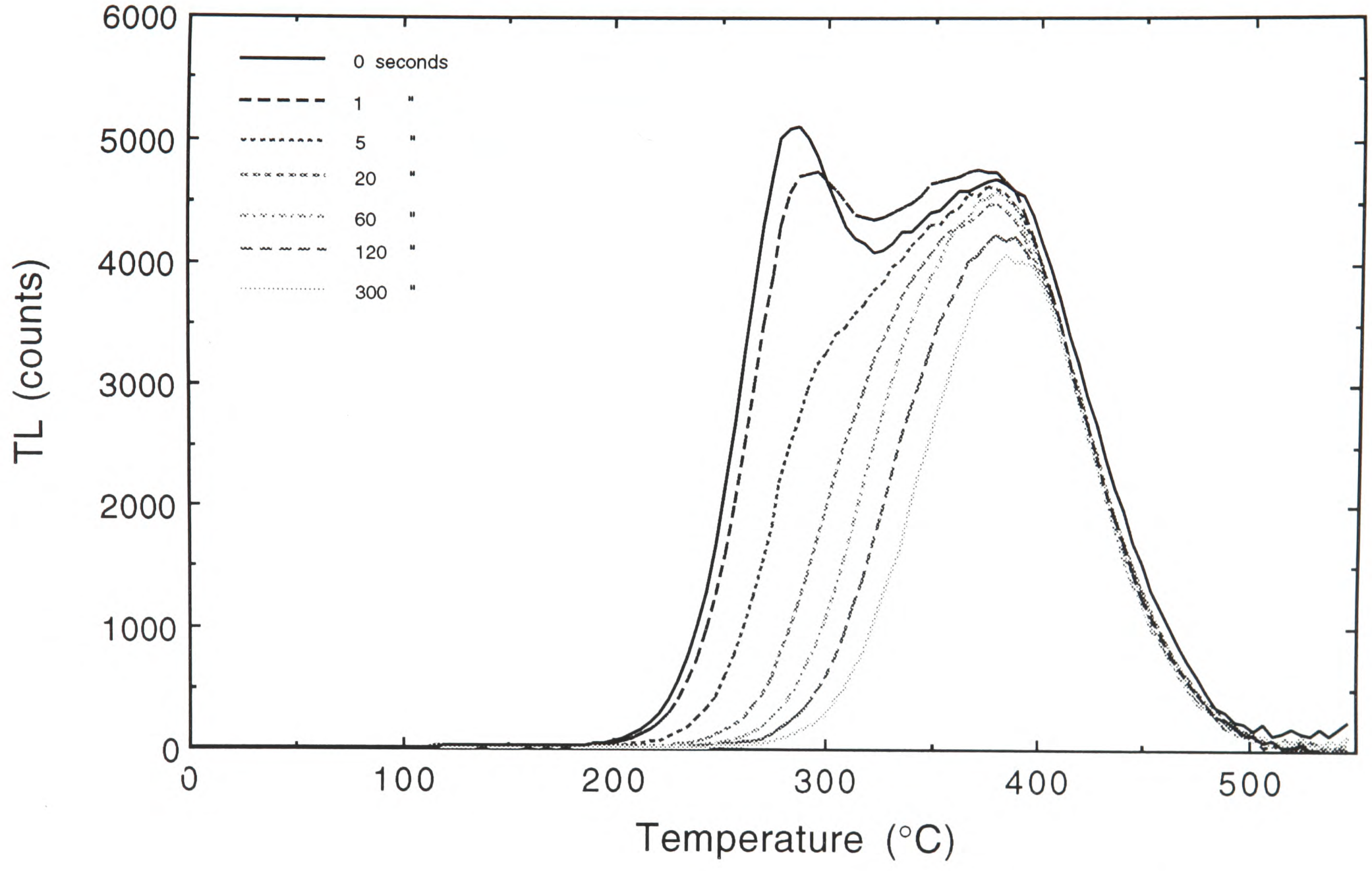


Fig.5.5.3.3 TL glow curves of 5. No.3062 microcline following various storage durations at 260°C. TL measurements were made at 5 K/s using a Risϕ automated TL reader; the data are second glow normalized and directly comparable to those of Fig.5.5.3.1. Note the thermal erosion on the rising portion of the glow curve in contrast to the thermal stability seen from the high temperature side.

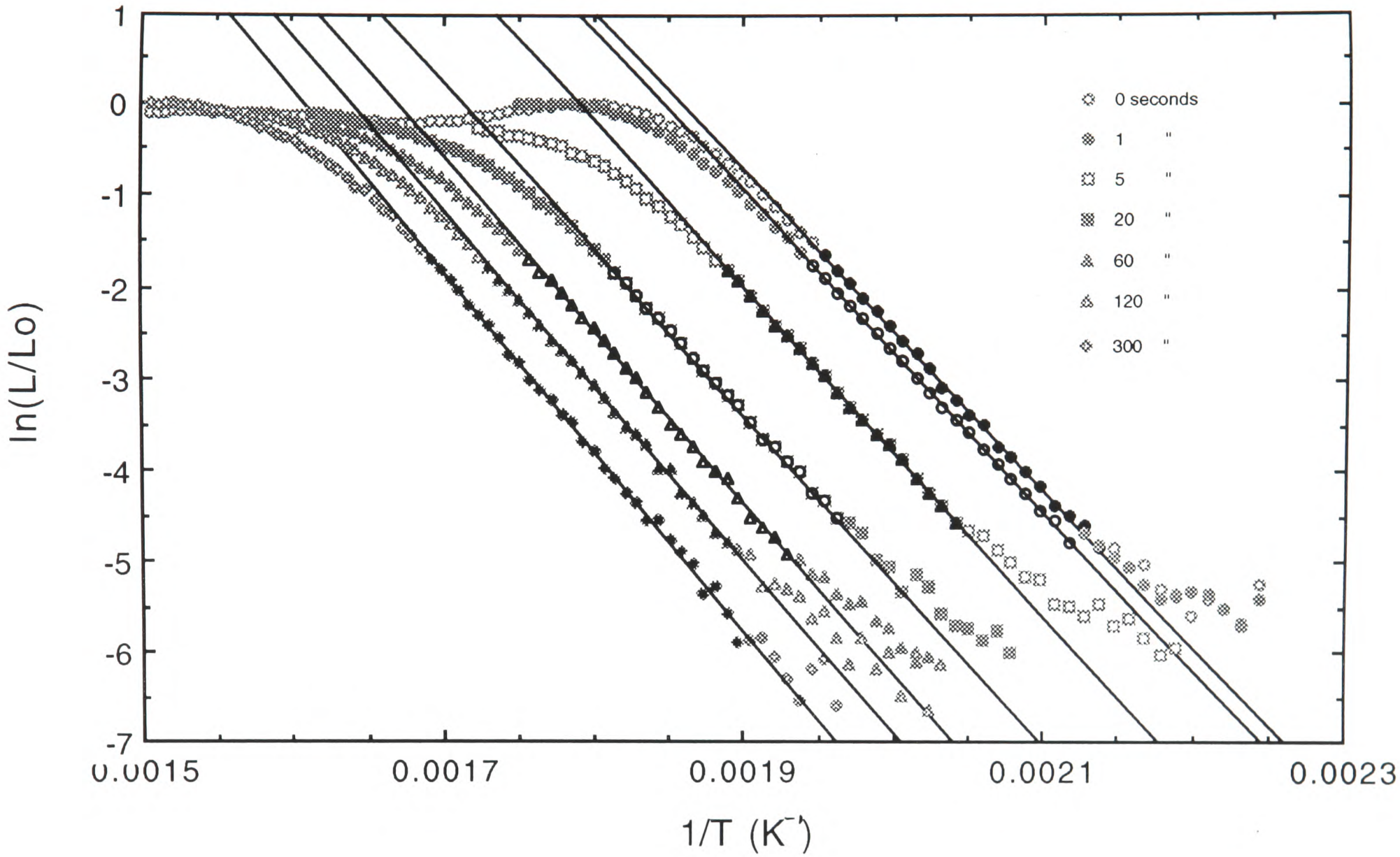


Fig.5.5.3.4 The initial rise portions of the TL glow curves of 5. No.3062 microcline following various storage durations at 260°C (see Fig.5.5.3.3) are shown overlain by the data fitted for initial rise analysis.

5.5.3 TL PEAK STRIPPING BY STORAGE AT 220°C AND 260°C: GLOW CURVES AND INITIAL RISE MEASUREMENTS

As a preliminary step to measurement of the trap parameters of the TL glow peaks useful for dating, a series of elevated temperature storage experiments were made to determine which TL glow peaks had the greater thermal stability. Comprehensive analysis of their stability should then reveal whether or not any of the feldspar TL glow peaks were in fact sufficiently stable for reliable dating.

Two sets of sample discs prepared as outlined in section 5.5.2 were stored for various durations at 220°C or at 260°C, following which the TL was measured. The glow curves following storage at 220°C are shown in Fig.5.5.3.1 and that resulting from storage at 260°C in Fig.5.5.3.3, in both cases along with the data fitted for initial rise analyses of the first rise of the glow curve (shown in Figs.5.5.3.2 and 5.5.3.4 respectively). Parameters calculated from these data are given in Table 5.5.3.1. As these data were unsuitable for the application of other methods, only the initial rise method was applied here. Additionally, as the fitted data are of the first rise of the glow curve and so relate to the lowest temperature TL peak surviving that preheat, then the lifetimes can be considered as minimum lifetimes for any TL surviving the preheat - the parameter of interest here.

Assignment of the temperatures at which to plot the measured activation energies was done by assuming association of the activation energies with the lowest temperature TL peak, of which the fitted data represents the lower temperature rising side. The T_{max} value of that TL peak is then the temperature assigned to the activation energy. This approach differs from that used in the computer simulations by Kierstead and Levy (1991), there the temperature midpoint of the fitted temperature range was used, though

with the result that the activation energy plateaux occurred to the lower side of the corresponding TL peak, and for the first rising peak lead to unrealistically long lifetimes attributed to the lower temperature TL peaks. That these lifetimes are demonstrable overestimations is proven by the absence of significant TL at these temperatures in natural samples (for example, the activation energy found following a "cut" preheat to 220°C would be assigned to the TL at ≈ 196°C; the lifetime of ≈ 45.1 ka determined for this TL predicts the occurrence of dating plateaux for samples up to ≈ 5 ka at this temperature - this behaviour is not seen, from which it is concluded that the temperature assignation used by Kierstead and Levy (1991) is not usable for real cases).

Preheat Temperature 220°C								
PH time (s)	E ± ΔE (eV)	T_m (°C)	(K)	S (s^{-1})	ΔS/S	S 1st order (s^{-1})	$\tau_{20°C}$ (s)	(ka)
0	1.439 ± 0.009	256	529	1.43 x 10^{13}	0.48	1.52 x 10^{13}	3.97 x 10^{11}	1.26 x 10^{1}
1	1.457 ± 0.009	260	533	1.66 x 10^{13}	0.48	1.77 x 10^{13}	6.95 x 10^{11}	2.20 x 10^{1}
5	1.473 ± 0.009	267	540	1.53 x 10^{13}	0.48	1.63 x 10^{13}	1.42 x 10^{12}	4.51 x 10^{1}
20	1.543 ± 0.007	278	551	3.58 x 10^{13}	0.43	3.80 x 10^{13}	9.72 x 10^{12}	3.08 x 10^{2}
60	1.535 ± 0.022	298	571	9.01 x 10^{12}	0.68	9.59 x 10^{12}	2.81 x 10^{13}	8.92 x 10^{2}
120	1.596 ± 0.015	312	585	1.42 x 10^{13}	0.56	1.51 x 10^{13}	2.00 x 10^{14}	6.34 x 10^{3}
300	1.620 ± 0.013	315	588	1.95 x 10^{13}	0.53	2.07 x 10^{13}	3.77 x 10^{14}	1.19 x 10^{4}
600	1.582 ± 0.010	315	588	8.99 x 10^{12}	0.47	9.56 x 10^{12}	1.81 x 10^{14}	5.75 x 10^{3}
1000	1.585 ± 0.012	320	593	7.21 x 10^{12}	0.51	7.68 x 10^{12}	2.55 x 10^{14}	8.07 x 10^{3}
Preheat Temperature 260°C								
PH time (s)	E ± ΔE (eV)	T_m (°C)	(K)	S (s^{-1})	ΔS/S	S 1st order (s^{-1})	$\tau_{20°C}$ (s)	(ka)
0	1.496 ± 0.011	285	558	8.45 x 10^{12}	0.50	8.99 x 10^{12}	6.40 x 10^{12}	2.03 x 10^{2}
1	1.507 ± 0.008	293	566	6.68 x 10^{12}	0.44	7.11 x 10^{12}	1.25 x 10^{13}	3.97 x 10^{2}
5	1.566 ± 0.010	303	576	1.29 x 10^{13}	0.48	1.37 x 10^{13}	6.72 x 10^{13}	2.13 x 10^{3}
20	1.565 ± 0.012	330	603	2.80 x 10^{12}	0.50	2.98 x 10^{12}	2.97 x 10^{14}	9.42 x 10^{3}
60	1.628 ± 0.011	355	628	2.59 x 10^{12}	0.47	2.76 x 10^{12}	3.89 x 10^{15}	1.23 x 10^{5}
120	1.655 ± 0.012	383	656	1.08 x 10^{12}	0.48	1.15 x 10^{12}	2.73 x 10^{16}	8.65 x 10^{5}
300	1.701 ± 0.015	388	661	1.96 x 10^{12}	0.53	2.09 x 10^{12}	9.26 x 10^{16}	2.94 x 10^{6}

Table 5.5.3.1 The kinetic parameters and lifetimes measured using the initial rise method following various durations of storage at 220°C and 260°C. Second order kinetics were used.

The trap depths were evaluated from the slopes of Arrhenius plots and the frequency factors subsequently calculated for the cases of both 1st and 2nd order kinetics, using the appropriate equations, given below:

$$S = \frac{\beta E}{kT_m^2} \exp\left(\frac{E}{kT_m}\right)$$

$$S = \frac{\beta E}{kT_m^2} \exp\left(\frac{E}{kT_m}\right) \left[(b-1)\frac{2kT_m}{E} + 1\right]^{-1}$$

The kinetic parameters and lifetimes (calculated assuming second order kinetics) are given in Table 5.5.3.1.

Initial consideration of the TL glow curves and corresponding trap parameters reveals the "280°C" TL peak seen in the "NTL" of this sample (and characteristic of potassium feldspar) to be simply the high-temperature remnant of a much greater TL peak seen in the ATL at ≈ 250°C (see Appendix I). The measured lifetimes explain its significance in NTL - in spite of thermal instability it retains charge sufficiently long for the fading remnant to be substantial, given typical natural dose rates.

Interpretation of the findings invokes either a spectrum of trap energies or the hypothesising of a band of trap energies around each of several distinct defect energy levels. The latter explanation is more plausible and appears intuitively the more likely on inspection of the TL glow curves. A hypothesis for the existence of such bands of energies rather than well defined trapping energies is offered by the range of perturbations to which each particular defect is exposed in the various configurations in which it can exist within the lattice; the band central energy is then the characteristic energy of that defect in its most common configuration.

It was apparent from the resistance to thermal erosion of the 330°C and 380°C TL peaks that they were the only features of these glow curves likely to prove sufficiently stable for dating applications; consequently further work was restricted to those peaks.

5.5.4 THE 380°C TL PEAK

5.5.4.1 INTRODUCTION

The TL peaks at 330°C and ≈ 380°C represented potentially thermally stable dating signals with the advantage of being readily isolable from less stable glow peaks by simple preheats; the 380°C TL glow peak was then chosen to test the thermal stability of feldspar TL. However, although earlier work (see section 3.5) had shown this TL glow peak to be readily bleachable by IR photons, it remained to show that this bleaching was accompanied by simultaneous emission of IRSL. The demonstration that the traps giving rise to this TL peak also emitted detectable luminescence under IR stimulation is described in the following section.

5.5.4.2 THE 380°C TL PEAK AS AN IRSL SOURCE

Given that the 380°C TL peak was potentially stable for dating purposes and bleachable by 880 nm IR illumination, it remained to prove that it did indeed emit detectable IRSL and so constitute a thermally stable IRSL source. As emission of IRSL does not necessarily follow from IR bleachability, a set of IR bleaching experiments with simultaneous IRSL detection were conducted to test that IRSL did accompany bleaching

of this TL peak. The approach was to compare the magnitude of the IRSL signals after successive TL peaks had been removed by increasingly strong preheats, in conjunction with a consideration of the corresponding IR-bleached and unbleached TL glow curves.

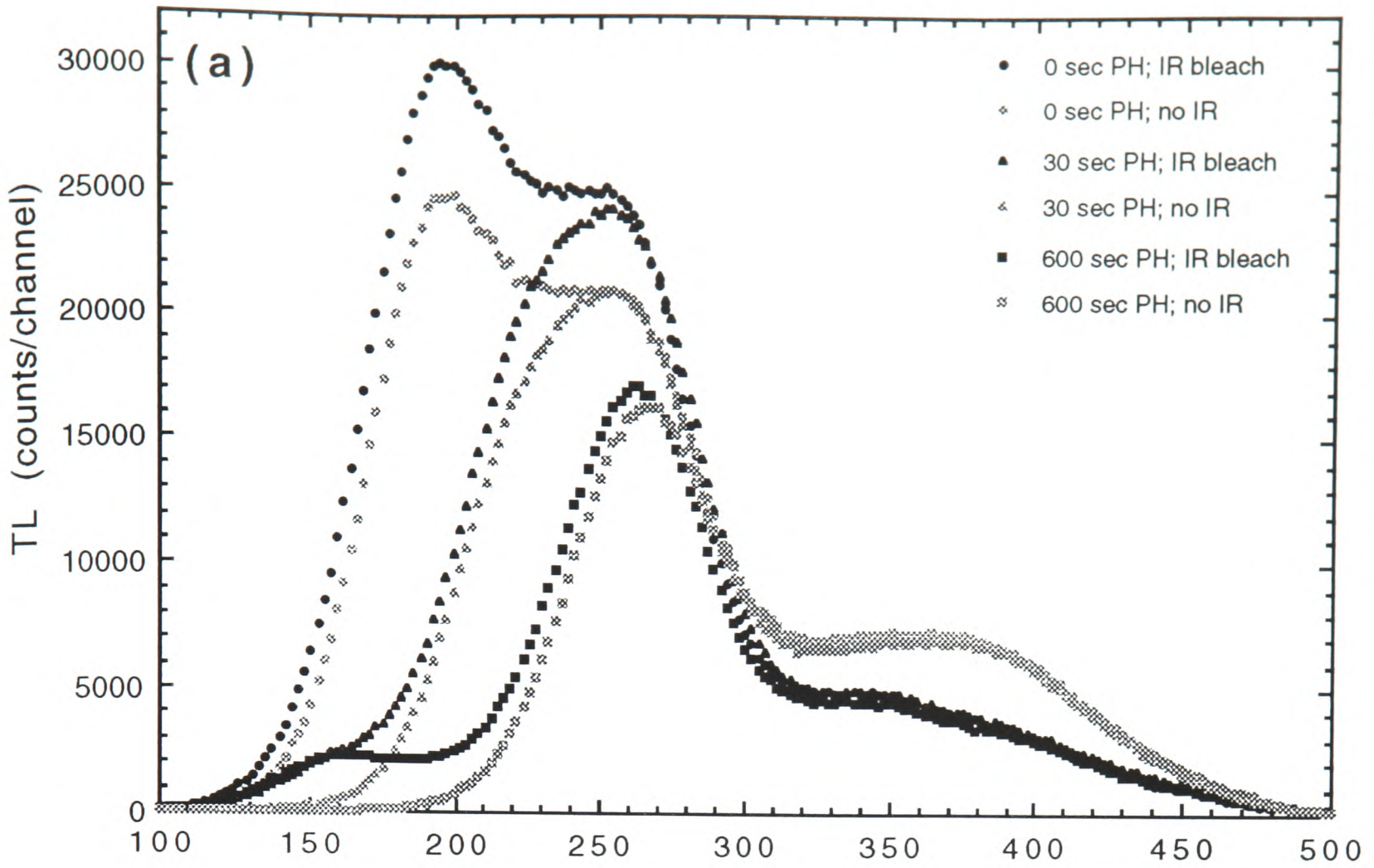
5.5.4.2.1 EXPERIMENTAL

Approximately 1 mg of sample 5. No.3062 microcline (90-180 μm grains) was attached to the central 3 mm of each of 16 rhodium-plated copper discs using silicone oil. The "NTL" was then thermally drained by heating at 5 K/s to 550°C and reheating, following which was administered a $^{90}Sr/^{90}Y$ β dose of ≈ 30 Gy using an Elsec Type 9022 automated β irradiator. A two day delay at ambient temperature then followed before the IRSL was monitored using a short exposure of ≈ 3 mJ of 880 ∆ 80 nm IR from an Elsec Type 9010 automated reader (IRSL emissions were detected by an EMI 9235Q PMT with a 2 mm Schott BG 39 filter) after which the various preheats were given using a Risϕ automated TL reader. Pairs of discs received the same preheats; the 16 discs were then divided into two sets - one set to be unexposed controls while the other 8 discs each received 5000 seconds (≈ 150 J) IR exposure using the Elsec reader. The TL of all portions was then measured, heating at 5 K/s to 550°C and reheating, using the Risϕ reader (TL emissions were detected by an EMI 9635Q PMT with Corning 7-59 and Chance-Pilkington HA3 filters). TL measurement was followed finally by a TL dose-normalization step, similarly measured.

5.5.4.2.2 RESULTS AND DISCUSSION

The TL dose-normalized glow curves measured after each treatment are shown in Fig.5.5.4.2.2.1.(a)-(c). Table 5.5.4.2.2.1. summarizes the IRSL data. An assessment of the role of each of the prominent TL peaks in this sample (at ≈ 160°C, 260°C, 330°C and 380°C) can be reached by inspection of the normalised long exposure data (the normalised IRSL light sum) in Table 5.5.4.2.2.1 in conjunction with the TL glow curves.

Considering each peak in turn: it appears that as there are no significant differences in the normalised IRSL light sums (normalised by IRSL light sums following test doses after the completion of the other measurements) measured when the corresponding glow curves differ only by the presence or absence of the 160°C peak, that peak plays no significant role in IRSL production, either as a source or sink of charge, (at the precision level of these measurements, estimated at ≈ 10 % from the TL variability). The role of the 260°C TL peak is less clear, because although the decline in the observed IRSL light sums coincides with the progressive erasure of that peak, the possibility exists that this is not due to the removal of the 260°C TL peak's contribution to the total IRSL light sum but through the increasingly significant competition for retrapping offered by the enlarged population of vacant 260°C TL peak traps; the 260°C TL peak traps in this interpretation do not necessarily contribute any IRSL component. Although the proportion of the IRSL signal originating from the 260°C TL peak traps cannot be precisely determined from the measurements reported here, an upper limit can be estimated: assuming the observed IRSL light sum is unaffected by retrapping, then from the reduction of ≈ 40 % in the IRSL light sum seen between those glow curves in which the 260°C TL peak is present (i.e., 0 second preheat at 220°C) and those in which



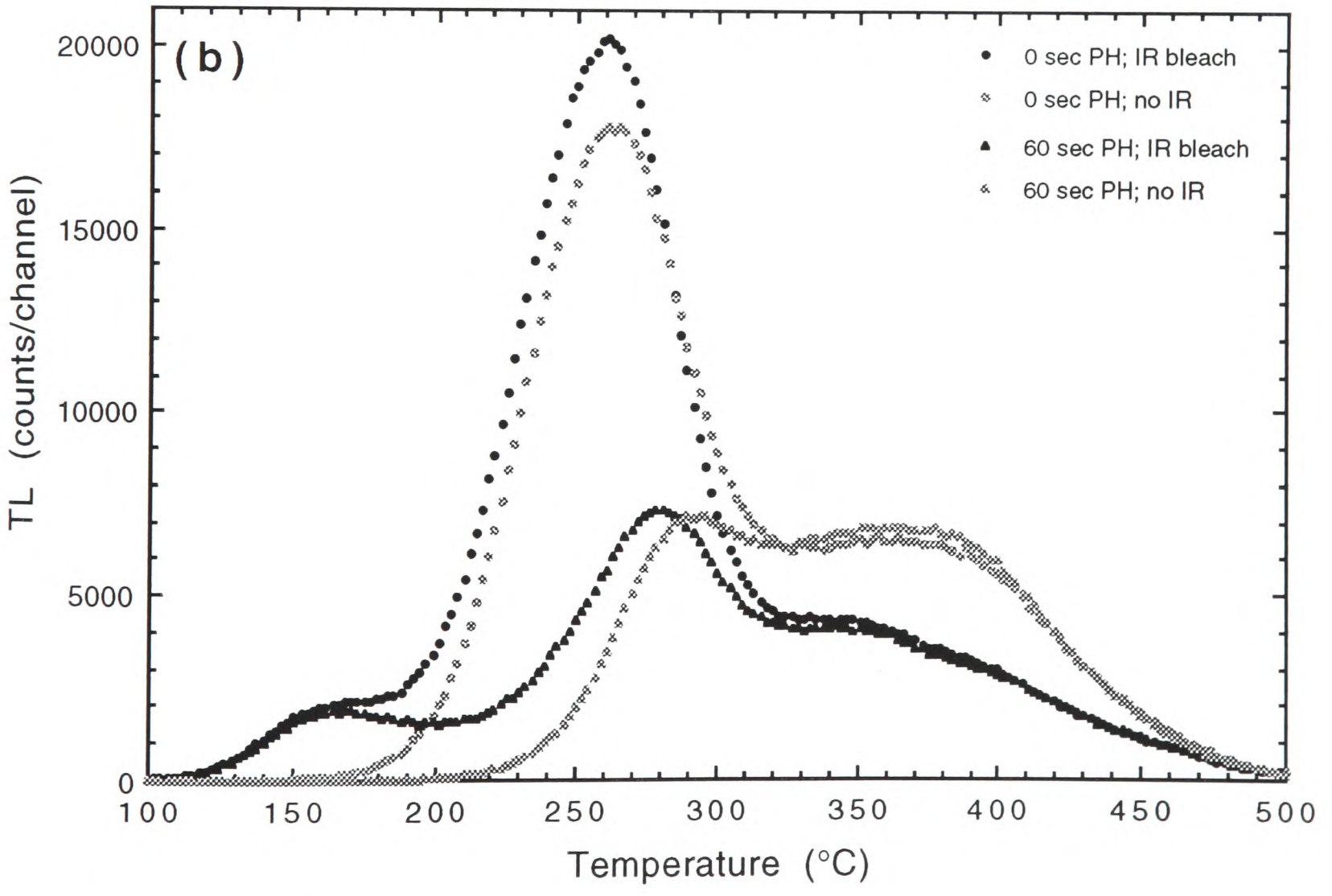
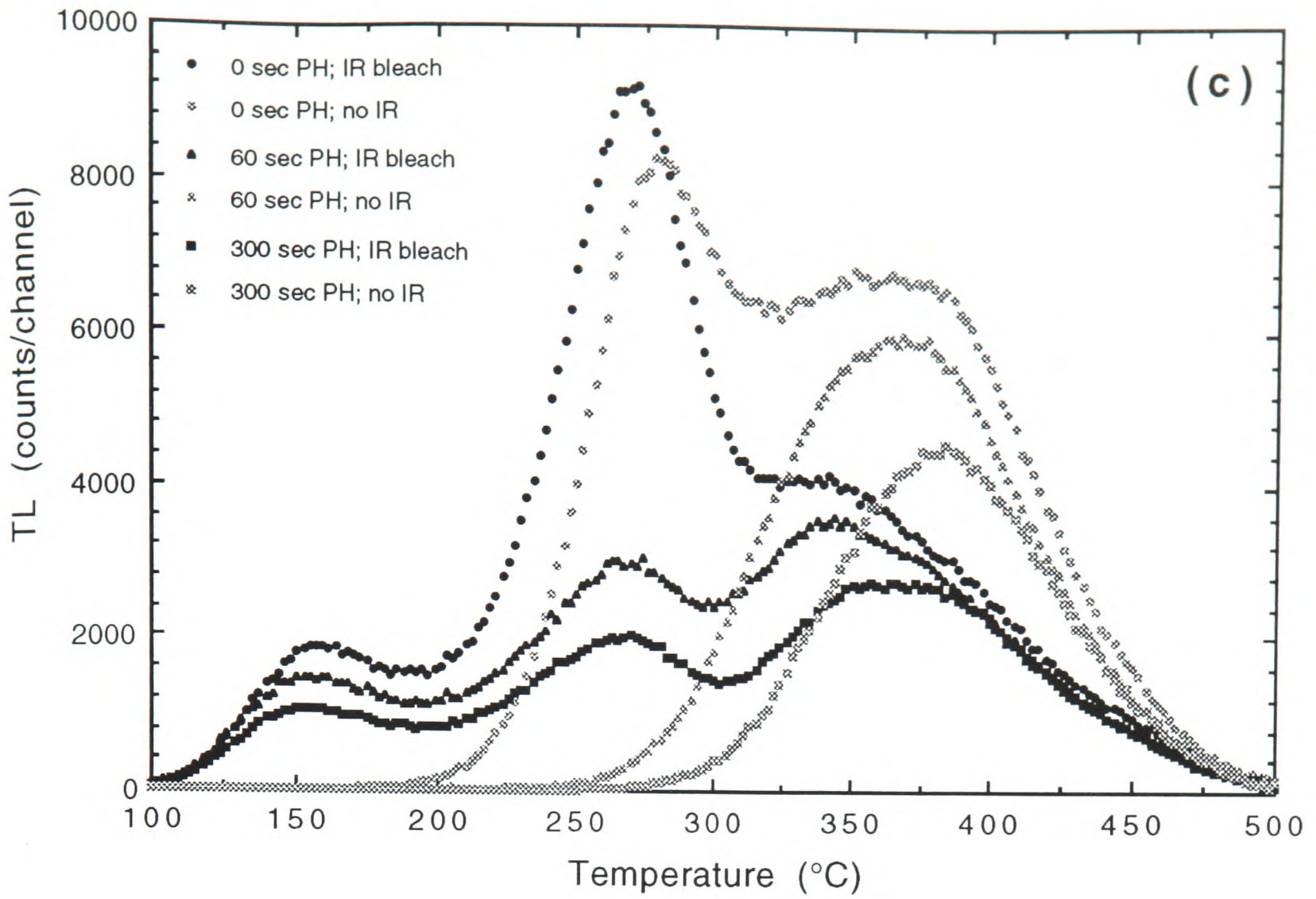


Fig.5.5.4.2.2.1.(a)-(c) Pairs of sample discs of 5. No.3062 microcline received various durations of storage at **(a)** 160°C, **(b)** 220°C and **(c)** 260°C. Following these storages one of each pair of discs was given ≈ 150 J exposure of 880 ▵ 80 nm IR and the TL of all discs then measured. Data shown are the second-glow normalized glow curves.



Preheat Temperature (°C)	Preheat time (s)	IRSL short exposure before preheat (cps)	IRSL long bleach	IRSL long exposure after preheat (counts)	Ratio long/short exposure	IRSL normalization factor (cps)*	normalized short exposure	normalized long exposure
160	0	432670	yes	81944586	189.4	36132	11.97	2268
	0	404920	no	-	-	41990	9.64	-
160	30	406670	yes	86183225	211.9	32285	12.60	2669
	30	483200	no	-	-	43167	11.19	-
160	600	429080	yes	97962954	228.3	38691	11.09	2532
	600	487480	no	-	-	44301	11.00	-
220	0	669700	yes	154865292	231.2	61616	10.87	2513
	0	656930	no	-	-	58286	11.27	-
220	60	528060	yes	125786488	238.2	61939	8.53	2031
	60	498400	no	-	-	56726	8.79	-
260	0	353050	yes	78990082	223.7	38379	9.20	2058
	0	379950	no	-	-	42377	8.97	-
260	60	214920	yes	54844286	255.2	35311	6.09	1553
	60	238130	no	-	-	44722	5.32	-
260	300	159990	yes	42872156	268.0	40134	3.99	1068
	300	120770	no	-	-	36832	3.28	-

Table 5.5.4.2.2.1 The IRSL light sums, and ratios, from the IRSL emitted by the various portions of 5. No.3062 microcline following differing preheats (see Fig.5.5.4.2.2.1.(a)-(c) for the corresponding glow curves, and the text for details).

it was removed by preheating prior to the IR long exposure (i.e., 60 seconds preheat at 260°C), it is deduced that this ≈ 40 % of the IRSL (at most) originates from these traps.

The higher temperature TL peaks (330°C and 380°C) appear to both contribute to the IRSL and account for the remaining ≈ 60 % of the total observed IRSL signal. This is concluded from the similar proportional reductions in the TL and IRSL light sums seen on extending the duration of preheat at 260°C from 60 seconds to 300 seconds, an increase which results in the removal of the 330°C TL peak. Note that the estimated 60 % component of the IRSL is a lower limit which will rise with increasing significance of retrapping competition from the lower temperature TL peaks. Indeed it is within the range of possibility allowed by these measurements that the 380°C TL peak traps are the *only* source of IRSL in this microcline.

The above interpretations necessarily avoid quantitative comparison between the TL light sums and corresponding IRSL light sums as such comparisons are precluded by the use of different detection systems for TL and IRSL. These instrumental factors (different detection spectral windows, PMT spectral sensitivities and detector collection efficiency) could not be accurately corrected for. Additionally, sample-dependent problems such as thermal quenching and initial-state-dependent changes in the competitive retrapping behaviour of the various trap populations present severe problems even when instrumental variables are allowed for.

Regarding the presence of thermal quenching: the magnitude of the TL light sums before and after IR bleaching of the glow curves and following preheats which isolate the 330°C and 380°C TL peaks (see Fig.5.5.4.2.2.1.(c)) appear irreconcilable without invoking thermal quenching. For example, following 60 seconds preheat at 260°C the unbleached glow curve has a light sum of 309,402 counts, compared to the post-bleach light sum of

326,204. The corresponding values when the preheat was 300 seconds at 260°C were 203,428 (unbleached) and 249,334 (IR bleached). Note that the bleached light sums do not include the IRSL light sums - these are seen from Table 5.5.4.2.2.1 to be in excess of 40,000,000 counts in each case. (The factor of ≈ 150-200 by which these values exceed the TL cannot accounted for by the broader spectral window monitored for IRSL and the superior detector collection efficiency of the Elsec system alone, and heating rate variation analysis shows no conclusive evidence for thermal quenching in this sample. It is therefore hypothesised that there is a degree of localization of the luminescence traps and recombination centres, and that the consequences of untrapping via the "IRSL" excited state pathway differ from untrapping by either TL or shorter wavelength (photoionization) untrapping. The crucial difference is that from the "IRSL" excited state pathway the electron reaches the conduction band with ≈ minimum energy needed for the untrapping process; thermalization will therefore take in the immediate vicinity of the hypothetical electron-trap/hole-centre pairing, so increasing the probability of radiative recombination (though admittedly now in competition with geminate neutralization of recombination (Noolandi, 1987)). Conversely, for untrapping by higher energy photons, the excess energy above the minimum needed for untrapping ensures that thermalization will now not occur in the locality of the electron/hole pairing, and consequently, significant transport of the untrapped electrons, by diffusion in the conduction band, should remove a greater proportion from proximity with the hole centre, so facilitating their loss at competing non-radiative recombination centres. A similar situation may hold for thermal untrapping: the greater crystal temperature, and hence the greater mean lattice-phonon energy, in this case will likewise ensure thermalization at distance from the electron/hole pairing, and again result in lower luminescence efficiency due to competition from the same (presumably)

non-luminescent centres as before). Finally, the possibility that the PTTL includes a component transferred by the IR from deep traps at glow curve temperatures > 550°C was previously eliminated, for this sample - the observed PTTL and IRSL originate from traps drained by heating to 550°C.

Considering the shapes of the IRSL shine curves: the steady decrease of the ratio of long:short IRSL exposures (see Table 5.5.4.2.2.1) indicates a decreasing IRSL decay rate with progressive removal of TL peaks by increasingly strong preheats. This apparently contradicts the suggestion above that most, if not all, of the IRSL is attributed to the 380°C peak traps alone (although it cannot be ruled out that a considerable IRSL signal also originates from the 280°C TL peaks). However this can be qualitatively reconciled by a consideration of the increasing significance of retrapping into the now-vacant lower temperature traps competing with luminescent recombinations. According to Levy (1982), the filling of initially empty lower temperature traps by phototransfer while simultaneously bleaching results first in a rise in the lower temperature TL followed by reduction as bleaching comes to dominate as the source traps are depleted. In this case where the lower temperature peaks may not bleach under the phototransfer illumination (IR), the observed shapes of the IRSL shine curves measured here (not shown) are consistent with Levy (1982) in that the lower temperature traps act as an electron sink throughout the bleaching process.

A consequence of such modification of the shine curve shapes by competition effects is that the question of whether the 380°C TL peak traps possess a smaller untrapping cross-section (due to their deeper excited state, for instance) cannot be answered from these data, as the possibility exists that the "slower" IRSL decay rate seen when only this peak is present following preheating is a competition effect rather than an

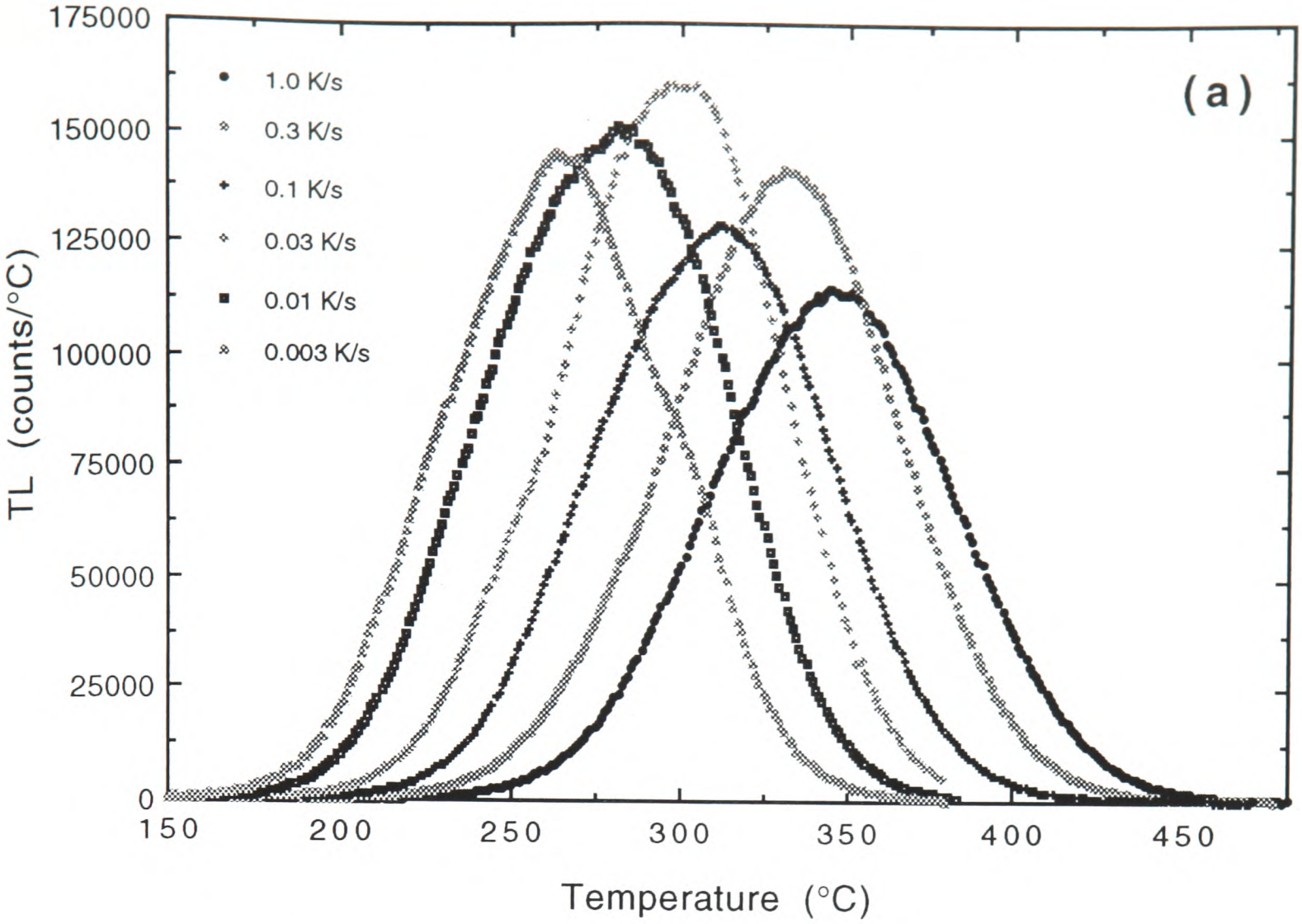
inherently slower rate of detrapping the electrons from the 380°C traps.

It is concluded that not only does the 380°C TL peak bleach when exposed to IR stimulation but that this bleaching is accompanied by relatively intense emission. This work parallels that on loessic material (D.G. Questiaux, pers. comm. 1992) in which similar results were found. Consequently the isolation of this peak by appropriate preheating should be an essential step in any optical dating procedure using samples in which this mineral is present, a conclusion equally valid for TL dating.

5.5.4.3 THE ISOLATED 380°C TL PEAK: ANALYSIS BY THE METHOD OF HEATING RATE VARIATIONS (HOOGENSTRAATEN'S METHOD)

Following confirmation that the isolated 380°C TL peak was a strong source of IRSL, measurement of its kinetic parameters was undertaken to provide, by association, a direct measurement of the thermal stability of the IRSL originating from that same trapped charge population. Given the self-evident significance of this TL peak as a potentially thermally stable IRSL source, accurate and precise determination of its kinetic parameters were of paramount importance. Therefore, as each kinetic method has specific deficiencies or restrictions on applicability all feasible methods were applied, under the philosophy that good accord between the findings is a strong validation of the common result.

Sample preparation and pretreatment are as described in section 5.5.2 except that the final procedural step before TL measurement was preheating for 300 seconds duration at 260°C, to isolate the 380°C TL peak. The kinetic methods then applicable to these data



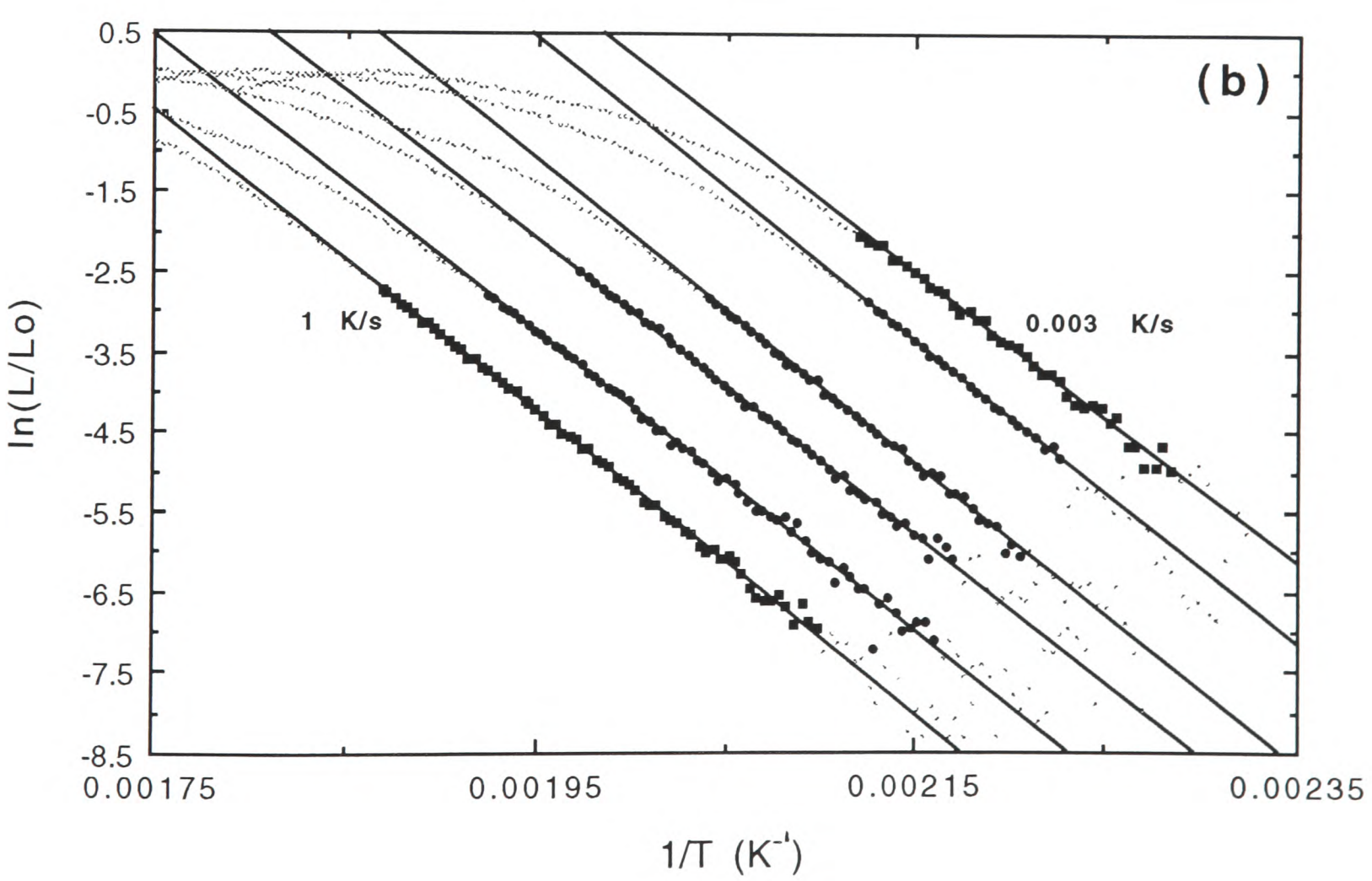


Fig.5.5.4.3.1.(a) Glow curves of 5. No.3062 microcline measured at the various heating rates shown following 300 seconds preheating at 260°C; second-glow normalization has been used. The distortion on the high temperature side of the "0.003 K/s" glow curve is believed to be an artifact. Note the absence of evidence for strong thermal quenching even when the "380°C" TL peak is shifted downwards in temperature by ≈ 90 K. **(b)** The initial rise portions of each glow curve, overlain with the portions fitted to determine trap parameters.

were variation of heating rate and the initial rise method.

The glow curves measured at each heating rate are shown in Fig.5.5.4.3.1.(a), and the initial rise portions of the glow curves overlain by the fitted sections for initial rise analysis are shown in Fig.5.5.4.3.1.(b). Kinetic results from the application of the initial rise method to glow curves measured at a range of heating rates for analysis also by the method of heating rate variations are presented in Table 5.5.4.3.1; results from the method of heating rate variations on that same data set are presented in Table 5.5.4.3.2..

Inspection of the glow curves in Fig.5.5.4.3.1.(a) reveals possible thermal quenching, although the scatter on the data reduces the certainty of this conclusion (even following normalization with factors derived from the "NTL"). Otherwise there is no "untoward" behaviour apparent and the initial rise portions of the curve (see Fig.5.5.4.3.1.(b)) show excellent uniformity, with the extracted trap parameters in close agreement with each other, as expected.

Heating rate (K/s)	E ± ΔE (eV)	T_m (°C)	(K)	S (s^{-1})	ΔS/S	S 1st order (s^{-1})	$\tau_{20°C}$ (s)	(ka)
1.000	1.627 ± 0.009	347	620	7.70 x 10^{11}	0.44	8.20 x 10^{11}	1.26 x 10^{16}	3.99 x 10^{5}
0.300	1.602 ± 0.017	332	605	3.15 x 10^{11}	0.58	3.35 x 10^{11}	1.14 x 10^{16}	3.63 x 10^{5}
0.100	1.588 ± 0.011	312	585	2.41 x 10^{11}	0.49	2.56 x 10^{11}	8.58 x 10^{15}	2.72 x 10^{5}
0.030	1.633 ± 0.013	299	572	3.98 x 10^{11}	0.54	4.22 x 10^{11}	3.09 x 10^{16}	9.80 x 10^{5}
0.010	1.636 ± 0.016	282	555	4.15 x 10^{11}	0.60	4.39 x 10^{11}	3.34 x 10^{16}	1.06 x 10^{6}
0.003	1.563 ± 0.023	265	538	7.71 x 10^{10}	0.72	8.17 x 10^{10}	9.96 x 10^{15}	3.16 x 10^{5}

Table 5.5.4.3.1 The kinetic parameters evaluated for 5. No.3062 microcline using the initial rise method applied to each glow curve measured at each of the given heating rates for later analysis by the method of heating rate variations. The frequency factor S was calculated by both first and second order kinetics; lifetimes were evaluated using second order S (note that these lifetimes differ from the first order case by <5%).

Sample	Preheat	E ± ΔE (eV)	S (s^{-1})	ΔS/S	$\tau_{20°C}$ (s)	(ka)
(1) 5. No.3062 microcline (280°C peak)	220°C, 60s	1.434 ± 0.097	4.40 x 10^{12}	10.0	1.05 x 10^{12}	3.32 x 10^{1}
(1) 5. No.3062 microcline (380°C peak)	220°C, 60s	2.019 ± 0.215	2.89 x 10^{15}	75.1	1.85 x 10^{19}	5.87 x 10^{8}
(2) 5. No.3062 microcline (380°C peak)	260°C, 300s	1.892 ± 0.031	1.27 x 10^{14}	1.63	2.75 x 10^{18}	8.73 x 10^{7}
(1) 9. Z15 sanidine	220°C, 60s	1.499 ± 0.153	7.39 x 10^{12}	32.8	8.15 x 10^{12}	2.58 x 10^{2}
(1) 12. Patmos albite	220°C, 60s	1.590 ± 0.157	1.28 x 10^{14}	21.0	1.75 x 10^{13}	5.53 x 10^{2}
(1) 18. Amelia albite	220°C, 60s	1.522 ± 0.032	2.78 x 10^{13}	2.00	5.40 x 10^{12}	1.71 x 10^{2}
(1) 23. Dup(B) oligoclase	220°C, 60s	1.659 ± 0.041	2.06 x 10^{14}	2.87	1.67 x 10^{14}	5.29 x 10^{3}

Table 5.5.4.3.2 Kinetic parameters evaluated using the method of various heating rates. Also shown are parameters determined for other feldspar samples from data in

section 4.2.5.3 for comparison, and for the 280°C and 380°C TL peaks of 5. No.3062 microcline measured in section 4.2.5.3 (indicated above as "(1)"). First order kinetics were assumed for S. Note that the apparent instability of the other feldspar mineral TL peaks may be a consequence of the less stringent preheat applied to these samples leaving less stable TL as the rising side of the glow curve. However, the 280°C TL peak of 5. No.3062 microcline is clearly less stable than the 380°C TL peak, as expected.

The data from which the values in Table 5.5.4.3.2 were derived are shown in Fig.5.5.4.3.2. The parameters presented in Table 5.5.4.3.2 lead to a number of observations: first is the clearly greater thermal stability of the 380°C TL peak of the microcline with respect to both the 280°C TL peak of that same sample and the peaks of the other measured feldspars. This is intuitively expected given the substantially greater temperature at which the 380°C TL peak occurs. Secondly, the trap depths for the 380°C microcline peak average $\approx$ 1.95 eV, which significantly exceeds any other trap depth estimate made here for that peak. Exclusion of these data from subsequent comparisons on the grounds that the excess of this value over other estimates is likely to be an experimental artifact is supported by consideration of the associated frequency factors. S in both cases exceeds $\approx 10^{14}$ s^{-1}, which is becoming unphysically large and appears to be in the nature of a compensating error resulting from a slightly incorrect curve fit. Although the data sets (see Fig.5.5.4.3.2) appear well fitted, nevertheless S is significantly discrepant with the consistently found value of $\approx 10^{12}$ s^{-1} elsewhere; however the calculated lifetimes are in reasonable accord with those from all other methods used here. The likelihood then is the analysis is valid with respect to the order of magnitude found for the lifetime, further emphasising the extreme thermal stability of this TL peak.

An important additional reason for using Hoogenstraaten's method was in an attempt to test the significance of the presence of the excited state in modifying the true total thermal trap depth to a lower value (this aspect is further discussed in section 5.6).

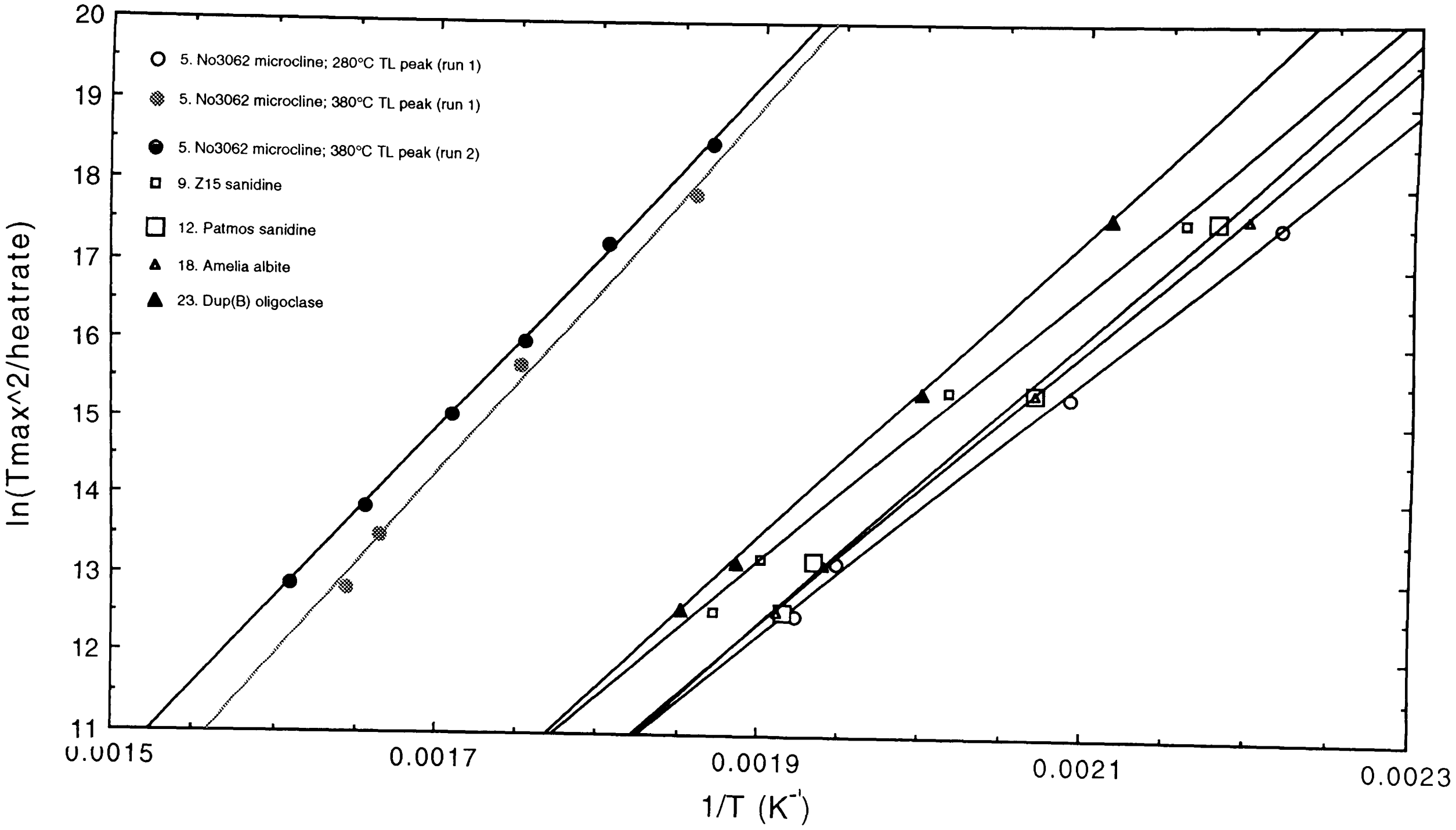
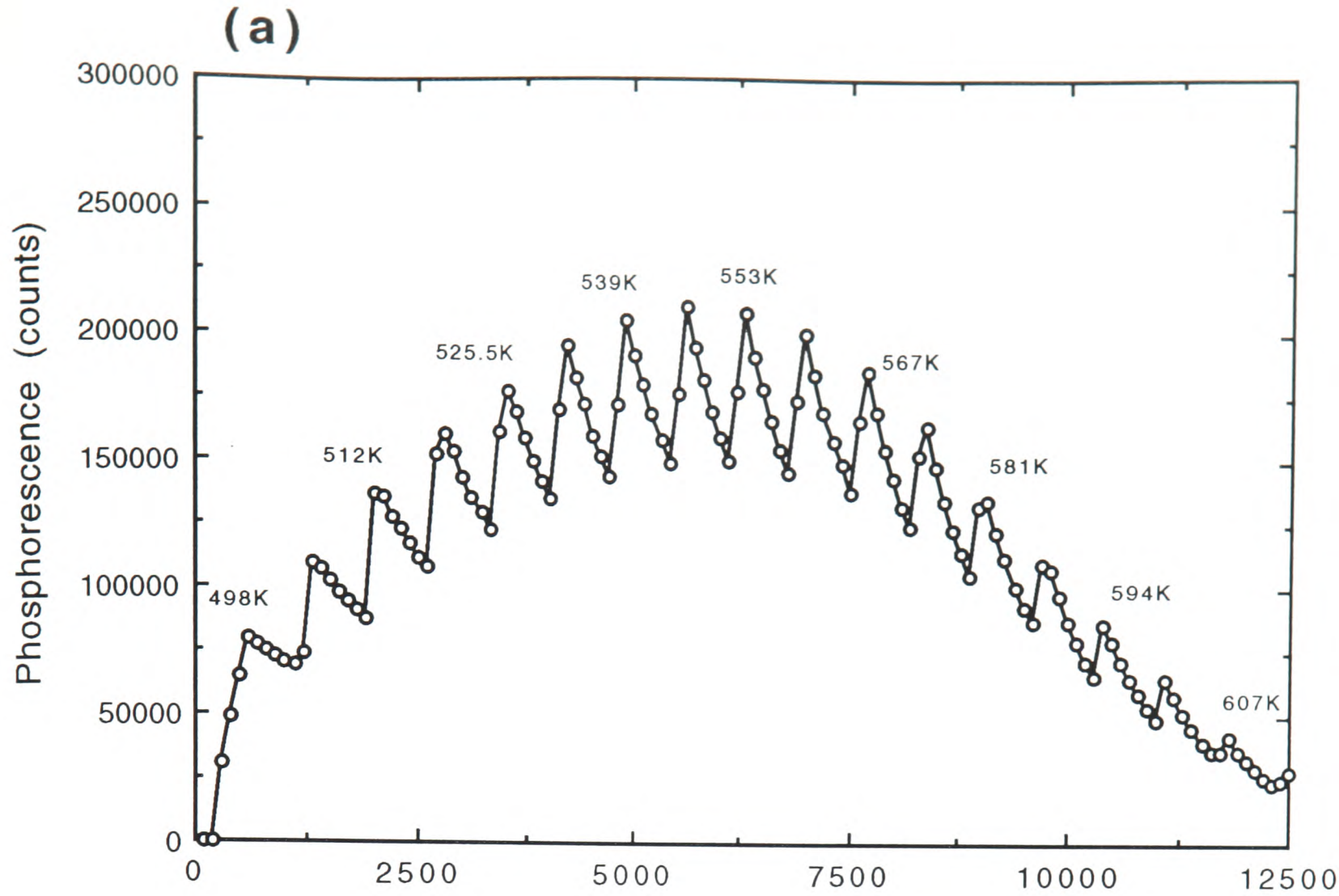


Fig.5.5.4.3.2 Hoogenstraaten analysis for the five feldspar samples (see text for details). Sample 5. No.3062 microcline (run 2) received a preheat of 300 seconds at 260°C (the T_{max} data used here is taken from the glow curves shown in Fig.5.5.4.3.1.(a)). All other data shown here was collected following preheats of 60 seconds at 220°C.

5.5.4.4 ISOTHERMAL DECAY AT 0.01 K/s

The isothermal decay method was attempted, in spite of its presumed inapplicability to this sample on account of the strong retrapping displayed (see for example section 5.5.4.2). However, instead of the "usual" mode of application, in which the sample is raised to a set temperature at which the phosphorescent decay is measured, with repetitions at different temperatures on different portions of sample, a novel approach was attempted. Here, each individual isothermal decay curve was generated as a separate temperature step of a stepped ultra-slow heating (following a suggestion by Wheeler, (pers. comm. 1988)). The optimistic prospect was that such a stepped measurement through the isolated 380°C TL peak may produce reliable parameters because the strong preheating successfully eliminated lower temperature satellite TL peaks, and so removed the source of retrapping interference. A typical stepped glow curve for 5. No.3062 microcline is shown in Fig.5.5.4.4.1 along with the corresponding isothermals recorded until just past T_{max}. Unfortunately, the phosphorescent lifetimes at increasing temperatures did not produce a linear plot of ln(I) Vs $1/T(K^{-1})$, either due to there being a spectrum of trap lifetimes or significant self-retrapping or both. A log-log plot of phosphorescence intensity Vs time also failed to produce a linear result, and data was not recorded over a sufficiently long time to permit the use of tI(t) Vs ln(t) analysis (Kirsh and Chen, 1991). These complications prevented meaningful analysis of the isothermals, and so precluded the use of this approach. However, these results do offer further support to the hypothesis of a band of trapping energies centred on a mean energy.



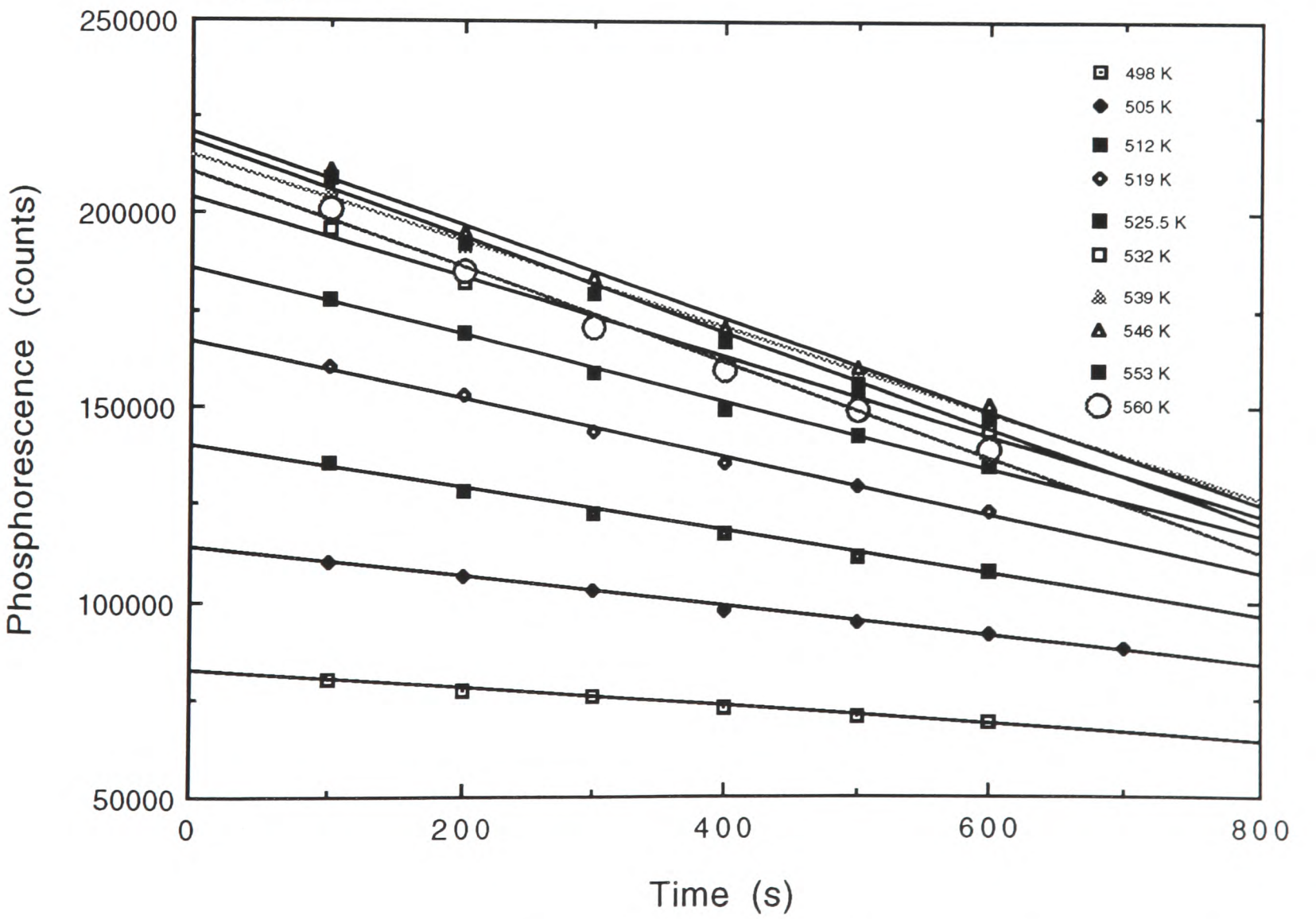


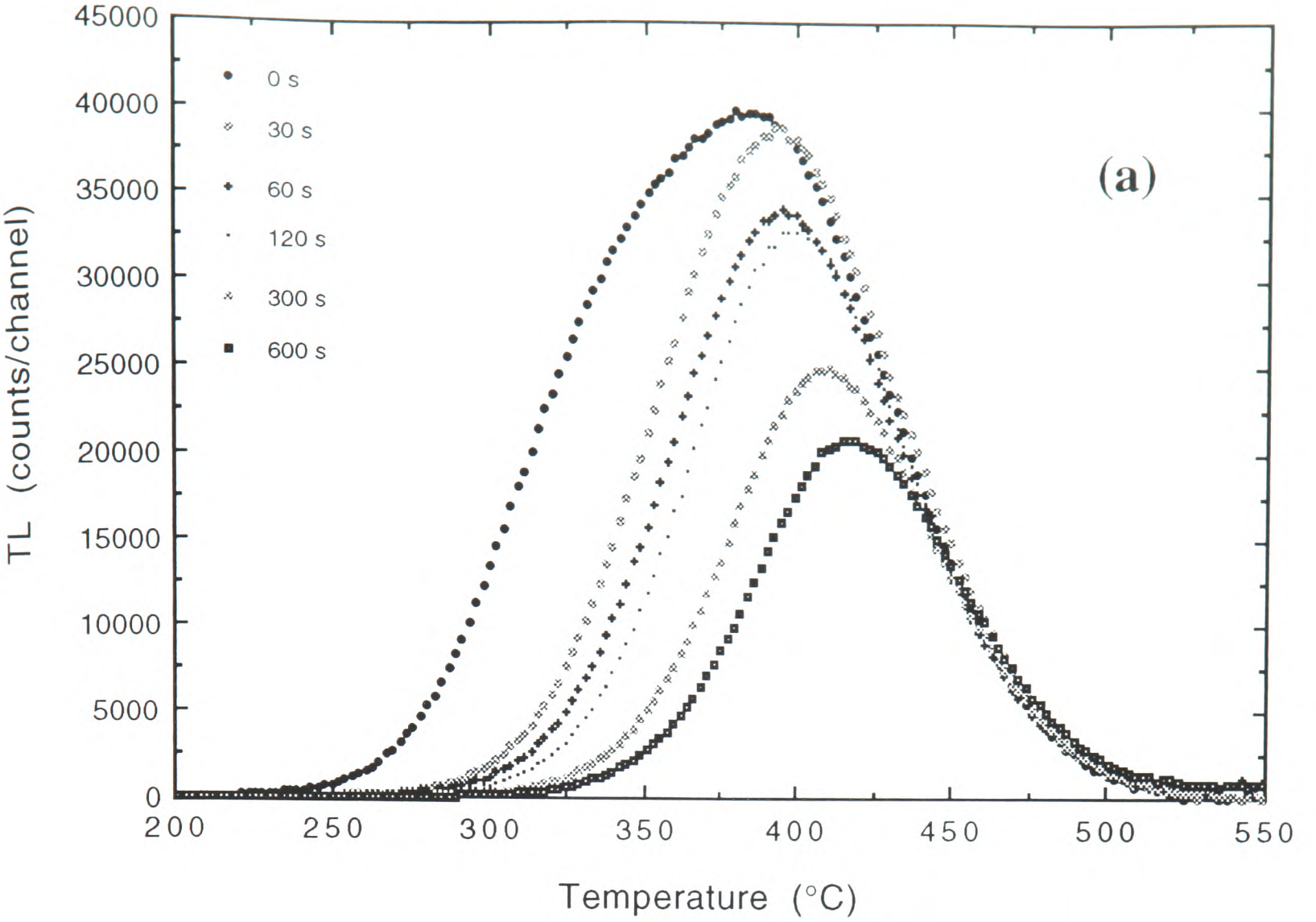
Fig.5.5.4.4.1.(a) The 380°C TL peak of 5. No.3062 microcline measured by the method of temperature-stepped isothermal decay. The ramp mean heating rate was 0.01 K/s with the temperature profile being a series of 8 K steps; the temperature at each step was held for 800 seconds, during which time the phosphorescence was measured to produce each isothermal. **(b)** A selection of the phosphorescence decay curves from which lifetimes were extracted. Unfortunately the data were not suitable for further analysis.

5.5.4.5 ANALYSIS OF THE 380°C TL PEAK FOLLOWING STORAGE AT 300°C: CHEN'S METHOD AND THE INITIAL RISE METHOD

Preceding work had revealed both the highly interactive nature of the kinetic processes occurring and the apparent complexity of the trap structure, in which a band of energies centred on a mean value seemed the most feasible model. Consequently, to investigate further the energetics of the 380°C TL peak, a final series of kinetic determinations on 5. No.3062 microcline were conducted, though now following the "hardest" preheats yet administered in this study: storage at 300°C for up to 600 seconds.

The intention was that this strong preheat would empty all trapping levels other than those at or deeper than the presumed mean trap depth; i.e., "cut" into the TL glow peak to enable initial rise analysis of TL at glow curve temperatures corresponding to the mean trap energy. However, given the possible occurrence of thermal quenching of this TL peak it was also determined to apply Chen's peak shape method (Chen, 1969a,b) to provide a second kinetic estimate from the same data. The applicability of Chen's method was anticipated for this data on the assumption that the strong preheats would successfully eliminate all lower temperature satellite TL peaks and so leave the 380°C TL peak "clean", as is essential for this method.

The glow curves measured for each of the various storage durations are shown in Fig.5.5.4.5.1.(a) and (b), along with the corresponding initial rise data fitted (see Table 5.5.4.5.2 for presentation of the results). Inspection of the TL glow curves shows the briefer preheats to be inadequate to eliminate the lower temperature (≈ 330°C) TL peak fully. Subsequent confirmation of this impression was given by the failure of Chen's



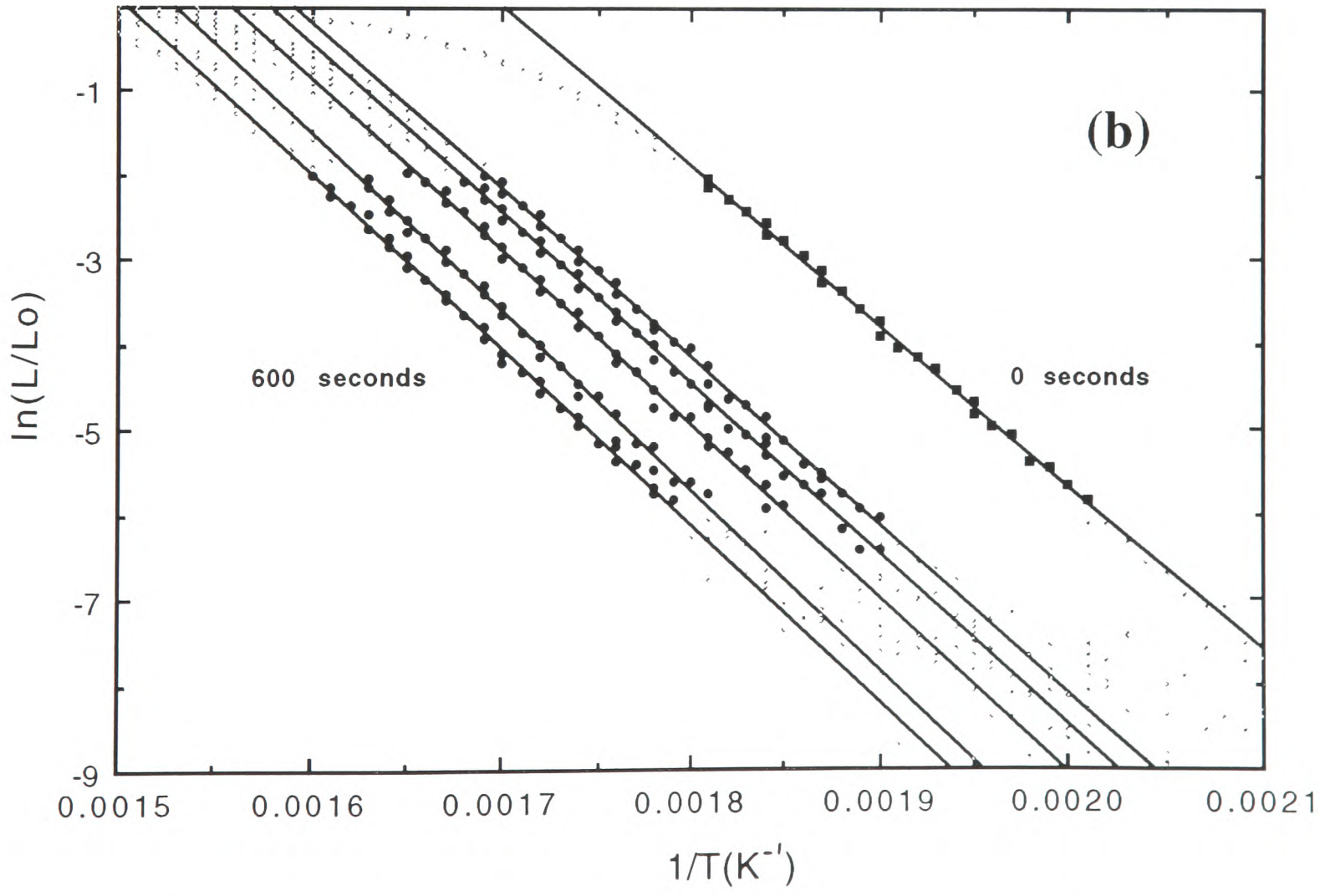


Fig.5.5.4.5.1.(a) Glow curves of 5. No.3062 microcline following various storage durations at 300°C. Note the early erasure of the 330°C TL peak, and that even after the longest storage the higher temperature side of the glow curve is unaffected. **(b)** The initial rise portions of each glow curve overlain by the data fitted to extract trap parameters.

method to produce realistic results for these glow curves - not until the preheats exceeded 120 seconds did the calculated parameters become reasonable (see Table 5.5.4.5.1). Finally, regardless of the kinetic findings, simply the survival of a significant residual TL peak following 600 seconds storage at 300°C demonstrates that this peak possesses great thermal stability.

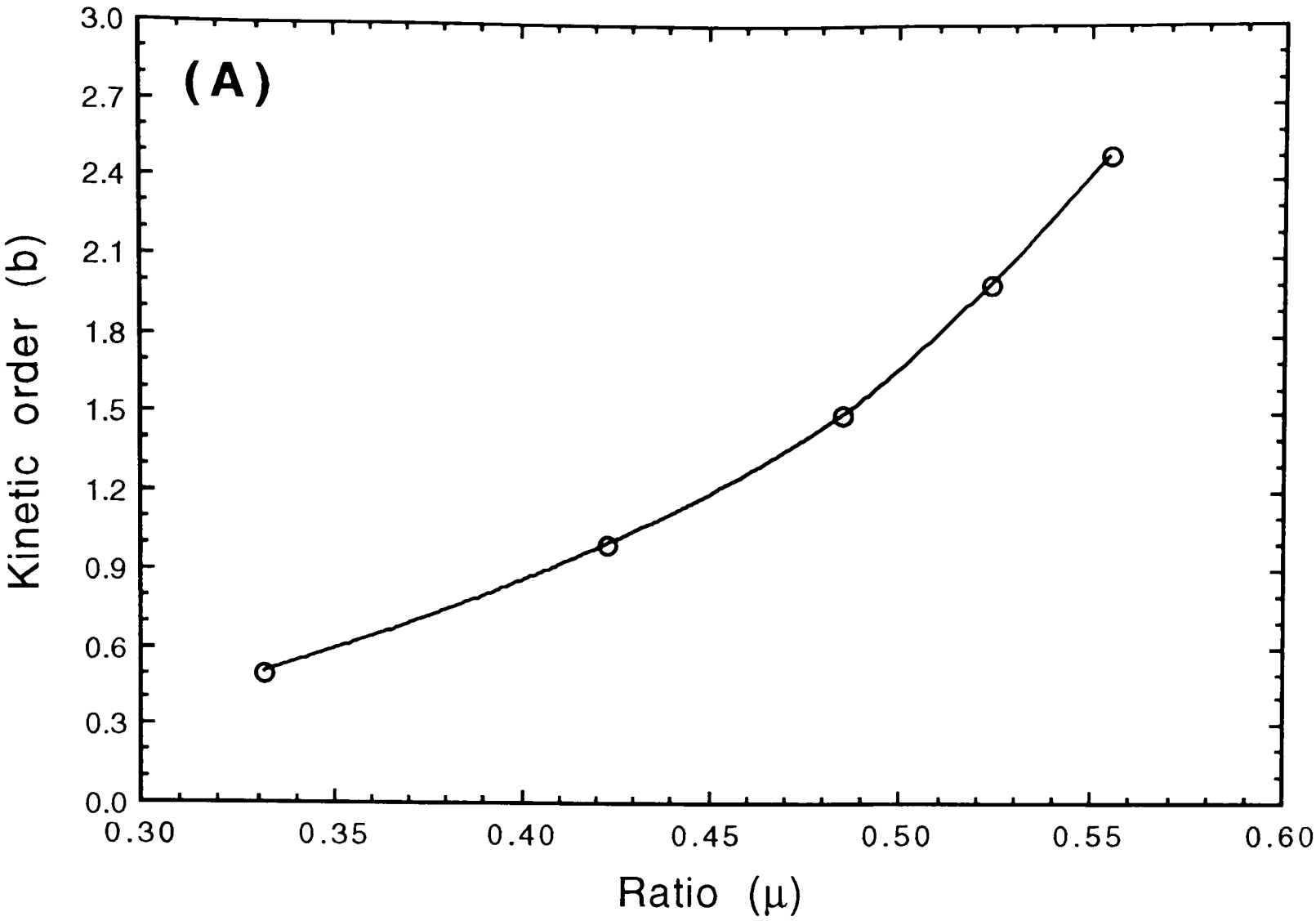
The version of Chen's formula used was based on the FWHM (ω) for the activation energy, to minimise the errors of precision associated with measuring the TL peak widths (shown below, see Table 5.5.4.5.1 caption for definitions of terms).

$$E_{activation} = \frac{A_\omega k T_m^2}{\omega} - B_\omega 2kT_m$$

PH time (s)	T_m (°C)	T_m (K)	ω	δ	τ	μ (δ/ω)	b	A_ω	E ± ΔE (eV)	S (s^{-1})	ΔS/S	$\tau_{20,C}$ (s)	(ka)
0	385	658	123.5	51.5	72	0.417	1.0	2.45	0.63 ± 0.23	4.49 x 10^3	2.05	1.34 x 10^7	4.26 x 10^{-4}
30	393	666	92.5	47.5	45	0.514	1.9	3.44	1.31 ± 0.23	1.21 x 10^9	2.02	2.46 x 10^{13}	7.81 x 10^2
60	395	668	88	46	42	0.523	2.0	3.52	1.42 ± 0.23	9.32 x 10^9	2.01	3.21 x 10^{14}	1.02 x 10^4
120	399	672	85	45	40	0.529	2.1	3.59	1.53 ± 0.23	5.23 x 10^{10}	2.01	3.63 x 10^{15}	1.15 x 10^5
300	408	681	79	43	36	0.544	2.3	3.73	1.77 ± 0.23	2.59 x 10^{12}	1.99	1.06 x 10^{18}	3.35 x 10^7
600	417	692	80	42	38	0.525	2.0	3.73	1.80 ± 0.23	2.86 x 10^{12}	1.98	3.86 x 10^{18}	1.22 x 10^8

Table 5.5.4.5.1 The determination of kinetic parameters using the method of Chen (1969a,b) based on the TL peak FWHM. The glow curves of 5. No.3062 microcline were measured following various storage durations at 300°C. Lifetimes were calculated using the kinetic orders tabulated above. δ and τ are respectively the high and low temperature wings of the FWHM. A_ω derives from the "triangle assumption" (Chen, 1969a), and B_ω accounts for the temperature dependence of S and is assumed to be unity here.

The parameters ω, δ and T_m were measured from the glow curves (see



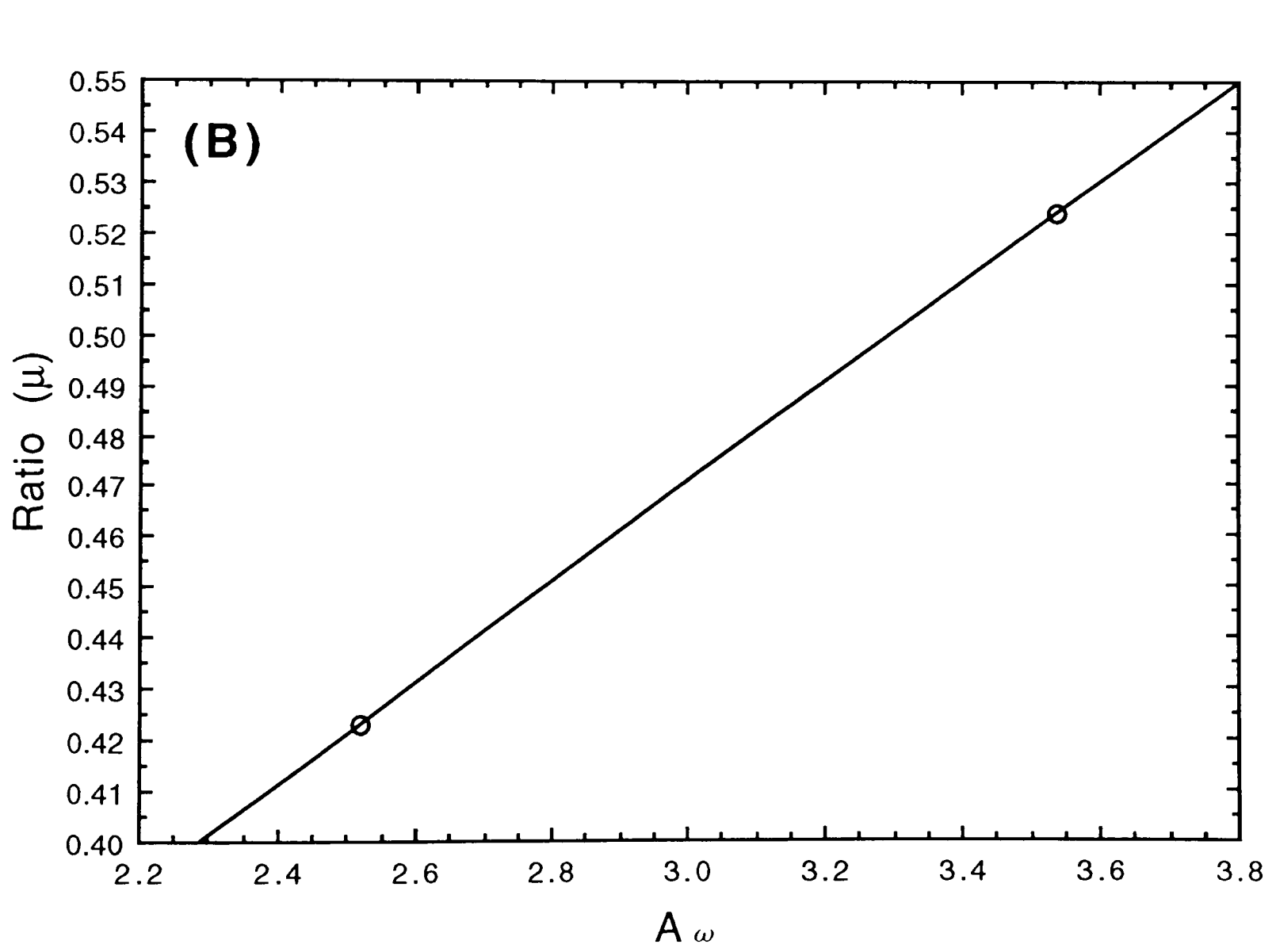


Fig.5.5.4.5.2.(A) The kinetic order b and **(B)** the parameter A_ω (Chen, 1969a) are shown as functions of the shape parameter μ.

Fig.5.5.4.5.1.(a)), μ is the ratio δ/ω and τ found from ω and δ. The ratio μ was then used to determine b and A_ω by interpolation from Figs.5.5.4.5.2.(A) and (B) respectively. These parameters and the derived E and S values are presented in Table 5.5.4.5.1.

While the shorter preheat times give clearly unrealistic lifetimes, due to interference from lower temperature satellite peaks, the results from the two longest preheats are in very good agreement with those from the initial rise analysis.

Preheat Temperature 300°C								
PH time (s)	E ± ΔE (eV)	T_m (°C)	T_m (K)	S (s^{-1})	ΔS/S	S 1st order (s^{-1})	$\tau_{20°C}$ (s)	$\tau_{20°C}$ (ka)
0	1.638 ± 0.017	340	613	6.92 x 10^{12}	0.58	7.36 x 10^{12}	2.17 x 10^{15}	6.87 x 10^{4}
30	1.720 ± 0.018	393	666	2.17 x 10^{12}	0.57	2.32 x 10^{12}	1.77 x 10^{17}	5.62 x 10^{6}
60	1.742 ± 0.018	395	668	2.93 x 10^{12}	0.57	3.13 x 10^{12}	3.14 x 10^{17}	9.95 x 10^{6}
120	1.762 ± 0.023	399	672	3.46 x 10^{12}	0.64	3.69 x 10^{12}	5.88 x 10^{17}	1.86 x 10^{7}
300	1.829 ± 0.030	408	681	7.34 x 10^{12}	0.72	7.81 x 10^{12}	3.94 x 10^{18}	1.25 x 10^{8}
600	1.795 ± 0.021	419	692	2.40 x 10^{12}	0.60	2.56 x 10^{12}	3.14 x 10^{18}	9.93 x 10^{7}

Table 5.5.4.5.2. The initial rise method applied following various durations of storage at 300°C. The value for S determined by assuming second order kinetics was used in the lifetime evaluations as being a better approximation to the real situation, note that use of the first order S reduces the lifetimes insignificantly (by < 5%).

The initial rise trap depths and lifetimes follow a trend of increasing with increasing preheat duration, with even the briefest preheat leaving a TL residual

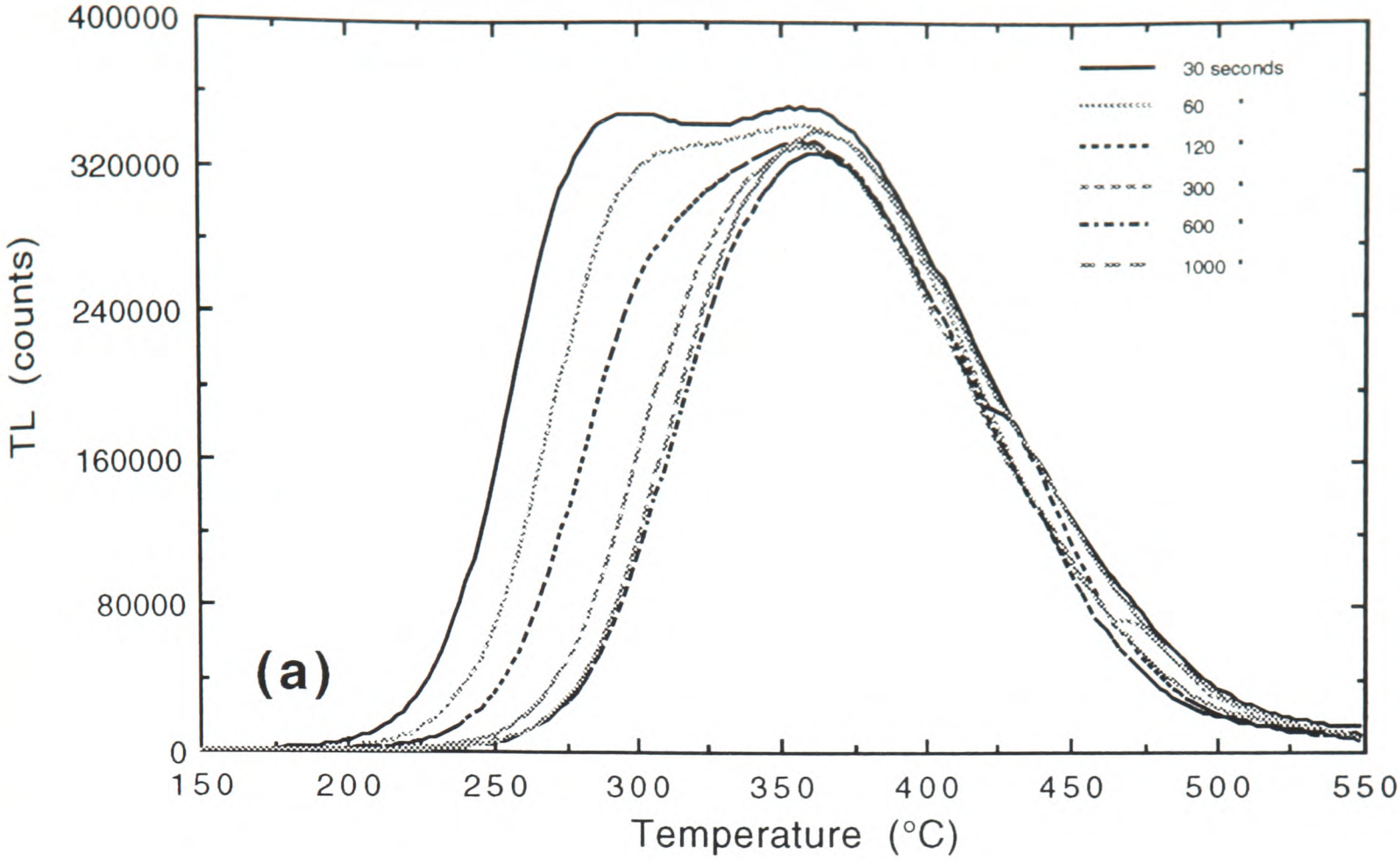
sufficiently stable to make dose saturation rather than thermal stability the limiting parameter on the useful dating age range of this TL peak (assuming the absence of other interferences). It is concluded from the above that a spectrum of trap depths is associated with the 380°C TL peak, and that preheating permits choice of residual stability. Indeed, the entire 380°C TL peak structure has thermal stability greatly in excess of the minimum requirements for archaeological dating, although this optimistic result must be qualified with the caveat that nothing in these measurements permits conclusions to be drawn regarding either the presence or effect of "long-term" fading.

5.5.5 SOME TRAP PARAMETERS OF SCANDINAVIAN FELDSPAR Z10b

Following the determination of the trap parameters for 5. No.3062 microcline, it remained to demonstrate that these values, having been determined from a single-crystal museum specimen, were concordant with the parameters of natural coarse-grain sedimentary potassium feldspars. To verify this was in fact the case a series of initial rise analyses were performed on the < 2.58 g/cm^3 coarse-grain fraction of a natural Scandinavian sediment, Z10b, kindly provided by V. Mejdahl.

A range of storage durations at 220°C were selected, so as to provide information on the NTL over a wide temperature range. These preheats, and subsequent TL measurements, were performed using a Risϕ automated TL reader (with an EMI 9635Q PMT and Corning 7-59 and Chance-Pilkington HA3 filters).

The glow curves measured are shown in Fig.5.5.5.1.(a), and the initial rise portions of the glow curves overlain with the fitted sections are shown in (b). The kinetic



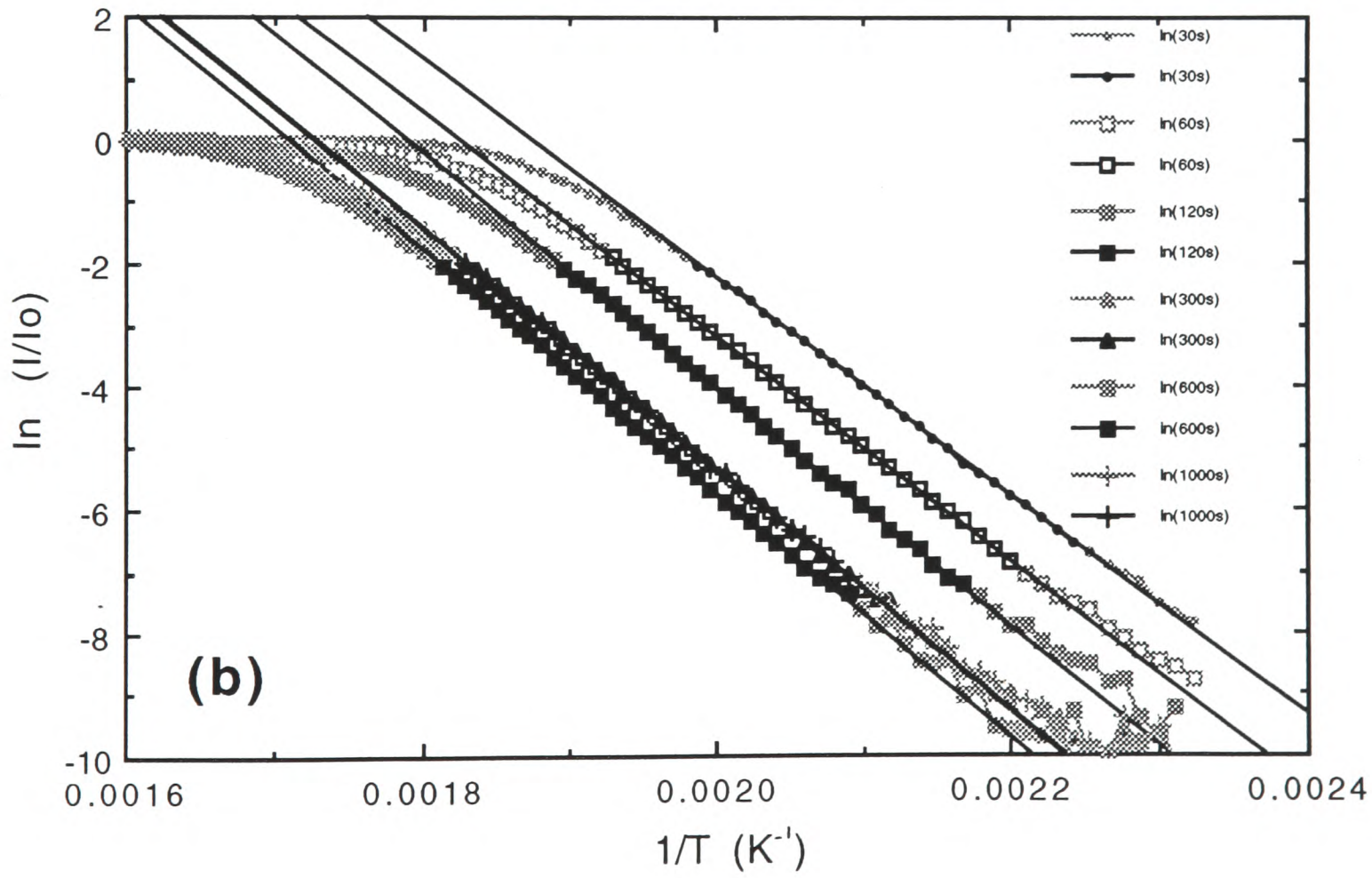


Fig.5.5.5.1.(a) The glow curves of sample Z10b (< 2.58 g/cm^3 coarse grain fraction extracted from Scandinavian sediment) following various storage durations at 220°C. The irregularities on the high temperature sides of several glow curves are system artifacts. **(b)** The initial rise portions of each glow curve overlain with the data fitted for each glow curve to determine trap parameters. The sedimentary origins of this sample prevent attribution of the glow curves to any particular mineral outcrop, or even species.

parameters evaluated from these curves are given in Table 5.5.5.1.. Values are in generally close agreement with those found for 5. No.3062 microcline (Table 5.5.3.1), from which it is concluded that the same defects are giving rise to the corresponding TL peaks in each sample, and consequently it is inferred that the values determined from 5. No.3062 microcline can be validly extrapolated to natural sedimentary feldspars.

Preheat Temperature 220°C								
PH time (s)	E ± ΔE (eV)	T_m (°C)	(K)	S (s^{-1})	ΔS/S	S 1st order (s^{-1})	$\tau_{20°C}$ (s)	(ka)
30	1.534 ± 0.003	292	565	1.26 x 10^{13}	0.36	1.34 x 10^{13}	1.94 x 10^{13}	6.15 x 10^{2}
60	1.576 ± 0.004	305	578	1.41 x 10^{13}	0.37	1.50 x 10^{13}	9.12 x 10^{13}	2.89 x 10^{3}
120	1.659 ± 0.005	310	583	5.82 x 10^{13}	0.39	6.17 x 10^{13}	5.92 x 10^{14}	1.87 x 10^{4}
300	1.694 ± 0.006	360	633	7.03 x 10^{12}	0.38	7.49 x 10^{12}	1.96 x 10^{16}	6.20 x 10^{5}
600	1.706 ± 0.006	358	631	9.81 x 10^{12}	0.39	1.04 x 10^{13}	2.26 x 10^{16}	7.15 x 10^{5}
1000	1.685 ± 0.005	363	636	5.08 x 10^{12}	0.36	5.41 x 10^{12}	1.90 x 10^{16}	6.02 x 10^{5}

Table 5.5.5.1. The initial rise method applied to Scandinavian sedimentary extract Z10b, following various durations of storage at 220°C. Second order kinetics are used in the lifetime evaluations (see caption to Table 5.5.4.5.2).

5.6 DISCUSSION AND SUMMARY

The preceding chapter examined the short term anomalous fading in the feldspar minerals and conclusively demonstrated that such fading is not treatable by any laboratory means. This chapter investigated the thermal stability of the IRSL signal and leads to a

guardedly optimistic conclusion: although the IRSL signal has been shown to originate from the trapped charge population associated with a range of TL glow peaks, great lifetimes with regard to thermal stability have been found for some of these. Furthermore, isolation of these TL peaks can be obtained by convenient preheats. (It can be seen from Table 5.5.4.5.2 that a simple ramping at 5 K/s to 300°C is sufficient to leave only TL possessing lifetimes in excess of 1 Ma; similarly, brief durations at 220°C (> 2 minutes) or at 260°C (> 20 seconds) will suffice).

The issue of the stability of feldspar luminescence signals has been approached here through an investigation of the trap energetics, and as two separate studies: (1) determination of trap depths by combined optical and thermal techniques, and; (2) kinetic measurements of an isolated IRSL source population.

The principal findings for the IRSL source traps are:

(1) optical resonance energy (1.44 ± 0.01 eV) + excited state depth (0.278 ± 0.004 eV) ≈ thermal trap depth (≈ 1.72 ± 0.01 eV, the approximate best-estimate for the thermal trap depth, as the range of values spans ≈ 1.68 - 1.82 eV)). It is therefore concluded that there is no clear evidence for untrapping processes requiring either greater photon energies than the thermal trap depth (see Mott and Gurney, 1953), or less than the measured available energy sum.

(2) thermal trap depths determined for the higher temperature (≈ 380°C) TL glow peaks of a microcline by kinetic means are sufficiently deep for use in dating applications. These large trap depths are found consistently and are independent of the kinetic method applied; it is therefore concluded they represent the true trap depths, so comprehensively precluding thermal instability as the cause of age shortfalls.

Agreement between the optical and thermal trap depths *per se* is interpreted as

strongly validating the trap parameters, and so also the calculated lifetimes. The crucial assumption here is that in the application of kinetic methods to estimating lifetimes on timescales of use to luminescence dating there are no processes occurring which remove trapped charge other than the thermal loss accounted for in the lifetime determination. Whether this assumption holds is not verifiable except through the dating of carefully selected known age samples. The value of this work is that it is unlikely there are any unrecognised processes operant which *extend* the lifetime beyond that estimated from kinetics, hence a TL peak designated kinetically as unstable is unlikely to prove useful for dating on closer examination. Kinetic studies are therefore a useful means of eliminating "marginal contenders" as dating signals and enabling better targeting of effort onto signals likely to prove useful. This is the rationale for their application here and intrinsically a strong justification for directing this effort towards kinetic measurements - the definitive rejection of the 280°C TL peak as anything other than a short range dating signal illustrates this.

Turning to the question of long-term trapping stability raised by the existence of the "IRSL" pathway: does it offer an energetic shortcut through which electrons can "leak" over long timescales? Simply, if the excited state-to-ground state transition probability is << than the probability of thermal detrapping from the excited state at ambient temperatures, then the electron remains in the excited state until it detraps, and so the electron only has to reach the excited state to detrap. Under these conditions the ground-to-excited state transition energy of ≈ 1.44 eV represents the effective thermal depth of the trap regardless of the depth below the conduction band of the excited state. The means of testing this hypothesis alluded to in section 5.5.4.3 is simply the determination of kinetic parameters, particularly by the method of heating rate variations in which the

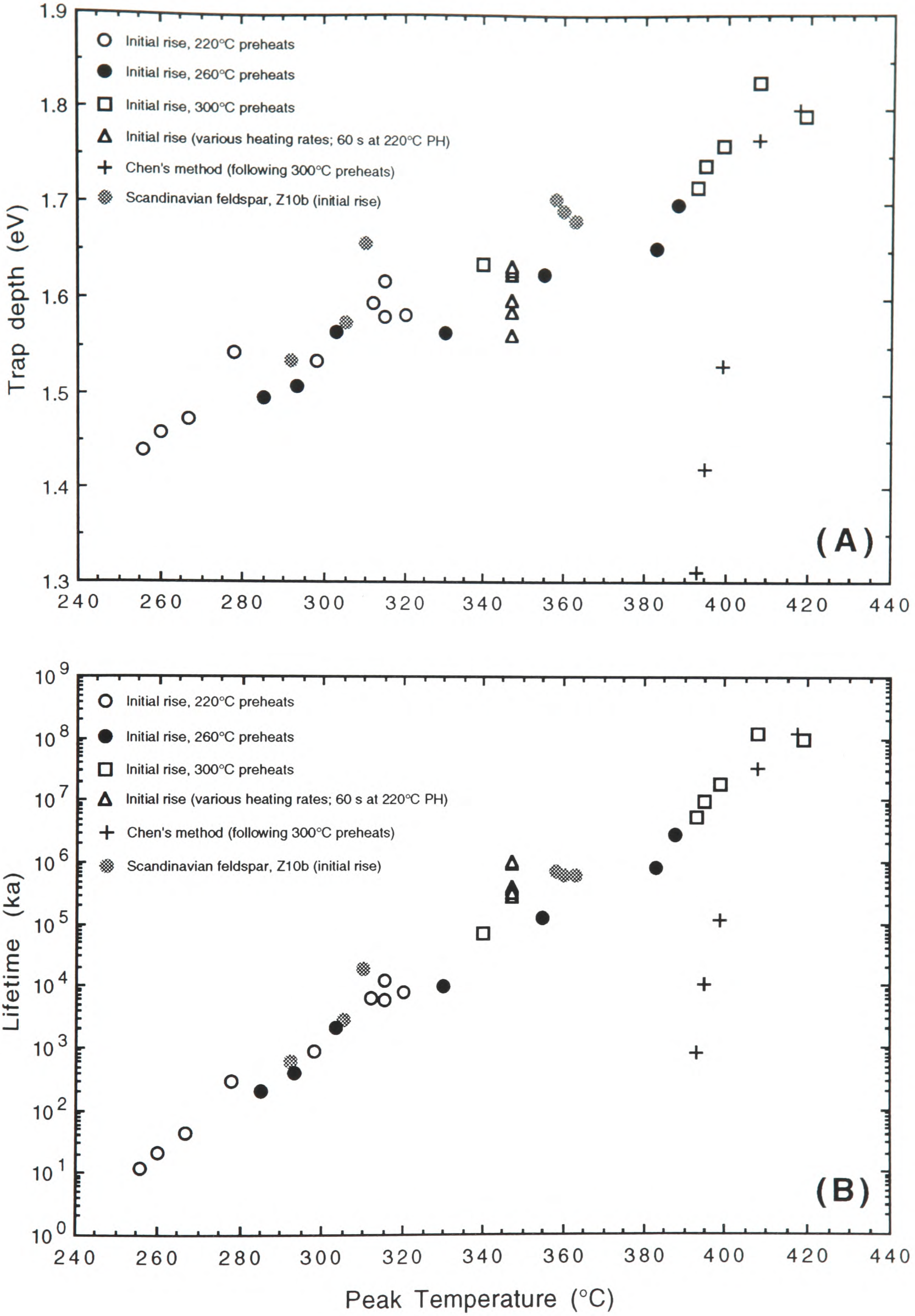


Fig.5.6.1.(A) The trap depths E (eV) for 5. No.3062 microcline are shown plotted against T_{max} of the corresponding TL peaks. **(B)** The lifetimes at 20°C calculated using the trap depths given in (A) along with the corresponding S values tabulated earlier.

samples are maintained at elevated temperatures for substantial periods of time - more than sufficient to permit each electron many attempts to reach the excited state and so detrap. This leads to the crucial inference that as there is no "step" or "plateau" in either of Fig.5.6.1.(a) or (b) then the electrons are effectively not "seeing" the excited state during thermal detrapping. Furthermore, from the deduction that the probability of detrapping from the excited state is << than that of retrapping, the electrons must reach the conduction band with a single phonon absorption step during thermal untrapping. It is therefore inferred that the excited state plays no role in reducing the effective total trap depth for thermal detrapping, and thus appears not to offer any pathway for thermally activated charge leakage over archaeological timescales. It therefore seems unlikely, fortunately, that thermal detrapping from "IRSL-capable" traps via the excited state is related to the long-term fading.

Considering the long-term fading problem from a different perspective: a serious concern must be reiterated: that of inadvertent bleaching in the laboratory. The bleaching susceptibility of the IRSL signal is seen in Fig.5.2.4.1.(a)-(e) to exceed that of the quartz 325°C TL peak by an order of magnitude at red wavelengths (Spooner, 1987 and Spooner *et al*, 1988). Furthermore it is noted that these wavelengths are precisely those which have moved into favour as laboratory "safelighting" in the past decade. This concern must not be understressed and it is the opinion of the author that inadvertent bleaching in the laboratory of the feldspar luminescence may contribute to a considerable proportion of the age underestimations found using these minerals.

Finally, with respect to coarse-grain K-feldspars, aside from the demonstration of *apparent* long-term fading by Mejdahl (1988 and 1989), no cases exist in which the presence of subsequently recognized complicating factors such as internal self-absorption

of luminescence could not offer a probable solution to that specific case (the conclusions of Mejdahl (1988 and 1989) require re-evaluation in this light). It is here speculated that unrecognized additional effects such as inadvertent bleaching in laboratories or dose-rate effects may in combination account for the problems. Further work is needed.

A question is raised when the apparent stability found from the kinetic results is set against the perception that feldspar luminescence (from fine-grains at least) is unstable over long timescales: can kinetic methods reveal anything further relevant to the 100 ka limit problem, as the conclusions here that some feldspar signals far exceed the stability required for dating *appears* to conflict with observation? The likelihood is that all the kinetic methods are correctly measuring the total trap depths, but that unidentified factors prevent the retention of trapped charge over the timespans potentially available from these traps. This prospect is further investigated in chapter 6.

It is concluded that there are no identified fundamental physical properties precluding the use of feldspars from optical dating applications. However, this optimistic conclusion must be tempered by recognition that the "long-term" fading phenomenon remains ill-defined, though with the pessimistic possibility that it is the manifestation of generally occurring long-term tunnelling processes. Only tentative steps have been possible here in the search for a solution to the problem, and the setting of definitive criteria (such as monitoring for tunnelling-type fading) has been attempted; hopefully this should ensure the future collection of data from which a solution may be forthcoming. Failing this, the applicability of optical dating to older feldspathic materials must be reviewed.

CHAPTER 6 SOME INVESTIGATIONS ON LONG-TERM STABILITY

6.1 INTRODUCTION

Previously in this work the stability of luminescence from feldspars has been examined from the perspectives of either well-known fading mechanisms or as a consequence of thermal instability. In this chapter a dating study aimed at breaching the "100 ka" limit is described. From this starting point a range of possible contributors to the observed dating age limitations are investigated. These include a hypothesis that multiple excited states exist, so providing a pathway by which electrons can "leak" from traps over geological timespans (a dating test using a loessic sample tested this). Following this, a range of complementary investigations are also reported, particularly into the nature of the "build-up" effect seen from some samples under short exposures to IR (Spooner and Questiaux, 1989), and also the potential for the "long range" limit in feldspathic dating to be caused by a dynamic equilibrium between accumulation of trapped charge and bleaching of the IRSL signal by environmental blackbody radiation.

6.2 AN ATTEMPT AT LONG RANGE OPTICAL DATING USING POLYMINERAL FINE GRAIN MATERIAL

Following the proposal and demonstration of dating using IRSL by Hütt *et al* (1988), the possibility was opened that this "new" signal may be free of the unknown effects giving rise to the "100 ka" limit. To test this hypothesis the 4-11 μm fraction of a loessic sample from Achenheim, France, was dated in a study in which a range of

experimental parameters offering prospects for circumventing the age limit barrier were varied. That work is described in Spooner and Questiaux (1989) and the variables tested were : (1) stimulation wavelength (514.5 nm and 880 ▲ 80 nm); (2) emission wavelength; (3) duration of preheat at 160°C; (4) energy deposited during measurement. Principal conclusions were that no combination of preheat duration and temperature, emissions monitored (spanning the effective detection range of the bialkali type EMI 9635Q PMT used) or stimulation wavelength (IR or green) enabled the 100 ka barrier to be convincingly breached using IRSL or OSL.

An additional parameter considered was that of inadvertent bleaching in the laboratory. Given the potential bleaching of the IRSL signal under exposure to any visible wavelengths (from a consideration of Hütt *et al* (1988) and Krϕnborg (1983)), the laboratory safe-light illumination was revised before this work was commenced. The optical response spectra of Hütt *et al* (1988) and the bleach spectrum of the 330°C TL of K-feldspar by Krϕnborg (1983), when considered against the spectral sensitivity of the human eye, indicated that no region of the spectrum was truly "safe", and that "safelighting" (perhaps more appropriately "minimum-damage lighting") could at best only be optimised to minimise the damage of inadvertent bleaching during laboratory work. Consequently, physiological considerations led to the introduction of low pressure sodium-lamp-based safelighting for all work involving feldspathic materials. The dominant emission line of these lamps, ≈ 589 nm, is close to the peak visual response wavelengths of the human eye (≈ 555 nm) yet not so short as to present a serious bleaching hazard from brief exposures (see Fig.5.2.4.1.(a)-(e)). The rationale then is that the greater sensitivity of the eye to 589 nm light over red light permits the use of much lower power densities, hence the bleaching rate under minimum visibility conditions of Na light is less

than that under corresponding red illumination. The above work was performed under ultra-low intensities of sodium light, so eliminating inadvertent bleaching as a significant factor contributing to the age underestimates in this case.

It was concluded from the failure of any of the tested combinations of experimental conditions to reasonably approach geological expectation that optical dating of fine-grain feldspathic materials was subject to a similar, apparently fundamental, age range limitation to that reported by Debenham (1985) and Wintle (1985) for the TL of fine-grain samples (see section 1.4.1). Additionally, in spite of the publication of TL ages from coarse grain K-feldspar of up to ≈ 250 ka (Balescu and Lamothe, 1992), the results of Mejdahl (1988 and 1989) invite speculation as to the existence of an upper age limitation for all feldspars, lower than that predicted from kinetic studies and regardless of grain size or composition. Some phenomena capable of giving rise to such general age shortfalls are investigated in the following sections.

6.3 CIRCUMVENTION OF FADING OF IRSL BY CHOICE OF STIMULATION WAVELENGTH - A DATING TEST OF THE SINGLE-EXCITED-STATE HYPOTHESIS

6.3.1 INTRODUCTION

The original work of Hütt *et al* (1988) presented a model for the detrapping mechanism governing IRSL: absorption of an IR photon raised a trapped electron to an excited state just below the conduction band, from where it promptly detrapped thermally to the conduction band. Two excited levels were proposed to account for the apparent

structure of the resonance absorption peak (observed there in microcline and unspecified K-feldspar). These excited levels were attributed energies above the ground state of 1.33 eV and 1.43 eV, corresponding to the resonance peaks at 932 nm and 866 nm respectively (no frequency factors were given).

In a later refinement to this model it was hypothesised (Hütt, pers. comm. October, 1990) that the two excited levels were not present in the same trap, but were each the single excited state of two separate but similar trap types. Furthermore, traps containing the shallower of these excited states were subject to thermal fading via this excited state over a lifetime too short for use in dating (assuming an S value of 10^{12} s^{-1} for the 1.33 eV ground state-to-excited state gap gives a lifetime at 10°C of $\approx$ 15.0 ka before the excited state is reached, and that same lifetime for the trap if all electrons reaching the excited state detrap). Consequently, thermal fading was predicted to erode, slowly, the 932 nm stimulable signal and maintain dynamic equilibrium with irradiation in the environment, so precluding the use of this signal for dating and possibly explaining some observed cases of age shortfall.

However, this hypothesis referred solely to the 932 nm stimulable signal and considered the 866 nm stimulable signal to be sufficiently stable for dating (assuming S $\approx 10^{12}$ s^{-1}, as above, gives a lifetime at 10°C of $\approx$ 902 ka). To perform successful dating therefore necessitated separating the two signals; implicit in the hypothesis were two means of doing so. First, by a preheat tailored to leave the 866 nm stimulable signal largely untouched while emptying the shallower, 932 nm stimulable traps, and second, by precise "tuning" of the stimulation wavelength to the resonance wavelength of the desired trap type (866 nm stimulable). (Hütt recommended the use of a narrow-band IR source with an optimum wavelength of $\leq$ 860 nm, provided by, for example, an IR laser diode).

Finally it was also proposed by Hütt that a procedure involving substantial delay at room temperature followed by measurement using short exposures only was necessary to obtain correct dates, ie, routines using raised temperature storage and long exposures for measurement may produce erroneous results.

If valid, these hypotheses were clearly of great importance to the successful use of IRSL for dating, and two series of experiments were conducted to test them. The first investigated the bleaching of the NTL of an old loess and the ATL of a characterised feldspar sample by two different wavebands of IR, while simultaneously recording the emitted IRSL. The second was the dating of a younger loess using various combinations of IR stimulation wavelength, delay at ambient temperature, differing preheat conditions and short and long measurement IR exposures. Both experiments are described below.

6.3.2 IRSL LIGHT SUMS AND TL BLEACHING - EFFECT OF DIFFERENT IR WAVELENGTHS

A consequence of the above hypothesis is that different light sums should be observed when different stimulation wavelengths are used, (as each wavelength would be expected to probe only those traps containing susceptible excited states). This prediction was tested using an old loess (lab. ref. 722t1, from Achenheim, France, expected age ≈ 220 - 320 ka), and 11. Z6 orthoclase (from the RLAHA mineral collection). The two wavebands selected, 831.8 ∆ 12.8 nm from a xenon lamp set (Spooner and Questiaux, 1989) and 950 ∆ 80 nm (from IR LED's), were at the lower and upper wavelength limits of the optical response resonance peak respectively, in order to minimize overlap of stimulation photon energies and so probe the discrete trapping levels, if they exist. These

wavebands are shown in Fig.6.3.2.1.

The old loess was chosen in the expectation that the natural signal would be dominated by the stable 866 nm-stimulable signal, with the supposedly unstable 932 nm-stimulable traps relatively empty due to thermal fading; dosing should then induce a relatively significant 932 nm component for comparison. The orthoclase was included as a known pure K-feldspar; added β doses were ≈ 200 Gy, followed by a preheat of 60 seconds at 220°C. The measurement routine comprised an initial short exposure using one of the two IR stimulation wavebands, followed by a long (bleaching) exposure using the other IR stimulation waveband, and finally another short exposure with the first IR stimulation waveband. Measurements were made at 20°C, and emissions detected using an EMI 9635Q PMT with Corning 7-59 and 2 mm Schott BG 39 filters; correction was made for detection geometry.

The remanent IRSL values (shown in Table 6.3.2.1) lead to two conclusions: firstly, both IR wavebands significantly bleach the signal probed by the other waveband (the different remanent levels reached are explicable by the lower bleaching efficiency of the 950 nm waveband as shown in Figs.5.2.4.1.(a)-(e)) demonstrating that clear resolution between the hypothetical two excited states by choice of stimulation wavelength is not possible; secondly, the ratios are unchanged for both natural and additive dose cases, contrary to the expectation of a lower proportion of the 932 nm-stimulable signal in the natural sample.

Sample	Treatment	Exposure sequence			Remanent IRSL
		Initial (short)	Long exposure	Final (short)	Final(short) /Initial(short)
722t1	N	831 nm	950 nm	831 nm	0.28
722t1	N	950 "	831 "	950 "	0.03
722t1	N+β+PH	831 "	950 "	831 "	0.26
722t1	N+β+PH	950 "	831 "	950 "	0.03
Z6	β+PH	831 "	950 "	831 "	0.26
Z6	β+PH	950 "	831 "	950 "	0.04

Table 6.3.2.1 The remanent IRSL following long exposures (1200 seconds duration, totalling ≈ 2.4 J of 831 nm and 12 J of 950 nm IR respectively).

The above data are consistent with the IRSL originating from one species of trap possessing a single excited state. A second, related, experiment compared the IRSL light sums observed, from the undosed loess, during long exposures to IR and the remanent TL measured following these exposures to confirm that the same total trapped charge population was being measured. The long exposures were of 5000 seconds duration, totalling ≈ 10 J of 831 nm IR and ≈ 50 J of 950 nm IR respectively.The normalized NTL, residual TL and IRSL light sums are given in Table 6.3.2.2, along with the ratio, Q, of IRSL to TL removed by the long exposures. Apparatus were as described above and correction was made for detection geometry.

Exposure waveband	IRSL - background (counts)	Residual TL (counts)	$Q - \frac{\text{IRSL}}{\text{NTL} - \text{Residual TL}}$
831.8 Δ 12.8 nm	8.672×10^6	3.862×10^6	3.66
950 Δ 80 nm	8.498×10^6	3.872×10^6	3.60
no bleach	-	NTL = 6.235×10^6	-

Table 6.3.2.2 The light sums observed following long exposures to these IR wavelengths, and the fractional excess of IRSL observed over TL removed by the bleaches from old loess sample 722t1.

The concordance of the light sums resulting from stimulation by either waveband was interpreted as confirming that both were untrapping only the same trapped charge population. To illustrate this, the TL removed (= NTL - residual TL) by 831.8 nm exposure and 950 nm exposure are shown overlain in Fig.6.3.2.2; there are no significant differences between the TL removed by these wavebands.

It was noted that quantitative comparison between the IRSL lightsums and the lightsums of the TL removed by the exposures gave the same ratio of ≈ 3.6 for both stimulation wavebands (within errors estimated at ≈ 5 %). Two possible explanations for the IRSL lightsum exceeding that of the bleached TL are that the TL has a proportion of its emissions lying outside the detection waveband, or that thermal quenching is present. (This latter explanation is of relevance to the assessment of the kinetic data obtained previously by the method of variation of heating rate (see sections 4.2.5 and 5.5.4.3) as the effect of thermal quenching would make the measured trap depths apparently greater at slower heating rates).

In conclusion the IRSL appears to originate from a single population of traps which can be probed using either of the wavebands tested here; consequently the

hypothesis does not appear true. However a final test - dating a known-age loess using IRSL - was undertaken to confirm this conclusion; the results are described below (dating a known-age sample was considered a more definitive test of signal stability than the obvious approach of monitoring the erosion during annealing of the IRSL signals stimulated by the various wavebands).

6.3.3 A DATING COMPARISON OF THE IRSL STIMULATED BY DIFFERENT IR WAVEBANDS

The palaeodose of a known age loess sample was measured using different IR stimulation wavebands and following various durations of ambient temperature storage and preheats at 160°C and 100°C. It was intended here to examine simultaneously various aspects of the dating procedure highlighted as potential sources of inaccuracy in age estimation or advocated as necessary, including: (1) long storage duration at room temperature, (2) preheating, (3) choice of IR stimulation waveband and (4) the effect of exposure duration on palaeodose, (ie, short vs long exposures; all measurements were made using short exposures except the final measurement which consisted of a long exposure immediately following the final short exposure).

The sample dated was the fine grain fraction of a loess (lab. ref. 72211, expected age ≈ 20 ka and expected palaeodose ≈ 55 Gy) from Achenheim, near Strasbourg, France, and kindly prepared by D.G. Questiaux. Three stimulation wavebands were used (see Fig.6.3.2.1) and 15 discs were used to construct additive dose growth curves for each of these wavebands (regarding disc-to-disc variability: the 1σ value for the natural IRSL measured for the full set of 45 discs in step (1) was ≈ 4 %).

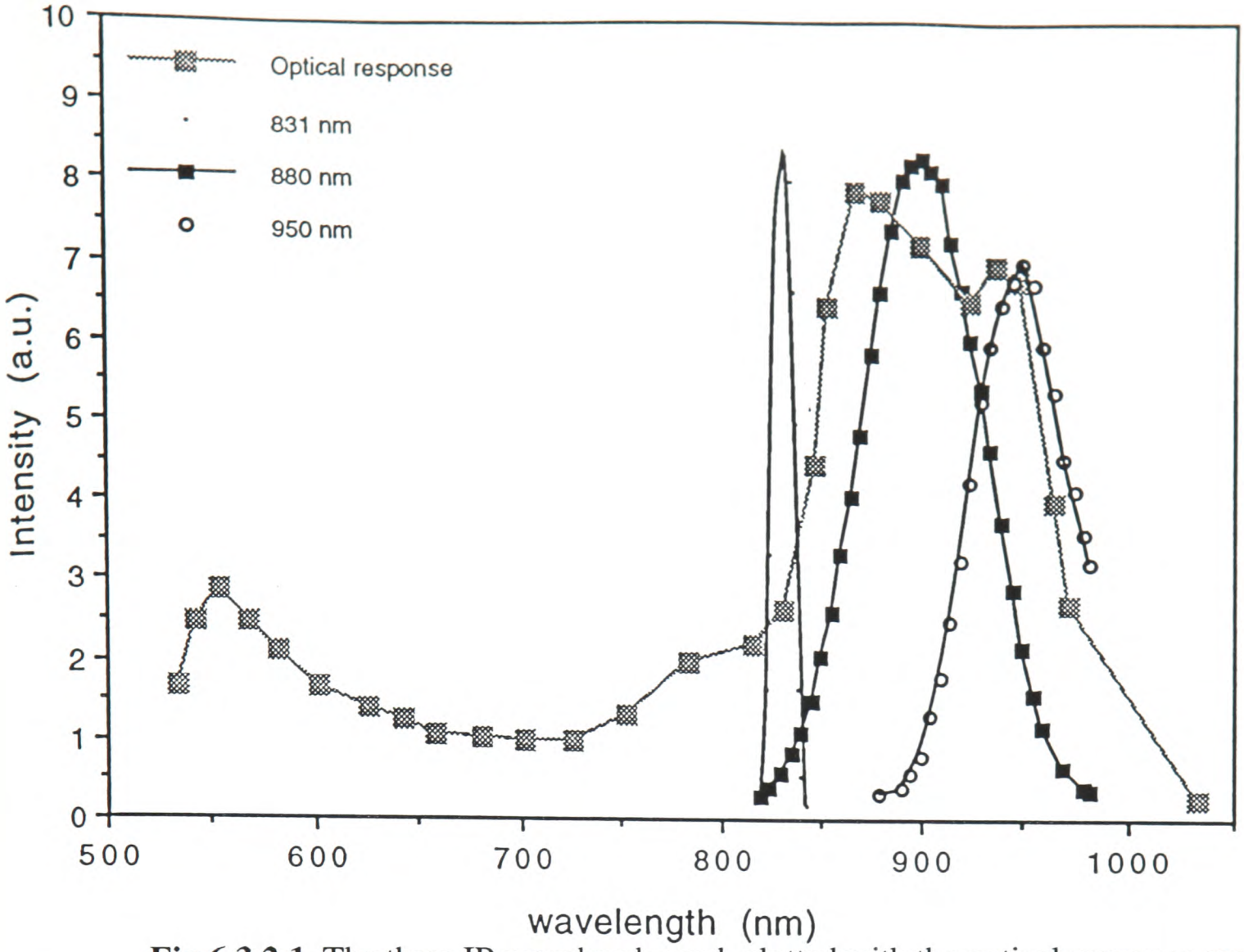


Fig.6.3.2.1 The three IR wavebands used, plotted with the optical response spectra of alkali feldspar (after Hütt *et al*, 1988).

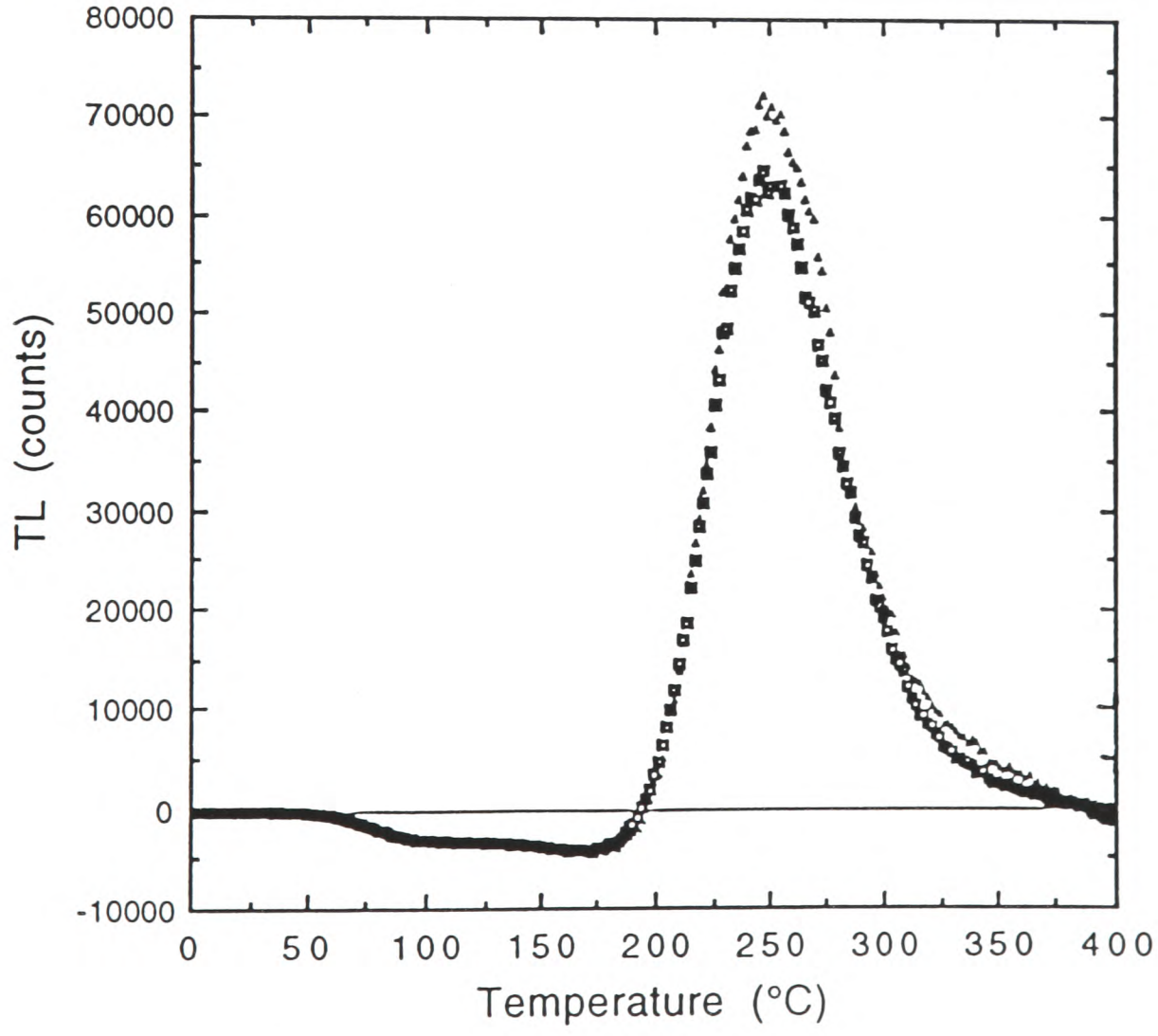


Fig.6.3.2.2 The TL removed from an old loess sample (lab. ref. 722t1) by long exposures to 831 nm (triangular symbols) and 950 nm (square symbols). These data result from subtraction of the residual TL from the NTL. For both wavebands the residual TL was ≈ 45 % of the NTL and measurements errors ≈ 5-8 %. Data plotted are counts / 2K.

The measurement routine is summarised below; the steps are cumulative:

1) 15 discs for each of the 831.8 ▵ 12.8 nm, 880 ▵ 80 nm and 950 ▵ 80 nm wavebands were each given a short normalization exposure

2) $^{90}Sr/^{90}Y$ β dosing

3) 2 day storage at ambient temperature, followed by short exposure

4) 7 day storage at ambient temperature, followed by short exposure

5) 43 day storage at ambient temperature, followed by short exposure

6) Preheat for 4 hours at 160°C (shown to be an adequate preheat for this sample to eliminate the unstable TL, pers. comm. D.G. Questiaux, 1990), followed by short exposure

7) Preheat for 1 week at 100°C, followed by short exposure

8) Long exposure to measure the majority of the IRSL signal

9) Residual TL measured by heating to 550°C at 5 K/s then reheating.

The growth curves constructed from the short exposure data for each of the wavebands are shown, with linear curve fitting, in Fig.6.3.3.1, and the palaeodoses found in each case are tabulated in Table 6.3.3.1 along with the palaeodoses found from the long exposures. Flat shine plateaux (not shown) were obtained from the long exposure data from all three IR stimulation wavebands.

Pretreatment	Stimulation Waveband		
	831.8 Δ 12.8 nm	880 Δ 80 nm	950 Δ 80 nm
(1) 2 day storage, ambient	- 9.9 10.9 + 11.8	- 12.5 12.8 + 13.1	- 8.5 9.5 + 10.5
(2) 9 day storage, ambient	- 10.1 11.0 + 11.8	- 12.3 12.8 + 13.2	- 8.6 9.7 + 10.7
(3) 54 day storage, ambient	- 10.0 11.1 + 12.1	- 12.3 12.7 + 13.0	- 9.6 10.5 + 11.4
(4) (3) + 4 hr at 160°C	- 21.5 22.2 + 22.5	- 26.6 26.8 + 26.9	- 24.1 24.4 + 24.7
(5) (4) + 1 week at 100°C	- 22.8 23.1 + 23.4	- 28.1 28.2 + 28.3	- 25.5 26.1 + 26.6
(6) Long exposure following (5)	- 21.7 23.5 + 25.3	- 20.5 22.0 + 23.5	- 18.0 19.5 + 21.0

Table 6.3.3.1 The ages (ka) found using the various cumulative pretreatments. Note the dramatic increase to approximately the correct ages following the first elevated temperature storage. The variability in ages subsequent to this preheat is attributed to errors of curve fitting given the limited number of sample portions used to construct each growth curve.

Several conclusions are drawn from these results:

(1) Prolonged ambient temperature storage following irradiation is not a viable preheat step for obtaining the correct palaeodose and will not lead to correct age determination within a feasible time; note that no significant increase in palaeodose was observed for storage of up to 54 days at room temperature. This is the expected result following a consideration of the feldspar glow curve shapes given in Appendix I: the prominent ATL peaks at temperatures < 250°C (particularly the 160°C and 240°C peaks)

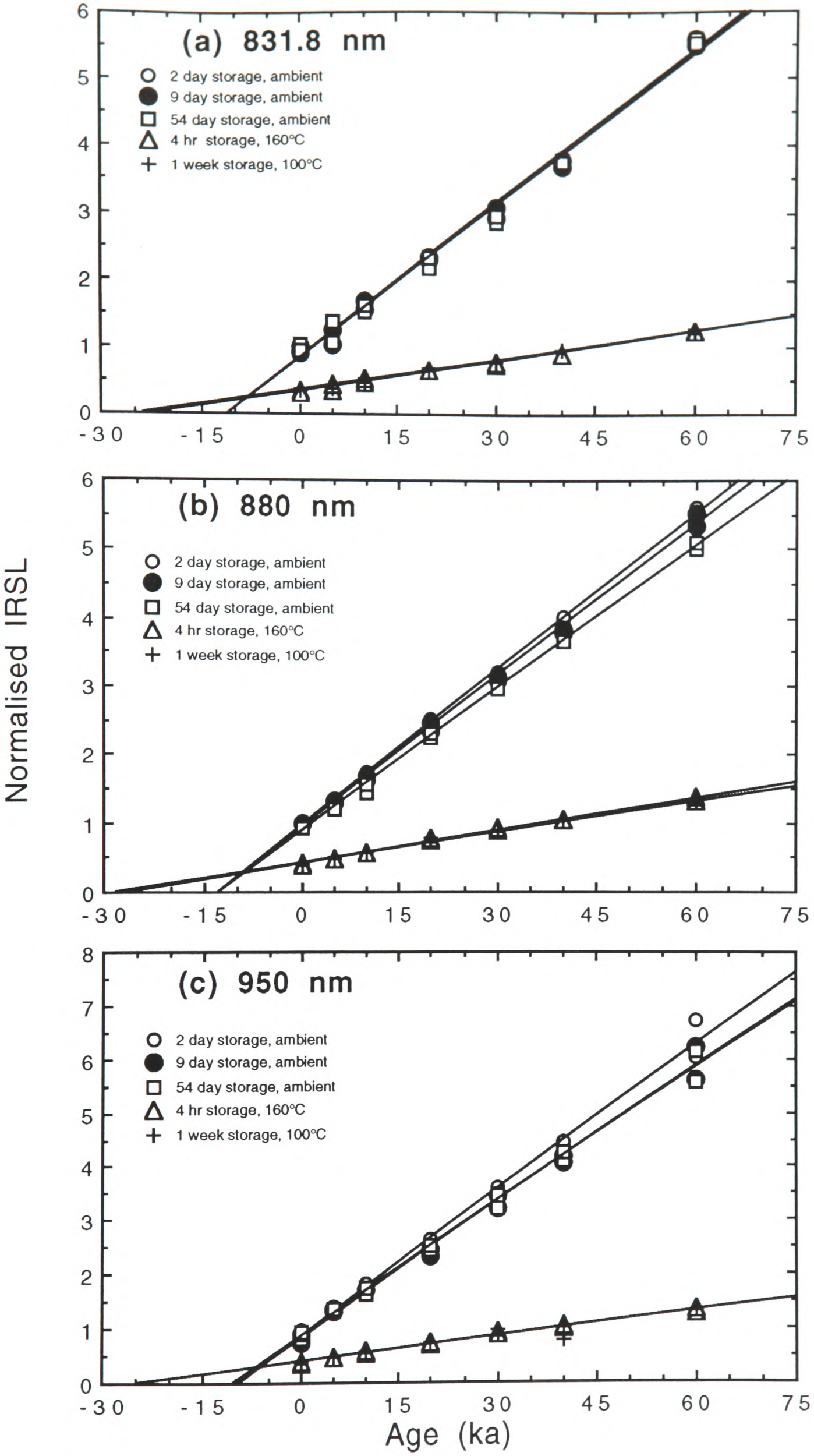


Fig.6.3.3.1 (a)-(c) The growth curves obtained from loess sample 72211 for each stimulation waveband, following each combination of pretreatment conditions.

not only contribute IRSL signal but also possess a spectrum of trapping lifetimes at room temperature that ensures their thermal decay is too slow for storage at that temperature to drain them. Additionally, retrapping into dating signal traps of a proportion of the charge untrapping thermally from the lower temperature ATL peaks must occur as a necessary charge transfer step to replicate the sensitivity with which the NTL was acquired. (The potential for such recuperation of the IRSL signal over broad timespans of days to millennia following deposition have been outlined in Appendix I).

(2) Following from (1), preheating must be sufficient to drain the low temperature ATL peaks, or severe age underestimation results. Conveniently here the first preheat, 4 hours at 160°C, drained these ATL peaks such that the palaeodose increased to a level commensurate with geological expectation. Subsequent storage at 100°C for 1 week gave no significant further palaeodose increase in this case (presumably no thermally accelerable fading component is present in this sample unless it was fully removed by the 4 hour preheat at 160°C).

(3) Palaeodose appeared independent of IR stimulation waveband used.

(4) Short and long exposures appear equivalent within measurement errors.

Finally, it is inferred from the above that the IR stimulable signal is originating from a single population of traps possessing a common stability with respect to detrapping to the conduction band and that preferential thermal erosion of a specific component of the IRSL signal is not a cause of age underestimations. This conclusion directs attention to this common stability, leading to the work of the following section in which the optical and thermal detrapping of feldspar luminescence are investigated.

6.4 AN INVESTIGATION OF A POSSIBLE INTERMEDIARY TRAP ACCESSIBLE BY PHOTOTRANSFER

6.4.1 INTRODUCTION

It was reported previously (Spooner and Questiaux, 1989) that the time-resolved (order of milliseconds) IRSL signal form observed from a sample of old European loess (Achenheim, lab. ref. 722t1) on giving a short IR exposure displayed both a characteristic "build-up" portion lasting from the commencement of illumination until equilibrium was reached, and a corresponding decay portion from the moment illumination ceased. An example of such behaviour is shown in Fig.4. (Spooner and Questiaux, 1989), where it was further noted that this effect seemed characteristic of the green/orange emissions only. A tentative explanation was proposed attributing this build-up effect to a detrapping mechanism in which recombination occurred following phototransfer to a shallow intermediary trap, in a manner analogous to that proposed for zircon luminescence (Smith, 1988). The nature of this hypothetical phototransfer-accessible trap was unknown, and the possibility that it revealed the presence of long-lifetime localised transition fading could not be ruled out; further delineation of its properties were therefore essential.

Consequently this effect was further investigated in Spooner (1992), from the perspective of sample composition, and the occurrence of the build-up behaviour was confirmed to be restricted to the green/orange emission ($\approx$ 570 nm). Build-up was only clearly observed in the sodic corner of the ternary diagram, as the more calcic plagioclases lacked sufficient signal intensity. Albite and oligoclase demonstrated the build-up effect most dramatically, in agreement with the significant presence of these minerals in the

Achenheim loess previously investigated (pers. comm., Questiaux, 1989).

The lifetime measured previously (Spooner and Questiaux, 1989) for the decay portion of this build-up curve was ≈ 8 ± 3 ms, but the trap depth of the hypothetical intermediary trap was not measured. Later, in order to define more fully the energetics of this system, and to investigate the possibility that it may offer a pathway by which charge might "leak" from otherwise apparently thermally stable traps over archaeological timescales, a more detailed study of this signal was commenced.

Following the earlier attribution of the build-up effect to thermal decay of TL phototransferred to the intermediary trap, the obvious initial step was to determine the trap depth of this intermediary trap using the isothermal decay method. As the lifetime at ≈ 20°C was of the order of 10 ms, which was approaching the time resolution limits of the IR illumination apparatus available (where illumination was actuated by Melles-Griot shutters), it was necessary also to measure the lifetime of this signal below room temperature in order to obtain a useful range of lifetimes for isothermal analysis. This experiment is described below.

6.4.2 EXPERIMENTAL

Two samples were chosen from the sodic region of the ternary diagram, 18. Amelia albite (displays no fading) and 23. Dup.(B) oligoclase (fades). The choice was based both on sample IRSL sensitivity, so as to enable good counting statistics to be obtained in the short exposure times necessary, and to enable comparison between the behaviour of a fading and a non-fading sample.

The xenon lamp set described previously was used to provide 861.1 ∆ 12.1 nm IR

illumination for these measurements, with the samples positioned on the cooling stage of a liquid nitrogen flow cryostat (Templer, 1986b). Emissions were detected using an EMI 9635Q PMT with Schott GG475 (2 mm) and BG39 (1.7 mm) colour glass filters, giving a transmission window from ≈ 470 nm to ≈ 580 nm (50% transmission points).

Both samples were prepared as 90-180 μm grains fixed to rhodium plated copper discs by silicone oil. Sample pretreatment consisted of thermal drainage of the "NTL" by heating at 5 K/s to 550°C and reheating, then administering a 300 Gy $^{90}Sr/^{90}Y$ dose. Then followed a "cut" preheat to 180°C (5 K/s), so as to eliminate phosphorescence at ambient temperatures from thermal decay of lower temperature TL.

Measurements were made by repeated short exposures at a range of temperatures from 129 K to 425 K and some results are shown for each sample in Figs.6.4.3.1.(a) and 6.4.3.2.(a). Also shown (in Figs.6.4.3.1.(b) and 6.4.3.2.(b)) are the decay portions of the build-up plotted so as to determine the decay time constants.

6.4.3 DISCUSSION

It is clear from Figs.6.4.3.1 and 6.4.3.2 that there is no apparent temperature dependence of the decay time constant. This was contrary to expectation and refutes the earlier interpretation of the build-up as thermal decay of phototransfer TL. Time constants were found for the decay portions of each of the short exposure pulses measured at each temperature, for both samples, using the equation

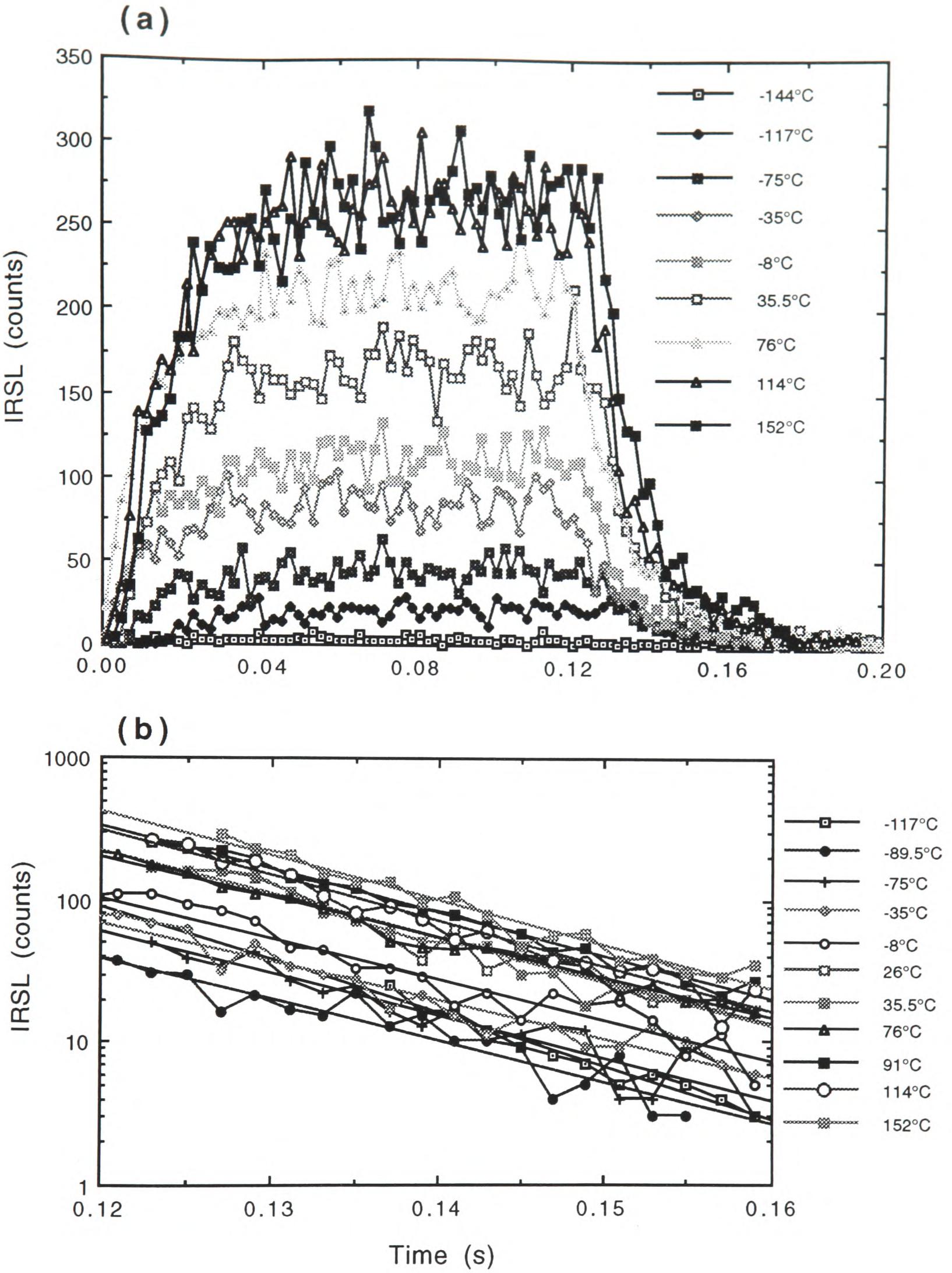


Fig.6.4.3.1.(a) The green/orange IRSL from a single aliquot of 18. Amelia albite, measured at the temperatures shown. Data plotted are counts/2 ms; the estimated background is ≈ 0.02 counts/ms, and has not been subtracted. Illumination commenced at time zero and ended at 12.5 ms. Note the symmetry of the build-up and decay portions of the curve. **(b)** The decay portions of each curve plotted against time. Note that the similarity and linearity of the slopes indicates a simple exponential decay with time and a similar time constant.

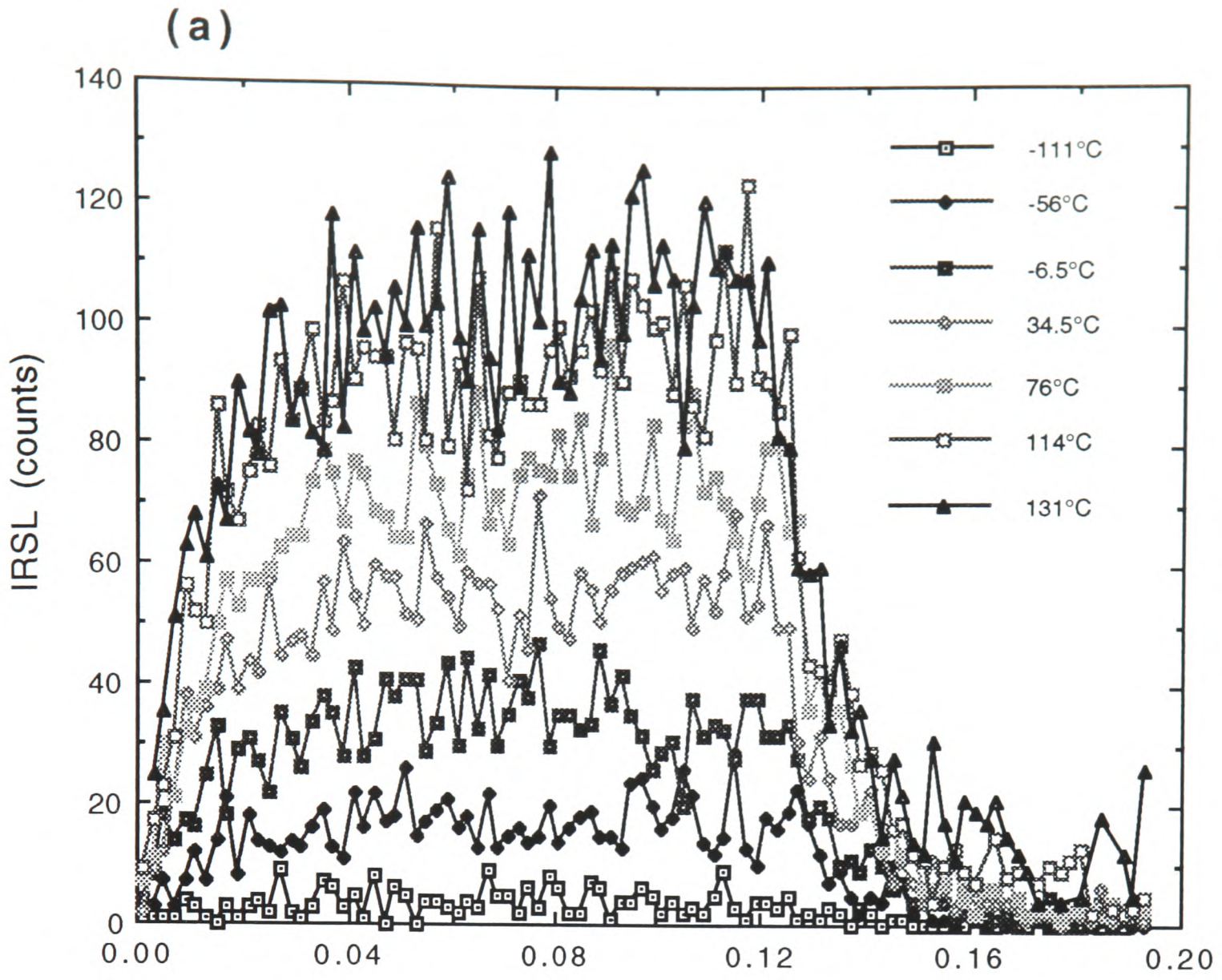


Fig.6.4.3.2.(a) The green/orange IRSL from a single aliquot of 23. Dup(B) oligoclase, measured at the various temperatures shown. Data plotted are counts/2 ms; details are as for Fig.6.4.3.1. **(b)** The decay portions of each curve plotted against time. The lower sensitivity of this sample resulted in insufficient counts at the lowest temperatures for acceptable precision in curve fitting.

$$I = I_o e^{-t/\tau}$$

where I = IRSL intensity
I_o= initial IRSL intensity
t = time
τ = decay time constant

The decay time constants found in each case are tabulated below:

Amelia albite	
Temp (K)	Time constant τ (ms)
183.5	14.85
198	14.69
238	15.84
265	15.18
299	14.25
308.5	13.98
349	15.23
364	14.19
387	13.55
425	13.85

Oligoclase	
Temp (K)	Time constant τ (ms)
217	13.46
241	13.66
266.5	13.65
307.5	14.49
349	13.46
387	14.34
404	14.95

The mean values found were: albite, T = 14.56 ± 0.72 ms, and oligoclase, T = 14.00 ± 0.59 ms. These values overlap at the one standard deviation confidence level and so it is concluded that there is no difference in the decay time constants between fading and non-fading feldspars.

The athermal nature of the decay time constant, along with the restriction of the

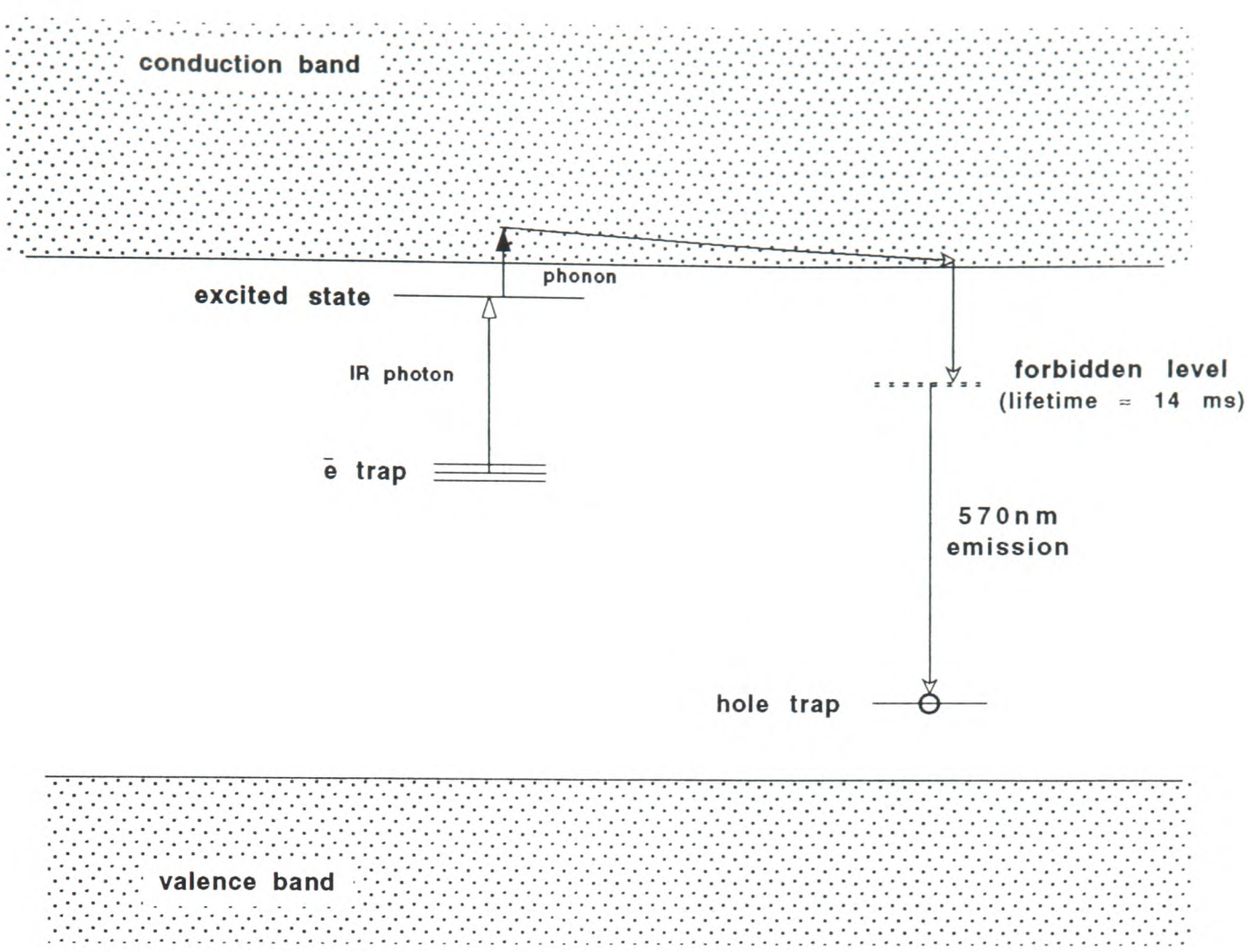


Fig.6.4.3.3 A simplified energy level diagram illustrating the interpretation of the signal "build-up" in the 570 nm emission observed under IR stimulation as electron transition into the recombination centres via a forbidden level.

Commencing with the initial exposure to IR photons, electrons are detrapped at an effectively constant rate to the conduction band and diffuse to recombination centres. However, at centres which characteristically emit 570 nm photons, recombination is delayed by the existence of a forbidden level through which the electrons must pass. Consequently the electron population in the forbidden level increases until dynamic equilibrium is reached between electrons arriving into these forbidden levels and those being lost by recombination transitions from these levels into the holes. When illumination ceases, the electron population in the forbidden level is no longer replenished, and so depletes with the characteristic time constant of $\approx$ 14 ms.

signal build-up behaviour to solely the 570 nm emission band, leads to a new interpretation of this effect. It is now hypothesised that electron transitions into the 570 nm recombination centres proceed via a forbidden level transition in that recombination centre. Fig.6.4.3.3 shows a simplified energy band diagram illustrating this interpretation.

A significant consequence of this interpretation is that the effect is restricted to one type of recombination centre only, and furthermore is a characteristic of the pathway the electron must take at the recombination centre. This eliminates the possibility that the build-up effect is related to electron retention at the electron traps, and so removes this effect as a possible alternative pathway for fading. The similarity in the decay time constants measured above for the fading oligoclase and non-fading albite reinforce this interpretation. It is therefore concluded that the build-up effect has no apparent relevance to signal stability.

6.5 BLEACHING BY ENVIRONMENTAL BLACKBODY RADIATION

6.5.1 INTRODUCTION

Following measurement of the optical energy for the ground-to-excited state transition, the way opened to assessing the possibility that the "100 ka" limit was a real and fundamental effect due to bleaching of the IRSL source traps via the excited states over the burial time. The bleaching photons in this case are the IR photons of the thermal radiation field, and the effect should attain dynamic equilibrium with trap filling of the susceptible traps. An attractive feature of this model is the ready explanation it offers of the "mid-term" fading reported by Xie and Aitken (1991) for Chinese loess. The

apparently athermal fading component hypothesised in that work is the IRSL signal undergoing slow bleaching in dynamic equilibrium with trap filling, whereas the "infinitely stable" component comprises the sum of non-IR bleachable feldspathic luminescence and that of other minerals, notably quartz. As this mechanism leads to a sub-saturation-level equilibrium, then the natural "saturation" level would be lower than that obtainable in the laboratory following high dose-rate irradiation. This difference between natural and laboratory saturation levels has been previously reported by others (Mejdahl, (1988), and Hütt and Jaek (1989)). Explanations based on dose-rate effects were proposed (Hütt and Jaek (1989), Mejdahl *et al* (1992)). Here however, the effect of exposure to environmental thermal radiation over archaeological timescales is assessed, in order to test the hypothesis that bleaching of the IR stimulable component of the TL accounts for these effects and consequently also the "100 ka" limit.

6.5.2 THERMAL RADIATION DOSAGE IN ANTIQUITY AND IN LABORATORY PROCEDURES

The spectral distribution of blackbody radiation follows the general functional form of Wien's law, and the wavelength of peak radiative intensity is found from Wien's displacement law, $b=\lambda_{max}T$, where $b=2.898\times10^{-3}$ mK. At 20°C the peak wavelength of the blackbody curve is ≈ 9990 nm, and 6693 nm at 160°C, clearly too long to affect the IRSL signal via the known excited states. Considering then the total energy: the emissive power of a black body is given by Stefan's equation, $I_T=\sigma eT^4$, where I_T = the radiant power (W/m^2), σ = Stefan-Boltzmann constant 5.670×10^{-8} $Wm^{-2}K^{-4}$, and e = emissivity. To assess the total energy available for bleaching over archaeological timescales: assume e = 1, the

maximum possible value, then the radiant power is ≈ 401 Wm^{-2} at 17°C, (and 1,993 Wm^{-2} at 160°C), meaning that over 100,000 years the total exposure at 17°C is 401 Wm^{-2} × 3.156×10^{12} seconds ≈ 1.27×10^{15} Jm^{-2}. Although these seem massive energies, the intensity of the short wavelength (near-IR) tail of this distribution required further evaluation, bearing in mind the rapid fall-off in flux at shorter wavelengths, to determine whether sufficient energy was actually available at the near-IR resonance wavelengths over the timescales of interest. The emissive power of a black body is given by Planck's formula:

$$E_{\lambda,T} = \frac{2\pi c^2}{\lambda^5} \cdot \frac{h}{e^{\frac{hc}{k\lambda T}} - 1}$$

where: $c = 2.997925 \text{ X } 10^{8}$ ms^{-1}
$h = 6.62618 \text{ X } 10^{-34}$ Js^{-1}
$k = 1.38066 \text{ X } 10^{-23}$ JK^{-1}

From this the flux in a frequency band ν to ν+dν can be shown to be:

$$R = \frac{c}{4}\int_{\nu}^{\nu+d\nu}\left(\frac{8\pi\nu^2}{c^3}\right)\left(\frac{h\nu}{e^{\frac{h\nu}{kT}} - 1}\right)d\nu$$

which, on substituting x=hν/kT and simplifying becomes:

$$R = \frac{2\pi k^4 T^4}{c^2 h^3}\left(\int_{\nu}^{\nu+d\nu}\frac{x^3}{e^x - 1}dx\right)$$

where the approximation $x^3/(e^x-1) \approx x^3e^{-x}$ can be used if hν>>kT, as is the case, and so gives:

$$\int_{\nu_1}^{\nu_2} x^3 e^{ax} dx = \left[e^{ax}\left(\frac{x^3}{a} - \frac{3x^2}{a^2} + \frac{6x}{a^3} - \frac{6}{a^4}\right)\right]_{\nu_1}^{\nu_2}$$

Evaluating this expression, over the wavelength range defined by the FWHM of the IRSL resonance (≈ 820-920 nm), and for storage at 17°C (290 K) gives:

$$R = [(2\pi k^4 T^4)/(c^2 h^3)](1.864 \text{ X } 10^{-18}) \approx 1.15 \text{ X } 10^{-16} \text{ W/m}^2.$$

Therefore, the total deposited energy over a period of 100,000 years in the "resonance" waveband is ≈ 0.036 $\mu J/cm^2$. This is an insignificant quantity of energy, and too low by ≈ 8 orders of magnitude to account for the long-term fading. (A similar calculation for storage at 160°C (433 K) finds the flux to be ≈ 6.552 X 10^{-10} mW/cm^2, which means that over a typical preheat duration of 4 hours at this temperature, the total deposited energy will be ≈ 9.43 X 10^{-6} mJ/cm^2; this is also clearly innocuous, from which it is concluded that bleaching by IR photons during preheating is insignificant).

Final confirmation of the insignificance of exposure to environmental thermal radiation photons comes from a consideration of the absorption cross section of an electron trapped in the dating trap with respect to 880 nm photons (calculated from data used in section 5.4). The probability for absorption is found from:

$$\frac{dN}{N} = n\delta\,dx$$

Where
N = IR photons/second incident on sample = 1.8×10^{16}
dN = photons emitted/second (corrected for DQE) = 2.2×10^{9}
n = number of trapped electrons/unit volume = $1.1 \times 10^{14}/cm^3$
dx = sample thickness = 0.01 cm

The absorption cross section δ was found from these values as $\delta = 1 \times 10^{-19}$ cm^2. This very small absorption cross-section indicates a very low likelihood of untrapping, in accord with the bleaching response curves presented earlier (see section 5.2).

Finally, although the above calculations show that long-term fading cannot be explained in terms of environmental blackbody radiation bleaching via the *identified*

excited state, an alternative form of this hypothesis is not ruled out: additional excited states exist in the IRSL traps which possess lower ground-to-excited state transition energies, so permitting the electron to detrap via a "ladder" of two or more of these hypothetical excited states. However, evidence for the existence of such a route is not apparent: measurement of TL levels following prolonged elevated temperature storage (160°C or 200°C) of natural loessic samples in an artificially high IR photon flux environment (D.G. Questiaux, pers. comm. 1992) reveals no significant erosion of luminescence other than from thermal causes. It is concluded that bleaching by the environmental blackbody radiation field neither causes the "100 ka" limit nor contributes significantly to age shortfalls obtained from larger grain sizes.

6.6 DISCUSSION AND SUMMARY

It appears that no attempts to breach the 100 ka limit for fine grain samples have been unambiguously successful, and no consensus exists as to physical explanations for this limit. Speculatively, several causes or contributing effects could be involved: fading of L centres (Debenham, 1985), mid-term fading components (Xie and Aitken, 1991), long-term fading (Hütt and Jaek, (1989) and Mejdahl, (1988)), long-term athermal (or near-athermal) tunnelling type behaviour (Spooner, this work). Although this is the case for fine grain materials, recent results (i.e., Balescu and Lamothe (1992)) from the use of coarse grains give more cause for optimism.

However, in the search for a physical explanation for observed age shortfalls in general, it is timely to explicitly state a hypothesis based on the work presented in this thesis: as the similarities of the measured fading and bleaching behaviours cut strongly

across the mineralogical classification of the feldspars into various mineral species, it is postulated that from the viewpoint of luminescence defect studies the feldspar minerals would be more usefully treated as a single system rather than as distinct minerals. From this new perspective, possible causes then broadly categorise as grain-size-dependent or grain-size-independent: a brief discussion of each follows.

Grain-size-independent effects: regarding the influence of anomalous fading: it is apparent from the fading measurements (see chapter 4) on characterised feldspars that there are some examples of high-potassium feldspars which do not show detectable fading over at least 4 decades of time. Clearly, as the known anomalous fading mechanisms predict that such feldspars will not then commence fading, a comprehensive explanation cannot be based on anomalous fading alone (the pessimistic position that the stability seen from the feldspars studied here is peculiar, and that fading is the normal behaviour in natural samples, is not supported by the comparisons of the properties of these samples with "natural" samples, made wherever possible).

Another possibility, raised by Mejdahl *et al* (1992), is that dose rate effects give rise to the age underestimates seen in coarse-grain K-feldspars, at least. Mejdahl *et al* (1992) constructed growth curves following irradiation at 130°C and found significantly greater palaeodoses when compared to room temperature dosing. The explanation given, based on competitive filling of traps, is that at elevated temperatures the lower temperature traps are maintained in an almost-empty condition during dosing, approximating the condition found in nature. Therefore the probability of trapping into the "dating" traps is also similar to that found in nature; however, when significant doses are administered at laboratory dose-rates at room temperature, the lower temperature traps rapidly saturate and cease to play the role of competitor. The "dating" traps now fill at a

greater rate, leading to underestimation of the palaeodose. This proposal is currently undergoing investigation by D.G. Questiaux, in an attempt to determine whether the effect is due to competition as hypothesised by Mejdahl *et al* (1992) or due to a temperature dependent trapping cross-section such as suggested by Aitken *et al* (1975) in respect of quartz: if the latter, it is irrelevant to dating.

Finally, the surprising bleachability of the feldspar luminescence (see section 5.2.4) by wavelengths across the visible and near-IR spectrum, and particularly at redder wavelengths, leads to the speculation that some age underestimations from feldspathic materials could be the result of inadvertent bleaching in the laboratory, rather than any intrinsic fading.

Turning to causes in which the grain size should determine the severity of the effects: firstly, there is the straightforward possibility of grain alteration - both the growth of grains by authigenic processes or surface degradation by weathering (and consequent loss of α-dosed material) would give rise to age shortfall. However, the expectation would be that the range of physico-chemical environments from which luminescence dates have been obtained should result in a corresponding range of regional age limits - this has not been observed.

Two other environmental aspects affect fine grains principally: firstly, they receive full-volume α irradiation, along with all the associated possibilities for enhanced fading (as discussed in section 4.2.4), radiation quenching and damage that such a high LET heavy-particle irradiation entails (Nambi, 1984). Secondly, the prospects for long-timescale diffusion into the grains from the environment of "killer" ions, with consequent neutralization of trapped charge, are greatly enhanced for fine grains. Diffusion rates of $\approx$ 1 μm / 20 ka would explain many of the observed shortfalls - however, these processes

are difficult to model realistically, depending critically as they do on surface conditions and concentrations of the diffusing species (speculatively, the diffusing species are likely to be either diatomic molecular ions or divalent metal ions, and not small mobile species such as H^+, Li^+ or Na^+). Generally, hypotheses based on diffusion from the environment constitute a very attractive solution to the problem of long-term age shortfalls, but may prove difficult to differentiate from the effects of α-irradiation.

However, a related class of model, based solely on volume effects such as long-timescale clustering of defects, are ruled out by the apparent grain size dependency.

Finally, dosimetric causes have not been excluded: and particularly the internal dose contributions from U and Th α-irradiation and K and Rb β-irradiation in K-feldspars require to be comprehensively reevaluated.

It remains for a detailed study to be made of feldspar luminescence down a deep (old) section in which a range of grain sizes are present (without likelihood of contamination by percolation from younger levels) to enable direct comparison of coarse and fine grain ages to test the hypothesis that the 100 ka limit and other age shortfalls are grain-size-dependent.

CHAPTER 7 CONCLUSIONS ON OPTICAL DATING USING FELDSPAR

The major findings of this work regarding the suitability of the feldspar minerals for optical dating applications can perhaps be condensed down to a few critical points. These are summarised as follows: (1) anomalous fading in feldspars is phenomenologically complex but appears to proceed predominantly by quantum mechanical tunnelling. (2) IRSL originates from only one type of defect - the variety of observed glow peaks in the high temperature (> 200°) TL is a consequence of the range of electronic environments within the crystal lattice in which this defect can exist. Some configurations of this defect possess great thermal stability. (3) Untrapping from the "IRSL" defect is dominated by photoionization to the conduction band at wavelengths < 750 nm, and by thermal eviction via an electron-trap excited state for wavelengths in the near-IR. As visible light appears to probe luminescence signals for which complete depositional bleaching is unlikely (in addition to the "IRSL" defect) then IR is the optimum waveband for measurement.

These findings give rise to three general rules to be followed in the dating application of feldspar or feldspathic materials: (1) Preheating is necessary to isolate a thermally stable dating signal (the findings presented in section 6.3 show that the presence of significantly populated thermally unstable traps results in serious age underestimations, either due to contributions of "unstable" IRSL or through the reduction of competition to recombination during measurement). A suitable preheat should thermally drain the lower temperature TL glow peaks, up to and including the 280°C TL peak. (2) Anomalous fading must be monitored for in any dating work using feldspathic samples. Presence of fading should be generally regarded as a rejection criteria for dating that sample; exceptions are only if the proportion of signal lost per decade of time is insignificant, i.e., if a very weak fading phosphorescence is detected from a sensitive sample. (3) Near-IR is the optimum stimulation waveband to sample thermally-stable, readily bleachable signal.

APPENDIX A. A FLUORESCENT MONITOR FOR OSL READERS

Monitoring of optical power delivered to a sample disc by the Oxford Ar-ion laser set (Smith *et al*, 1988) relied previously on the Fresnel reflections from a beam splitter (anti-reflection coated optical flat - "cube detector") inserted in the beam line being detected by a photodiode (RS large area silicon photodiode, cat # 303-674, with beam attenuation by a 2 ND Kodak Wratten filter). As the reflected beam was a constant proportion of the incident beam, this gave a relative measure of beam power. Absolute power was then found from calibration with a pyroelectric radiometer (Molectron Corp. model PR-20). However the location of the optical flat was such that the beam passed through several further optical elements before reaching the sample, so leaving this arrangement vulnerable to component misadjustment.

Earlier work using the Xe-lamp system had showed intense red fluorescence from various Schott glass sharp cut filters. Utilizing this finding, a disc of suitably fluorescent filter glass of sample disc dimensions was positioned on-plate, analogous to a sample. Such a monitor simultaneously constitutes a non-depleting (countrate unchanged by $\approx$ 350 J exposure to 514.5 nm light) check of both laser power incident on the sample disc and the correct functioning of the detector electronics. Schott glass OG-530 was chosen from several types tested, for reasons of fluorescence intensity and resistance to temperature change (measured at -0.4 %/°C at 20°C). Additionally, no phosphorescence which could constitute a background component was detected. Usage simply required the Schott glass disc to be placed on-plate and illuminated as if it were a sample, while observing the fluorescence with a PMT (four Corning 7-59 and 0.5 mm Schott BG-39 filters - a limit to applicability being strong suppression of the red fluorescence by Corning 7-51 filters).

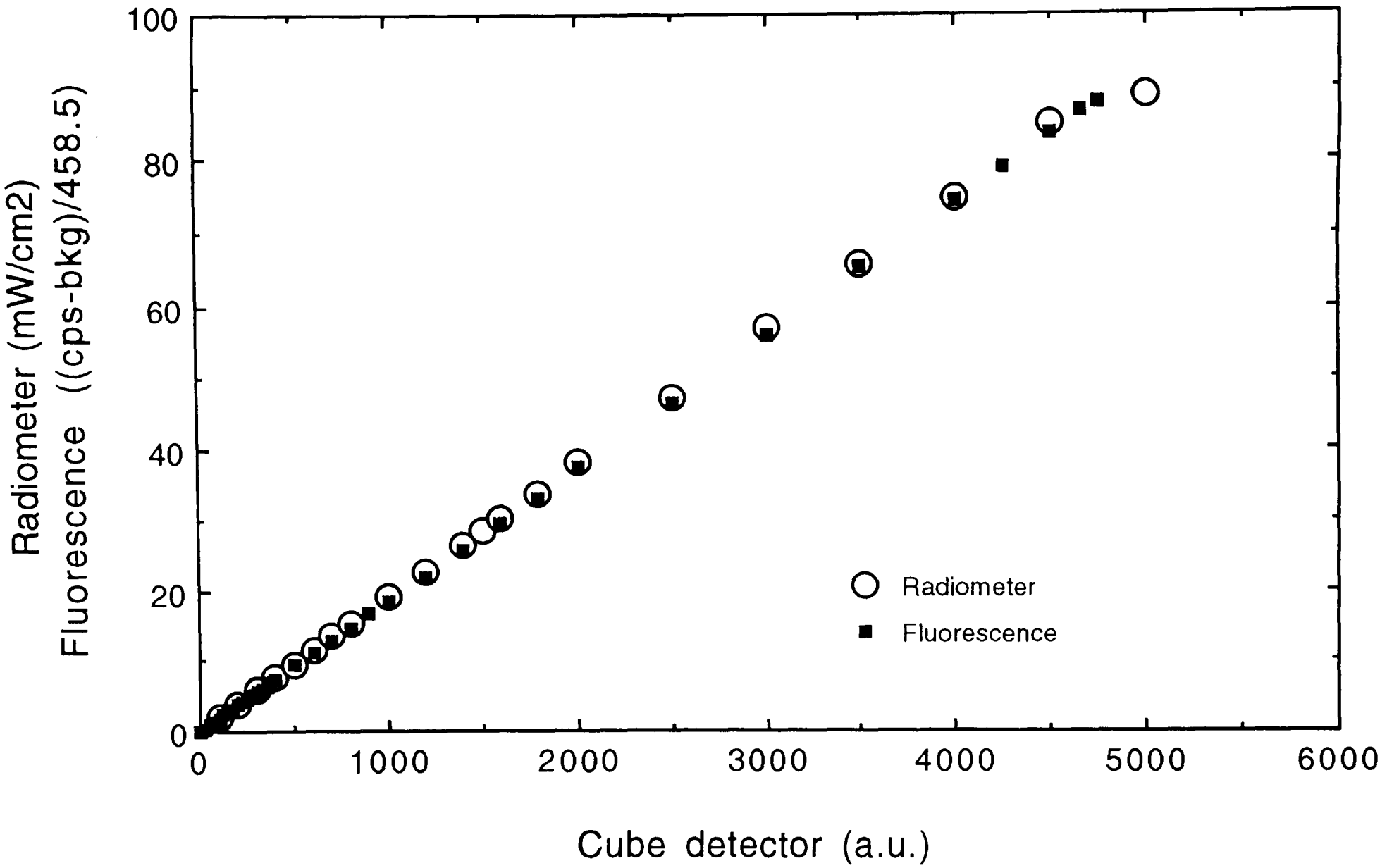


Fig.A1 Schott glass fluorescence as a function of cube detector reading, along with absolute power measurements made by radiometer. The concordance of the data sets is excellent, justifying reliance on this monitor as a convenient illumination-detector system check.

APPENDIX B AN INVESTIGATION OF CERAMIC-SUBSTRATE SOURCES FOR BETA IRRADIATIONS

At the time when the Elsec automated β irradiator project was commenced the future availability of silver $^{90}Sr/^{90}Y$ plaques (from Amersham International) was in doubt. The reduced external levels of bremsstrahlung radiation if the radioisotopes were instead carried on a ceramic substrate made the succession of silver-type plaques by ceramic seem attractive (Pers. comm. M.J. Aitken, 1991). However the advantage of obtaining a suitable source with the reduced shielding required by ceramic sources to lower the external leakage dose-rate to safe levels was offset in the luminescence application by the possibility of poorer sample disc centre-edge dose uniformity as a consequence of a smaller active source area (5 mm ϕ for ceramic, compared with 12 mm ϕ for silver type). Consequently the dose-rate profile across a sample disc was measured and compared to that from a silver plaque to find the minimum source-sample distances needed for equivalent and acceptable dose-rate uniformity. A second consideration was to estimate the likely dose-rate delivered from a ceramic source if used - the available activities being 50 mCi and 100 mCi.

An outline of this work follows and further details can be found in Allsop and Spooner (in preparation).

Fig.B1 Shows the radioluminescence apparatus. The test source was traversed in a 2 mm X-Y grid pattern above a 1 mm^3 crystal of CaF_2 (attached by "Viscasil" to a glass optical fibre light guide) using X-Y micrometer screws. The induced radioluminescence was transmitted by the optical fibre to an EMI 9635 PMT through one Corning 4-96 filter (50 % pass from 380 nm to 560 nm). Photon counts were integrated

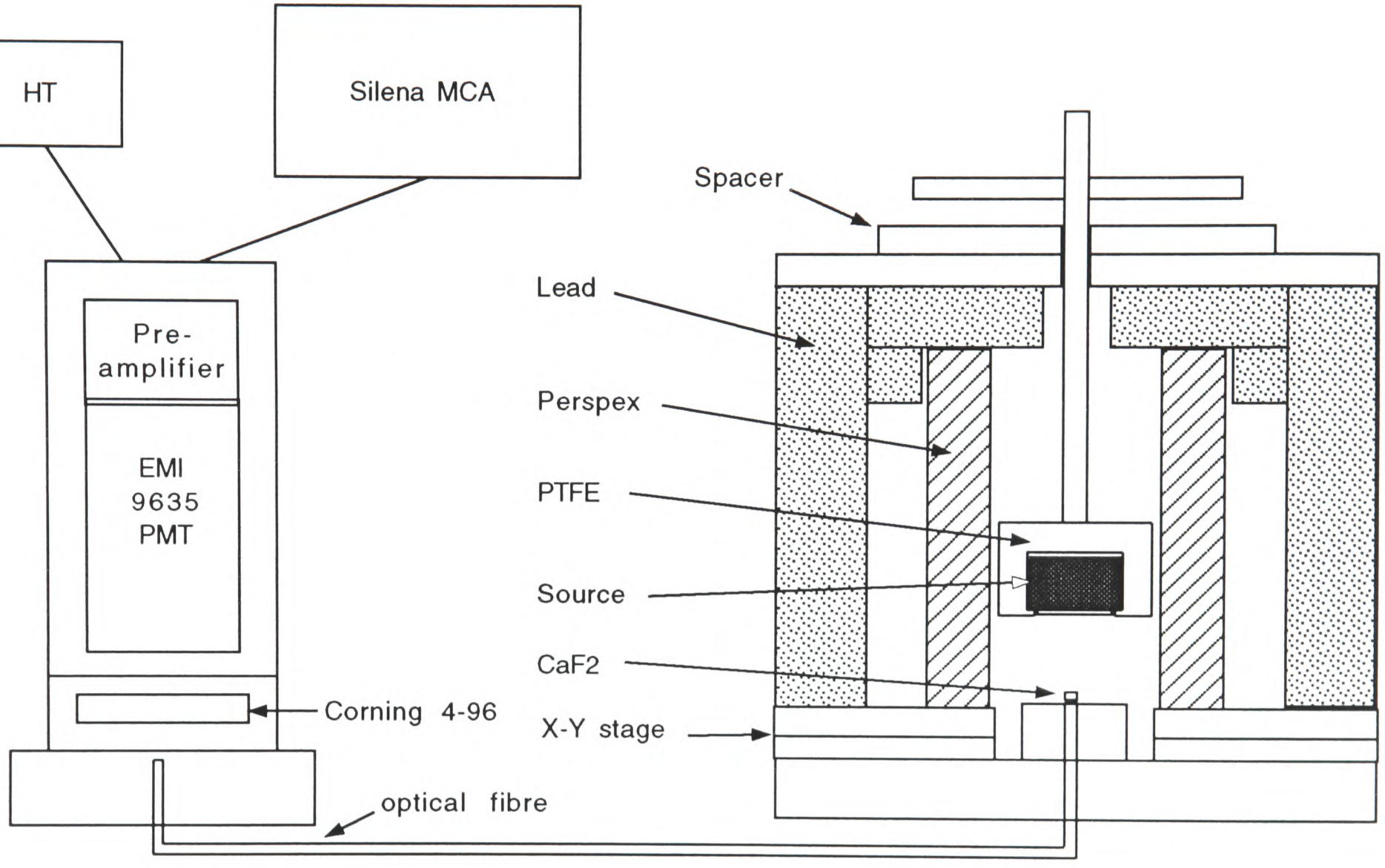


Fig.B1 The apparatus used to measure dose-rate spatial uniformity by observing the radioluminescence induced in a CaF_2 crystal.

over periods of either 2 sec or 5 sec and manually recorded along with the corresponding X-Y coordinate. Several chips of natural CaF_2 were screened to select a crystal having intense blue-yellow emission. The filters were chosen to pass this waveband and to bias against UV-wavelength Cerenkov radiation induced in the glass fibre, the detected signal therefore originated dominantly from the CaF_2. The crystal received two hours irradiation immediately prior to measurements being made so as to minimize sensitivity changes during the procedure.

Fig.B2 Shows results for a 40 mCi silver plaque and 50 mCi ceramic plaque at several source-sample distances. The data represent single transverses through the irradiation beam and exhibit the predicted increasing uniformity with increasing source-sample distance. Inspection of the complete data set (not shown) revealed no apparent " fine-structure" to the irradiation profile (as would have been expected from inhomogeneous distribution of radioisotope on the source active area).

The principal conclusion was there was no significant difference between the two types of source with respect to spatial variation of dose rate across the sample disc surface. A second finding was the apparent lower dose-rate delivered per mCi of activity from the ceramic sources. Comparison of mean countrates induced in the CaF_2 crystal by 50 mCi and 100 mCi ceramic sources with that induced by a 40 mCi silver plaque gave:

50 mCi ceramic = 8,807 cps, = 176 cps/mCi and relative source strength 1.00

100 mCi ceramic = 15,600 cps, = 156 cps/mCi " 1.77

40 mCi silver = 12,000 cps, = 300 cps/mCi " 1.36

Following consideration of typical total dose requirements for sediment dating

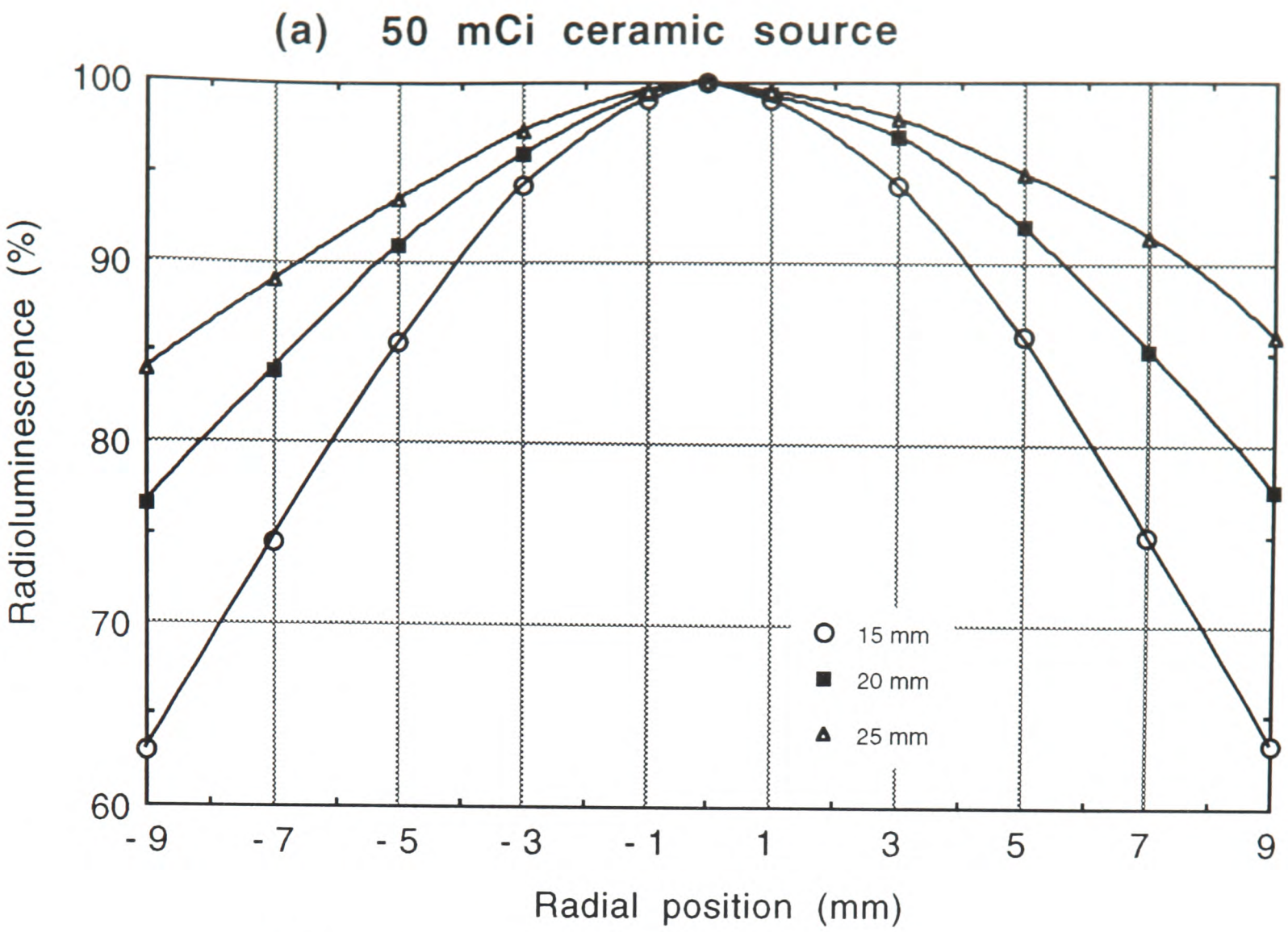
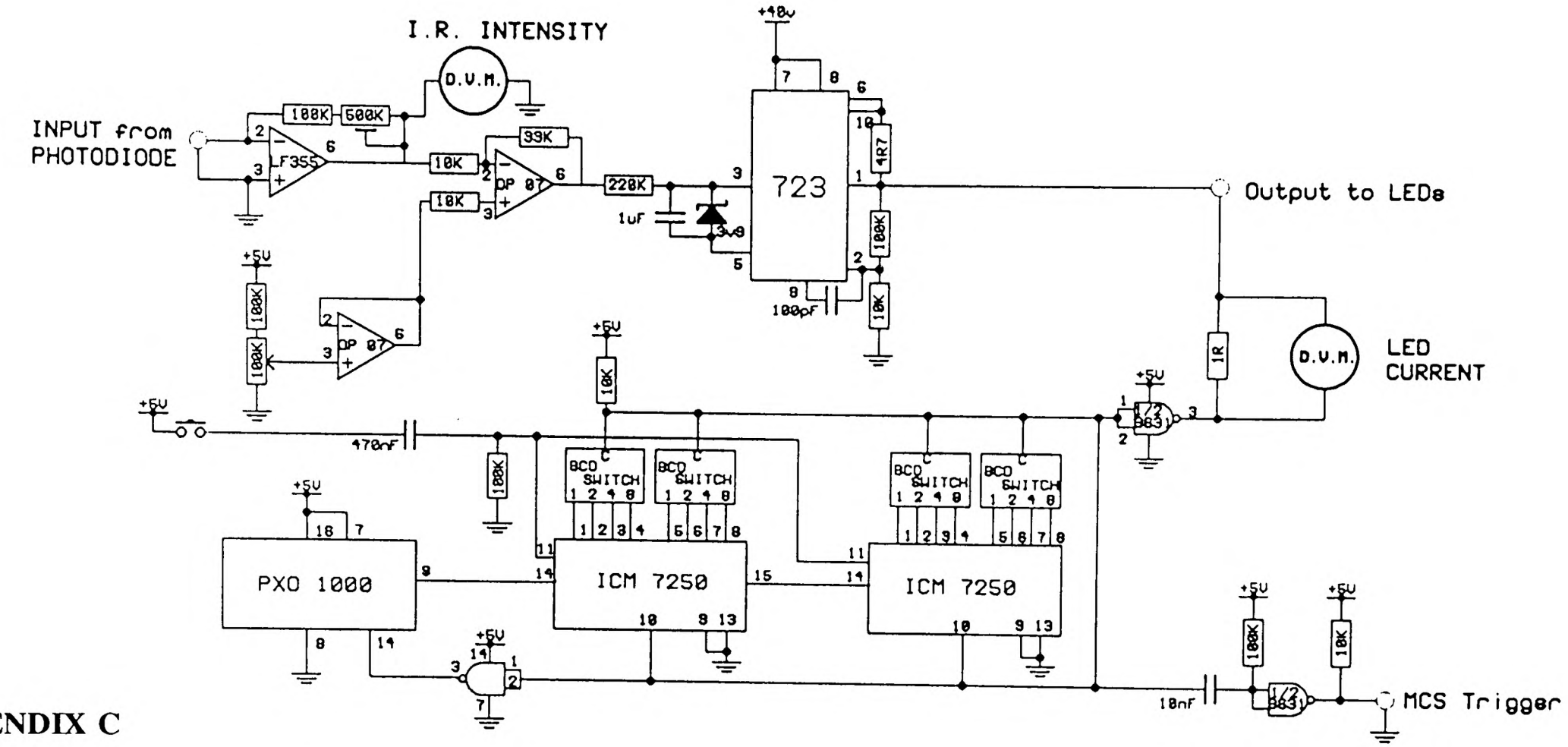


Fig.B2 The radioluminescence plotted as a percentage of the central position countrate for **(a)** the 50 mCi ceramic source and **(b)** the 40 mCi silver source. Source-to-sample distances cover the range of separations likely to be used in practice.

growth curves, a 100 mCi source was installed in the Elsec automated irradiator. Leakage dose rates external to a fire proof box enclosing the irradiator were measured to be within safe levels. Preliminary calibrations found dose rates of 0.058 Gy/sec (3.5 Gy/minute) to fine grain CaF_2 on aluminium discs and 0.088 Gy/sec (5.3 Gy/minute) to 90-125 μm quartz on stainless steel discs. As the ceramic source has a different energy spectrum from the silver type source, a 0.05 mm thick titanium foil was interposed between the source and the sample to attenuate the contribution from lower energy radiation and so make the energy spectra more equivalent. This was expected to lower the dose rate by ≈ 20 %. Recalibration found dose rates :

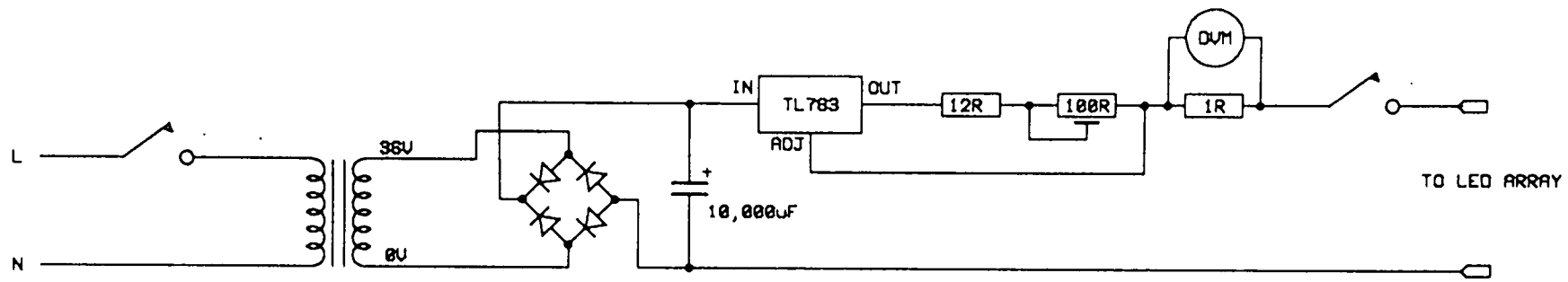
fine grain (4-11 μm) quartz on aluminium = 2.63 ± 0.07 Gy/minute (D.G. Questiaux, May, 1992)

coarse grain (90-125 μm) quartz on stainless steel = 3.32 ± 0.07 Gy/minute (R. Roberts, March, 1992)



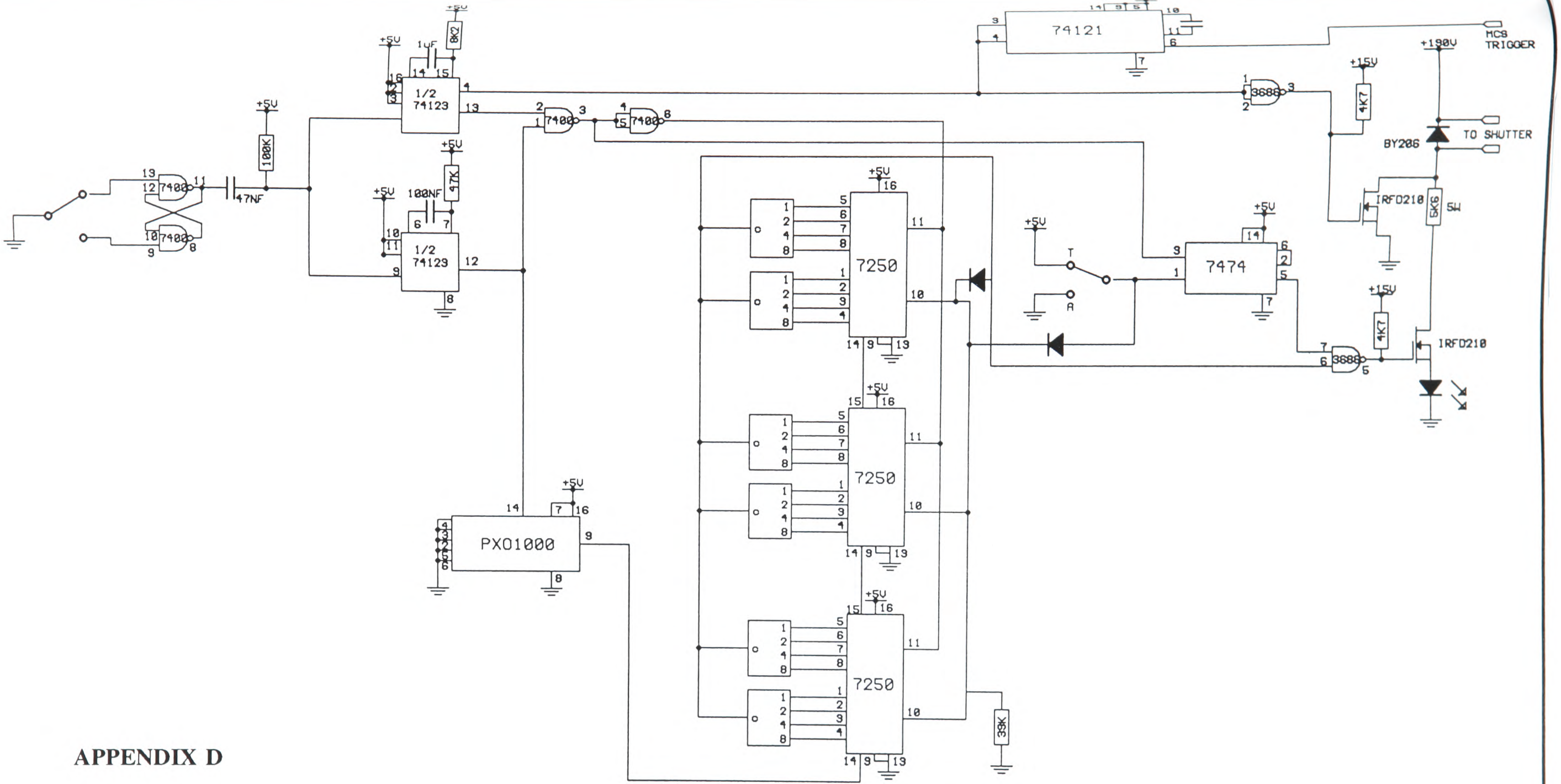
APPENDIX C

Fig.C1 The circuit diagram for the Mk III LED module



APPENDIX D

Fig.D1 MK IV diode module - constant current supply.



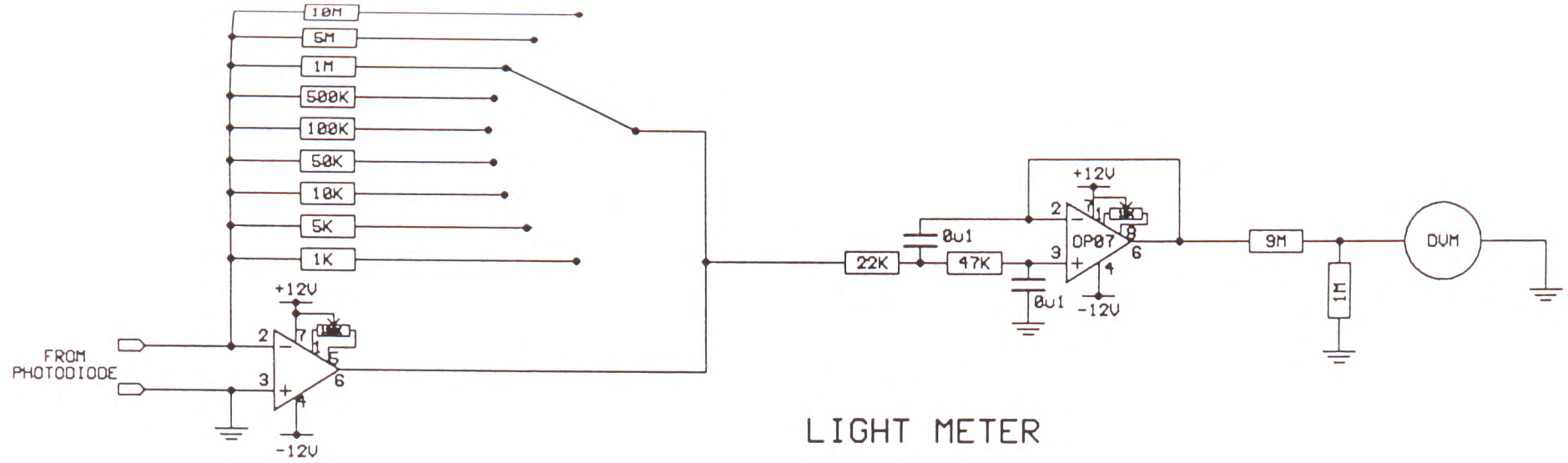
APPENDIX D

Fig.D2 MK IV diode module - shutter controller.

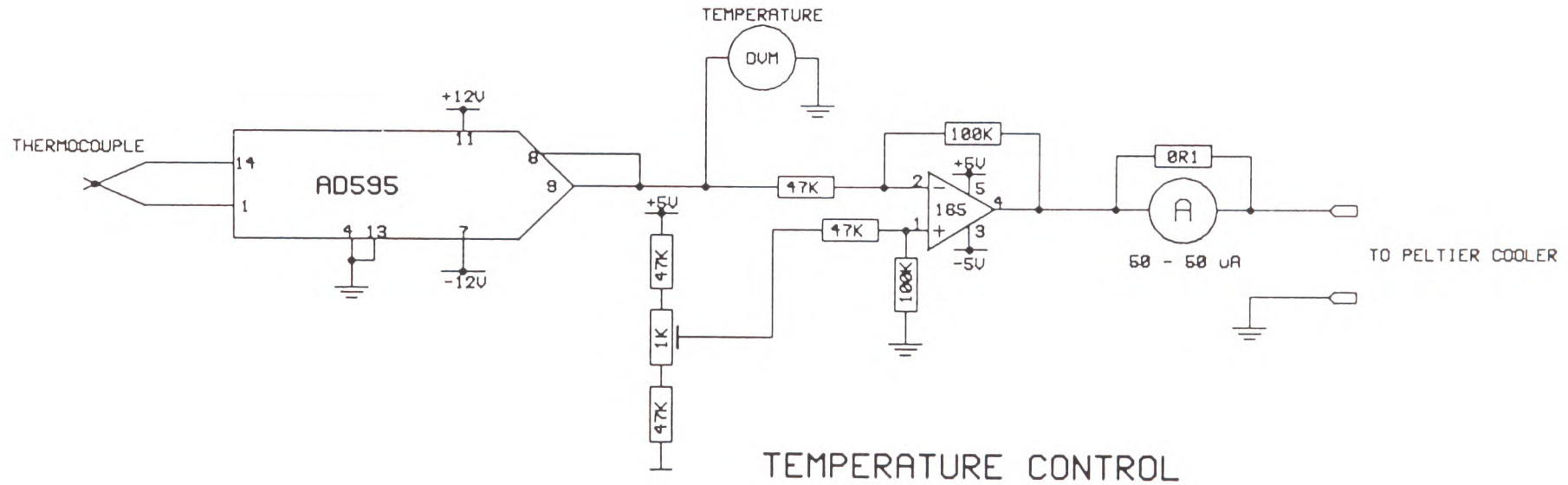
RESEARCH LAB. FOR ARCHAEOLOGY, OXFORD

LED SHUTTER CONTROLLER

ALL MAINS AND HIGH VOLTAGE CONNECTIONS TO BE SHROUDED SO THAT ACCIDENTAL CONTACT IS AVOIDED WHEN COVER IS REMOVED



LIGHT METER



TEMPERATURE CONTROL

APPENDIX D

Fig.D3 MK IV diode module - temperature-controlled light meter

	RESEARCH LAB. FOR ARCHAEOLOGY, OXFORD
TEMPERATURE CONTROLLED LIGHT METER	
	ALL MAINS AND HIGH VOLTAGE CONNECTIONS TO BE SHROUDED SO THAT ACCIDENTAL CONTACT IS AVOIDED WHEN COVER IS REMOVED

APPENDIX G FELDSPAR SAMPLE COMPOSITION

FELDSPAR	P	Si	Ti	Al	Fe	Mg	Ca	Mn	Ba	Na	K
5. No. 3062 microcline	0.0357	32.8671	0.0109	10.2185	0.0000	0.0068	0.0077	0.0136	0.0000	0.3558	7.2756
"	0.0000	32.8845	0.0000	10.4320	0.0048	0.0095	0.0000	0.0655	0.0000	0.3120	7.1741
" (minor phase)	0.0262	35.1421	0.0094	11.0956	0.0158	0.0066	0.0206	0.0000	0.0317	8.5381	0.1038
22. orthoclase	0.0248	31.3811	0.0000	9.1802	1.3488	0.0893	0.0000	0.0000	0.0575	0.1391	13.2471
3. Z5 microcline	4.4024	32.1379	0.0000	10.2524	0.0715	0.0000	0.0000	0.0284	0.0028	0.4035	6.5943
" (minor phase)	0.0053	34.2657	0.0027	10.9379	0.0618	0.0000	0.0014	0.0185	0.0078	8.5628	0.0778
11. Z6 orthoclase	0.0000	33.0929	0.0000	10.3691	0.0618	0.0258	0.0095	0.0000	0.0766	0.3842	5.9231
"	0.0205	33.0333	0.0000	10.4279	0.0049	0.0014	0.0272	0.0000	0.0028	0.5044	5.7870
" (minor phase)	0.0000	33.6319	0.0047	11.9481	0.0000	0.0000	1.1010	0.0111	0.0557	7.7742	0.0307
21. Z9 microcline	0.0155	31.1239	0.0000	10.1540	0.0000	0.0000	0.0253	0.0161	0.2489	0.5095	5.4855
" (minor phase)	5.8418	31.1395	0.0000	10.4832	0.0133	0.0000	0.1509	0.0000	0.0000	8.2329	0.0400
14. Z11 microcline	0.0052	33.0998	0.0027	10.4912	0.0303	0.0000	0.0316	0.0074	0.0348	0.5365	6.3212
" (minor phase)	0.0000	34.3229	0.0067	11.7192	0.0970	0.0051	0.3291	0.0000	0.0000	8.2377	0.2046
13. Dup(C) microcline	0.0000	32.2462	0.0000	10.4352	0.0303	0.0000	0.0000	0.0074	0.4686	0.5426	6.2795
"	0.0154	32.1807	0.0311	10.4471	0.0000	0.0075	0.0081	0.0000	0.5089	0.5450	6.1184
" (minor phase)	0.0104	35.0853	0.0000	11.3622	0.0303	0.0000	0.1729	0.0000	0.0000	8.4295	0.0443
1. adularia	0.0102	32.1019	0.0000	10.2358	0.0206	0.0014	0.0187	0.0000	0.1582	0.9300	5.8712
"	0.1282	32.6950	0.0190	10.3381	0.0000	0.0000	0.0070	0.0074	0.1398	0.8033	6.1237
20. Z9N microcline	0.0052	30.8022	0.0000	9.8565	0.0436	0.0000	0.0077	0.0815	0.1930	1.1095	7.1998
" (minor phase)	5.5684	31.5745	0.0047	10.9492	0.0048	0.0000	0.8058	0.0259	0.0000	6.1633	0.0059
9. Z15 sanidine	0.0000	32.3143	0.0000	10.3598	0.0508	0.0000	0.0317	0.0000	0.1707	1.0176	10.6743
"	0.0155	32.2181	0.0567	10.9047	0.1914	0.0000	0.4431	0.0000	0.2433	2.9991	4.1080
"	0.0359	32.1258	0.0547	10.7748	0.1356	0.0000	0.3577	0.0000	0.4048	2.1563	4.9733
12. Patmos sanidine	0.0000	32.0009	0.0365	10.6514	0.1502	0.0000	0.3944	0.0469	0.3337	3.1281	3.8236
"	0.0929	33.0280	0.0344	10.8672	0.1126	0.0000	0.3612	0.0000	0.3797	3.1646	3.8214
16. 1947,199(2) anorthoclase	0.0156	32.0483	0.0485	11.2982	0.2009	0.0000	0.7794	0.0185	0.6455	5.5847	1.9042
17. albite	0.0000	35.2533	0.0000	11.1541	0.0413	0.0000	0.0370	0.0000	0.0000	5.6992	0.0385
18. Amelia albite	0.0263	36.1188	0.0067	11.5096	0.0000	0.0035	0.0765	0.0000	0.0254	4.9429	0.0721
15. Dup(A) albite	0.0103	31.3341	0.0007	12.7142	0.0097	0.0000	2.3013	0.0049	0.0078	6.9377	0.0627
"	0.0000	32.4229	0.0067	12.9461	0.0000	0.0000	2.2274	0.0111	0.0226	6.9710	0.1094
4. 17 oligoclase	0.0000	33.0437	0.0000	11.8942	0.0642	0.0000	1.3278	0.0000	0.0106	7.4673	0.1502
7. 18 oligoclase	0.0154	32.7251	0.0102	10.3121	0.0303	0.0000	0.0228	0.0161	0.0000	0.7242	6.6709
23. Dup(B) oligoclase	0.0000	33.3535	0.0000	12.6391	0.0279	0.0000	2.3307	0.0074	0.0000	4.9682	0.0855
19. BA6 labradorite	0.5448	28.3302	0.0298	15.6490	0.2070	0.0000	5.7062	0.0000	0.0560	4.1278	0.0023
6. 23 labradorite	0.0356	27.2756	0.0068	15.2390	0.1816	0.0000	6.1900	0.0074	0.0525	3.8506	0.1761
" (minor phase)	0.0000	19.8115	0.0865	14.3063	6.3659	0.0000	14.0355	0.0963	0.0253	0.0074	0.0202
24. Dup(D) labradorite	0.0152	27.1636	0.0088	16.1624	0.1864	0.0000	8.6983	0.0025	0.0000	3.9112	0.2623
"	2.1901	25.9209	0.0319	15.8101	0.2021	0.0000	8.2292	0.0000	0.0284	4.1890	0.2410
"	0.0203	26.1702	0.0109	15.8914	0.2179	0.0000	8.3299	0.0000	0.0561	3.5887	0.2528
2. 25 bytownite	0.0251	22.3494	0.0242	15.6461	2.6294	2.7192	7.3811	0.0319	0.0000	1.5293	0.0020
" (minor phase)	0.0472	19.7596	0.0216	0.2503	3.9991	21.0417	0.1260	0.0399	0.0201	0.0075	0.0029
8. 26 bytownite	0.0202	24.6380	0.0272	17.9335	0.2094	0.0000	9.7822	0.0000	0.0107	1.9019	0.0356
"	0.0251	24.4191	0.0210	17.7277	0.2735	0.0000	9.1130	0.0296	0.0256	1.8488	0.0378
10. Z4 bytownite	0.0400	23.4035	0.0156	18.5099	0.3315	0.0000	10.0943	0.0074	0.0000	1.0915	0.0110
" (minor phase)	0.0252	21.1052	0.0000	16.2258	0.0097	0.0000	7.4355	0.0000	0.0213	1.9695	0.0482

Table G1 The feldspar sample compositions as determined by wavelength dispersive X-ray analysis (WDS) using a Cameca SU30 scanning electron microscope, (see section 3.2). Further details, including the estimated fractional volumes of the minor phases, may be found in Table 3.2.1.

Feldspar	294 Δ 23	310 Δ 10	322 Δ 22	341 Δ 22	360 Δ 25	386 Δ 28	410 Δ 19	412 Δ 18	437 Δ 36	460 Δ 10	476 Δ 15	497 Δ 28	517 Δ 12	536 Δ 28	558 Δ 15	572 Δ 18	594 Δ 28	618 Δ 33
1. Adularia	2260.2	1081.8	1545.1	2816.0	8631.6	212064.4	135776.3	121840.9	121633.7	9405.9	10558.2	7229.6	1273.9	1329.9	310.3	176.5	51.4	19.0
2. Bytownite	0	0.0	0.0	0.0	0.0	0.0	0.0	0.0	0.0	0.0	0.0	0.0	0.0	0.0	0.0	0.0	0.0	0.0
3. Microcline	14653.9	4922.8	5793.9	2152.6	3981.9	12778.3	5051.6	5548.0	8116.4	1314.2	2791.4	2720.4	805.9	1554.0	483.0	226.5	105.2	7.5
4. Oligoclase	1246.3	418.9	3342.3	2419.2	1841.5	12020.8	6745.3	8449.8	9091.0	0.0	1651.9	512.7	845.7	3081.2	6466.1	4106.8	2044.7	213.7
5. Microcline	25653.5	10831.6	35046.8	35170.5	33411.5	143322.2	119569.1	115820.4	253504.0	42573.2	59675.0	62217.2	14684.6	20438.0	5843.8	3063.1	1624.7	307.5
6. Labradorite	64.1	42.9	110.4	0.0	177.1	527.2	457.4	133.8	426.2	0.0	77.7	63.6	0.0	31.1	30.4	0.0	15.1	0.0
7. Oligoclase	438.2	165.5	592.3	948.1	1091.1	4177.3	2442.0	2463.5	3460.7	96.9	324.0	344.3	166.7	471.4	817.9	423.5	241.1	21.1
8. Bytownite	0.0	21.5	32.1	47.9	13.7	95.8	110.3	115.0	74.3	14.8	49.3	9.4	0.0	183.0	59.0	21.6	13.0	0.0
9. Sanidine	313.2	131.8	333.8	367.7	218.1	2777.6	1908.1	2129.2	3771.6	720.0	874.4	925.7	216.7	205.8	43.9	23.8	5.8	0.0
10. Bytownite	0.0	162.8	88.3	254.4	358.7	1841.2	556.8	852.7	295.6	34.7	84.3	63.6	0.0	0.0	83.8	17.8	5.4	11.2
11. Orthoclase	2272.0	1660.2	4788.3	3814.7	3738.7	56563.1	45394.7	45138.8	51206.0	4270.1	5759.9	4350.0	1427.9	2469.9	1453.0	702.8	335.1	38.3
12. Sanidine	1014.6	0.0	1271.0	1367.9	2699.5	14529.7	8365.7	8400.5	23376.0	3270.6	4187.4	3262.5	645.7	491.8	102.8	44.4	2.4	0.0
13. Microcline	1428.6	819.3	1261.7	1374.5	4674.5	149933.8	143465.0	125604.7	145146.1	15886.6	17292.3	14134.9	2604.7	3512.5	969.2	437.0	209.5	45.0
14. Microcline	15782.7	10809.7	45977.2	36694.3	17665.6	164087.1	145759.1	137676.3	150008.3	15232.2	18351.1	16270.5	4356.5	9025.9	4144.8	2514.2	1232.8	181.6
15. Albite	53084.1	33730.1	156907.7	129508.2	46880.1	409397.0	528776.0	493502.2	745983.3	74393.0	89802.3	69383.2	27993.5	71151.6	56663.6	33688.0	16092.4	1808.1
16. Anorthoclase	0.0	0.0	0.0	0.0	0.0	0.0	0.0	0.0	0.0	0.0	0.0	0.0	0.0	0.0	0.0	0.0	0.0	0.0
17. Albite	0.0	0.0	0.0	0.0	0.0	19.6	5.5	2.1	0.0	0.0	7.9	1.3	0.0	0.0	12.0	0.0	0.0	1.1
18. Albite	32524.9	11599.4	27272.1	23796.2	16660.7	81521.7	29307.0	45547.0	69099.7	0.0	18017.6	17264.9	41683.2	146533.9	93389.9	46424.9	18250.8	1643.0
19. Labradorite	25.0	0.0	0.0	0.0	0.0	62.7	62.1	27.6	57.5	0.0	33.9	0.0	0.0	0.0	5.7	0.0	0.0	0.0
20. Microcline	5532.4	3374.9	10650.1	9981.1	13324.6	233432.9	219637.6	207306.7	269831.0	33952.6	45513.8	42317.1	10154.5	17729.1	8643.0	5531.9	3119.1	535.4
21. Microcline	8460.0	4878.3	15186.9	14188.1	19048.1	338178.0	330560.1	300082.1	436571.4	54130.9	77594.7	72933.0	18944.8	32328.3	15375.0	8629.7	4492.4	665.5
22. Orthoclase	0.0	0.0	0.0	0.0	0.0	0.0	0.0	0.0	0.0	0.0	0.0	0.0	0.0	0.0	0.0	0.0	0.0	0.0
23. Oligoclase	62707.3	40190.6	181416.8	150221.1	48083.8	64619.8	36083.7	38336.0	67899.9	1436.7	14264.6	4778.9	6476.3	13924.7	32029.3	19385.4	8662.2	930.2
24. Labradorite	0.0	0.0	106.8	0.0	0.0	131.6	23.1	159.2	33.7	15.5	27.9	0.0	0.0	2.0	6.5	0.0	0.0	0.0
Spec. Corr. factor	12.7	13.0	17.6	18.2	27.0	5.8	4.8	5.1	5.8	6.6	6.6	8.4	10.6	14.7	24.1	48.3	153.1	809.1

APPENDIX H The counts measured in each waveband for the various feldspars shown with backgrounds subtracted and corrected for electronic "pile-up" and signal depletion by the repeated short exposures (the counts in each waveband were determined by sequential subtraction). These data therefore represent the signals observed uncorrected for detector spectral response; their significance is that the proportion of total counts seen here in a given waveband gives an indication of the significance of that waveband with respect to the integrated signal. This enables assessment of the relative importance of each waveband when observed by a spectrally uncorrected detector, i.e., a "normal" broadband luminescence detector system.

Multiplication by the spectral correction factors (shown separate from the body of the table, and derived from the filter transmissivities and PMT spectral response) gives correction for detector spectral response.

APPENDIX I "NATURAL" AND REGENERATED FELDSPAR GLOW CURVES

It was hypothesised that, as found by Templer (1985b) for a low temperature TL peak in zircon, a relation may exist between peak width and the distribution of trapping state energy levels and fading (for example a more disordered lattice may result in a "smearing" out of energy levels, manifest as broader glow peaks due to the greater range of electronic environments experienced by the members of a given trap type population). In an attempt to quantify this the FWHM of the glow peak complex was measured following test doses, for later correlation with fading behaviour. The compound nature of many of the lower temperature peak complexes introduced a degree of subjectivity into the FWHM estimates (in the absence of peak stripping software) and both the TL peak-widths of the compound peaks and the peak-widths and T_{max} data of the most prominent peaks are given in Table I1. For purposes of correlating peak-width with fading, the latter data was used.

I.1 EXPERIMENTAL

Initially, the TL present in the "as received" samples was drained by heating at 5 K/s to 550°C, with reheat. As most of the samples originate from museum collections their prior light exposure history was unknown, making this particular measurement of limited utility only. Following this thermal draining, test doses of 1 Gy then 100 Gy were given to each sample, with similar TL measurement routines after each dose. These irradiations were intended to display the glow curve structure in the temperature range upwards from ambient, both to indicate the magnitude of the populations of unstable traps

present in this range (of direct relevance to optical dating as competitor traps for retrapping during optical readout and irradiation, and as source traps for thermally transferred TL during preheats) and to assess the potential of using the low temperature glow curve structure as a "signature" for characterization purposes.

I2 RESULTS AND DISCUSSION: POTENTIAL FOR RECUPERATION

The "natural" TL glow curves are given in Fig.I1 with selected regenerated glow curves overlain. The extreme sensitivity of some of the high Na and high K feldspars resulted in the exclusion of the corresponding "100 Gy" data due to excessive "pile-up" signal loss in the TL reader (no "neutral" density filters were used so as to maintain the same spectral detection window throughout).

Apart from the question of correlation with fading, as discussed in chapter 8, it is noteworthy that all samples exhibit their greatest sensitivities, at the doses used, at glow peaks which would not be expected to retain charge over time spans of interest to dating. The inference drawn here is that the traps corresponding to these lower temperature peaks are either intrinsically more numerous than those giving rise to the glow peaks seen in the natural signals, or they possess far greater trapping cross sections. This is of significance for any charge transfer processes. An example of a potential problem raised by this sensitivity in conjunction with the temperature range of these peaks, and therefore their lifetimes at ambient temperatures, is that of recuperation (Aitken and Smith, 1988). Under certain transportational and depositional conditions the bleaching of the geological TL will result in significant PTTL peaks which will not be bleached to insignificance because of the absence of repeated bleaching cycles. In these cases thermal decay of this PTTL

following depositional burial may result in a long term on-going recuperation with the magnitude of the recuperated signal being dependent on the time elapsed since burial (this is in contrast to the case of quartz where the only significant recuperation will occur with the decay of the 110°C peak within ≈ 1 day). Competition during irradiation or readout are additional situations in which the relative prominence of the lower temperature peaks may play a role.

Finally, the absence of prominent 110°C peaks supports the inference drawn from the TAC curves (section 3.6) that feldspars do not ordinarily play a significant role in pre-dose dating.

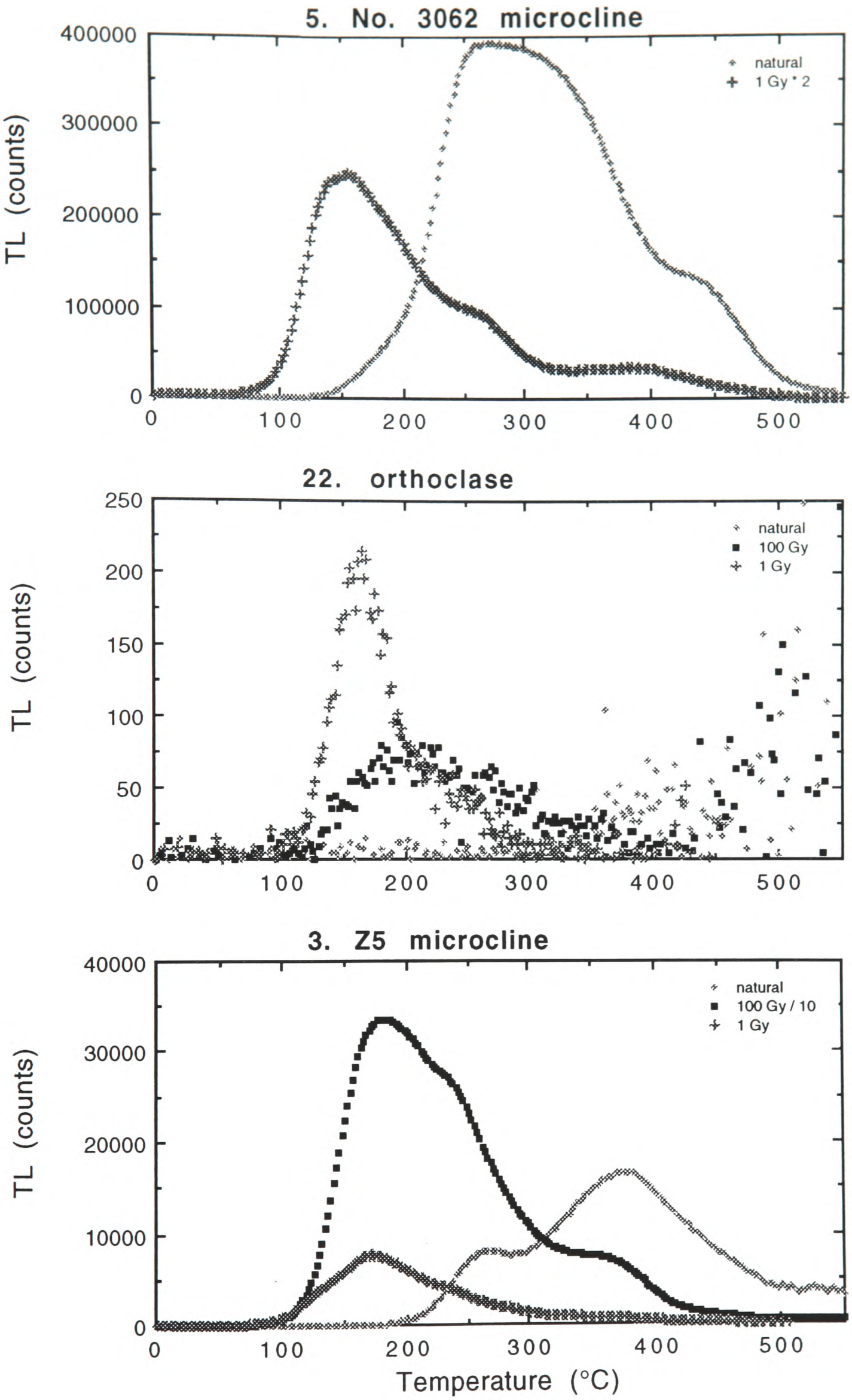
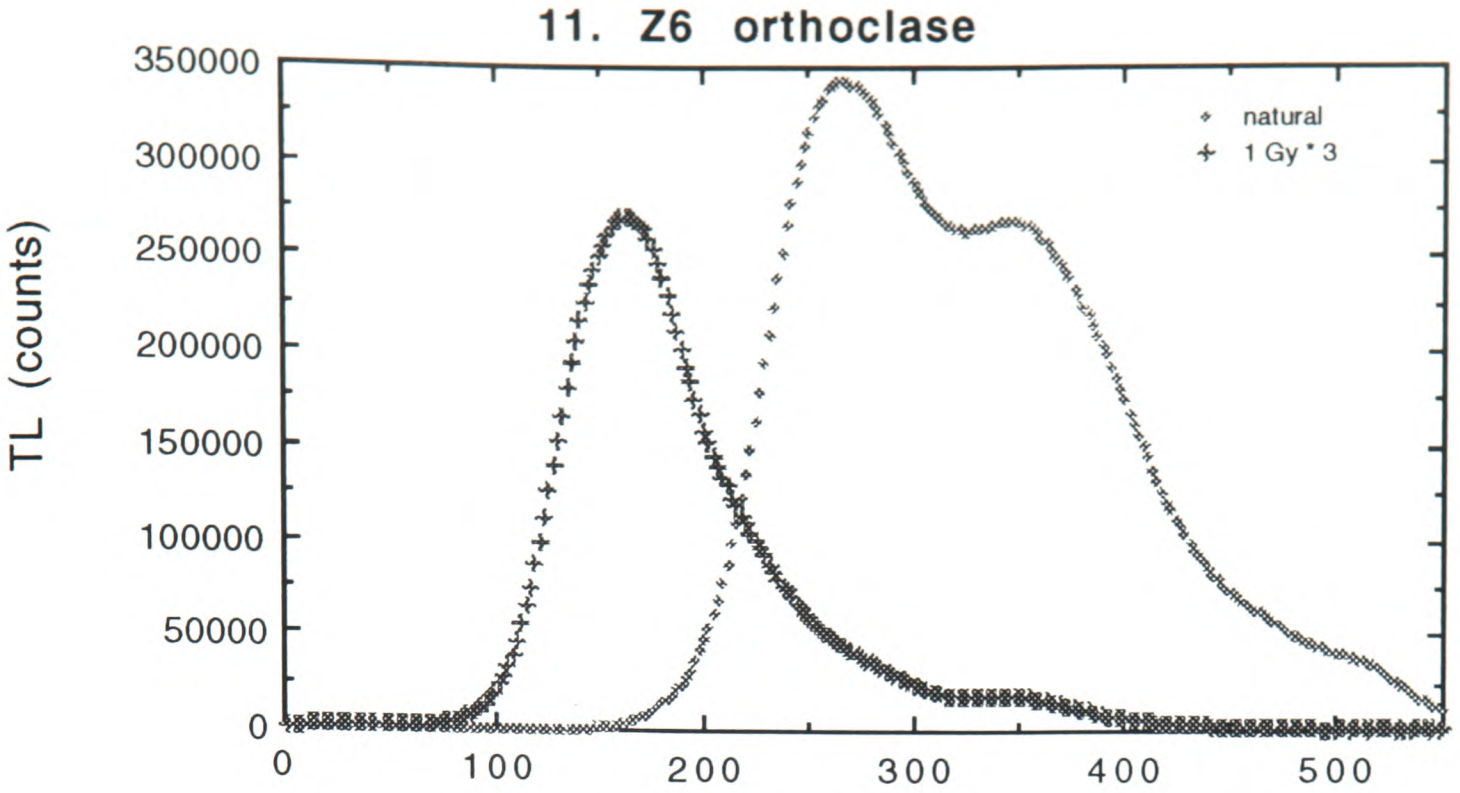
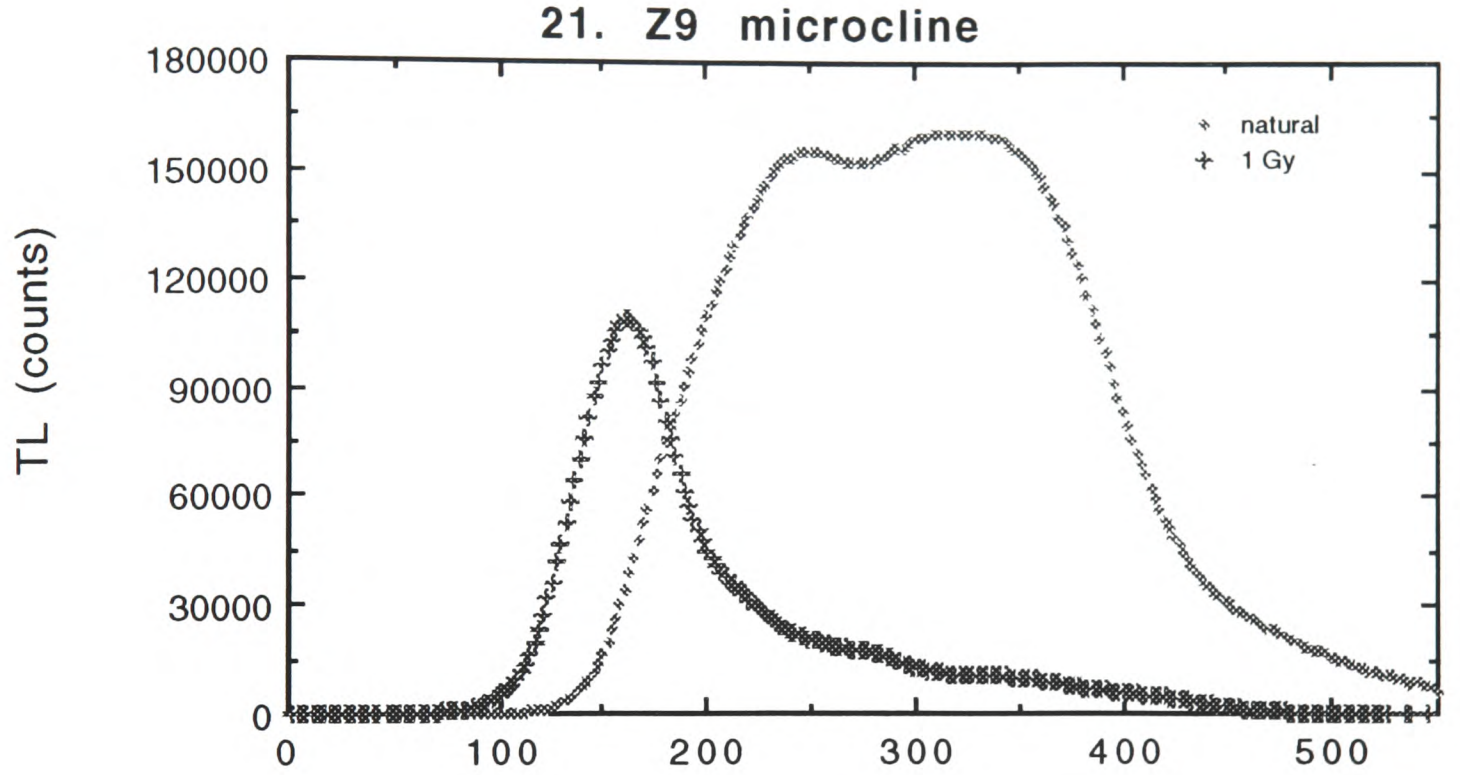
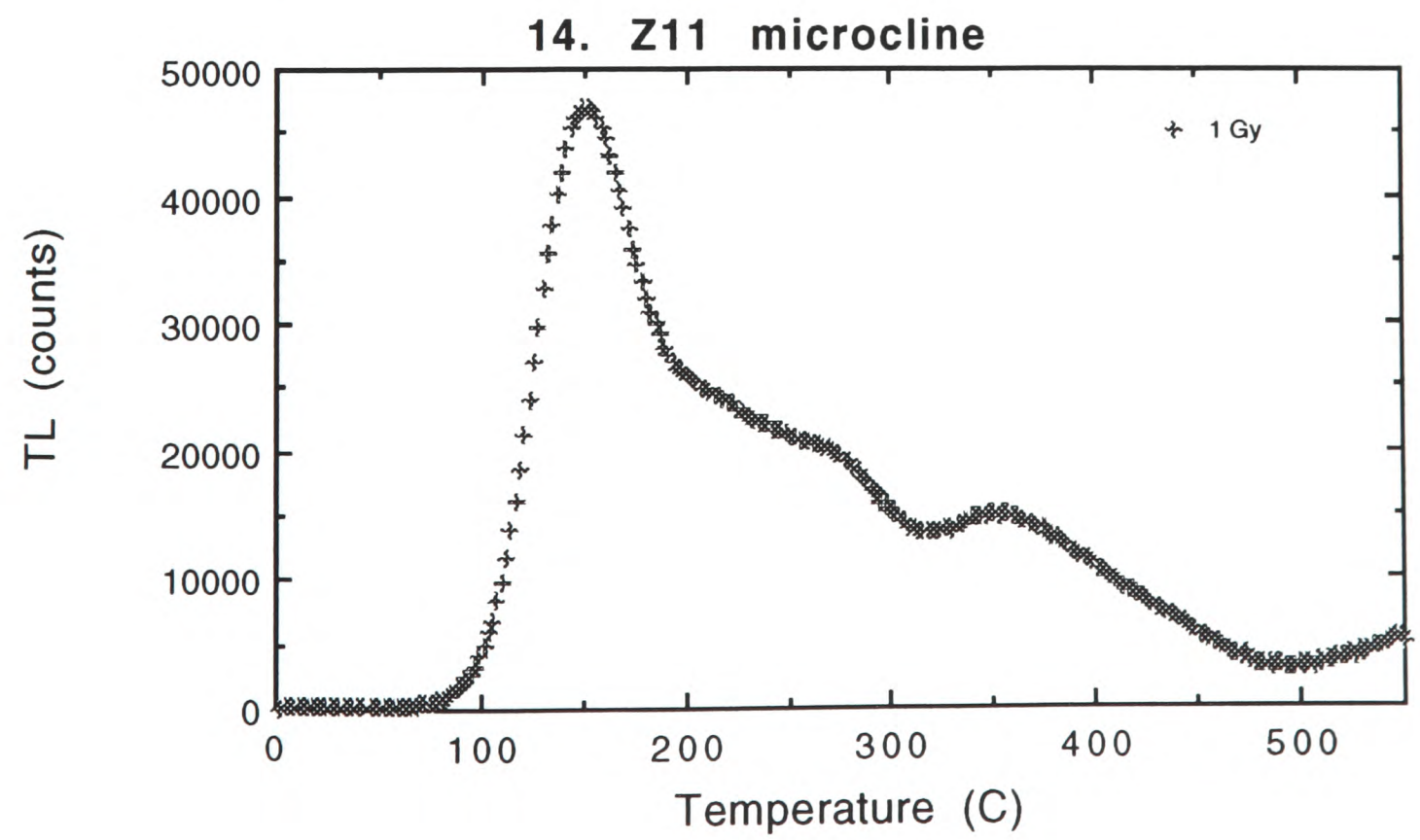
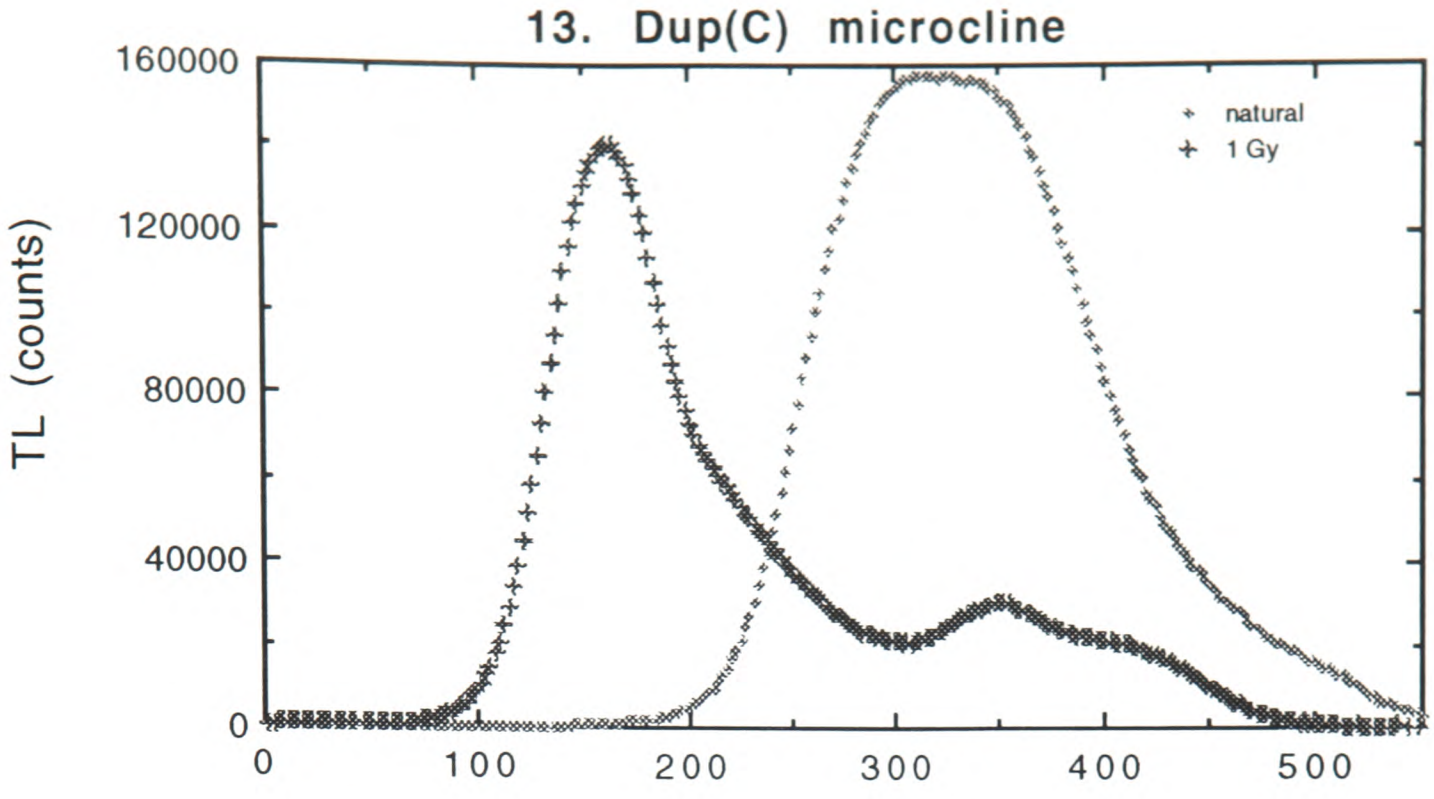


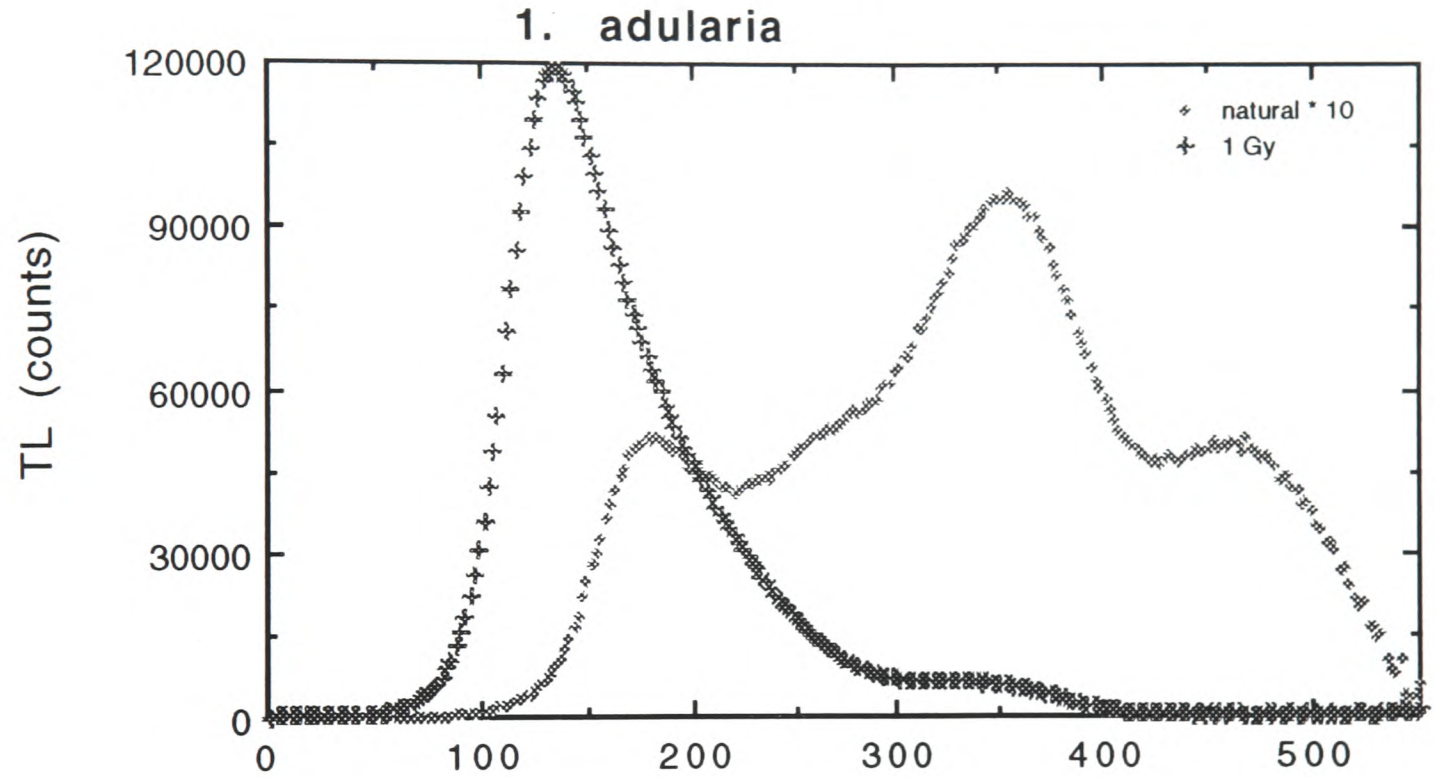
Fig.I1 The natural TL glow curves, along with TL induced by 1 Gy or 100 Gy irradiations. The regenerated TL was measured promptly, with no preheat. Data are counts/2K. Scaling has occasionally been necessary to permit clear comparison between overlain glow curves; in these cases the scaling factors are given in the legend.

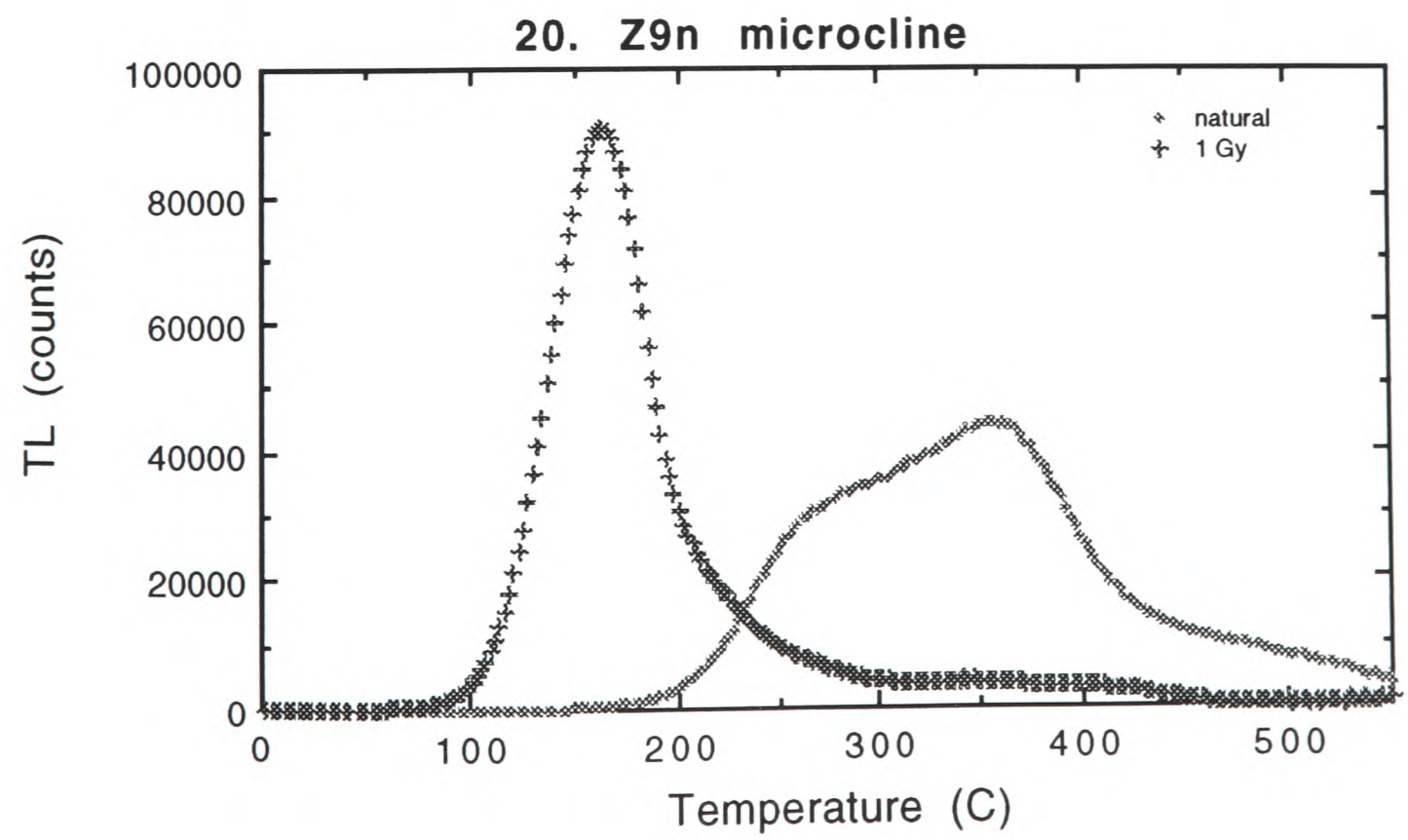

11. Z6 orthoclase
TL (counts)
350000
300000
250000
200000
150000
100000
50000
0
natural
1 Gy * 3
0
100
200
300
400
500


21. Z9 microcline
TL (counts)
180000
150000
120000
90000
60000
30000
0
natural
1 Gy
0
100
200
300
400
500

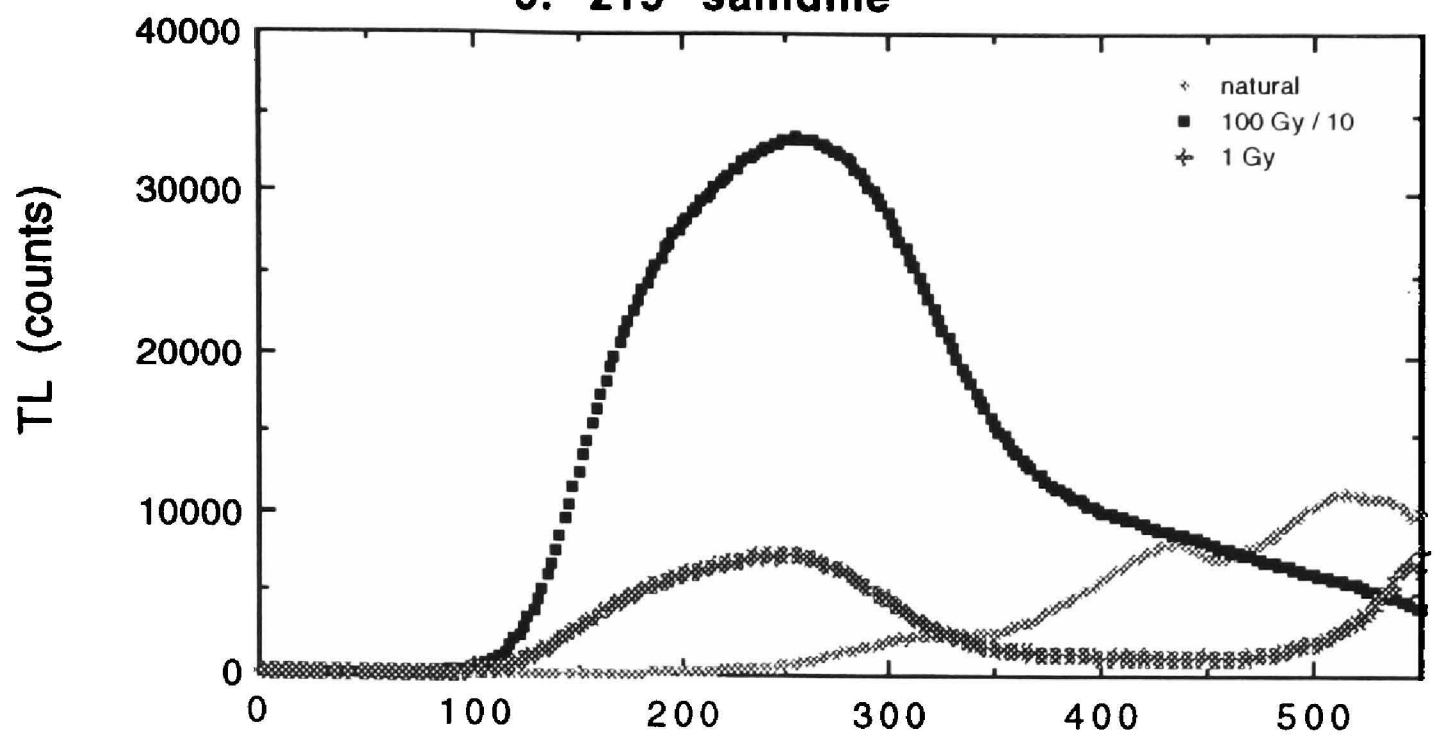

14. Z11 microcline
TL (counts)
50000
40000
30000
20000
10000
0
1 Gy
0
100
200
300
400
500
Temperature (C)


13. Dup(C) microcline
TL (counts)
160000
120000
80000
40000
0
0
100
200
300
400
500
natural
1 Gy

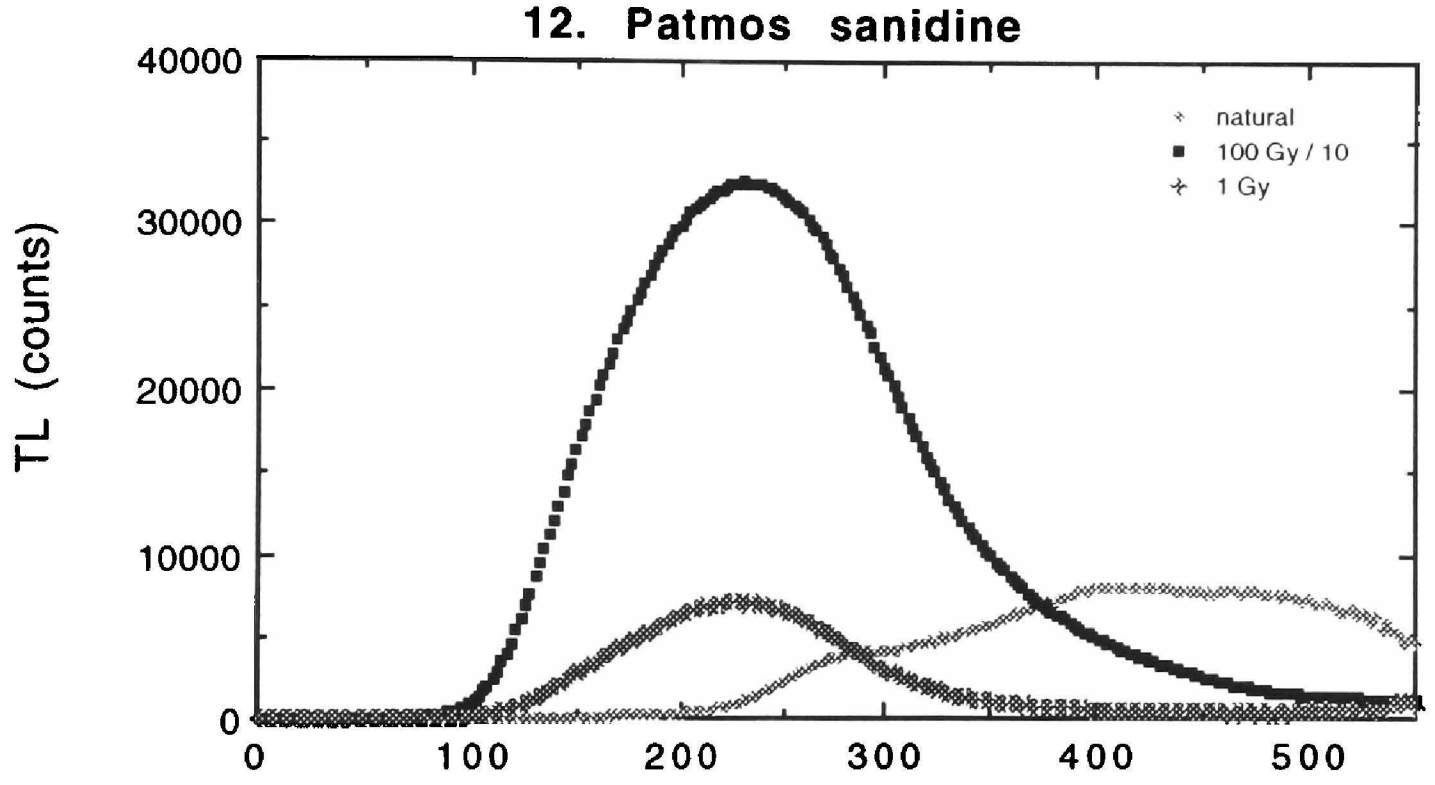

1. adularia
TL (counts)
120000
90000
60000
30000
0
0
100
200
300
400
500
natural * 10
1 Gy


20. Z9n microcline
TL (counts)
100000
80000
60000
40000
20000
0
0
100
200
300
400
500
Temperature (C)
natural
1 Gy

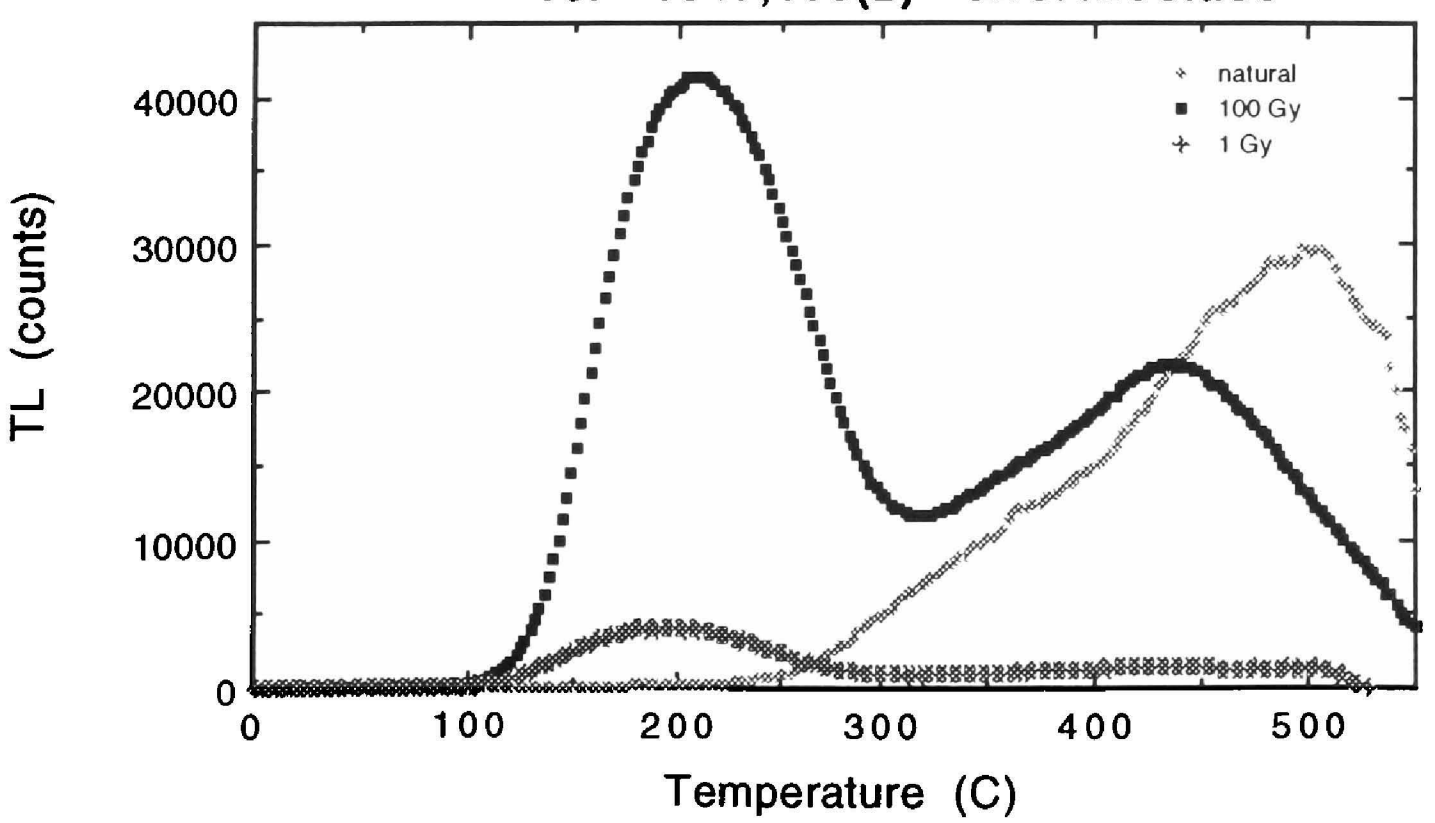
9. z15 sanidine

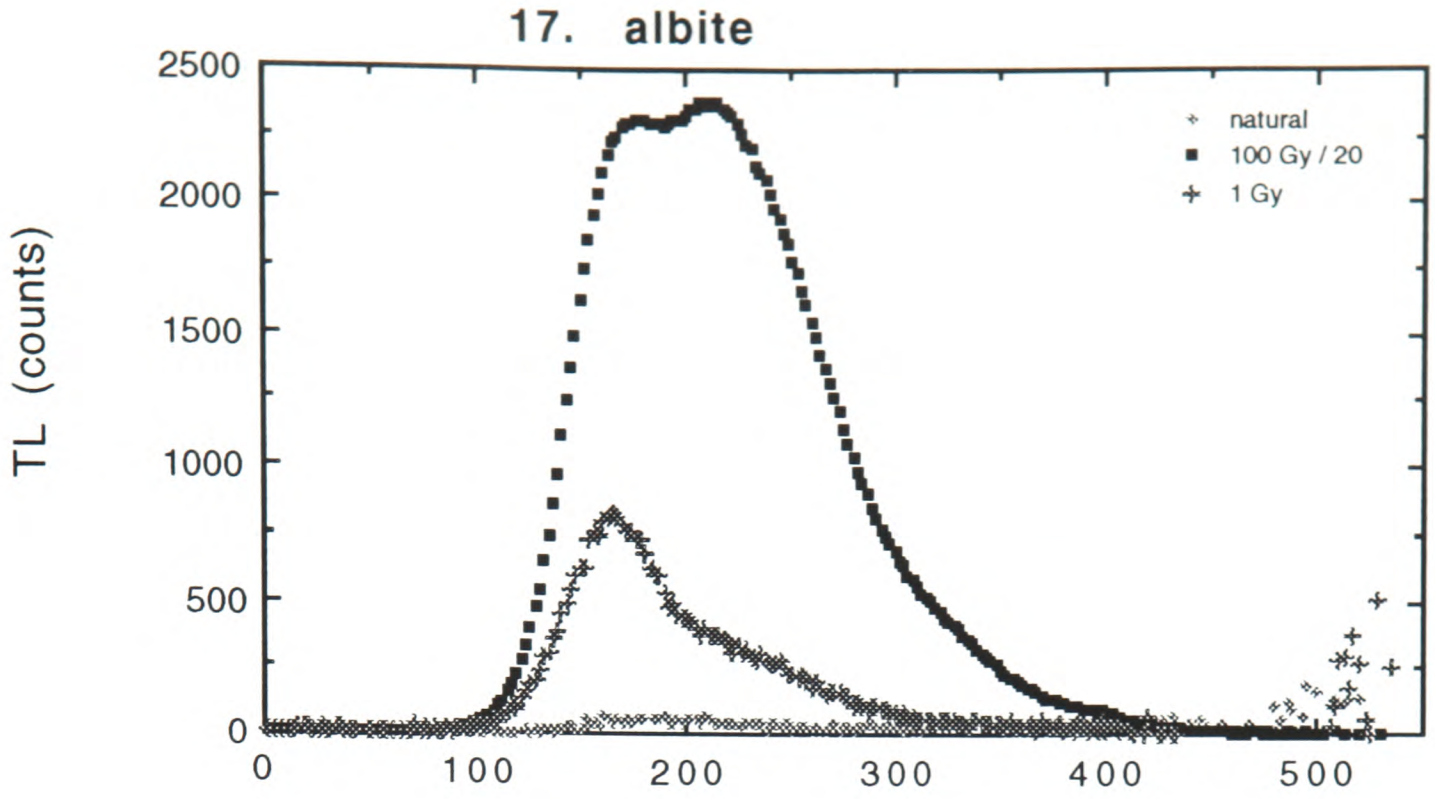


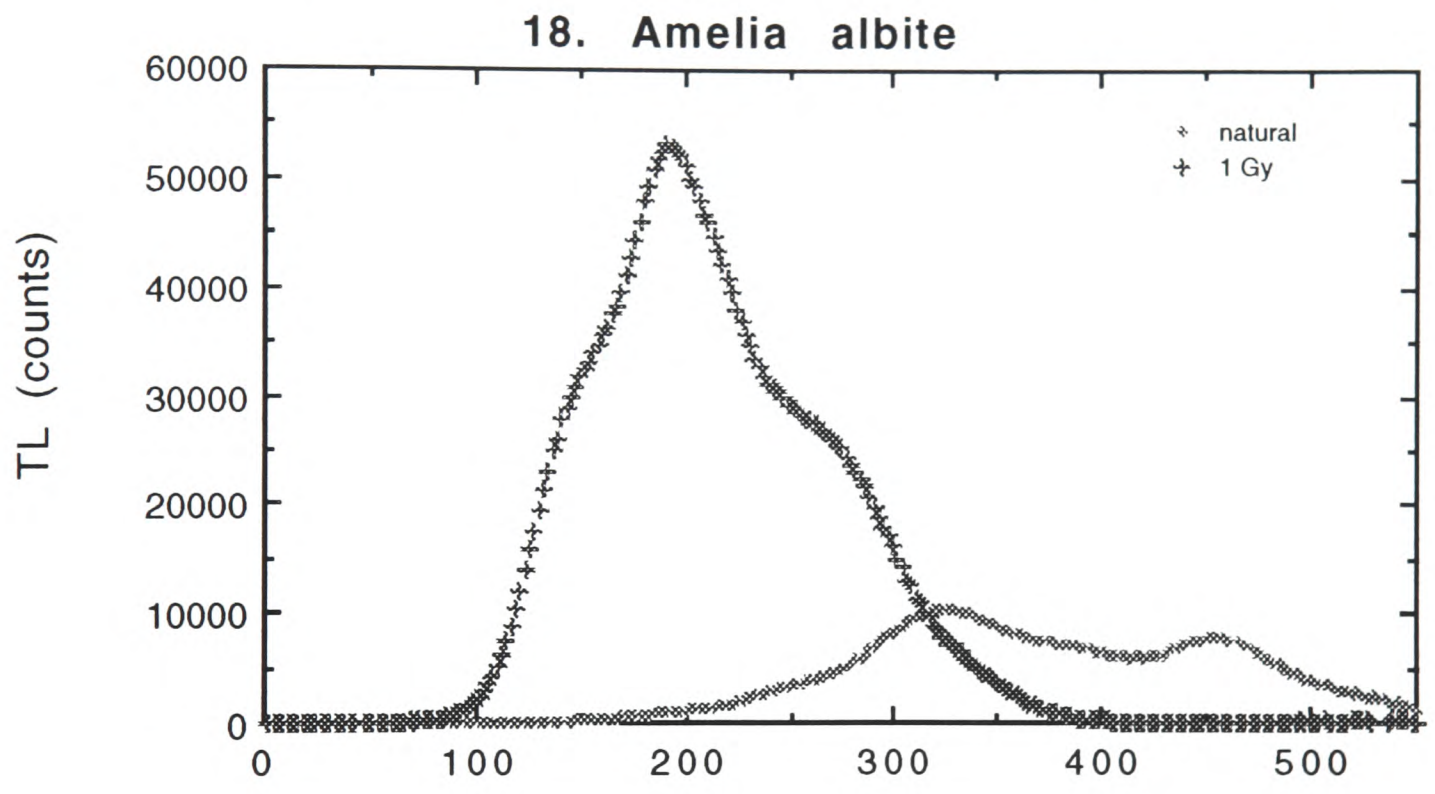
12. Patmos sanidine

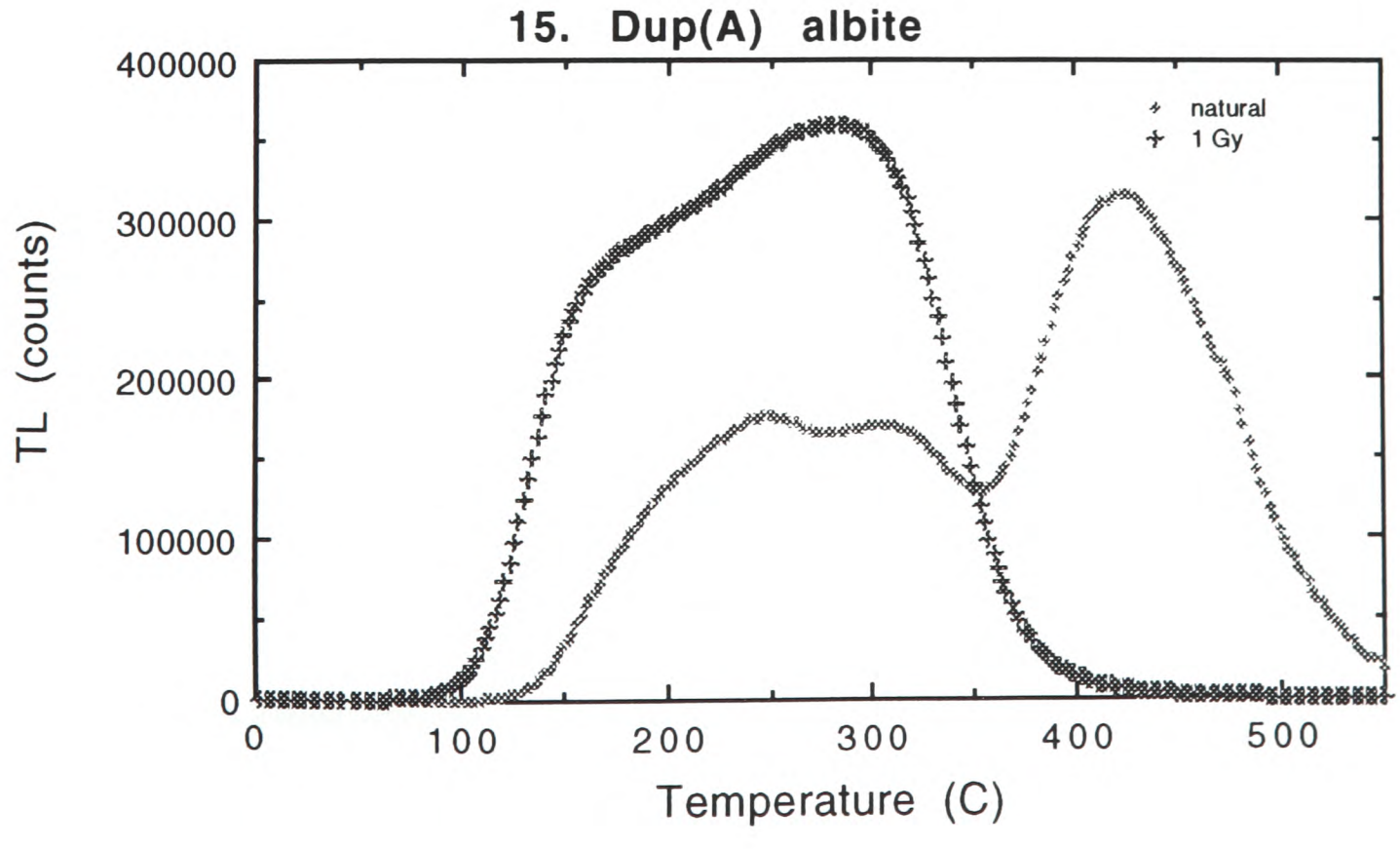


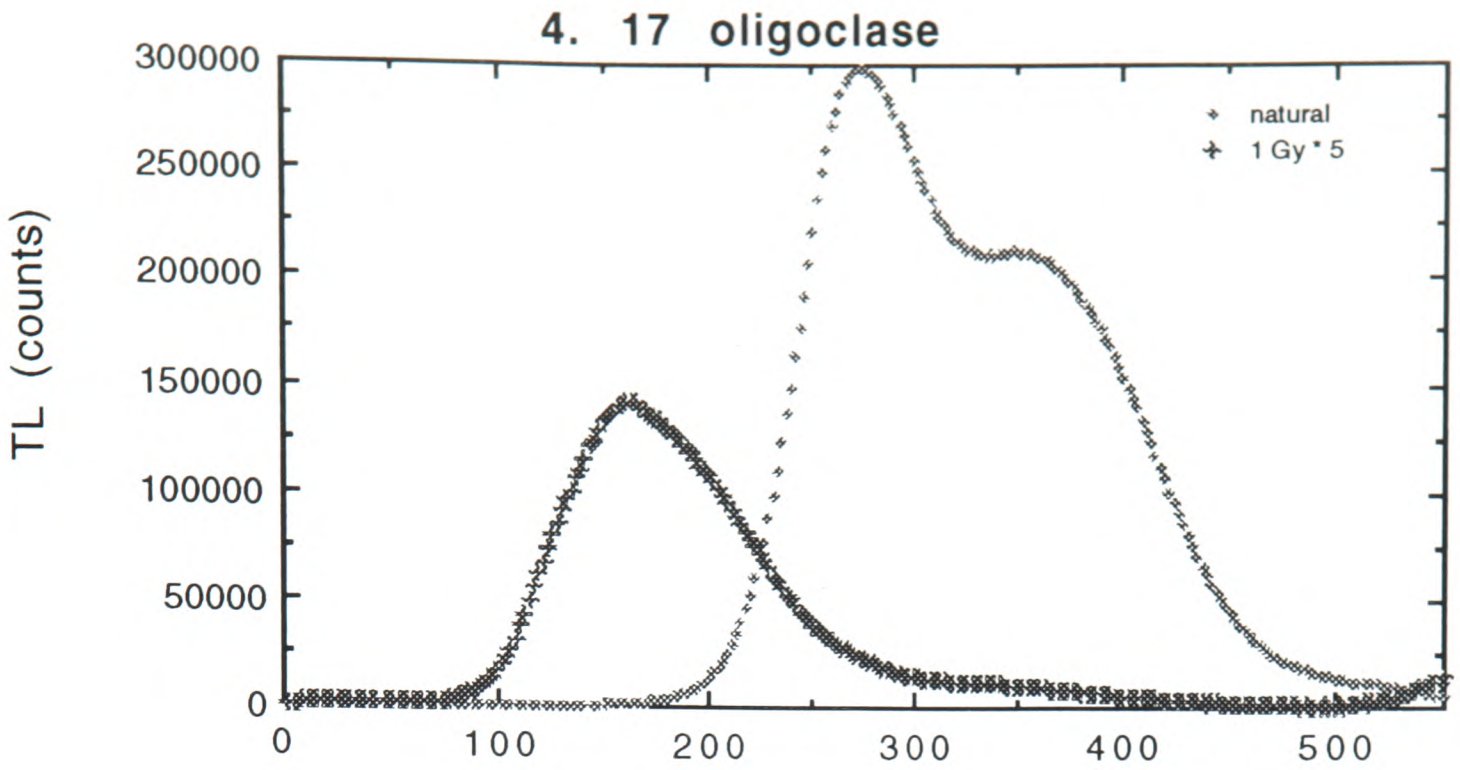
16. 1947,199(2) anorthoclase

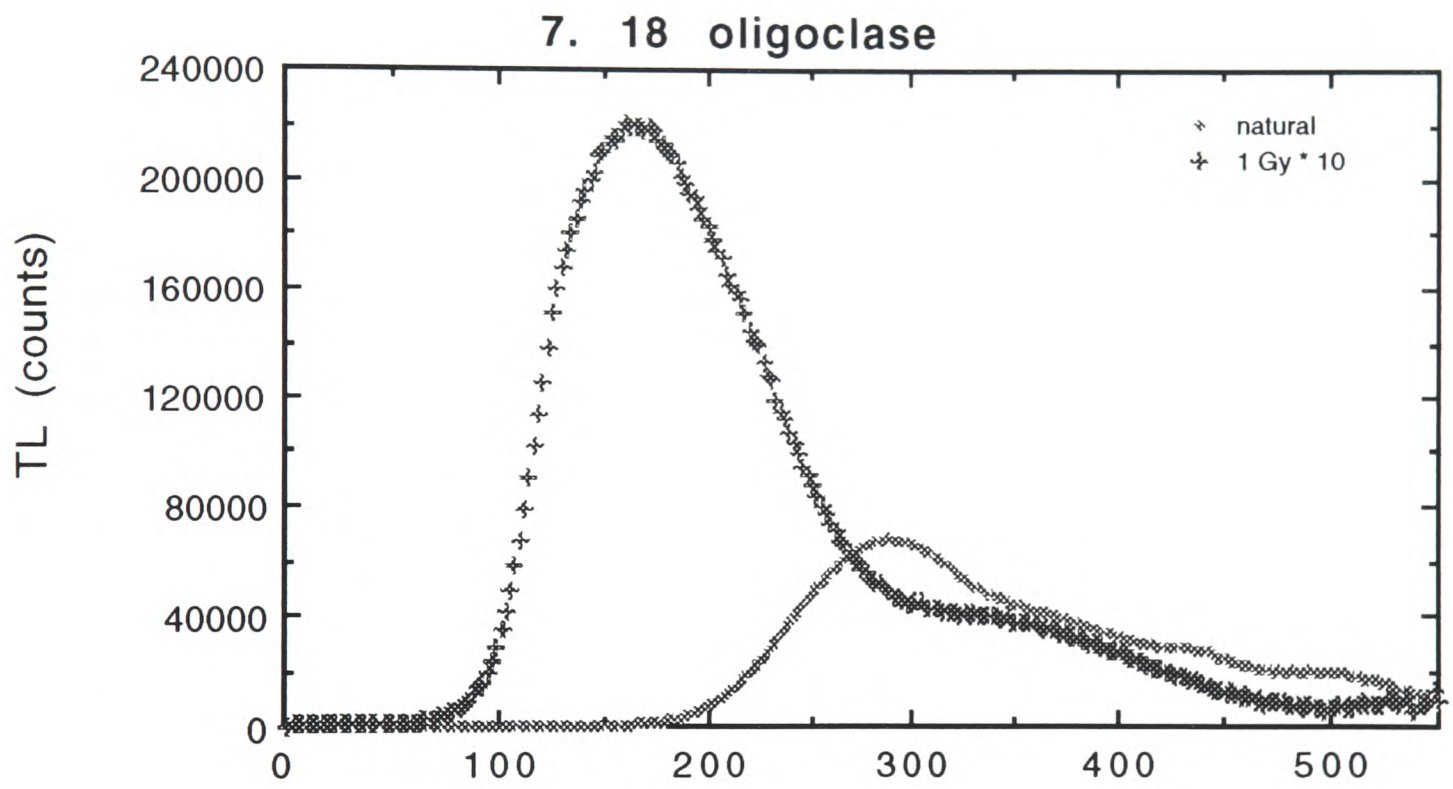


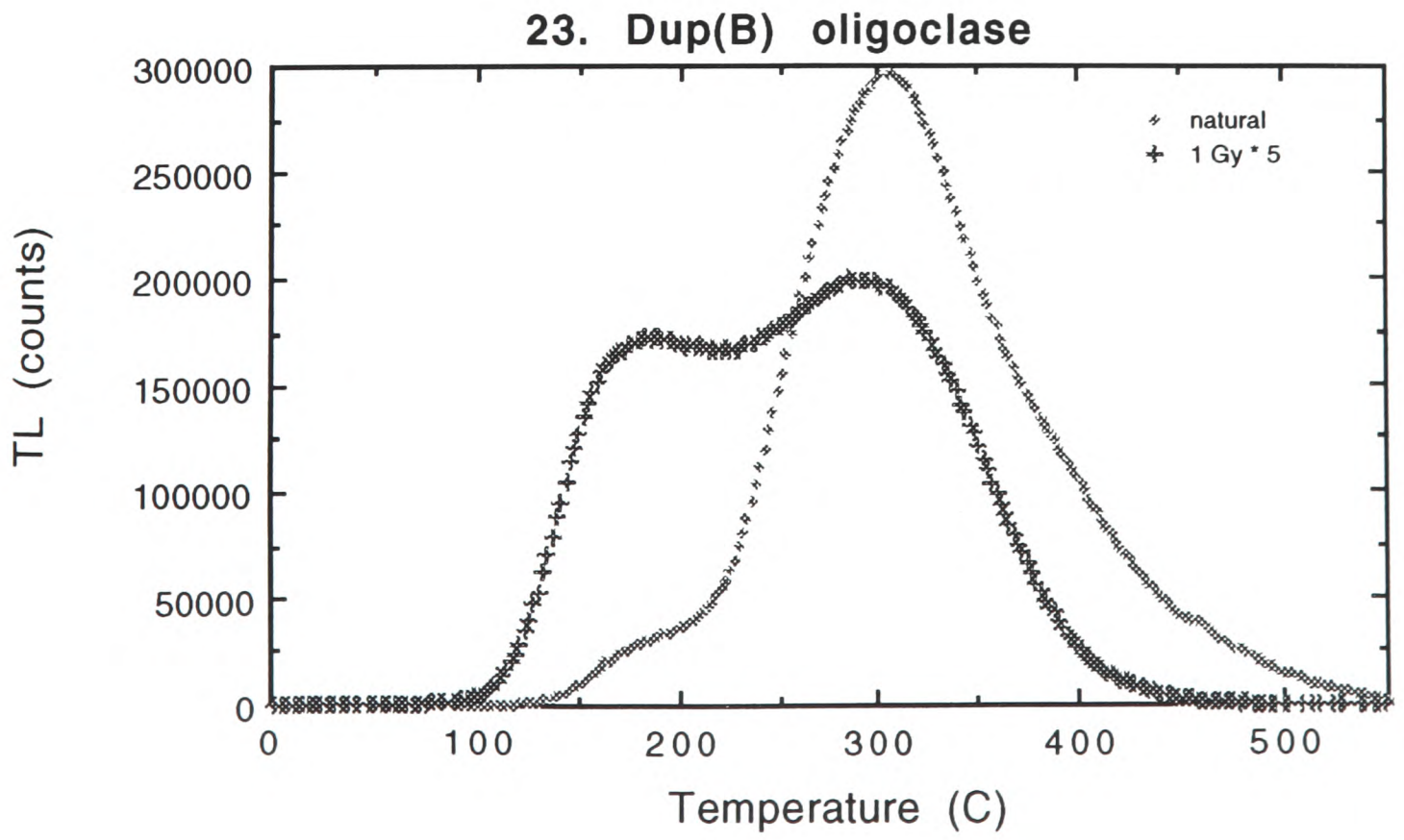

17. albite
TL (counts)
2500
2000
1500
1000
500
0
0
100
200
300
400
500
natural
100 Gy / 20
1 Gy

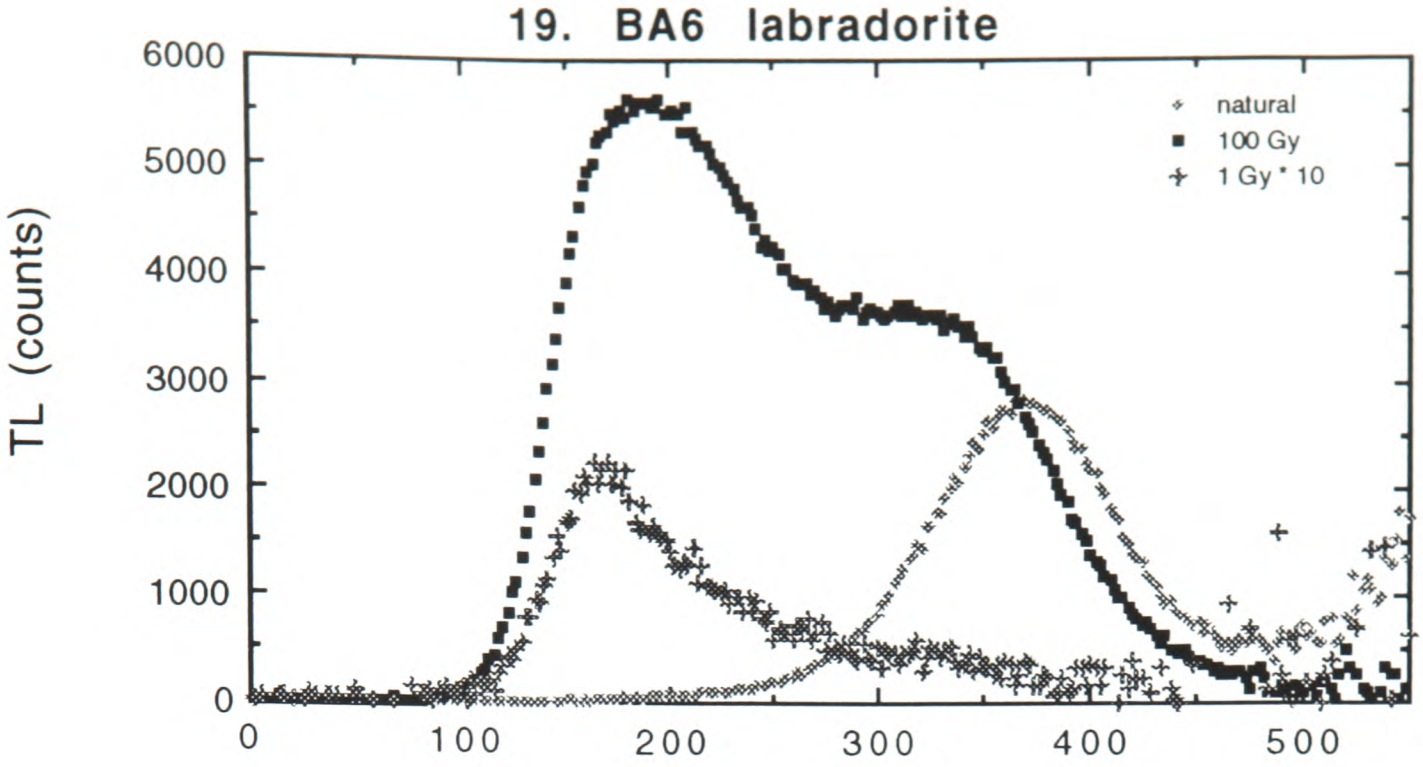

18. Amelia albite
TL (counts)
60000
50000
40000
30000
20000
10000
0
0
100
200
300
400
500
natural
1 Gy

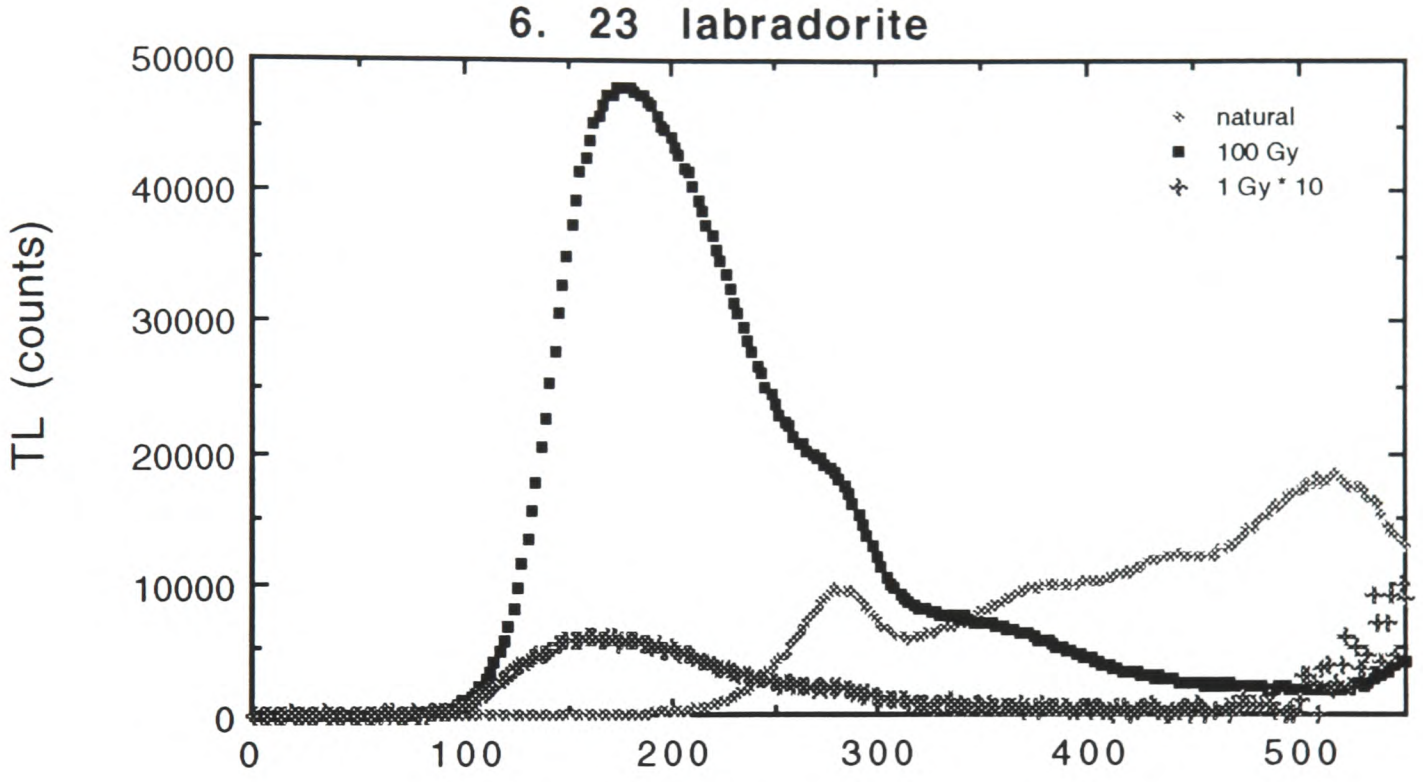

15. Dup(A) albite
TL (counts)
400000
300000
200000
100000
0
0
100
200
300
400
500
Temperature (C)
natural
1 Gy

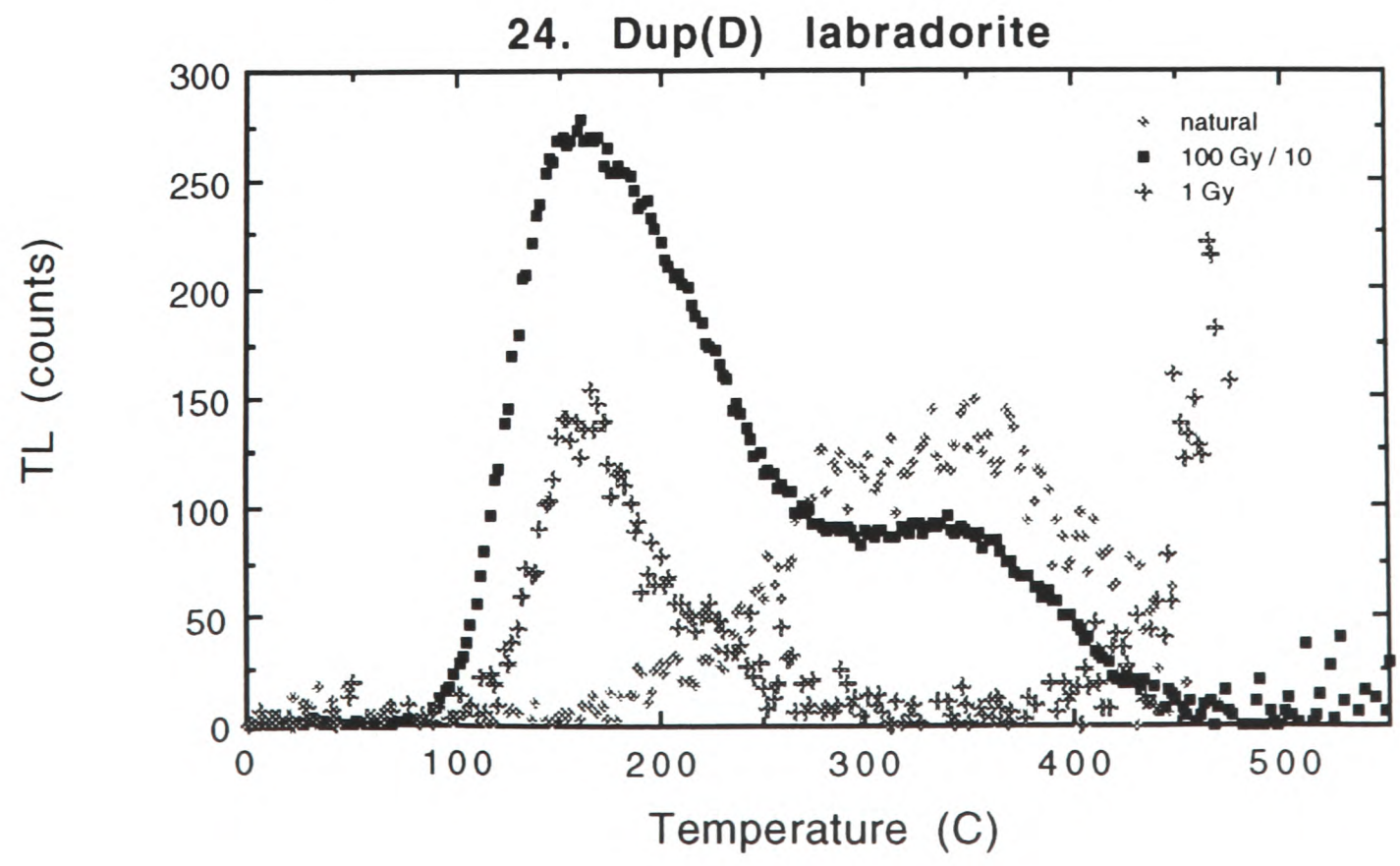

4. 17 oligoclase
TL (counts)
300000
250000
200000
150000
100000
50000
0
0
100
200
300
400
500
natural
1 Gy * 5

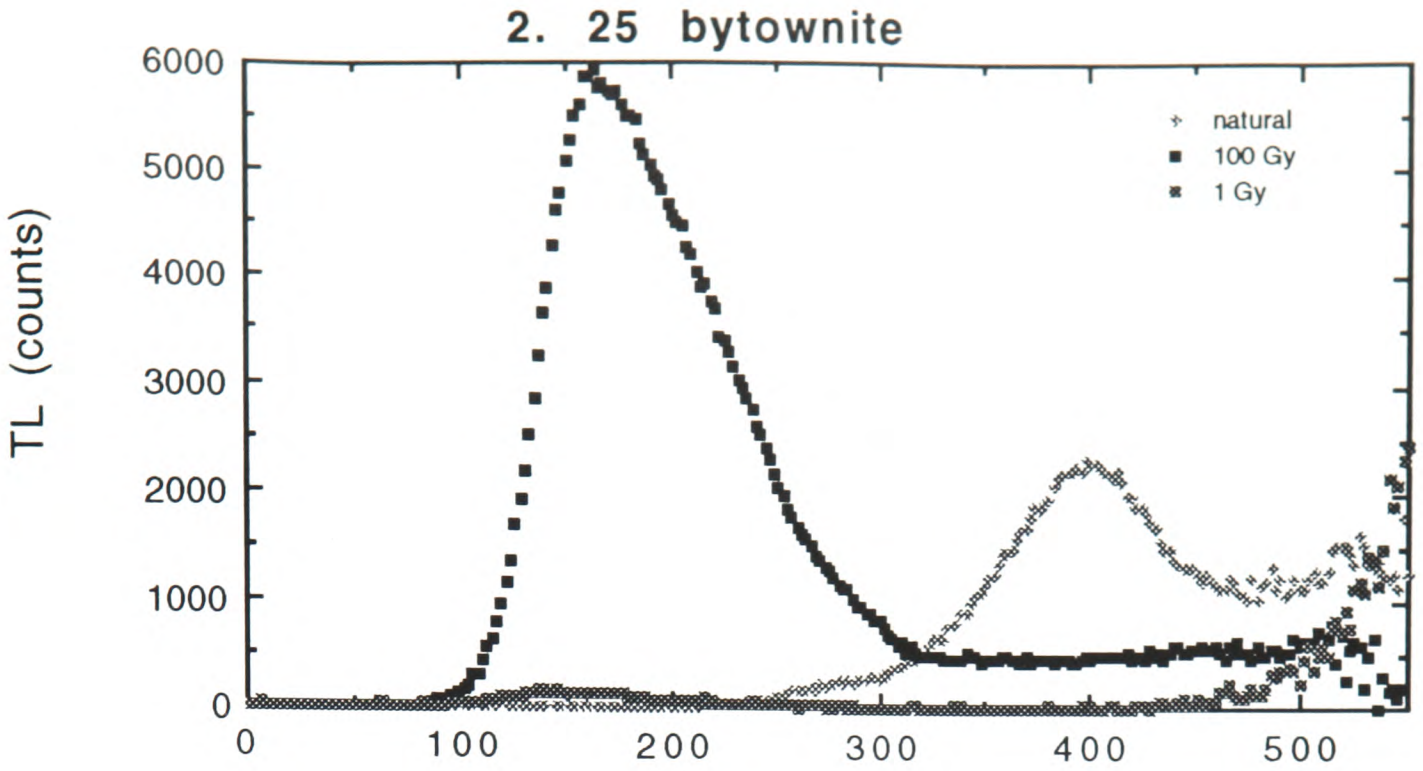

7. 18 oligoclase
TL (counts)
240000
200000
160000
120000
80000
40000
0
0
100
200
300
400
500
natural
1 Gy * 10

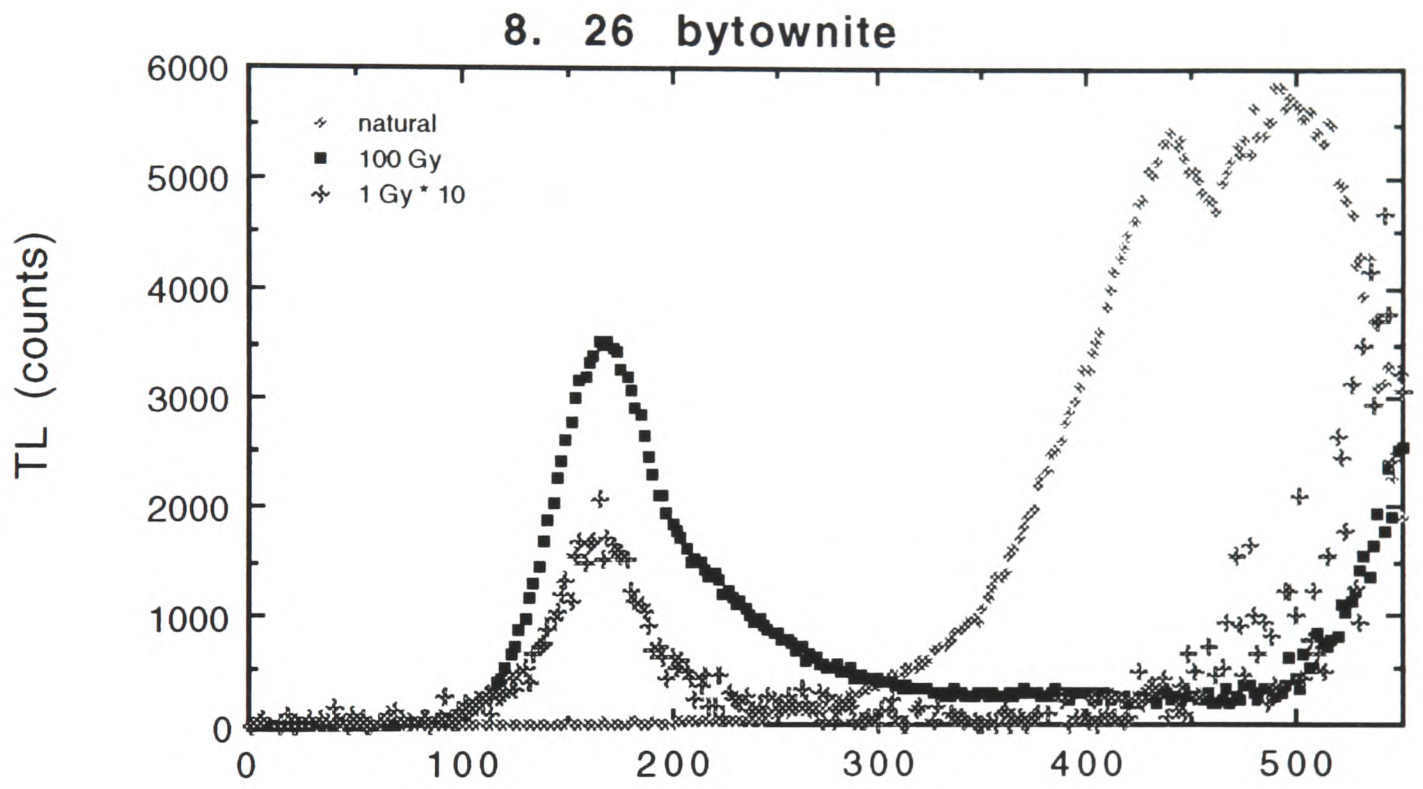

23. Dup(B) oligoclase
TL (counts)
300000
250000
200000
150000
100000
50000
0
0
100
200
300
400
500
Temperature (C)
natural
1 Gy * 5

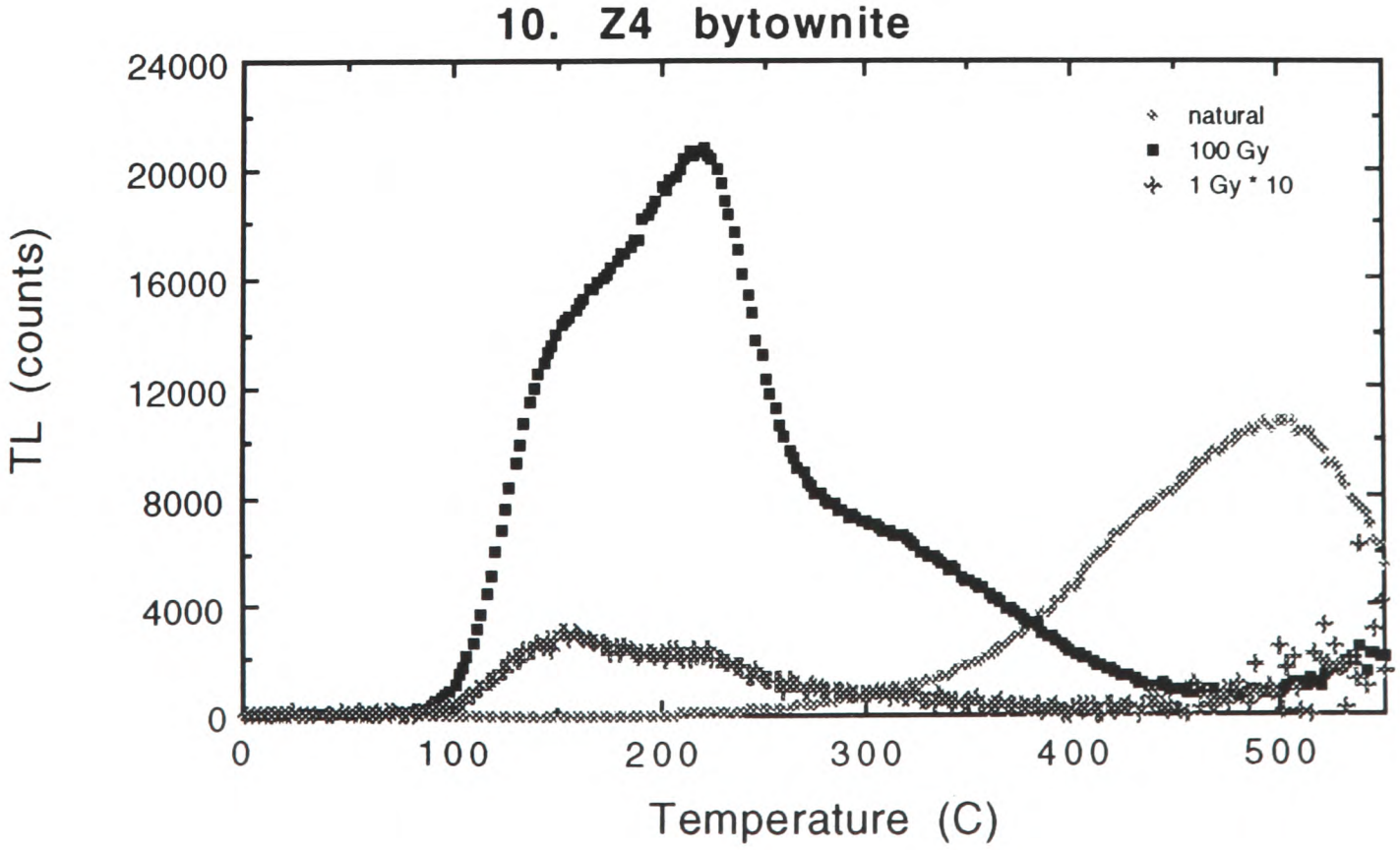

19. BA6 labradorite
TL (counts)
6000
5000
4000
3000
2000
1000
0
0
100
200
300
400
500
natural
100 Gy
1 Gy * 10


6. 23 labradorite
TL (counts)
50000
40000
30000
20000
10000
0
0
100
200
300
400
500
natural
100 Gy
1 Gy * 10


24. Dup(D) labradorite
TL (counts)
300
250
200
150
100
50
0
0
100
200
300
400
500
Temperature (C)
natural
100 Gy / 10
1 Gy


2. 25 bytownite
TL (counts)
6000
5000
4000
3000
2000
1000
0
0
100
200
300
400
500
natural
100 Gy
1 Gy


8. 26 bytownite
TL (counts)
6000
5000
4000
3000
2000
1000
0
0
100
200
300
400
500
natural
100 Gy
1 Gy * 10


10. Z4 bytownite
TL (counts)
24000
20000
16000
12000
8000
4000
0
0
100
200
300
400
500
Temperature (C)
natural
100 Gy
1 Gy * 10

FELDSPAR	TL peak Temp. (°C)	FWHM (°C)	"Stripped" TL peak Temp. (°C)	"Stripped" FWHM (°C)
5. No. 3062 microcline	155	100	155	71
22. orthoclase	164	50	164	50
3. Z5 microcline	183	129	183	71
11. Z6 orthoclase	164	83	164	83
21. Z9 microcline	163	62	163	62
14. Z11 microcline	150	100	150	60
13. Dup(C) microcline	162	74	162	74
1. adularia	137	79	137	79
20. Z9N microcline	163	57	163	57
9. Z15 sanidine	256	186	256	186
12. Patmos sanidine	230	174	230	174
16. 1947,199(2) anorthoclase	210	117	210	117
17. albite	214	131	177	57
18. Amelia albite	193	129	193	60
15. Dup(A) albite	285	205	171	67
4. 17 oligoclase	161	105	161	105
7. 18 oligoclase	165	121	165	121
23. Dup(B) oligoclase	294	217	180	93
19. BA6 labradorite	190	229	190	98
6. 23 labradorite	179	110	179	110
24. Dup(D) labradorite	160	117	160	117
2. 25 bytownite	165	100	165	100
8. 26 bytownite	166	64	166	64
10. Z4 bytownite	221	124	221	74

Table I1. The T_{max} values for the lower temperature TL peak complexes, along with their measured FWHM. Also shown are the corresponding values estimated for the dominant peak of each sample.

Synopses from a Workshop on

LONG & SHORT RANGE LIMITS

in

LUMINESCENCE DATING

Oxford, April 11-13, 1989

The Research Laboratory for Archaeology
& the History of Art
Oxford University

Occasional publication no 9

OPTICAL DATING - ACHENHEIM BEYOND THE EEMIAN USING GREEN AND INFRA-RED STIMULATION

Nigel A. Spooner and Danielle G. Questiaux
Research Laboratory for Archaeology and the History of Art,
Oxford University, 6 Keble Road, Oxford OX1 3QJ, U.K.

INTRODUCTION

Given the apparent existence of an upper age limit of ≈ 100ka (Debenham, 1985) for the thermoluminescence (TL) dating of the fine grain fraction of aeolian deposits, an attempt was made to determine if the technique of optically-stimulated luminescence (OSL) dating could exceed this "100ka barrier".

To this end, a series of trials were conducted on a pre-Eemian loessic sample in which stimulation wavelength, emission wavelengths detected and duration of pre-heating at 160°C were varied.

The sample (Laboratory reference 722t1) was collected from the loessic sequence of Achenheim, near Strasbourg. The layer from which it was collected was situated in the sequence above the Achenheim III pedocomplex related to the Holsteinian Interglacial (>320ka) and below the Achenheim II pedocomplex (<220ka). Further details of this sequence can be found in Lautridou et al, (1985), or Packman, (1989).

Two optical stimulation wavelengths were used : 514.5nm (blue-green) from an Ar-ion laser, and 853 Δ 82nm (infra-red (IR)) from a xenon lamp set, the latter following the work of Hütt, (1988) who reported the use of IR for dating at the 1987 Cambridge meeting.

A significant benefit of IR stimulation of polymineral samples is the degree of selectivity obtainable between mineral species; quartz, calcite and zircon have been found not to emit detectable luminescence under similar IR exposure conditions, either from natural or β dosed and pre-heated samples. Work by Hütt, (1988), and by the authors, on various known composition feldspars, leads to the attribution of the observed signal to feldspar minerals. Although there may be some luminescence contribution from other mineralic components of loess, such as amphiboles, pyroxenes or tourmalines, their low TL sensitivity and abundance makes this unlikely to be significant.

Assuming then that the signal originates from feldspar minerals, and that the TL and OSL emission spectra are congruent, it follows from the work of Akber (1986), Pasternack and Levy (1978) and Prescott (pers. comm.) that discrimination between alkali feldspar and plagioclase can be made by suitable choice of emission wavelengths observed. Consequently, five emission wavebands were chosen when IR stimulation was used,principally to observe the prominent feldspar emission peaks. However, under 514.5nm stimulation, the necessity of rejecting scattered stimulation photons restricted emission detection to blue/UV wavelengths.

The set of samples was divided into subsets, each treated identically except for receiving a different duration of pre-heat at 160°C.

THE OPTICAL STIMULATION LIGHT SOURCES

The Ar-ion laser unit is described elsewhere (Smith et al, 1986) and will not be discussed here. IR stimulation was provided by a xenon lamp unit, described at the U.K. TL Seminar, Paisley, September 15-16th, 1988, and shown in Fig.1.

The set consists of a 1000W short arc xenon lamp, lamp housing and power supply,(Oriel Corp., models 66021 and 8540) along with an optical assembly for the selection, by filters, and delivery to the sample, by either optical fibres or fluid light guide, of the stimulation waveband of interest. The optical configuration was designed to maximize power/nm delivered to the sample within constraints imposed by the need to remove "waste heat" - off-band optical power - and to prevent stray and off-band photons entering the optical fibre guide and hence the photomultiplier. The additional problem of imaging an extended source - the arc itself - with consequent loss of power through beam divergence, was minimized by reducing to a minimum the optical path length between the condensing lens (lamp housing) and focussing lenses (minibench).

In these experiments, IR power received by the sample was
20mW cm^{-2}, in the waveband 853 ± 27nm.

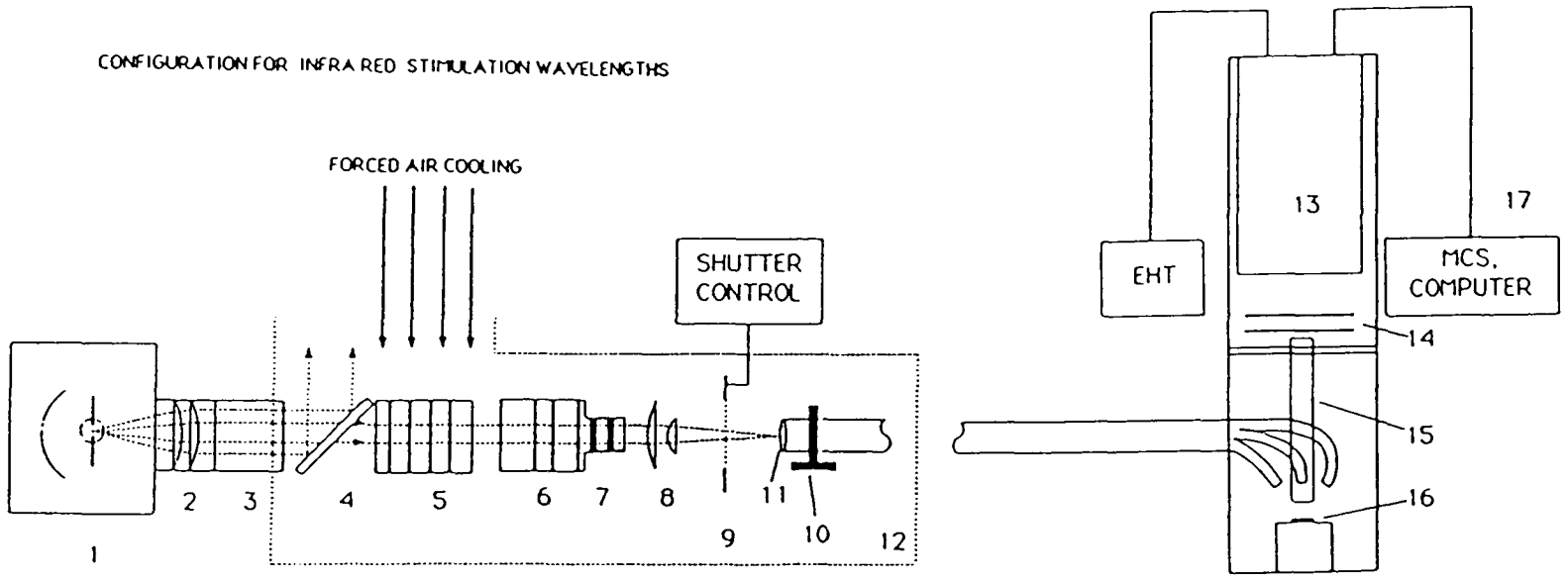


Fig.1. Schematic diagram of the xenon lamp OSL unit.

1. 1000W standard xenon lamp and spherical reflector in lamp housing #66021 (Oriel).
2. Condensing lens (Oriel).
3. Distilled water filter (Oriel) - absorbs IR >900nm.
4. "Cold mirror" interference filter (Ealing) used when IR wavelengths are to be selected - reflects ≈400-700nm light to water-cooled heat sink (not shown).
5. "Optical heat sink" - 2mm thick Schott edgecut colour glass filters in loose stack, cooled by forced air - removes off-band optical power from the beam line.
6. 3 x 2mm Schott edgecut colour glass filters, gasket-sealed to prevent light leakage.
7. Interference filters (Ealing) for final selection of stimulation waveband.
8. Focussing lenses (Ealing)

9. Ilex electronic shutter (Melles - Griot)
10. Three axis miniature stage (Ealing)
11. 6mm glass fibre bundle (Schölly), trifurcated, transmits ≈400-1400 nm light, (interchangeable with fluid light guide for UV transmission).
12. Optical assembly is mounted on an optical minibench (Ealing) within a light-proof box. Baffling eliminates stray light.
13. EMI 9635 QA PMT
14. Quick-change filter holder.
15. Spectrosil B light guide (U.Q.G.)
16. Sample, positioned on dimpled plate.
17. "Innovator" MCS card, Research Machines Nimbus VX minicomputer.

EXPERIMENTAL

The sample preparation, conducted under very low intensity red light, consisted of : dilute HCl (0.1 N) treatment for 5 days, multiple rinses with distilled water followed by hydrogen peroxide treatment for 7 days, multiple rinses with distilled water then acetone. Finally, the 4-11μm grain fraction, separated by sedimentation, was settled from acetone onto Al discs. The disc-to-disc variability, as assessed from short normalization shines (blue-green and IR stimulation), gave a 1 σ for the full set of discs as ≈ 3.6% and 6% of the mean respectively.

The additive dose (β) technique was used throughout, and all discs, whether natural or natural+β, were pre-heated. Pre-heats were conducted in two purpose-built thermostat ovens, with the various 160°C pre-heats being followed by 5-7 days at 100°C to remove the anomalous fading component.

The emission wavebands observed and the necessary filters are shown in Fig.2, along with the stimulation wavelengths and the principal feldspar TL emission bands. In all cases, regardless of stimulation wavelength, emissions were detected by EMI 9635 QA bialkali photomultiplier tubes.

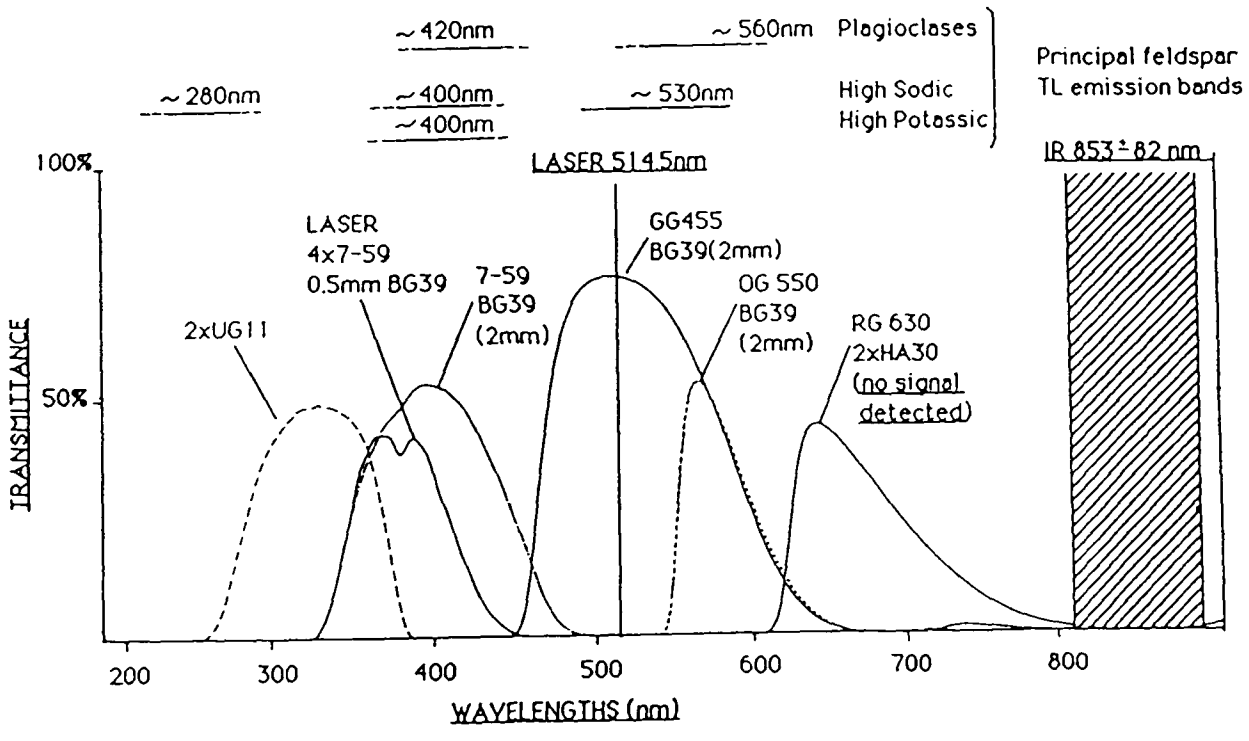


Fig.2. The blue-green and IR stimulation wavelengths, the filters used and the corresponding emission bands observed, and the principal feldspar TL emission bands.

Experimental procedure varied depending on whether IR or 514.5nm stimulation was used.

For IR stimulation:

0.05sec short shine (SS) for normalization → β dose → 160°C pre-heat for one of 0,1,2,4,8,16,88 hours → 5 days at 100°C → four SS (one for each emission band observed)

For blue-green stimulation:

0.04sec short shine for normalization → β dose → 0.5 hours at 160°C → 1 week at 100°C → SS → 1.5 hours at 160°C → cycles of 100°C (2 hours), 160°C, SS until the cumulative 160°C pre-heat reaches 16 hours

Exponential curves were fitted to the normalised data, using an exponential fitting program authored by B.W.Smith.

Normalisation was of the form of: $\frac{\text{SS light sum}}{\text{normalization SS light sum}}$

Dosimetry : the provisional dose rate was determined as 2.77 ± 0.18 Gy ka^{-1} using field γ-ray spectrometry and α counting. Laboratory γ-ray analysis by germanium γ-ray spectrometer indicated the sample was not in disequilibrium.

RESULTS AND DISCUSSION

Table 1 shows the equivalent doses (ED) and ages found for each emission band and 160°C pre-heat time, for both IR and blue-green stimulation; some corresponding families of growth curves are shown in Fig.3. The provisional dose rate of 2.77 ± 0.18 Gy ka^{-1} and the expected age of ≈220 - 320ka give an expected ED range of ≈610-890 Gy. This is clearly not approached by any of the combinations of stimulation wavelength, emission wavelength and 160°C pre-heat duration.

However, while there are no obvious trends suggesting that variations in these parameters will give ages more in concordance with geological expectation, a number of possibilities do exist. Although varying the duration of pre-heat at 160°C was unproductive, other pre-heat times and temperatures need investigation.

Only the additive dose technique was used here; others (Zöller and Wagner, 1989) have reported success in the dating of similar old loessic material by variants of the regeneration technique. Work along these lines is continuing. Preliminary findings from the application of the "strong thermal wash" treatment following bleaching (4 hours Sol 2) and regenerative β dosing are not encouraging - approximately 250 Gy ED was obtained.

160C Pre heat times (hours)	infrared 853 ±82 nm: 2 X UG-11	infrared 853 ±82 nm: 7-59 +BG39	infrared 853 ±82 nm: GG455 +BG39	infrared 853 ±82 nm: OG 550 +BG39	blue-green 514.5nm: 4 X 7-59 5mm BG 39
0	/	/	146 +55 -37	/	/
1/2	/	/	/	/	298 +53 -36
1	239 +90 -66	212 +100 -66	128 +32 -22	95 +14 -11	/
2	278 +38 -37	243 +45 -77	165 +44 -75	190 +74 -95	459 +50 -52
4	178 +61 -56	180 +50 -44	233 +23 -10	271 +28 -22	384 +71 -80
8	258 +123 -125	276 +87 -110	278 +51 -59	320 +48 -49	276 +39 -93
16	336 +71 -90	325 +119 -165	327 +123 -215	215 +53 -128	388 +104 -106
88	/	/	401 +90 -100	/	/

ED's in GRAYS

160C Pre heat times (hours)	infrared 853 ±82 nm: 2 X UG-11	infrared 853 ±82 nm: 7-59 +BG39	infrared 853 ±82 nm: GG455 +BG39	infrared 853 ±82 nm: OG 550 +BG39	blue-green 514.5nm: 4 X 7-59 5mm BG 39
0	/	/	53 +20 -13	/	/
1/2	/	/	/	/	108 +19 -13
1	86 +32 -24	76 +36 -31	46 +12 -8	34 +5 -4	/
2	100 +14 -14	87 +16 -28	60 +16 -75	69 +27 -34	166 +18 -19
4	64 +22 -20	65 +18 -16	84 +8 -4	108 +10 -8	139 +26 -29
8	93 +44 -45	100 +31 -40	100 +18 -21	115 +17 -18	100 +14 -34
16	121 +26 -32	117 +43 -56	118 +44 -78	78 +19 -46	140 +38 -38
88	/	/	145 +32 -36	/	/

AGES in ka

Table 1. Equivalent doses and ages for various combinations of pre-heat times at 160°C, emission wavebands and stimulation wavelengths.

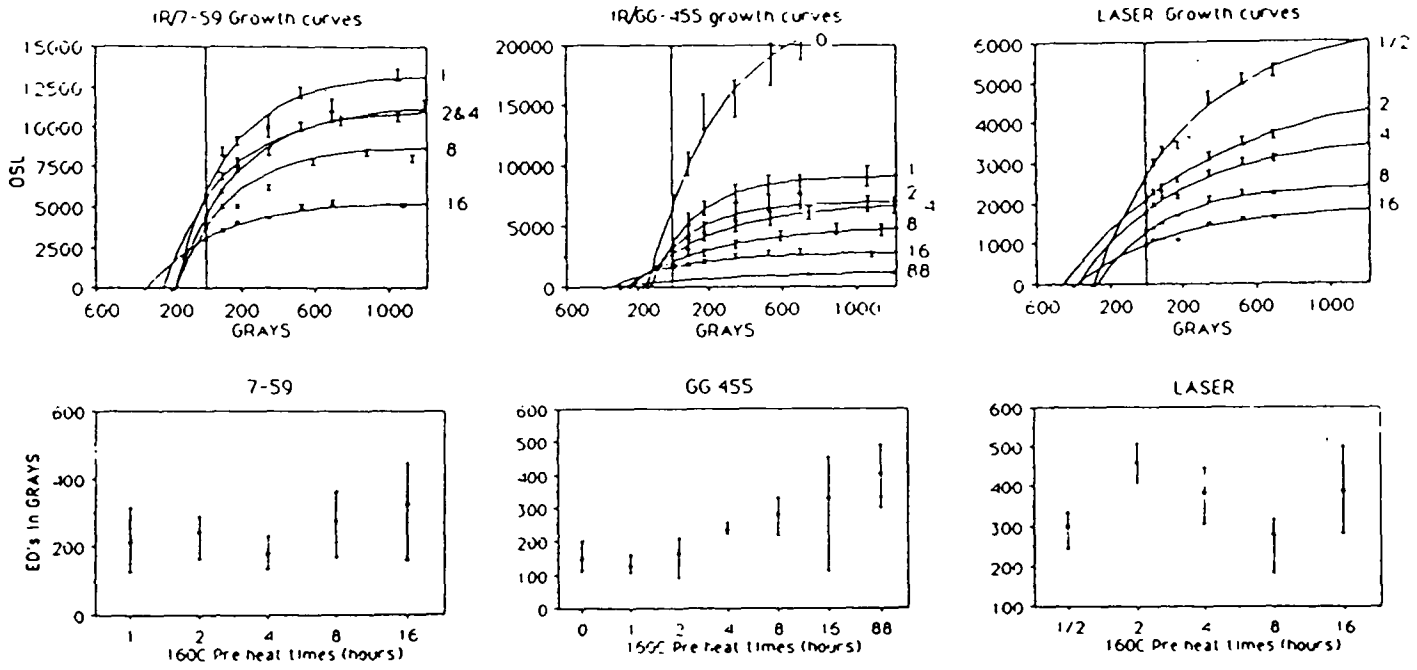


Fig.3. Growth curves and corresponding ED's for IR and blue-green stimulation, for the given wavebands and pre-heat times.

Another possibility is suggested by the observation that the blue-green stimulation produces ages which are significantly older than those from IR stimulation. An obvious explanation is that the signal contribution from the presumably saturated quartz in the sample adds a component to the age. However, studies on alkali feldspars have revealed that after a long IR exposure has removed the IR stimulable signal, there remains a substantial blue-green stimulable signal. Whilst this may also contribute to the discrepancy with the IR age, its greater optical stability may indicate greater thermal stability. The utility of this signal for dating is under investigation, both by blue-green and blue stimulation wavebands.

A difference in the shape of luminescence pulses produced by IR short shines was noted and seen to depend on the emission waveband observed (see Fig.4). Blue/UV emissions (BG-39 + 7-59 filters and 2xUG11

filters) showed pulse rise and fall within the shutter action time, whereas green/orange emissions (BG-39 + GG 455 filters and BG-39 + GG 550 filters) showed marked build-up and decay behaviour. The proposed correlation of emission waveband with feldspar species suggests that IR stimulated emission from plagioclase is dominated by a mechanism involving initial phototransfer to short lifetime traps (half-life 8±3ms at 19°C) followed by thermal untrapping and luminescent recombination, analogous to the model proposed for zircon luminescence (Smith, 1988).

It may be that the procedure of short shines by which the luminescence was measured leads to a systematic underestimation of the age, as opposed to ages determined by integrating to obtain the entire light sum. Preliminary results show ED's and ages found both by short shines and integrals of successively greater proportions of the luminescence agree within error limits. Further work is planned.

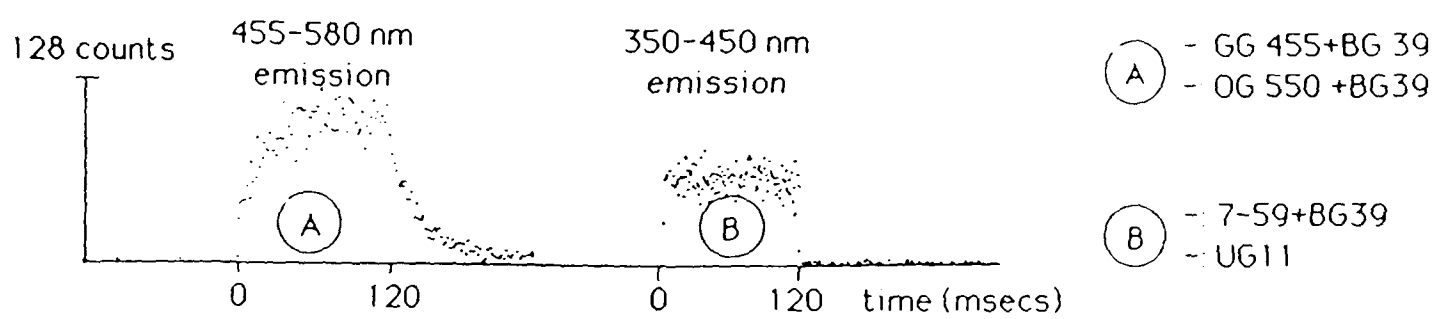


Fig.4. IR Stimulated Luminescence (0.12 sec. pulses) observed through (a) BG-39 + GG455 filters and (b) BG-39 + 7-59 filters

The effect of a long IR exposure (853 Δ 82nm, total energy 80Jcm^{-2}, final OSL rate ≈0.05% of initial rate) on the TL glow curves of both natural samples and additive dose samples (N + 360Gy β +24 hour delay) was briefly examined (see Fig.5). TL measurements were kindly made by Cate McElroy, using a Risø automated TL reader, heating rate 10Ksec^{-1} to 500°C maximum.

The extent of bleaching of the broad natural TL peak by IR exposure indicates that a significant proportion of the natural luminescence may be sampled by IR stimulation, suggesting a widespread applicability of the method, to feldspathic materials. The additive dose glow curve shows significant TL reductions at all glow curve temperatures, with notably greater erosion of signal on the high temperature edge. This is interpreted as due to the emptying of the stable IR bleachable traps, such as contribute to the natural TL, and also effectively an "optical washing" removal of the short term anomalous fading component, (Templer, 1985).

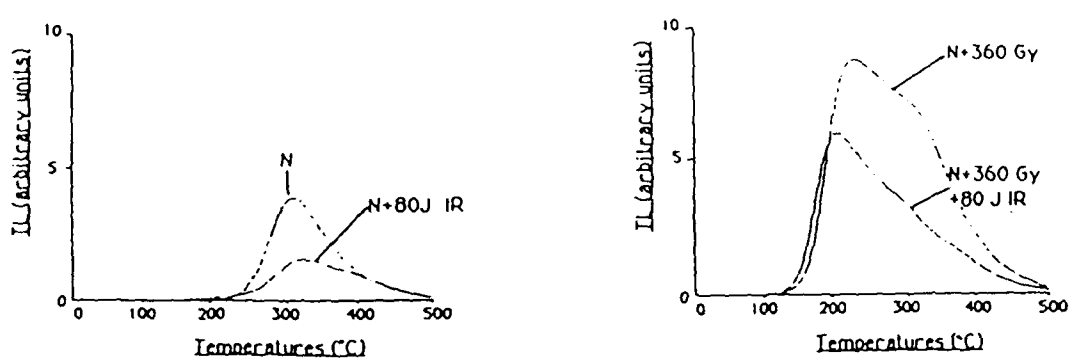


Fig.5. The IR bleaching of natural and additive dose TL.

CONCLUSIONS

No age determination, regardless of stimulation wavelength, emission wavelength or 160°C thermal pre-treatment, approached the supposed age of the sample, and the 100 ka limit was not convincingly exceeded. More work is needed to investigate the effects of various pre-heats, particularly in combination with regeneration techniques.

Discrimination is obtainable between mineral species under IR stimulation and furthermore, judicious choice of the luminescence emissions observed appears to discriminate between alkali feldspars and plagioclase. These findings open many possibilities, not the least being the prospect of IR dating from a selected feldspar component of a sample, followed by blue-green dating of the quartz component.

Also suggested is the monitoring for an IR stimulated signal from a "quartz" separate, as a convenient check for feldspar contamination.

ACKNOWLEDGEMENTS

We wish to thank Professors J Sommé and J-P Lautridou for collaboration in sampling, and Scott Wheeler, Dave Seeley, Martin Franks and John Fenton for their assistance in the construction of the xenon lamp unit.

REFERENCES

Akber, R.A., (1986), "Materials and techniques for thermoluminescence dating." Unpub. PhD thesis, University of Adelaide.

Debenham, N.C., (1985) "Use of UV emissions in TL dating of sediments". Nucl. Tracks, 10, No 4-6, 717-724.

Hütt, G., Jaek, I. and Tchonka, J., (1988), "Optical dating : K-feldspars optical response stimulation spectra." Quat. Sci. Rev., 7, 381-385.

Lautridou, J-P., Sommé, J., Heim, J., Puisségur, J-J., and Rousseau, D-D., (1985), "La Stratigraphie des loess et formations fluviatiles d'Achenheim (Alsace): Nouvelles Données Bioclimatiques et Corrélations avec les Séquences Pléistocènes de la France du Nord-Ouest. Bull. de l'Assoc. Francaise pour l'Etude du Quaternaire, 2-3, 125-132.

Packman, S.C., and Grün, R., (1989), "TL dating of loess samples from Achenheim", this volume.

Pasternack, E.S. and Levy, P.W., (1978), "Changes in TL emission spectra accompanying thermal disorder in Amelia albite". Geological Abstracts with Programs, 10, 468.

Smith, B.W. (1988), "Zircon from sediments: a combined OSL and TL auto-regenerative dating technique". Quat. Sci. Rev., 7, 401-406.

Smith, B.W., Aitken, M.J., Rhodes, E.J., Robinson, P.D. and Geldard, D.M., (1986), "Optical Dating: Methodological Aspects". Rad. Prot. Dos., 17, 229-233.

Templer, R.H. (1985), "The removal of anomalous fading in zircon". Nucl. Tracks, 10, No. 4-6, 531-537.

Zöller, L. and Wagner, G.A.(1989), "Partial thermal washing or strong thermal washing in TL dating of sediments?". This volume.

BIBLIOGRAPHY

Accorsi, C.A., Aitken, M.J., Cremaschi, M., Ferraris, M., McElroy, C., Questiaux, D.G. and Van Vliet Lanoe, B., (1990)
The loess deposits of the Rivoli moraine system
In "The loess in Northern and Central Italy: a loess basin between the Alps and the Mediterranean region", 21-39

Aitken, M.J., Huxtable, J., Wintle, A.G. and Bowman, S.G.E., (1975)
Age determination by TL: review of progress at Oxford
Proc. of the 4th Int. Conf. on Luminescent Dosimetry, Krakow, 1005-1010

Aitken, M.J., (1985)
Thermoluminescence Dating.
Academic Press, London

Aitken, M.J., (1992)
Optical dating.
Quat. Sci. Rev., 11, 127-131

Aitken, M.J. and Xie, J., (1992)
Optical dating using infrared diodes: young samples.
Quat. Sci. Rev., 11, 147-152

Aitken, M.J. and Smith, B.W., (1988)
Optical dating: recuperation after bleaching.
Quat. Sci. Rev., 7, 387-393

Akber, R.A., (1986)
Materials and techniques for thermoluminescence dating
Unpublished PhD thesis, University of Adelaide (Dept. of Physics)

Akber, R.A. and Prescott, J.R., (1985)
Thermoluminescence in some feldspars: Early results from studies of spectra
Nucl. Tracks Radiat. Meas., Vol. 10, 575-580

Akber, R.A. and Prescott, J.R., (1987)
Thermoluminescence dating: can we date all types of feldspars?
In: Archaeometry: Further Australasian Studies
Ed. Ambrose, W.R. and Mummery, J.M.J., 177-180, A.N.U., Canberra

Allsop, A. and Spooner, N.A., (0000)
A ceramic-substrate radiation source for luminescence applications
To be submitted to Rad. Prot. Dosim..

Bailiff, I.K., (1980)
Emission spectrum of the 'Facey' light source
Ancient TL, No. 12, 2-3

Bailiff, I.K., (1987)
TL analyses of ceramic tile
In: US / Japan joint reassessment of atomic bomb radiation dosimetry in Hiroshima and Nagasaki
Final Report, Vol. 2, Chapter 4, App. 7, 172-183, (1987)

Bailiff, I.K. and Poolton, N.R.J., (1989)
Charge transfer in quartz and feldspar: factors affecting the dating of young sediments
In Long and short range limits in luminescence dating,
Occasional Publication No. 9, Research Laboratory for Archaeology and the History of Art

Bailiff, I.K. and Poolton, N.R.J., (1991)
Studies of charge transfer mechanisms in feldspars
Nucl. Tracks Radiat. Meas., Vol. 18, No. 1/2, 111-118

Balescu, S., Packman, S.C. and Wintle, A.G., (1991)
Chronological separation of interglacial raised beaches from Northwestern Europe using thermoluminescence
Quaternary Research, Vol. 35, 91-102

Balescu, S. and Lamothe, M., (1992)
The blue emission of K-feldspar coarse grains and its potential for overcoming TL age underestimation.
Quat. Sci. Rev., Vol. 11, No. 1/2, 45-51

Balescu, S., Packman, S.C., Wintle, A.G., and Grün, R., (1992)
Thermoluminescence dating of the Middle Pleistocene Raised Beach of Sangatte (Northern France)
Quaternary Research, 37, 390-396

Berger, G.W., (1988)
TL dating studies of tephra, loess and lacustrine sediments
Quat. Sci. Rev., Vol. 7, 295-303

Berger, G.W., Pillans, B.J. and Palmer, A.S., (1992)
Dating loess up to 800 ka by thermoluminescence
Geology, V.20, 403-406

Bϕtter-Jensen, L., (1988)
The automated Risϕ TL dating reader system
Nucl. Tracks Radiat. Meas., Vol. 14, 177-180

Bϕtter-Jensen, L., Ditlefsen, C and Mejdahl, V., (1991)
Combined OSL (infrared) and TL studies of feldspars
Nucl. Tracks Radiat. Meas., Vol. 18, No. 1/2, 257-263

Bowman, S.G.E., (1988)
Observations of anomalous fading in maiolica
Nucl. Tracks Radiat. Meas., Vol. 14, 131-137

Chen, R., (1969a)
On the calculation of activation energies and frequency factors from glow curves
J. Appl. Phys., Vol. 40, No. 2, 570-585

Chen, R., (1969b)
Glow curves with general order kinetics
J. Electrochem. Soc., Vol. 116, No. 9, 1254-1257

Chen, R. and Winer, S.A.A., (1970)
Effects of various heating rates on glow curves
J. Appl. Phys., Vol. 41, No. 13, 5227-5232

Chen, R. and Kirsh, Y., (1981)
Analysis of thermally stimulated processes.
Pergamon Press, Oxford

Clark, P.A. and Templer, R.H., (1988a)
Thermoluminescence dating of materials which exhibit anomalous fading
Archaeometry, Vol. 30, 19-36

Clark, P.A. and Templer, R.H., (1988b)
Dating thermoluminescence samples which exhibit anomalous fading
Nucl. Tracks Radiat. Meas., Vol. 14, 139-141

Dalal, M.L., Kirsh, Y., Rendell, H.M. and Townsend, P.D., (1988)
TL emission spectra of natural feldspar
Nucl. Tracks Radiat. Meas., Vol. 14, Nos. 1/2, 57-62

Debenham, N.C., (1985)
Use of UV emissions in TL dating of sediments
Nucl. Tracks Radiat. Meas., Vol. 10, No. 4-6, 717-724

Delbecq, C.J., Toyozawa,, Y. and Yuster, P.H., (1974)
Tunnelling recombination of trapped electrons and holes in KCl:AgCl and KCl:TlCl
Phys. Rev. B9, No. 10, 4497-4505

Dijkmans, J.W.A. and Wintle, A.G., (1989)
Fractional bleaching of potassium feldspar from sediments and its role in equivalent dose determination
Ancient TL, Vol. 7, 5-10

Duller, G.A.T., (1991)
Equivalent dose determination using single aliquots
Nucl. Tracks Radiat. Meas., Vol. 18, No. 4, 371-378

Duller, G.A.T. and Wintle, A.G., (1991)
On infrared stimulated luminescence at elevated temperatures
Nucl. Tracks Radiat. Meas., Vol. 18, No. 4, 379-384

Fleming, R.J., (1990)
Activation energies and temperature-dependent frequency factors in thermally stimulated luminescence
J. Phys. D: Appl. Phys., Vol. 23, 950-954

Frechen, M., (1992)
Systematic thermoluminescence dating of two loess profiles from the Middle Rhine Area (F.R.G.)
Quat. Sci. Rev., Vol. 11, 93-101

Frechen, M, Brückner, H. and Radtke, U., (1992)
A comparison of different TL-techniques on loess samples from Rheindahlen (F.R.G.)
Quat. Sci. Rev., Vol. 11, 109-113

Galloway, R.B., (1991)
A versatile 40-sample system for TL and OSL investigations
Nucl. Tracks Radiat. Meas., Vol. 18, No. 1/2, 265-271

GE/RCA, (1987)
Optoelectronics Data Book

Gobrecht, H. and Hofmann, D., (1966)
Spectroscopy of traps by fractional glow technique
J. Phys. Chem. Solids, Vol. 27, 509-522

Godfrey-Smith, D.I., Huntley, D.J., and Chen, W.H., (1988)
Optical dating studies of quartz and feldspar sediment extracts.
Quat. Sci. Rev., Vol. 7, 373-380

Godfrey-Smith, D.I., (1991)
Optical dating studies of sediment extracts
Unpublished PhD. thesis, Simon Fraser University, Canada

Grün, R., Packman, S.C. and Pye, K., (1989)
Problems involved in TL-dating of Danish Cover sands using K-feldspar
In Long and short range limits in luminescence dating,
Occasional Publication No. 9, Research Laboratory for Archaeology and the History of Art

Guerin, G. and Valladas, G., (1980)
Thermoluminescence dating of volcanic plagioclases
Nature, Vol. 286, 697-699

Hayes, W. and Stoneham, A.M., (1985)
Defects and defect processes in non-metallic solids.
John Wiley and Sons, Inc., New York

Huntley, D.J., (1985)
A note on the temperature dependence of anomalous fading
Ancient TL, Vol. 3, No. 1, 20-21

Huntley, D.J., Godfrey-Smith, D.I. and Thewalt, M.L.W., (1985)
Optical dating of sediments
Nature, Vol. 313, 105-107

Huntley, D.J., Godfrey-Smith, D.I., Thewalt, M.L.W. and Berger, G.W., (1988)
Thermoluminescence spectra of some mineral samples relevant to thermoluminescence dating
Journal of Luminescence, Vol. 39, 123-136

Huntley, D.J., McMullan, W.G., Godfrey-Smith, D.I., Thewalt, M.L.W., (1989)
Time-dependent recombination spectra arising from optical ejection of trapped charges in feldspars
Journal of Luminescence, Vol. 44, 41-46

Huntley, D.J., Godfrey-Smith, D.I. and Haskell, E.H., (1991)
Light-induced emission spectra from some quartz and feldspars
Nucl. Tracks Radiat. Meas., Vol. 18, 127-131

Hütt, G., Jaek, I. and Tchonka, J., (1988)
Optical dating: K-feldspars optical response stimulation spectra.
Quat. Sci. Rev., Vol. 7, 381-385

Hütt, G. and Jaek, I., (1989)
Infrared photoluminescence (PL) dating of sediments: modification of physical model, equipment and some dating results
In Long and short range limits in luminescence dating,
Occasional Publication No. 9, Research Laboratory for Archaeology and the History of Art

Hütt, G. and Jaek, I., (1989)
The validity of the laboratory reconstruction of palaeodose
Ancient TL, Vol. 7, No. 2, 1989

Jungner, H. and Huntley, D.J., (1991)
Emission spectra of some potassium feldspars under 633 nm stimulation
Nucl. Tracks Radiat. Meas., Vol. 18, 125-126

Kierstead, J.A. and Levy, P.W., (1991)
Validity of repeated initial rise thermoluminescence kinetic parameter determinations
Nucl. Tracks Radiat. Meas., Vol. 18, No. 1/2, 19-25

Kirsh, Y. and Townsend, P.D., (1988)
Speculations on the blue and red bands in the TL emission spectrum of albite and microcline
Nucl. Tracks Radiat. Meas., Vol. 14, No. 1/2, 43-49

Kirsh, Y., (1992)
Kinetic analysis of thermoluminescence: theoretical and practical aspects
Phys. Stat. Sol.(a), Vol. 129, 15-48

Kirsh, Y., Shoval, S., Yariv, S. and Kristianpoller, N. (1989)
Natural and β-induced Thermoluminescence in Microcline
Phys. Stat. Sol. (a), Vol. 113, 631-636

Kirsh, Y., Kristianpoller, N. and Shoval, S., (1990)
Kinetic analysis of natural and beta-induced TL in albite
Rad. Prot. Dosim., Vol. 33, No. 1/4, 63-66

Kirsh, Y. and Chen, R., (1991)
Analysis of the blue phosphorescence of X-irradiated albite using a TL-like presentation
Nucl. Tracks Radiat. Meas., Vol. 18, No. 1/2, 37-40

Krϕnborg, C., (1983)
Preliminary results of age determination by TL of interglacial and interstadial sediments
PACT 9, Part II, 595-605

Levy, P.W., (1982)
Thermoluminescence and optical bleaching in minerals exhibiting second order kinetics and other charge retrapping characteristics
PACT Vol. 6, 224-242

Lewandowski, A.C. and McKeever, S.W.S., (1991)
Generalised description of thermally stimulated processes without the quasiequilibrium approximation
Phys. Rev., Vol. B43, No. 10, 8163-8178

Li, S.H. and Wintle, A.G., (1991)
Sensitivity changes of luminescence signals from colluvial sediments after different bleaching procedures.
Ancient TL, Vol. 9, No. 3, 50-53

Li, S.H. and Wintle, A.G., (1992)
A global view of the stability of luminescence signals from loess
Quat. Sci. Rev., Vol. 11, 133-137

Li, S.H., (1992)
Development and application of stimulated luminescence dating methods for sediments
Unpublished PhD thesis, University College of Wales, Aberystwyth

Lu Yanchou, Zhang Jingzhao and Xie Jun, (1988)
Thermoluminescence dating of loess and palaeosols from the Lantian section, Shaanxi Province, China
Quat. Sci. Rev., Vol. 7, 245-250

Luff, B.J. and Townsend, P.D., (1992)
High sensitivity thermoluminescence spectrometer
Meas. Sci. Technol., Vol. 3, 1-7

Mathur, V.K., Gasiot, J., Abbundi, R.J., and Brown, M.D., (1986)
Optically stimulated luminescence in MgS:Ce,Sm
Radiat. Prot. Dosim., Vol. 17, 333-336

McKeever, S.W.S.. (1985)
Thermoluminescence of solids.
Cambridge University Press, Cambridge

Mejdahl, V. and Winther-Nielsen, M., (1982)
TL dating based on feldspar inclusions
PACT Vol. 6, 426-437

Mejdahl, V., (1983)
Feldspar inclusion dating of ceramics and burnt stones
PACT Vol. 9, 351-364

Mejdahl, V., (1986)
Thermoluminescence dating of sediments
Rad. Prot. Dos., Vol. 17, 219-227

Mejdahl, V. (1988)
Long-term stability of the TL signal in alkali feldspars
Quat. Sci. Rev., Vol. 7, 357-360

Mejdahl, V. (1989)
How far back: life times estimated from studies of feldspars of infinite ages
In Long and short range limits in luminescence dating,
Occasional Publication No. 9, Research Laboratory for Archaeology and the History of Art

Mejdahl, V., Shlukov, A.I., Shakhovets, S.A., Voskovskaya, L.T., and Lyashenko, H.G.. (1992)
The effect of shallow traps: a possible source of error in TL dating of sediments.
Ancient TL, Vol.10, No.2, 22-25

Melles-Griot., (1988)
Optics Guide 4

Mott, N.F. and Gurney, R.W., (1953)
Electronic processes in ionic crystals
Oxford University Press

Nambi, K.S.V., (1984)
Alpha-radioactivity-related upper age limit for thermoluminescence dating
Procs. of the Indian Academy of Sciences-Earth and Planetary Sciences
Vol. 93, Iss. 1, 47-56

Noolandi, J., (1987)
Stochastic theory of electron-hole transport and recombination in amorphous materials
In: Kinetics of non-homogeneous processes
Ed. G.R. Freeman., J. Wiley & Sons, 465-532

Packman, S.C. and Grün, R., (1989)
TL dating of loess samples from Achenheim
In Long and short range limits in luminescence dating,
Occasional Publication No. 9, Research Laboratory for Archaeology and the History of Art

Packman, S.C. and Grün, R., (1989)
TL analysis of loess samples from Achenheim
Quat. Sci. Rev., Vol. 11, 103-107

Pasternack, E.S. and Levy, P.W., (1978)
Changes in TL emission spectra accompanying thermal disorder in Amelia albite
Geological abstracts with programs, 10, 468

Poolton, N.R.J. and Bailiff, I.K.. (1989)
The use of LEDs as an excitation source for photoluminescence dating of sediments.
Ancient TL, Vol. 7, 18-20

Questiaux, D.G.. (1991)
Optical dating of loess: comparisons between different grain size fractions for infrared and green excitation wavelengths
Nucl. Tracks Radiat. Meas., Vol. 18, 133-139

Rendell, H.M. and Townsend, P.D., (1988)
Thermoluminescence dating of a 10 m loess profile in Pakistan
Quat. Sci. Rev., Vol. 7, 251-255

Rendell, H.M., (1992)
A comparison of TL age estimates from different minerals fractions of sands
Quat. Sci. Rev., Vol. 11, 79-83

Robertson, G.B., Prescott, J.R. and Hutton, J.T., (1991)
Bleaching of the thermoluminescence of feldspars by sunlight
Nucl. Tracks Radiat. Meas., Vol. 18, No. 1/2, 101-107

Robertson, G.B., Prescott, J.R. and Hutton, J.T., (0000)
Bleaching of the thermoluminescence of feldspars by selected wavelengths present in sunlight
Nucl. Tracks Radiat. Meas., Vol. 00, No. 0, 000-000

Sanderson, D.C.W., Clark, R.J., Slater, C. and Cairns, K.J., (1989)
TL dating using alkali feldspars: high dose characteristics and stability estimates
In Long and short range limits in luminescence dating,
Occasional Publication No. 9, Research Laboratory for Archaeology and the History of Art

Smith, B.W., (1983)
New applications of thermoluminescence dating and comparisons with other methods
Unpublished PhD thesis, University of Adelaide, Australia

Smith, B.W., Aitken, M.J., Rhodes, E.J., Robinson, P.D. and Geldard, D.M., (1986)
Optical Dating: Methodological Aspects
Radiat. Prot. Dosim., Vol. 17, 229-233

Smith, B.W.. (1988)
Zircon from sediments: a combined OSL and TL auto-regenerative technique.
Quat. Sci. Rev., Vol. 7, 401-406

Smith, B.W., Wheeler, G.C.W.S., Rhodes, E.J. and Spooner, N.A.. (1991)
Luminescence dating of zircon using an imaging photon detector.
Nucl. Tracks Radiat. Meas., Vol.18, No. 1/2, 273-278

Spooner, N.A.. (1987)
The effect of light on the thermoluminescence of quartz.
Unpublished MSc Thesis, University of Adelaide, Australia

Spooner, N.A., Prescott, J.R. and Hutton J.T., (1988)
The effect of illumination wavelength on the bleaching of the thermoluminescence (TL) of quartz
Quat. Sci. Rev., Vol. 7, 325-329

Spooner, N.A., Aitken, M.J., Smith, B.W., Franks, M., and McElroy, C., (1990)
Archaeological dating by infrared-stimulated luminescence using a diode array.
Rad. Prot. Dos., Vol. 34, No. 1/4, 83-86

Spooner, N.A. and Questiaux, D.G., (1989)
Optical Dating - Achenheim beyond the Eemian using green and infrared stimulation
In Long and short range limits in luminescence dating,
Occasional Publication No. 9, Research Laboratory for Archaeology and the History of Art

Spooner, N.A. and Franks, M., (1990)
Some characteristics of infrared emitting diodes relevant to luminescence dating
Ancient TL, Vol. 8, No.3, 16-19

Spooner, N.A., (1992)
Optical dating: Preliminary results on the anomalous fading of luminescence from feldspars
Quat. Sci. Rev., Vol. 11, 139-145

Stoneham, D. and Winter, M.B., (1988)
The removal of anomalous fading in authenticity samples
Nucl. Tracks and Radiat. Meas., Vol. 14, 127-130

Strickertsson, K., (1985)
The thermoluminescence of potassium feldspars - glow curve characteristics and initial rise measurements
Nucl. Tracks and Radiat. Meas., Vol. 10, Nos 4-6, 613-617

Strickertsson, K. (1989)
Trap spectra and mean life determinations for potassium feldspars from Nordic sediments; Nordic bedrock and Scottish vitrified forts
In Long and short range limits in luminescence dating,
Occasional Publication No. 9, Research Laboratory for Archaeology and the History of Art

Templer, R. H., (1985)
The removal of anomalous fading in zircon
Nucl. Tracks and Radiat. Meas, Vol. 10, Nos 4-6, pp. 531-537

Templer, R. H., (1985b)
The dating of zircons by auto-regenerated TL at low temperatures
Nucl. Tracks and Radiat. Meas, Vol. 10, Nos 4-6, pp. 789-798

Templer, R. H., (1986a)
The localised transition model of anomalous fading
Radiation Protection Dosimetry, Vol. 17,pp. 493-497

Templer, R. H., (1986b)
Thermoluminescence techniques for dating zircon inclusions
Unpublished D.Phil thesis, University of Oxford

Townsend, P.D. and Kirsh, Y., (1989)
Spectral measurement during thermoluminescence - an essential requirement
Contempory Physics, Vol. 30, No. 5, 337-354

Tyler, S. and McKeever, S.W.S., (1988)
Anomalous fading of thermoluminescence in oligoclase
Nucl. Tracks and Radiat. Meas., Vol. 14, 149-154

Urbach, F., (1953)
The long-wavelength edge of photographic sensitivity and of the electronic absorption of solids
Phys. Rev., 2nd series, Vol. 92, 1324

Visocekas, R., Ceva, T., Marti, C., Lefaucheux, F. and Robert, M.C., (1976)
Tunnelling processes in afterglow of calcite
Physica Status Solidi (a), Vol. 35, 315-327

Visocekas, R., (1979)
Miscellaneous aspects of artificial TL of calcite: emission spectra, athermal detrapping and anomalous fading
PACT 3, 258-265

Visocekas, R., (1985)
Tunnelling radiative recombination in labradorite: its association with anomalous fading of thermoluminescence
Nucl. Tracks Radiat. Meas., Vol. 10, 521-529

Visocekas, R., (1993)
Tunnelling radiative recombination in K-feldspar sanidine
Nucl. Tracks Radiat. Meas., Vol. 21, No. 1, 175-178

Wheeler, G.C.W.S., (1990)
Luminescence studies relevant to archaeological dating
Unpublished D.Phil thesis, University of Oxford

Wintle, A.G., (1973)
Anomalous fading of thermoluminescence in mineral samples
Nature, Vol. 245, 143-144

Wintle, A.G., (1974)
Factors determining the thermoluminescence of chronologically significant materials
Unpublished D.Phil thesis, University of Oxford

Wintle, A.G., (1977)
Detailed study of a thermoluminescent mineral exhibiting anomalous fading
Journal of Luminescence, Vol. 15, 385-393

Wintle, A.G., (1985)
Sensitization of TL signal by exposure to light.
Ancient TL, Vol. 3, 16-21

Wintle, A.G. and Packman, S.C., (1988)
Irradiation of loess samples at elevated temperatures
Ancient TL, Vol. 6, 22-23

Wintle, A.G. and Duller, G.A.T., (1991)
The effect of optical absorption on luminescence dating
Ancient TL, Vol. 9, No. 3, 37-39

Wintle, A.G., Questiaux, D.G., Roberts, R. and Spooner, N.A., (1993)
Comments on "Dating loess up to 800 ka by thermoluminescence"
Geology, Vol. 000, 000-000

Xie, J. and Aitken, M.J., (1991)
The hypothesis of mid-term fading and its trial on Chinese loess
Ancient TL, Vol. 9, No. 2, 21-25

Zhou, Li-Ping and Wintle, A.G., (1989)
Underestimation of regeneration ED encountered in Chinese loess
In Long and short range limits in luminescence dating,
Occasional Publication No. 9, Research Laboratory for Archaeology and the History of Art

Zöller, L. and Wagner, G.A., (1989)
Strong or partial thermal washing in TL-dating of sediments?
In Long and short range limits in luminescence dating,
Occasional Pub. No. 9, Research Laboratory for Archaeology and the History of Art